Structural and functional investigation of the cytoplasmic domain of the Fas death receptor

Gemma Claire Wildsmith

University College London

A thesis submitted for the degree of Doctor of Philosophy

June 2014

I, Gemma Claire Wildsmith confirm that the work presented in this thesis is my own. Where information has been derived from other sources, I confirm that this has been indicated in the thesis.

Abstract

Activation of the transmembrane death receptor Fas (CD95/APO-1) by a membrane bound ligand (FasL/CD95L) activates the extrinsic pathway of apoptosis. Intracellular Fas death domains (DDs) are induced to oligomerise enabling binding to the adaptor protein FADD, thereby leading to the recruitment of procaspase 8 and other proteins to form the death inducing signalling complex (DISC).This thesis describes an investigation of the structure and function of the cytoplasmic Fas-DD.

A model for the solution structure of the Fas-DD was published in 1996, it has since been reported that the death domain can form at least one other conformation when in complex with FADD. As a foundation to the work in this thesis, modern multidimensional NMR techniques have been used to solve the structure of the Fas-DD, to further probe the potential for alternative conformations.

It has previously been reported that Fas can be phosphorylated at Tyr291, providing a platform for the recruitment of binding partners that can affect non-apoptotic signalling. The second part of this thesis details the development of an expressed protein ligation methodology to prepare a Tyr291 phosphorylated Fas DD to provide a basis for *in vitro* studies of the structural, dynamic and functional effects of phosphorylation.

It is widely accepted that Fas is palmitoylated at Cys199 and recognised by the membrane cytoskeletal protein, ezrin. Fas palmitoylation is important for clathrin-mediated internalisation of the DISC, and amplification of the caspase cascade. There are multiple reports detailing the binding of ezrin to Fas, but it is not clear whether this interaction occurs in a palmitoylation-dependent manner. Efforts to characterise an interaction between bacterially expressed intracellular Fas and ezrin proteins were carried out using a number of biophysical assays, described in the third part of this thesis. Building upon this, the fourth section explores the preparation of a palmitoylated Fas construct suitable for biophysical analysis by incubating recombinant Fas with palmitoyl-CoA.

Acknowledgements

To start, I would like to thank my supervisor Dr Paul Driscoll for giving me the opportunity to pursue such a varied project. I also would like to acknowledge my Thesis Committee: Dr Annalise Pastore, Dr Katrin Rittinger and Dr Steve Smerdon for taking the time during my PhD to critically examine my project, and the Medical Research Council for funding this work.

I would like to thank Dr Steve Martin, Dr Ian Taylor, Dr Pete Coombes and Dr Katrin Rittinger for their help and guidance with a number of the biophysical techniques carried out within this project. Dr Tom Frienkiel, Dr Alain Oregioni and Dr Geoff Kelly from the NMR centre have offered a world of help and information whenever I have been panicked and for that I am very grateful. My gratitude also to our collaborators in Dr John Offer's laboratory who shared their knowledge on peptide chemistry, in particular Caroline Morris who I can safely say taught me everything peptide I know.

I don't think I will ever be able to thank the members of the Driscoll lab (both past and present) enough for all they have done for me to make this thesis come about. In particular to Dr TJ Ragan for consistently moving the goal posts and teaching me so much (one day I want to just 'search' without the 're'), Dr Diego Esposito for his huge effort on helping the structure to converge and Dr Christine Richter for her kind reassuring words and the final proof reading of this thesis. Dr Acely Garza-Garcia I cannot thank you enough for the mammoth, rich tea biscuit fuelled effort you have put into making sure I was progressing, I am eternally grateful, you have taught me so much. Thank you to Dr Lily Nematallohi for being there, for teaching me so much and being my lab mum and Lucy Murfitt, Thari Fernando and Dr Masooma Rasheed for ensuring there was never a dull moment. Thank you all for holding me together, challenging me and being there for me I couldn't have asked for a friendlier more knowledgable working environment. If I ever know a mear fraction of what these people do about life and science I would be amazed.

My thanks also go to all my friends, both within NIMR and out, for being there to support me and for their continual encouragement. In particular to 'Team Thesis', who really kept me going in those final 24 hours. Thank you to my parents, your example, support and belief in me to succeed has never faltered.

Last but by no means least I would like to thank James Ellis, your continued support and just being there when I was struggling meant the world to me. Thank you!

Table of contents

List of figures

List of tables

Abbreviations

ACBP	acyl-coA binding protein
ALPS	Autoimmune lymphoproliferatave syndrome
AMPK	AMP-activated protein kinase
APT	acyl protein thioesterase
ARIA	Ambiguous Restraints for Iterative Assignment
ASC	apoptosis-associated speck like protein containing a CARD)
AUC	Analytical ultracentrifugation
BAX	BCL-2-associated X protein
BBB	blood brain barrier
BLAST	Basic Logical Alignment Search Tool
BLI	Biolayer interferometry
BSA	Bovine serum albumin
cAMP	cyclic adenosine monophosphate
CARD	Caspase recruitment domain
CBD	Chitin binding domain
cDNA	complementary DNA
c-FLIP	Cellular - Flice like inhibitory protein
CHCA	*α-cyano-4-hydroxycinnamic acid*
CoA	coenzyme A
CSI	Chemical shift index
CV	Column volume
DCM	Dichloromethane
DD	Death domain
ddH2O	double distilled?? Water
DDsf	Death domain superfamily
DED	Death effector domain
DEF	Death effector filament
DHHC-CRD	Asp-His-His-Cys- cysteine rich domain
DIC	1,3-diisopropylcarbodiimide
DIEA	N,N-diisopropylethylamine
DISC	death inducing signalling complex
DMF	Dimethylformamide
DMSO	Dimethyl sulfoxide
DNA	Deoxyribonucleicacid
DR	death receptor
DRM	detergent resistant microdomains
DTNP	2,2′-Dithiobis(5-nitropyridine)
DTT	Dithiothreitol
E coli	*Escheria coli*
EBD	ezrin binding domain

EBP50	ERM binding phosphoprotein 50
EDT	1,2-ethanedithiol
EDTA	ethylenediaminetetracetic acid
EGFR	extra cellular growth factor receptor
EMP	Exponential megapriming
EPL	Expressed Protein Ligation
ERM	Ezrin, radixin, moesin protein family
ERMAD	ezrin, radixin, moesin association domain
ESI-TOF-MS	Electrospray ionisation - time of flight - mass spectrometry
FADD	Fas associated death domain
FAP-1	Fas associated phosphatase-1
Fas-DD	Fas death domain
FasL	Fas ligand
FERM	four point one, ezrin, radixin, moesin domain
Fmoc	9-fluorenylmethyoxycarbonyl
g	grams
G	G-force
GB1	Gl Binding domain of immunoglobulin 1
GST	Glutathione-S-transferase
H6	Hexa-histidine
H**B**TU	N-[(1H-benzotriazol-1-yl)(dimethylamino)methylene]-N-methylmethanaminium hexafluorophosphate N-oxide
HCl	Hydrochloric acid
HOBt	hydroxybenzotriazole
HPLC	High pressure liquid chromatography
HSQC	Hetronuclear single quantum coherence
Htmb	2-hydroxy-3-thio-4-methoxy)benzy
ICAM	Intracellular adhesion molecule
IMAC	Immobilised metal affinity chromatography
IMPACT	intein mediated purification with an affinity chitin binding tag
IPAP	in-phase anti-phase
IPTG	Isopropyl β-D-1-thiogalactopyranoside
IRAK	interleukin-1 receptor associated kinase
ITC	Isothermal titration calorimetry
IVP	in vitro palmitoylation
JNK	Janus kinase
LB	Luria broth
LDS	lithium dodecyl sulfate
LIC	Ligation independent cloning
LRR	lyscine rich region
MALDI-TOF-MS	*Matrix-assisted laser desorption ionisation time of flight mass spectrometry*
MAPK	Mitogen activated protein kinase
MBP	Maltose binding protein

MEND	massive endocytosis
MES	2-(N-morpholino)ethanesulfonic acid
MPAA	mercaptophenylacetic acid
MRC	Medical Research Council
MWCO	molecular weight cut off
Mxe	Myx Gyr A intein
NCBI	National Centre for Biotechnology Information
NEB	New England Biolabs
NF-κB	Nuclear Factor kappa B
NHERF	Na/H exchange regulatory cofactor
NIMR	National Institute for Medical Research
Ni-NTA	Nickle Nitrilotriacetic acid
NMP	N-methyl-2-pyrrolidone
NMR	nuclear magnetic resonance
NOE	Nuclear overhouser effect
NOESY	Nuclear overhouser effect spectroscopy
Nt-Fas-DD	N-terminal Fas- death domain
PAT	protein acyl transferase
PCD	programmed cell death
PCR	polymerase chain reaction
PDB	protein data bank
pH	power hydrogen
PIDD	p53-induced death domain
PIP2	phosphatidylinositol 4,5-bisphosphate
PPT	protein palmitoyl thioesterase
pY	phospho-tyrosine
pY-Ct-Fas-DD	phospho-tyrosine C-terminal Fas death domain
PYD	pyrin domain
RAIDD	RIP-associated Ich-1 protein with a death domain
RDC	Residual dipolar coupling
RP-HPLC	Reverse phase high pressure liquid chromatography
SDS-PAGE	sodium dodceylsuphate polyacylramide gel elctrophoresis
SEC	Size exclusion chromatography
SH2	Src-Homology 2
SH3	src homology 3
SHP	(SH2)-containing tyrosine phosphatase
SPPS	Solid phase peptide synthesis
SW	sweep width
TCEP	Tris-(2-Carboxyethyl)phosphine, hydrochloride
TCR	T cell receptor
TEV	Tobacco etch virus
TFA	trifluoroacetic acid
TM	melting temperature

TNF	Tumor necrosis factor
TNFR1	tumour necrosis factor receptor 1
TRAIL	TNF-related inducing ligand
TROSY	Transverse relaxation- optimised Spectroscopy
UV	Ultra violet
ψP	pseudo proline

Chapter 1

Introduction

1.1 T-cell stimulation eliminates infected cells and activates the adaptive immune response

The development of the adaptive immune system is undeniably one of the greatest milestones in the evolution of jawed vertebrates. Innate immunity provides a non-specific first line of defence against potentially harmful microorganisms and molecules. In contrast, the adaptive immune system is more specific resulting in a highly specialised, pathogen-specific immune response and a long-lasting immunological memory of each infection. The functions of the adaptive immune response are carried out by the lymphocytes. There are two main classes of lymphocytes, T-cells and B-cells; B-cells are involved in antibody production and response while T-cells carry out cell-mediated immune responses.

Upon pathogen detection and initiation of the cell mediated immune response, antigen presenting cells, such as B-cells, dendritic cells and macrophages internalise and degrade the pathogen. Peptide fragments of the pathogen are then incorporated into major histocompatibility complexes (MHC) which are trafficked to and presented on the cell surface. T-cell activation occurs through the recognition and direct interaction with an antigen upon an MHC by the T-cell receptor (TCR).

Much like antibodies, T-cell receptors are hypervariable, with the T-cell only becoming active when the TCR is able to bind the antigen fragment bound to the MHC. An activated T-cell can either go on to initiate cell death in cells infected with intracellular pathogens or produce signalling molecules that amplify the immune response. T-cell signalling acts by stimulating and activating immune cell proliferation, antibody production, phagocytosis, and elimination of the infected cell.

1.2 The population of activated T-cells is tightly regulated by apoptosis

In order to prevent an excessive immune response, T-cell homeostasis is achieved through programmed cell death (PCD), also known as apoptosis. PCD results in the systematic breakdown of the cell by the cysteine proteases known as caspases. The final outcome of PCD is the formation of membrane-enclosed cellular breakdown products called apoptotic bodies, which are eliminated by phagocytosis. Unlike necrosis, which is the result of cell injury or external factors, PCD is a highly regulated planned cell death and, because it does not result in the leakage of cell contents, it does not cause inflammation of the surrounding tissues.

Apoptosis can be initiated intrinsically, when started internally from the mitochondria, or extrinsically when triggered via the activation of a transmembrane receptor. These two mechanisms are not mutually exclusive and they can probably influence one another[1]. In both pathways the outcome is cellular breakdown, culminating in the formation of the apoptotic bodies (Figure 1.1).

In the case of T-cell homeostasis, intrinsic apoptosis is triggered by the absence of survival stimuli such as growth factors and cytokines, whereas in other cell populations the intrinsic pathway can be triggered by external stimuli such as radiation, toxins and hypoxia. The removal of pro-survival signalling molecules triggers cytochrome C release from the mitochondria, inducing activation of caspase 9 through the formation of a complex known as the apoptosome and activation of caspase 2 through the formation of a complex known as the PIDDosome. The extrinsic pathway is triggered by ligand biding to one of the members of the tumour necrosis factor receptor (TNFR) family. These transmembrane receptors are formed by several cysteine-rich extracellular domains, and a cytoplasmic region comprising a death domain[2]. Upon activation, the death domain of the receptor is able to recruit other death-domain containing cytoplasmic adaptor proteins which in turn activate the caspases. The most well studied death receptor/ligand interactions are the ones between Fas (CD95) and Fas ligand (FasL) and TNFR1 and TNF-α, although many others exist (e.g. Death Receptor 3 (DR3) and TNF12, DR4 and TNFSF10).

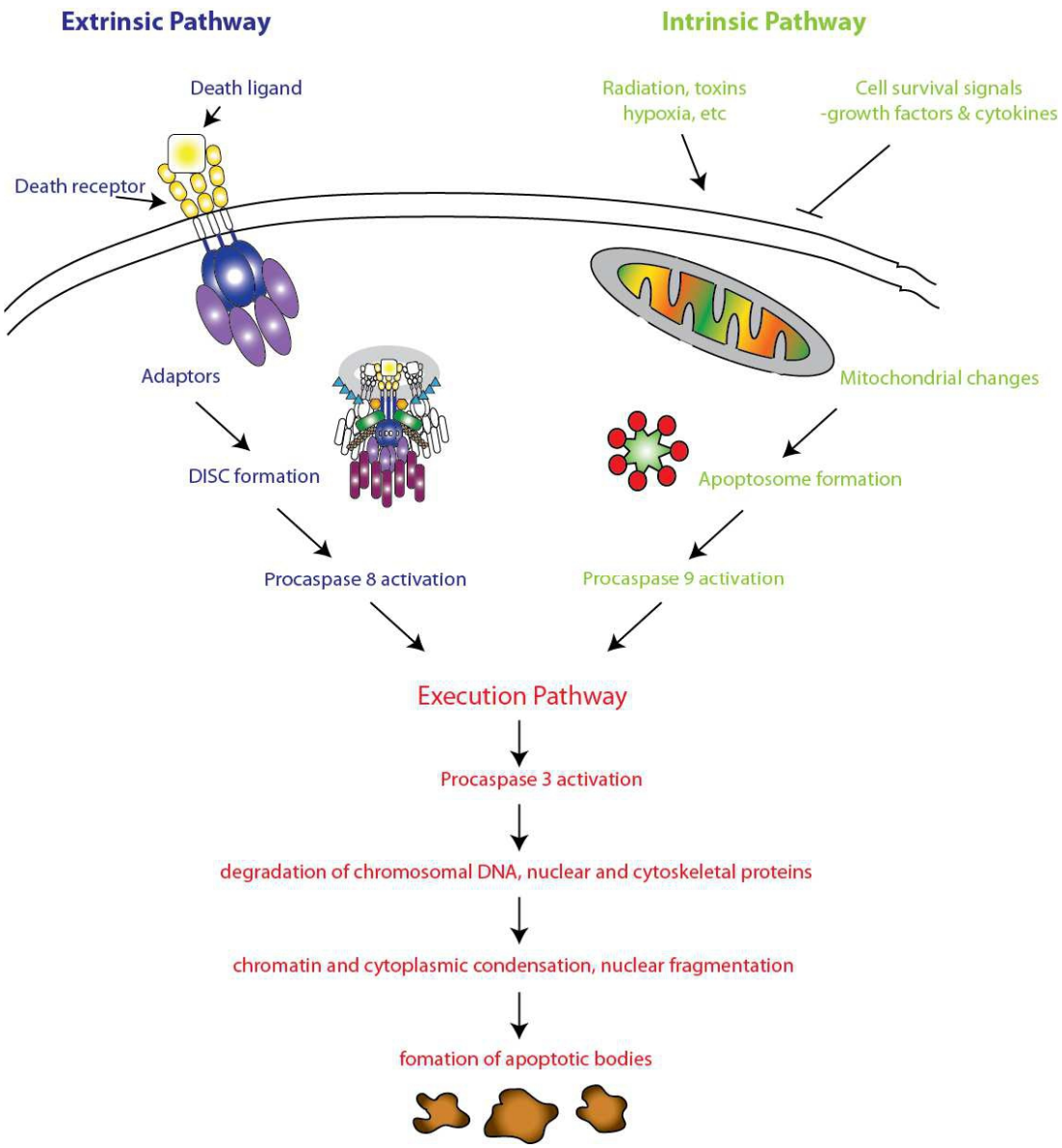

Figure 1.1 – Schematic representation of apoptotic pathways

The extrinsic and intrinsic pathways are the two main apoptotic pathways. Extrinsic apoptosis is activated through death receptor mediated signalling activating procaspase 8. Intrinsic apoptosis is initiated through cell stress which affects the mitochondria inducing apoptosome formation and activation of procaspase 9. Procaspases 8 and 9 initiate the execution pathway resulting in cell breakdown. DISC – death inducing signalling complex. Adapted from Elmore 2007.

The extrinsic and the intrinsic PCD pathways converge on the execution pathway that results in activation of the highly regulated process of caspase activation known as the caspase cascade. Caspases exist in the cell in an inactive 'procaspase' form until cellular signalling enables the release of the active enzyme through an autocatalytic mechanism (discussed in more detail below). Caspases 8, 10, 2 and 9 are known as 'initiator' caspases as they are the first members of the caspase cascade to be activated. Caspases 8 and 10 are activated in the extrinsic pathway, while 2 and 9 are activated in the intrinsic pathway.

The initiator caspases have limited target specificity, cleaving and activating the 'effector' caspases, 3, 6 and 7. Effector caspases execute cell death by digesting cellular components such as the cytoskeleton and nuclear lamins. This specific order of caspase activation enables tight regulation of the enzymes that are responsible for cellular breakdown, with initiator caspases acting as a check point to ensure that the effector caspases are only activated under the correct stimuli. Caspases are not just involved in cell death, there are other 'inflammatory' caspases (1, 4, 5, 11, 12, 14) that are activated in response to pathogenic infection and autoimmune disorders[3].

1.3 Homotypic interactions between death domain superfamily members are widespread in apoptosis and inflammation signalling

TNFRs and initiator caspases are some of the many proteins involved in apoptosis signalling that interact with each other through a domain belonging to the death domain superfamily (DDsf). Although there is up to 90% sequence divergence between members of this domain superfamily, they all fold to form a 80-100 residue long globular antiparallel six helical Greek key motif[4] with a minimal hydrophobic core.

Subtle differences between each domain in the length and orientation of the helices and the location of surface charge affect their mechanisms of interaction and are used to classify them into four families[5]: Death domain (DD), death effector domain (DED), caspase recruitment domain (CARD) and pyrin domain (PYDs). Figure 1.2 and Figure 1.3 illustrate structural and sequence differences between the members of the four subfamilies. According to the SMART database, DD and CARD families are present in all metazoan phyla, but only deuterostomes possess proteins with PYD domains and only chordates, cnidarians and echinoderms have proteins with DEDs. The human proteome has 27 proteins with DDs, 7 proteins with DEDs, 29 proteins with CARDs, and 22 proteins with PYDs. Some families of double-stranded DNA viruses possess proteins with DEDs and PYDs; this is thought to have occurred through horizontal gene transfer[4]. A distinctive and puzzling feature of the DDsf is that they only interact in a homotypic manner, *i.e.* DD-DD, DED-DED, CARD-CARD or PYD-PYD[5].

Figure 1.2 Sequence alignments of members of the death domain superfamily

Conserved residues are shaded dependent upon percentage identity (PID) - the percentage of the residues in the column that agree with the consensus sequence. Secondary structure representations are shown above each of the alignments. Protein sequences were downloaded from UniProt aligned using the MAFFT algorithm and visualised using Jalview.

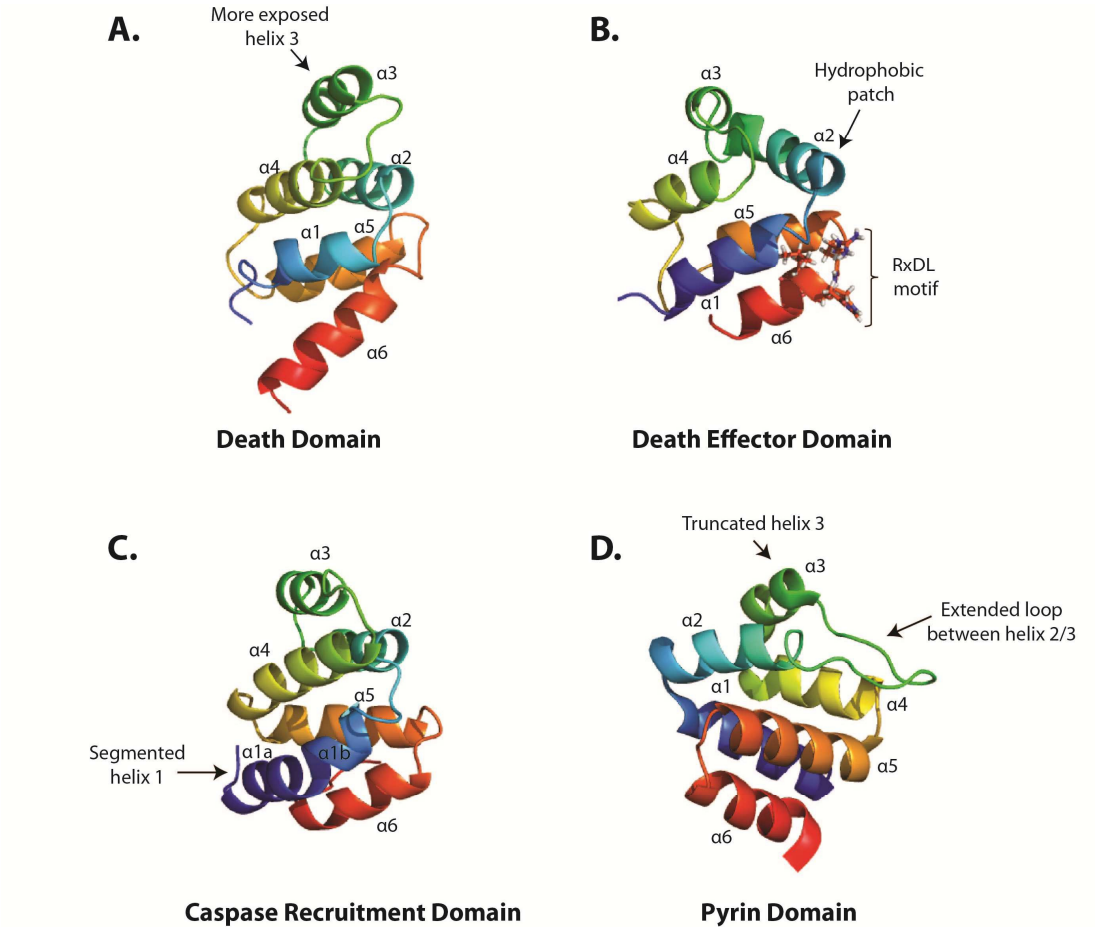

Figure 1.3 Schematic representations of the structures of representative members of the death domain superfamily

A, the death domain of Fas (PDB:1DDF); B, the death effector domain of FADD (PDB:1A1W); C, the caspase recruitment domain of Apaf1 (PDB:3YGS); D, the pryin (PYD) domain of ASC (PDB:1UCP). Helix colour corresponds to helix number. A, B and C are positioned in the same orientation. D is rotated 180^{o} along the Y axis to highlight the shorter helix 3.

1.3.1 Death domains assemble to form large signalling complexes

Death domains (DDs) were the first members of the DDsf to be identified both structurally and functionally[5]. They are found in the intracellular region of the family of transmembrane death receptors and of the UNC5 netrin receptors, as well as in intracellular proteins involved in apoptosis, necrosis and inflammation, such as Receptor-interacting protein 1 kinase (RIP1K), interleukin-1 receptor-associated kinase (IRAK) 3 and 4, THO complex subunit 1 (THOC1), Myeloid differentiation primary response protein MyD88, and the p100 subunit of the nuclear factor kappa-B. Adaptor proteins with DDs that are involved in apoptosis activation or modulation include FAS-associated death domain protein (FADD), RIP-associated Ich-1 protein with a death domain (RAIDD), Tumour necrosis factor receptor type 1-associated death domain protein (TRADD), and p53 induced protein with a death domain (PIDD).

The solution structures of the isolated DDs of Fas, FADD, TNFR1, and TNFR16 and the crystal structures of the IRAK4, RAIDD, PELLE, TUBE, MyD88 death domains have highlighted common features within this domain family[5]. The overall structure of the death domain forms a six amphipathic helical structure that is considered a perpendicular arrangement of two three-helix bundles. The feature that is characteristic of the DDs is that helix one and two are centrally located and helix three is more flexible and surface exposed. The surfaces of the DDs are characteristically charged, and it is thought that DD-DD interactions are predominantly mediated through electrostatic interactions[4,6].

Some proteins with death domains form heteromeric complexes that activate effector molecules. For example, the DDs of Fas and FADD have been identified as the core blocks of the death inducing signalling complex (DISC), a structure that leads to the activation of caspases 8 and 10 in the extrinsic apoptotic pathway. Also, the DDs of RAIDD and PIDD form the core of the PIDDosome, a structure responsible for the activation of caspase 2 in the intrinsic apoptotic pathway. Death domains show a tendency to self-aggregate and this is thought to be important for function. For example, for DISC progression the Fas death domains must initially homo-oligomerise prior to interacting with FADD[5]. Based on extrapolation of the crystal structure data of the death-domain containing complexes PIDDosome, MyDDosome

and the DISC, it has been proposed that each DD has six potential interaction surfaces. These surfaces arise by a combination of three non-overlapping interaction types[4]. Chapter three presents more in depth information about the 3D structure of the Fas death domain and other known death domain structures.

1.3.2 Death effector domains interact via hydrophobic interactions

There are only seven known human proteins with death effector domains (DEDs): activator caspases 8 and 10; adaptor proteins FADD, DEDD and DEDD2, anti-apoptotic protein PEA-15 and the apoptotic regulator cellular FLICE-like inhibitory protein (c-FLIP). DEDs contain shorter and more irregular loop structures than DDs as well as a characteristic beta-turn in the loop between helices four and five[7]. DEDs have two distinctive motifs: An Arg-X-Asp-Leu motif (R-X-D-L, X denoting any amino acid) in helix six, and a hydrophobic patch on the surface of helix two (Figure 1.3).

Little is known about DED-DED interactions because no structure of a complex has been solved, but it is thought that DEDs interact mainly through hydrophobic interactions[8]. Some extrapolations about general modes of interaction can be made from observations in individual members. For example, the RXDL motif enables FADD to self-associate, an event that is necessary for apoptosis onset[7]. Furthermore, mutagenesis studies have shown that this motif is essential for the anti-apoptotic properties of the viral FLIP protein MC159[9]. Caspases 8 and 10 as well as c-FLIP have tandem DEDs and this arrangement is believed to enable the assembly of chains of DEDs. In the case of the caspases the chains form higher order structures called death effector filaments (DEF), that are able to recruit more caspases and amplify the apoptotic stimulus[10,11].

1.2.3 Caspase recruitment domains form heterodimers or rings

Proteins with a CARD domain include the activator caspases of the intrinsic pathway (caspases 2 and 9) and the inflammatory caspases 1, 4, 5, 11 and 12. Also, several apoptosis regulators and adapter proteins have this domain, including RAIDD, Caspase recruitment domain-containing protein 16 (CARD16), Apoptotic protease-activating factor 1 (APAF1), and Baculoviral IAP repeat-containing protein 3 (BIRC3).

It was not until the NMR solution structure of the RAIDD death domain was solved that the common origin of DDs, DEDs and CARDs became evident[5]. CARDs are characterised by a highly conserved polar surface, in which one side of the domain is basic and the other is acidic[12], as well as by a bent or interrupted helix 1 (named H1a and H1b), and increased variability in helix length and orientations, including the stacking of three of the helices in a vertical direction[5,12]. Only one structure of a CARD-CARD domain complex has been solved, that of APAF1 with procaspase 9. Their mode of interaction is predominantly mediated by electrostatic charges and shape complementation[13] and is thought to be conserved throughout the family.

CARD domains are frequently found in large oligomeric complexes including, as part of the innate immune response complexes the NODosome and the inflammasome, and also as part of the PIDDosome. In the PIDDosome, PIDD and RAIDD interact through their DDs and RAIDD interacts via its CARD with the CARD of procaspase 2 . However, the CARD-mediated complexes that have been studied so far have a different topology from those involving DDs, as CARDs typically present one or two interaction sites per domain forming rings[14,15], while DDs have up to six interaction surfaces.

1.2.4 Pyrin domains may interact in the same mode as DEDs

The pyrin domain is the most recently identified and least well characterised of the DDsf[5]. PYD-containing proteins are involved mainly in the innate immune response, mediating inflammation and apoptosis. The best characterised proteins with PYDs are the NOD-like receptors (NLRPs). NLRPs are cytoplasmic proteins that are activated by stress signals and pathogen-associated molecular patterns. Once active, NLRPs are able to recruit adaptor proteins through their PYD and/or CARD domains, leading to the assembly of NODosomes and inflammasomes, and activation of NFκB and caspase 1, respectively. Other proteins with PYD domains include the apoptosis and inflammation mediator Apoptosis-associated speck like protein containing a CARD (ASC) and pyrin itself, which is one of the components of the inflammosome.

It was hypothesised from sequence analysis that pyrin domain containing proteins were related to death domains[16], however this was not confirmed until the structures of the PYD domains of ASC and NLRP protein NALP1 were solved[17,18]. The

solution structure of NALP1 revealed the overall helical fold of the death domain superfamily, however, helix three was found to be completely disordered[17]. Whereas in the solution structure of ASC, helix three was much smaller than expected for a DD, with the stability for the domain coming from hydrophobic interactions located in the loop region between helices two and three[18]. A bipolar distribution of charge on the surface of the PYD is another identifying feature; helices 1 and 4 show acidic properties, whereas helices two and three show basic properties. There is currently no structural information about the mode of interaction between the PYD domains. However, being more closely related to DEDs, it is possible that they have a similar mode of interaction[19].

1.4 Activation of Fas by FasL results in the formation of the death inducing signalling complex

Fas is a ubiquitously expressed 335-residue type I transmembrane protein. Fas is synthesised containing an N-terminal sixteen residue signal peptide that is cleaved from the mature protein prior to plasma membrane association. The extracellular region of Fas contains three disulphide-bonded cysteine rich-domains responsible for ligand binding, these are referred to as tumour necrosis factor receptor/nerve growth factor receptor repeats (TNFr). Fas resides in the membrane as a pre-associated homotrimer, trimerisation initiated by the preligand assembly domain (PLAD) location at residues 17 to 82[20]. The intracellular region of Fas contains the 90 residue death domain (DD), formed by six antiparallel amphipathic alpha helices joined by short loops[6] (Figure 1.3A).

Activation of Fas occurs by Fas Ligand (FasL). FasL is a 281-residue type II transmembrane protein, expressed primarily by cytotoxic T cells and natural killer cells, but also in tissues where immune cell presence needs to be suppressed to prevent inflammation, such as the eye[21]. The extracellular region of FasL forms a tumour necrosis factor domain, and it is thought that FasL needs to trimerise to be active. FasL can be processed by metalloproteases to form a soluble ligand[22]. In soluble form only the hexamer is highly cytotoxic[23], suggesting that high concentrations are needed *in vivo* for the soluble ligand to be active. Fas can also be activated by cross-linking with agonistic antibodies[24].

Upon Fas ligation, the death domain recruits the adaptor protein FADD and procaspase 8 in an actin dependent manner. This recruitment results in the formation of microaggregates that are called death inducing signalling complexes (DISC)[25]. The DISC acts as a molecular platform to recruit and activate initiator caspases triggering extrinsic apoptosis[26] (Figure 1.1 and Figure 1.4). FADD is a 208 amino acid cytoplasmic protein, with the function of coupling receptors with DDs to effector proteins. FADD contains two functional domains, a C-terminal DD to interact with Fas and other TNFRs and an N-terminal DED enabling binding to other DED-containing proteins such as procaspase 8 and 10. FADD self-association seems to be required prior to interaction with other DED-containing molecules[27,28] followed by procaspase 8 being recruited to Fas-bound FADD, via a DED-DED interaction[29]. Autoproteolytic cleavage of the procaspases occurs after proximity-induced dimerisation resulting in the formation of an active heterotetramer of two p18 and two p10 subunits[30] (Figure 1.4). The activated form of the caspase is released from the DISC, transducing the primary apoptotic signal by cleaving and activating the effector caspases (caspases 3, 6 and 7)[31]. Caspases initially cleave cytoskeletal components, which is followed by the cleavage of nuclear lamins and the fragmenting of DNA. The final stages of cell death are characterised as cellular fragmentation, observed as membrane blebbing and resulting in the formation of apoptotic bodies[32].

At the point of DISC formation, the molecule c-FLIP (cellular FLICE inhibitory protein) acts as a regulator of extrinsic apoptosis[29]. c-FLIP is a structural homologue of procaspase 8. It contains two DEDs which enable it to bind to the initial DISC but are lacking the critical protease active site Cys residue and, thus, prevent autoproteolytic activation[32]. It has been suggested that c-FLIP-mediated prevention of DISC progression and caspase activation can result in alternative signalling via non apoptotic pathways[33], which will be discussed further below. cFLIP-mediated inhibition of procaspase 8 and 10 activation is illustrated in Figure 1.4.

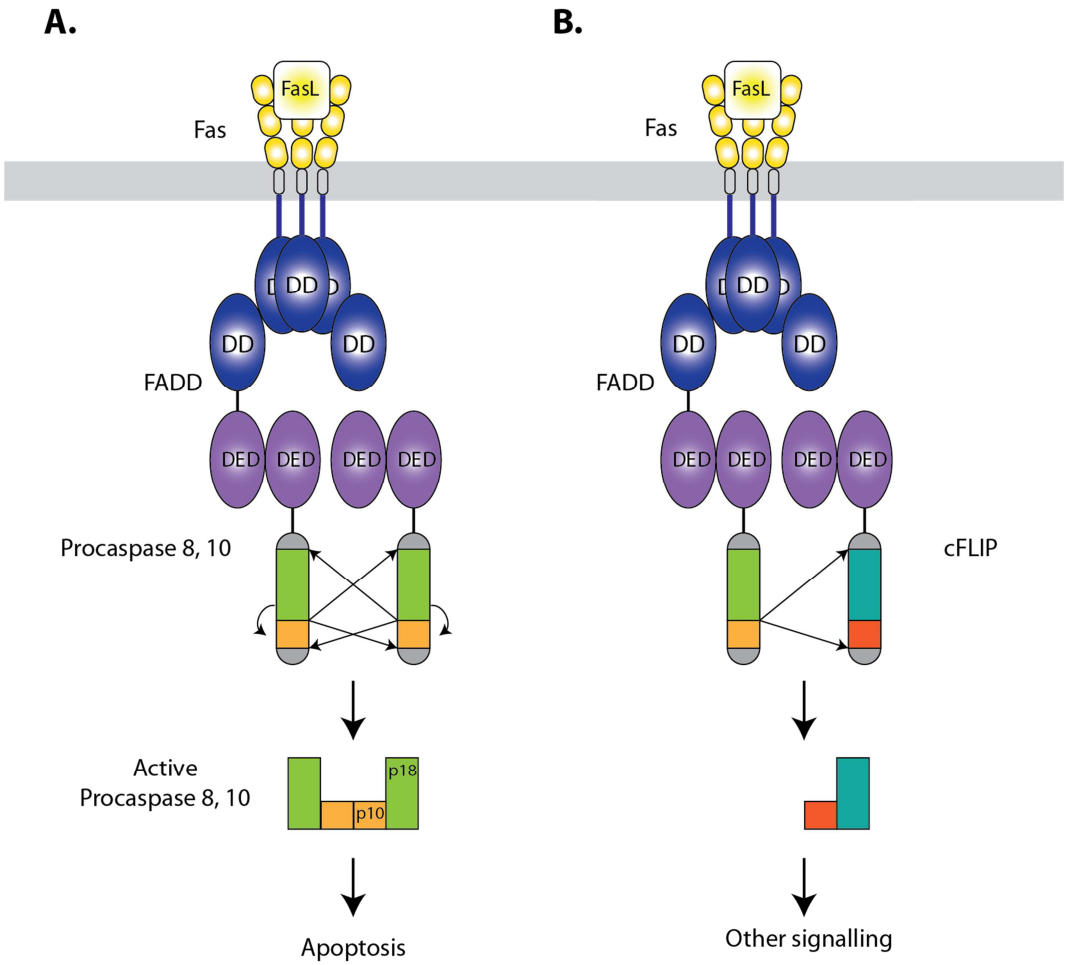

Figure 1.4 Initiator caspase processing, activation and inhibition

A; Schematic representation showing adaptor proteins FADD and procaspase associating with Fas-DD to form the DISC. Proximity induced dimerization enables the procaspase molecules to undergo autoproteolytic cleavage forming an active heterotetramer of two p18 and two p10 subunits. Arrows indicate autocatalytic cleavage and rearrangement to form an active caspase B; cFLIP recruitment inhibits procaspase processing resulting in the onset of alternative signalling pathways.

Mathematical modelling and quantitative mass spectrometry have been used in an attempt to elucidate the stoichiometry of the DISC. Through doing this, Schleich and colleagues discovered that upon DISC formation, there is a much higher concentration of caspase 8 present when compared to the amount of FADD. In conjunction with this, procaspase 8 can hetereodimerise with cFLIP which is present in lower abundance than procaspase 8[34]. This sub stoichiometric concentration of FADD:procaspase 8 at the DISC was also observed by Dickens and colleagues who observed up to nine times more procaspase 8 compared to FADD[10]. The authors postulate that this mechanism of recruitment acts as a method of amplification of the apoptosis response in which a small amount of initial DISC is able to activate a large number of caspases. As explained above, it is thought that DEDs are able to form long death-effector filaments that can recruit more caspases and amplify the apoptotic response away from the cell membrane[11].

1.4.1 The response to Fas stimulation is cell type dependent

The speed and order of events that occur upon receptor stimulation during Fas-mediated apoptosis are somewhat variable dependent on the cell type. Two categories of immune cells have been designated: Type I and Type II. Type I cells undergo rapid procaspase 8 activation with high detectable volumes of DISC formation, and caspase 3 activation occurring within thirty minutes. Type II cells show a reduced level of DISC formation with evidence of little caspase 8 recruitment, and depend on the intrinsic pathway to amplify the caspase cascade. It is important to point out that this classification was a result of experiments carried out in stable cell lines, so it may not reflect Fas signalling in an organism. However, the authors who proposed this classification have argued that that peripheral T-cells do undergo apoptosis when Fas is induced[35], but hepatocytes do not[36], and therefore are Type I and II respectively[37]. It is important to take into account that any experimental observations of the Fas signalling pathway may be influenced by the type of cell line used.

1.4.2 Full DISC activation is dependent upon oligomerisation and subsequent internalisation

The first step in DISC formation depends on the ability of the Fas homotrimers to oligomerise. This step has been characterised experimentally by the formation of SDS/β-merceptoethanol stable Fas aggregates, which correspond to a high molecular weight form of Fas, approximately 180 kDa in size, termed $CD95^{hi}$ [30,38]. Once aggregated, Fas is thought to be targeted to lipid rafts enabling FADD and procaspase 8 recruitment. This step is characterised by the formation of immunofluorescence-visible SPOTs (signalling protein oligomerisation transduction structures)[30]. SPOTs are able to recruit more Fas receptors and adaptor proteins, leading to co-localisation into "caps" on one pole of the cell and the formation of megadalton DISC complexes (hiDISCs). It is from this point that clathrin-mediated internalisation can occur[30,38] (Figure 1.5). It is not until internalisation takes place that full caspase 8 activation occurs[38,39].

The initial recruitment of Fas into lipid rafts is a contentious issue. However, there have been a number of studies showing that upon TCR activation Fas is redistributed into lipid microdomains containing low density lipoproteins (LDLs), cholesterol and glycosphingolipids[40,41], a structure they named detergent resistant microdomains[42]. Chakrabandhu and coworkers also show that perturbing lipid rafts by cholesterol depletion reduces the level of cell death occurring[25]. It is hypothesised that clustering around lipid rafts favours the lateral interaction between Fas in the membrane, increasing the efficiency of receptor stimulation[40], with minimal caspase 8 activation being observed prior to Fas recruitment into membrane microdomains[38]. However, the membrane localisation of Fas may not be conserved throughout all cell types. Eramo and colleagues have reported that in Type I cells at a resting state Fas is preferentially found in lipid raft locations, whereas in Type II cells Fas is only trafficked into lipid rafts upon receptor stimulation[43].

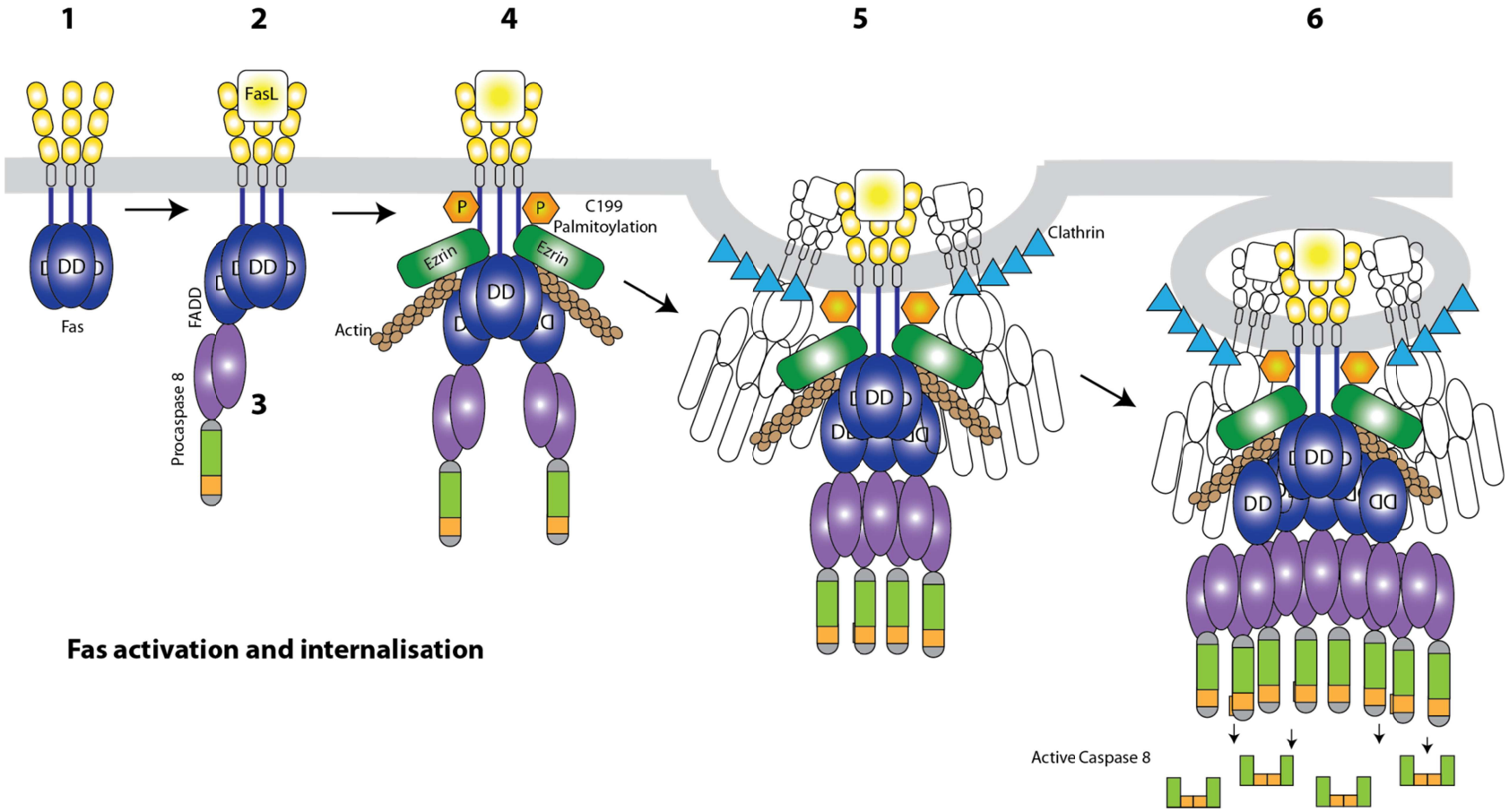

Figure 1.5 Schematic representation of Fas activation and internalisation

1, inactive membrane bound trimerised receptor; 2, FasL binding induces;3 , FADD and procaspace 8 binding forming low levels of the DISC. 4, DISC progression is followed by actin/palmitoylation dependent recruitment to lipid rafts. 5, The DISC is internalised through clathrin mediated mechanisms as the DISC grows in size. 6, Once internalised endosomal trafficking results in high levels of caspase activation.

The membrane location of Fas may therefore play a role in the differing of the speed in the onset of apoptosis that is observed within different cell line types. It is unclear how Fas is repositioned into lipid rafts, but it has been suggested that this process is mediated by lipidation. This is discussed in more detail below.

Clathrin mediated internalisation and DISC recruitment into an endosome is thought to enable maximum adaptor protein interaction and caspase activation. For efficient clathrin mediated internalisation, an interaction between the DISC and the endocytic machinery must be required. Lee and colleagues suggest an interaction between AP2 (crucial scaffold protein for membrane distortion) and the Fas-DD and Chakrabandhu and colleagues report that an extracellular glycophospholipid motif could play a role in the clustering of the Fas receptor and clathrin mediated internalisation, commenting that compartmentalisation and internalisation is a method to regulate cell surface signals[44]. It has also been reported that the association of the actin cytoskeleton is critical to DISC activation and progression[45]. With Kulms suggesting that the distribution of the cytoskeleton is mediated by Fas activation, showing clustering between Fas and actin, which may also be linked to the onset of internalisation of the receptor[46]. The relationship between Fas and the actin cytoskeleton will be discussed further below.

1.5 Post translational modifications of Fas tune the strength and nature of the response

It is thought that the degree of oligomerisation and the occurrence or absence of certain post translational modifications play an important role in directing the recruitment of components, internalisation, activation and resulting signalling pathways of the DISC[38]. A number of post translational modifications in the cytoplasmic region of Fas have been studied; their location and the organisation of the intracellular region of Fas is illustrated in Figure 1.6.

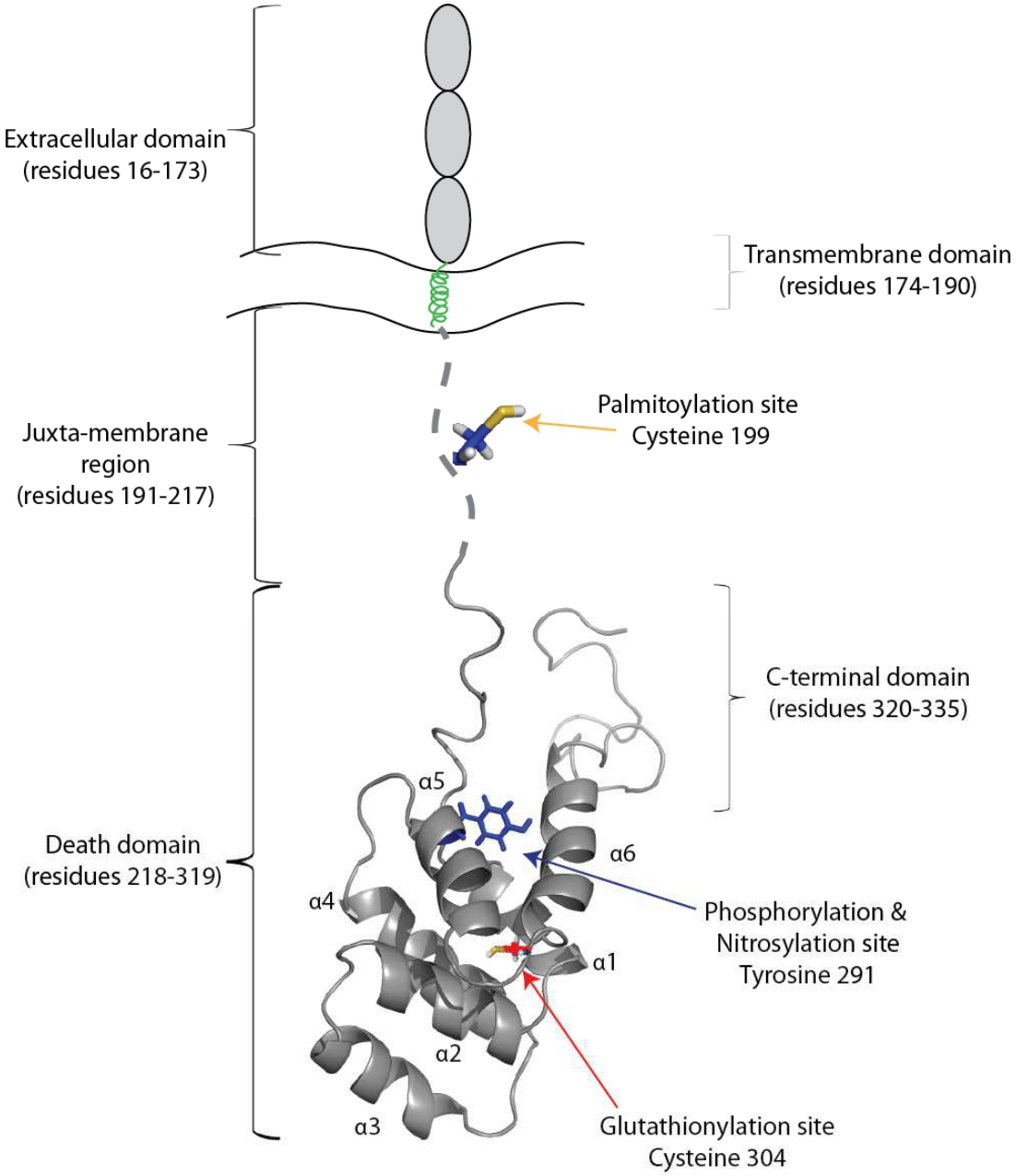

Figure 1.6 Cartoon representation of the Fas death domain and the locations of the reported post translational modifications

Cartoon representation based upon the Fas structure published by Haung *et al* (1996), PDB accession code, 1DDF. The site of phosphorylation and nitrosylation, Tyr291 is highlighted in blue. The site of palmitoylation Cys199 is highlighted in yellow The site of glutathionylation, Cys304 is highlighted in red. Schematic representation of the protein is not to scale.

1.5.1 Fas palmitoylation is required for the onset of cell death

Fas is S-palmitoylated on the membrane proximal cysteine 199[25]. S-palmitoylation is the reversible addition of the saturated sixteen carbon palmitate moiety to a cysteine residue through a thioester linkage. Palmitoylation is carried out *in vivo* by a class of enzymes known as protein acyl transferases (PAT) and removed by protein palmitoyl thioesterases. The addition of a hydrophobic lipid group is most commonly associated with the trafficking of soluble proteins to membranous locations around the cell. The effect of palmitoylation in already membrane bound proteins such as Fas is less intuitive, but it is thought to be able to alter the conformation of the transmembrane domain creating a tilt[47] that might expose otherwise inaccessible residues, encourage recruitment to lipid rafts[38] and influence protein:protein interactions[48], effects such as these might influence DISC formation. Due to the difficulties associated with studying a lipidated protein in solution, palmitoylation is one of the least well characterised protein post-translational modifications.

Palmitoylation on Cys 199 is thought to redistribute and partition Fas into lipid raft regions of the cell membrane prior to receptor internalisation, and to influence the events that lead to DISC internalisation. The first detectable event following Fas ligation is the formation of $CD95^{hi}$. Upon palmitoylation Fas is reported to aggregate more efficiently with increased oligomer stability enhancing $CD95^{hi}$ formation. Feig and colleagues have shown that mutation of Cys199 to Ser conserves lipid raft localisation but significantly reduces DISC internalisation and caspase activation[30], suggesting that the role of palmitoylation in DISC progression is not restricted to raft recruitment. It has also been proposed that the redistribution of Fas into lipid rafts is a prerequisite for Fas internalisation by orientating the receptor to engage with the actin cytoskeleton via the membrane cytoskeletal protein ezrin[25].

Cysteine 199 was identified as the palmitoylation site in the Fas intracellular region through mutational studies and investigating the effect of the C199S mutation on the onset of apoptosis[30]. This cysteine is located within the membrane proximal /juxtamembrane region of Fas, eight amino acids from the transmembrane domain (Figure 1.7).

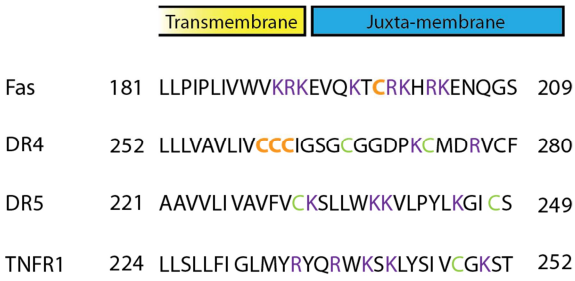

Figure 1.7 Sequence comparison of the membrane proximal regions of death receptors

Sequence comparison of the membrane proximal region of Fas (UniProt:P25445), TNFR1 (UniProt:P19438), DR4 (UniProt: O00220) and DR5 (UniProt:O14763). The transmembrane and juxtamembrane regions of the proteins are represented above the sequences. Cysteine residues highlighted in orange have been shown to be palmitoylated, putative palmitoylation sites are highlighted in green and basic residues in purple. The sequence comparison is adapted from the sequence comparison carried out by Rossin *et al.* (2009).

Cys199 is surrounded by a number of basic residues which is a common feature of palmitoylation sites, as this environment greatly reduces the pKa of the cysteine[49]. Rossin and collaborators showed that the five lysines located around C199 (K191, 193, 197, 201 and 204) are also required for Fas localisation into lipid rafts. By creating a mutant Fas in which these lysines were changed into asparagines, they showed that the mutant does undergo palmitoylation but does not get recruited to lipid rafts and perhaps as a consequence, is unable to signal cell death, but actives other non-apoptotic pathways through ERK and AKT pathways instead[25,50].

Fas is not the only member of the DDsf that has been shown to require palmitoylation to function, the death receptor DR4 is also palmitoylated on either transmembrane or membrane proximal cysteines[51]. DR4 is activated by TRAIL (TNF-related inducing ligand) and like the Fas DISC, the DR4 DISC is thought to progress through a series of activation steps involving oligomerisation and lipid raft recruitment, and results in cell death. Rossin and colleagues identified that palmitoylation of DR4 was required for the receptors lipid raft location and its ability to oligomerise upon activation[51]. However, the same authors demonstrated that DR5 and TNFR are not palmitoylated during activation, suggesting that palmitoylation is not a general feature of death receptors[51].

The palmitoylation of the membrane bound form of the Fas ligand (FasL) also seems to be essential for efficient ligand processing and the onset of cell death. Palmitoylation on Cys82 targets FasL to lipid rafts where it undergoes processing to become active. It is reported that palmitoylation of FasL is required upstream of Fas receptor binding, as ligand:receptor interactions are abnormal when FasL palmitoylation is limited[52]. The requirement for tight regulation of FasL due to its cytotoxic role is therefore perhaps palmitoylation dependent, illustrating another role of palmitoylation within Fas-mediated apoptosis.

1.5.2 Fas tyrosine phosphorylation is involved in both apoptosis and cell proliferation

The Fas death domain is reported to be phosphorylated upon tyrosine 291. Although this post translational modification of Fas has been reported in a number of cell types and a number of different situations, with variable downstream effects[53]. Upon pro-apoptotic stimuli, phosphorylation of Tyr291 has been observed to result in an increase in Fas oligomerisation and a faster onset of apoptotic pathways[54,55]. It is unclear which tyrosine kinases are involved in Fas phosphorylation, but p56Lck[56] is recruited to the membrane upon Fas activation and 59fynT[57] has been found to be physically associated with Fas. The epidermal growth factor receptor (EGFR) might also be able to phosphorylate Fas. Treatment with FasL in hepatocytes, leads to Fas association with the EGFR, phosphorylation[58] and DISC formation. The authors also showed that only the double mutation Y232/291F supresses Fas apoptotic signalling, suggesting that Y232 might become phosphorylated as well.

Tyrosine 291 is located in the residue formation EA**Y**DTL, which resembles the immunoreceptor tyrosine inhibitory (ITIM) motif S/I/V/Lx**Y**xxI/V/L (where x can be any amino acid), a known SH2 (src-homology 2) domain target binding site. The presence of the YxxL motif suggests that phosphorylated Fas can recruit SH2 domain containing proteins, expanding the signalling capabilities of the death domain[54]. SH2 domain containing phosphatases, SHP1 and SHP2 can be recruited to the Fas death domains, after Tyr291 phosphorylation. Gradl and colleagues describe the YxxL motif present in death domains as a 'functionally active tyrosine-based inhibition motif' as their results link the association of SHP1/2 with Fas as a mechanism to disrupt anti-apoptotic pathways and cell survival in neutrophils, linking Fas phosphorylation to cell death pathways[59]. This mechanism is still a matter of debate, because other authors have shown that in B cells SHP1 is associated with Fas, but that upon Fas activation, it down modulates Fas-internalisation and thus cell death by dephosophorylating Vav, a protein involved in the regulation of cytoskeleton rearrangements[45]. Other phosphatases without SH2 domains have also been implicated in apoptosis tuning by Fas dephosphorylation, notably Fas associated phosphatase (FAP-1) [60,61].

In other contexts, tyrosine phosphorylation of Fas can result in the onset of non-apoptotic effects involving the SH2 domain containing protein PI3K (phosphoinositide 3 kinase). The molecular link between Fas and the activation of PI3K was seen in the context of glioblatome multiforme[62], the most common form of malignant primary brain tumour. Kleber and collaborators reported that upon Fas stimulation by FasL a PI3K-Activation-Complex (PAC) is formed, containing the PI3K regulatory subunit p85 and the Src family kinase Yes. The authors showed that by knocking down Yes kinase and inhibiting PI3K they could block phosphorylation of AKT/PKB, inactivating glycogen synthase kinase 3β (GSK3 β) resulting in migration and cellular proliferation. The authors also showed that formation of the PAC inhibited DISC formation and apoptosis, speculating that the PAC outcompetes FADD and procaspase 8 in binding to Fas. Therefore the stoichiometry of the PAC may have an impact on cell fate[63,64,65]. The activation of PI3K upon Fas stimulation and other non-apoptotic signalling pathways are illustrated in Figure 1.8.

Ser/Thr phosphatase inhibitors have been shown to block Fas receptor oligomerisation and caspase 8 activation, suggesting that Fas also undergoes Ser/Thr phosphorylation[66]. The signalling cascade involved in this event is not known, but the inhibitors increase the level of ERK activity, a pathway that is believed to promote cell survival[67].

These results show that Fas phosphorylation and dephosphorylation are crucial mechanisms in the modulation of Fas signalling both in cell death, cell survival and proliferation cascades. However it is possible that the precise nature of the response depends on cell type and activation status as well as the type and intensity of Fas stimulation.

1.5.3 Other post translational modifications modulate Fas activity

Glutathionylation refers to the reversible addition of the glutathione tripeptide to a cysteine side chain thiol, enabling the formation of a disulphide bond. Anathy and coworkers have reported that Fas ligation is able to trigger S-glutathionylation at C295 in mouse Fas[68], a position equivalent to human C304, and that S-glutathionylated Fas enhances DISC assembly.

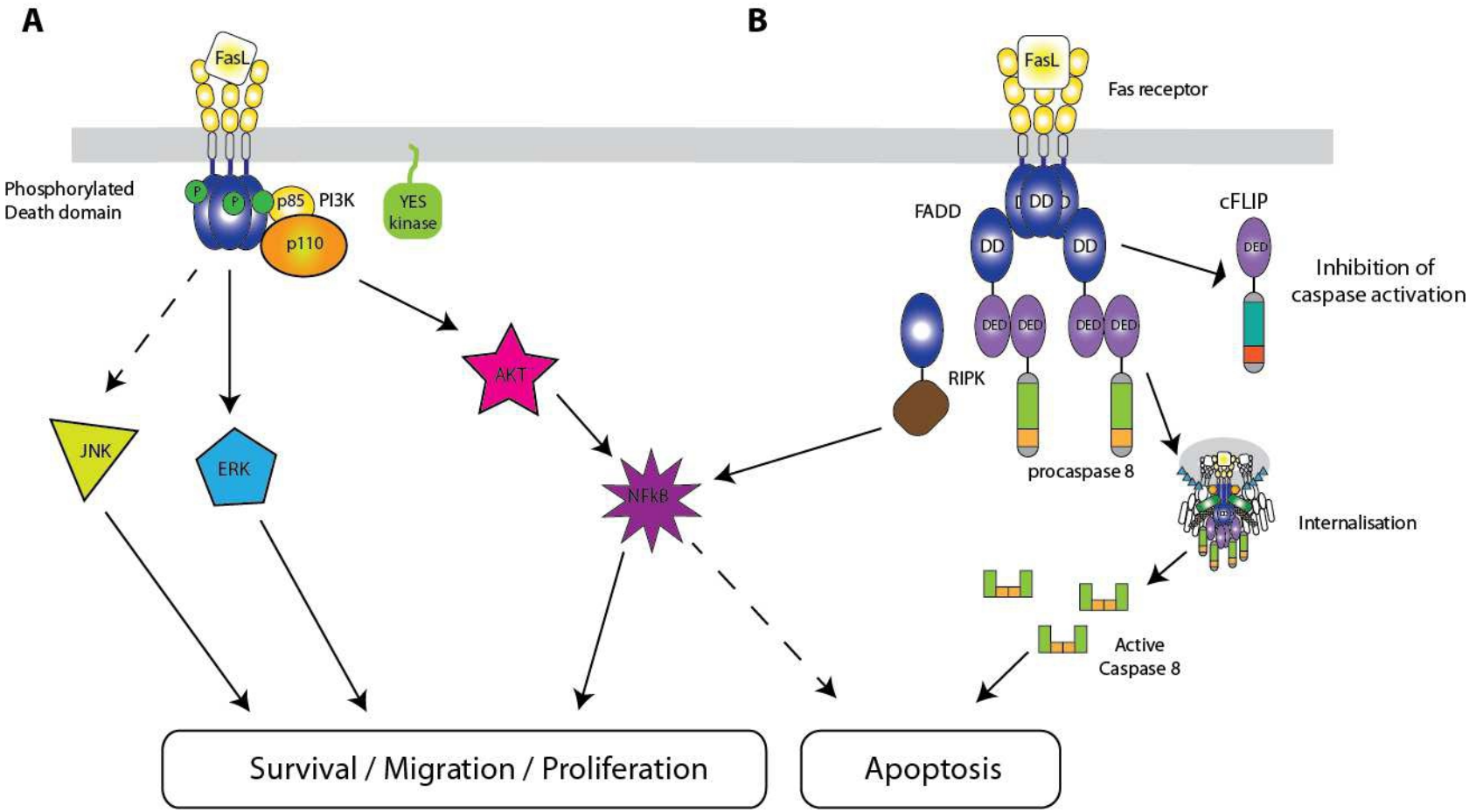

Figure 1.8 Schematic representation of the non-apoptotic signalling pathways involving Fas.

A. Non apoptotic Fas cell death pathways which rely upon phosphorylation of Y291 of the Fas-DD and SH2 domain containing protein recruitment. B. Apoptotic and non-apoptotic Fas cell death pathways which rely on the ratio and components forming the death inducing signalling complex. Adapted from Martin-Villalb*a et al. (2013)* and Schneider-Brachert *et al* (2013).

In a subsequent paper, they provided evidence that glutathionylation of Fas occurs in the ER upon FasL stimulation, and that it functions as a switch to target reservoir pools of Fas located in the ER to the membrane and thus control the extent of the apoptotic response[68].

S-nitrosylation refers to the reversible addition of a nitroso group to a cysteine side chain thiol, forming a nitrosothiol (R–S–N=O). Leon-Bollotte and collaborators have reported that when colon and mammary cancer cell lines are treated with NO donors, Fas undergoes S-nitrosylation on both cysteines 199 and 304. However, only nitrosylation at C304, promotes recruitment to lipid rafts and DISC assembly[69]. Whether this effect has a biological implication remains to be studied; however, it is known that some protein:protein interactions are NO dependent. For example, Talbot and collaborators reported that S-nitrosylation of cFLIP is necessary for recruitment of RIP1K and the activation of NFκB [70].

1.6 Fas activation can also trigger non-apoptotic signalling cascades

Under certain circumstances the formation of the DISC does not lead to its internalisation and instead triggers non-apoptotic signals from the cell membrane that result in cell survival, proliferation, migration and inflammation. Some of the alternative signalling pathways have been elucidated through the study of Fas signalling in cancer cell lines, which are known to be able to avert Fas-induced apoptosis. Therefore, it is not possible to generalise on the prevalence of these pathways or their relevance in healthy cell functions. Nevertheless, their study is providing valuable information on possible alternative targets for cancer therapy[71].

As described previously, in glioblastoma cells the phosphorylation of the Fas death domain on tyrosine 291 results in AKT activation, suppression of apoptosis, and increased cell mobility and migration[62]. In other systems Fas activation results in the recruitment of other adaptor proteins triggering different signalling effects. Starved fibroblasts and CD3-activated T cells respond to FasL by activating NFκB via mitogen-activated protein kinases ERK and/or JNK. NFκB activation was found to induce the expression of cytokines able to promote proliferation, migration and inflammation[72,73,74]. Other cell lines and a variety of primary tumour cells have

recently been shown to activate transcription factor AP-1 via JNK kinase, resulting in cell growth[75,76]. However, in regulatory dendritic cells, pERK production following Fas activation via T cells led to the production of immunosuppresive agents[77]. Accordingly, activation of MAPK kinases cannot be directly associated with cell proliferation pathways.

A number of studies have shown that the stoichiometry of the adaptor proteins recruited to the DISC can affect cellular fate, for example, an increased level of c-FLIP or decreased levels of caspase 8 and FADD at the DISC prevent apoptosis and promotes proliferation[78,79]. The fact that c-FLIP is involved in proliferative signalling pathways has been considered following evidence that in Jurkat cells cFLIP appears to inhibit NF-κB activity[73] with activation occurring in a procaspase 8 and FADD dependent manner[80]. However, both pathways of NF-κB activation rely on the recruitment and activation of RIP1K via its DD domain. Therefore, it seems plausible that RIP1K can be recruited by both cFLIP and procaspase 8 and that additional signals and/or the stoichiometry of the DISC influence the outcome. For example, it has recently been proposed that RIP1K recruitment by cFLIP is dependent on cFLIP nitrosylation[70]. In TNFR signalling RIP1K activity is also controlled by ubiquitination[81], a factor which has yet to be explored in the case of Fas.

The examples described above illustrate that the Fas death receptor is able to initiate cellular signalling through a number of different apoptotic and non-apoptotic signalling pathways. Evidence has been presented that both pathways may be occurring at the same time involving cross-talk between formations of the DISC[33]. For example, in Jurkat cells the NF-κB and the PI3K pathways are both active at the same time, and both cFLIP and Akt can inhibit NF-κB activity[82]. Also Fas activation of NF-kB is a self-perpetuating signalling pathway, with NF-kB directly regulating the transcription of Fas in a positive feedback loop[83]. A summary of these alternative DISC signalling pathways is shown in Figure 1.8. Most probably, the components and stoichiometry, local concentration, level of oligomerisation, the degree of the activation, the signalling of other death receptors and the spatiotemporal location of the DISC influence one another to define the final outcome of the signalling events[38,84]. What is clear is that, in light of the pleiotropic signals that Fas can

initiate, the label of “death receptor” is not as explicit to its function as originally thought.

1.7 Germline and somatic mutations in Fas cause deregulation of cell homeostasis

1.7.1 Mutations in Fas are the most common cause of autoimmune lymphoproliferative syndrome

Autoimmune lymphoproliferative syndrome (ALPs) is caused by detrimental mutations in apoptotic genes leading to the dysregulation of Fas-mediated apoptosis, which results in an unbalance in immune cell homeostasis[85]. Patients present a proliferation of polyclonal T lymphocytes that respond poorly to antigens and fail to produce cytokines upon activation, they also present increased levels of the anti-inflammatory cytokine IL-10 and γ-interferon. The accumulation of excess leukocytes causes enlargement of the liver, the spleen (hepatosplenomegaly) and the lymph nodes (lymphadenopathy) as well as autoimmune disorders such as anaemia and decreased platelets (thrombocytopenia)[85,86]. Patients with ALPs also have a greater risk of developing lymphoma and other types of cancer. In order to control the symptoms, patients are generally treated with immunosuppresive drugs such as glucocorticoids, and blood transfusions with the use of intravenous globulin in cases of severe anaemia. The antimalarial drug ‘Fasidar’ has been tested as a possible alternative treatment. The authors reported reduction in the levels of the inflammation cytokine IL-10 and induction of apoptosis via the intrinsic pathway[85].

ALPs is classified according to the genotype of the defective protein involved in apoptosis signalling. Type 0 ALPS is defined by homozygous mutations in the Fas gene; it causes high levels of lymphoproliferation and spontaneous apoptosis and it is only treatable with a complete bone marrow transplant. Type I ALPS is divided into two subtypes, Type Ia and Ib, depending on whether the heterozygous detrimental mutation is located in Fas or FasL. The mutations found in these patients are generally point mutations and small deletions. Abnormal Fas or FasL proteins act in a dominant negative manner, forming trimeric receptors that are a combination of wild type and mutant proteins, resulting in reduced binding and/or reduced

recruitment or activation of caspase 8[87,88]. Type Ia ALPS is the predominant form of ALPS. Type II ALPS is characterised by heterozygous mutations in the initiator caspases 8 or 10, therefore both Fas expression and signalling are normal. Mutations in caspase 10 that impair the auto processing and activation are most common. In these patients DISC formation is normal but the initiation of apoptosis is prevented. Mutations in caspase 8 are more severe, because they also cause defects in the activation of T cells, B cells and natural killer cells. Type II ALPS results in a more severe autoimmune outcome than the other forms of the disease. ALPS is categorised as type III, when the ALPS symptoms are present, but no molecular defects can be found in Fas, FasL, caspases 8 or caspase 10[85,86].

The study and characterisation of ALPS has been greatly aided by the existence of the natural MRL *lpr* mouse mutant strain. The MRL *lpr* mouse mutant strain was initially used as a model for human lupus however as the mice age they develop $CD4^-$ $CD8^-$ T cells resulting in a phenotype similar ALPS. The use of this mouse model and the underlying disease mutations in ALPS have greatly increased our knowledge of the protein:protein interactions that occur at the Fas DISC, identifying the point mutations that can abrogate binding[86]. For example ALPS point mutations identified in both systems revealed the location of FADD binding on helix 3 of the Fas death domain[6].

1.7.2 Mutations in Fas have been associated with cancer

As inferred from the non-apoptotic and proliferative effects of Fas stimulation described above, Fas stimulation has been associated with a number of cancers[42,89,75]. A study suggested that people with germ line mutations in the *FAS* gene, even if they do not develop ALPs, have a higher risk of developing B-cell and T-cell lymphomas[90]. Somatic mutations in Fas have been also been detected in Hodgkin and non-Hodgkin lymphoma[91].

1.8 Ezrin is crucial for Fas internalisation and transmission of the apoptotic signal

The endosome machinery plays a very important role in Fas-mediated apoptosis. Current understanding of the mechanism of Fas activation suggests that internalisation only takes place in the apoptotic route and not when the activation of Fas leads to the non-apoptotic outcomes. Of special interest is the interaction of Fas with the cytoskeletal elements that are responsible for attachment to the plasma membrane. In many cell types, these elements are the members of the ERM family (named after the first three proteins in the family: ezrin, radixin and moesin), which act as a bridge between proteins in the membrane and actin. In the case of Fas, a number of reports implicate ezrin specifically as the crucial link between Fas and the actin cytoskeleton.

1.8.1 Extracellular and intracellular signals regulate the attachment of actin to the proteins in the cell membrane through the ERM proteins

Proteins belonging to the ERM family (ERMs) have been associated with a number of processes at the cell membrane, such as cell adhesion, cell motility, cell shape and the progression of endocytosis and exocytosis as well as specific protein localisation, membrane transport and signal transduction[92]. ERMs are structurally and functionally related showing a high level of sequence and structural similarity (illustrated in Figure 1.9), which is most probably the result of a gene duplication in the last common ancestor of all vertebrates. The great similarities within this protein family make the functions of ERMs both similar and redundant[93], making cell based studies of this family challenging, as the knockout of one protein is compensated for by one of the others. However, in an organism, only moesin seems redundant[93], this is probably a result of non-overlapping tissue distributions for radixin and ezrin. The absence of radixin results in liver damage[94] and the absence of ezrin is incompatible with life[95]. ERM proteins have also been shown to be structurally and functionally related to the tumour suppressor protein Merlin, which shows essential but non overlapping functions to the other ERMs[92].

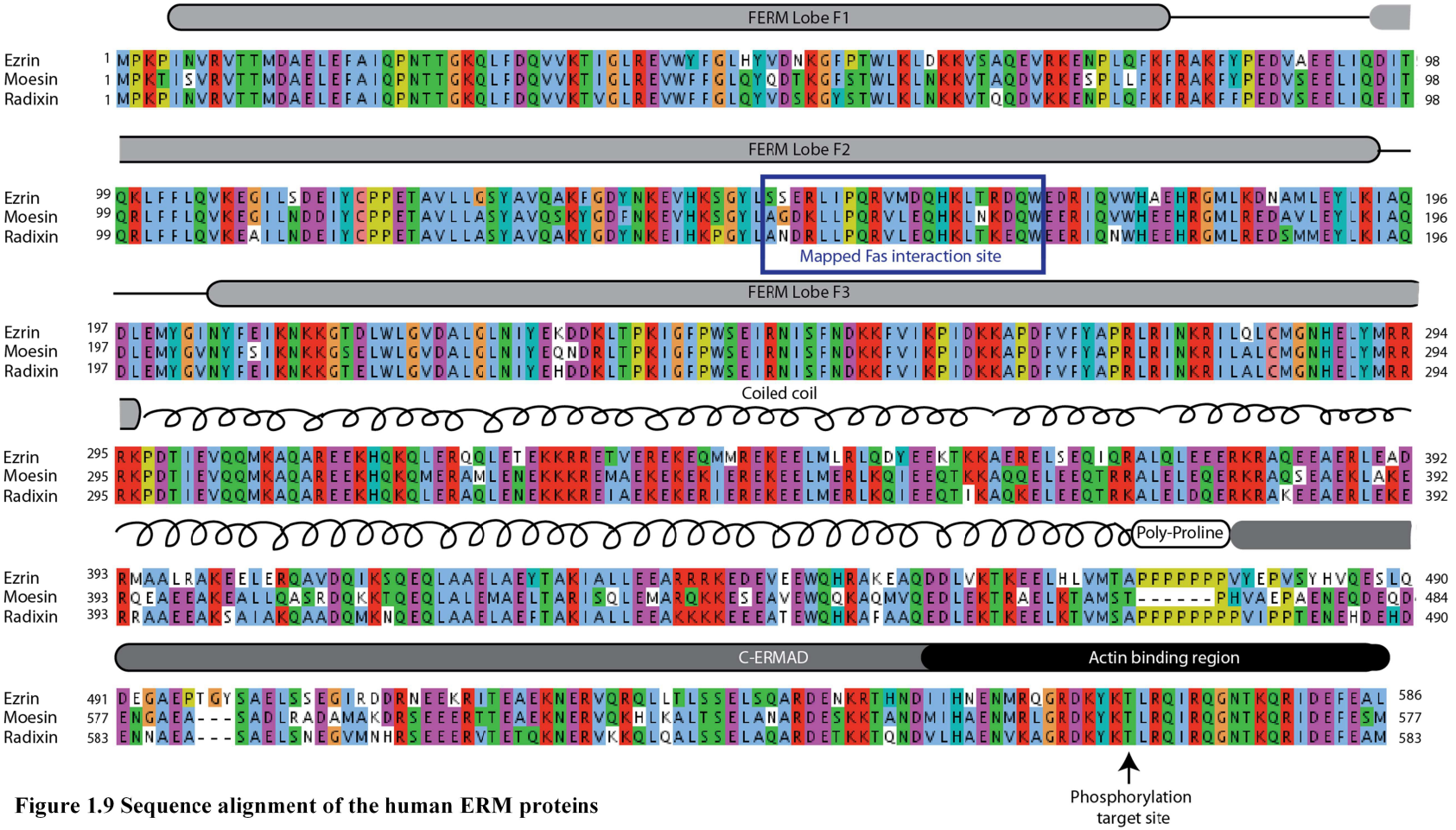

Figure 1.9 Sequence alignment of the human ERM proteins

Sequence alignment carried out using MAFFT alignment protocol. Coloured according to clustalx parameters in Jalview. Structural features are annotated above each of the sequences. The FERM domain is shown split into the labelled three lobes, F1, F2 and F3. The blue box highlights residues 149-168, these residues of ezrin have been indicated to bind Fas.

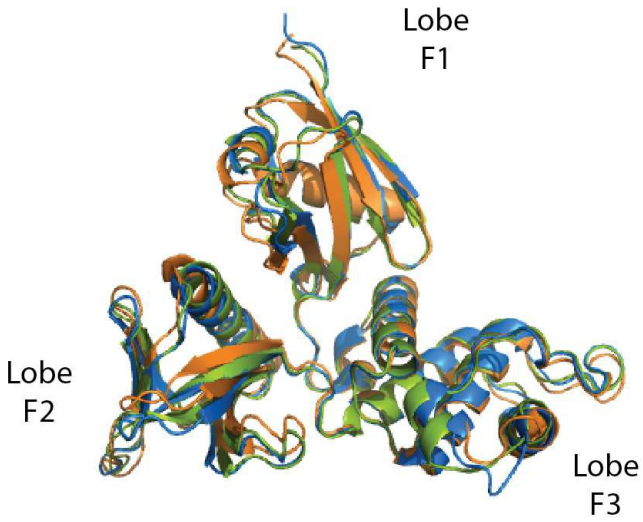

Figure 1.10 Structural alignment of the FERM domains of ezrin radixin and moesin

Ezrin shown in green (PDB:1NI2); radixin shown in blue (PDB:1GC7); moesin shown in orange (PDB:1E5W). Structures aligned within Pymol.

ERMs have three functional domains: an N terminal globular FERM (four point one, ezrin, radixin, moesin) domain, a central coiled-coil region and a C terminal tail[96,97]. ERMs are negatively regulated by intramolecular interactions between the N and C termini of the molecule. In the resting state, ERMs adopt a compact closed structure in which 90 residues from the C-terminus bind to the N-terminal FERM domain, thereby masking both the F actin-binding site, formed by the most C-terminal 34 residues, and the different protein interaction sites in the FERM domain[92,98]. This interaction between the N-ERMAD (ezrin, radixin, moesin association domain) and the C-ERMAD also enables homo- and heterodimerisation of ERMs forming large intracellular complexes[99]. Inactive ERMs are predominantly found in the cell cytosol.

To enable activation and membrane protein association, the ERMs need to undergo post translational modifications as well as a large structural reorganisation, adopting an extended conformation. Phosphorylation of threonine 567, which is present in the C-ERMAD, by either ROCK, PKCα or PKCθ reduces the affinity between the N- and C-ERMADs and allows the ERMs to open[98]. Besides phosphorylation, an interaction of the FERM domain with phospholipids is necessary for the activation of the ERMs[100]. In particular, phosphatidylinositol 4,5-bisphosphate (PIP_2) binding to the ezrin FERM domain has been reported to be necessary for an interaction to occur *in vitro*[101].

The crystal structures of the FERM domains of ezrin, moesin and radaxin have been solved both in isolation[96,102,103] and in association with known binding partners. Of particular interest to elucidate their mechanisms of activation, structures have been solved of radixin in complex with the PIP_2 mimic, IP_3[104], moesin FERM domain in complex with the C-terminal tail[98] and moesin with a portion of the coiled coil region directly C terminal to the FERM domain[103]. These structures have provided valuable information about the possible modes of interaction and the effects that these interactions have on the molecule. The FERM domain is formed of three lobes (named F1-F3) orientated in a clover shape, each with distinct structural homology to other known protein folds. Lobe F1 contains a structure similar to ubiquitin, lobe F2 shows similarity to acyl CoA-binding protein whereas lobe F3 contains a pleckstrin homology (PH) domain like that found in protein kinase B[98]. The variety of folds in the FERM domain enables a number of different modes of binding to

occur. The structures of the free FERM domains of ezrin radixin and moesin are shown in Figure 1.10. The structure of the radixin FERM domain in complex with IP_3 showed no difference in structure between the free and bound forms. In the crystal, IP_3 was bound inside a basic groove between F1 and F3[104]. However, this location was different to the PIP_2 binding site that has been mapped using site directed mutagenesis[101], so the mechanism by which lipids mediate ERM protein activation is still unclear. The presence of the C-ERMAD in complex with moesin[98] showed that there are great changes in the F3 lobe, with the C terminal β-strand moving by about 6 angstroms. This F3 region was the location where IP_3 was found bound in the radixin FERM[104], so perhaps the change in conformation of F3 is indeed involved in the transition from the inactive to the active state.

Two modes of interaction with membrane proteins have been observed for the ERMs, either through direct ERM:membrane protein interactions, or through indirect association of the ERM protein and the membrane protein, mediated via a scaffold protein[92]. Direct ERM:membrane protein interactions have predominantly been described with adhesion receptors, such as the positively charged juxtamembrane region of the hyaluronate receptor – CD44 and the Ig like domains of ICAM2 (intracellular adhesion molecule 2). These interactions are discussed in more detail below[105,106]. Scaffold protein mediated interactions involve the NHERF1 (Na^+/H^+ exchange regulatory factor 1 also called EBP50) and NHERF2 (also called E3KARP) proteins as the link between the ERMs and the cytoplasmic tail of a membrane protein. NHERF1 and NHERF2 fold into two PDZ domains and a thirty amino acid C terminal region which is recognised by the ERMs[107,92]. Proteins that are known to be bound to ERMs in this fashion are the β2-adrenergic receptor[108] and podocalyxin, a sialoglycoprotein important for maintaining the structural organization and blood plasma filtration in kidney cells[109]. Figure 1.11 illustrates the activation and two binding mechanisms of ERM proteins at the cell membrane.

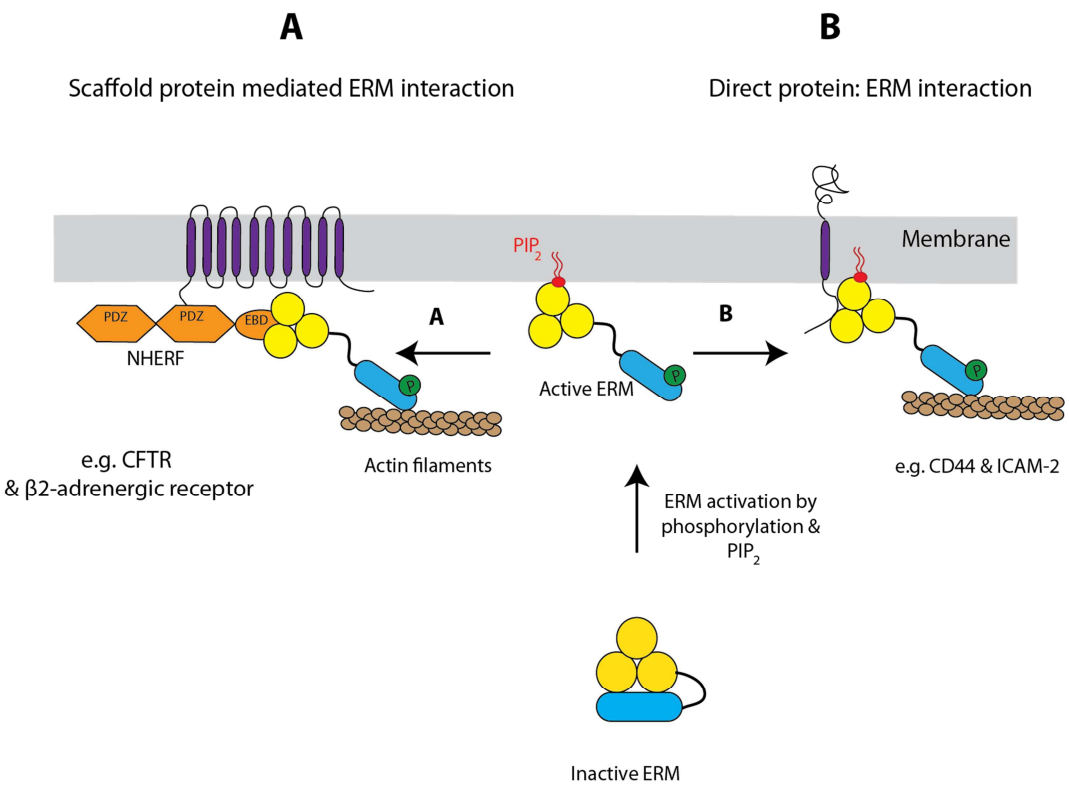

Figure 1.11 Activation and interaction of ERM proteins

ERM proteins exist in an inactive closed conformation in the cytosol. Upon activation by phosphorylation and interactions with PIP_2 they are recruited to the plasma membrane to enable either A, scaffold protein mediated interactions with membrane proteins or B, direct membrane protein interactions. Adapted from Bretscher *et al* (2002). EBD – Ezrin binding domain.

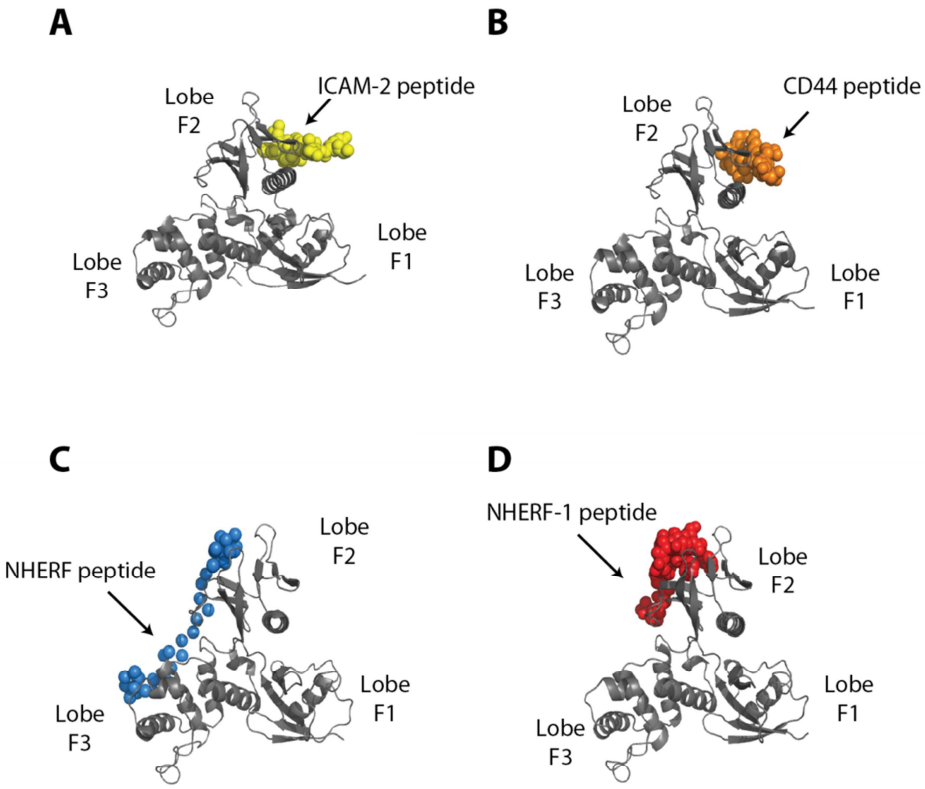

Figure 1.12 Structural representations of known radixin FERM domain:ligand interactions

Crystal structure of the Radixin FERM domain (grey) crystallised with peptides from four different protein binding partners. A, ICAM-2 peptide in yellow (PDB:1J19); B, CD44 peptide in orange (PDB:2ZPY); C, NHERF peptide in blue (PBD:1SGH); D, NHERF1 peptide in red (PDB:2D10). Abbreviations, ICAM-2 – intracellular adhesion protein 2, NHERF1 – Na^+/H^+ exchanger regulatory factor.

1.8.2 ERMs bind their targets using a variety of binding modes

Some of the interactions between ERMs and their targets and scaffold proteins have been extensively characterised. Structures have been solved showing the mode of interaction of moesin FERM with NHERF1, radixin FERM with both NHERF1 and NHERF2 as well as with the target proteins adhesion molecule PSGL-1, adhesion molecule CD43, neutral endopeptidase 24.11, the ICAM2 cytoplasmic peptide, and a CD44 cytoplasmic peptide[110–112]. Despite the fact that these structures have been solved with radixin, the sequence conservation among the ERMs is so high that similar modes of interaction are expected for all of the ERMs. Some of these structures are shown in Figure 1.12. The binding region recognised by the FERM domain is usually a short, basic twenty to thirty amino acid stretch with little regular secondary structure. In Chapter Five of this study some of these well-characterised ERM interactions have been used as positive controls for ezrin binding and as a model for the interaction between Fas and ezrin.

1.8.3 The interaction of Fas with ezrin is necessary for DISC internalisation and apoptosis onset

The first report linking the ERMs to Fas-mediated apoptosis observed that FasL stimulation in fibroblasts resulted in the translocation of ezrin from the plasma membrane to the cytoplasm, and that absence of ezrin from the plasma membrane was concomitant with the breakdown of the cell microvilli[113]. It was later observed that ezrin knockdown protected cells from undergoing apoptosis and that Fas and ezrin co-immunoprecipitated in $CD4^+$ T-cells lysates[114], suggesting that the interaction of ezrin with Fas was key to the onset of apoptosis. Hèbert and coworkers further built upon this work, showing that in Jurkat and peripheral blood T cells not only ezrin, but also moesin is involved and necessary for Fas-mediated apoptosis. The authors also observed that upon Fas stimulation both ezrin and moesin are phosphorylated by Rho activated ROCK1, and that inhibition of either Rho or ROCK1 was sufficient to stop the formation of Fas aggregates[115]. In contrast, Parlato and colleagues did not find moesin in association with Fas in lymphoblastoid CD4+ T cells and day 6 activated lymphocytes[114]. Both Hebert and collaborators and Parlato and colleagues found that the association between Fas and ezrin was constitutive, as it was observed without any stimulation. However, Hebert and

coworkers found that immediately after Fas activation, there is a transient dephosphorylation of ezrin and moesin, presumably to allow membrane remodelling. Rho-ROCK1 ezrin phosphorylation at the onset of Fas-mediated apoptosis was also observed by Rebillard and collaborators in colon cancer cells treated with cisplatin[41]. Kuo and colleagues also observed that in T cells, Fas and ezrin association was constitutive[116]. However, in their system ezrin deficiency facilitated DISC formation and increased the level of apoptosis in Type I cells, having no detrimental effect on the endocytosis of the DISC. This illustrates that there is not a consensus on the role of the interaction between Fas and ezrin during apoptosis. These discrepancies could be due to experiments being done in a variety of cell types and with different types of stimulating reagents, for example, FasL vs activating Fas antibodies.

Lozupone and colleagues mapped the Fas binding site on ezrin to the central lobe of the ezrin FERM domain at residues 149-168[117] (Figure 1.13). They arrived to this conclusion through performing GST pull down assays, in which short ezrin fragments were immobilised upon GST beads to pull down the whole cytoplasmic domain of recombinant *E. coli* expressed Fas and full length Fas from Jurkat cell lysates, respectively. To verify their results, the authors made a chimeric ezrin in which the region 149-168 was replaced with that of moesin and transiently co-transfected into HeLa and Hut78 cells containing both wild type and chimeric ezrin. Upon Fas activation, cells with chimeric ezrin, but not those with wild type ezrin, showed protection against apoptosis. Fas could also be co-immunoprecipitated with GST-tagged wild type ezrin but not GST-tagged chimeric ezrin from Hut78 lysates[117]. Given that Hèbert and colleagues did observe Fas binding to moesin, the fact that the moesin peptide 149-168 cannot interact with Fas suggests that there is more than one mode of interaction taking place.

Subsequently, Ruan and coworkers performed the reciprocal experiment to locate the region of Fas that was being recognised by ezrin. Their experimental design consisted of making GST-tagged constructs comprising different regions of the intracellular portion of Fas and using them as prey in pull-down assays with COS-7 cell lysates as bait. They could pull down ezrin with all Fas constructs except those lacking residues 191-204 in the juxtamembrane region, a region they called the membrane proximal domain[118] (MPD; Figure 1.13).

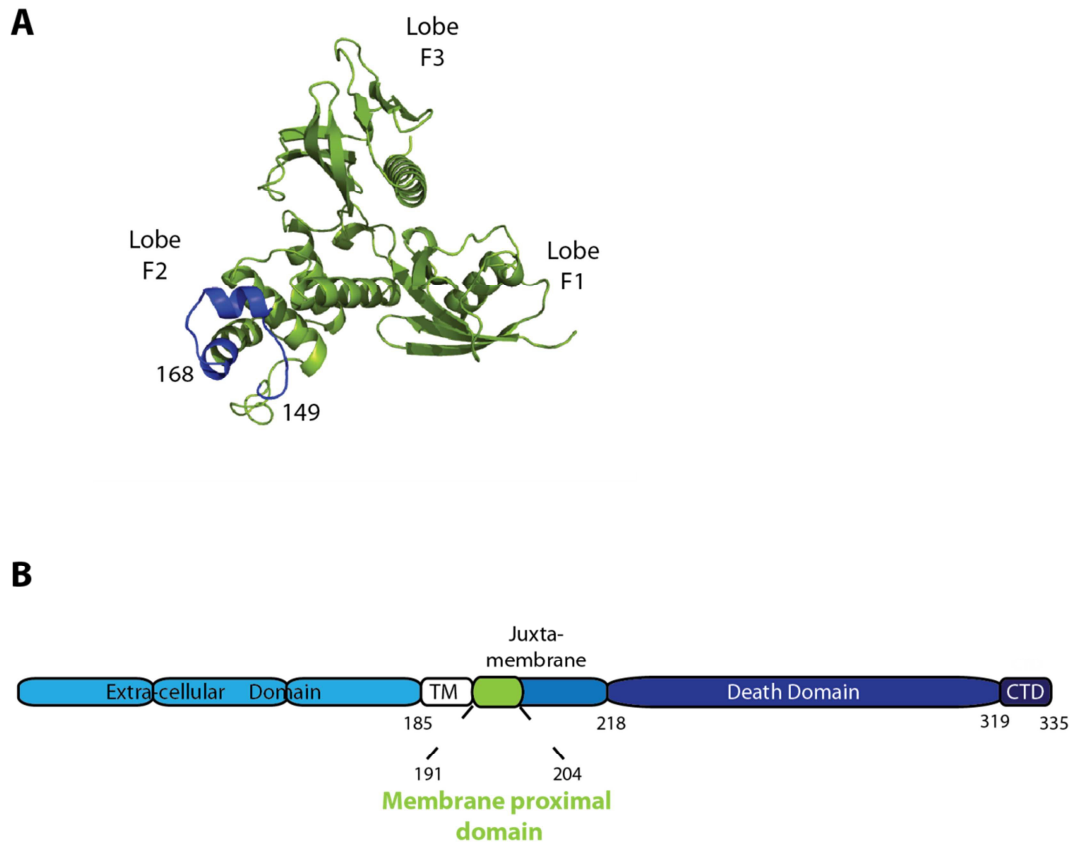

Figure 1.13 Schematic diagrams of the reported Fas and ezrin interaction sites

A, FERM domain of ezrin (PDB:1NI2) shown in green, with the reported Fas binding site, residues 149-168 highlighted in blue. B, schematic representation of the Fas protein highlighting the different domains. The reported ezrin binding site, the membrane proximal domains (MPD), is highlighted in green.

Ruan and colleagues went on to transfect a version of Fas lacking the MPD and found that this construct was unable to activate the apoptotic and non-apoptotic Fas signalling pathways. Others have pointed out that the region they deleted contains the palmitoylation site C199 and the lysine-rich region that have been shown to be necessary for lipid raft targeting and activity[50,25]. Nevertheless, binding of ezrin to the positively charged juxtamembrane region of Fas would be in agreement with the mode of binding observed in other ezrin targets[100,119].

The interaction of Fas with other molecules has also been reported to affect the association of Fas with ezrin. The disialoganglioside GD3 is reported to colocalise with ezrin, and has been suggested to play an early role in Fas oligomerisation, possibly mediating DISC progression[120]. Moreover, the phosphorylation of the guanine exchange factor (GEF) vav1 has been hypothesised to act as a fine tuning mechanism to terminate receptor internalisation by down modulating the Fas:ezrin:actin linkage[45].

1.9 Aims, objectives and scope of this study

Fas receptor stimulation activates the Fas death domain (Fas-DD), resulting in receptor clustering, and recruitment of adaptor proteins and formation of the DISC. The DISC is assembled through homotypic interactions between members of the death domain superfamily, DD:DD interactions between Fas and FADD and DED:DED interactions between FADD and procaspase 8[38]. This oligomerisation is crucial for the onset of both apoptotic or non-apoptotic cell signalling pathways[71], as it enables autoproteolytic activation of procaspase 8 and initiation of the caspase cascade. The Fas-DD is at the heart of these interactions, being the activating molecule and the nucleation point for FADD, procaspase 8 and also other proteins with death domains. The 3D structure of the Fas-DD was solved in 1996 by nuclear magnetic resonance[6]. It was the first 3D structure of a member of the death domain superfamily. Ever since, much work has been carried out to characterise the modes of interaction of the Fas-DD and the molecular mechanisms of DISC formation[121–124]. Throughout these structural studies of the Fas-DD and of other DDs a debate has arisen regarding the structural plasticity of this fold. The original NMR solution structure of the Fas DD depicts the canonical DD fold composed of six antiparallel

alpha helices in a bundle arrangement. Years later, a crystal structure of the Fas and FADD death domain complex was published showing the Fas-DD in a different, more open conformation[121]. In this new arrangement, helices 5 and 6 merged creating a long stem helix formation with an extra α–helix at the C-terminus. A number of studies have since disproved that this arrangement is biologically relevant[122–124]. However, it does indicate that the Fas-DD has the potential to exist in a different conformation to the canonical death domain fold.

Different lines of evidence suggest that structural plasticity is a feature of death domains. For example, it is clear that Tyr291 in the DD of Fas can become phosphorylated, but in the canonical structure this residue is not solvent accessible. The question arises as to how a kinase can access Tyr291 and to what extent this negatively charged modification can have upon the death domain fold[54]. Along the same lines, a recent structure of calmodulin with a peptide derived from Fas-DD indicates that the opening of the death domain would be necessary for calmodulin binding[125]. The first results chapter of this thesis reports the use of nuclear magnetic resonance techniques to explore the possibility that the Fas-DD exists in different conformations. This objective was approached by measuring the dynamic behaviour of the Fas-DD at different timescales and in destabilising conditions, i.e. in the presence of the buffer used to obtain the crystal structure of the open conformation and after the introduction of a phosphomimetic mutation at Tyr291.

Being a transmembrane receptor, it is not surprising that posttranslational modifications in the intracellular region of Fas are important for signalling, but given that Fas lacks enzymatic activity, the nature and consequences of these modifications are more difficult to explore. The evidence suggesting that the structure of Fas-DD is flexible makes it tempting to hypothesise that these modifications are able to alter the structure and dynamics of the Fas-DD. To the best of my knowledge, there are no previous studies exploring the molecular effects that any posttranslational modification might have on a death domain structure. Unfortunately, the necessary methodology to enable the study of posttranslational modifications using biophysical techniques has yet to become standard. Chapters Four and Six of this thesis describe my efforts to establish protocols to prepare tyrosine phosphorylated and palmitoylated death domains respectively.

Chapter Four documents the development of techniques to prepare phosphorylated Fas death domain *in vitro* using expressed protein ligation technology. Expressed protein ligation is a technique that creates a native peptide bond between a fragment prepared using recombinant expression and a fragment obtained using peptide synthesis. The chemical flexibility of peptide synthesis enables the incorporation of modified residues, non-natural amino acids and a variety of molecular probes into the synthetic peptide; while the convenience, plasticity and economy of bacterial expression allows for better yields and the generation of much longer proteins than by chemical synthesis alone. Established methods of chemical ligation are restricted by the need of a cysteine at the C-terminus of the junction[126]. However, developing molecules with cysteine mimicking properties is a promising development to lift this limitation in the near future[127]. Part of my objective in Chapter Four was to assess the applicability of a novel cysteine mimic for expressed protein ligation.

Internalisation of the DISC is understood to be the point at which the cell commits to apoptosis; it is the undisputable event that differentiates apoptotic from non-apoptotic Fas signalling cascades. It is believed that this internalisation requires interactions between the cytoplasmic region of Fas and the cytoskeleton adaptor proteins ezrin and/or moesin, which function as a bridge between transmembrane proteins and actin. It is not clear whether the interaction with ezrin is necessary to enable or disable DISC internalisation. However, it is clear that ezrin interaction with Fas is important in Fas-mediated signalling. Possible sites of interaction in both Fas and ezrin have been mapped using deletion constructs[117,118] but no structural or biophysical confirmation of this interaction has been reported. Chapter Five describes my efforts to replicate this interaction *in vitro* and to detect binding using nuclear magnetic resonance spectroscopy, analytical ultracentrifugation and biolayer interferometry.

Finally, Chapter Six describes my brief experience with *in vitro* protein palmitoylation. Palmitoylation of a cysteine thiol is the only acylation modification that is reversible, and as such enables dynamic partition of proteins in and out of membrane compartments within the cell. Given that Fas is a transmembrane protein, the effects are less straightforward to understand, and the behaviour of a palmitoylated version of Fas would certainly provide valuable and novel information regarding the effects on the structure and dynamics of such a modification. In

particular, I was interested in addressing the possibility that upon palmitoylation, Fas experiences a change in configuration that allows interaction with ezrin to occur.

Chapter 2

Materials and Methods

2.1 General equipment and chemicals

Chemicals used were purchased from Sigma or Fisher Scientific, unless otherwise stated. Oligonucleotides were purchased from Integrated DNA Technologies or Sigma. Isotope labelled chemicals were purchased from Cambridge Isotope Laboratories, Inc. All enzymes for DNA manipulation were acquired from New England Biolabs, unless otherwise stated.

Polymerase chain reactions (PCRs) were carried out in a Mastercycler Gradient S thermal cycler (Eppendorf). Plasmid mini-preparations, DNA gel extractions and PCR purifications were carried out using the Qiagen Qiaprep and Qiaquick kits.

UV/Visible absorbance was measured using BioMate3 or Nanodrop 2000 UV/Vis spectrophotometers (Thermo Scientific).

Protein concentration was carried out by centrifugal ultrafiltration with a molecular weight cut off (MWCO) of either 3 kDa, 5 KDa or 10 KDa (Vivaspin 20, Vivaspin 2 Sartorious Stedim Biotech GmbH). Unless otherwise stated, centrifugation up to a speed of 4500 rpm and a volume of 50 ml was carried out using Universal 320R, for larger samples or higher speeds in either a J2-21 or an Avanti J26-XP Beckman centrifuge, and JA-10 or JA-20 rotors (Beckman Coulter). All buffers and solutions were prepared using deionised water from Arium611VF Ultrapure water system (Sartorious Stedim Biotech GmbH).

2.2 Bioinformatics

Nucleotide sequences of target proteins were obtained from the NCBI website (www.ncbi.nlm.nih.gov), protein and DNA homologues were identified using the

NCBI BLAST tool. Protein sequences and domain boundary information was found at the Uniprot database (www.uniprot.org). DNA and protein sequence alignments were carried out using the MAFFT algorithm[128] as implemented in their server (mafft.cbrc.jp/alignment/server/) and analysed with Jalview[129]. Theoretical extinction coefficients were calculated from the primary amino acid sequence of the relevant protein using the Protparam tool on the Expasy Bioinformatics Resource Portal (web.expasy.org/protparam/), which uses a modified version of the Edelhoch method[130], but with the extinction coefficients for Trp and Tyr suggested by Pace and collaborators[131]. The Expasy translator was used to translate DNA to protein sequences. The Scripps Mass calculator (protcalc.sourceforge.net/) was used to calculate ^{15}N averaged masses for mass spectrometry analysis. Peptidemass (web.expasy.org/peptide_mass) on the Expasy server was used to calculate theoretical peptide masses following trypsin digestion.

2.3 General molecular biology techniques

2.3.1 Expression plasmid construction

The expression plasmid for Fas death domain and Fas death domain and C terminal tail constructs were constructed by Dr Diego Esposito prior to the start of this project. The constructs comprise residues 202-302 and 202-319 of the intracellular region of Fas respectively. The vector incorporates an N-terminal hexa-histidine sequence to allow for immobilised metal affinity purification of the expression construct.

pTWIN1 is a commercial vector from New England Biolabs. pET-His_1a was a kind gift from Dr Gunter Stier, then at the European Molecular Biology Laboratory Heidelberg (babel.ucmp.umu.se/cpep/web_content/Pages/CPEP_09_vectors.html). pET-His-Bio was generated in-house from pET-His_1a. pNIC vectors were a kind gift from Dr Charles Allerston and Dr Opher Gileadi, at the Oxford site of the Structural Genomics Consortium (www.addgene.org/Opher_Gileadi/), pNIC-GB1 was constructed in-house from pNIC-GST.

Variations on the Fas expression constructs as well as other constructs used throughout this project (ezrin, moesin, radixin and others) were generated by PCR

amplification from human neural cDNA (DV Biologics). This was followed by either enzymatic digestion and ligation into the multiple cloning site (MCS) of the vector, or by ligation independent cloning (LIC) as specified for each construct throughout this report. PCR primers were designed using the Oligocalc website[132](www.basic.northwestern.edu/biotools/oligocalc.html) to calculate melting temperature and likelihood of secondary structure formation, in order to ensure they fitted within the following parameters: primer length <50 bp, GC content 40-60% and a melting temperature (TM) of ~55 ^{o}C (nearest neighbour score on OligoCalc website). For cloning into pTWIN the SapI and NdeI restriction sites were incorporated into the 5' and 3' end of the primers respectively. For cloning into pET-His_1a and pET-His-Bio vectors the NcoI and XhoI restriction sites were incorporated into the 5' and 3' end of the primers. For cloning into pNIC vectors 5' and 3' LIC sequences were incorporated into the 5' and 3' end of the primers. Vectors used throughout this study are shown in table 2.1

Table 2.1 Expression vectors used throughout this study

Vector	Antibiotic Resistance Marker	Promoter	Purification and/or protein tag	Protease cleavage site
pNIC-GST	Kan	T7	GST (N-terminal)	TEV
pNIC-GB1	Kan	T7	His_6-GB1(N-terminal)	TEV
pNIC-MBP	Kan	T7	His_6-MBP(N-terminal)	TEV
pNIC-Zb	Kan	T7	His_6-Zb(N-terminal)	TEV
pET-His_1a	Kan	T7	His_6(N-terminal)	TEV
pET-His-Bio	Kan	T7	His_6-Avi (N-terminal)	TEV
pTWIN1	Amp	T7	*Mxe* intein-CBD (C-terminal)	

2.3.2 Competent cell transformation

Chemically competent cells were either purchased or prepared using the standard Maniatis $CaCl_2$ protocol[133]. *E. coli* competent cells were transformed as follows: 50 µl of thawed competent cells were incubated on ice for 30 minutes with 1-5 µl of purified plasmid. Cells were then subjected to a 30 second heat shock at 42 ^{o}C and then kept on ice for 5 minutes. 950 µl of warmed SOC medium was then added and cells were incubated in a shaking incubator at 37 ^{o}C for one hour. The culture was

then spread onto an agar plate containing the appropriate antibiotic. For supercoiled plasmids, 50-100 µl of culture were plated out, whereas for ligations and plasmids which had undergone site directed mutagenesis, the culture was spun down at 5000 rpm for 1 minute, the supernatant discarded and the whole cell pellet was plated out. Plates were incubated at 37 ^{o}C overnight (12-16 hours) to allow colony growth.

2.3.3 Preparation of E. coli glycerol stocks

A well isolated colony from a fresh transformation was used to inoculate 10 ml of sterile LB medium containing the appropriate antibiotics in a 50 ml centrifuge tube (BD Falcon). The culture was grown in a shaking incubator at 37 ^{o}C for 4-6 hours until the optical density at 600 nm had reached 0.6, 1 ml of culture was mixed vigorously with 400 µl of sterile glycerol (40% w/v) in 1.5 ml cryovials and stored at -80 ^{o}C.

2.3.4 Plasmid DNA preparation

Plasmid DNA was transformed into *E. coli* NEB5α strain (New England Biolabs) as described in section 2.3.2. A fresh isolated colony was used to inoculate 10 ml of sterile LB medium containing the correct antibiotic and incubated at 37 ^{o}C overnight in a shaking incubator at 250 rpm. Following overnight incubation, cells were harvested by centrifugation at 4500 rpm for ten minutes. Plasmid DNA was prepared from the cell pellet using the Qiaprep miniprep kit following manufacturer's instructions. The concentration was determined using a Nanodrop 2000 UV-Vis spectrophotometer.

2.3.5 Agarose gel electrophoresis

Agarose gels were cast at 0.8% or 2% w/v in Tris-acetate-EDTA (TAE) buffer (40 mM Tris acetate pH ~8.5, 1 mM EDTA) containing 1:10,000 Sybrsafe (molecular probes) for DNA visualisation. DNA samples were prepared with the addition of 6X gel loading buffer (30% w/v glycerol containing trace amounts of bromophenol blue or xylene cyanol FF, for DNA fragments at <1 kbp or >4 kbp respectively). Appropriate molecular weight markers (100 bp or 1 kbp, NEB) were also prepared in this way. Electrophoresis was carried out at 50-100 V in TAE buffer. Gels were visualised under UV light.

2.4 Cloning and mutagenesis

2.4.1 Cloning using restriction enzymes

2.4.1.1 Insert preparation

DNA for the proteins of interest was amplified by PCR from cDNA, synthetic genes or from an expression plasmid previously cloned in our laboratory. PCR reactions were prepared in thin walled PCR tubes on ice using the KOD Hotstart Polymerase kit (Novagen). An example of a typical PCR reaction is shown in table 2.2. A typical PCR program is shown in table 2.3

Table 2.2 PCR reaction for insert preparation in 100 µl

Reagent	Final Concentration	Volume
Template DNA	20 ng	Up to 1 µl
KOD Hotstart buffer	1x	10 µl
dNTP mix	200 µM	10 µl
$MgSO_4$	1.5 mM	6 µl
Forward primer	0.5 µM	5 µl of 10 µM stock
Reverse primer	0.5 µM	5 µl of 10 µM stock
KOD enzyme	1 U	2 µl
H_2O	N/A	Up to 100 µl

Table 2.3 A typical PCR program for insert preparation

Step	Time	Temperature (^oC)	Cycles
Denaturation	2 min	95	1
Denaturation	30 sec	95	30
Annealing	30 sec	56	
Extension	30 sec*	72	
Extension	10 min	72	1
Hold		4	1

* 1 min per 1kB

PCR reactions were set up in 100 µl volumes to ensure a large amount of insert was amplified. PCR products were analysed in a 2% agarose gel. If the template DNA was a vector, it was digested by adding 1 µl of the endonuclease DpnI to the reaction and incubated at 37 ^oC in a water bath for two hours. PCR products were finally purified using the QIAquick PCR cleanup kit according to the manufacturer's instructions, eluted in 50 µl of deionized H_2O.

2.4.1.2 Vector preparation

Cloning vectors were prepared by the plasmid DNA preparation method described in section 2.3.4. To ensure enough plasmid DNA was purified, larger overnight cultures (10-20 ml) were separated into 5 ml aliquots and treated as separate preparations up to precipitation and pelleting of the proteins and chromosomal DNA. A this point all supernatants were sequentially loaded onto the same spin column, in order to increase the final yield and concentration of the eluted DNA.

2.4.1.3 DNA digestion and purification by agarose gel electrophoresis

Both plasmid vector and insert were digested with compatible restriction enzymes at 37 ^{o}C for three hours. Digestions were set up according to the manufacturers recommendations including a compatible buffer and (where appropriate) 1 mM BSA to a total volume of 60 µl. The digestions contained less than 10% total v/v of restriction enzyme to avoid the star activity of the enzyme. Following digestion, the vector DNA was treated with Antarctic phosphatase (3 µl) at 37 ^{o}C for three hours, in order to remove the 5´ phosphate groups from the vector and prevent vector re-circularisation.

Following digestions and phosphatase treatment of the vector preparative agarose gel electrophoresis was carried out to purify the digested products. Vector DNA was run and excised from 0.8% agarose gels and the insert DNA from 2% gel. To increase the efficiency of the ligation/transformation, gels were stained with 2% v/v methylene blue to enable gel extraction without the use of UV light. DNA was purified from excised gel fragments using a QIAquick gel extraction kit following the manufacturer's instructions.

2.4.1.4 DNA ligation and transformation

Ligation reactions were done with T4 DNA ligase. The set up was commonly ~50 ng of digested plasmid DNA and a molar vector:insert ratio of 1:3 and 1:6. A typical ligation reaction is shown in table 2.4. To control for vector re-circularisation and/or inefficient digestion, as well as for improper purification of the insert and vector, control ligations were also set up containing vector or insert only.

Table 2.4 Typical DNA ligation reaction

Reagent	Concentration	Volume
Insert	3-6x more than vector (molar ratio)	X µl
Vector	50 ng	Y µl
T4 DNA ligase buffer	1x	1 µl
T4 DNA ligase	1 Unit	1 µl
H_2O		Up to 10 µl

Ligation reactions were set up on ice and incubated overnight at 16 ^{o}C. Following overnight incubation the ligase was inactivated by heating at 65 ^{o}C for ten minutes. 5 µl of each ligation reaction was then transformed into NEB5α competent cells as described in 2.3.2

2.4.2 Ligation Independent Cloning (LIC)

Ligation independent cloning was used for the majority of cloning for Fas and ezrin constructs into a number of pNIC vectors containing TEV cleavable purification tags (see table 2.1).

2.4.2.1 LIC vector preparation

5 µg of pNIC vector were linearised by digestion with BsaI at 50 ^{o}C for 2-3 hours. The digested product was purified by preparative gel electrophoresis as described in 2.4.1.3

2.4.2.2 LIC insert preparation

Inserts for LIC cloning need to contain complementary overhangs to those found in the target vector. In the case of the pNIC vectors with N-terminal purification tags, as are all the ones used in the study, the following 5' extensions are added to the primers: TAC TTC CAA TCC ATG to the 5' end of the upstream primer, in which ATG is in-frame with the desired coding sequence; and TAT CCA CCT TTA CTG to 5' end of the downstream primer.

Insert amplification was carried out in a 50 µl reaction volume using the methods described in 2.4.1.1, and 2.4.1.3. If the template was a plasmid, the PCR reaction was treated with DpnI for 1-2 hours prior to preparative gel electrophoresis.

2.4.2.3 T4 DNA polymerase treatment of LIC insert and vector

Reactions for controlled digestions exploit the 3' - 5' exonuclease activity of T4 DNA polymerase. T4 DNA polymerase treatment was carried out at 22 ^{o}C for thirty minutes and then the polymerase was inactivated by incubation at 75 ^{o}C for twenty minutes. Typical T4 DNA polymerase treatments of vector and insert are shown in tables 2.5 and 2.6.

Table 2.5 Vector T4 DNA polymerase treatment reaction

Reagent	Concentration	Volume
BsaI digested plasmid	600 ng	X µl
Buffer NEB2	1x	2 µl
DTT	100 mM	0.5 µl
dGTP	25 mM	0.5 µl
BSA	1x	0.2 µl
T4 DNA polymerase	1x	0.4 µl
H_2O		Up to 20 µl

Table 2.6 Insert T4 DNA polymerase treatment set up

Reagent	**Concentration**	**Volume**
Insert	0.2 pmole	Y µl
Buffer NEB2	1x	2 µl
DTT	100 mM	1 µl
dCTP	25 mM	0.5 µl
BSA	1x	0.2 µl
T4 DNA polymerase	1x	0.4 µl
H_2O		Up to 20 µl

2.4.2.4 Annealing and transformation

To anneal insert and vector, 0.02 pmol of insert was incubated with 25-50 ng of prepared vector for 5 mins at room temperature. 1 µl 25 mM EDTA was then added and the reaction incubated at room temperature for a further 5 minutes. 1 µl of annealed product was transformed into BL21 (DE3) Gold competent cells (Agilent Technologies) as described in 2.3.2.

2.4.3 Site-directed mutagenesis

Point mutations were inserted into the construct of interest using the linear amplification technique, with completely overlapping complementary mutagenic primers. Primers were designed according to Agilent's Quikchange Primer Design Guidelines, i.e. with a length between 25 and 45 bp, minimum GC content of 40% and a melting temperature more than or equal to 78 ^{o}C, using the formula:

Tm = 81.5+ 0.41(%GC) (675/N) - % mismatch.

Where N is the length of the primer. The base mutation of interest was usually placed within the centre of the oligonucleotides. A typical PCR reaction and program used for site directed mutagenesis are shown in tables 2.7 and 2.8 respectively.

Table 2.7 Typical reaction mixture for site-directed mutagenesis (50 µl)

Reagent	Concentration	Volume
Template DNA	50 ng	
KOD Hotstart buffer	1x	5 µl
dNTP mix	200 µM	5 µl
$MgSO_4$	1.5 µM	3 µl
Forward primer	0.14 µM	0.7 µl of 10 µM stock
Reverse primer	0.14 µM	0.7 µl of 10 µM stock
KOD enzyme	1U	1 µl
H_2O		Up to 50 µl

Table 2.8 Typical PCR program used for site- directed mutagenesis

Reaction step	Time	Temperature (^{o}C)	Cycles
Denaturation	2 min	95	1
Denaturation	20 sec	95	20
Annealing	20 sec	55	
Extension	2 min 30 sec	70	
Extension	10 min	72	1
Hold		4	1

Following PCR amplification, in order to digest the parent DNA, 1 µl of the endonuclease DpnI was added to the reaction and incubated at 37 ^{o}C in a water bath for two hours. A 5 µl aliquot was removed before digestion to control for the DpnI digestion. PCR amplification and DpnI digestion was verified by running a 0.8%

agarose gel. Positive reactions were transformed into NEB5α as described in section 2.3.2. Selected colonies were used to inoculate 10 ml of sterile LB medium and cultured overnight in a shaking incubator at 37 ^{o}C. Plasmid DNA was extracted using the Qiaprep spin miniprep kit and mutations verified by DNA sequencing.

Fas-DD is known to aggregate *in vitro*. It has been shown that the K247A point mutation reduces this aggregation allowing increased concentrations to be achieved[50]. All Fas-DD constructs contain this mutation unless otherwise stated.

2.4.4 Colony PCR for detection of positive clones

Following cloning, colonies were screened by colony PCR method using 5 PRIME Taq DNA polymerase MasterMix. A suitable number of isolated colonies (typically 10-12) were picked and independently re-suspended in 20 µl of LB medium which was split into two 10 µl aliquots. One of the aliquots was stored at 4 ^{o}C for propagation and storage in case the colony was positive. The other aliquot was lysed by heating to 95 ^{o}C for five minutes and centrifuged at 13000 rpm for 1 minute. This cleared lysate was used as template for the colony-PCR. A typical colony-PCR reaction is shown in table 2.9. PCR program/protocol used for colony PCR is shown in Table 2.10.

Table 2.9 Typical reaction mixture used for colony PCR

Reagent	Concentration	Volume
5 PRIME Master Mix	1x	10 µl
Forward primer	0.2 µM	0.5 µl of 10 µM stock
Reverse primer	0.2 µM	0.5 µl of 10 µM stock
Colony	N/A	1 µl
H_2O	N/A	Up to 25 µl

Table 2.10 PCR program for colony PCR

Reaction step	Time	Temperature (^{o}C)	Cycles
Denaturation	2 min	95	1
Denaturation	30 sec	95	35
Annealing	45 sec	55	
Extension	1 min	72	
Extension	2 min	72	1
Hold		4	1

The reaction products were analysed in a 2% w/v agarose gel to verify whether a correctly sized PCR product had been generated. Positive colonies were used to seed 10 ml of sterile LB medium containing appropriate antibiotics and grown overnight at 37 ^{o}C in a shaking incubator. Plasmid DNA was purified from overnight cultures using the Qiaprep miniprep kit and purified plasmids sent for sequencing to verify the sequence of the DNA product.

2.4.5 Megaprimer insertion of MBP into Fas-DD-Mxe-CBD

The exponential megapriming (EMP) PCR method of Ulrich *et al*. 2012[134] was used to incorporate the MBP solubility tag into the pTWIN1 N-terminal Fas construct to improve solubility.

2.4.5.1 Megaprimer preparation

Three primers are needed, named F1, R1 and R2. F1 and R1 are for initial amplification of the megaprimer from the target, they are complementary to the 5' and 3' (respectively) ends to the insert, R1 also contains 20-25 nucleotide overlap to the target plasmid, 3' to the insertion site. R2 is used to clone the insert into the target vector and is complementary to the 5' end of the insertion site on the target plasmid. Amplification of the megaprimer was carried out using the PCR program described in table 2.10 using the reaction set up detailed below in table 2.11. Following megaprimer amplification it was gel extracted as described in 2.4.1.3

Table 2.11 Reaction mixture for megaprimer preparation

Reagent	**Concentration**	**Volume**
buffer for KOD hot start polymerase	1x	5 µl
dNTP mix	200 µM	5 µl
MgSO4	1.5 µM	3 µl
F1	0.5 µM	2.5 µl
R1	0.5 µM	2.5 µl
Template DNA	50 ng	
KOD hot start polymerase	1U	1 µl
ddH_2O		Up to 50 µl

2.4.5.2 Insertion of megaprimer into target vector

The megaprimer was inserted into the target vector by PCR using the reaction and PCR program shown below.

Table 2.12 Reaction mixture for megaprimer insertion into target vector

Reagent	Concentration	Volume
Buffer for KOD Hot Start master mix	1x	25 µl
R2	0.5 µM	2.5 µl
Template DNA	25 ng	X µl
Megaprimer	200 ng	Y µl
DMSO	5%	2.5 µl
ddH_2O		Up to 50 µl

Table 2.13 PCR program used for megaprimer insertion into target vector

Reaction Step	Time	Temperature (^oC)	Cycles
Denaturation	2 min	95	1
Denaturation	20 sec	95	20
Annealing	20 sec	46-55 #	
Extension	2 min 30 sec *	70	
Extension	10 min	72	1

*dependant on size of vector, # annealing temperature was varied in respect to primer R2.

The final product was further amplified using the reaction mixture in table 2.14 and the PCR program shown in table 2.10.

Table 2.14 Reaction mixture to amplify EMP product

Reagent	Concentration	Volume
Buffer for KOD Hot Start master mix	1x	25 µl
F1	0.5 µM	2.5 µl
R2	25 ng	2.5 µl
Previous PCR reaction		5 µl
ddH_2O		Up to 50 µl

This PCR reaction was purified using the method described in 2.4.1.1 with the final DNA eluted in 30 µl 10 mM Tris-HCl pH 8, 1 mM EDTA.

2.4.5.3 In vitro ligation and transformation

To improve transformation efficiency, *in vitro* ligation was carried out. 16.5 µl of purified EMP product was incubated at 37 ^{o}C with 5 units of PNK kinase in 1x PNK kinase buffer to phosphorylate the 5' end of the DNA. Ligation was carried out by adding 200 U of T4 DNA ligase and incubating at room temperature for one hour. To ensure no retransformation of original plasmid, DpnI treatment was then carried out at 37 ^{o}C for 1-2 hours. 5 µl of the ligation mixture was transformed into NEB5α competent cells as described in 2.3.2, plating out all of the cells.

2.4.6 DNA sequencing

Plasmid DNA was sent away to the GATC sequencing service (GATC Biotech AG, Germany) for Sanger sequencing. Plasmids were typically sequenced using the T7 or T7 reverse primers available at the sequencing facility. Plasmid DNA was sent away at the concentration of 30-75 ng/µl in 30 µl aliquots.

2.5 Protein expression

2.5.1 Bacterial strains and storage

Expression constructs were transformed into the BL21 (DE3) Gold expression strain of *E. coli* (Agilent Technologies). Single colonies from fresh transformation plates were used to prepare glycerol stocks as described in section 2.3.3.

2.5.2 Small scale expression test

A small flake from a glycerol stock was used to inoculate 10 ml LB containing the appropriate antibiotics. Cultures were grown until the OD_{600} was 0.6 and then induced with 0.5 mM isopropyl-β-D-thiogalactopyranoside (IPTG). Cultures were tested for expression at 37 ^{o}C for four hours or at 22 ^{o}C overnight. Four hour and overnight cultures were harvested by centrifugation at 4500G for ten minutes and resuspended in 1 ml of lysis buffer (50 mM Tris-HCl, 300 mM NaCl, pH 8) followed by cell lysis by sonication on ice. 15 µl of lysed cells were taken as a total protein sample while the rest of the sample was clarified by centrifugation at 13000 rpm in a micro centrifuge for 5 minutes; 15 µl of this was taken as the soluble protein sample.

Samples corresponding to total and soluble protein were assayed for protein expression by SDS-PAGE. The expression level and amount of soluble protein was increased when expressed at 22 ^{o}C overnight. If the construct was not adequately expressed the insert was subcloned into a vector containing an alternative solubility tag.

2.5.3 Large scale protein expression

2.5.3.1 Rich medium

100 ml LB medium containing 60 mg/ml kanamycin (LB-kanamycin) were inoculated using a flake from a glycerol stock. The culture was grown overnight at 37 ^{o}C, cells harvested, the medium decanted and the pellet used to inoculate four 2-litre flasks with 500 ml of LB-kanamycin each. Cultures were grown at 37 ^{o}C and 275 rpm until an OD_{600} of 0.6 was reached. Induction was initiated with 0.5 mM IPTG and cultures were grown overnight at 22 ^{o}C. Cells were harvested by centrifugation at 6370G for 20 minutes using a Beckman Coulter 'JSP F500' rotor.

2.5.3.2 PG minimal medium for ^{15}N and/or ^{13}C isotope labelling

Recombinant ^{15}N-labelled proteins were expressed in cells grown in a modified Studier PG medium[135] with 60 mg/ml kanamycin and $(^{15}NH_4)_2SO_4$ and/or $^{13}C_6$-D glucose, as sole nitrogen and carbon sources respectively.

10 ml of LB-kanamycin medium containing appropriate antibiotics were inoculated with a flake from a glycerol stock or a fresh well isolated colony and cultured by shaking at 250 rpm at 37 ^{o}C. After 6-8 hours, the cells were harvested by centrifugation at 3000 rpm for ten minutes. The supernatant was discarded and the cell pellet resuspended into 100 ml of non-isotope labelled PG medium-kanamycin in a 500 ml flask. This seed culture was grown overnight at 37 ^{o}C and 250 rpm. Overnight cultures were harvested by centrifugation at 3000 rpm for ten minutes and used to inoculate two 2-litre flasks containing 500 ml of isotopically labelled PG medium-kanamycin. Cultures were grown at 37 ^{o}C and 275 rpm until an OD_{600} of 0.7-0.8 was reached, they were then induced with 0.5 mM IPTG and grown overnight at 22 ^{o}C to allow for protein expression.

2.5.3.3 M9 minimal medium for $^{15}N/^{13}C$-labelled Fas-DD

The recombinant $^{15}N/^{13}C$-labelled Fas-DD construct for structural data collection was expressed in *E. coli* (DE3) Rosetta (Novagen). The expression protocol was the same as for the PG medium, but in this case the medium was modified M9[133] with $^{13}C_6$-D-glucose and $(^{15}NH_4)_2SO_4$ as sole carbon and nitrogen sources. Modified M9 minimal medium contains: Na_2HPO_4 6 g/l, KH_2PO_4 3g/l, NaCl 5 g/l, $(^{15}NH_4)_2SO_4$ 1 g/l , 2 mM $MgCl_2$, 0.1 mM $CaCl_2$, 0.01 mM $FeSO_4$, 0.2% $^{13}C_6$-D-glucose, 40 µM H_3BO_3, 3 µM $CoCl_2$, 1 µM $CuSO_4$, 0.8 µM $MnCl_2$, 1 µM $ZnSO_4$, 0.3 µM $(NH_4)_6Mo_7O_{24}$, 0.4 mg/l choline chloride, 0.5 mg/l folic acid, 0.5 mg/l pantothenic acid, 0.5 mg/l nicotinamide, 1 mg/l myo-inositol, 0.5 mg/l pyridoxal HCl, 0.5 mg/l thiamine HCl, 0.05 mg/l riboflavin, 1 mg/l biotin.

2.5.3.4 Large scale expression of $^{2}H/^{15}N$-labelled protein

Expression of ^{2}H-labelled protein was carried out as described in 2.5.3.2 with the addition of 20 mM sodium succinate and $^{15}NH_4Cl$. Instead of H_2O 99.9% $^{2}H_2O$ was used.

2.6 Protein purification for NMR and biophysical studies

2.6.1 Cell lysis and clarification

Cell pellets were resuspended in either IMAC lysis buffer (50 mM Tris-HCl, 300 mM NaCl, pH 8) or GST lysis buffer (20 mM Tris-HCl, 100 mM NaCl, 1 mM EDTA, pH 8), containing Complete EDTA-free protease inhibitor tablet (Roche) and lysed on ice by sonication (Branson Sonifier 250, power output 50 W, 50% duty cycle, 2x 180 seconds). Lysed samples were clarified at 39,200G for 30 minutes using a Beckman Coulter ‘JA-20’ rotor.

2.6.2 Immobilised metal affinity chromatography (IMAC)

Hexahistidine-tagged proteins were affinity purified using Ni-IDA metal affinity resin (Generon). Per 1 litre of overnight cell culture, 4 ml of Ni-IDA metal affinity resin was packed into a gravity-driven column (BioRad Econopac) and equilibrated with 10 column volumes (CV) of lysis buffer. The supernatant of clarified cell lysate

was applied to the resin and the flow-through loaded onto the column for a second time. The resin was washed with 5 CV of lysis buffer followed by 5 CV of wash buffer (20 mM Tris-HCl, 300 mM NaCl, 50 mM imidazole, pH 8) and eluted with elution buffer (20 mM Tris, 150 mM NaCl, 300 mM imidazole, pH 8). Elution was monitored used Bio-rad Bradford protein assay. Elution buffer was applied until protein was no longer detected. 15 µl of each step was collected and analysed by SDS-PAGE.

2.6.3 Glutathione sepharose affinity chromatography

GST-tagged proteins were purified by batch Glutathione sepharose (GE Healthcare) affinity chromatography. Beads were first equilibrated with 10 CV of GST lysis buffer (20 mM Tris-HCl, 100 mM NaCl, 1 mM EDTA, pH 8), added to the lysate and incubated with gentle stirring for one hour. The resin was then packed into a gravity driven column and washed with 5 CV GST lysis buffer and eluted with GST elution buffer (20 mM Tris-HCl, 100 mM NaCl, 1 mM EDTA, 50 mM reduced glutathione, pH 8).

2.6.4 TEV protease cleavage

All protein expression constructs contained the tobacco etch virus (TEV) protease recognition site ENLYFQ*S which was used to remove the tags from the constructs to yield as constructs with only an N-terminal extra serine. Recombinant H_6-TEV protease was prepared in-house.

TEV protease was added in an approximate mass ratio of 1:100 to the eluate obtained from the IMAC purification. The eluate was then dialysed for sixteen hours at 18-22 ^{o}C in Specta/Por Dialysis Membrane 3500 MWCO (Spectrum Laboratories) in 200x the sample volume of 20 mM Tris-HCl, 300 mM NaCl, 1 mM DTT pH 8. In order to be able to use IMAC again to remove the H_6-TEV and any uncleaved protein, is necessary to remove the DTT. To achieve this removal the dialysis bag was then transferred into 200x the sample volume of 20 mM Tris-HCl, 150 mM NaCl, pH 8 and dialysed at 4 ^{o}C for 4-16 hours. The TEV-cleaved sampled was then loaded into a pre-equilibrated the Ni-IDA column and washed with 5 CV of 20 mM Tris-HCl, 300 mM NaCl, pH 8. Samples of the flow-through and wash were analysed by SDS-PAGE.

2.6.5 Size exclusion chromatography (SEC)

Samples from affinity chromatography were concentrated to 10 ml by centrifugal concentration using Vivaspin concentrators of appropriate MWCO and dialysed overnight in 2 litres of the corresponding NMR buffer. The buffer for NMR samples of Fas was 20 mM MES, 100 mM NaCl, 0.5 mM TCEP, 1 mM EDTA, 3 mM NaN_3 pH 6.2. The buffer for ezrin samples was 20 mM Tris-HCl, 150 mM NaCl, 1 mM TCEP, 1 mM EDTA, 3 mM NaN_3, pH 7.4. Samples were finally concentrated again to less than 2 ml.

Size Exclusion Chromatography (SEC) was carried out using an AKTA purifier chromatography system (GE Healthcare) with a prepacked 16/600 Superdex 200 or 75 XK column (GE Healthcare), equilibrated in the respective NMR buffer. Fractions were analysed by SDS-PAGE. Fractions containing pure protein were pooled and concentrated by centrifugal concentration to the desired concentration.

2.6.6 SDS-PAGE

SDS-PAGE analysis was carried out using pre-cast Novex 4-12% 1.0 mm, 15 well Bis-Tris gels (Life Technologies) in an XCell SureLock (Invitrogen) gel tank and power source. Gels were run in 1x MES buffer (Life Technologies) at a constant current of 200 V for 35 minutes. Samples were prepared by mixing 15 µl protein sample with 5 µl NuPAGE LDS sample buffer (Life Technologies) and heating at 90 ^{o}C for 5 minutes. A typical gel was loaded with 10 µl of each protein sample and 5 µl of Mark12 molecular markers (Life Technologies). Gels were stained in Coomassie stain (45% methanol, 10% acetic acid, 0.25% comassie blue R-250) for up to 2 hours and de-stained overnight in de-stain solution (20% methanol, 10% acetic acid). Gels were recorded using a GeneFlash gel documentation system (Syngene).

2.6.7 Protein concentration for NMR, buffer exchange and storage

Pure protein samples were concentrated by centrifugal concentration. Depending upon sample start volume, Vivaspin tubes of either 2 or 20 ml were used. Prior to sample addition, tubes were washed with 2-10 ml of ddH_2O to remove storage additives. Centrifugal concentration was typically carried out at 3800 rpm for variable time intervals in order to minimise the concentration gradient that forms inside the tube.

Buffer exchange was typically carried out by dialysis as described in section 2.6.5. When buffer exchange was required into D_2O buffer for NMR side chain experiments, samples were lyophilised at the correct concentration and volume and resuspended in the same volume of D_2O.

For long term storage, protein samples were aliquoted, snap frozen by immersion in dry ice/methanol, lyophilised and stored at -20 ^{o}C until required.

2.6.8 Protein concentration determination

Protein concentration was determined using a Nanodrop2000 UV/Vis spectrophotometer (Thermo Scientific) recording protein absorbance at 280 nm. This is used to calculate protein con centration using the Beer-Lambert Law.

$$A=\varepsilon CL.$$

A is the absorbance at 280nm, C is the protein concentration, ε is the molar extinction coefficient and L is the path length. Molar extinction coefficients for each protein constructs were predicted using the Expasy ProtParam server.

2.7 Biochemical and biophysical analysis

2.7.1 Analytical size exclusion chromatography

Analytical SEC was carried out in a Superdex 75 analytical size exclusion column (GE Healthcare) attached to an AKTA Purifier chromatography system (GE Healthcare). The column was equilibrated in 20 mM Tris-HCl, 100 mM NaCl, 0.5 mM TCEP, 1 mM EDTA, pH 7.4. Samples were injected in 100 µl volumes. Co-injection of samples involved co-concentration of proteins in the ratio specified in each section.

2.7.2 Co-precipitation assays

2.7.2.1 GST pulldown

The binding buffer for GST-tagged ezrin (residues 1-365) experiments was 30 mM Tris-HCl, pH 7.5, 150 mM NaCl, 10% glycerol, 1% Triton X-100. Beads equilibrated in binding buffer were added to cleared GST-ezrin lysate and incubated

for an hour. Beads were rinsed twice with binding buffer and the bead slurry was added to the solution of the expected binding partner and incubated overnight at 4 ^{o}C with gentle rotation. After washing three times with binding buffer, pelleted beads were resuspended in LDS sample buffer and loaded onto an SDS-PAGE gel which was run and stained with Coomassie blue as described in 2.6.6.

2.7.2.2 Ni-NTA pulldown

Hexa-histidine tagged Fas and untagged ezrin expression lysates were separately incubated with cOmplete Ni-NTA beads (Roche) in IMAC binding buffer and the pull down carried out as described in 2.7.2.1.

2.7.2.3 Immunoprecipitation

Hexa-histidine tagged Fas and untagged ezrin expression lysates were precleared by incubation with Protein G coated Dynabeads (Life Technologies) for one hour at 4 ^{o}C. After preclearing the cell lysate, 5 μg/ml penta-His Mab (Abchem) was added to the lysate and incubated at 4 ^{o}C for one hour. Untagged ezrin was then added and incubated overnight at 4 ^{o}C. Protein G Dynabeads were then added and incubated for one hour at 4 ^{o}C to pull down any potential binding partners. After three washes, the beads were resuspended in LDS sample buffer and loaded onto an SDS-PAGE gel which was run and stained with Coomassie blue as described in 2.6.6.

2.7.3 Biolayer interferonmetry (BLI)

Enzymatic *in vitro* biotinylation was carried out using the Avidity Biotin-protein ligase kit. The kit consists of the BirA biotin ligase, and a two part 10x biotinylation buffer. the first containing 0.5 M bicine buffer, pH 8.3, and the second 100 mM ATP, 100 mM MgOAc, 500 μM d-biotin. The final biotinylation reaction had 40 μM protein, 50 mM bicine, 10 mM ATP, 10 mM magnesium acetate, 50 μM d-biotin and 10 μg of BirA. The mix was incubated for two hours at 30 ^{o}C.

All experiments were carried out in PBS, 0.5 mM TCEP, 0.005% Tween20, 0.5 mg/ml BSA, pH 7.4 on an Octet Red BLI instrument (ForteBio) operated at 25 ^{o}C. Streptavidin-coated biosensors with immobilised biotinylated Fas (residues 202-335) or Fas (residues 194-335) were exposed to different concentrations of ezrin (residues 1-365) [0-400 μM], ezrin (residues 1-297) [0-200 μM], and radixin [0.7-100 μM] and readings were taken. Positive controls of immobilised NHERF2 and

FasDD+CTD were exposed to different concentrations of ezrin (residues 1-365) [0-0.8 μM], and FADD (residues 93-192) respectively. Dissociation constants were calculated by fitting the experimental data in SEDPHAT[55].

2.7.4 Isothermal titration calorimetry (ITC)

Complex formation was measured by ITC using a MicroCal VP-ITC microcalorimeter. Fas (residues 194-335) and ezrin (residues 1-362) were dialysed overnight in the same buffer (20 mM Tris-HCl, 150 mM NaCl, 0.5 mM TCEP, pH 8). The sample cell contained ezrin (1-362) [50 μM] and the syringe contained Fas (194-335) [500 μM]. Experiments were conducted at 10 ^{o}C, 20 ^{o}C and 25 ^{o}C. Heat of dilution measurements were not taken as no heat of interaction was observed.

2.7.5 Analytical ultracentrifugation (AUC)

A Beckman Optima XL-I analytical ultracentrifuge was used to perform sedimentation velocity measurements. Experiments were carried out in aluminium double sector sapphire cells using an AN50-Ti rotor at a speed of 35,000 rpm at 293 K. Prior to the beginning of each run, the rotor temperature was equilibrated at 293 K for 1-2 hours in the vacuum chamber. Interference images were collected every 60 s during the sedimentation run. The recorded data was analysed using SEDFIT[54] in terms of discrete species and continuous distribution function of sedimentation coefficient [c(s)].

The concentration of protein used with the experiments ranged from 0.5-2 mg/ml for Fas (202-335) and ezrin (1-365) ran in isolation and mixed together at equal concentrations of 20 μM, 50 μM, 100 μM. Prior to the experiments, samples were dialysed overnight against the experimental buffer blank solution, 20 mM Tris, 150 mM NaCl, 0.5 mM TCEP, pH 7.4.

2.7.6 Mass spectrometry (MS)

2.7.6.1 Sample preparation

Mass spectrometry samples were prepared using C4 Ziptips (Merck-Millipore) for desalting and concentration. Ziptips were activated with 5 CV of acetonitrile, equilibrated in 5 CV of 0.1% acetic acid which was followed by sample addition. This was followed by 5 CV 0.1% acetic acid wash, 5 CV 5% methanol, 0.1% acetic

acid wash, 0.1% acetic acid wash and the protein sample was eluted in 65% acetonitrile, 0.1% acetic acid.

2.7.6.2 ESI-TOF

Electrospray ionisation time of flight mass spectrometry was carried out in a Bruker Dalronics MicroTOF instrument. Data were analysed using the Bruker Daltonics DataAnalysis program.

2.7.6.3 MALDI-MS

Analysis by Matrix-assisted laser desorption ionisation time of flight mass spectrometry (MALDI-TOF-MS), (Bruker Microflex) was carried out using α-cyano-4-hydroxycinnamic acid (CHCA) matrix. For all analysis, ion positive linear mode was used. Data were processed using FlexAnalysis program (Bruker).

2.8 *In vitro* palmitoylation

2.8.1 Palmitoylation of intracellular Fas

The palmitoylation reaction was carried out by incubating intracellular Fas (residues 194-335) in a final concentration of 200-300 μM, at 37 ^{o}C with 1 mM palmitoyl Co-A in acylation buffer (10 mM HEPES, pH 7, 1 mM EDTA, 1 mM $MgCl_2$, 10 mM NaCl, 130 mM KCl, 1 mM DTT). Reactions were incubated for variable amounts of time. Reaction progression was monitored by ESI-TOF mass spectrometry with the samples prepared as described in 2.7.6.1. This method is based upon the acylation reaction carried out by Bano and collaborators[136].

2.8.2 Tryptic digestion

100 μg of protein samples were digested with 2 μg of trypsin overnight at 37 ^{o}C. Reactions contained 10% acetonitrile and were prepared for mass spectrometry using C4 Ziptips as described in 2.7.6.1.

2.9 NMR spectroscopy

2.9.1 Sample preparation, D_2O addition/concentration

NMR protein samples were prepared by protein expression in minimal medium followed by IMAC and SEC purification as described in 2.6. Samples were typically concentrated to between 100-700 μM (depending on the experiment) at a volume of 550 μl by centrifugal concentration as described in 2.6.7. To obtain the lock signal on the instrument 10% of the final volume was ^2H_2O.

2.9.2 Spectrometers

NMR spectra were recorded at the MRC Biomedical NMR Centre at the National Institute for Medical Research (NIMR), London, using Bruker Avance 600 and 700 or Varian INOVA 600 and 800 MHz spectrometers with cryogenic probes. Pulse sequences had been adapted 'in house' by the staff of the MRC Biomedical NMR Centre. HSQC experiments were set up by the author alone, more complex experiments were set up under the guidance of Dr Tom Frenkiel, Dr Geoff Kelly, Dr Diego Esposito or Dr TJ Ragan.

2.9.3 NMR data processing

NMR data processing was carried out using NMRPipe[137] and initially visualised using NMRDraw[137] using processing scripts which had been developed within the Driscoll laboratory by Dr Diego Esposito or Dr TJ Ragan or supplied by the MRC Biomedical NMR Centre. Processed spectra were viewed and analysed using the CCPN Analysis software[138].

2.9.4 Heteronuclear single quantum coherence (HSQC) spectroscopy

Two-dimensional $^1H/^{15}N$-HSQC[139] experiments were recorded with 1024 complex points in the direct dimension and 128 complex points in the indirect dimension unless otherwise stated. During titration experiments, the number of scans per increment was kept constant for each point in the titration.

2.9.4.1 Titration experiments

To avoid dilution effects, titration experiments were carried out using two separate 550 µl NMR samples, one containing 100-300 µM of ^{15}N labelled protein (Sample A) and a second containing the same concentration of labelled protein with a higher molar concentration (usually double) of the unlabelled putative binding partner (Sample B). ^{1}H/^{15}N-HSQC experiments were collected for both sample A and sample B independently which would correspond to the first and last titration points. Following the initial HSQC experiments, equal volumes of samples A and B were simultaneously swapped between sample A and sample B, producing two new mixtures still containing the same volume of ^{15}N labelled protein sample. NMR spectra were then recorded for these new samples. This mutual swapping of aliquots between samples A and B was continued until an equimolar concentration of the unlabelled protein and the ^{15}N labelled protein was reached, which completed the titration series. Tracking the changes in chemical shift and intensity of cross peaks across the HSQC spectra of the labelled component of the samples determines the involvement of particular residues in any specific protein-protein interaction.

2.9.5 Fas-DD backbone assignments

2.9.5.1 NMR experiments for backbone resonance assignment

For sequence-specific resonance assignments, a number of two and three dimensional NMR experiments were carried out. A 2D ^{1}H/^{15}N-HSQC experiment was used as the basis and all other spectra referenced to this one. Three dimensional experiments collected for backbone assignments were HNCA[140], HNCACB[141], HNCO[140], HN(CA)CO[142], CBCA(CO)NH[143]. All spectra were recorded with 600 µM ^{15}N/^{13}C Fas-DD construct at 298 K, the magnetic field strength each experiment was collected at is shown in Table 2.15. Dr Diego Esposito collected the initial data and initialised the assignments on a sample expressed and purified prior to the author starting in the laboratory.

2.9.5.2 Sequence specific backbone resonance assignments

To assign the backbone resonances in a sequence-specific manner, intra-residue ^{13}C chemical shifts are identified for a particular NH group, followed by sequential chemical shifts which are identified from a different NH group. The three

dimensional spectra recorded for the backbone assignments are rooted on the ^{15}N-^{1}H correlations. Sequence assignments are obtained by correlating inter and intra-residue resonances of Cα and Cβ chemical shifts and generating connected segments of sequential connected spin sub-systems using the CCPN Analysis software.

Combined analysis of HNCA, HNCACB and CBCA(CO)NH spectra were used to designate the sequence specific resonance assignments for the Fas death domain. Table 2.15 contains the experimental details for these three dimensional experiments.

Table 2.15 Experimental details for the 3D NMR experiments acquired for sequential backbone assignments

Experiment	**Magnetic Field Strength (MHz)**	**^{1}H**		**^{15}N**		**^{13}C**	
		Complex Points	**SW (Hz)**	**Complex Points**	**SW (Hz)**	**Complex Points**	**SW (Hz)**
HSQC	800	926	9620	80	2757		
HNCA	800	1024	9620	40	2757	56	6036.3
HN(CO)CA	700	1024	8427.5	20	2411.9	55	5636.9
HNCACB	800	1024	9620	40	2757	112	14084.5
CB(CACO)NH	600	1024	9620	40	2757	64	14084.5

SW – sweep width

2.9.6 NMR experiments for Fas-DD side-chain resonance assignments

To assign the Fas-DD side-chain resonances, a number of two and three dimensional experiments were collected to detect through-bond and through-space interactions. ^{15}N-TOCSY[144] and HCCH-TOCSY[145,146] experiments were collected to identify side-chain proton resonances. The HCCH-TOCSY experiment allows correlation between $^{13}C\alpha$, Hα with aliphatic side-chain protons and carbon nuclei within an individual residue. The ^{15}N-TOCSY correlates side chain protons with the amide proton and nitrogen. A ^{13}C-constant time HSQC was collected which correlated the resonances of each residue found using these experiments. Interproton NOEs arising from through-space dipolar interactions were identified by recording ^{15}N-NOESY and ^{13}C aliphatic and aromatic NOESY[144] experiments. These experiments were carried out on a ^{15}N ^{13}C Fas-DD sample at 600 μM in $^{2}H_2O$, experimental details are shown in table 2.16 and table 2.17.

Table 2.16 Experimental details for ^{13}C through-bond and through-space side-chain experiments

Experiment	Magnetic Field Strength (MHz)	^{1}H		^{13}C		^{1}H-indirect		% sampled
		Complex points	SW (Hz)	Complex points	SW (Hz)	Complex points	SW (Hz)	
^{13}C HSQC	600	853	10000	388	14084			
HCCH-TOCSY	600	1024	7183	32	11314	64	7199	100
^{13}C - ali NOESY	600	960	9600	60	14084	180	9600	100
^{13}C – aro NOESY	600	1024	9600	46	5231	160	9600	100
Non-uniform sampled								
HCCH-TOCSY	600	838	8389	2	11636	3800	4201	32%
^{13}C-ali NOESY	600	1120	8012	2	10204	5800	6024	41%
^{13}C -aro NOESY	600		1561		1024		6024	41%

Table 2.17 Experimental details for ^{15}N through-bond and through-space side-chain experiments

Experiment	Magnetic Field Strength (MHz)	^{1}H		^{15}N		^{1}H- indirect		% sampled
		Points	SW (Hz)	Points	SW (Hz)	Points	SW (Hz)	
^{15}N TOCSY	700	960	9615	32	2310.5	63	2310.5	100%
	700	1372	9803	3700	2483	120	8403	50%

These experiments were also collected using a non-uniform sampling, weighted Poisson disk sampling scheme to improve signal to noise under the guidance of Dr Tom Frenkiel. Experimental information is detailed in table 2.16. Spectra were reconstructed using MDDnmr[147,148] under the guidance of Dr TJ Ragan. Through-space NOE data was used for structural calculation.

2.9.7 Residual dipolar couplings

For residual dipolar coupling (RDC) collection, ^{15}N Fas-DD was aligned in Pf1 bacteriophage (ASLA biotech Pf1 co-solvent P100-P)[149], 10 mg/ml and dialysed against Fas NMR buffer. For NHH couplings, IPAP (in-phase, anti-phase) type HSQC[150] experiments and for HACA couplings HNCOCA experiment (with no

proton decoupling) were collected for aligned and non-aligned Fas samples. The ^{1}H-^{15}N residue dipolar coupling values (RDC) were calculated for each residue (using CCPN Analysis[138]) by subtracting the difference between ^{15}N frequencies in the spectra of the isotropic sample from the bacteriophage aligned sample. Module[151] was used to compare experimental RDC's with simulated RDC values from the published Fas-DD solution structure (pdb:1DDF). RDC values were used within the structure calculation to help restrain the structure.

2.9.8 Methyl-TROSY spectroscopy

ILV-Fas-DD with Ile, Leu and Val residues specifically $^{13}CH_3$ labelled at one single methyl position was kindly provided by Dr Diego Esposito. NMR samples (110 μM) were prepared in buffer containing 20 mM Tris, 150 mM NaCl, 0.5 mM TCEP, 1 mM EDTA, 3 mM NaN_3 pH 6.2 in $^{2}H_2O$. Methyl-TROSY[152] spectra were recorded on a 800 MHz spectrometer.

2.9.9 NMR relaxation experiments

2.9.9.1 ^{15}N Relaxation experiments

T_1, T_2 and $^{1}H/^{15}N$ heteronuclear NOE data was collected for Fas-DD in three conditions:

- Fas-DD in NMR buffer (20 mM MES, 100 mM NaCl, 0.5 mM TCEP, 1 mM EDTA, 3 mM Sodium azide pH 6.2)
- Fas-DD Y291E in NMR buffer (20 mM MES, 100 mM NaCl, 0.5 mM TCEP, 1 mM EDTA, 3 mM Sodium azide pH 6.2)
- Fas-DD in Crystal buffer (0.95 M citric acid, 1.9 M ammonium sulphate, pH 4.0)

T_1, T_2 and $^{1}H/^{15}N$ heteronuclear NOE data for Fas-DD construct was collected and analysed by Dr Diego Esposito prior to the author starting in the laboratory. Spectra were acquired at 25^{o}C. Relaxation delays are shown below in table 2.18.

Table 2.18 Parameters used in ^{15}N relaxation experiments at 600 MHz for Fas-DD

Experiment	**Number of relaxation delays**	**^{15}N relaxation delay times (s)**
T_1	10	0, 0.1, 0.2, 0.3, 0.4, 0.6, 0.8, 1, 1.25, 1.5
T_2	10	0.01, 0.02, 0.03, 0.04, 0.05, 0.06, 0.08, 0.1, 0.125, 0.15

T_1, T_2 and $^{1}H/^{15}N$ heteronuclear NOE data were recorded at 600 MHz using experiments based on published pulse sequences[153], but optimised by the MRC Biomedical NMR Centre, for Fas-DD Y275E and Fas-DD in crystal buffer. Spectra were acquired at 25 ^{o}C using 1024 and 864 complex points in the direct and indirect dimensions. The spectral width in the direct and indirect dimensions was 9615.3 and 2066.9 Hz. Relaxation delays are shown below in table 2.19. R_1 and R_2 values were determined for each residue by fitting an exponential decay (fitting function: Aexp(-Bx)) to the peak intensity of data collected in an interleaved manner. In each case the error was determined from the fit according to a covariance procedure implemented in CCPN Analysis[138] assuming a normal distribution. Residues were excluded when overlap in the data precluded accurate measurement of peak intensity and where the chemical shift no longer matched the wild type assignment.

Table 2.19 Parameters used in ^{15}N relaxation experiments at 600 MHz for Fas-DD Y275E and Fas-DD in crystallisation buffer

Experiment	**Number of relaxation delays**	**^{15}N relaxation delay times (s)**
T_1	9	0.01, 0.05, 0.1, 0.3*, 0.6, 1, 1.5, 2,
T_2	9	0.008, 0.016, 0.024, 0.040*, 0.064, 0.096, 0.144, 0.2

* - denotes repeated delay time

2.9.9.2 Relaxation dispersion experiments

CPMG based relaxation dispersion experiments were carried out upon Fas-DD, Fas-DD Y275E and Fas-DD in crystallisation buffer. Spectra were acquired at 25^{o}C at 600 MHz using 1024 and 600 complex points in the direct and indirect dimensions.

The spectral width in the direct and indirect dimensions was 8417.5 and 2000 Hz. CPMG field strengths of 40, 100, 200, 400, 600, 800 and 1000 Hz (where one point was used for no relaxation) were applied during a 50 ms relaxation period. Peak intensities were extracted using CCPN Analysis[138] and fitted to a single exponential curve to look into the dispersion on a residue by residue basis.

2.9.10 ARIA structural calculations for the Fas-DD

Inter-proton distance restraints were derived from 3D ^{15}N-NOESY-HSQC and ^{13}C-NOESY-HSQC spectra. A proportion of the resonances were successfully assigned in a manual fashion without ambiguity. Backbone φ and ψ torsion angle restraints were derived from the pattern of ^{1}Hα, ^{13}Cα, ^{13}Cβ, ^{13}C′ and ^{15}NH chemical shifts and extracted from CCPN Analysis[138]. Hydrogen bond restraints for amide protons were derived from assessment of the helices of the protein from the current model (PDB: 1DDF). RDCs were collected as described in 2.9.7.

All structure calculations were carried out using the default settings from version 2.3 of the ARIA (Ambiguous Restraints for Iterative Assignment) software package[154–156]. Ambiguous NOEs were calibrated and assigned iteratively, with automatic assignments being checked manually throughout the refinement. Per calculation, nine iterations of ARIA were carried out, with 20 structures calculated at each iteration. After refinement of the 50 lowest-energy structures in explicit solvent, the final ensemble contained 20 structures with no distance restraint violations >0.5 Å and no dihedral angle restraint violation >5°. Figures were generated using PyMOL.

2.10 Expressed protein ligation (EPL)

2.10.1 Solid phase peptide synthesis (SPPS)

The C-terminal phospho-tyrosine Fas peptide was synthesised by standard Fmoc (9-fluorenylmethyoxycarbonyl) solid phase peptide synthesis (SPPS) techniques at a 0.1 mmol scale using Rink Amide resin (0.1 mmol loading) (PL Rink Resin, 0.39 mmol/g loading). The first 32 amino acids (DTLIKDLKKANLCTLAEKIQTIILKDITSDSE) were synthesised on a CEM Liberty1 automated microwave peptide synthesiser with DIC/HOBt (1,3-

diisopropylcarbodiimide/hydroxybenzotriazole) coupling reagents, with a ten-fold excess of Fmoc amino acids relative to the amount of resin. Amino acid deprotection was carried out using 20% piperidine in DMF. To reduce secondary structure formation IT (Fmoc-Ile-Thr(psiMe,Mepro)-OH) and QT (Fmoc-Gln(Trt)-Thr(psiMe,Mepro)-OH) pseudoproline amino acids (Novabiochem) were inserted at positions five and twelve (C to N-terminal) of the peptide respectively.

Fmoc phosphotyrosine (Fmoc-Tyr(PO-(OBzl)OH)-OH, Novabiochem) and the final six residues (GKKEA) were incorporated into the peptide using a CS Bio 336 automated synthesiser with coupling reagents HBTU/DIEA (N-[(1H-benzotriazol-1-yl)(dimethylamino)methylene]-N-methylmethanaminium hexafluorophosphate N-oxide/N,N-diisopropylethylamine) with Fmoc amino acids at ten-fold excess relative to the resin. The reaction was followed by a final deprotection step to remove the N-terminal Fmoc group. One equivalent of 2-hydroxy-3-thio-4-methoxy)benzyl (Htmb) auxiliary was coupled to the deprotected N-terminus of the peptide using microwave coupling, followed by treatment with sodium borohydride to reduce the peptide.

The peptide was cleaved from the resin in trifluoroacetic acid (TFA) with 5% trielthysilane, 5% H_2O, 2% 1,2-ethanedithiol (EDT), for 1.5 hours. The TFA was filtered from the resin and sparged under nitrogen. The peptide was precipitated with sodium-dried diethyl ether and resuspended in 200 mM sodium phosphate pH 7.0-7.5, 2 mM EDTA, 6 M guanidine-HCl, prior to freeze drying or preparation.

Peptide preparation was carried out by semi-preparative High Pressure Liquid Chromatography (HPLC), using a RP-C18 column (22x250 mm, Vydac) and the linear gradient, 15-35% B in 5 minutes, 35-70% B in thirty minutes at a flow rate of 15 ml/min. Pure peptide fractions were pooled, lyophilised and stored at -20 ^{o}C prior to deprotection.

The auxiliary protecting group was removed from the full peptide in TFA with 2% thioanisole and 0.167 mM 2,2′-Dithiobis(5-nitropyridine) (DTNP)[157,158]. Each deprotection reaction consisted of 5 mg of lyophilised peptide was treated in 600 µl TFA. The deprotection reaction was incubated for one hour at room temperature; TFA was sparged away with nitrogen and precipitated using ice cold sodium-dried diethyl ether, resuspended in buffer A and prepared using semi-preparative HPLC as

described above. Pure peptide fractions were pooled, lyophilised and stored at -20 ^{o}C.

At each stage of the synthesis, small aliquots of resin were removed and test cleaved (using the cleavage conditions described above) to check the synthesis was progressing correctly. Samples were analysed by RP-HPLC and MALDI-MS.

2.10.2 Intein mediated protein preparation

2.10.2.1 Expression, chitin purification and on-column cleavage

Fas N-terminal constructs were expressed in BL21 (DE3) Gold as described in 2.5.1.1. Protein expression was induced by the addition of 0.5 mM of IPTG once the cell density had reached an optical density of 0.6 at 600 nm. Optimal expression was achieved when expressed overnight at 20 ^{o}C. Cells were lysed and clarified as described in 2.6.1.

Per 1 litre of overnight cell culture, 7-10 ml of chitin resin (New England Biosciences) was packed into a gravity-driven column and equilibrated in 10 CV of chitin binding buffer. For the N-terminal Fas chitin binding buffer was 20 mM sodium phosphate, pH 6, 0.5 M NaCl, 1 mM EDTA, 1.5 M urea; for the MBP-N-terminal Fas chitin binding buffer was 20 mM sodium phosphate, pH 6, 0.5 M NaCl, 1 mM EDTA. The supernatant of the clarified cell lysate was applied to the resin and the flow through was loaded a second time. The resin was washed with 5 CV of chitin binding buffer followed by 1 CV wash in chitin cleavage buffer, (degased chitin binding buffer containing 16.67 mM TCEP and 5 mM benzyl mercaptan). The column was incubated overnight in 1.5 CV of chitin buffer for on-column intein cleavage to occur. Following incubation, the column was washed in 5-10 CV of chitin buffer to elute cleaved product. 15 µl of each step was collected and analysed by SDS-PAGE. H269G mutant constructs were left incubating with chitin cleavage buffer for 72 hours to increase the yield of cleaved protein.

2.10.2.2- N-terminal fragment preparation

When the elution from the chitin column contained urea, the protein was concentrated by centrifugal concentration to 5 ml. Final purification was achieved by semi-preparative high performance HPLC using a reverse phase C18 column

(22x250 mm Vydac) with a linear gradient of A and B (15-35% in five minutes, 35-75% in 30 minutes) at a flow rate of 15 ml/min. Fractions were analysed by MALDI-MS.

For non-urea containing chitin eluted proteins, fractions were lyophilised, resuspended in purified water and desalted using PD10 desalting columns (GE Healthcare) equilibrated in 10 mM HCl. The final step of purification was using semi-preparative HPLC as described above. Fractions were analysed by ESI-TOF-MS. Pure N-terminal Fas protein was lyophilised and stored at -20 ^{o}C prior to ligation reactions.

2.10.3 Expressed protein ligation of N and C terminal Fas

The ligation of pY291-Fas-DD was performed as follows: 200 mM sodium phosphate buffer (pH 7.4) containing 2 mM EDTA and 6 M guanidine was degassed with argon for 20 min before use. 50 mM TCEP was added and the pH adjusted to 7. Protein thioester and auxiliary conjugated peptide were dissolved at a final concentration of 0.5 mM-5 mM. The ligation reaction was performed in a heating block at 30 ^{o}C unless otherwise stated. Before analysis, 2 µl of the ligation reaction was quenched in 8 µl buffer A. The ligation was monitored by reverse phase HPLC with a C18 or C4 column, using a linear gradient of (30-60% and 30-50% respectively) of buffer B in buffer A over 30 minutes. Confirmation of HPLC peaks was carried out by MALDI-MS.

2.10.4 RP-HPLC

Analytical reverse phase HPLC was carried out using C4 (Vydac, 214TP C4 5 µM 150 mmx4.6mm) or C18 columns (Vydac, 218 TP C18 5µ 150x4.6 mm) in an Agilent 1200 series, or Hitachi elite LaChrom HPLC machines. Flow rates at 1 ml/ml and thirty minute linear gradients were used as standard where buffer A was 0.1% TFA and buffer B was 90% acetonitrile with 0.1% TFA.

Chapter 3

Exploration of the propensity of the Fas death domain to form alternative conformations in solution

3.1 Introduction

3.1.1 Death domain structures are inherently difficult to solve

Solving the three dimensional structures of death domains has been used to inform our understanding of the basis of death receptor signalling. The classical death domain fold is a bundle of six alpha helices in a Greek key topology: the nature of the domains surface features confer protein-protein signalling capabilities through homotypic interactions[159].

The classical route of protein structure determination is to isolate the domain of interest from a whole protein, then to solve the structure by NMR spectroscopy or X-ray crystallography. However, as the native function of a death domain is to undergo oligomerisation and interact with other proteins, the isolation and study of death domains *in vitro* has proved challenging[160]. Out of the 24 death domain structures deposited in the Protein Data Bank (both isolated domains and from interacting complexes), those that are involved in apoptotic signalling were only able to be solved under non-physiological conditions or with the presence of stabilising mutations preventing self-association as illustrated in Table 3.1. For example, to obtain a monomeric Fas-DD at the concentrations needed to solve the structure by NMR, the solution structure was solved at the non-physiological pH 4. However the authors reported that the non-aggregating D260A mutant formed the same structure at a pH of 6[6].

Table 3.1 Conditions that death domain structures have been solved in

Death domain	PDB code	Technique	Conditions	Complex (Y/N)	Reference
Ankryin	2YVI	X-Ray	200mNaCl, 100mM Tris, pH8.5, 25% PEG 3350	N	N/A 2007
Ankryin-1	2YQF	NMR	20mM Tris pH7, 100mM NaCl, 1mM DTT, 0.02% NaN3	N	N/A 2007
FADD	1E3Y	NMR	50mM potassium phosphate, pH6.2, 150mM NaCl, 1mM DTT	N	Berglund *et al* 2000
FADD	2GF5	NMR	50 mM potassium phosphate (pH 4), 150mM NaCl, and 1mM DTT - F25Y mutation	Y	Carrington *et al* 2006
Fas	1DDF	NMR	pH4	N	Huang *et al* 1995
Fas:FADD (4:4)	3EZQ	X-Ray	0.95M citric acid, 1.9M ammonium sulphate, pH4	Y	Scott *et al* 2009
Fas:FADD (5:5)	3OQ9	X-Ray	100mM Tris, pH8.5, 100mM $MgCl_2$, 5% glycerol, 6-10% PEG4000	Y	Wang *et al* 2010
Interleukin-1 receptor associated kinase-4	2A9I	X-Ray	100mM HEPES pH7.5, 25% PEG3350, 10mM $MnCl_2$	N	Lasker *at al* 2005
IRAK-4	1WH4	NMR	20mM Tris pH7.5, 100mM NaCl, 1mM DTT, 0.02% NaN_3	N	N/A 2009
mFADD	1FAD	NMR	50mM sodium acetate pH4	N	Jeong *at al* 1999
Myddosome (MyD88-IRAK4-	3MOP	X-Ray	50mM tris pH8.5, 250mM $MgCl_2$, 8-	Y	Wang *at al* 2012

IRAK2)			15% ethanol		
NFkB p100 subunit	2D96	NMR	200mM Tris, pH7, 100mM NaCl, 1mM DTT, 0.02% NaN_3	N	N/A 2005
NFkB p105 subunit	2DBF	NMR	200mM Tris, pH7, 100mM NaCl, 1mM DTT, 0.02% NaN_3	N	N/A 2005
Nuclear matrix protein p84	1WXP	NMR	20mM Tris pH7, 100mM NaCl, 1mM DTT	N	N/A 2005
p45	2IB1	NMR	PBS pH7	N	N/A 2005
p75 Neurotrophin receptor	1NGR	NMR	pH6 and pH7 dependent on experiment	N	Liepinsh *et al* 1997
Pelle	IYGO	NMR	20mM sodium phosphate pH7.6, 100mM NaCl, 0.5mM EDTA, pH7.6	N	Moncrieffe *et al* 2005
Pelle and Tube complex	1D22	X-Ray	20%–25% PEG 2K monomethyl ether, 100 mM EPES at pH 7.2–8.4, 0–200 mM NaCl	Y	Xiao *et al* 1999
PIDDosome	2OF5	X-Ray	100mM Na/K phosphate pH6.5, 200mM NaCl, 5.5% PEG3350	Y	Park *et al* 2007
RAIDD	2O71	X-Ray	20mM Tris pH8, 150mM NaCl mixed 2M Na/K phosphate pH7		Park and Wu 2006
TNFR1	1ICH	NMR	10mM sodium acetate pH4, 10mM DTT - R347K mutation	N	Sukits *et al* 2001
UNC5b	3G5B	X-Ray	0.1M MES, pH6.5		Wang *et al* 2009
UNC5H2 (netrin1 Receptor)	1WMG	X-Ray	100mM MES pH6.4, 1.8M $MgSO_4$	Y	Handa *et al* 2006

3.1.2 The currently available Fas-DD structures show diverse polypeptide topologies, suggesting some plasticity in the domain

The solution structure of the Fas death domain (Fas-DD) was solved in 1996[6]. However, only a single coordinate set was deposited in the Protein Data Bank, with no resonance assignments, restraints or alternative conformations placed in the public domain. At the time this solution structure of the Fas-DD was the first observation of the death domain fold.

The Fas-DD is made up of six antiparallel amphipathic helices, containing a disordered C-terminal tail as shown in Figure 3.1A. This conformation will be referred to as the 'closed' Fas formation.

In recent years a debate has begun regarding the possibility that the Fas-DD could form alternative conformations to the published solution structure. In part, this debate derives from the publication of two papers detailing different oligomeric states of the complex formed between the Fas and FADD death domains which illustrate different formations of the Fas-DD[121,123,124].

In 2009 the crystal structure of a complex containing four Fas and four FADD death domains (4:4 complex) indicated that the interaction was dependent upon the remodelling of the structure of Fas-DD. This crystal structure suggests that the interaction with FADD-DD causes a conformational change within the Fas death domain, in which the Fas α5 and α6 helices rearrange to form an elongated stem helix paired with a structured C terminus of the domain[121] (shown in Figure 3.1B). This remodelling formed the main interaction surface between Fas-DD and FADD-DD in the 4:4 hetero-oligomer[121]. The more open conformation of Fas-DD exposes the hydrophobic core of the domain enabling an interaction with a hydrophobic patch upon the surface of FADD-DD. Whereas the FADD-DD retains a six helical Greek key topology expected from a death domain. The elongation of Fas-DD helices 5 and 6 form what the authors describe as a Fas-Fas bridge within the structure suggesting that this interaction stabilises the more open conformation and could act in a regulatory role in the formation of the DISC. Although this complex was formed by mixing cell lysates at physiological pH (pH 7.8) the crystallisation conditions were at pH 4. From this point onwards this will be described as the 'open' Fas conformation. Interestingly, it has previously been reported that Fas-DD was unable to self-associate at pH 4[6].

In the Fas-DD solution structure also at pH 4, the C-terminus of Fas is unstructured, with no evidence of fusion of helix five and six.[6] (Figure 3.1A). In depth biophysical analysis has since shown that the C-terminal twelve residues of intracellular Fas are not required for the formation of the Fas:FADD complex in solution[122,123], with this C terminus remaining in a disordered formation upon interaction. Sequence alignment illustrated that the C terminus of Fas is not conserved between orthologues suggesting that the stem loop formation at helices 5 and 6 is not a universal mechanism for DISC formation[123]. In solution, the predominant stoichiometry observed by NMR spectroscopy and ESI-MS of the Fas:FADD complex was in a 5:5 ratio[123], as illustrated in in Figure 3.2C.

The crystal structure of a 5:5 Fas:FADD complex (not involving the C terminal tail) has since been reported, shown in Figure 3.1D[124], corroborating the stoichiometry observed in solution[123]. This crystal structure was solved in less harsh pH and salt conditions (0.1 M Tris pH 8.5, 100 mM $MgCl_2$, 5% glycerol, 6-10% PEG 4000) compared to the 4:4 crystal structure perhaps suggesting this is a more relevant Fas:FADD oligomer. Within this complex, the Fas-DD formed a fold identical to that reported in the original solution structure. Although identified in both crystallographic and solution studies a 5:5 Fas complex also struggles to rationalise trimeric Fas interacting with FADD, as Fas is widely accepted to exist in the membrane in a trimeric form. Ultimately none of the Fas:FADD complex models which are currently in existence fully explain the results from *in vivo* experimental observations upon the formation of the Fas DISC.

A comparison of the three observed Fas-DD conformations is shown in Figure 3.2, illustrating each death domain using a ribbon cartoon. Although the 4:4 crystal structure was obtained in non-physiologically relevant conditions (pH 4)[121], the variation in the Fas-DD structure highlights scope for conformational plasticity of the domain, which may be relevant to further aspects of DISC formation and downstream events.

3.1.3 Post translational modifications within the Fas-DD may infer domain flexibility

It has been reported that the Fas death domain is phosphorylated upon Tyr 291, resulting in Fas oligomerisation and non-apoptotic signalling[55]. Tyr 291 is located within a suspected SH2 domain target site (a YxxL motif) which would suggest that

upon phosphorylation Fas is able to recruit protein domains which are not involved with the usual cell death pathways[62]. In the current Fas-DD solution structure, Tyr291 and Leu294 have a relatively low surface accessibility which is illustrated in Figure 3.3A&B. The addition of a phosphate group upon Tyr291 would disrupt the structure of the Fas-DD both by adding steric bulk as well as changing the properties of the region. This could be taken as an indication that the Fas death domain is able to tolerate some level of flexibility in its structure.

A rigid death domain would further be challenged by the recruitment of SH2 domain containing signalling proteins as in the canonical model, an SH2 domain would require Leu 294 to also be exposed, which in this conformation would not be possible. The location of this post translational modification further highlights the scope for flexibility within the Fas death domain which was not observed in the previous solution studies. In the ‘open’ Fas death domain observed in the crystal structure, (had the domain not been in complex) Y291 and L294 would be positioned in a surface exposed location which could aid in phosphorylation and recruitment of alternative signalling proteins. A comparison of Y291 surface accessibility in both the solution death domain structure and the ‘open’ crystal structure is shown in Figure 3.3

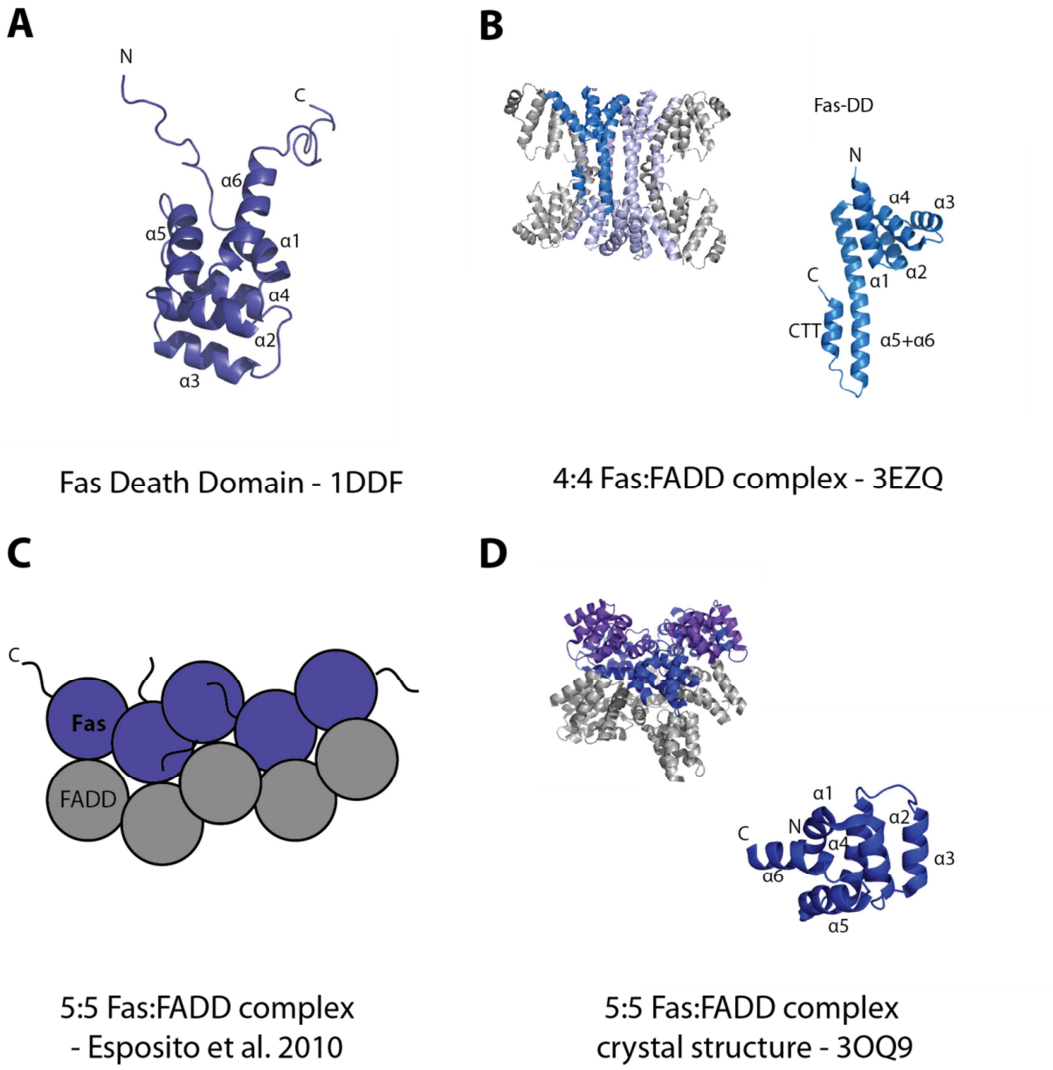

Figure 3.1 The published structures of Fas-DD and Fas-DD:FADD-DD

A, The solution structure of Fas-DD (PDB:1DDF) showing the classical 6 helical bundle with a disordered C terminal tail. B, The crystal structure of the 4:4 Fas:FADD complex (PDB:3EZQ). Fas is highlighted in blue shades and FADD in grey. An individual Fas-DD is also shown, highlighting elongation of α5 and α6 helices and an ordered C terminal tail. C, Schematic representation of the 5:5 Fas:FADD complex inferred from solution techniques by Esposito et al. D, Crystal structure of the 5:5 Fas:FADD, (PDB:3OQ9). Fas-DD in blue shades and FADD-DD shown in grey. An individual Fas-DD is shown in blue showing a similar domain organisation to that in 1DDF.

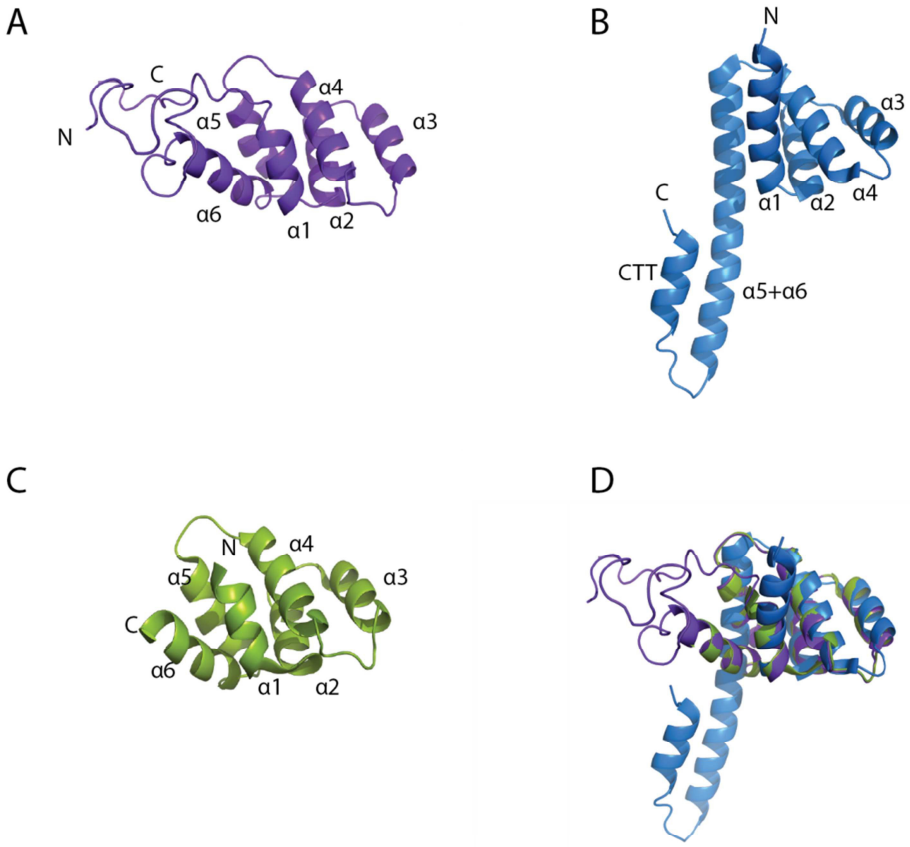

Figure 3.2 Comparison of the three published structures of Fas-DD

A, NMR structure of the Fas-DD, PDB:1DDF. B, Structure of Fas-DD taken from the 4 Fas:4 FADD crystal structure, PDB: 3EZQ. C, Structure of mFas-DD taken from the 5 Fas: 5 FADD crystal structure, PDB: 3OQ9. D, Overlay of the three Fas-DD structures which have been solved.

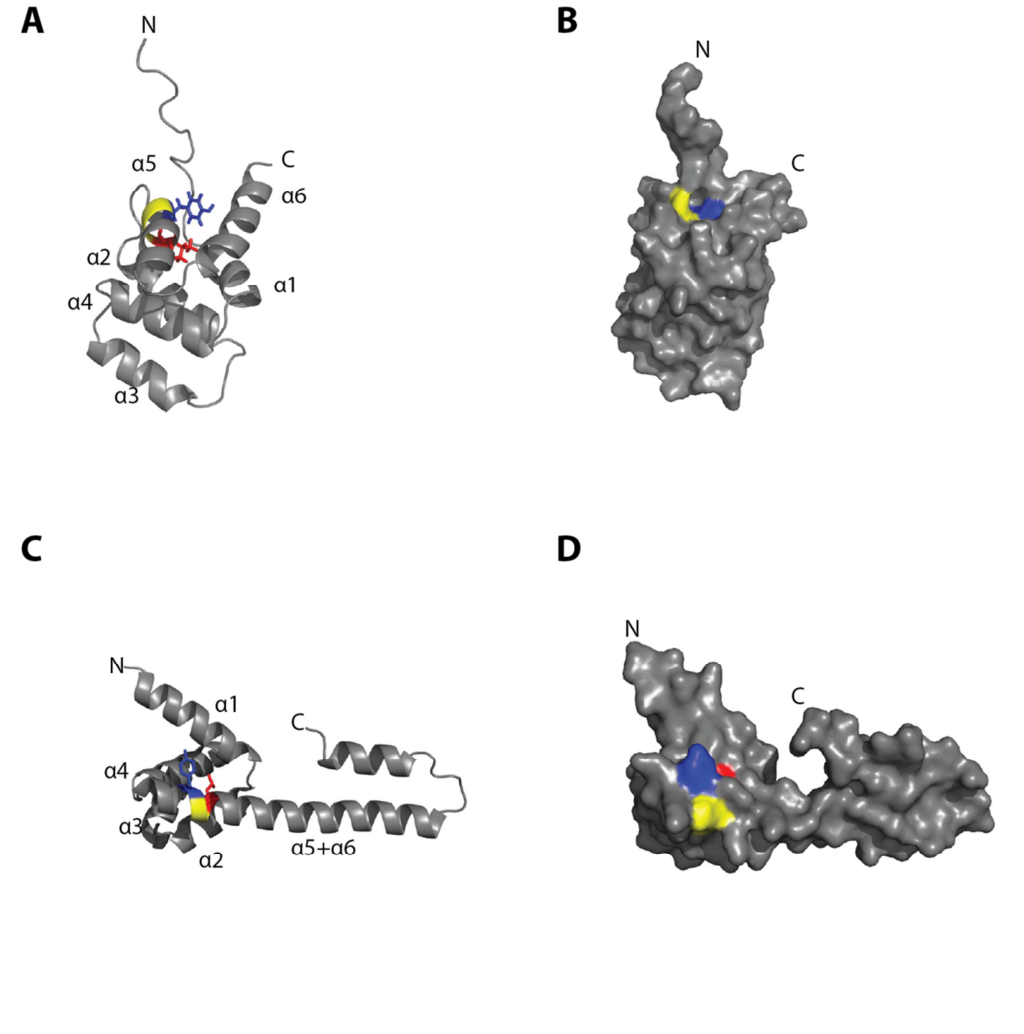

Figure 3.3 Location of Y291 within the current Fas-DD models

Cartoon (A) and surface (B) representations of Fas-DD in the closed conformation (PDB:1DDF). Cartoon (C) and surface (D) representations of Fas-DD in the open conformation (PDB:3EZQ). The YxxL motif is highlighted, Y291 is highlighted in blue, D292 and T293 are highlighted in yellow and L294 in red.

3.1.4 Structural similarity between the known death domain structures

The remodelling of the Fas death domain shown in the 4:4 crystal structure of Fas-DD and FADD-DD appears to be unique throughout the known structures of death domain containing proteins.

Sequence analysis published by Feinstein and Kimchi described two different subtypes of death domains, relating to the structures predicted through sequence analysis. Death domain subtype 1 was described as having a less conserved α1 helix, and included the death domains involved in apoptosis and cytotoxic effects such as Fas, FADD, RIP and TRADD death domains[161]. Subtype 2 was described as having longer loop regions between helices α3-α4 and α4-α5 and conserved prolines between helices, describing proteins DAP (death associated protein) kinase related proteins and the NGFR (nerve growth factor receptor) death domain. From the eighteen isolated death domain structures deposited in the protein data bank, these differences in helix conservation and loop length appear to be the only major difference between the death domain structures. Examples of the similarity in the death domain structures are illustrated in Figure 3.4 in which the overall globular six helix shape is conserved with minimal differences between the globular structures.

The structure of the FADD death domain has been published a number of times from both human[162] and murine[163] sources as well as in tandem with its death effector domain[27]. Each structure shows an overall similarity to Fas-DD even though the sequence similarity between human Fas and FADD death domains is only around 14%. However in the other death domains, there are some subtle differences within their structures compared to Fas-DD. The death domain of TNFR shows an example of some rearrangement in that helices α2 and α4 become more compact when compared to Fas-DD[160] (Figure 3.4D). This has also been shown for the death domain of the p75 neurotrophin receptor which is involved in neuronal growth and migration. P75 death domain was categorised as a subtype 2 death domain, showing reorientation of helix one to be perpendicular to its equivalent location in the Fas-DD, with the authors commenting that this is a large rearrangement for a conserved death domain[164]. The crystal structure of IRAK4 (interleukin-1 receptor-associated kinase 4) also highlights that the loop regions amongst death domains can be variable, with an eleven amino acid loop between helices two and three[165](Figure

3.4E). Just to note, none of the known death domain structures other than Fas-DD describe any helical rearrangement between helices five and six either in isolation or when in a complex. Observed helical rearrangements have only been described to have occurred between helices α1 to α4.

A number of death domain structures have been solved in their hetero-oligomeric form as well as in isolation, much like the known structural data for Fas-DD. The complex structures of both the Myddosome[166] (oligomeric complex containing death domains of MyD88, IRAK2 and IRAK4) and the Piddosome[79] (oligomeric complex containing the death domains of PIDD and RAIDD) showed no difference in structure of the death domain subunits found in the complexes compared to the individual structures of the IRAK4[165] and RAIDD (RIP-associated Ich-1 protein with a death domain)[167] subunits respectively. However, there is one example of a death domain complex other than Fas and FADD which illustrates some level of structural rearrangement between crystal and solution forms. The death domain complex containing *Drosophilia* proteins Pelle and Tube have been shown to be involved in the dorsal-ventral patterning of the *Drosophilia* embryo. The crystal structure of the complex describes the three dimensional folds of the proteins involved as death domains, highlighting the hydrophobic core which is preserved throughout the family of proteins. The complex contained a linear arrangement of four domains (two Pelle and two Tube) showing two distinct interaction sites with the authors describing the interaction as 'plastic'[168]. Both further crystallographic and NMR spectroscopic analysis suggested some differences between the isolated Pelle domain to the one which had been crystallised. An attempt to crystallise Pelle resulted in the observation of a non-classical death domain shaped protein, with the domain rearranging into a single helix which formed an antiparallel dimer. However in solution, results obtained from NMR spectroscopy still suggested the protein formed a six helical bundle. It was finally concluded that the single helical formation was possibly due to the conditions that the crystal was grown in[169], whereas in the NMR solution structure the structure of the Pelle death domain was similar to the death domain topology shown in the crystal complex. The authors went on to comment that they saw no evidence of the plastic nature of the interaction with Tube in the NMR, putting into doubt that the crystallographic tetramer was a suitable model for the interaction of Pelle and Tube[170]. Parallels between this example of a death

domain forming a different structure under different methodological conditions and the two known structural forms of Fas-DD could be drawn, as this is an example of another death domain showing some level of structural rearrangement upon interacting with another death domain.

3.1.5 Aims

This chapter documents the approaches taken to validate whether the ‘open’ Fas-DD conformation is relevant to a functioning death domain in solution. Initial NMR characterisation of the Fas-DD has previously been carried out within the laboratory, providing information about the Fas death domain in complex with FADD. This chapter expands on that work to investigate whether Fas-DD can exist in the reported open, crystal conformation in isolation, in a solution environment.

This chapter describes (a) the collection and assignment of modern multidimensional NMR structural experiments for the Fas-DD to assess the intramolecular interactions within the domain and (b) the exploration of the dynamic properties of the Fas-DD in solution. Fas-DD dynamic properties were assessed using traditional spin-relaxation and relaxation dispersion measurements in conditions designed to mimic the presence of a phosphorylated Y291 and in the crystal environment that the ‘open’ Fas structure was reported in.

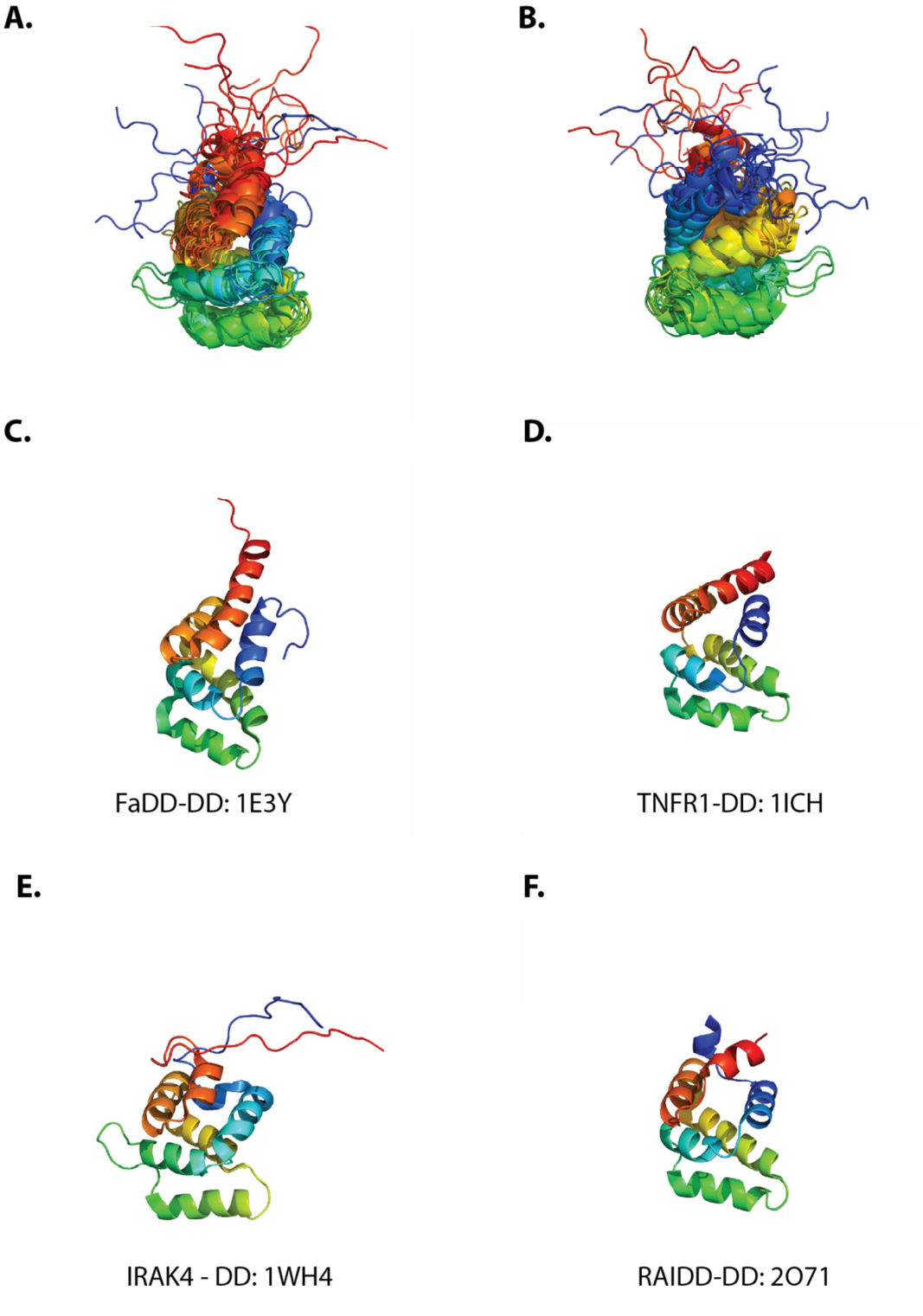

Figure 3.4 Examples of Fas-DD structures

A and B, overlay of 15 separately determined death domain structures, PDB accession codes: 1DDF, Fas-DD;1FAD, 1E41, 1E3Y, FADD-DD; 1ICH, TNFR1-DD; 1NGR, p75 neutrotrophin receptor-DD; 1WH4, 2A9I, IRAK4-DD; 1WXP, nuclear matrix protein p84-DD; 2D95, NFkB p100-DD; 2DBF, NFkB p105-DD; 2IB1, P45-DD; 2O21, RAIDD-DD; 2YQF, ankryin-1-DD; 2YVI, ankryin-DD. C, isolated DD of FADD, 1E3Y. D, isolated DD of TNFR1, 1ICH. E, isolated DD of IRAK4, 1WH4. F, isolated DD of RAIDD, 2O71. Helices are coloured from N to C termini. Helix 1, red; helix 2, orange; helix 3; yellow; helix 4, green; helix 5, cyan; helix 6, blue.

3.2 ^{15}N ^{13}C Fas-DD expression and purification

Vectors expressing Fas-DD (residues 218-319) and Fas-DD+CTD (residues 218-335) with an N-terminal TEV cleavable hexa-histidine tag and GB1 solubility tag were kindly donated by Dr Diego Esposito. These constructs were used for the biophysical studies of Fas-DD published previously[123].

BL21 (DE3) Gold *E. coli* expression strains were used for the expression of both Fas constructs. Expression had been previously optimised by Dr Diego Esposito. Both Fas constructs were expressed with 0.5 mM IPTG for sixteen hours at 22 ^{o}C. These were the conditions used for large scale expression of the proteins. Isotopic labelling of the constructs for NMR spectroscopy was carried out by expression in either ^{15}N labelled and ^{15}N,^{13}C-labelled minimal medium as detailed in Section 2.5.

Purification was carried out using the N-terminal hexa-histidine tag for Ni-NTA affinity purification which was followed by purification tag removal using TEV protease. A final clean-up of the preparation was carried out by size exclusion chromatography, as described in Section 2.6. Figure 3.5 shows SDS-PAGE analysis for each steps of the purification and the size exclusion chromatogram for $^{15}N^{13}C$ Fas-DD.

The solubility of Fas constructs was enhanced by the presence of the K263A mutation which has been shown to enable Fas-DD constructs to be concentrated up to 700 μM without aggregation occurring[6]. This enabled preparation of protein at concentrations suitable for NMR samples. For NMR experiments, the protein was typically concentrated by centrifugal concentration to between 500 μM and 700 μM. The presence of the K263A mutation ensured that the constructs were monomeric and soluble at these concentrations.

3.3 Backbone resonance assignments

In order to obtain residue-specific information from HSQC based experiments, assignment of the cross peaks in the $^{15}N/^{1}H$-HSQC spectrum is required. This is traditionally the first step in NMR characterisation of a protein. The $^{1}H/^{15}N$-HSQC spectrum is considered the fingerprint of a protein, with each peak within the spectrum corresponding to the NH of a single amino acid.

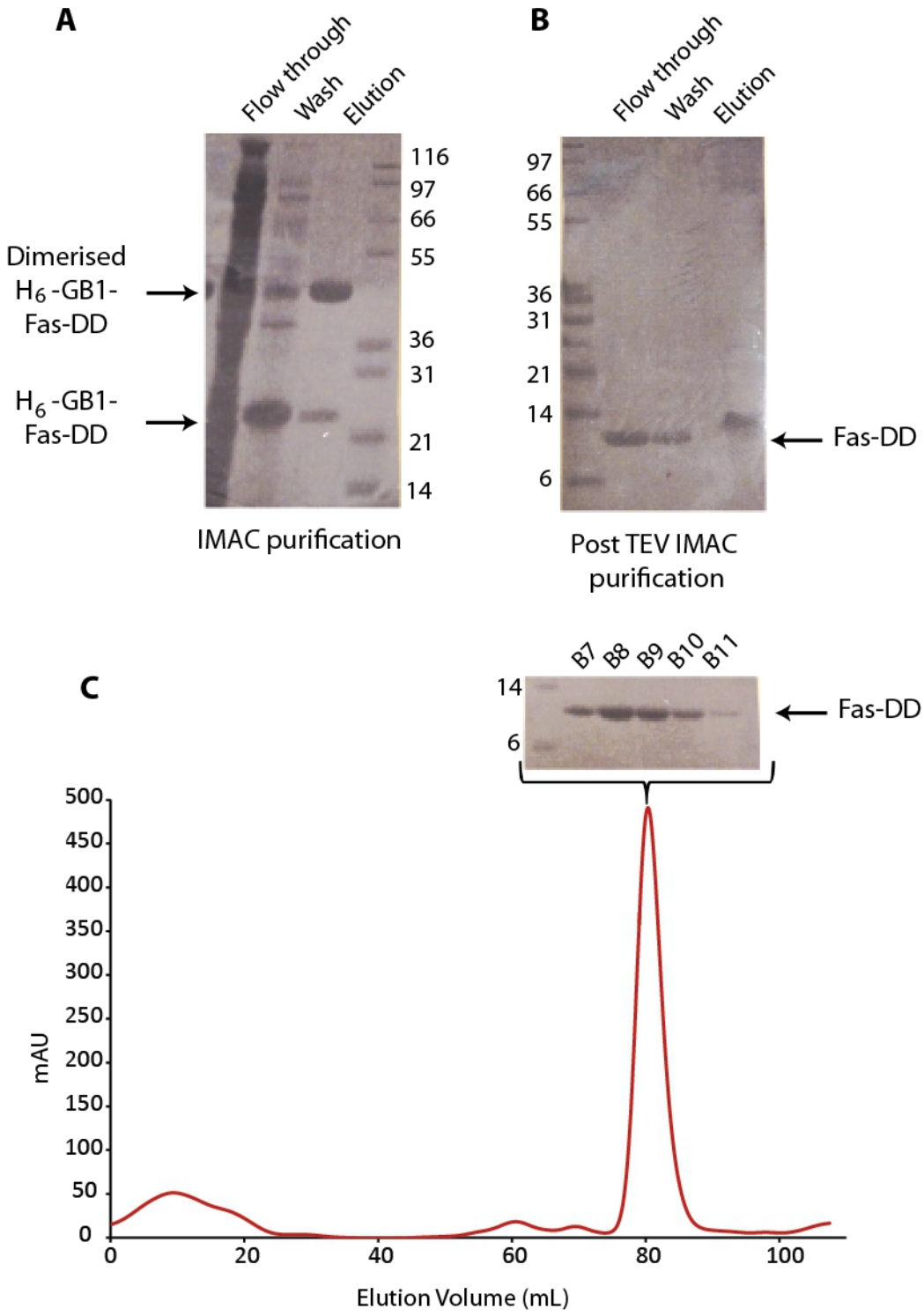

Figure 3.5 Purification of Fas-DD

SDS-PAGE analysis of the IMAC purification of $^{15}N^{13}C$ Fas-DD is shown in A. The elution was taken and TEV cleaved prior to running back over an IMAC column, SDS-PAGE analysis post TEV cleavage is shown in B. The flowthrough and wash from the post TEV IMAC purification was taken, concentrated to 5ml and loaded upon a Superdex 75 SEC column. The elution profile (monitored by UV absorbance at 280nm) and SDS-PAGE analysis of the peak are shown in C. The pure fractions were taken and concentrated for NMR.

Assignment of the resonances in the $^{1}H/^{15}N$-HSQC corresponds to the backbone resonance of the construct. Identification of the backbone NH cross peaks in the $^{1}H/^{15}N$-HSQC spectrum was necessary for further assignment of the structure of Fas-DD as well as analysis of the dynamic properties of Fas-DD. Throughout this thesis $^{1}H/^{15}N$-HSQC based experiments of Fas-DD have been used to assay protein:protein interactions. The assignment of the backbone NH cross peaks of Fas-DD inferred binding information to these experiments as well.

The backbone resonance assignment for Fas-DD+CTD had previously been carried out within the laboratory by Dr Diego Esposito. Due to the highly overlapped nature of the spectra, backbone assignment remained incomplete. As a basis for training in protein NMR and to attempt to complete backbone assignment for Fas-DD+CTD, I repeated the assignment process, starting from the raw data which had previously been collected by Dr Diego Esposito.

Through-bond triple resonance NMR experiments to correlate backbone amide resonances to the C_{α}, C_{β} and C' atoms of the same and previous residues were recorded to establish a stretch of sequential cross peak connections. Dr D. Esposito collected HNCA, HN(CA)CB, HNCO, HN(CA)CO and CBCACONH 3D heteronuclear experiments to enable these connections to be made. The details of these experiments are shown in Chapter 2. The experiments were recorded upon a ^{15}N ^{13}C-labelled sample at 25 ^{o}C at 600, 700 and 800 MHz. Field strength and experimental parameters are detailed in Chapter 2, the raw data was processed using in house generated NMRPipe[137] scripts and analysed using CCPN-Analysis[138].
Through my own analysis of these datasets within the CCPN-Analysis software package, I assigned 109 backbone NH resonances out of 117, corresponding to 93% completeness. Assignment was carried out by sequential linkage of the $^{13}C\alpha$, $^{13}C\beta$ and ^{15}NH frequencies as illustrated in Figure 3.6. The dotted lines represent the correlation of the selected NH peak (the region of the spectrum the strip corresponds to) with the respective intra- (i) and inter-residue (i-1) $^{13}C\alpha$ and $^{13}C\beta$ atoms. The amide NH cross peak assignment is illustrated upon the $^{1}H/^{15}N$-HSQC spectrum of Fas-DD+CTD shown in Figure 3.7.

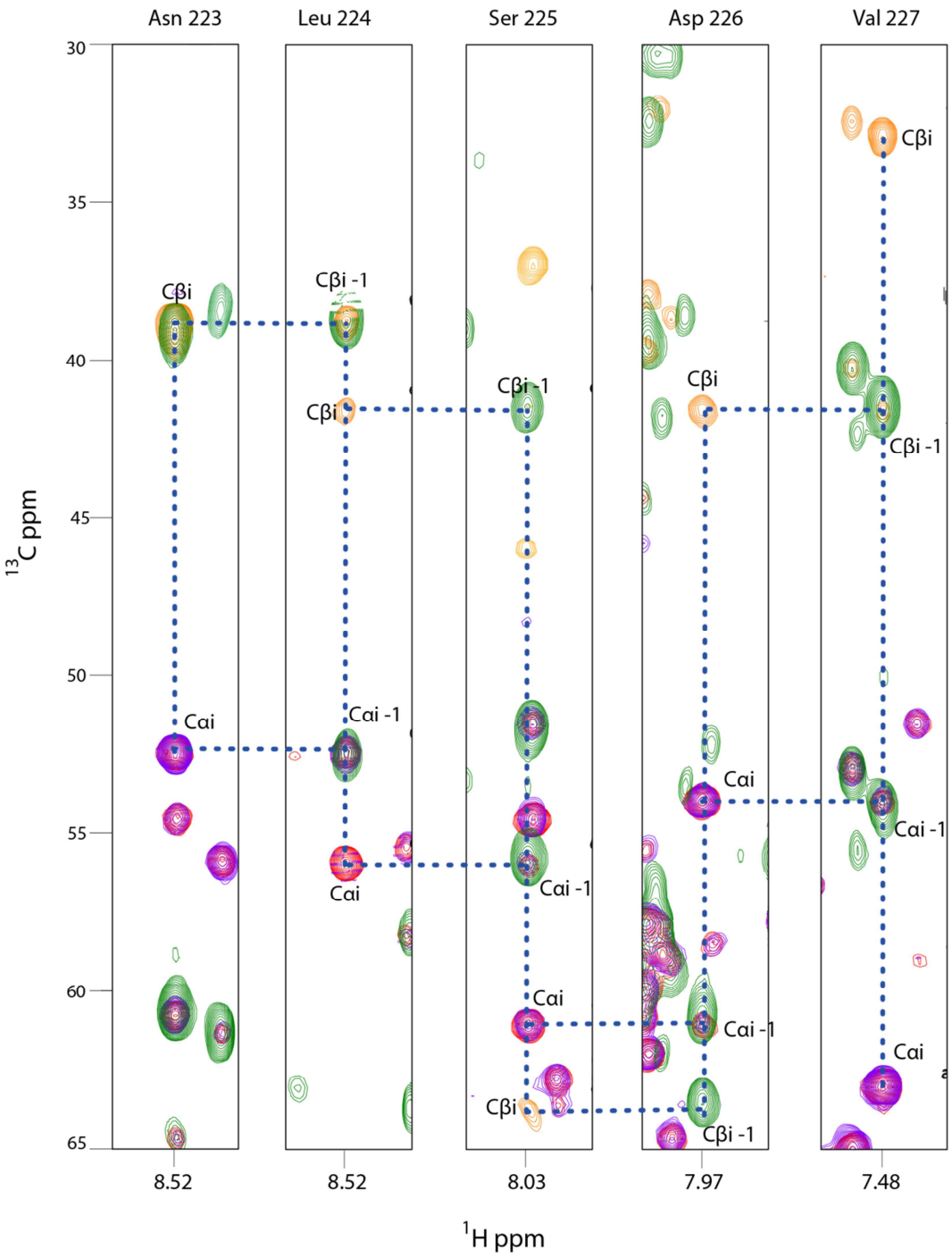

Figure 3.6 Example of the strategy of sequential assignment used to assign the backbone resonances of Fas-DD

Strip plots of the HNCA (red), HNCACB (purple and orange) and CBCACONH (green) spectra, showing examples of ^{1}H ^{15}N ^{13}C correlations from residues Asn 223 to Val 227 of Fas-DD. Cross peaks are labelled corresponding to whether they originate from Cα or Cβ and intra (i) or inter (i-1) residue carbon atom correlations. The blue dotted line depicts the sequential connections across these residues.

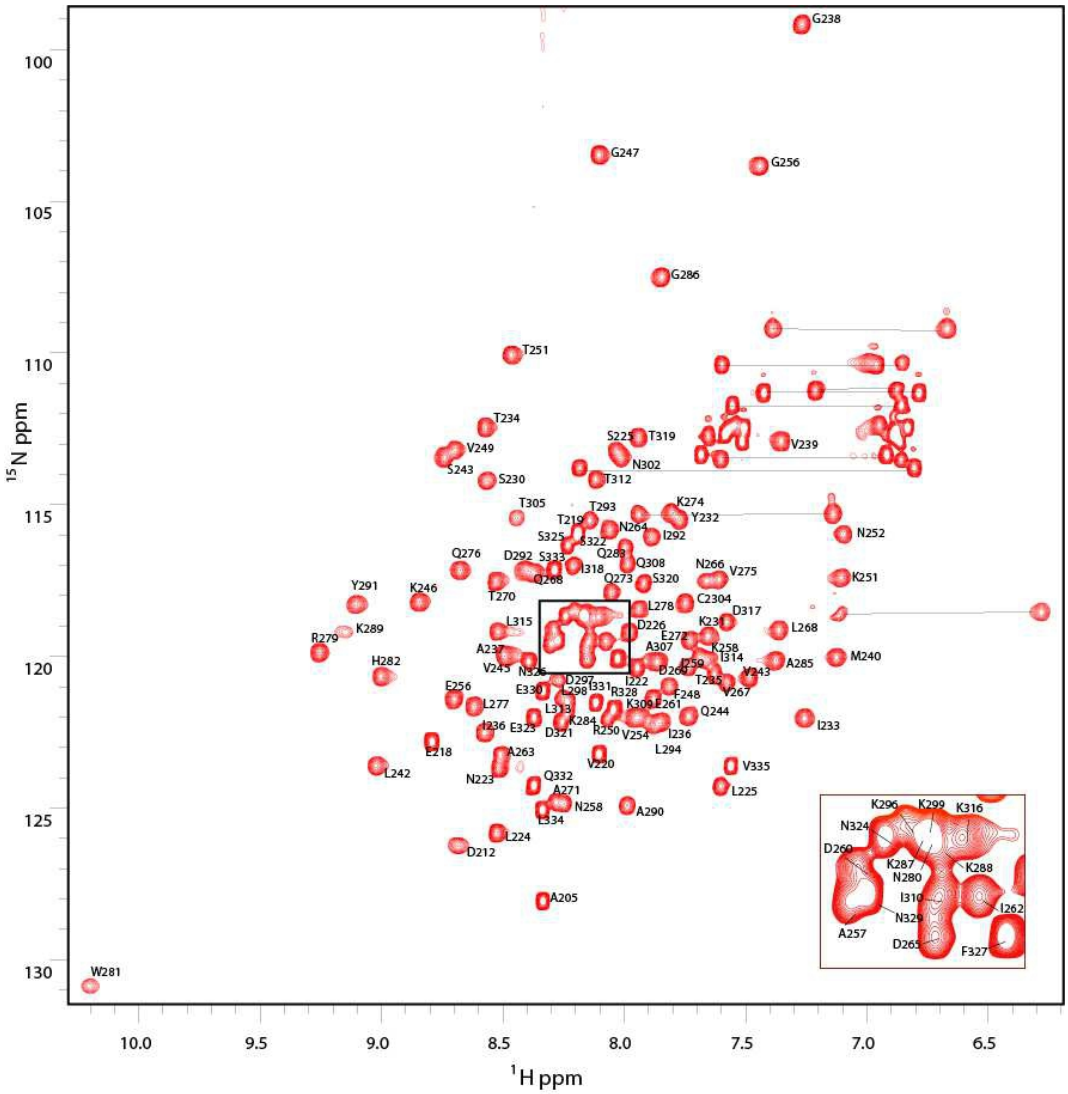

ETVAINLSDVDLSKYITTIAGVMTLSQVKGFVRKNGVNEAKIDEIANDNV
QDTAEQKVQLLRNWHQLHGKKEAYDTLIKDLKKANLCTLAEKIQTIILK
DITSDSENSNFRNIQSLV

Figure 3.7 Assigned ^{1}H/^{15}N-HSQC spectrum of ^{15}N ^{13}C Fas-DD+CTD

A, ^{1}H/^{15}N-HSQC spectrum. Each red peak corresponds to the backbone NH from one amino acid in the sequence. The centre of the spectrum is enlarged to highlight the peaks in this overlapped region. B, sequence of Fas-DD+CTD with the residues with backbone assignments highlighted in red. Buffer conditions: NMR buffer (20 mM MES, 100 mM NaCl, 20 mM MES, 100 mM NaCl, 0.5 mM TCEP, 1 mM EDTA, 3 mM Sodium azide pH 6.2).

The reasons for less than complete assignment of the cross peaks shown in the $^{1}H/^{15}N$-HSQC spectrum include unresolved NH cross peaks and lack of tractable HN(CA)CB correlations. In conjunction with the alpha helical nature of Fas-DD, the non-folded flexible N and C termini of the constructs resulted in regions of spectra which were impossible to fully resolve.

3.4 The Fas-DD forms a compact structure in solution

To build upon the possibility that Fas-DD could exist in alternative forms in solution, modern multidimensional NMR techniques were implemented to solve the solution structure of the Fas-DD.

3.4.1 NMR structural experiment rationale

The NMR experimental work flow used to get to the point of structure calculation is summarised in Figure 3.8. The backbone resonance assignment was carried out using HNCA, HNCACB and CBCAcoNH experiments as described in Section 2.9.5. As mentioned above, these experiments were carried out upon the Fas-DD+CTD construct. These assignments were used as the basis for Fas-DD structure assignment as the cross peaks in the $^{1}H/^{15}N$-HSQC spectrum of Fas-DD overlaid perfectly with the $^{1}H/^{15}N$-HSQC of Fas-DD+CTD making for facile transfer of the resonance assignments to the spectrum of the former construct.

The next step was to assign resonances to the ^{13}C and ^{1}H atoms of the protein side chains. ^{15}N-TOCSY and HCCH-TOCSY experiments were used to assign side-chain proton atoms. This was achieved using the resonance of the NH peak in the $^{1}H/^{15}N$-HSQC in conjunction with the location of the Cα and Cβ resonances from the backbone experiments to inform the location of the correct ^{13}C strips in the HCCH spectrum to yield the side chain proton connectivities.

To obtain restraints for structure calculations, through-space ^{15}N- separated-NOESY and ^{13}C-separated aromatic and aliphatic NOESY spectra were collected. NOESY experiments show correlations between atoms that are relatively close in space, up to a separation of approximately 5Å. Figure 3.8 illustrates the magnetisation transfer pathways under each of these experimental conditions to obtain this information.

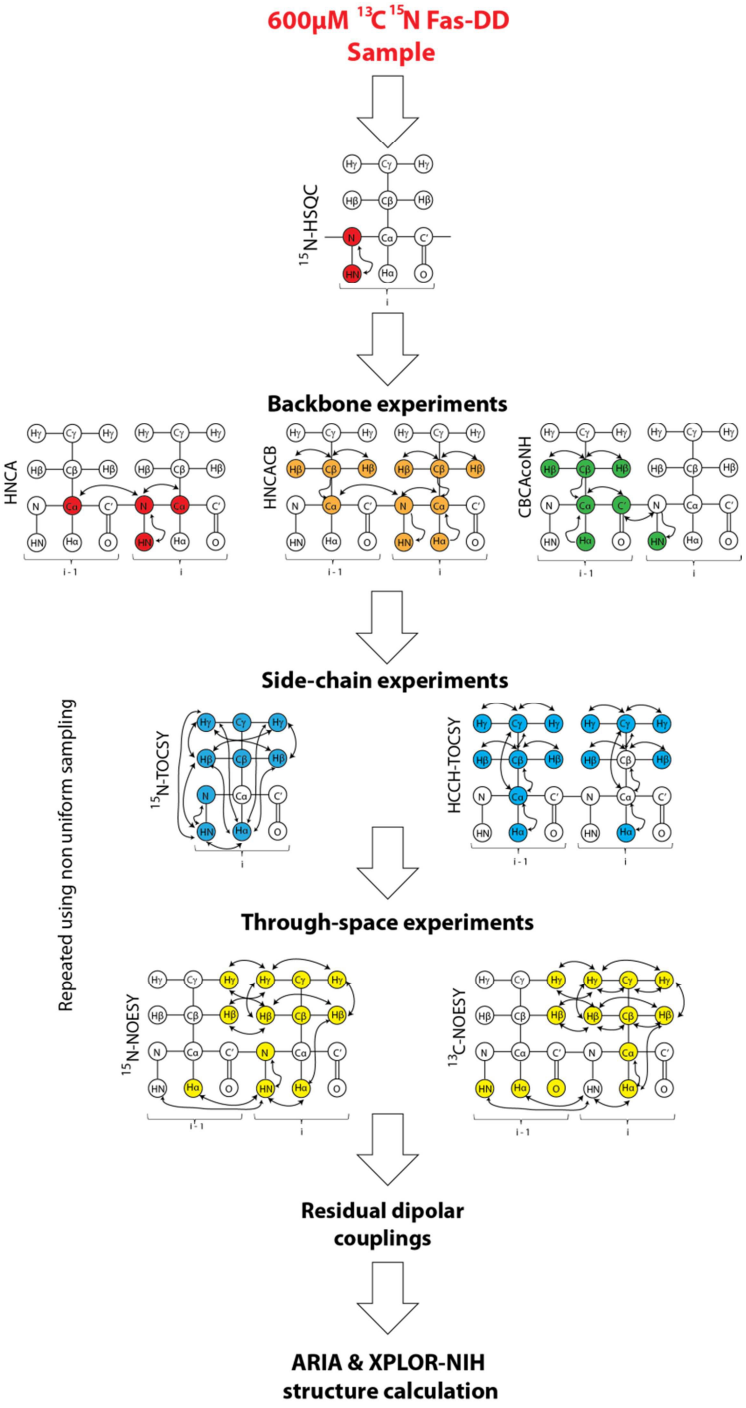

Figure 3.8 Flow chart for structural data collection of the Fas-DD

Diagram showing the experiments used to collect atomic assignments for Fas-DD. Schematic diagrams show the transfer of magnetisation between atoms for each NMR experiment collected. Atom colour corresponds to how the spectra are represented elsewhere in this study. Side-chain experiments (^{15}N-TOCSY, HCCH-TOCSY, ^{15}N NOESY and ^{13}C-NOESY) were repeated using both uniform and non-uniform sampling to obtain a better signal to noise for assignment. Information has been adapted from www.protein-nmr.org.uk.

3.4.2 Fas-DD side chain resonance and through-space resonance assignment were greatly improved with the use of non-uniform sampling schemes

Side chain resonance assignments were initially attempted using traditional uniformly sampled ^{15}N-TOSCY and ^{13}C-HCCH-TOCSY spectra in which all data points in the indirect dimensions are systematically sampled, and the data is processed using standard Fourier transform methods. In practice assignment was hampered due to low resolution within the HCCH-TOCSY spectrum combined with limited chemical shift dispersion resulting in peak overlap. 30% of the side chain resonances could be assigned using these spectra.

The data was re-acquired for the same protein samples using non-uniform sampling as detailed in Section 2.9.6. Non uniform sampling (NUS) relies on the collection of a carefully selected subset of the indirect dimension data points of an experiment which is followed by the reconstruction of the full experimental dataset using sophisticated signal processing methods. The application of non-uniform data sampling allows the extension of the effective acquisition time in the indirect dimension(s), without extending the overall measuring time of the experiment. Because the effective signal acquisition times are extended, NUS combined with non-standard signal processing results in a higher signal resolution in the indirect dimensions than is achievable by traditional methods. The Fas-DD NMR data recorded with NUS spectral reconstruction was carried out by Dr TJ Ragan using the IRLS function of MddNMR. The increased spectral resolution achieved through the NUS methods reduced peak overlap and facilitated the extension of the side chain assignments. This is illustrated for the resonances corresponding to Ile222 in the HCCH-TOCSY spectrum in Figure 3.9. To date the implementation of the NUS method of spectral sampling has enabled 91% of the side chain resonances to be assigned.

Nuclear Overhauser effect spectroscopy (NOESY) spectra are used to obtain distance restraints. In a NOESY spectrum, each cross peak corresponds to the correlation of two (sets of) protons that are close in space. Due to the high number of cross peaks present in a NOESY spectrum there is often a high degree of overlap, leading to potential for ambiguity in the assignment. For Fas-DD, the uniform sampled ^{13}C-NOESY spectrum was particularly crowded, which hindered the assignment of ^{1}H resonances.

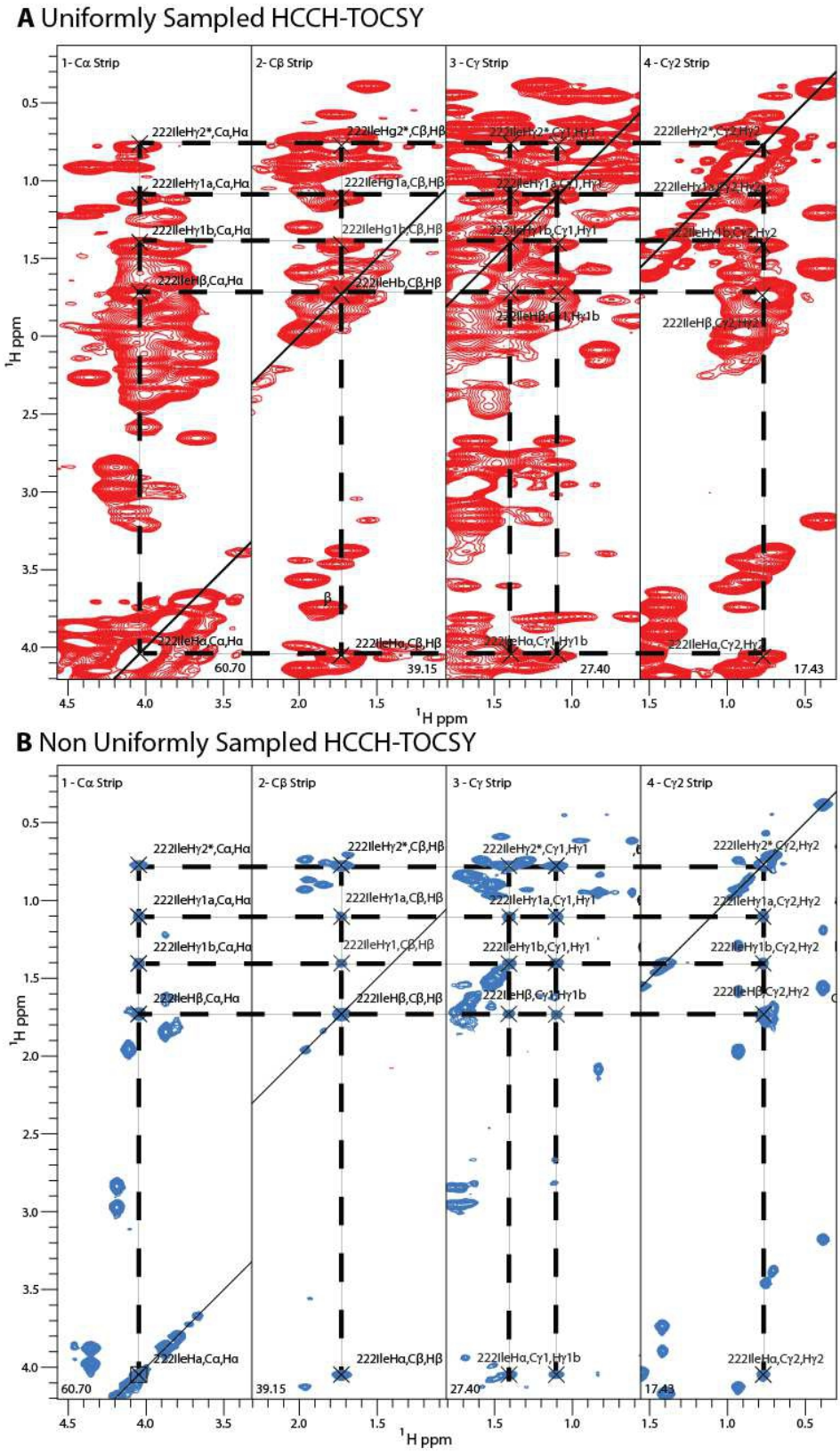

Figure 3.9 Non-uniform sampling increases resolution in side-chain spectra which simplified side-chain proton assignments

Strip plots from HCCH-TOCSY experiments which were uniform sampled (A) and non-uniform sampled (B) which were assigned to Ile 222. Non-uniform sampling markedly increased the resolution of peaks in the spectrum (B) allowing more assignments to be made.

To overcome this problem, the NOESY data was also re-acquired using NUS techniques and reconstructed by Dr TJ Ragan using the MDD function of mddNMR. The use of NUS again improved peak resolution, reducing overlap, which enabled an increased number of unambiguous NOE assignments to be made.

3.4.3 Secondary chemical shift index (CSI) infers a compact death domain structure

Backbone resonance assignment of a protein assigns a ^{13}C and ^{1}H chemical shift to the Cα, Cβ and H atoms of the amino acids which make up the protein. Each amino acid has a known propensity to reside within a particular chemical shift window; a property that is exploited in the assignment of the backbone resonances. As is true throughout all protein NMR applications, the chemical shift of an atom is modulated by the chemical environment in which it resides, whether that is the external solution or the amino acids surrounding the residue of interest. Thus, the chemical shift of a particular atom of an amino acid is dependent upon the nature and character of the local secondary structure of the protein. Exploiting this observation, Wishart and Sykes described what they called the 'chemical shift index' (CSI) as a technique to predict the local secondary structure of a protein from the backbone ^{1}H and ^{13}C chemical shifts[171,172]. CSI exploits the deviation in chemical shifts of certain nuclei relative to known random coil chemical shifts as a method to detect secondary structure, assigning an index value of 1 if the amino acid is in a position expected to form an α helix or -1 if in a β-strand. Using the CSI profile it is possible to assess the secondary structure content of a protein using just the backbone resonance assignments and no NOESY through space assignments. Mapping the chemical shifts in such a manner is an accurate method to obtain a consensus estimate of the secondary structure of the molecule[171,172].

Following backbone resonance assignment, the CCPNAnalysis program, was used to extract the chemical shifts of the $^{13}Cα$, $^{13}Cβ$ and ^{1}H atoms and assign a chemical shift index score to each of the residues. The CCPNAnalysis readout of chemical shift perturbation and chemical shift index scores for Fas is shown in Figure 3.10. The carbonyl chemical shift difference (Δδ) has been omitted from the plot as assignments were made using the HNCO and HNcaCO spectra.

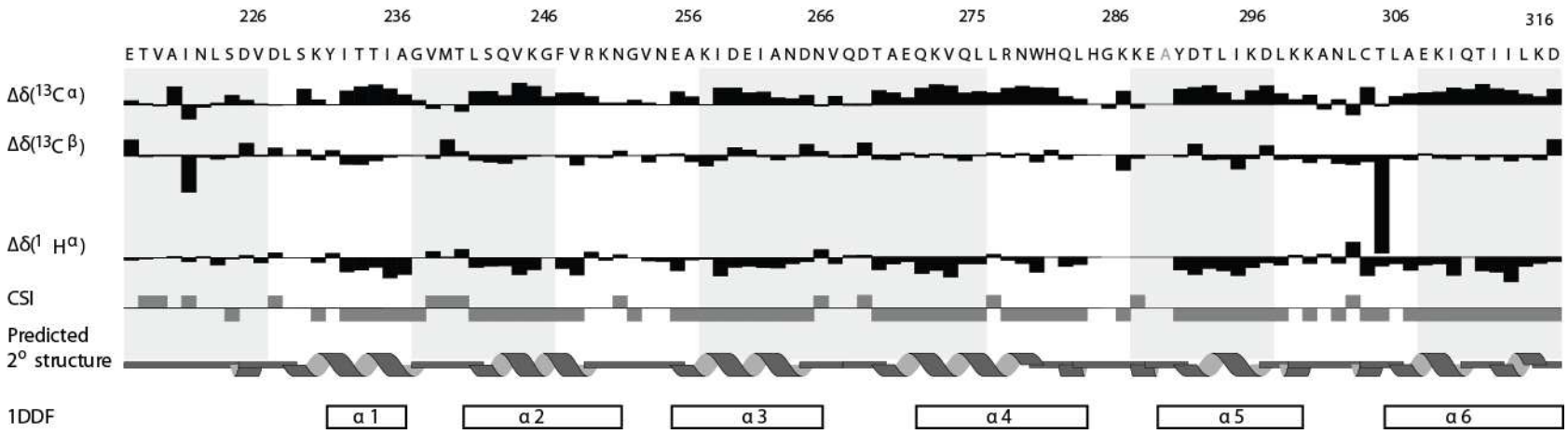

Figure 3.10 Secondary chemical shift analysis for Fas-DD

Chart illustrating the chemical shift difference (Δδ) between the recorded ^{13}Cα, ^{13}Cβ and ^{1}Hα and a random coil chemical shift for each assigned residue, labelled as ($\Delta\delta^{13}$Cα), ($\Delta\delta^{13}$Cβ) and ($\Delta\delta^{1}$H) respectively. Also shown is the chemical shift index (CSI) relating the residue chemical shift to secondary structure propensity in the selected region. Predicted secondary structural features are illustrated at the base of the chart. As expected the Fas-DD secondary chemical shifts imply a domain with six helices. Data and graphs were extracted from CCPNAnalysis project used for Fas assignments. The location of the helices in the Fas solution structure (PDB:1DDF) are shown as boxes below the graphic.

The chemical shift difference (Δδ) for Fas-DD in solution shows that the secondary structure contains six alpha helices in the locations expected from the previously published Fas-DD NMR structure. This suggests that the domain forms a compact death domain fold unlike the open Fas-DD reported in the 4:4 crystal structure. The secondary structure prediction indicates that in solution helices five and six are separate helices. The results characterise a more flexible loop between helices five and six rather than an elongated helical shape as would be expected in the open conformation.

3.4.4 ^{13}C aromatic and aliphatic NOESY spectral analysis infers that Y291 is in a buried location

NOESY spectra give information about which atoms are close in space. The experiment takes advantage of the nuclear Overhauser effect (NOE) between nuclear spins during a mixing period to establish correlations between atoms corresponding to their distance apart in space. NOESY pulse sequences record the exchange of ^{1}H polarization (longitudinal magnetisation) as a result of dipolar coupling between ^{1}H nuclei in different regions of the protein structure. Thus the NOE depends upon a fundamentally different type of mechanism to that exploited in NMR experiments that depend upon though-bond J-coupling dependent transfer of antiphase or in-phase transverse magnetisation. The magnitude of a particular NOE cross peaks depends upon the inverse-6th power of the internuclear separation ($1/r^{6}$), the details of the reorientational dynamics of the internuclear vector, and the NOE build-up time. However for most globular proteins, it has been found that for short NOESY mixing times one can make a semi-quantitative estimate of the relative internuclear distances from the comparison of NOE cross peak intensities. The resulting NOESY spectra contain autocorrelation peaks along a diagonal and a number of cross peaks, each identifying atoms which are close to each other in space. The other cross peaks, (in a vertical line from the diagonal) correspond to atoms which are close to the atom identified upon the diagonal. The assignment of NOESY spectra is traditionally used to generate distance restraints between atoms within a protein to be used to generate a 3D model of the structure. To identify whether Y291 is in a buried or a solvent exposed location within the Fas-DD being used in this study, the NOEs which had been assigned to the ^{1}H atoms of Y291 were analysed.

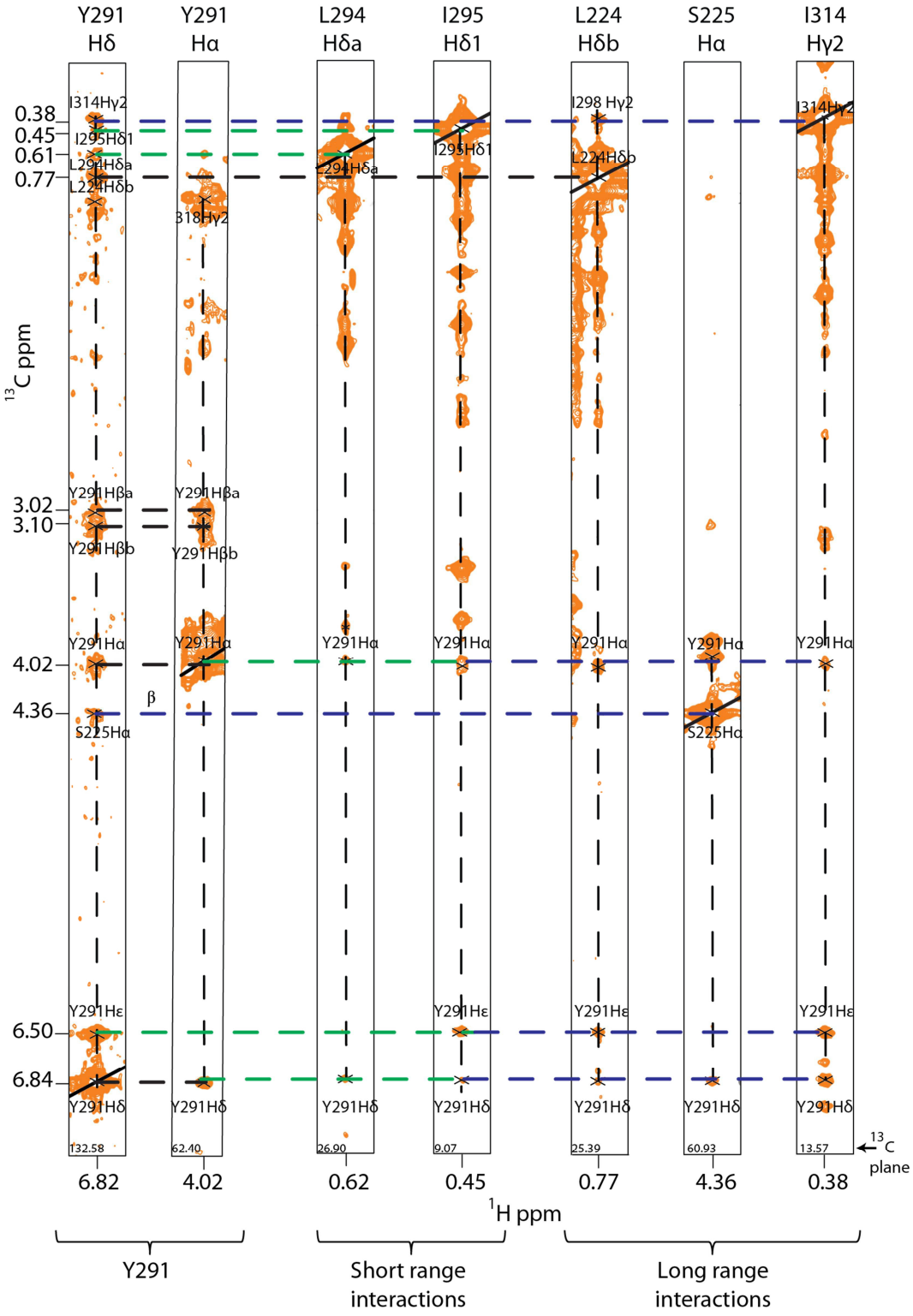

Figure 3.11 Strips from ^{13}C aromatic and aliphatic NOESY-HSQC spectra showing atoms which are close in space to Y291

Each NOE strip corresponds to the nucleus highlighted at the top of the strip. Off diagonal peaks in the spectrum correspond to an NOE between two a nuclei which are close to each other in space. Strips corresponding to Y291 Hδ and Hα are shown with assigned intra and inter-residue NOEs. Strips relating to interacting nuclei are also shown, confirming the NOE connectivity to Y291. Black lines represent NOE heteronuclei in Y291 which are close in space. NOEs to residues that are close in the primary sequence and in space are represented with green lines. NOEs to residues that are further away in the primary sequence and close in space are shown with blue lines.

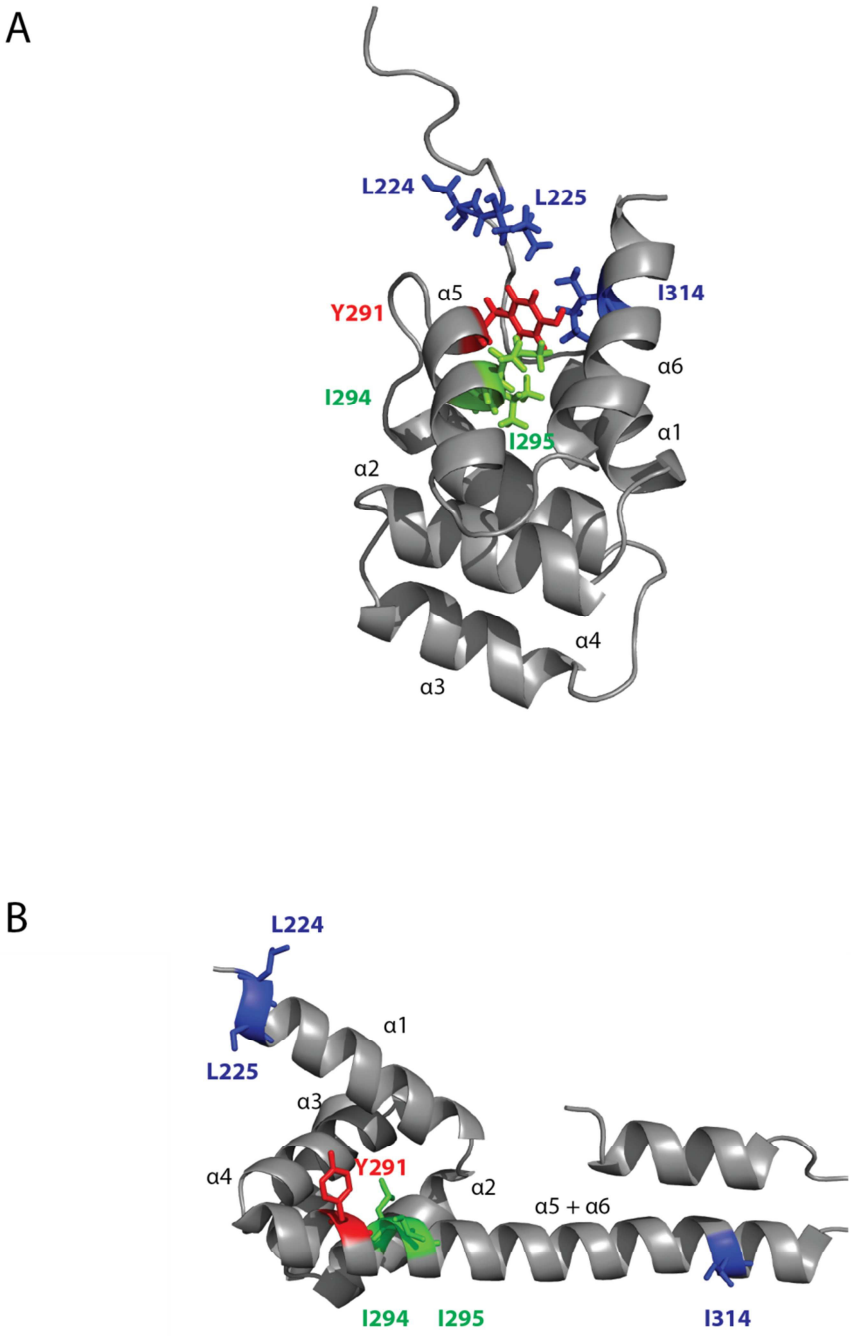

Figure 3.12 The location of the residues showing NOEs to Y291

A, Fas solution structure (PDB:1DDF) and B, Fas-DD in 'open' structure from crystal structure (PDB:3ZQ) with Y291 highlighted in red. Residues containing short range NOE's to Y291 illustrated in green. Residues showing long range NOE's to Y291 shown in blue.

Strips from the ^{13}C aromatic and aliphatic NOESY spectra corresponding to Y291 and those atoms showing NOE connectivity are shown in Figure 3.11. Each of the strips shown in Figure 3.11 corresponds to a ^{13}C plane in the spectrum (plane location highlighted within each strip) of the residue and atom shown at the top of the figure. Peaks on the diagonal line correspond to autocorrelations that correspond to the chemical shifts in the 1D ^{1}H NMR spectrum; vertical lines show peaks corresponding to atoms which are close in space to the atom shown on the diagonal. NOE connectivity is considered when the cross peaks are at the same ^{1}H chemical shift but at different ^{13}C chemical shifts. The horizontal lines in Figure 3.11 highlight the connectivity between different ^{13}C planes of the ^{13}C-NOESY spectrum, indicating the ^{1}H atoms which are close to each other in space. For example the I294Hδ strip, shows that the Hδ protons of I294 is close to both the Hα and the Hδ atoms of Y291.

NOE cross peaks are present which show that the side chain of Y291 is close in space to residues I294 and I295, constituting medium range NOEs. This outcome would be expected as the latter residues are close in the primary sequence to Y291. NOE cross peaks are also present between Y291 and L224, L225 and I314, residues much further away from Y291 in the primary amino acid sequence constituting long range NOEs. The presence of NOE peaks between Y291 and these residues suggest that Y291 is in a buried/folded location within the domain. When the locations of these five residues are highlighted on the published ‘open’ and ‘closed’ Fas-DD 3D structures (Figure 3.12) the pattern of NOEs is clearly more consistent with the more buried ‘closed’ form of Fas-DD. The NOE data agrees with the residues which have been shown to be close to Y291 in the solution structure (PDB:1DDF). If Y291 was present in Fas in the ‘open’ conformation one would expect to observe fewer NOEs for this residue as it is predominantly solvent exposed.

3.5. Working towards a Fas-DD high resolution solution structure

The structure calculations presented in this section were carried out with equal contribution between the author and Dr Diego Esposito.

3.5.1 Using ARIA to calculate the Fas-DD structure

The assignment of NOE cross peaks is the critical step in determining the 3D structure of a protein using NMR data. ARIA (ambiguous restraints for iterative assignment) is a program which can be used to inform NOE assignment through the process of iterative NMR structure calculations. It involves NOE assignment as an integral part of the structure calculation process. NMR structures are predominantly based upon the cross relaxation rates between nuclei which are close in space; these interactions are measured through NOESY spectroscopy. Traditionally a set of unambiguously assigned NOE resonance assignments would be incorporated into a NMR calculation that comprising a combination of simulated annealing and energy minimisation molecular dynamics protocols. Using the ARIA method, the whole NOESY spectrum is taken into account, in which the unambiguously assigned NOEs as well as unassigned and ambiguous cross peak assignments are included in the calculation. The core protocols of ARIA derive distance restraints from the NOESY spectra to define molecular conformations which are compatible with the cross peaks in the original data set. To do this, ARIA creates ambiguous distant restraints (ADR) from the chemical shift lists, in which the alternative possibilities for an NOE peak are combined into one restraint which impacts the generated structure. The use of ARIA involves an iterative process in which each ARIA calculation is used to inform the assignment of more ambiguous NOE cross peaks from the spectrum. This function is built into the CCPNAnalysis program to aid in NOE assignment[173].

3.5.2 Residual dipolar couplings were collected in Pf1 bacteriophage alignment medium

As well as the experiments described above, residual dipolar couplings (RDCs) were collected in magnetically-aligned Pf1 bacteriophage solution. The magnitudes of an RDC is dependent upon the distance and angle in which a bond vector is orientated relative to the applied magnetic field. When RDCs can be measured for a set of internuclear vectors within a molecule these data can provide information about the

spatial arrangement of those vectors and aids the determination of the overall shape of that molecule.

RDCs arise from the partial alignment of a macromolecule with a magnetic field. A molecule in solution undergoes isotropic tumbling, in this situation the RDC value averages to zero. To obtain a situation in which the sample does not undergo isotropic tumbling and an RDC can be measured, the sample is introduced into a compatible dilute liquid crystalline environment such as lipid bicelles or in the presence of filamentous bacteriophage. Solutions of filamentous pf1 bacteriophage spontaneously align in a magnetic field, due to the magnetic susceptibility anisotropy of the lipid bilayer head groups. Cosolute macromolecules, by dint of random collisions with the aligned phage, are induced to undergo non-random reorientational (tumbling) dynamics, the nature of which is dependent on the overall molecular shape. Thus in the presence of the dilute liquid crystalline environment provided by the phages, a co-dissolved protein will be, in effect, partially aligned (albeit very weakly) and give rise to non-zero dipolar couplings. In practice RDCs are detected as a contribution (positive or negative, depending upon the direction of the internuclear vector relative to the alignment tensor) to the measured J-couplings between the nuclei involved. In-phase anti-phase (IPAP) NMR experiments were acquired to extract N-H effective one-bond J-couplings and HNCOCA experiments with no proton decoupling were recorded to extract HA-CA one-bond J-couplings for both Fas-DD in isotropic (unaligned) and anisotropic (bacteriophage aligned) environments. To determine the RDC values, the difference in ^{15}N frequency of the isotropic and anisotropic samples was measured. 64 RDC values were obtained for N-H couplings and 58 values for CA-HA couplings. RDC values were not obtained for every residue in the construct due to spectral overlap which meant that some of the peaks in the spectra overlapped too much to be able to identify which residue they corresponded to.

The calculated RDC values were analysed prior to inclusion in the structure calculation using the program Module. Within this program the experimentally derived RDC values were compared to RDC values which had been predicted from the published Fas-DD structure (PDB:1DDF). The output from this analysis is shown in Figure 3.13. Both the experimentally derived HN-H and CA-HA couplings show a reasonable fit to those which were simulated by the program.

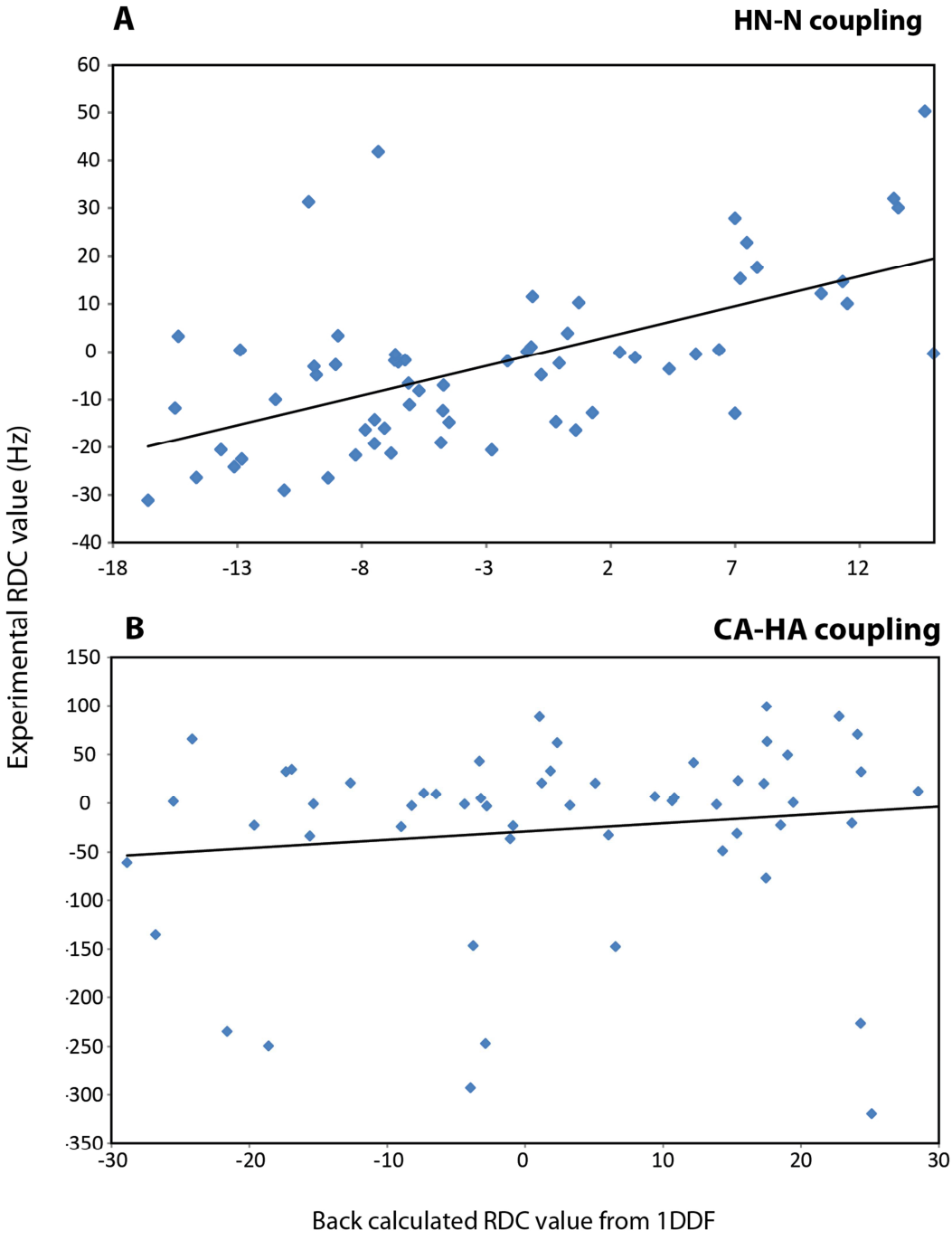

Figure 3.13 Experimental RDC data showed a reasonable fit to the 1DDF structure of Fas-DD data

RDC values collected for HN-N couplings using IPAP type HSQC experiments and HA-CA couplings collected using HNCOCA with no proton decoupling were fitted against the current published model of the Fas-DD (pdb:1DDF) using the program Module. A shows the fit of the NH couplings, which appear to follow the trend expected from the 1DDF structure more closely than the CA couplings shown in B.

3.5.3 Preliminary structural calculation

The software ARIA[174] was used for automatic assignment of ambiguous NOEs and to obtain a starting set of restraints to use in a refinement protocol created for the program XPLOR-NIH[175]. CCPN data were input directly into ARIA. Initial interproton distance restraints lists were created by the software starting from the cross peaks picked manually in the 3D ^{1}H-^{13}C NOESY-HSQC, ^{1}H-^{13}C aromatic NOESY-HSQC and ^{1}H-^{15}N NOESY-HSQC spectra. Backbone ϕ and ψ torsion angle restraints were derived from the pattern of ^{1}Hα, ^{13}Cα, ^{13}Cβ, ^{13}C' and ^{15}NH chemical shifts using the program DANGLE[176] in CCPN analysis. Hydrogen bond restraints for amide protons deriving from the assessment of the regular secondary structure helical segments in the available Fas-DD structure, coupled with the absence of the relative water cross peak in the ^{1}H-^{15}N NOESY-HSQC spectrum, were also used in the ARIA calculations.

Unfortunately, due to the incomplete side chain resonance assignment the first set of conformers generated by ARIA did not converge to a single tertiary fold. In order to improve convergence in the final ARIA iteration we simulated a small subset (500) of NOE restraints from the available deposited coordinates of Fas-DD (PDB:1DDF). The insertion of simulated NOE restraints was used to calibrate the NOE distances used by ARIA to calculate NOE distances from the ambiguous peak lists.

ARIA outputs, consisting of a set of unambiguous and ambiguous restraints were used, together with the hydrogen bonds, dihedral and experimental HN residual dipolar couplings, in a standard XPLOR-NIH refinement protocol. The subset of 500 inserted NOE restraints used to calibrate ARIA were removed prior to this calculation. The final structures were calculated using PARALLHDG[177] force field parameters, with PROLSQ non-bonded energy function[155]. The dynamic simulated annealing protocol consisted of a high temperature (3000 K) torsion angle molecular dynamics followed by a Cartesian dynamics whilst cooling from 3000 K to 25 K in 12.5 K steps. A final 200 steps Powell minimization followed the simulated annealing protocol. The axial and rhombic components of the molecular alignment tensor were left floating during the calculations. The final ensemble consisted of the 20 lowest energy structures from the refinement protocol. Structural quality of was assessed with PROCHECK[178].

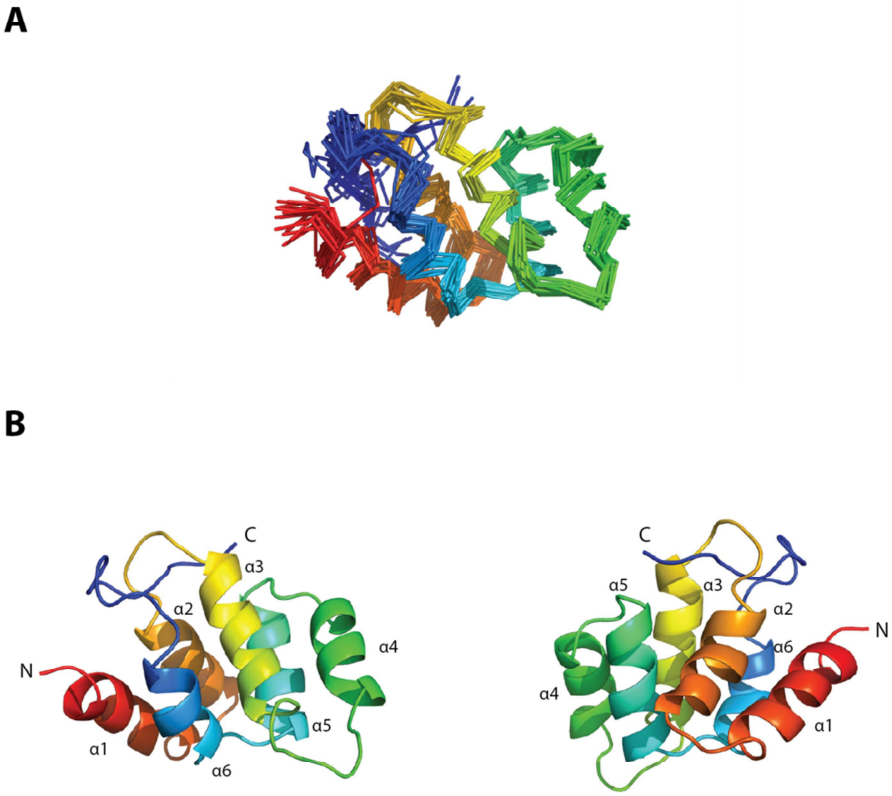

Figure 3.14 NMR solution structure of Fas-DD at pH 6.4 and 298 K

A, Backbone atoms of the ensemble of the twenty lowest energy conformers obtained after refinement in explicit water. B, Two orthogonal views of a ribbon representation of the structure of the lowest energy conformer of the ensemble. The helices are numbered from N (red) to C terminal (blue).

Table 3.2 Restraints and structural statistics for the Fas-DD ensemble

	Ensemble (n=20)	*Lowest energy conformer*
Number of experimental restraints		
Unambiguous distance restraints		1332
Ambiguous distance restraints		130
Dihedral angles		213
Residual dipolar couplings		130
Root mean square deviation from experimental data		
Unambiguous NOE distances (Å)	1.59 ±0.03	1.60
Residual dipolar couplings	0.33 ±0.04	0.342
R factor	0.48 ±0.06	0.485
Average root mean square deviation to the mean structure		
Backbone atoms (residues 221-319)	1.75 ±0.66	
Root mean square deviation from idealised covalent geometry		
Bond (Å)	0.0206 ±0.0007	0.02
Angle (^{o})	1.723 ±0.07	1.647
Improper (^{o})	1.99 ±0.08	1.93
Ramachandran plot statistics (PROCHECK)		
Residues in most favoured regions (%)	70.42±0.02	70.8
Residues in additionally allowed regions (%)	24.12±0.02	22.9
Residues in generously allowed regions (%)	2.92±0.01	3.1
Residues in disallowed regions (%)	2.56±0.01	3.1

The restraints and structural statistics for our preliminary Fas-DD structure are shown in Table 3.2. Our preliminary Fas-DD structure shows the canonical six helical bundle death domain fold, with no major deviation from the six helix bundle presented in the 1DDF structure. Figure 3.14 illustrates the twenty lowest energy conformers obtained after refinement in explicit water and a ribbon representation of the lowest conformer of the ensemble.

3.6 Dynamic investigation of Fas-DD using NMR relaxation experiments

Secondary chemical shift/CSI data and analysis of NOESY through-space connectivity indicates that in our hands Fas-DD in solution forms the 'closed' death domain structure. However, it cannot be ignored that the Fas death domain would need to be able to form alternate conformations to enable non apoptotic signalling through the recruitment of adaptor proteins to phosphorylated Y291. The crystal structure shows that Fas can exist in an alternate conformation in a solid state environment. We embarked upon an investigation of the dynamics of Fas-DD in solution in conditions which we hypothesised could induce the death domain to form different conformations.

To investigate the ability of Fas-DD to sample the alternate conformations in solution, two sets of NMR relaxation measurements were acquired for Fas-DD in three different conditions. Classical ^{15}N spin relaxation measurements were acquired to observe Fas-DD dynamics on the picosecond-nanosecond timescale and relaxation dispersion (CPMG-based) experiments were acquired to sample whether Fas-DD dynamics could be observed upon the microsecond-millisecond timescale.

Experiments were initially acquired with a sample of Fas-DD in the same conditions used for the structural experiments; this was considered to be the equivalent of 'wild-type' Fas-DD and used as a reference with which to compare other conditions. To investigate the effects of tyrosine phosphorylation upon the dynamics of Fas-DD, an Y291E phosphomimetic mutant Fas-DD+CTD construct was generated. ^{15}N nuclear relaxation measurements were also acquired for Fas-DD+CTD in the buffer used in the Fas;FADD crystal structure reported by Scott *et al.* (2009) (0.95 M citric acid, 1.9M ammonium sulphate, pH4 - in which a massive rearrangement of Fas-DD

helices five and six was observed) to see whether such dramatic effects might be observed in solution by NMR spectroscopy. These experimental conditions will be referred to throughout the chapter as Fas-DD, Fas-DD Y291E and Fas-DD in crystal buffer respectively.

The theory that underpins the basis for extracting information concerning molecular dynamics from nuclear relaxation data is particularly challenging and beyond the scope of this thesis. It should suffice to note that many of the experimental observables that relate to nuclear relaxation fundamentally depend upon the nature of fluctuating local magnetic fields that induce nuclear spin transitions. For a typical globular macromolecule the fluctuations arise as a result of both the overall molecular motion (tumbling) and any 'superposed' internal motion that can either be faster or slower than the overall tumbling. Whilst in principle the relaxation of ^{1}H, ^{13}C and ^{15}N magnetisation can inform the researcher of the underlying dynamics, this is most readily teased out with measurements that focus upon ^{15}N nuclei, for which the relaxation is dominated by the influence of the directly attached H^N proton. 'Classical' relaxation measurements comprise pulse sequences designed to allow measurement of: a) the longitudinal ^{15}N relaxation rate constant R_1; b) the transverve ^{15}N relaxation rate constant R_2; and c) the $\{^{1}H\}^{15}N$ heteronuclear NOE. The value of R_1 characterises the rate of return of ^{15}N Z-magnetisation following a perturbation away from equilibrium (e.g. by a ^{15}N radiofrequency pulse). The R_2 value characterises the rate of decay in the X-Y plane of in phase transverse ^{15}N magnetisation, following excitation (e.g. by a 90° ^{15}N pulse). Finally the heteronuclear NOE (hNOE) measures the influence on the equilibrium polarisation of the ^{15}N Z-magnetisation of radiofrequency saturation of the NMR transitions for the directly bonded proton nucleus. It turns out that in each case the magnitude of the NMR observable (R_1, R_2, hNOE) is a sensitive function of the temporal dynamics of the NH bond vectors. Because spontaneous emission at NMR spectral frequencies is negligible, relaxation of spin-1/2 nuclei relies upon the influence of local magnetic field fluctuations operating through instantaneous dipole-dipole interactions or the motion of the nucleus within a non-spherically symmetric electronic environment (known in NMR as chemical shift anisotropy). Thus an excited ^{15}N nucleus experiences fluctuating magnetic fields, including at specific frequencies that can effect spin-state transitions, and thereby a return to equilibrium. It turns out that the

dynamics of the molecule (more strictly the NH vectors) can be related to the observed relaxation parameters via specific values of the so-called 'spectral density function' that encodes the dynamics in terms of a frequency-dependent time correlation function. The spectroscopist can choose from various levels of sophistication for the analysis of the relaxation data, from attempting to map out the complete spectral density function, to the adoption of simplified models, as in the 'model-free approach' and its variants. Complicating factors in such analyses include rotational anisotropy of the molecular system under investigation, and the contribution to R_2 rates that arise from chemical exchange processes that modulate the chemical shift on a timescale that is long compared to the overall tumbling and are expressed in the theory as contributions to the spectral density at zero frequency. Properly disentangling these influences requires the application of a complex and time-consuming series of NMR experiments, followed by detailed data analysis beyond the scope of the work presented in this thesis. However the presence of chemical exchange, that might arise as a result of a low population of ligand bound protein molecules or from the existence of a low-lying excited state (i.e. alternate conformation) can be readily inferred from either: a) high outlier instances of ^{15}N R_2 values in an otherwise unremarkable profile across the protein chain; or (more reliably) b) from the presence of ^{15}N 'relaxation dispersion' in experiments designed to measure the influence of radiofrequency fields on the effective R_2 relaxation rate constant. In this work I have performed preliminary ^{15}N relaxation dispersion measurements for ^{15}N-labelled Fas-DD using the paradigm of Carr-Purcell-Meiboom-Gill (CPMG) trains of ^{15}N 180° pulses. Dispersion is identified when the measured effective transverse relaxation rate R_2^{eff} displays a characteristic non-zero dependence on the rate of application of CPMG pulses (the CPMG 'field strength').

3.6.1 Sample preparation for relaxation studies

The three conditions used for relaxation measurements were:

- Fas-DD in NMR buffer (20 mM MES, 100 mM NaCl, 0.5 mM TCEP, 1 mM EDTA, 3 mM Sodium azide pH 6.2).
- Fas-DD+CTD Y291E in NMR buffer (20 mM MES, 100 mM NaCl, 0.5 mM TCEP, 1 mM EDTA, 3 mM Sodium azide pH 6.2).

- Fas-DD+CTD in Crystal buffer (0.95 M citric acid, 1.9 M ammonium sulphate, pH 4.0) in a 3mm diameter tube.

Dr Diego Esposito had previously collected R_1, R_2 and Het NOE data for ^{15}N labelled Fas-DD+CTD (218-335) construct, this was used as the wild-type control to compare the perturbed conditions to using classical relaxation measurements. The Fas-DD (residues 218-319) construct donated by Dr Diego Esposito was used for the remaining relaxation experiments, samples and experiments were prepared/executed by the author. Fas-DD was expressed in ^{15}N-labelled minimal medium and purified as described in Section 2.5. Protein from the same preparation of ^{15}N-Fas-DD was used for both crystal buffer conditions and 'wild-type' conditions for relaxation dispersion experiments. The Y291E phosphomimetic mutation was generated from the Fas-DD plasmid using site directed mutagenesis methods as described in Section 2.4.3 and expressed and purified as described in Section 2.6. All samples were concentrated by centrifugal concentration to 500μM with 10% $^{2}H_2O$ for field frequency lock.

The Fas sample in crystal buffer conditions was achieved by dialysis of Fas-DD against crystal buffer overnight, as described in Section 2.6.7. Fas-DD was not as soluble in crystal buffer resulting in limited precipitation; the sample concentration was therefore lower and undetermined. Data was collected upon this sample using a glass NMR tube with a diameter of 3 mm. Using a tube with a diameter of 3 mm enhances the sensitivity of experiments collected in high salt conditions by reducing the concentration of salt present in the active sample. In doing this, the pulse length is reduced and the sensitivity of an experiment carried out on a sample containing up to 4 M salt is comparable to a sample in a conventional NMR buffer in a 5 mm diameter tube[179].

The use of a Tyr-Glu phospho mimetic mutation is not fully representative of the addition of a phosphate group upon a tyrosine side chain. Glutamate mimics the negative charge incorporated upon a tyrosine when phosphorylated, but this does not take into account the steric bulk of the phosphate upon the surrounding structure. Therefore the tyrosine to glutamate mutation does not fully recapitulate the effects of phosphorylation upon a protein. Incorporation of a phosphotyrosine into the Fas

death domain would be the only method to confirm that this post translational modification had an effect upon the domain *in vitro* (see Chapter 4).

3.6.2 $^{1}H/^{15}N$-HSQC projections of relaxation data for protein samples used for relaxation measurements show they are folded and suitable for relaxation analysis

Both spin relaxation and relaxation dispersion experiments are on a $^{1}H/^{15}N$-HSQC based format of experiment. Spectral analysis is carried out by the extraction of peak heights from the spectra collected at different ^{15}N internal relaxation delay times or CPMG field strengths. The relaxation of ^{15}N magnetisation is in effect projected onto the cross peak intensities of a $^{1}H/^{15}N$-HSQC. Spectral analysis is carried out on a residue by residue (peak location) basis therefore, cross peak assignments are required. $^{1}H/^{15}N$-HSQC spectrum assignments for Fas-DD were transferred from the structural work upon Fas-DD detailed above, however the other two Fas-DD conditions perturbed the spectra therefore tentative assignments were made in these conditions and in some cases cross peaks remained unassigned.

Mutation of Tyr291 to Glu resulted in minimal changes to the overall $^{1}H/^{15}N$-HQSC spectrum compared to Fas-DD (Figure 3.15), suggesting that the mutant Fas-DD is still folded. However a number of the peaks which corresponded to the residues immediately proximal to Y291 shifted or disappeared. 84% of the assignments were transferred from Fas-DD to this spectrum to enable relaxation analysis; the portion of the sequence confidently assigned is highlighted in Figure 3.15.

As described above, upon dialysis into crystal buffer, Fas-DD partly precipitates. Due to this, the $^{1}H/^{15}N$-HSQC projection for this sample showed poor signal to noise (Figure 3.16). Buffer conditions are well known to affect the $^{1}H/^{15}N$-HSQC spectrum for a particular protein, therefore it was unsurprising to observe a number of peak shifts for Fas-DD in these conditions. It is possible to tell that Fas-DD was still folded as the spectrum still possesses a high degree of dispersion; for example the four Gly cross peaks are still notable at the top of the spectrum. 45% of the assignments were transferred from Fas-DD to this spectrum to enable relaxation analysis (highlighted in Figure 3.16). Having less than 50% of the protein assigned meant that only general trends could be observed in the relaxation data obtained for this sample

Figure 3.15 $^{1}H/^{15}N$-HQSC projection of the T1 relaxation spectra for Fas-DD Y291E showing which assignments were transferred from Fas-DD+CTD

There were some chemical shift differences caused by the Y291E mutation, resulting in peak shifts of a number of residues. 84% of assignments were transferred and relaxation analysis carried out upon these residues. The residues assignments were transferred for are highlighted in blue upon the Fas sequence below the spectrum.

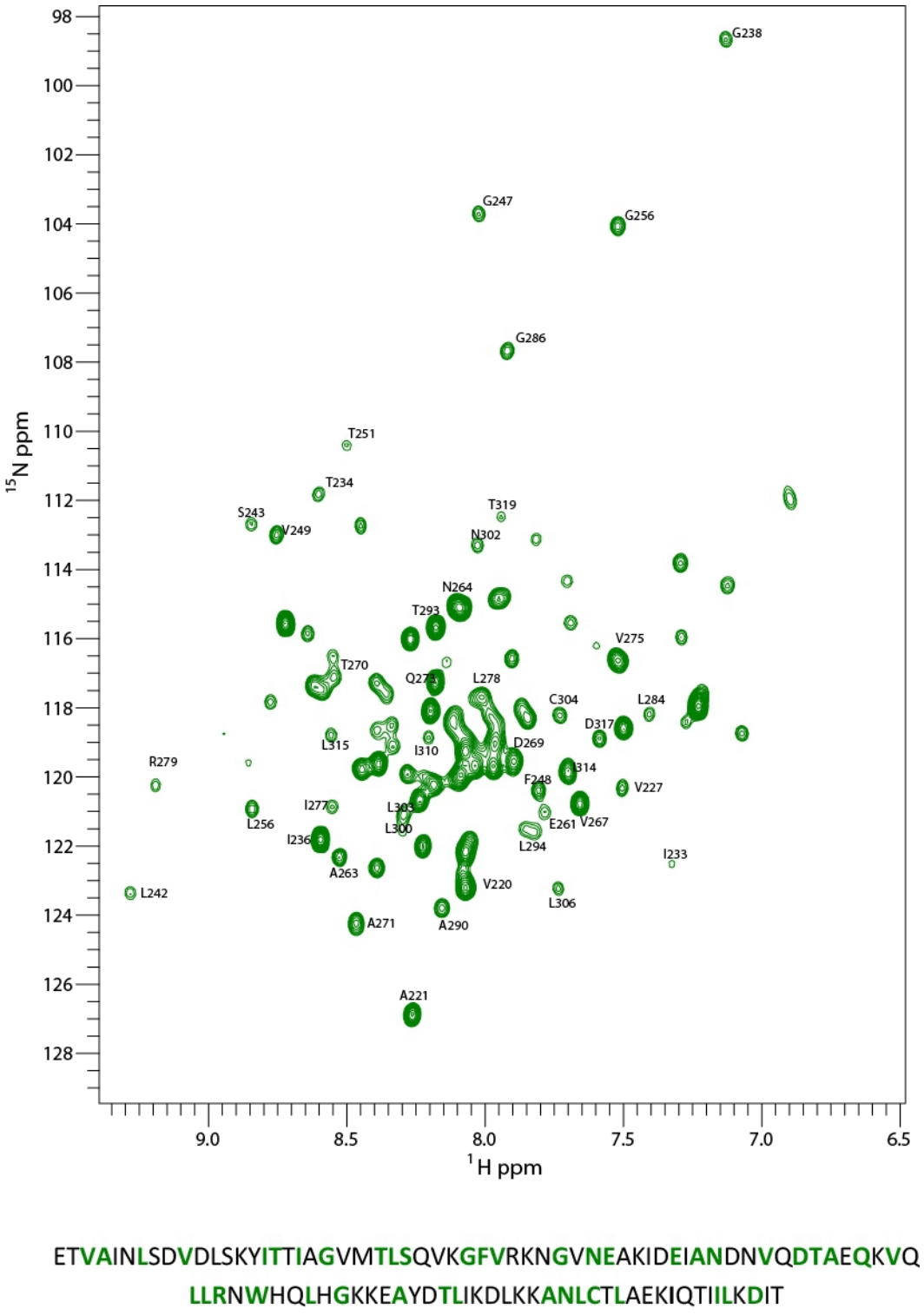

ETVAINLSDVDLSKYITTIAGVMTLSQVKGFVRKNGVNEAKIDEIANDNVQDTAEQKVQ
LLRNWHQLHGKKEAYDTLIKDLKKANLCTLAEKIQTIILKDIT

Figure 3.16 $^{1}H/^{15}N$-HQSC projection of the T1 relaxation spectra for Fas-DD in crystal buffer showing which assignments were transferred from Fas-DD+CTD

Fas-DD was less stable in crystal buffer compared to NMR buffer. There were a substantial number of peak shifts and a significant reduction in signal to noise of the spectra. 45% of the resonance assignments were transferred and relaxation analysis carried out upon these residues. The residues assignments that were transferred are highlighted in red upon the Fas sequence below the spectrum.

3.6.3 Classical ^{15}N spin relaxation measurements were acquired to explore Fas flexibility upon the picosecond-nanosecond timescale

The ^{15}N longitudinal and transverse relaxation rate constants (R_1 and R_2 respectively) and the $^{1}H/^{15}N$ steady state heteronuclear NOE were measured to assess the overall rotational diffusion and internal mobility of Fas-DD in the conditions described above. The measurements were made at 600 MHz with a sample temperature of 25 ^{o}C. The sample concentration was essentially identical for the Fas-DD and the Fas-DD Y291E samples at 500 μM.

The ^{15}N relaxation experiments were recorded using standard pulse sequences as described by Kay, Bax, Torchia and colleagues[180,153]. CCPN Analysis[138] was used to fit the R_1, R_2 and $^{1}H/^{15}N$ NOE values and their associated uncertainties. For the R_1 and R_2 datasets, single exponential decays of the peak heights were assumed (Figure 3.17). The fit of the exponential decay is then plotted as a function of residue number for both R_1 and R_2. $^{1}H/^{15}N$ NOE values obtained from the ratio of peak intensities in spectra measured with and without ^{1}H saturation are illustrated in a similar residue by residue manner. Collectively, from these data, the correlation times (τc, representative of the time it takes for a molecule to tumble through one radian in any arbitrary direction) for each Fas-DD sample was estimated from the mean trimmed R_2/R_1 ratios using in house software written by Dr Paul Driscoll.

3.6.3.1 Fas-DD shows little flexibility throughout the whole death domain

^{15}N R_1, R_2 and $^{1}H^{15}N$ heteronuclear NOE data recorded for Fas-DD+CTD had been previously recorded at 600 MHz by Dr Diego Esposito. This data was used for training purposes in the analysis of classical ^{15}N spin relaxation measurements. The quality of the spectra was excellent allowing for high quality fitting of the R_1 and R_2 decay curves and a high precision estimation of the corresponding decay constants and the heteronuclear NOE. Figure 3.18 shows the derived values for R_1, R_2 and $^{1}H^{15}N$ heteronuclear NOE and Figure 3.21A shows the computed R_2/R_1 ratios on a per residue basis.

The most part of the R_2/R_1 plot is flat which is consistent with a globular fold with relatively low rotational diffusion anisotropy. Preliminary estimates of the predicted

isotropic rotational correlation time τ_c from the trimmed R_2/R_1 ratios was 8.2 ns. It is generally considered that for a globular protein the correlation time is approximately 0.5 ns per kDa of atomic weight. Thus the estimated τ_c for Fas-DD (11 kDa) is on the high side for a monomeric protein and could indicate that the protein experiences some weak self-association, or possesses 'rougher' surface characteristics that lead to relatively slow tumbling. Resolution of the precise origin of this behaviour would require substantial additional experimentation and analysis.

3.6.3.2 Fas-DD Y291E shows similar flexibility to Fas-DD

^{15}N R_1, R_2 and $^{1}H^{15}N$ heteronuclear NOE data were also recorded for Fas-DD Y291E as described above. The quality of the spectra was adequate for the fitting of the R_1 and R_2 decay curves (examples shown in Figure 3.17) and estimation of the corresponding decay constants and heteronuclear NOEs. Figure 3.19 shows the derived values for R_1, R_2 and $^{1}H^{15}N$ heteronuclear NOE and Figure 3.21B shows the computed R_2/R_1 ratios on a per residue basis.

Due to having only 85% of the cross peak assignments for this construct there is not data for every residue throughout the construct, but there are sufficient to observe global trends. From the heteronuclear NOE it is observable that the mutation does not destabilise the whole protein. The profile of R_1 and R_2 magnitudes is more dispersed compared to Fas-DD, with the R_2/R_1 values spread over a greater range. Assignments for the residues closest to the mutation were understandably the ones which could not be transferred with confidence. However, it is observable that values of relaxation parameters corresponding to residues within helix 5 (the location of Y291E mutation) are more perturbed throughout each of the datasets collected compared to Fas-DD, which may suggest some change in dynamics in this region.

Preliminary estimates of the predicted isotropic rotational correlation time τ_c for the Fas-DD Y291E was 8.3 ns, which was similar to the wild type protein indicating no overall change in the shape of the protein.

3.6.3.3 Fas-DD in crystal buffer showed an increase in the range of R_1, R_2 and heteronuclear NOE values

^{15}N R_1, R_2 and $\{^1H\}^{15}N$ heteronuclear NOE data was recorded for Fas-DD in crystal buffer as described above. Compared to the other samples, the quality of the spectra was poor due to a reduced level of signal to noise caused by the apparent instability of the construct under these conditions, witnessed as a tendency to precipitate. R_1 and R_2 decay curves were fitted for the well resolved cross peaks in the spectrum and for which the assignments of Fas-DD could be transferred (45% of the residues), enabling estimation of the corresponding decay constants and fitting of the heteronuclear NOE. Figure 3.20 shows the derived values for R_1, R_2 and $^1H^{15}N$ heteronuclear NOE and Figure 3.21C shows the computed R_2/R_1 ratios on a per residue basis. Fas-DD in crystal buffer showed elevated values of R_2/R_1 compared to the other Fas-DD conditions sampled suggesting some dynamics within the construct upon the nanosecond timescale.

Preliminary estimates of the predicted isotropic rotational correlation time τ_c from the R_2/R_1 trimmed ratios was 12 ns. The distinctly higher value of τ_c for the protein under these conditions compared to standard NMR buffer is noteworthy and could result from a number of factors that includes the adoption of an expanded monomeric conformation, enhanced self-association and possible homodimer formation, a higher solvent viscosity due to the buffer conditions, or a combination of these influences. Further experiments would be required to specifically identify the origin(s) of the higher τ_c value.

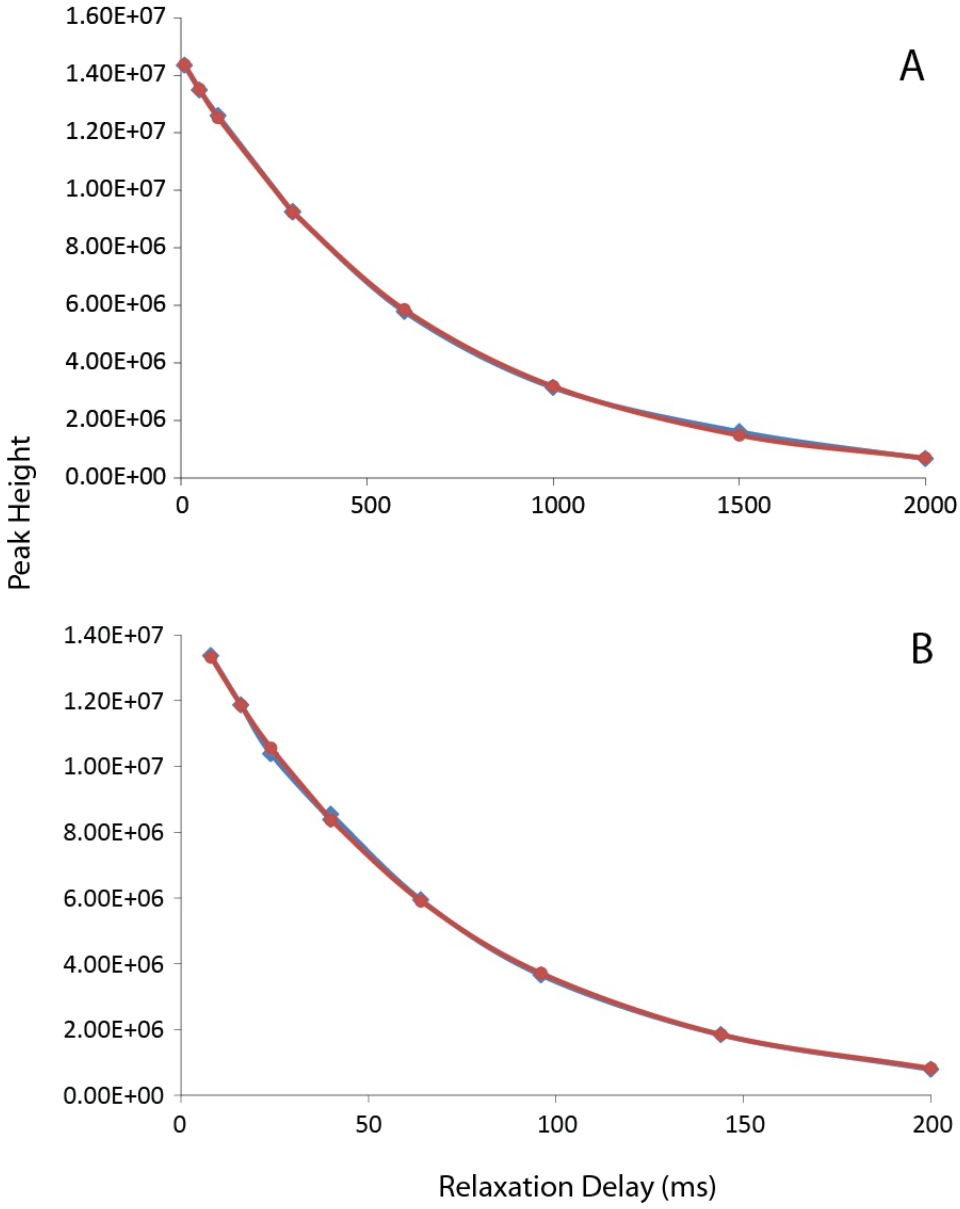

Figure 3.17 Example of the relaxation decay graphs for Fas-DD Y291E used to extract values for R_1 (A) and R_2 (B) using CCPN analysis

Delay curves used to extract the R_1 (A) and R_2 (B) for Serine 209 from Fas-DD Y291E. The relaxation data were collected at 600MHz at 25^{o}C. CCPN analysis was used to fit the data using the fitting function 'A exp (-Bx)'. The extracted peak heights are shown in blue and the fitted values in red.

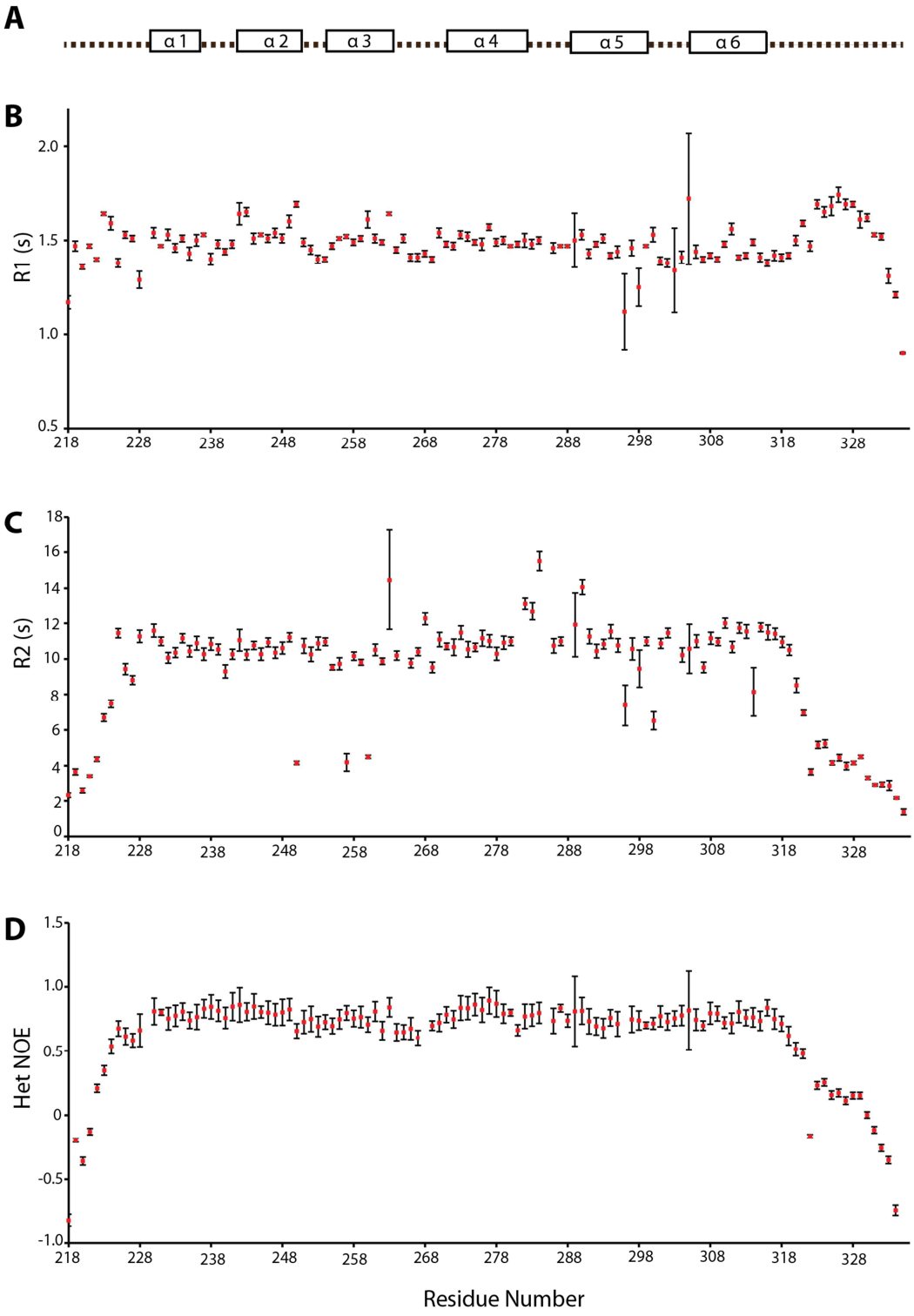

Figure 3.18 Longitudinal, transverse and ^{1}H-^{15}N Heteronuclear NOE relaxation rates for Fas-DD

Secondary structural elements of Fas-DD (A) are represented by rectangles indicating alpha helices with loops and less structured regions shown by the dashed line. Longitudinal ^{15}N relaxation rates R_1 (B), Transverse ^{15}N relaxation rates R_2 (C) and ^{1}H-^{15}N heteronuclear NOE values (D) for Fas-DD are plotted as a function of residue number. Values were extracted at 600MHz and fitted using CCPN Analysis.

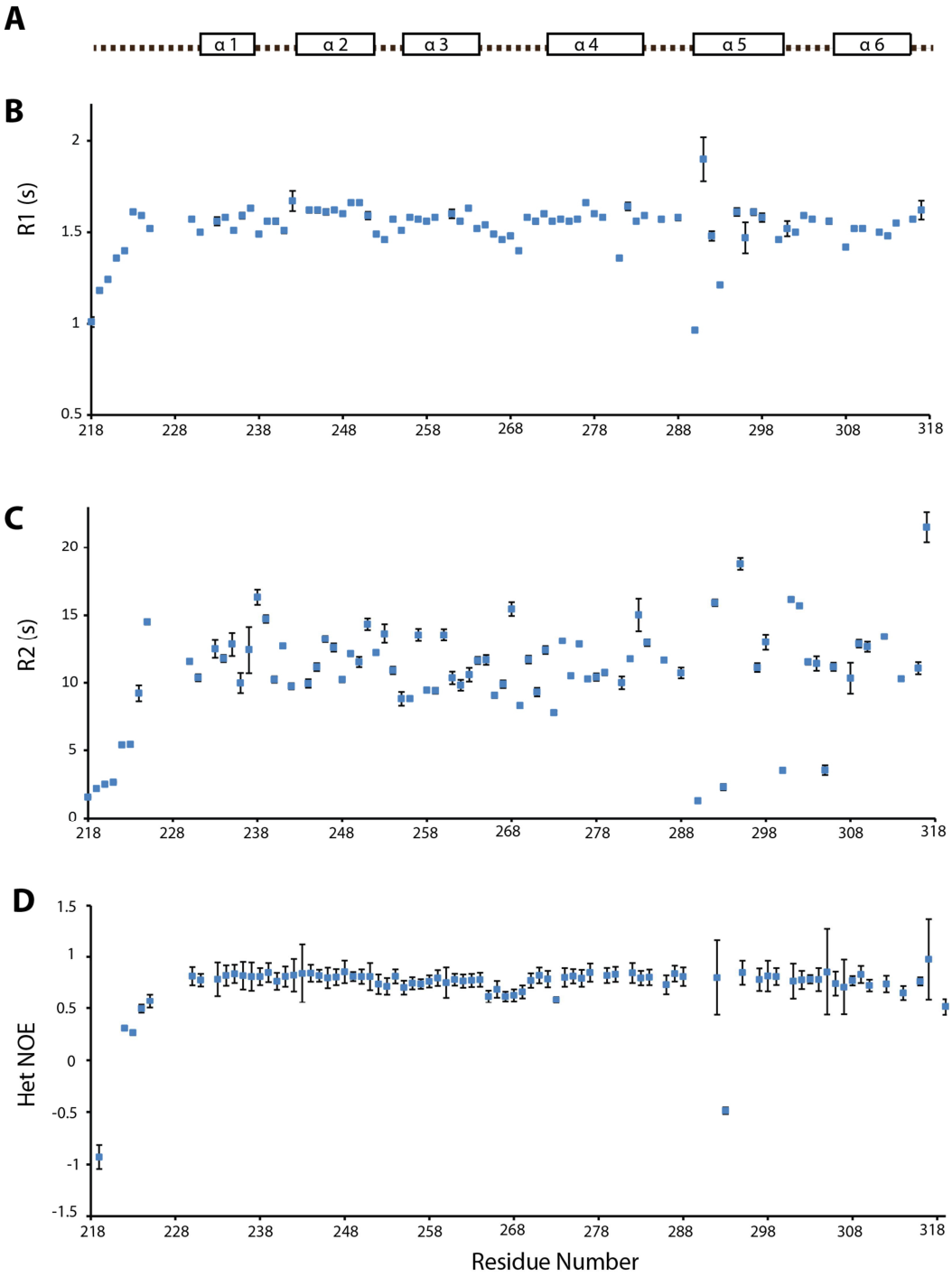

Figure 3.19 Longitudinal, transvers and ^{1}H-^{15}N Heteronuclear NOE relaxation rates for Fas-DD Y291E

Secondary structural elements of Fas-DD (A) are represented by rectangles indicating alpha helices with loops and less structured regions shown by the dashed line. Longitudinal ^{15}N relaxation rates R_1 (B), Transverse ^{15}N relaxation rates R_2 (C) and ^{1}H-^{15}N heteronuclear NOE values (D) for Fas-DD Y291E are plotted as a function of residue number. Values were extracted from spectra recorded on a 600MHz spectrometer and fitted using CCPNAnalysis.

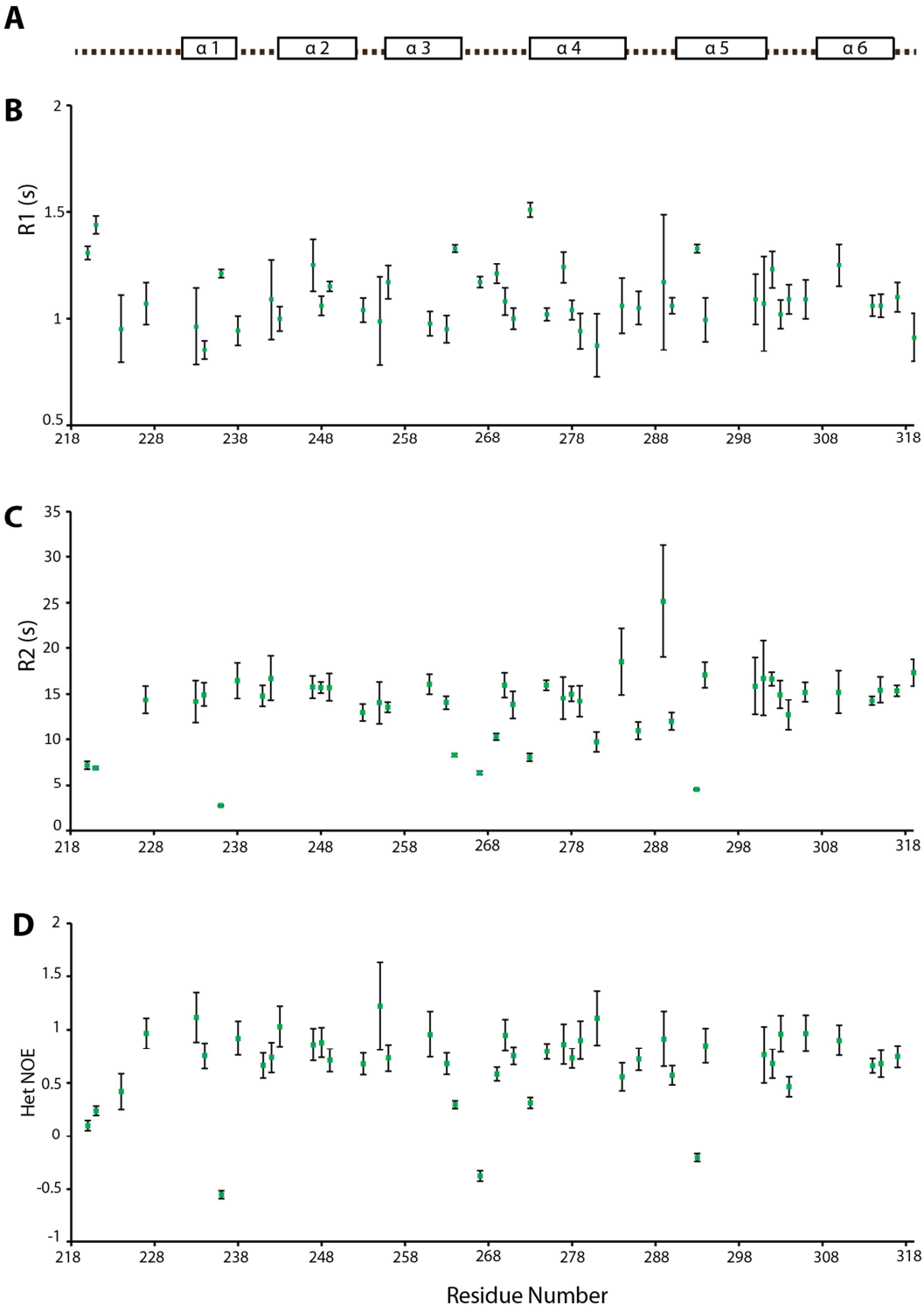

Figure 3.20 Longitudinal, transverse and ^{1}H-^{15}N Heteronuclear NOE relaxation rates for Fas-DD in crystallisation buffer

Secondary structural elements of Fas-DD (A) are represented by rectangles indicating alpha helices with loops and less structured regions shown by the dashed line. Longitudinal ^{15}N relaxation rates R_1 (B), Transverse ^{15}N relaxation rates R_2 (C) and ^{1}H-^{15}N heteronuclear NOE values (D) for Fas-DD in crystallisation buffer are plotted as a function of residue number. Values were extracted from spectra recorded on a 600MHz spectrometer and fitted using CCPNAnalys

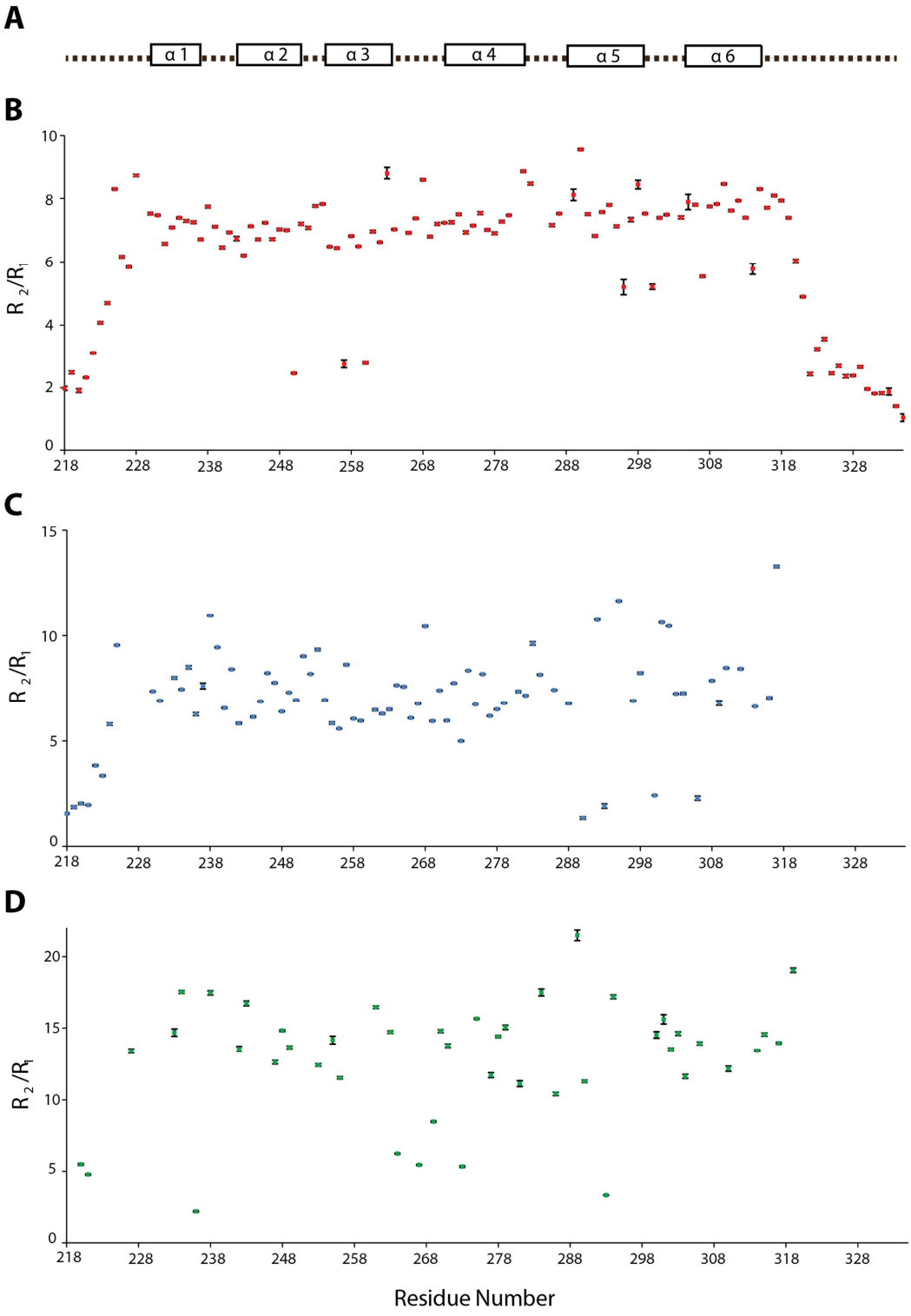

Figure 3.21 R_2/R_1 for Fas-DD, Fas-DD Y291E and Fas-DD in crystal buffer

Secondary structural elements of Fas-DD (A) are represented by rectangles indicating alpha helices with loops and less structured regions shown by the dashed line. A plot of R_2/R_1 for A, Fas-DD; B, Fas-DD Y291E and C, Fas-DD in crystal buffer.

3.6.4 Relaxation dispersion measurements were acquired to explore Fas flexibility on the microsecond-millisecond timescale

Relaxation dispersion data were acquired at seven CPMG field strengths (40, 100, 200, 400, 600, 800 and 1000 Hz) to assess the potential presence of possible intermediate states of Fas-DD which cannot be detected using classical ^{15}N spin relaxation measurements. The data was acquired at 600 MHz with a sample temperature of 25 ^{o}C upon the three Fas-DD conditions described above. A new sample of ^{15}N-Fas-DD was expressed and purified as this data had not been previously collected by Dr Esposito. The samples used for the classical ^{15}N spin relaxation measurements described in Section 3.4.3 were the same as for Fas-DD Y291E and Fas-DD in Crystal buffer acquisition.

The relaxation dispersion experiments were recorded using standard pulse sequences as described by Palmer and colleagues[181]. CCPN Analysis was used to measure the peak heights in the ^{1}H-^{15}N correlation spectra as a function of the applied ^{15}N radio frequency (CPMG) field. The effective transverse relaxation rate constants R_2^{eff} were calculated by measuring two point change in peak intensity between a dataset with no CPMG relaxation period and another data set with a 40 relaxation ms delay comprising up to 1000 Hz of CPMG modulated transverse relaxation. Data were analysed for specific cross peaks corresponding to residues of interest either within close proximity to Y291 or at the boundary between helix 5 and helix 6.

Relaxation dispersion experiments interpret the classical relaxation experiments described above in terms of the overall rotational diffusion of the molecule. It is a measure of motions which are slower than the overall molecular tumbling of the whole molecule[182]. Due to the readout relating to internal motion on relatively slow micro-to millisecond timescales, these types of experiments are commonly used to study protein refolding[183], the effects of mutations upon protein folding[184], and the allosteric transitions within proteins. The experiments themselves monitor the return of transverse magnetization in the X-Y plane following perturbation by and appropriate excitation train. In effect the observation of RF-field dependence of the effective transverse relaxation rate R_2 in these experiments enables the detection of weakly-populated alternate states of the protein corresponding to either ligand-bound, or ‘excited’ conformational states[185].

3.6.4.1 Selected residues in close proximity of Y291E mutation show increased flexibility compared to Fas-DD

The effective transverse relaxation rate constants R_2^{eff} were calculated for a subset of six cross peaks (Tyr232, Asp292, Leu294, Ile295, Ile310 and Ile314) from both the Fas-DD and the Fas-DD Y291E relaxation dispersion spectra. These residues were judged to be in the closest proximity to Y291 in the published Fas-DD solution structure and therefore should be sensitive to the substitution of Tyr for Glu. The R_2^{eff} was calculated for Glu261, as a control that the effects were localised to the region of interest, not a global change throughout the whole domain. This analysis in conjunction with an illustration of the location of the analysed residues upon the Fas-DD structure is displayed in Figure 3.22, highlighting Tyr291 in black, with the other analysed residues highlighted in colours corresponding to the associated dispersion profile.

The dispersion profiles for residues extracted from experiments upon wild type Fas-DD are flat: that is the difference between the effective transverse relaxation rates at low and high RF field $R_2^{eff}{}_{(40Hz)}$ and $R_2^{eff}{}_{(1000Hz)}$ is close to zero. This result indicates that this construct is unlikely to be undergoing exchange on the microsecond to millisecond timescale with a significant population of an excited state. Mutation of Tyr291 to glutamate led to an increased R_2^{eff} at low CPMG field strengths of residues in close proximity to Tyr291 (Tyr232, Asp292, Ile295). This observation is consistent with the appearance of dynamics on the microsecond to millisecond timescale for the mutant protein. However this effect is not a global one upon the whole protein. Glu261, which is not within the region of interest, exhibits a profile of R_2^{eff} values similar to those obtained for wild type Fas-DD.

3.6.4.2 Sub microsecond dynamics are observed throughout Fas-DD in crystal buffer

The effective transverse relaxation rate constants R_2^{eff} were calculated for a subset of five cross peaks (Ala301, Leu303, Cys304, Leu306, Ala307) from both the Fas-DD and the Fas-DD in crystal buffer relaxation dispersion spectra. These peaks correspond to the residues in the loop region between helices 5 and 6 in Fas-DD. The analysis focused upon this region because within the published 4:4 Fas:FADD crystal structure it is within this part of the structure that the polypeptide chain is

reoriented to form an elongated helix. It would have been ideal to have been able to analyse the surrounding helix regions of this loop, however assignments for this region of the construct were not transferrable between spectra, as highlighted in Figure 3.16, which suggests that this region of the protein has been affected by the buffer conditions.

The analysis of relaxation dispersion data for Fas-DD in crystal buffer is illustrated with the location of the analysed residues upon the Fas-DD structure in Figure 3.23. Fas-DD within the conditions used to crystallise Fas and FADD in a 4:4 complex exhibits a a globally higher value of R_2^{eff} compared to wild type Fas-DD throughout all of the residues analysed. This result is consistent with the results of the classical relaxations analysis where the true ^{15}N R_2 values were significantly higher than for the same protein in standard buffer conditions. However, the quality of the Fas-DD in crystal buffer relaxation dispersion data is not particularly high. The calculated experimental error is larger throughout the Fas-DD in crystal buffer samples compared to all of the rest of the Fas-DD acquisitions. This is due to the poor signal to noise within the spectra collected for these conditions, resulting in a drop off in peak height prior to reaching the longest CPMG value. The poor signal to noise is a consequence of the lower protein concentration coupled with the loss of signal due to dielectric losses associated with the high ionic strength of the buffer and aggregation of the sample. This greatly reduced the data that were available to analyse for this experiment. As a result it is essentially impossible to definitively infer the presence of relaxation dispersion for Fas-DD under these buffer conditions.

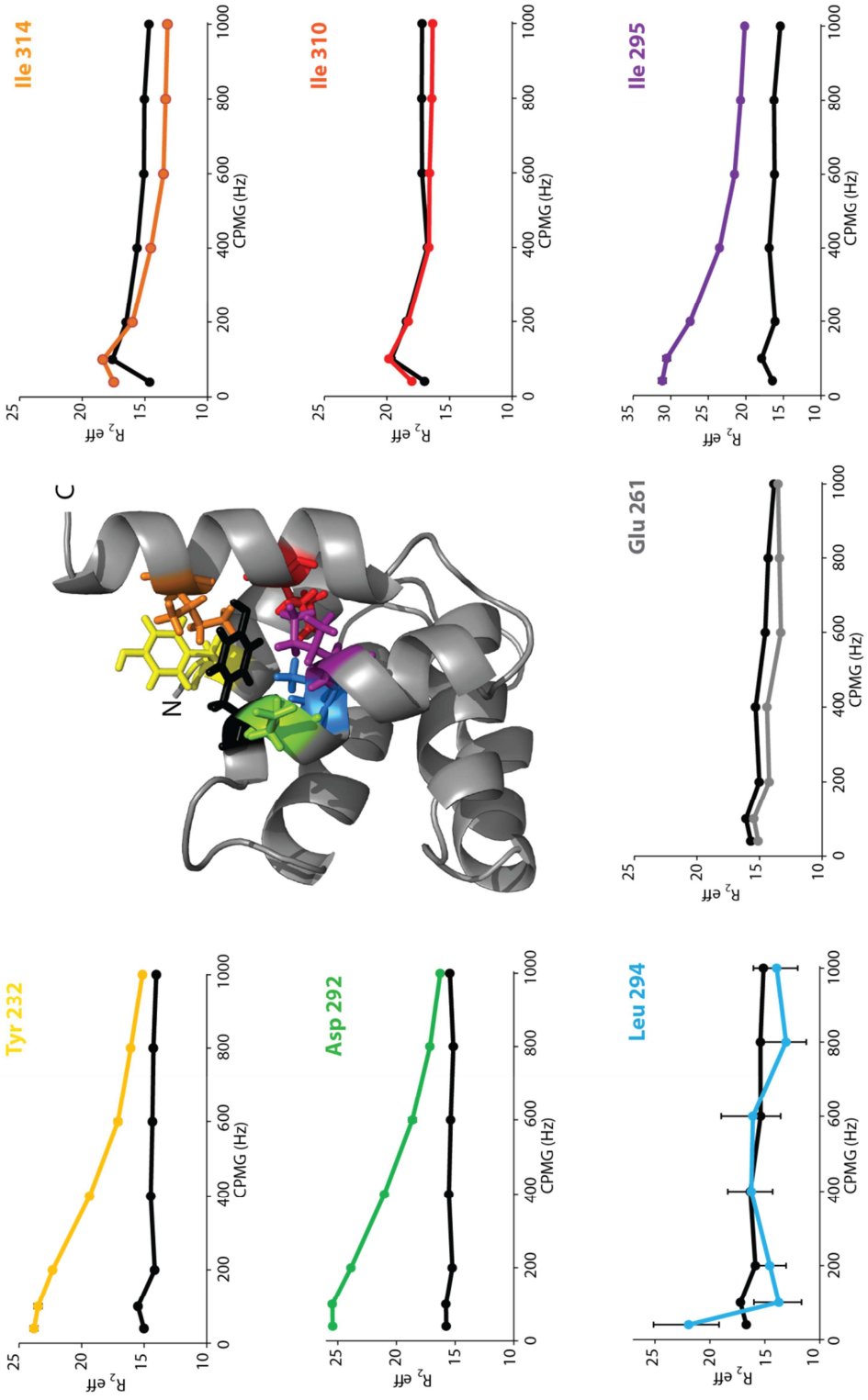

Figure 3.22 CPMG relaxation dispersion curves and the Fas-DD structure highlighting the six amino acids in the closest proximity to the Y291.

Data extracted from relaxation dispersion experiments upon Fas-DD Y291E recorded at 600MHz and 25^{o}C, with the $R_{2\ effective}$ measured relaxation rate and CMPG field strength applied indicated. Six residues were analysed for their proximity to Y291. Insert, published Fas-DD structure (PDB:1DDF) highlighting each of the residues for which dispersion curves were calculated by colour. The dispersion curve for E261 (grey) is included to illustrate that dispersion differences are specific to the location of the mutation rather than global effects upon the domain.

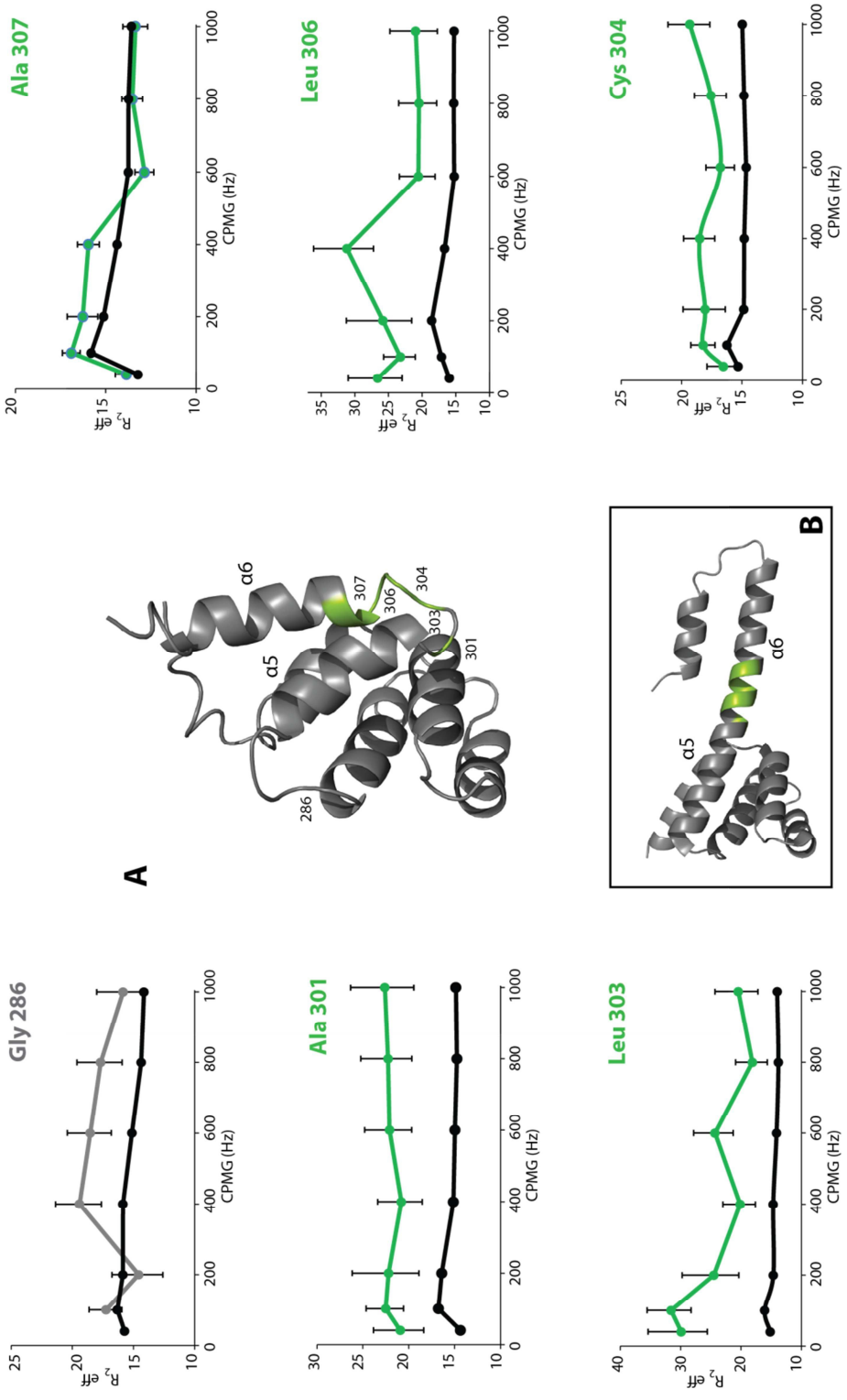

Figure 3.23 CPMG relaxation dispersion curves for the 6 amino acids present in the loop between helices five and six in the Fas-DD

Dispersion curves for Fas-DD in crystallisation buffer recorded at 600MHz and 25°C, with the $R_{2\ \text{effective}}$ measured relaxation rate and CMPG field strength applied indicated. Data collected from Fas-DD shown as black curves, data collected for Fas-DD in crystallisation buffer shown as grey curves. A, Fas-DD published structure (pdb:1DDF) highlighting the residues for which dispersion curves were calculated. B, Fas-DD structure taken from Fas:FADD crystal structure (PDB:3EZQ) highlighting the same residues. The dispersion curve for G286 (grey) is included as a representative of the dispersion differences to another area of the domain..

3.7 Discussion

The Fas death domain structure was first described in 1996 by Haung and colleagues documenting a bundle of six antiparallel amphipathic helices. Since then a number of other death domain structures have been determined, all showing this now canonical death domain fold. The interaction with Fas and the adaptor protein FADD is mediated by a death domain-death domain interaction which provides the basis for the formation of the death inducing signalling complex and the onset of apoptosis. Much work has been carried out to elucidate the mechanism of interaction between the Fas and FADD death domains. Crystallisation of the Fas-DD and FADD-DD complex has elucidated two very different structures with different stoichiometry. In one of the structures (showing a 4:4 Fas:FADD complex), the Fas-DD is shown to undergo a rearrangement resulting in the fusion of helices α5 and α6, thus deviating from the classical death domain fold. Although this complex has been suggested to be an unfeasible mechanism of interaction between Fas and FADD *in vivo*, it does illustrate that the death domain may not be as rigid as was previously thought and rather might undergo plastic deformation under prescribed circumstances. A phosphorylation site has been documented within Fas-DD at Tyr291, an observation that provides additional support that the Fas death domain may have some level of flexibility in its shape. Due to the relatively buried location of Tyr291, the death domain may need to reorganise to accommodate the presence of a phosphate group. The work described in this chapter has used NMR spectroscopy to explore the propensity of the Fas-DD to form other structures in solution.

Almost invariably the starting point for any protein NMR analysis is the assignment of the protein backbone resonances. Backbone assignment initially involves the identification of which cross peak in the $^{1}H/^{15}N$-HSQC spectrum corresponds to which amino acid in the protein's primary sequence. The backbone assignment forms the basis of all further side chain chemical shift and structural (NOE, RDC, etc.) assignments for the molecule. The assignment of the protein backbone signals was also required for the analysis of the polypeptide dynamics as the experiments used are all based on an HSQC-type readout which enables analysis of the data on a residue by residue basis. The backbone correlation NMR experiments for Fas-DD+CTD had already been acquired within the laboratory by Dr Diego Esposito. I repeated the task of backbone assignment using the same raw data as a training

exercise in protein NMR spectroscopy, assigning 93% of the backbone NH in the HSQC spectrum. Assignment was incomplete due to unresolved NH cross peak resulting from flexible N and C-termini of the construct and lack of a tractable HN(CA)CB spectrum.

Structural restraints which are used in the calculation of solution structures are mainly derived from the collection and analysis of NOESY spectra. ^{15}N- and ^{13}C-NOESY spectra can be used to calculate the relative distances between pairs of protons which are close in space. To enable assignment of the NOESY spectrum the side chain ^{1}H resonances of the amino acids are required to be assigned. This task is usually achieved by acquisition of a 3D HCCH-TOCSY spectrum followed by ^{13}C-aromatic and aliphatic NOESY spectra. The side chain spectra recorded using traditional methodology and parameters were highly crowded with poor signal-to-noise. To overcome this problem experiments were re-acquired using a non-uniform sampling schedule which significantly improved the resolution of the spectra enabling a more complete and efficient assignment. The application of non-uniform sampling (NUS) is rapidly becoming a more everyday occurrence throughout the NMR community. In the world of protein NMR the trade-off is consistently between the amount of instrument time available and the achievable signal to noise within a spectrum. An NUS sampled spectrum offers an increase in resolution (particularly in the indirect dimension) in a much shorter space of time than a traditionally sampled spectrum[186], and helps to overcome the traditional bottleneck of NMR data acquisition[187]. In this study, NUS particularly improved the resolution in the ^{13}C NOESY experiments. NOESY spectra are notorious for the presence of overcrowding of the peaks, due to the sheer number of correlations and the range of cross peak intensities which are within the aliphatic region of the spectrum. Often the weakest cross peaks carry a disproportionate amount of information in terms of structural restraints. Therefore there is a premium on optimising the ability of the NOESY-type spectra. The implementation of NUS methods has been shown to enhance considerably the approach to extracting the maximum utility from NOESY data without compromising on experimental sensitivity[187], something that we were able to exploit throughout this work.

Secondary chemical shift information taken from the chemical shifts of the ^{13}Cα, ^{13}Cβ and ^{1}H atoms point towards the domain forming six helices which are located

in the equivalent positions as in the PDB:1DDF (Figure 3.10). NOE spectral analysis also highlighted that Tyr291 is in a buried location, with NOE correlations between itself and residues which have been shown to be located nearby in the Fas-DD 'closed' solution structure. Unfortunately we had an incomplete set of side chain resonance assignments and therefore pursued solving the structure with the aid of restraints from the deposited co-ordinates of Fas-DD (PDB:1DDF). Due to this we can only consider our structure as a preliminary representation of the data we collected from the structural NMR experiments; there is much scope for further refinement of the NOE dataset which we used to calculate our structure in its current form. However, the preliminary structural results unambiguously indentify that in our hands in solution Fas-DD forms the canonical death domain fold, almost identical to the Fas-DD structure published by Huang and colleagues in 1996.

To test the likelihood that Fas-DD can exist in a more open conformation in solution within different environments, the dynamics of Fas-DD containing a phospho-mimetic mutation (Y291E) and in the buffer Fas was crystallised in were explored using NMR relaxation experiments. The problem with the introduction of a mutation or variation of the buffer environment of a protein is that it can disrupt the secondary structure of a protein, to this the NMR spectrum should be sensitive to such changes. The presence of the Y291E mutation resulted in a number of peak shifts within the Fas-DD $^{1}H/^{15}N$-HSQC spectrum, preventing full transfer of backbone resonance assignments. This could be considered to have limited the analysis of the relaxation data acquired in these conditions. Peak shifts in the $^{1}H/^{15}N$-HSQC should have been expected due to the additional formal negative charge due to the mutation, Fas-DD backbone resonance assignments should be repeated with this mutant construct to be able to fully analyse the effect of this mutation on the relaxation properties of Fas-DD. The Fas-DD construct, once dialysed into crystallisation buffer (0.95 M citric acid, 1.9 M ammonium sulphate, pH 4) showed, signs of instability. Upon dialysis a proportion of the protein partly precipitated resulting in a lower concentration of protein and a knock-on effect upon the achievable quality of the NMR data. Changing the buffer conditions of a protein also has a large effect upon the local environment of each NMR active nucleus and a global effect on the chemical shifts; again for these conditions only a subset of the resonance assignments could be transferred. As these experiments were designed to recapitulate the conditions the

death domain was exposed during crystallisation, there is little improvement to the quality of this sample that could be made.

Despite the difficulties posed by the constructs used to look at Fas dynamics, a number of observations were able to be made. The overall rotational diffusion and internal mobility of Fas-DD in these three different conditions were assessed using the standardised set of NMR spin relaxationion experiments: ^{15}N R_1, ^{15}N R_2 and $\{^1H\}^{15}N$ heteronuclear NOE. These 'classical' experiments are most useful for assessing the overall dynamic characteristics of the target protein. In particular for the globular part of a folded protein the ratio of R_2/R_1 values relates directly to the overall rotational correlation time τ_c. Outlier low values of the hNOE (<~ 0.6) combined with small values of R_2 typically indicate regions of the protein that are more flexible on the nano-to-picosecond timescale. And outlier high values of R_2 may indicate the presence of an exchange contribution to the ^{15}N linewidth and thereby the presence of multiple states (conformations) that fluctuate on the milli- to microsecond timescale.

Chemical exchange is more reliably identified in CPMG relaxation dispersion measurements. Such experiments were performed for all three Fas-DD conditions described above. The data was analysed on a residue by residue basis for each of the conditions, focusing upon residues which are in suspected areas of increased flexibility/rearrangement. The effective transverse relaxation rate, R_2^{eff}, of the residues of interest was plotted against the CPMG frequency. These were plotted in conjunction with the same analysis from peaks corresponding to the Fas-DD data to make a comparison between the conditions and what was considered globular Fas-DD. Of note, each of the dispersion curves shown in Figure 3.21 and 3.22 show an initial dip in the R_2^{eff} values. This is considered to have been an unexplained and unresolved artefact of the pulse sequence used when the experiments were acquired, similar effects were observed using ^{15}N ubiquitin as a control protein (Dr Tom Frienkel, personal communication).

The R_1, R_2 and heteronuclear NOE analysis of Fas-DD+CTD all showed essentially flat dynamic profiles. This pattern of relaxation and dynamic parameters is characteristic of a stable, globular protein fold, coupled with the estimate of τ_c (8.2 ns) determined from the trimmed average R_2/R_1 ratio these results are in line with

Fas-DD forming a globular structure consistent with the canonical death domain fold. In conjunction with the structural results observed for Fas-DD in solution in our hands, these conditions were considered wild type or Fas in a closed conformation. This categorisation was to aid in the analysis of the other conditions tested to act as a comparison.

The profiles of R_1, R_2 and heternonuclear NOE of Fas-DD Y291E are mostly flat, indicating that this mutant Fas-DD maintained the globular fold. The R_2 values throughout the protein were significantly more dispersed than both the R_1 and NOE profiles. The dynamic profiles indicate that there are some localised differences in all three parameters around helix five and the loop between helix five and six which may suggest some flexibility in this region. This is the location of the Y291E mutation and could therefore indicate local rearrangement of Fas-DD, however there is not a continued stretch of residues affected. The classical readout for a region of a protein with increased flexibility would be an increase/decrease in the parameters of all three experiments for a contiguous stretch of amino acids. Complete assignment of Fas-DD Y291E would give a clearer picture as to whether these anomalies are due to local unfolding or plasticity. For Fas-DD Y291E, the assignments for six of the peaks in the closest proximity to Y291 were available. The R_2^{eff} of these peaks and the associated peaks for Fas-DD in NMR buffer calculated from relaxation dispersion measurements were compared. The Y291E mutation increased the R_2^{eff} at the lowest CPMG frequencies of residues in the closest proximity to residue 291 (Tyr232, Asp292, Ile295). This effect is consistent with the presence of dynamics in the micro- to millisecond timescale for these residues. However, for the residues slightly further away and a ‘control’ residue (Glu261) which is in a region distinct from that containing Tyr291, the R_2^{eff} values were essentially indistinguishable from those obtained for the wild type protein. These results are consistent with the presence of local dynamic refolding or orientation of the domain close to the location of the mutation, suggesting that the Fas-DD Y291E is capable of some level of deformation or rearrangement. The experiments with this mutant were carried out with a view to crudely model the effect of phosphorylation of the side chain of Tyr291. At face value the results for Fas-DD Y291E suggest that the introduction of a negative charge at that position can be accommodated without very significant disruption of the overall fold of the protein as evidenced by the overall high level of

conservation of chemical shifts, the essentially identical rotational correlation time, and only limited evidence of ^{15}N relaxation dispersion patterns. Rather it seems probable that, given the larger dimensions of the Tyr side chain compared to Glu residue, and the fact that the putative phosphoryl group would be appended onto the solvent exposed extremity of the former, the modification would have very limited influence on the stability and folded-ness of the Fas death domain.

It is well known that buffer conditions can have a large effect upon the position of NH peaks observed in a $^{1}H/^{15}N$-HQSC spectrum. The high salt conditions of the crystal buffer resulted in a number of dramatic peak shifts throughout the $^{1}H/^{15}N$-HQSC spectrum which resulted in only 45% of the backbone resonance assignments being able to be transferred for the spectrum. This dramatically reduced the number of data points which could easily be sampled. As observed from the formation of the 'open' Fas conformation, the crystal conditions (if this is what caused the rearrangement) could encourage helical rearrangement of the Fas-DD. Analysis of the R_1, R_2 and heteronuclear NOE showed dispersed, 'non flat' dynamic profiles, suggesting that Fas-DD in crystal buffer is more flexible upon the nanosecond timescale than Fas-DD in NMR buffer. Interestingly, the estimated value of τ_c (12 ns) is significantly higher for Fas-DD in crystal buffer when compared to wild type (8.2 ns) and the Y291E mutant (8.3 ns). This could be an indication that in crystal buffer, Fas-DD tends to strongly self-associate and possibly forms a dimer, or tumbles more slowly as a result of the heightened viscosity of the buffer conditions, or a combination of these effects. Both the observed ^{15}N R_2 and R_2^{eff} values for Fas-DD in crystal buffer were all significantly higher than the corresponding values obtained in standard NMR buffer. Unfortunately it is difficult to make definitive conclusions from the relaxation dispersion data from the experiments collected in crystal buffer. The lower solubility of Fas-DD in these conditions is consistent with the use of these conditions to crystallise the protein. However, it is noteworthy that a number of the cross peaks remained essentially unshifted compared to Fas-DD in standard NMR buffer. Those cross peaks which could be assigned were distributed throughout the length of the protein which would indicate that the overall fold of the construct in the crystal buffer conditions is essentially that of a canonical death domain fold. Taken as a whole we have not obtained any substantive evidence that Fas-DD can rearrange in these conditions, although an exhaustive investigation for a

conclusive outcome is warranted. Unfortunately, due to the time and resource commitment applied towards the other strands of activity described in this thesis, at the time of writing it has not proved possible to devote further effort towards this objective.

In summary, this chapter has given a clear indication that in our hands, the Fas-DD does in fact form a six helical, compact bundle like the reported solution structure. Dynamic analysis of Fas-DD in conditions to induce alternative conformations has on the whole proved inconclusive, with some local rearrangements possible with the introduction of a phosphomimetic mutation and global changes in crystallisation conditions. In general there was no definitive evidence for the spontaneous formation of any significantly different structures similar to those observed *in crystallo*. Further work would focus upon the possibility of generating a phosphorylated Fas-DD to test whether this post translational modification confers structural rearrangement to the death domain.

Chapter 4

Semi-synthesis of pY Fas Death Domain using frontier methods in expressed protein ligation

4.1 Introduction

4.1.1 Phosphorylation of the death domain of Fas could alter the structure and dynamics of the domain

The death domain of Fas (Fas-DD) has been reported to be phosphorylated on tyrosine 291.[54] It has been proposed that this phosphorylation is crucial for Fas oligomerisation and the commitment to apoptotic signalling[55]. Furthermore, reports have suggested that Fas phosphorylation triggers a variety of non-apoptotic signalling pathways, including the PI3 kinase and ERK pathways[63].

Y291 is present within a region with homology to the known SH2 domain target sites (YxxL). Co-precipitation of SH2-domain containing phosphatases SHP1/2 and SHIP[45] and the activation of PI3K through its SH2 domain containing regulatory subunit[62] further implicate the phosphorylation of the death domain to have a role within cellular signalling. The kinase(s) able to phosphorylate Fas have not been unambiguously identified, but the src family YES kinase has been implicated, at least as part of the PI3K activation pathway[62].

Two, highly divergent, 3D structures of Fas-DD have been reported, exhibiting different degrees of solvent accessibility for Y291[6,121]. As described in Chapter 3, NMR studies with wild type and a phospho-mimetic mutation of Fas-DD indicated that, at least in solution, both constructs behave in a manner compatible with the structure in which Y291 is buried. This fact prompts a plethora of questions regarding how this tyrosine can be phosphorylated and the consequences this might have on the structure of the domain. The addition of a phosphate group would certainly disrupt the compact structure of the death domain possibly having 'knock-on' effects upon the functional interactions of Fas.

The implementation of a methodology for the semi-synthetic preparation of a Tyr-phosphorylated death domain would have merits in its own right. Development of novel chemical-biology based methods would generate transferrable protocols to introduce post translational modifications into other proteins within the laboratory. Moreover, the introduction of pY291 into Fas-DD might reveal interesting structural and dynamical information about death domains and their ability to modulate their interaction with other proteins.

4.1.2 The use of expressed protein ligation to generate a Tyr291 phosphorylated Fas construct in vitro

It is extremely challenging to synthesise peptides longer than 60 residues in length using standard methods due to the formation of secondary structure (primarily β-sheets) within the peptide chain. Regular secondary structure elements normally cause aggregation, reducing the efficiency of the amino acid coupling reaction[188]. A common method to overcome this problem is the insertion of pseudo proline (ψP) units into the peptide sequence throughout synthesis. A ψP is a dipeptide unit constituted of any amino acid followed by a serine, threonine or cysteine derivatised as an oxazolidine. This derivatisation creates an amino acid with a similar structure to proline, resulting in a kink in the backbone of the peptide preventing any ordered structure from forming. Acid treatment following peptide synthesis, converts the ψY into the two native amino acid structures, leaving no trace in the peptide chain. ψY are routinely used to enable the synthesis of long peptides thus allowing the synthesis of longer peptides by solid phase peptide synthesis[188,189]. Fas-DD itself has previously been fully synthesised with the use of eight pseudo proline (ψP) units[190]. Although very interesting, syntheses based on using multiple pseudo proline units are laborious, resulting in a low yield of peptide and, at least for the present time, are not suitable to be used for preparative purposes in structural biology laboratories.

Expressed protein ligation (EPL) is a technique which merges the biochemical techniques of recombinant protein expression and purification with the organic chemistry techniques of peptide synthesis. EPL overcomes the peptide length limitation in peptide synthesis by the ligating a protein, or a fragment of a protein, expressed in *E. coli* with a synthesised peptide. It is a powerful method, enabling the semi-synthesis of cytotoxic proteins, the incorporation of non-native amino acids and

post translational modifications, as well as fluorescent and isotopic site-specific protein labelling for NMR, of the type that are either difficult or impossible to achieve with peptide synthesis or protein expression alone[191].

Established technologies of EPL are currently limited by the need to have a cysteine residue at the N-terminus on the second C-terminal fragment in the ligation junction. This is because the ligation occurs via a thioester exchange reaction. The work described here includes the validation of a novel Nα auxiliary ((2-hydroxy-3-thio-4-methoxy)benzyl; Htmb) that bypasses the requirement for a cysteine at the ligation junction[192].

The strategy used to generate a pY Fas Death Domain by expressed protein ligation was carried out in three steps. First, the N-terminal fragment (residues 218-285) of Fas-DD (Nt-Fas-DD) was expressed in *E. coli* in a form that contained a reactive C-terminal thioester. Then, the C-terminal fragment (Ct-Fas-DD residues 286-323) was synthesised by Fmoc solid phase peptide synthesis (SPPS) to include a phosphorylated tyrosine at position 291 (pY-Ct-Fas-DD) and a novel auxiliary group (Htmb) attached at the N-terminus. The N- and C-termini were then ligated by thioester exchange. The following sections will extend on the principles of each of these stages of generating pY291 Fas-DD *in vitro*.

The phospho-tyrosine of interest is in the C-terminal part of the death domain thus, the peptide forms the C-terminus of the construct. The location of the ligation site within the protein is crucial for the yield of the ligation, as the rate of the thioester exchange reaction depends on factors such as the nucleophilicity of the C-terminal reactive thioester, which is the attacking nucleophile, and the steric hindrance at the site. It has been shown that the rate of exchange of C-terminal glycine or histidine thioesters is enhanced compared to that for other natural amino acids[193,194]. Also, it is thought that the presence of a glycine at the N-terminus of the second fragment optimises the ligation yield because it minimises the steric hindrance due to the absence of a side chain. Residues 285 and 286 in the Fas death domain are His and Gly respectively, so this peptide bond was the chosen location to be the ligation junction. The decided Fas-DD construct designs for EPL are shown in Figure 4.1.

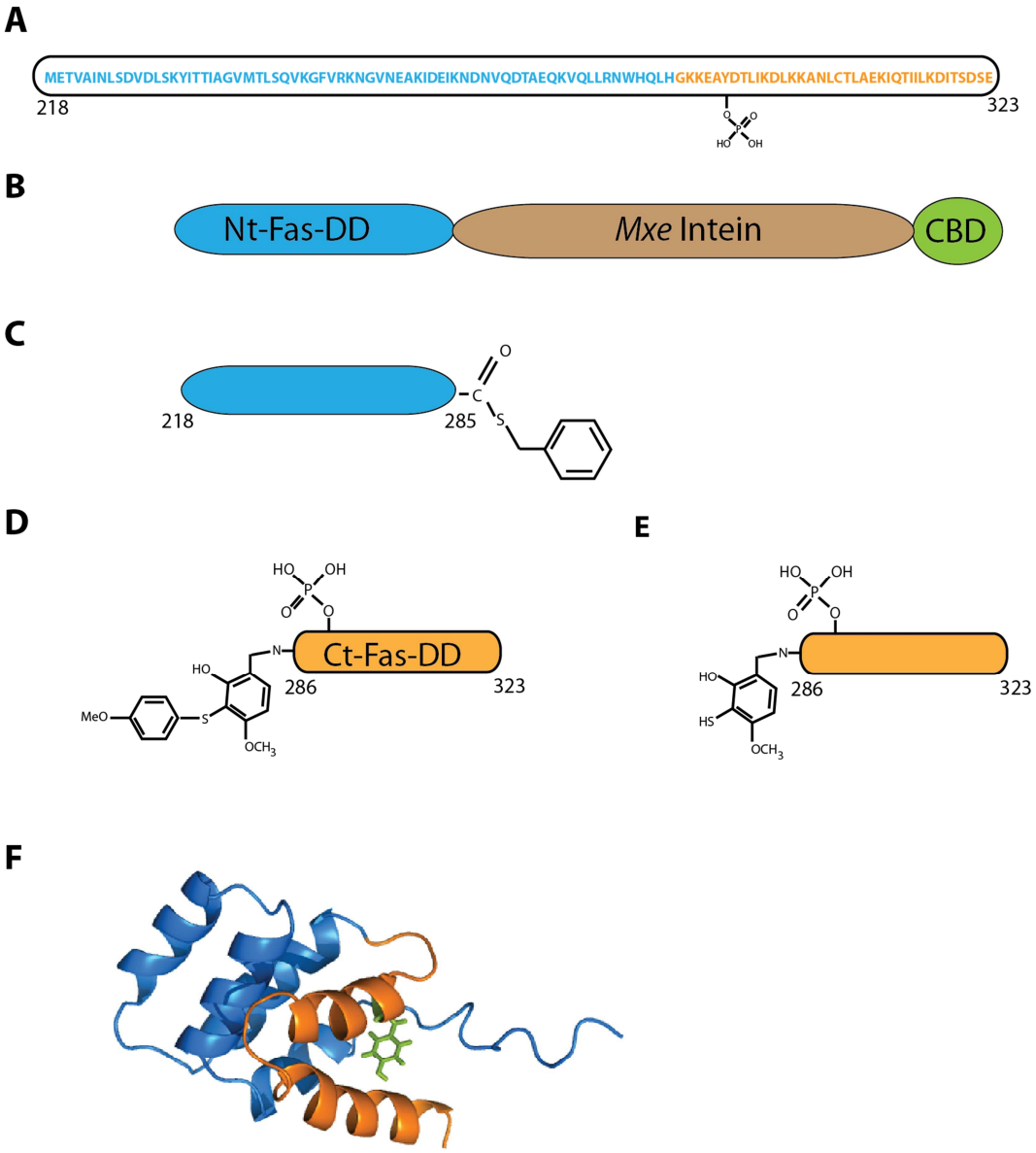

Figure 4.1 Schematic representation of the division of the Fas-DD for expressed protein ligation

A, Schematic representation of the full Fas Death domain, to be recreated using expressed protein ligation. The sequence of the N-terminal construct is highlighted in blue and the C-terminal peptide is highlighted in orange. The N-terminal methionine will be left over from E coli expression. B, Representation of the Nt-Fas-DD construct cloned using the NEB IMPACT system. C, The Nt-Fas-DD benzyl mercaptan thioester produced following on column cleavage. (CBD – chitin binding domain.) D, representation of protected Htmb- Ct-Fas-DD. E, Representation of deprotected Htmb-pY-Ct-Fas-DD. The numbers below illustrations correspond to the residue number of Fas. F, Cartoon representation of Fas-DD (pdb:1DDF) highlighting the N-terminal (blue), C-terminal (orange) and Tyr291 (green)

4.1.3 The Nt-Fas-DD fragment with a C-terminal reactive thioester is produced by intein excision

An intein is a self-splicing protein. Protein splicing is a post translational processing event in which the intein domain catalyses its own excision from a larger polypeptide. The excision is followed by the ligation of the two flanking regions (termed exteins) via the formation of a native peptide bond between them (Figure 4.2). Protein self-splicing enables the formation of two distinct proteins from one gene transcript[195]. Although inteins have been identified in all domains of life, there is little sequence similarity, other than a conserved N-terminal cysteine residue (or Serine) and a C-terminal asparagine followed by a cysteine, threonine or serine[196]. Intein-mediated protein splicing is initiated at the N-terminus of the intein, with an N-S (or N-O) acyl rearrangement that replaces the peptide bond between the N-terminal extein and the intein with a thioester (or ester) linkage. The next step is a transesterification reaction in which the C-terminal Cys, Thr or Ser attacks the carbonyl group of the newly formed thioester (or ester) cleaving the bond between the N-terminal extein and the intein, yielding a branched intermediate. Then, the side chain nitrogen of the C-terminal Asn residue undergoes cyclisation by attacking its own backbone carbonyl group, which breaks the peptide bond between the intein and the C-terminal extein, releasing the intein and leaving a thioester (or ester) bond between the exteins. Finally, the exteins undergo an spontaneous S–N (or O–N) acyl shift to form a native peptide bond (Figure 4.2A) [197,198].

In order to use inteins for the generation of proteins with a C-terminal reactive thioester, the intein needs to be located C-terminal to the protein of interest. Also, the C-terminal Asn of the intein must be mutated to Alanine. This mutation halts the intein cleavage at the level of the formation of the thioester between the protein of interest and the intein. The reaction is carried out in the presence of a thiol reagent such at 2-mercaptoethanesulfonic acid (MESNA), DTT or thiophenol[199,200]. The thiol reagent attacks the carbonyl group in the newly formed thioester, releasing the target protein from the intein and resulting in the formation of a polypeptide product containing a C-terminal thioester (Figure 4.2B).

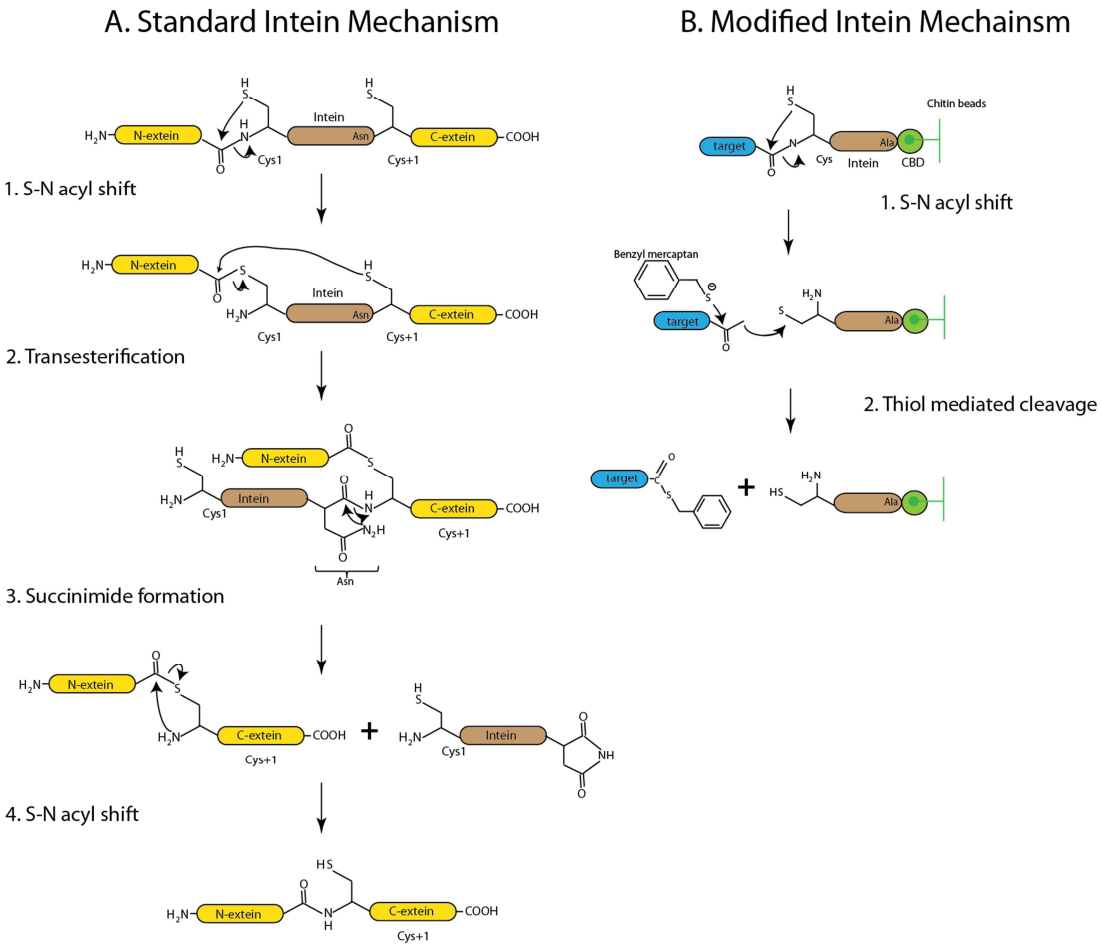

Figure 4.2 Comparison of standard intein cleavage and modified intein cleavage used within the IMPACT system

A, Standard intein mechanism. 1, N-S acyl shift between the side chain of a cysteine residue and the carbonyl of the C-terminal amino acid of the N-extein, which is followed by, (2) transesterification to shift the N-extein to the side chain cysteine in position +1. 3, Succinimide formation caused by the presence of the Asn at position -1 releases the intein, this is followed by a S-N acyl shift which recapitulates the native peptide bond and the side chain of the cysteine in the +1 position. B, Modified intein mechanism. 1, undergoes S-N acyl shift like a native intein. 2, benzyl mercaptan thiol attacks the carbonyl in the newly formed thioester, releasing the target protein from the intein and results in the formation of a protein construct containing a C-terminal thioester. Due to there being no Asn in the -1 position, succinimide formation and intein excision is prevented causing the intein to remain bound to the C-terminal CBD and chitin bead. More information on this process is shown in Figure 4.3. Adapted from Southworth and Perler 2004.

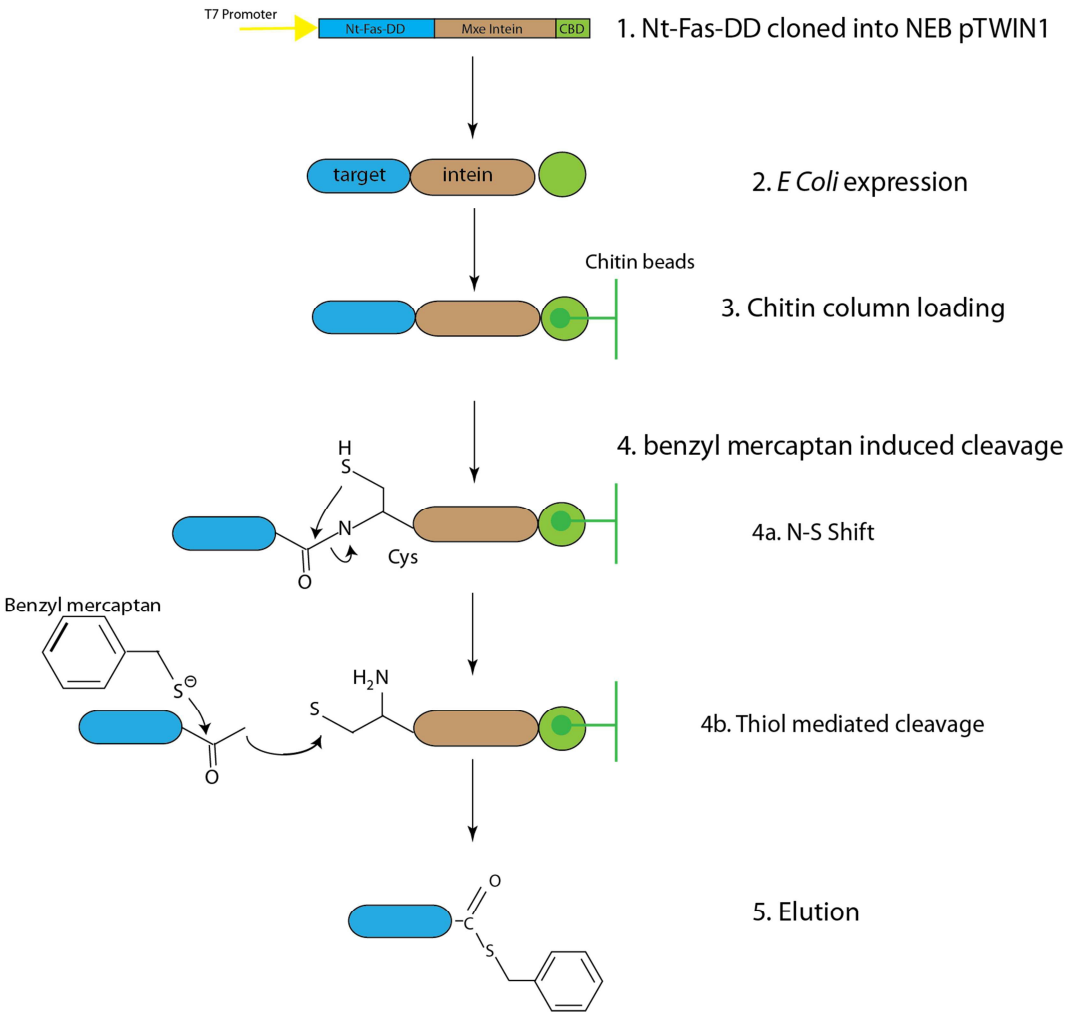

Figure 4.3 Schematic diagram illustrating the protocol used for Nt-Fas-DD purification, including the mechanism for intein cleavage

Schematic diagram showing benzyl mercaptan induced on column intein cleavage of the Nt-Fas-DD construct from the intein and chitin binding domain. Nt-Fas-DD is shown in blue, the intein in brown and the chitin binding domain (CBD) in green. Briefly, after *E. coli* expression (2), the lysate is clarified and the construct is affinity purified using chitin beads (3). Upon the beads, intein cleavage is induced by the presence of benzyl mercaptan. This induces thiol mediated cleavage via a N-S acyl shift (4), allowing the freed Fas-DD thioester to be eluted from the column (5). (adapted from NEB Biolabs literature on the IMPACT system).

The thiol chosen for this study was benzyl mercaptan. The benzyl thioester is considered a robust group which is less susceptible to hydrolysis than other thioesters therefore has advantages for the storage of the prepared protein thioester[201].

New England Biolabs incorporated the intein-mediated cleavage technology in their IMPACT (intein mediated purification with an affinity chitin binding tag) system of products, in which an intein is fused to the chitin binding domain (CBD) of chitinase A1 from *Bacillus circulans*[202] . The DNA insert of the protein of interest can then be cloned either N or C-terminal to the intein-CBD to exploit these properties[203]. The vector chosen to prepare the Nt-Fas-DD thioester contains the coding sequence for the naturally occurring Mxe GyrA mini intein which was originally isolated from *Mycobacterium xenopi*. This intein is 198 residues in length. When it was discovered, this was the smallest naturally occurring protein splicing element identified[204]. The presence of the CBD in the expressed protein not only enables affinity purification using chitin beads, but also on-column cleavage of the target protein. The released protein of interest (containing the reactive thioester) elutes from the column, while the intein and CBD remain on the beads. This procedure aims to yield a purified protein containing a C-terminal thioester and no vector derived amino acids[199,205]. The process and mechanism of thiol mediated intein cleavage which was used to generate Nt-Fas-DD is illustrated in Figure 4.3.

4.1.4 The C-terminal Y-phosphorylated fragment was synthesised using Nα 9-fluorenylmethylozycarbonyl solid phase peptide synthesis

Nα 9-Fluorenylmethylozycarbonyl (Fmoc) solid phase peptide synthesis (SPPS) is a widely used methodology for the generation of peptide fragments from amino acid constituents on a solid support. It builds upon the SPPS technique originally described by Merrifield in 1963[206], in which Nα-derivatised amino acids are sequentially coupled to form the peptide of interest. Following each coupling, the reagents and by-products are removed by filtration as the peptide is built up from the C to the N terminus. A schematic of the Fmoc-SPPS process used to synthesise pY-Ct-Fas-DD is shown in Figure 4.4.

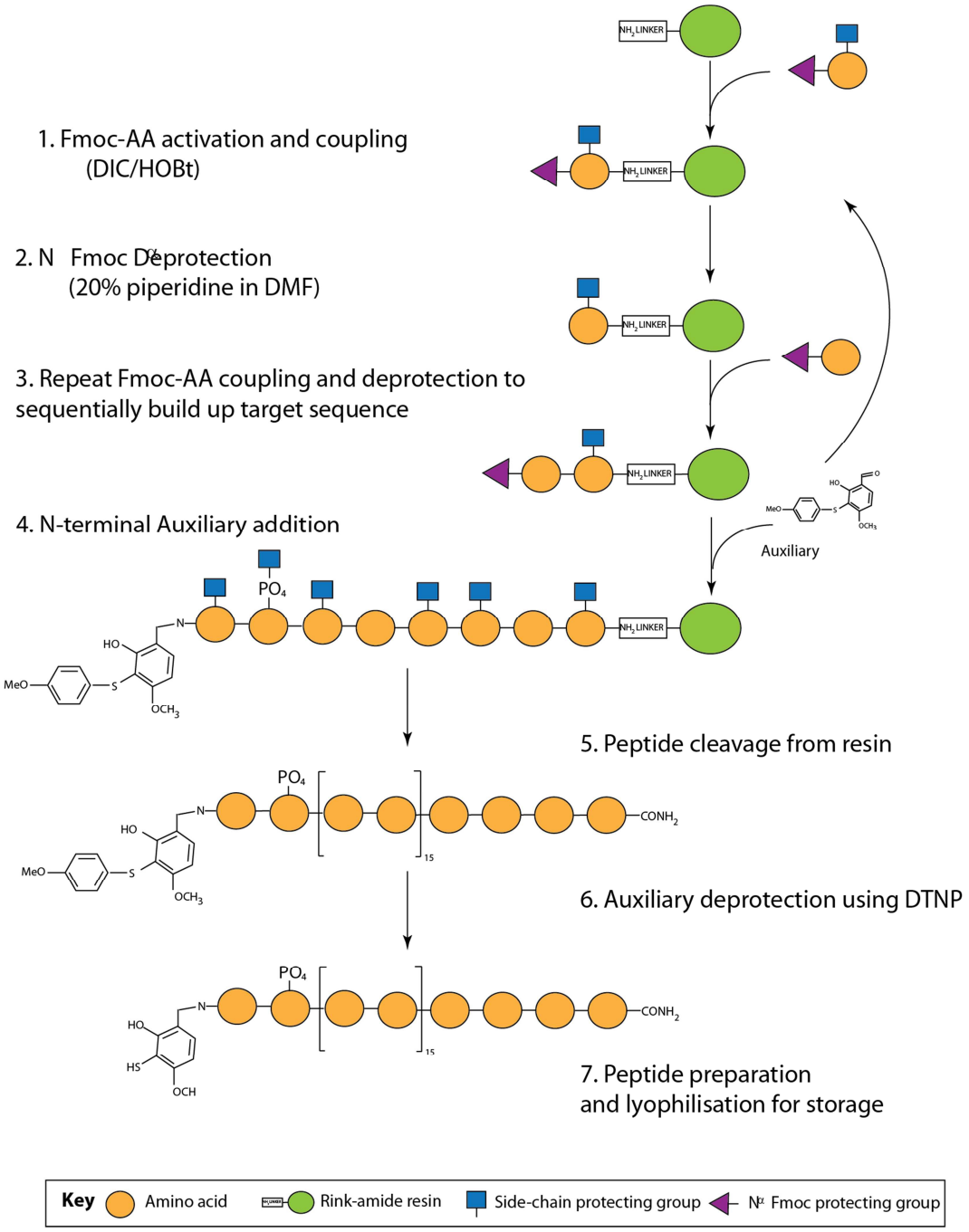

Figure 4.4 Synthesis of pY-Ct-Fas-DD peptide

Schematic representation of the process used to make the Ct-Fas-DD phosphopeptide by Fmoc-SPPS, followed by auxiliary addition and deprotection. Briefly, Rink resin, containing a free amide group is swelled in DMF. The first Fmoc protected amino acid is coupled to the resin using DIC/HOBt coupling methods (HBTU/DIEA for the phosphotyrosine and last five amino acids) (1), followed by the removal of the Fmoc protecting group using 20% piperidine in DMF (2). The amino acid coupling and deprotection is repeated sequentially to build up the target protein sequence (3). This is followed by the chemical addition of the auxiliary by a 1, 2 addition, elimination reaction (4) The phosphopeptide was cleaved from the resin using TFA and appropriate side-chain protecting group scavengers (5). Following preparation the auxiliary deprotecting group was removed using DTNP (6), re-prepped and lyophilised for storage (7).

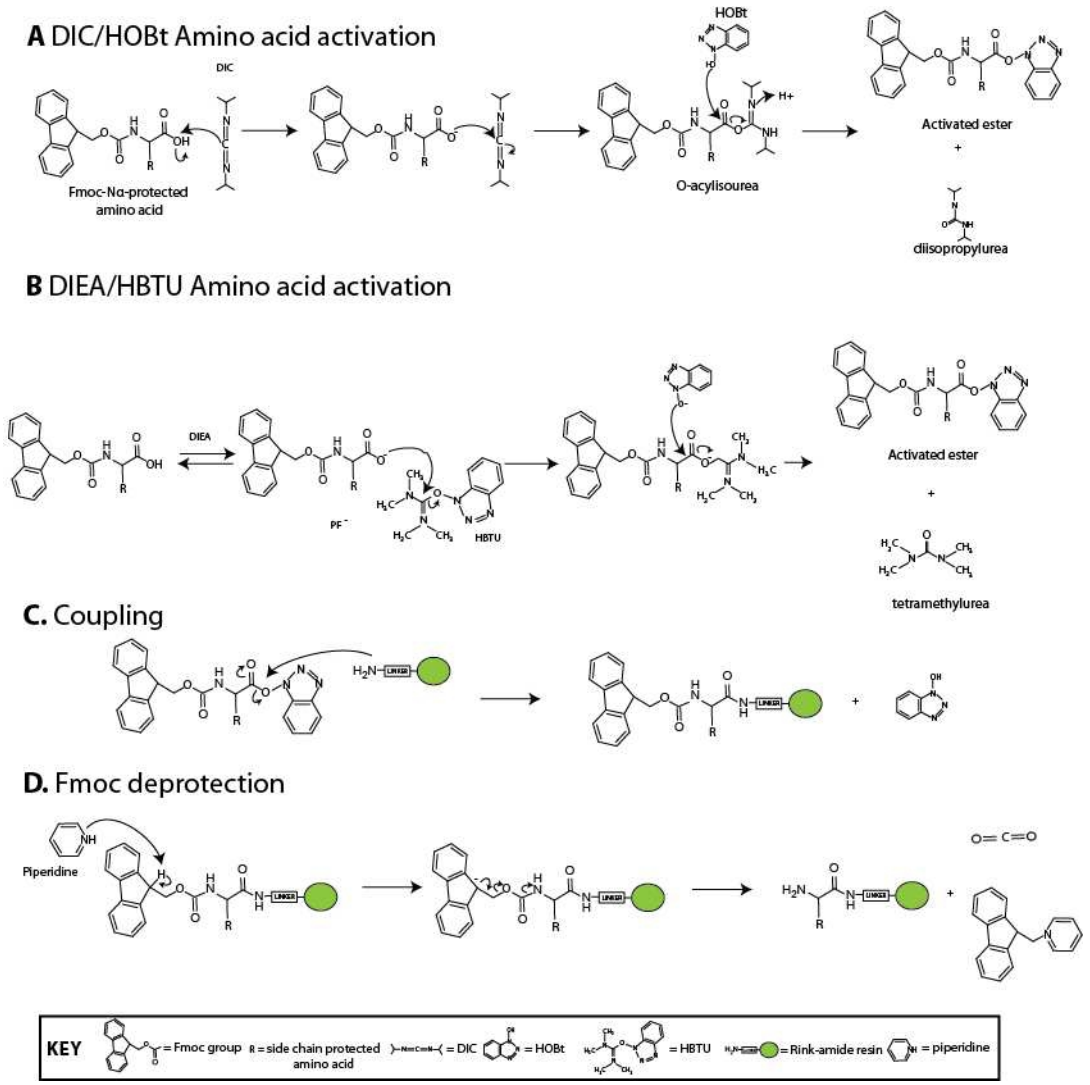

Figure 4.5 Chemical mechanisms involved in solid phase peptide synthesis

The three main reactions involved in solid phase peptide synthesis. A, Activation of Fmoc protected amino acid using DIC/HOBt coupling. Carboxylic acid needs activating to enable coupling. DIC converts the amino acid to O-acylisourea which is spontaneously converted to the reactive 1-hydroxybenzotriazole ester by HOBt. B, Activation of Fmoc amino acids using DIEA/HBTU coupling works along a similar mechanism. C, Coupling reaction to form an amide bond. D, Fmoc deprotection. The Nα-Fmoc protecting group is removed through a β-elimination reaction with piperidine. More in depth description of the reaction is found in the main text.

Amino acids used for SPPS contain side chain and N-terminal modifications designed to protect the functional groups and limit side reactions. Side-chain protecting groups are designed to prevent the peptide chain growing through side-chain linkages whereas the N-terminus is protected by an Fmoc group which ensures that only one amino acid is incorporated to the chain in a given reaction cycle. To enable amide (peptide) bond formation between the resin-linker and the carbonyl group of the amino acid to be coupled, the carbonyl of the amino acid needs to be activated. The activity of the activated species is one of the most important factors to affect the coupling yield. One of the most common 'activators' is a combination of N,N-diisopropylcarbodiimide (DIC) and the catalytic auxiliary N-hydroxy-benzotriazole (HOBt). The HOBt presence is primarily to reduce the occurance of side reactions, especially racemisation. DIC reacts with the carboxylic acid of the amino acid to form a highly reactive O-acyl isourea. The O-acyl isourea reacts with HOBt to form an activated benzotriazolyl ester of the amino acid which can readily react with the deprotected amine in the existing peptide chain to form an amide bond (Figure 4.5A).

Other activation chemistries exist, one of them using O-(benzotriazol-1-yl)-1,1,3,3-tetramethyl-uronium hexafluorophosphate (HBTU) and N,N-diisopropylethylamme (DIEA). HBTU does not require the generation of the O-acyl isourea in order to form the benzotriazolyl ester of the amino acid. The incorporation of benzyl protected phosphoamino acids using DIC/HOBt results in incomplete incorporation[207], so HBTU was used for the activation of Fmoc protected phosphor-tyrosine used to synthesise Ct-pY-Fas-DD. The mechanism of amino acid activation is shown in Figure 4.5B. Once the amino acid is activated, the first coupling reaction can be carried out.

The very first coupling reaction in Fmoc SPPS is the coupling of the most C-terminal amino acid to an insoluble support (resin) which contains a specific functional group such as free acids, amides or hydrazide[208]. For Ct-Fas-DD synthesis, a PL-Rink amide resin, containing an amide functional group was chosen in order to create generate a natural amino C-terminus following synthesis. The coupling reaction is shown in Figure 4.5C. The amide group upon the resin attacks the carbonyl group of the activated benzotriazolyl ester forming an amide bond

between the resin and the amino acid. Prior to the second amino acid coupling, the Nα Fmoc group is removed in a process known as deprotection. This is carried out by washing the resin/solid support in the weak base, piperidine, thus exposing the N-terminus of the amino acid that has just been incorporated. The basic properties of piperidine abstracts the acidic proton from the Fmoc fluorenyl ring system resulting in β-elimintation of the Fmoc group from the peptide chain (Figure 4.5D). The next Fmoc protected amino acid is then activated and coupled to this new N-terminus using the same series of reactions[208,209]. The cycle of amino acid coupling and deprotection is repeated until the desired amino acid sequence has been synthesised.

In the case of pY-Ct-Fas-DD, the N-terminal auxiliary group Htmb was additionally coupled to the most N-terminal residue in order to allow for ligation without the requirement for a cysteine at the C-terminus of the junction. For all Fmoc-SPPS resin supports, the resin-peptide link is acid labile. This property enables simultaneous cleavage of the full peptide from the support and removal of side chain protecting groups. This process is done by the addition of trifluoroacetic acid (TFA) supplemented with scavengers such as H_2O and phenol. Scavengers trap and prevent reactive co-products from reacting with the synthesised peptide[208,210]. Following cleavage, the peptide is purified using reverse phase high pressure liquid chromatography (RP-HPLC).

4.1.5 The Htmb auxiliary group enables the ligation of fragments without an N-terminal cysteine at the junction

Native chemical ligation (NCL) refers to the general method of coupling large unprotected peptides to form a natural amide bond at the reaction site. This reaction is illustrated in Figure 4.6. In NCL a thioester-containing peptide reacts with a second peptide that has a cysteine residue at its N-terminus. In an analogous manner to the N-S acyl shift reaction that occurs during intein cleavage, the side chain thiol of the cysteine attacks the carbonyl group of the C-terminal thioester, forming a new thioester-linked intermediate. The thiol moiety can then spontaneously rearrange to form an amide bond[211].

The development of NCL has revolutionised the field of peptide chemistry, greatly extending the size of the peptides which could be generated by SPPS alone. The

reaction is also advantageous as it is a 'one pot' reaction in which the formation of the natural amide bond occurs both in neutral and denaturing aqueous conditions. The ability to carry out the reaction in a denaturing environment permits an increased concentration of reactants to be used and increases the overall rate of reaction[211]. However the requirement for a cysteine residue at the ligation junction is a significant drawback to the technique. Cysteine is the second lowest abundant amino acid in native proteins. Therefore a protein may not have an adequate number of cysteine residues, or they might be located at an inconvenient location in the peptide chain, this greatly limits the application of NCL to native sequences. Moreover, NCL does not perform well when certain amino acid residues are present at the ligation junction. For example β-branched amino acids result in steric hindrance[212] and Asp and Glu cause ligation to occur between side chains rather than in the peptide backbone[213]. In this context it is estimated that only half of the natural amino acids are suitable for efficient NCL[127].

To overcome this problem, the method of auxiliary-mediated NCL was developed. The general strategy is to include at the N-terminus of the C-terminal peptide, a chemical auxiliary that is able to undergo the same reactions as the side chain thiol group of cysteine, but that can be removed from the protein after the ligation. This strategy was initially mentioned by Canne at al[193], highlighting X-Gly or Gly-X ligation sites, and then put into practice by Low et al.[214] and Offer et al.[192,215] who respectively synthesised cytochrome b562 and SH3 domains using an auxiliary-mediated ligation approach. The auxiliary used in this study, 2-hydroxy-3-thio-4-metoxy-benzaldehyde (Htmb) acid, and the mechanism of auxiliary-mediated ligation using this compound are illustrated in Figure 4.7. The adoption of Nα-linked auxiliary has two advantages: first it might, in principle, expand the number of amino acids that can be used at the ligation junction and second, it is broadly compatible with SPPS techniques[214].

A number of different auxiliaries have been developed to improve the yield of the ligation reaction between different combinations of amino acids. When designing an auxiliary, there are two desirable features: first, following addition to a peptide which is still attached to the resin, an auxiliary is required to be able to withstand the strong acid treatment used to finally cleave the synthetic peptide from the resin;

second, it needs to be acid labile to enable successful removal following the ligation reaction. Auxiliaries have been designed around substituted derivatives of benzaldehyde because this framework fits these requirements[192].

The auxiliary used in this study, Htmb, is illustrated in Figure 4.7B. Due to its high reactivity, and in a similar manner to the side chains of natural amino acids, the thiol group of Htmb needs to be protected during peptide synthesis[216]. The protected Htmb, 2-hydroxy-3-[(4-methoxyphenyl)thio]-4-metoxy-benzaldehyde, is shown in Figure 4.7A. The protected Htmb was coupled to the N-terminus of the pY-Ct-Fas-DD peptide prior to the peptide being cleaved from the resin. The first step of auxiliary coupling to the peptide is a nucleophilic addition to give a carbinolamine intermediate that dehydrates to form an imine. Next, sodium borohydride is added to reduce the imine to an amine (Figure 4.8).

The 4-methoxyphenyl protecting group has to be removed from the auxiliary prior to the ligation reaction taking place. The removal (deprotection) of this group prior to ligation adds another step after the elution of the peptide from the solid support. The mechanism of DTNP (2,2'-dithiobis(5-nitropyridine)) deprotection used within this study is shown in Figure 4.9[157]. The first step in the reaction is the formation of a highly reactive DTNP-thioanisole conjugate. The conjugate reacts with the protected sulphur of Htmb to form an unstable sulphonium intermediate that is resolved by the removal of the 4-methoxyphenyl group, while the disulphide bond between the sulphur of Htmb and 2-(5-nitropyridyl) (5 Npys) intermediate group remains. Finally, TCEP is added in excess to reduce the disulphide bond.

Once the peptide is cleaved from the resin and the auxiliary is deprotected, the NCL between the Nt-Fas-DD thioester and Hmb-pY-Ct-Fas-DD can be carried out. As illustrated in Figure 4.7, there are three basic steps in auxiliary-mediated NCL: (1) an initial capture step in which the protein and peptide undergo thioester exchange which links the two peptide chains together via the auxiliary; (2) the intermediate then undergoes two acyl transfer steps, in which the N-terminal fragment is transferred from the auxiliary to the C-terminal fragment forming a terminal secondary amine; (3) the release of the auxiliary by acid treatment generates the native peptide bond[127].

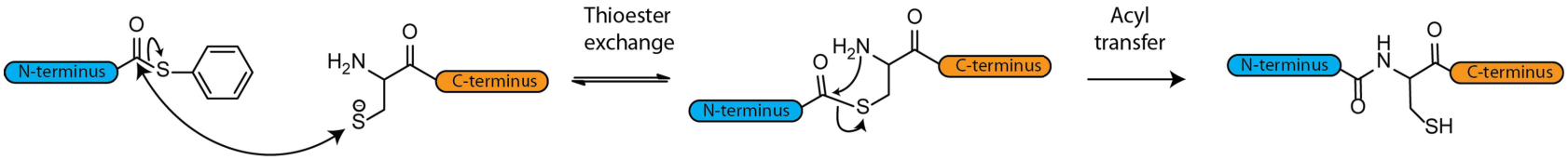

Figure 4.6 Native chemical ligation reaction (NCL)

NCL is the joining of two unprotected peptides, one containing a C-terminal thioester and the other containing a N-terminal cysteine (or cysteine mimic) to form a native amide bond. N-terminal peptide is represented in blue. C-terminal peptide is represented in orange. The unprotected peptides undergo thioester exchange forming a transient thioester linked ligation product, which undergoes acyl transfer to form a native amide bond between the peptides.

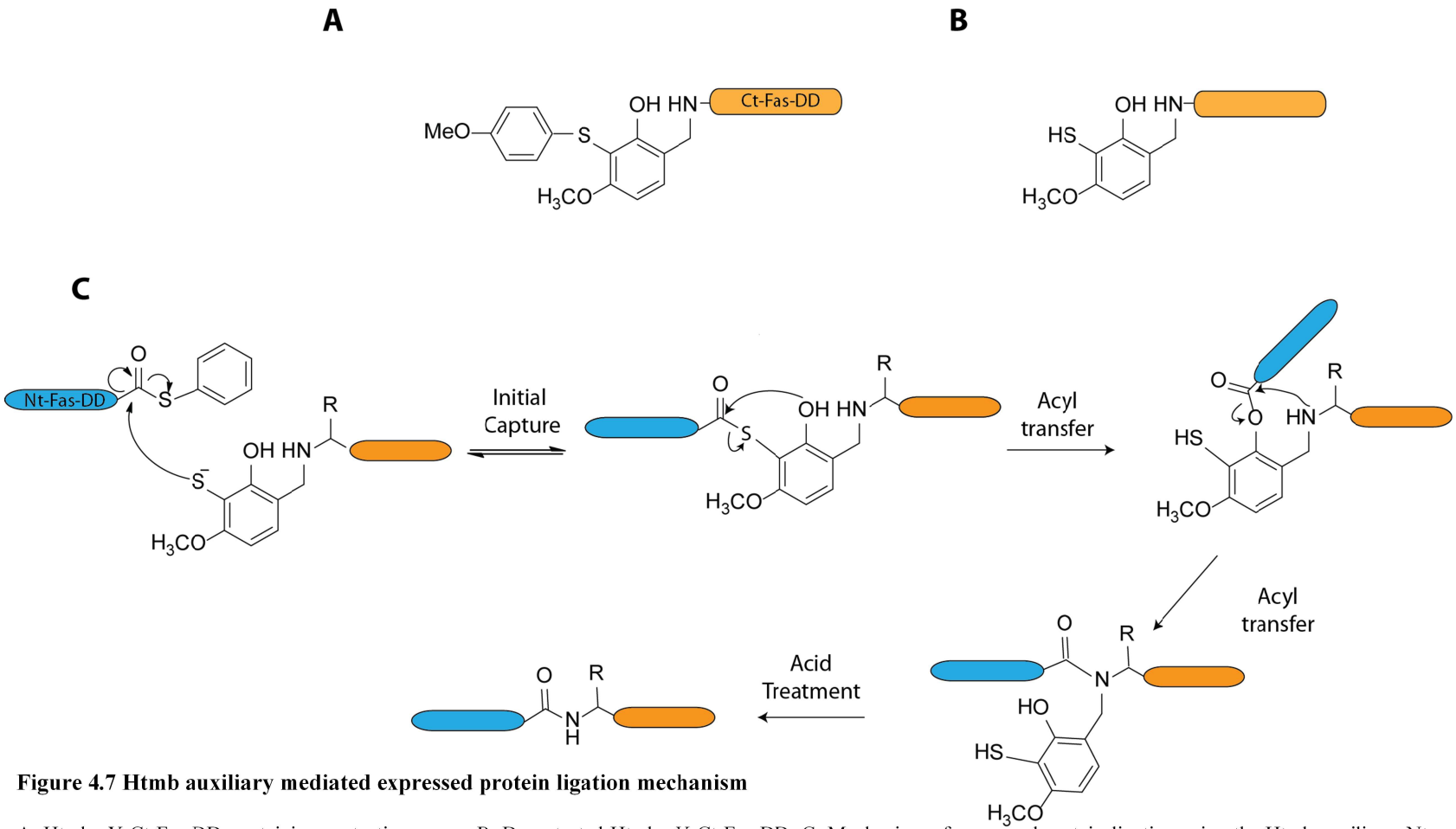

Figure 4.7 Htmb auxiliary mediated expressed protein ligation mechanism

A, Htmb-pY-Ct-Fas-DD containing protecting group. B. Deprotected Htmb-pY-Ct-Fas-DD. C, Mechanism of expressed protein ligation using the Htmb auxiliary. Nt-Fas-DD and pY-Ct-Fas-DD are represented in blue and orange respectively. Peptide and protein undergo thioester exchange, linking the N and C-termini. The acyl group if then transferred along the auxiliary to form a terminal secondary amine. The final amide release is catalysed by an acid treatment which removes the auxiliary from the ligated product.

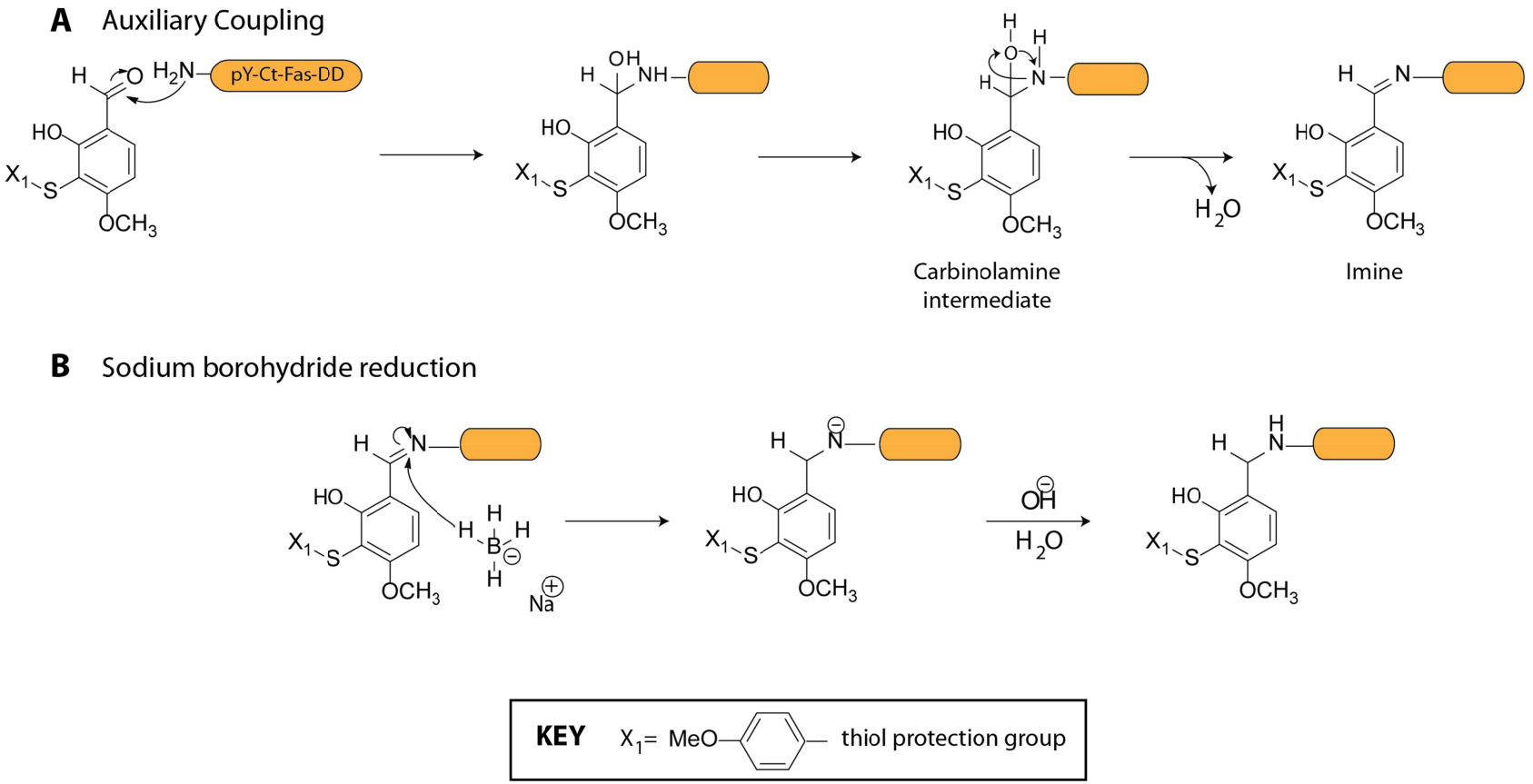

Figure 4.8 Chemical coupling of the Htmb auxiliary to the peptide and sodium borohydride reduction

A, Auxiliary coupling to the peptide. The auxiliary undergoes nucleophilic attack from the amide of the peptide, which results in proton transfer and the formation of a carbinolamide between the auxiliary and the N-terminus of the peptide. Upon the loss of H_2O, the peptide and auxiliary are coupled with an imidium ion forming between the two components. B, Sodium borohydride reduction. The imidium ion is reduced by sodium borohydrate enabling the auxiliary to be attached via the amide of the peptide.

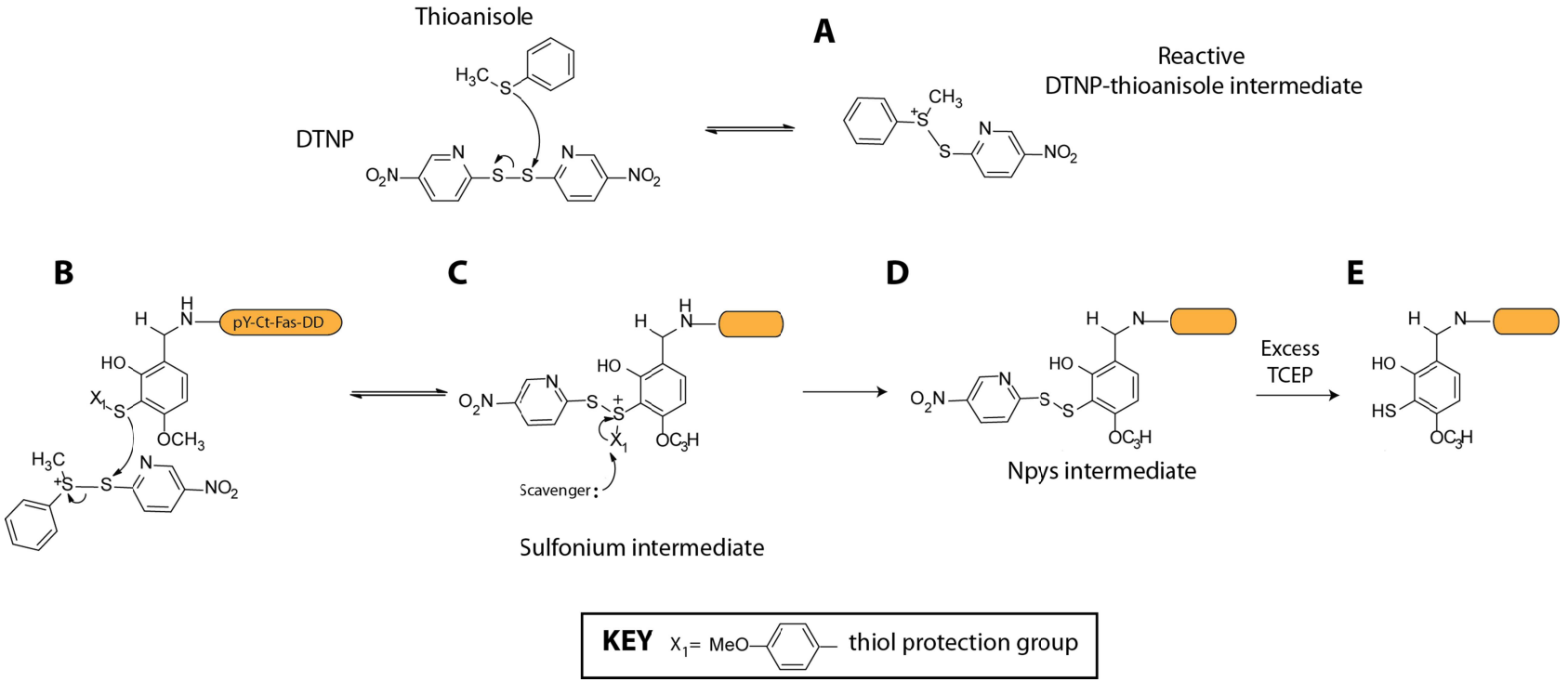

Figure 4.9 Deprotection of auxiliary prior to reaction

Figure adapted from Schroll et al (2012). X_1 corresponds to the protecting group upon the thiol moiety. The thioanisole sulfer attacks the electron deficient disulphide of DTNP, forming a reactive trivalent sulfonium thioanisole 2-(5-nitropyridyl) (Nphys) conjugate (A). The protected cysteine sulfer then induces attack on the reactive sulfer in the conjugate (B). This forms a trivalent solfonium intermediate at the cysteine (C), which ultimately collapses into the auxiliary - Nphys conjugate (D). Upon TCEP reduction, the conjugate collapses into the desired thiol group (E). Mechanism adapted from Schroll et al (2012).

4.1.6 Aims

This part of the thesis documents the semi-synthesis of phosphorylated Y291 Fas-DD using expressed protein ligation (EPL). Our aim was to investigate whether it was feasible to use this methodology to produce samples for structural biology studies, as well as to validate a novel native chemical ligation auxiliary which avoids the need for a cysteine at the ligation junction. Death domains prepared by this method could then be used to investigate the effect of post translational modifications on the structure, dynamics and binding. This work was performed in collaboration with the laboratory of Dr John Offer in the Division of Physical Biochemistry, to exploit the novel methods of peptide ligation which they are aiming to develop.

4.2 N-terminal Fas-DD can be expressed with a good yield but can only be purified after cleavage using denaturing conditions

4.2.1 Cloning of the Nt-Fas-DD-Mxe intein-chitin binding domain construct

To generate a protein construct suitable to undergo expressed protein ligation, the first 67 residues of the Fas-DD (residues 218-285) were cloned into the NEB pTWIN1 expression vector as described in Section 2.4. The DNA template was kindly provided by Dr Diego Esposito and contained the K263A mutation which has been shown to enhance the solubility of Fas-DD constructs. The pTWIN1 vector allows either an N-terminal chitin binding domain and *Ssp* intein or a C-terminal *Mxe* intein (or both) and chitin binding domain (CBD).

In order to insert the N-terminal Fas-DD (Nt-Fas-DD) sequence, the N-terminal *Ssp* intein-CBD was excised from the vector resulting in an Nt-Fas-DD construct containing a C-terminal *Mxe* intein and CBD (Nt-Fas-DD-*Mxe*-CBD). The molecular weight and extinction coefficient of the different protein products that were obtained with this construct were calculated using the EXPASY Protparam server, as shown in Table 4.1.

Table 4.1 Properties of the Nt-Fas-DD-Mxe-CBD expressed protein products

Protein construct	Residues of Fas	Predicted molecular mass (Da)	Extinction coefficient (M^{-1} cm^{-1})
Nt-Fas-DD-Mxe-CBD	218-285	35593	42650
Nt-Fas-DD (with active thioester)	218-285	7852	6990
Nt-Fas-DD (without active thioester)	218-285	7752	6990
Mxe-CBD	-	27858	35660

4.2.2 Expression and purification of N-terminal Fas-DD with a reactive thioester at the C-terminus

E. coli BL21(DE3) Gold expression strain was used for the expression of Nt-Fas-DD-*Mxe*-CBD. Small scale expression tests were performed as described in Section 2.5 assaying expression by SDS-PAGE. Optimal expression was obtained when induced with 0.5 mM IPTG for sixteen hours at 20 ^{o}C. These were the conditions used for large scale expression of the proteins, carried out as described in Section 2.10.2.

Expressed Nt-Fas-DD-*Mxe*-CBD was affinity purified using chitin beads which bind to the C-terminal CBD. Elution of the Nt-Fas-DD thioester from the beads was achieved by benzyl mercaptan-induced intein cleavage (as described in Section 4.1. and Figure 4.3). Column incubation in cleavage buffer was optimal after 16 hours at room temperature. Following this time little uncleaved Nt-Fas-DD-*Mxe*-CBD remained, as assessed by resuspending the chitin beads in SDS-PAGE loading buffer before SDS-PAGE analysis, however only a minimal amount of Nt-Fas-DD eluted from the column.

The most plausible explanation of the minimal elution of cleaved Nt-Fas-DD is that Nt-Fas-DD was binding to the beads. Due to the construct being a truncation of the death domain we would presume that it is unable to fold properly, possibly exposing hydrophobic residues to the solvent and rendering the construct insoluble and/or able to interact strongly with the bead matrix once the *Mxe* intein and CBD had been removed. In order to elute Nt-Fas-DD from the chitin column, cleavage was carried out in denaturing conditions (1.5 M urea for cleavage, and 8 M urea washes

following cleavage). Denaturation enabled the elution of the Nt-Fas-DD benzyl mercaptan thioester from the column. SDS-PAGE analysis of optimised Nt-Fas-DD purification is shown in Figure 4.10A. The presence of the thioester was confirmed by QTOF mass spectrometry as shown in Figure 4.10B.

The elution and washes from the chitin column were pooled and concentrated by centrifugal concentration. A final clean-up step was done by semi-preparative C18-RP-HPLC, the chromatogram is shown in Figure 4.10C. The mass spectrum of purified Nt-Fas-DD benzyl mercaptan thioester is shown in Figure 4.10D. Between 3 and 5 mg of Nt-Fas-DD thioester was purified for each litre of bacterial culture.

4.3 The C-terminal pY-Fas-DD peptide was synthesised by SPPS

The 38-mer phospho-tyrosine 291 containing C-terminal Fas-DD (Ct-pY-Fas-DD) peptide (residues 286-323) was synthesised by FMOC-SPPS on a PL-Rink amide solid support as described in Section 2.10.1. The synthesis was carried out in five stages. At each stage a small portion of resin was cleaved and analysed by C18-RP-HPLC and MALDI-MS in order to confirm that the correct peptide had been obtained; this is illustrated in Figure 4.11. In order to reduce the formation of regular secondary structure elements, two pseudo-proline units were incorporated into the peptide. The location of the amino acids substituted with pseudo-proline dipeptides are highlighted in bold in the peptide sequences shown in Figure 4.11J. The initial 32-mer was synthesised with microwave coupling using DIC/HOBt. The most N-terminal six amino acids were incorporated onto the chain using HBTU/DIEA coupling. DIC activation results in incomplete incorporation of benzyl-protected pY as discussed in Section 4.1.4.

The Htmb auxiliary was coupled to the deprotected N-terminus of the full-length peptide using microwave coupling, followed by sodium borohydride treatment to reduce the imine group formed during the coupling reaction (Figure 4.8 and Figure 4.9). After auxiliary coupling, the peptide was cleaved from the resin and the side chain protecting groups removed using TFA plus scavengers. Finally, the peptide was purified by semi-preparative C18-RP-HPLC as described in Section 2.10.1.

Fractions containing pure Ct-pY-Fas-DD peptide were pooled and lyophilised prior to auxiliary deprotection.

Deprotection of the Htmb auxiliary (Figure 4.9) was obtained by incubation with DTNP as described in Section 2.10.2 and assayed by C18-RP-HPLC (Figure 4.11G-I). The deprotected product could be detected after reduction with TCEP (Figure 4.11H and I). It should be noted that the MALDI-MS of the final product shows two species corresponding to the predicted masses of peptides both with and without the auxiliary, despite appearing pure judging by the RP-HPLC profile; we believe this is due to the auxiliary coming off the peptide during ionisation. The deprotected peptide was purified by semi-preparative C18-HPLC. Fractions containing one species of peptide were pooled and lyophilised. The C18-RP-HPLC chromatogram and ESI-QTOF mass spectrum of the pure Htmb-Ct- pY-Fas-DD peptide is shown in Figure 4.12. Following deprotection, the overall peptide yield was 1.5%.

4.4 pY-Fas-DD can be obtained by auxiliary mediated expressed protein ligation

4.4.1 pY-Fas-DD is produced by auxiliary mediated EPL at low yield

To perform the ligation, Nt-Fas-DD thioester and Htmb-Ct-pY-Fas-DD peptide were mixed to a final concentration of 2 mM each in pH 7 ligation buffer, as detailed in Section 2.10.3. The ligation reaction was monitored over time using analytical RP-HPLC. Product peaks were identified by MALDI-TOF-MS as illustrated in Figure 4.13. A peak (peak labelled 4) corresponding to the ligated pY-Fas-DD began to form within two hours of the reaction and marginally increased up until the eight hour time point. As can be seen from Figure 4.13, a peak (peak labelled 3) which is not the desired product begins to form. This peak corresponds to the hydrolysis product of the Nt-Fas-DD thioester, showing that the thioester start material for the ligation is being depleted by hydrolysis.

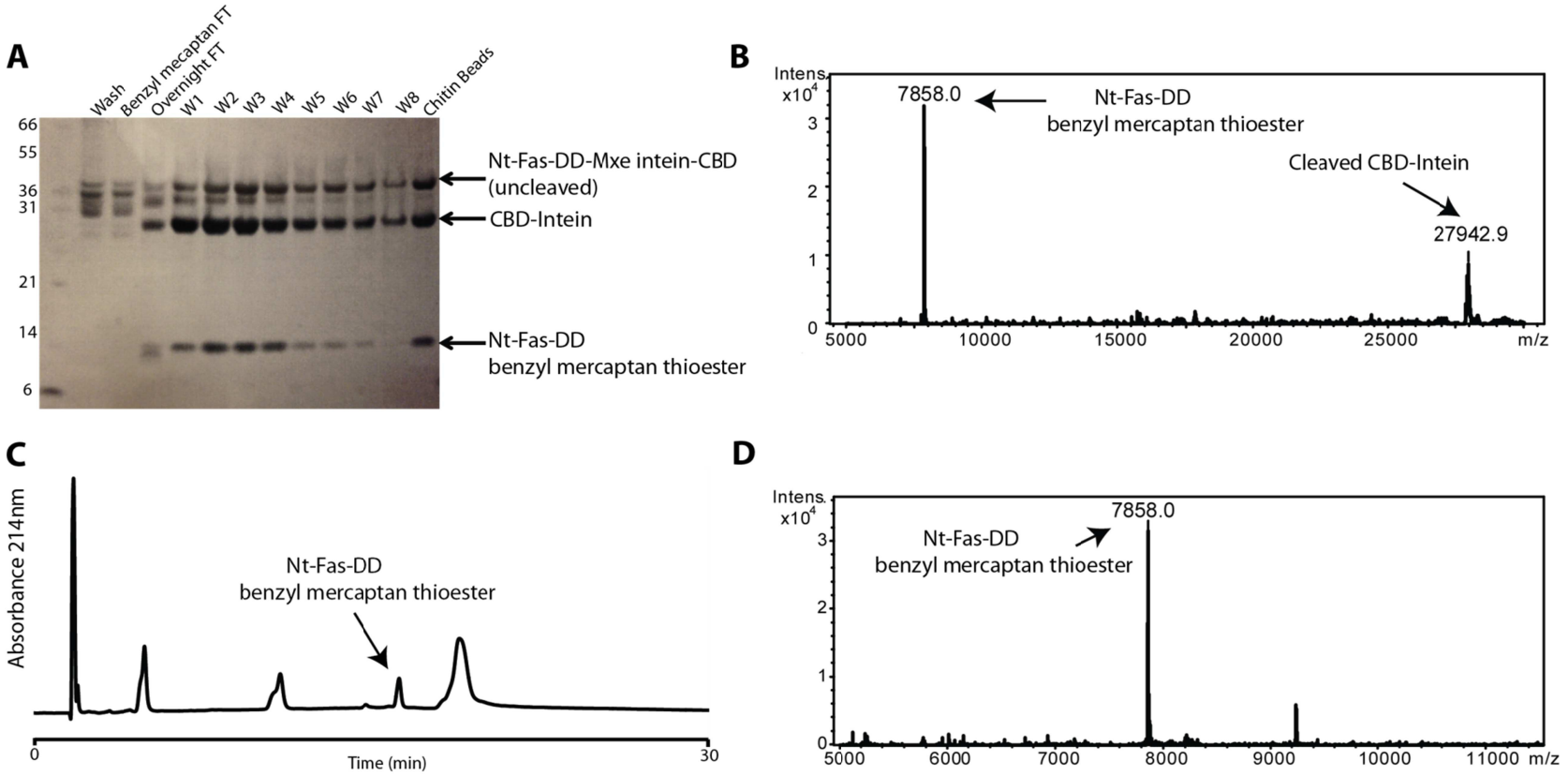

Figure 4.10 Purification of Nt- Fas-DD benzyl mercaptan thioester

A. SDS-PAGE of Nt-Fas-DD chitin purification, highlighting the three species remaining following benzylmercaptan cleavage; uncleaved start protein (Nt-Fas-DD-Mxe intein-CBD), cleaved intein-CBD and the released benzyl mercaptan thioester. Wash refers to the initial wash of non-specifically bound impurities from the lysis. Benzyl mercaptan flowthrough (FT) corresponds to when the column was equilibrated with chitin cleavage buffer. Overnight flowthrough corresponds to elution of buffer incubated upon the column overnight. W1-W8 corresponds to urea buffer washes (W). Chitin bead sample is shown to illustrate the difficulty removing all the sample from the beads. B. Q-TOF mass spectrum following chitin column elution and PD10 desalting. C. RP-HPLC of chitin column fractions ran upon a C18 column using a 35-70% gradient over thirty minutes. The elution profile was monitored by UV absorbance at 214nm. D. Q-TOF mass spectrum of purified Nt-Fas-DD.

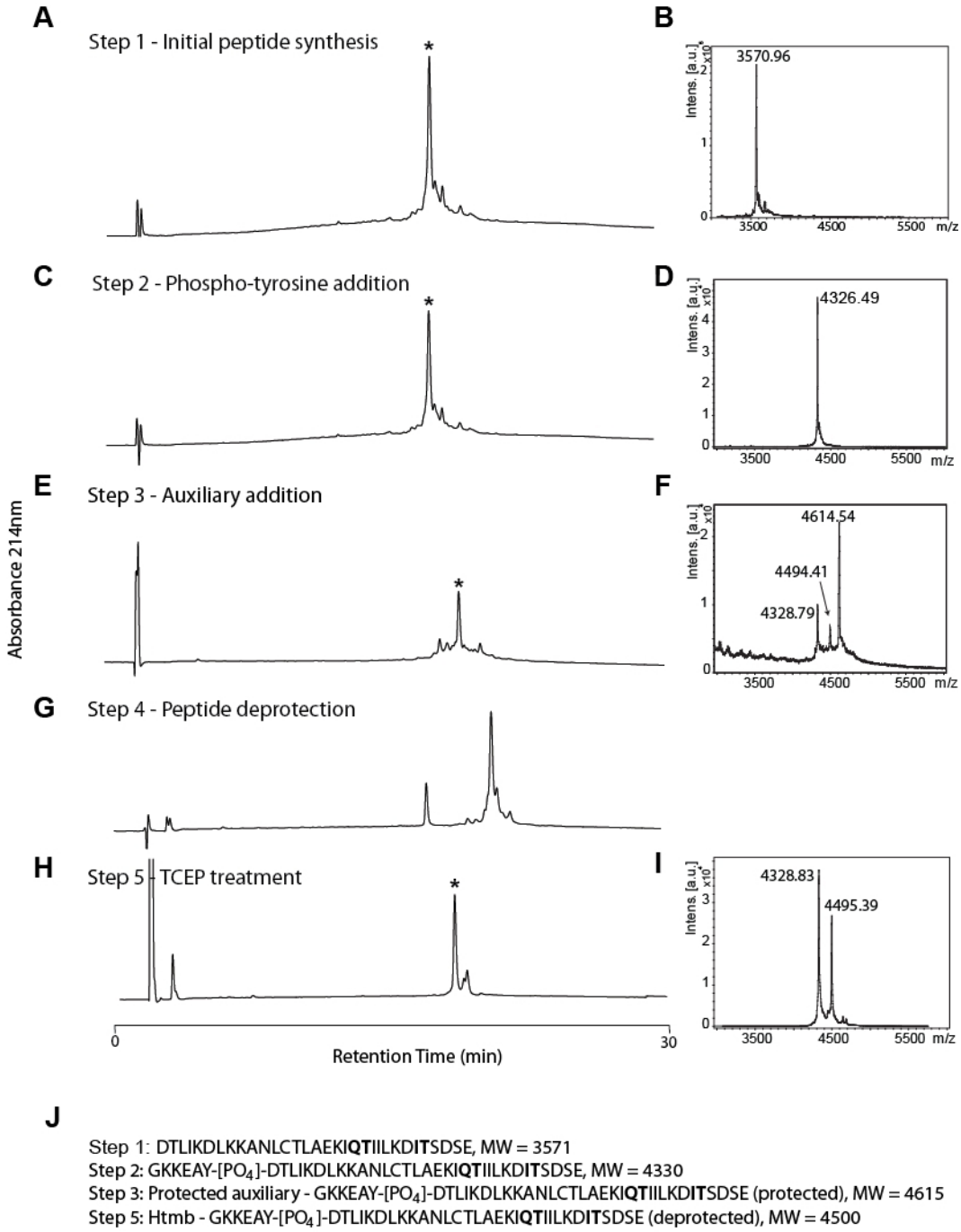

Figure 4.11 Sequential Ct-Fas-DD synthesis and auxiliary addition

A, C, F, G, H show C18 RP-HPLC profiles from each step in the C-terminal peptide synthesis. A gradient of 20-70%B over thirty minutes was used with the absorbance recorded at 214nm. The step of the synthesis is indicated above the HPLC profile. B, D, F, I, MALDI-TOF-MS results for each of the HPLC profiles.* denotes the HPLC peak corresponding to the mass spectrometry result illustrated. J, shows the peptide sequence and expected mass at each step in the synthesis. Amino acids in bold were coupled as Fmoc pseudo-proline amino acids to reduce secondary structure. During the mass spectrometry analysis, the auxiliary comes off the peptide, therefore the non- auxiliary and or deprotected mass of the peptide and auxiliary is observed in F and I

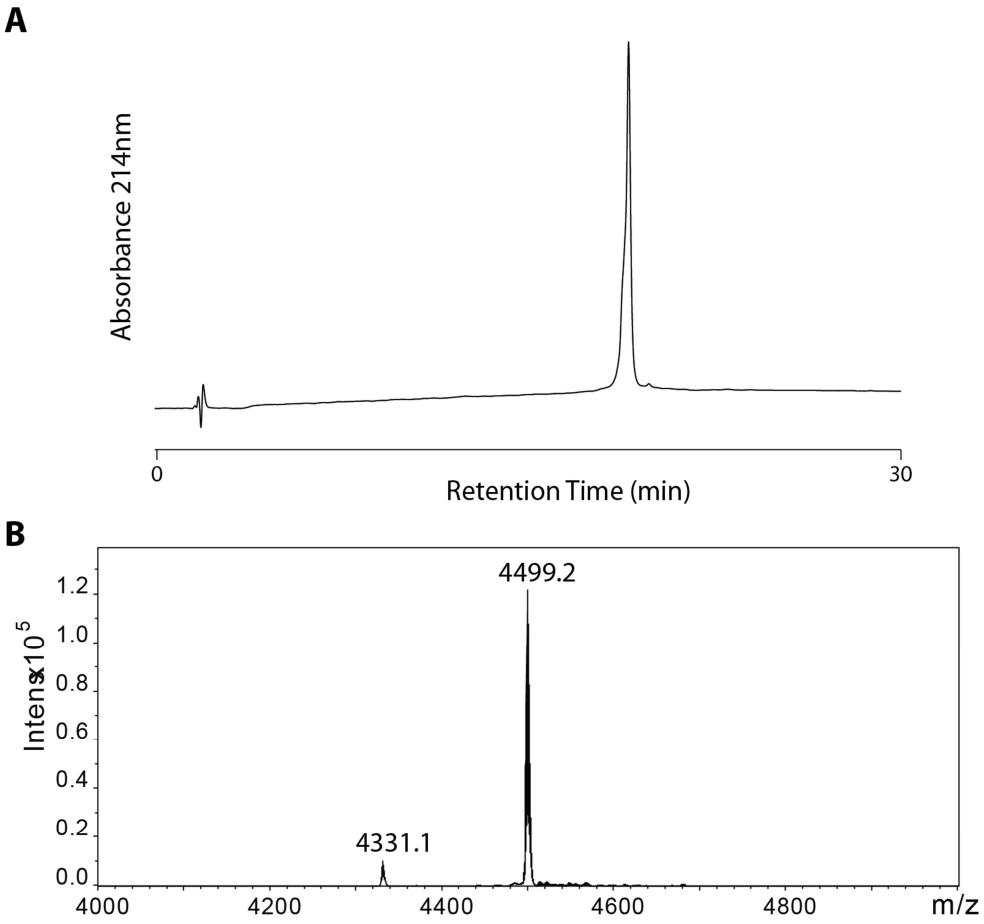

Figure 4.12 Pure preparation of Htmb-pY-Ct-Fas-DD C-terminal phosphopeptide.

A. A typical C18 RP-HPLC profile of pure Htmb-pY-Ct-Fas-DD. A gradient of 20-70%B over thirty minutes was used with the absorbance recorded at 214nm. B, QTOF mass spectrum showing the pure mass of the phosphopeptide (4500) as well as a peak corresponding to the loss of the auxiliary in the instrument (4331).

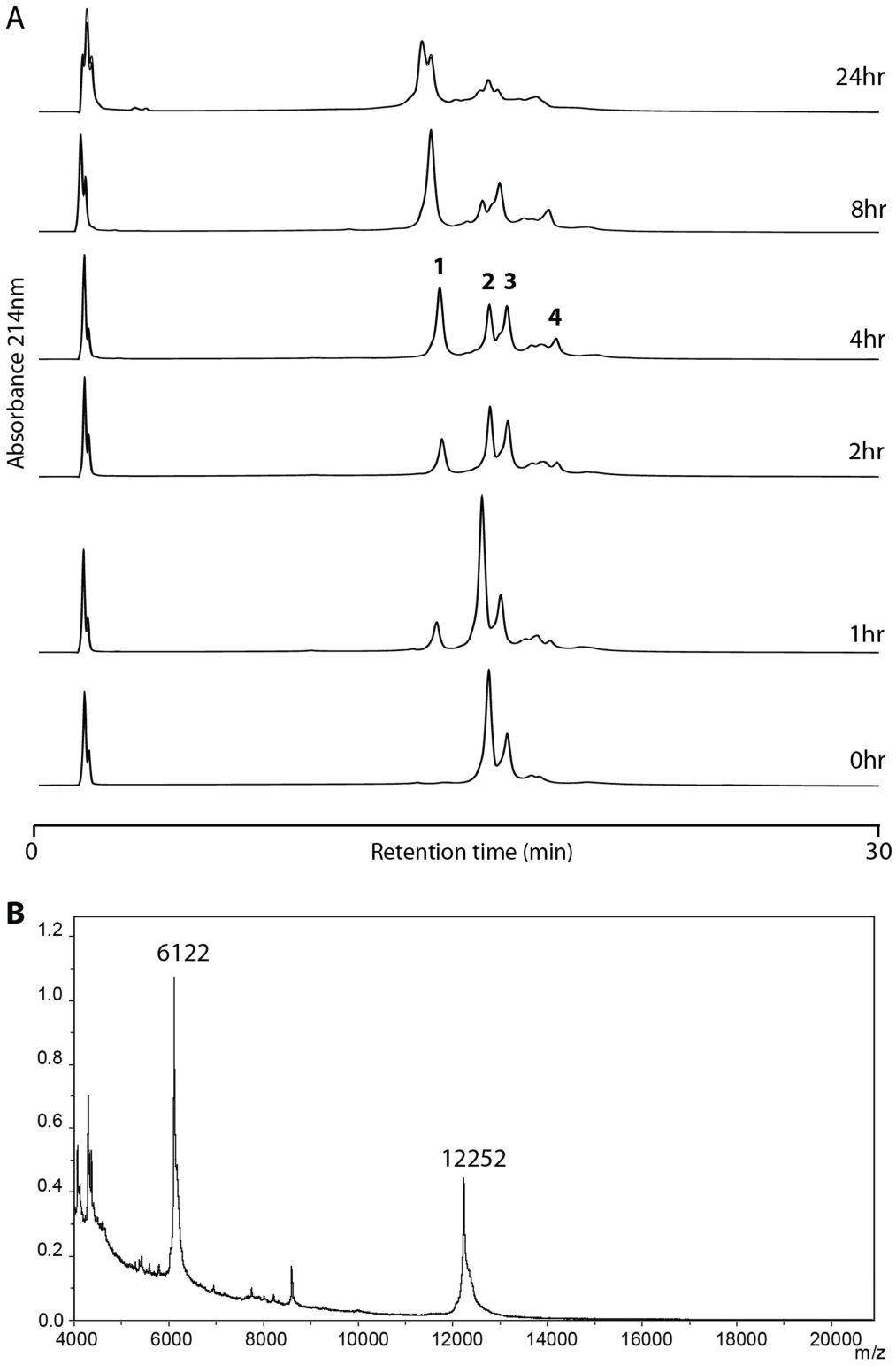

Figure 4.13 pY291-Fas-DD can be obtained using auxiliary mediated EPL although a lot of N-terminal start material is lost to hydrolysis

A, Analytical C18 HPLC of the time-course for a ligation reaction between 1mM N-terminal Fas-DD and 1mM C-terminal Fas-DD phosphopeptide with TCEP in degassed 200 mM NaH_2PO_4 and 6 M Guanidine chloride at pH 7.5. Peaks are numbered corresponding to the species that were present; 1, hydrolysed N-terminal Fas-DD thioester, 2, N-terminal Fas-DD thioester, 3, C-terminal Fas-DD phosphopeptide, 4, ligated phospho-Y291-Fas-DD product B, MALDI-TOF MS of the product. 1^+ and 2^+ ions can be observed, 12,252 and 6122 respectively.

4.4.2 Attempts to optimise the ligation reaction were not successful

The initially selected ligation conditions led to the formation of the product, but considerable hydrolysis of the N-terminal Fas-DD thioester as well. In order to minimise hydrolysis I performed the reaction in an organic solvent and explored variation of the pH.

It has previously been reported that ligation reactions can be carried out in the presence of high concentrations of organic solvents[217–219], and that this could reduce the level of hydrolysis observed. To perform the ligation in organic solvent, Nt-Fas-DD thioester and Htmb-Ct-pY-Fas-DD were mixed to a final concentration of 4 mM each in a ligation buffer consisting of 80% N-methyl-2-pyrrolidone (NMP) and 20% ligation buffer v/v. The N and C termini were solubilised and mixed in the 20% ligation buffer prior to combing with the NMP. The reaction was monitored over time by analytical RP-HPLC. As can be seen from Figure 4.14, no ligation occurred in high solvent conditions. After six hours, the ligation reaction was diluted 1:2 with ligation buffer at pH 7, reducing the NMP concentration to 40% v/v. Reduction of the NMP concentration did not result in ligation either, however by 24 hours, a peak corresponding to hydrolysed N-terminal thioester could be observed.

The ligation reactions discussed above were all at pH 7. We hypothesised that increasing the pH might slow the hydrolysis. A ligation was carried out in which 2 mM Nt-Fas-DD was mixed with 2 mM Htmb-Ct-pY-Fas-DD in ligation buffer at pH 8 as described in Section 2.10.3. The reaction was monitored over a time course in which the ligation was followed by analytical RP-HPLC and products analysed by MALDI-TOF-MS. Increasing the pH of the reaction did not improve either product formation or decrease the amount of hydrolysis observed when compared to the same reaction at pH 7 (data not shown). Although this observation suggests that the thioester hydrolysis maybe base-catalysed, the pH of the ligation could not be reduced below pH 7 as this value is below the pKa of the auxiliary. Ligation reactions from this point were maintained at pH 7.

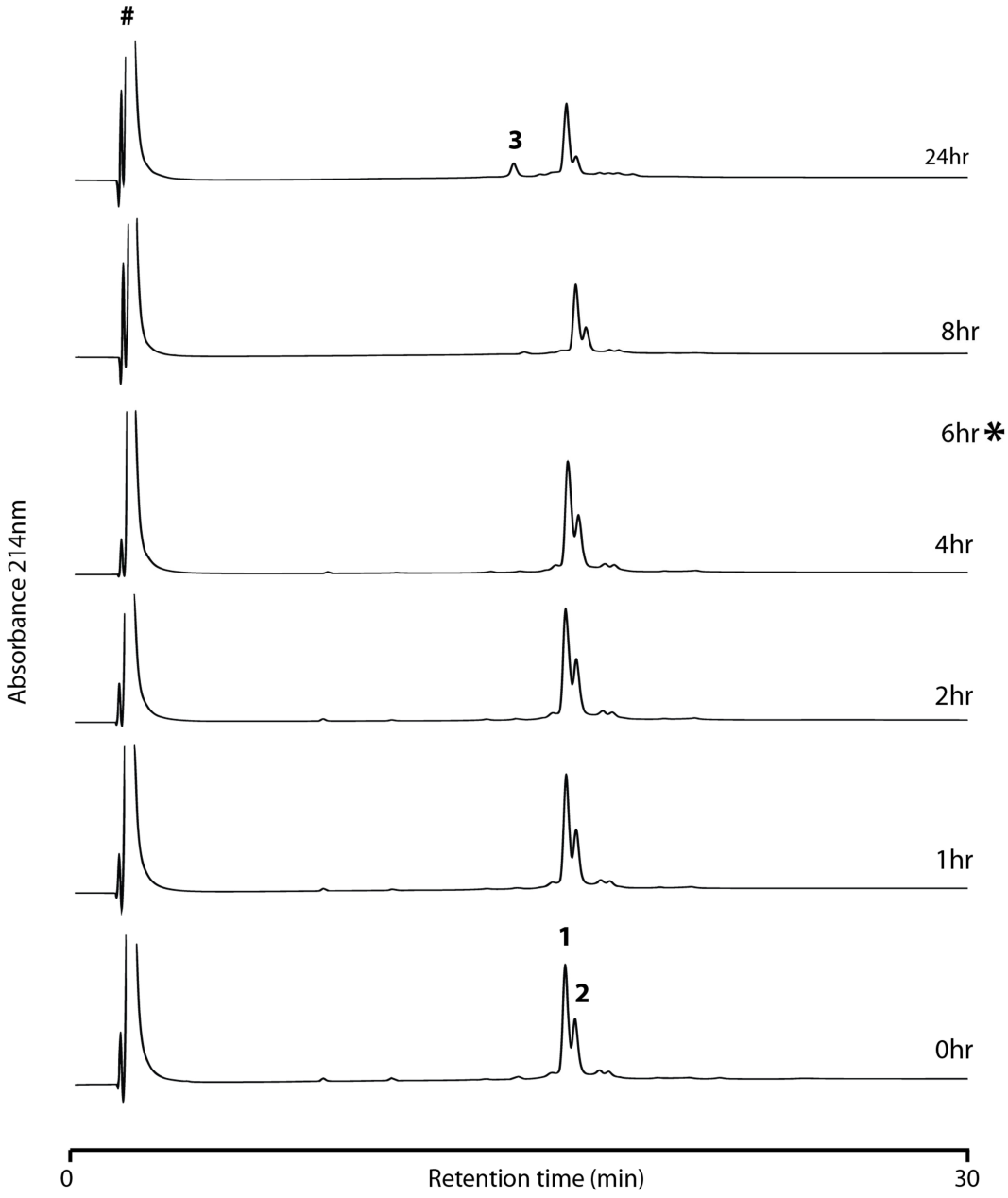

Figure 4.14 Hydrolysis is prevented by carrying out the ligation in the solvent NMP however the ligation reaction does not occur.

Analytical C18 HPLC of the time-course for a ligation reaction between 4mM N-terminal Fas-DD and 4mM C-terminal Fas-DD phosphopeptide in 80% NMP (N-methyl-2-pyrrolidone) with TCEP in degassed 200 mM NaH_2PO_4 and 6 M Guanidine chloride at pH 7.5 and 30^{o}C. Due to lack of ligation, reaction was diluted to 40% NMP using phosphate buffer at 6hours. This only encouraged hydrolysis. Peaks are numbered corresponding to the species that were present: 1, N-terminal Fas-DD thioester, 2, C-terminal Fas-DD phosphopeptide, 3, hydrolysed N-terminal Fas-DD thioester. #, buffer/NMP peak

4.5 Introduction of a solubility tag in Nt-Fas-DD simplifies purification and a mutation increases ligation yield

4.5.1 Fusion of maltose binding protein to Nt-Fas-DD makes the protein soluble after cleavage, increasing purification yield

4.5.1.1 Cloning of MBP- Nt-Fas-DD-Mxe-CBD construct

With the aim of increasing the solubility of the Nt-Fas-DD thioester, maltose binding protein (MBP) was inserted at the N-terminus of the Nt-Fas-DD construct. MBP is well known for its ability to make protein constructs soluble in solution[220]. Therefore the aim was to create a soluble Nt-Fas-DD construct which would increase the yield of the protein purified from the chitin beads and simplify the purification protocol.

MBP was amplified from the pNIC-MBP vector developed at the Oxford site of the Structural Genomics Consortium[221]. The construct contains an N-terminal hexa-histidine tag, MBP and a tobacco-etch virus protease cleavage site, all these features were inserted into pTWIN-Nt-Fas-DD using the exponential megaprimer technique followed by DNA ligation as described in section 2.4.5. The protein construct generated is illustrated in Figure 4.15 with the predicted properties shown in Table 4.2. Inserting the H_6-tag and TEV protease site along with the solubility tag would enable the MBP tag to be removed from the ligated pY-Fas-DD product following *in vitro* protein folding after ligation using the TEV cleavage protocol outlined in Section 2.6.4.

Table 4.2 Properties of H_6-MBP-TEVp-Nt-Fas-DD-Mxe-CBD expressed protein products

Protein construct	Residues of Fas	Predicted molecular mass (Da)	Extinction coefficient (M^{-1} cm^{-1})
MBP-Nt-Fas-DD-Mxe-CBD	218-285	78362	110490
MBP-Nt-Fas-DD (with active thioester)	218-285	50610	74830
MBP-Nt-Fas-DD (without active thioester)	218-285	50510	74830
Mxe -CBD	-	27858	35660

4.5.1.2 MBP-Nt-Fas-DD can be purified in non-denaturing buffer with good yield

E. coli BL21(DE3) Gold cells were used for the expression of MBP-Nt-Fas-DD-Mxe-CBD. An expression test was carried out and assayed by SDS-PAGE as described in Section 2.5.1. The addition of the MBP solubility tag did not alter the expression profile observed for Nt-Fas-DD-Mxe-CBD. Optimal expression continued to be achieved with induction using 0.5 mM IPTG for sixteen hours at 20 ^{o}C.

Expressed MBP-Nt-Fas-DD-Mxe-CBD was affinity purified using chitin beads. Intein-mediated cleavage of the construct was induced by incubation of the column in cleavage buffer. The addition of MBP to the construct did not affect the rate of intein-mediated cleavage of the construct (shown in Figure 4.16A). SDS-PAGE analysis of the elution of MBP-Nt-Fas-DD after overnight cleavage (Figure 4.16B) shows a great improvement compared to a similar sample with the initial Nt-Fas-DD construct (Figure 4.10A). The MBP tag had therefore improved the solubility of Nt-Fas-DD and reduced its affinity for the bead matrix.

As MBP-Nt-Fas-DD was no longer eluted from the chitin column in buffer containing urea, pooled elution and wash fractions could be concentrated by lyophilisation. To mitigate problems with semi-preparative RP-HPLC, such as construct aggregation and buffer salt crystallisation, the lyophilised MBP-NT-Fas-DD was resuspended in H_2O and desalted using a PD10 size-exclusion column equilibrated in 10 mM HCl. The final clean up step after desalting was carried out using semi-preparative C18-RP-HPLC. The chromatogram and ESI-QTOF-MS analysis of a pure fraction are shown in Figure 4.16C and D. As a result of the introduction of the desalting step, the resolution of the peaks in the RP-HPLC was improved, allowing the separation of the MBP-Nt-Fas-DD thioester from the uncleaved MBP-Nt-Fas-DD-Mxe-CBD. 13 mg of MBP-Nt-Fas-DD thioester was purified per litre of *E.coli* culture, thereby the insertion of the MBP tag had improved the yield of purified active thioester by nearly three fold.

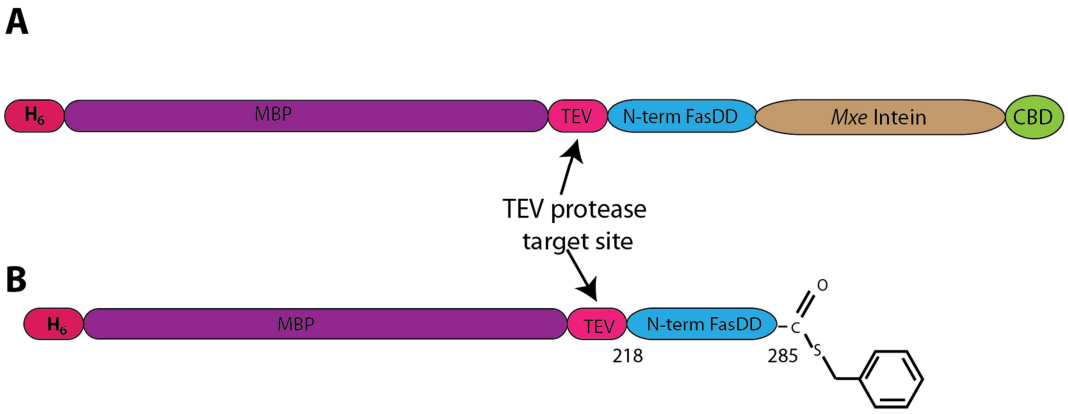

Figure 4.15 – Schematic representation of MBP-Nt-Fas-DD construct.

The MBP solubility tag was cloned N-terminal to Nt-Fas-DD to improve solubility. A and B; represent the MBP-Nt-Fas-DD construct cloned using the NEB pTWIN1 vector and the benzyl mercaptan thioester of this construct produced following on column cleavage. H_6 – hexahistidine tag, MBP – maltose binding protein, TEV – recognition sequence for TEV protease, CBD – chitin binding domain.

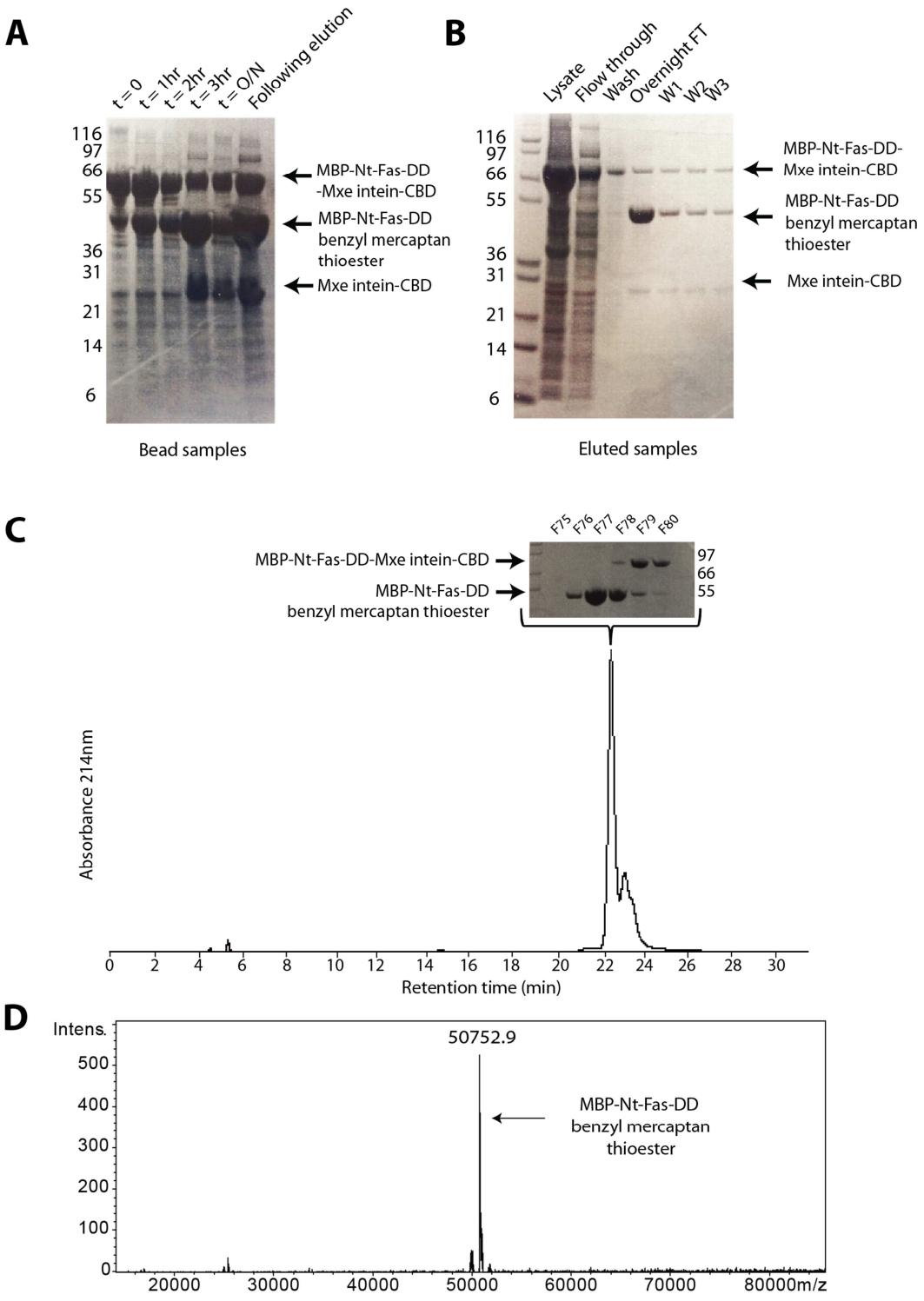

Figure 4.16 Purification of MBP-Nt-Fas-DD

A, SDS-PAGE analysis of samples corresponding to bead samples taken at hour (hr) timepoints (t) once chitin cleavage buffer had been put onto the column and following elution and washes of the column, illustrating there was still protein on the beads. 15µl samples of the chitin beads were taken and denatured. B, SDS-PAGE analysis of MBP-Nt-Fas-DD chitin purification, the three resulting species are highlighted. Overnight flowthrough corresponds to the elution of buffer incubated upon the column overnight. W1-W3 corresponds to buffer washes (W) to collect the rest of the sample. C, semi-preparative C18 RP-HPLC of desalted chitin column pooled elution and wash. The elution profile was monitored by UV absorbance at 214nm, using a method 15-35%B in 5minutes, followed by 35-70%B in thirty minutes. SDS-PAGE analysis of fractions (F) corresponding to the peaks is shown above the elution profile. D, Q-TOF mass spectrum of fraction 76.

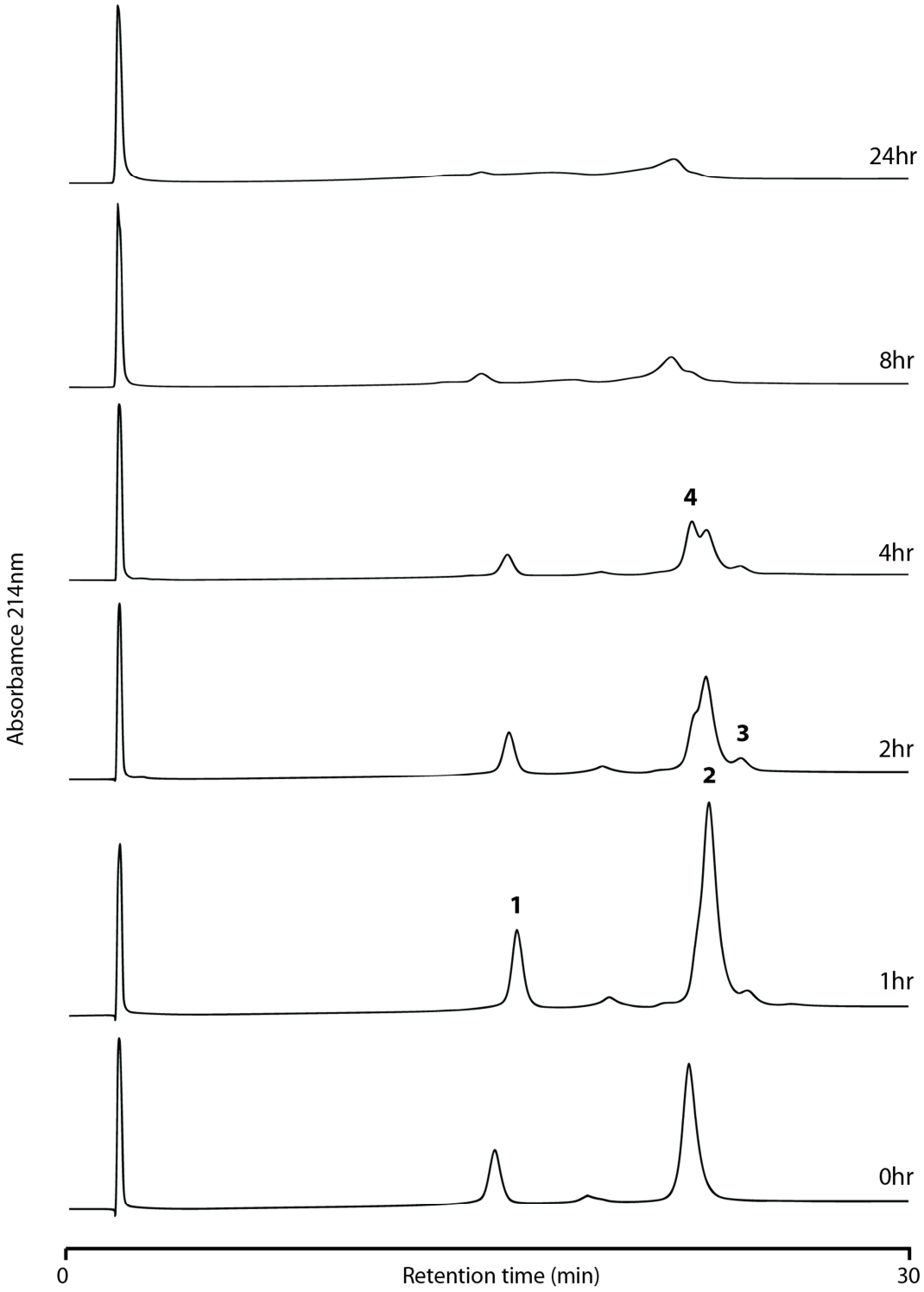

Figure 4.17 MBP-N-terminal Fas-DD construct does not sufficiently improve the ligation but causes solubility problems

Analytical C4 HPLC (gradient: 30-60% B in 30 minutes) of the time-course for a ligation reaction between 1mM N-terminal MBP-Fas-DD and 1mM C-terminal Fas phosphopeptide with TCEP in degassed 200mM NaH_2PO_4 and 6 M Guanidine chloride at pH7. Peaks are numbered corresponding to the species that were present; 1, Htmb-pY-Ct-Fas-DD, 2, Nt-MBP-Fas-DD, 3, Ligated pY291 MBP-Fas-DD product, 4, hydrolysed Nt- MBP-Fas-DD

4.5.2 MBP-Nt-Fas-DD also undergoes hydrolysis during ligation

To perform the ligation, MBP-Nt-Fas-DD thioester and Htmb-Ct-pY-Fas-DD peptide were mixed to a final concentration of 1 mM each in pH 7 ligation buffer, as detailed in Section 2.10.3. The reaction was monitored over time by analytical RP-HPLC and product peaks identified by QTOF-MS, as illustrated in Figure 4.17. A peak corresponding to the ligated phospho-Y291-Fas-DD product began to form by two hours but after this time the MBP-Nt-Fas-DD thioester started hydrolysing and the ligation did not proceed further.

It is relevant to notice that the relative intensity of the peaks in Figure 4.17 at 0 hours is very different to the one observed in Figure 4.12. This difference shows that I inadvertently added a lower amount of Htmb-Ct-pY-Fas-DD in the former case. According to Le Chatelier's Principle, the lower loading should have shifted the equilibrium towards hydrolysis instead of ligation, so perhaps at equimolar concentrations the outcome might have been better. Nevertheless, it is possible to conclude that whilst the presence of MBP greatly improves the yield of N-terminal fragment, the ligation reaction does not proceed to completion and the thioester readily undergoes hydrolysis limiting the reaction yield.

4.5.3 The H285G mutation improves the yield of the ligation reaction

Previous studies report that peptides with histidine or glycine thioesters show better ligation yields than other amino acids[193,194,222]. As our ligation using the histidine thioester had demonstrated limited success, we decided to attempt the ligation with a glycine thioester instead. Histidine 285 is located in the loop between helices α4 and α5, and it is not conserved in other death domains, suggesting that a His-Gly substitution should not cause major disruption in the folding of the domain.

4.5.3.1 MBP-Nt-Fas-H285G-Mxe-CBD has very slow intein cleavage kinetics

The H285G mutation was introduced into the MBP-Nt-Fas-DD-Mxe-CBD expression vector by linear cyclic amplification as described in Section 2.4.5. Properties of the new construct are shown in Table 4.3. BL21 (DE3) Gold *E. coli* cells were used for the expression of MBP-NT-Fas-DD-H285G. An expression test assayed by SDS-PAGE was carried out as described in Section 2.5.2. The insertion of the H285G mutation did not alter the expression profile of MBP-Nt-Fas-DD

construct, optimal expression still being observed when expressed with 0.5 mM IPTG for sixteen hours at 20 ^{o}C.

Table 4.3 Properties of H_6-MBP-TEVp-Nt-Fas-DDH285G-Mxe-CBD expressed protein products

Protein construct	**Residues of Fas**	**Predicted molecular mass (kDa)**	**Extinction coefficient (M^{-1} cm^{-1})**
MBP-TEVp-Nt-Fas-DD-H285G-Mxe -CBD	218-285	78285	110490
MBP-Nt-Fas-DD H285G (with active thioester)	218-285	50530	74830
MBP-Nt-Fas-DD H285G (without active thioester)	218-285	50430	74830
Mxe -CBD	-	27858	35660

Although expression of the protein was not affected by the H285G mutation, the performance of intein-mediated cleavage was extremely poor. Figure 4.18A shows SDS-PAGE analysis of the fractions taken from chitin column purification following overnight incubation with chitin cleavage buffer. Reports show that glycine at this position reduces the rate of intein cleavage. NEB literature documents that after sixteen hours incubation at room temperature, only 40% of a protein with a C-terminal glycine was cleaved, compared to 80-95% cleavage with a C-terminal histidine. However, cleavage of up to 60% of the glycine C-terminal construct can be achieved with incubation times of over 40 hours[223].

To optimise the on-column cleavage of MBP-Nt-Fas-DD-H285G-Mxe-CBD, a chitin column loaded with MBP-Nt-Fas-DD-H285G-Mxe-CBD was incubated in chitin cleavage buffer for 60 hours with samples of the beads being taken at specified time points. SDS-PAGE analysis of these samples is shown in Figure 4.18B. By 60 hours, a large proportion of the loaded MBP-Nt-Fas-DD H285G thioester had been formed. SDS-PAGE analysis of fractions from the optimal chitin purification of MBP-Nt-Fas-DD-H285G-Mxe-CBD is shown in Figure 4.18C. Incubation of the

column for 72 hours resulted in an equivalent amount of reactive thioester as was observed for the corresponding wild type construct during overnight cleavage. Elution and wash fractions were pooled, lyophilised, desalted and purified by semi-preparative C18-RP-HPLC in the same manner as for the wild type construct. The RP-HPLC chromatogram and QTOF-MS spectra for purified fractions are shown in Figure 4.18D-F. The fractions and mass spectra make apparent the difficulty separating cleaved and non-cleaved MBP-Fas-DD-H285G constructs using a C18 column, which was apparent for the wild type construct also. It is possible that columns with lower hydrophobicity would be more suitable for this purpose due to the less hydrophobic properties of this construct. Only the fractions containing the desired thioester species were used for the ligation reactions. 7 mg of active MBP-Nt-Fas-H285G thioester were purified per litre of *E.coli* culture.

4.5.3.2 Ligation of MBP-Nt-Fas-DD-H285G, increases yield but hydrolysis still competes

To perform the ligation reaction, MBP-Nt-Fas-DD H285G thioester and Htmb-Ct-pY-Fas-DD peptide were mixed to a concentration of 1 mM each in ligation buffer at pH 7, as detailed in Section 2.10.3. The reaction was monitored over time by analytical RP-HPLC and the product peaks identified by QTOF-MS, as illustrated in Figure 4.19. A peak corresponding to the ligated MBP-pY291-Fas-DD product began to form much more rapidly than in the previous ligation reactions. A product peak more than half the area of that corresponding to the MBP-Nt-Fas-DD H285G thioester had formed by two hours. The amount of ligated product increased until four hours, after this point thioester hydrolysis became the predominant reaction.

To confirm that the MBP-pY291-Fas-DD product was ligated by an amide bond and not a thioester, an aliquot of the four hour time point was taken and reduced with hydroxylamine. This test confirmed that the product peak was the final product and not an intermediate species (shown in Figure 4.7C). Hydroxylamine is a strong reducing agent, therefore would reduce and non-covalently bonded product or unreacted thioester. By analytical RP-HPLC, the pY291 product peak remained unchanged following reduction however the remaining MBP-Nt-Fas-DD H285G thioester had all been converted into the hydrolysed product. These RP-HPLC traces can be seen in the appendix.

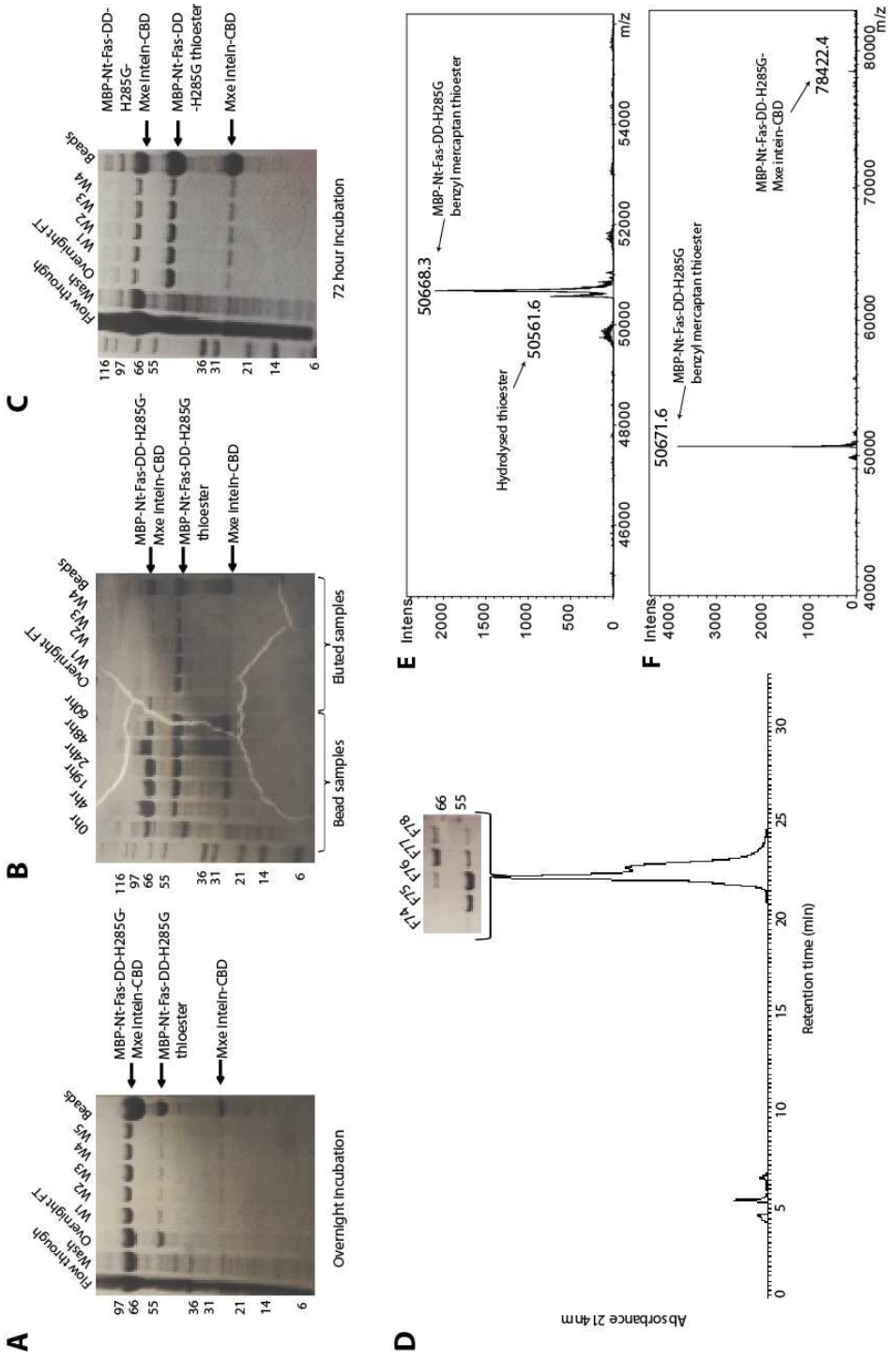

Figure 4.18 Purification Optimisation of MBP-N-terminal Fas-DD-H285G

A, SDS-PAGE analysis of initial MBP-Nt-Fas-DD-H285G chitin purification, when incubated overnight in chitin cleavage buffer. B, SDS-PAGE analysis of samples corresponding to bead samples taken at hour (hr) timepoints during chitin column incubation in chitin cleavage buffer (left) and flow through samples following chitin elution (right). C, SDS-PAGE analysis of optimised incubation time for MBP-Nt-Fas-DD-H285G chitin column cleavage. Overnight flowthrough corresponds to the buffer left incubating on the column overnight. D, semi-preparative RP-HPLC of desalted chitin column pooled elution and wash. The elution profile was monitored by UV absorbance at 214nm. SDS-PAGE analysis of fractions corresponding to the peaks is SHOWN. E, Q-TOF mass spectrum of F75 showing both MBP-Nt-Fas-DD-H285G thioester and hydrolysed product. F, Q-TOF mass spectrum of F76 showing both MBP-Nt-Fas-DD-H285G thioester as well as the uncleaved MBP-Nt-Fas-DD-H285G-Mxe intein-CBD

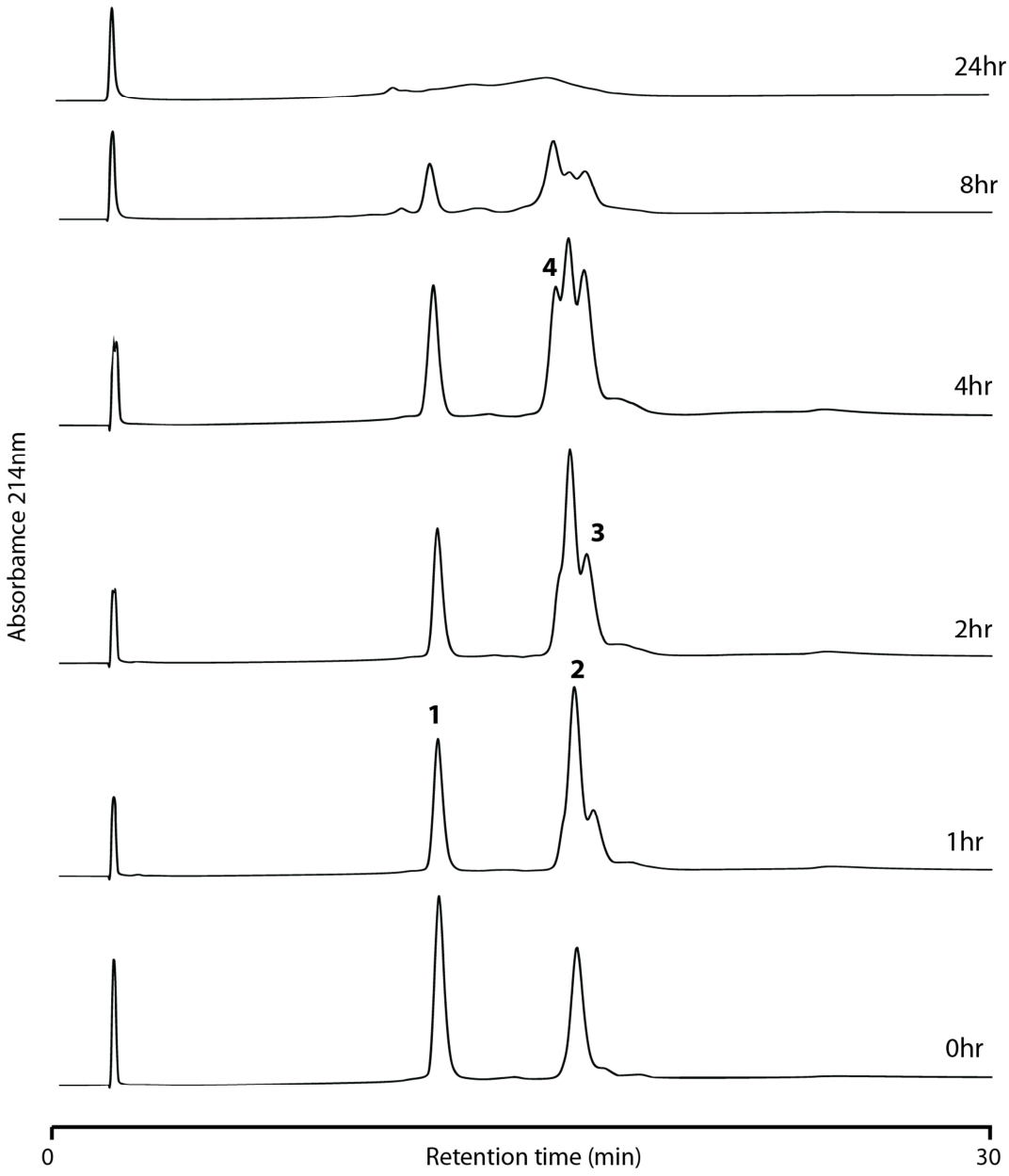

Figure 4.19 Ligation between MBP-Nt-Fas-DD-H285G and Htmb-pY-Ct-Fas-DD at equimolar concentrations

Analytical C4 HPLC (gradient: 30-60% B in 30 minutes) of the time-course for a ligation reaction between 1mM N-terminal MBP-Nt-Fas-DD-H285G and 1mM Htmb-pY-Ct-Fas-DD with TCEP in degassed 200mM NaH_2PO_4 and 6 M Guanidine chloride at pH 7. Peaks are numbered corresponding to the species that were present; 1, Htmb-pY-Ct-Fas-DD, 2, MBP-Nt-Fas-DD-H285G thioester, 3, Ligated pY291-MBP-Fas-DD-H285G product, 4, hydrolysed MBP-Nt-Fas-DD-H285G.

Although the kinetics and yield of the ligation of the MBP-Nt-Fas-DD H285G thioester were much improved compared to the corresponding wild-type construct, this construct still underwent undesirable side reactions under the standard ligation conditions.

4.6 Dissection of the ligation reaction variables gave little clue as to the origin of thioester hydrolysis

The mutation H285G at the site of the ligation greatly improved the yield of the ligation reaction, but the hydrolysis side reaction was still prevalent under standard ligation conditions. A variety of conditions were changed in an attempt to reduce hydrolysis and understand the underlying causes.

4.6.1 Increasing the ratio of C to N-terminal Fas-DD increases the rate of the ligation reaction but still results in hydrolysis

The ligation reactions described above were limited by the breakdown of the N-terminal Fas-DD thioester construct by hydrolysis over time. If the ligation reaction could be engineered to progress faster, it would enable more pY291-Fas-DD product to form. Ligation reactions were performed in which the ratio of Htmb-pY-Ct-Fas-DD to MBP-Nt-Fas-DD H285G was increased. The rationale being that this would shift the equilibrium towards forming product and outcompete hydrolysis. Ligation reactions containing the concentration ratios of 1:2 and 1:10 of MBP-Nt-Fas-DD H285G and Htmb-Ct-pY-Fas-DD were performed at pH 7 in ligation buffer as described in Section 2.10.3. The time course of these ligations monitored by analytical RP-HPLC is shown in Figures 4.20 and 4.21 respectively.

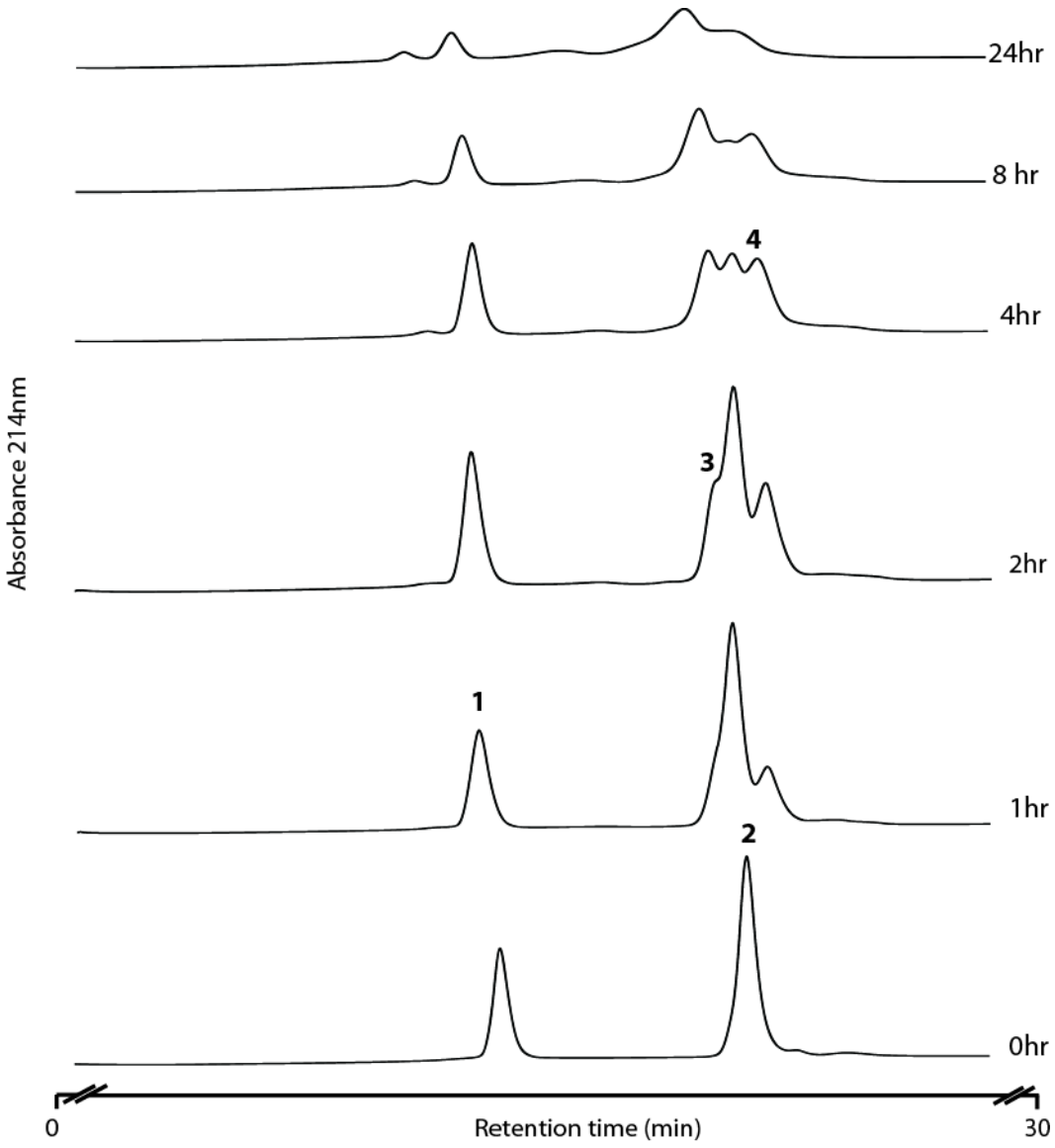

Figure 4.20 Ligation between MBP-Nt-Fas-DD-H285G and Htmb-pY-Ct-Fas-DD at a 1:2 concentration ratio

Analytical C4 HPLC (gradient: of 30-50%B in 30 minutes) of the time-course for a ligation reaction between 0.5mM N-terminal MBP-Fas-DD-H285G and 1mM C-terminal Fas phosphopeptide with TCEP in degassed 200mM NaH_2PO_4 and 6 M Guanidine chloride at pH 7. Peaks are numbered corresponding to the species that were present; 1, Htmb-pY-Ct-Fas-DD, 2, MBP-Nt-Fas-DD-H285G thioester, 3, hydrolysed MBP-Nt-Fas-DD-H285G, 4, ligated pY291 MBP-Fas-DD-H285G product

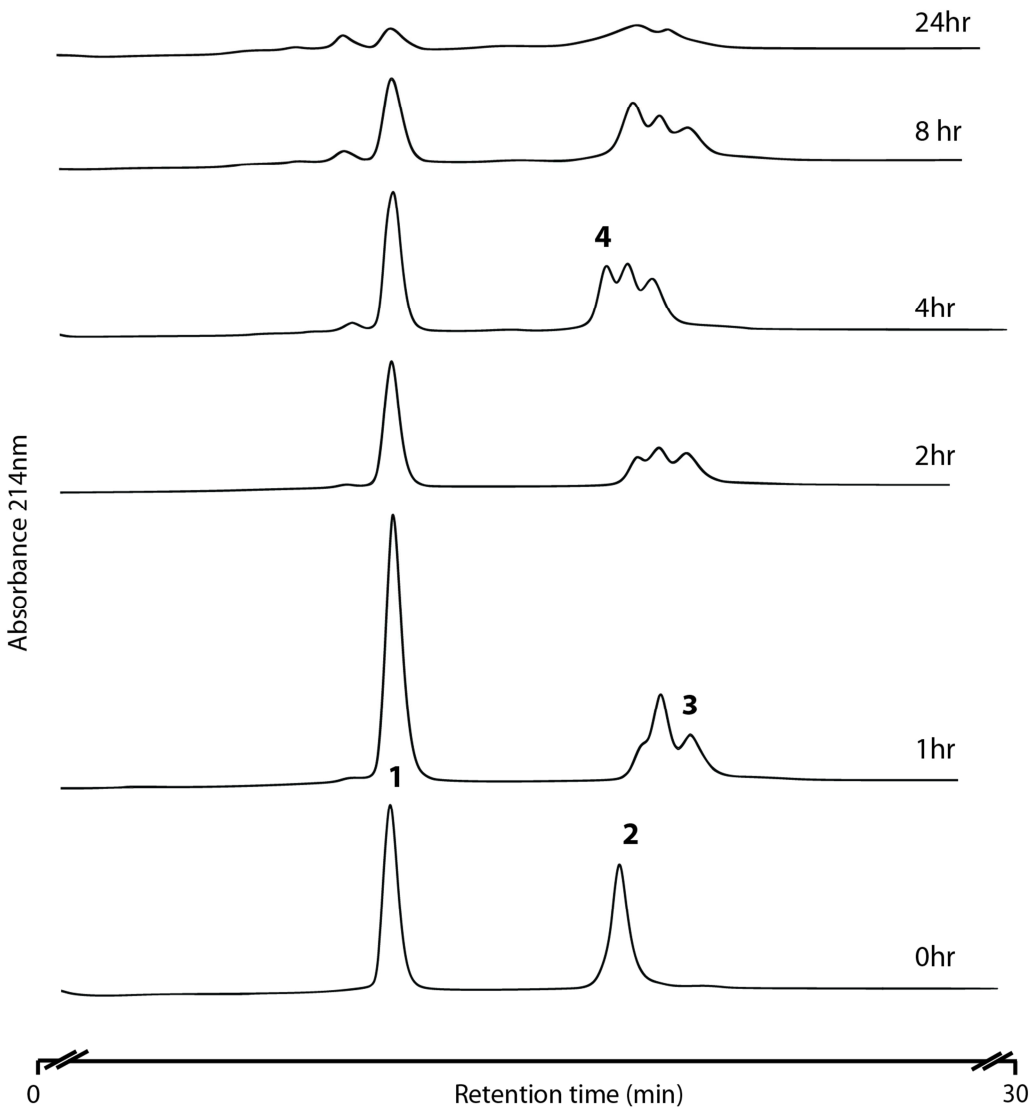

Figure 4.21 Ligation between MBP-Nt-Fas-DD-H285G and Htmb-pY-Ct-Fas-DD phosphopeptide at a 1:10 concentration ratio

Analytical C4 HPLC (gradient: of 30-50%B in 30 minutes) of the time-course for a ligation reaction between 0.1mM N-terminal MBP-Fas-DD-H285G and 1mM C-terminal Fas phosphopeptide with TCEP in degassed 200mM NaH_2PO_4 and 6 M Guanidine chloride at pH 7. Peaks are numbered corresponding to the species that were present; 1, Htmb-pY-Ct-Fas-DD, 2, MBP-Nt-Fas-DD-H285G thioester, 3, hydrolysed MBP-Nt-Fas-DD-H285G, 4, ligated pY291 MBP-Fas-DD-H285G product.

As before, the ligations result in a similar distribution of peaks corresponding to the N and C termini of Fas as well as the ligation product and hydrolysis peaks. However it is possible to see that the ligation reaction occurs at an increased rate when there is more C-terminal than N-terminal Fas. For example, by the two hour time point in the 1:10 ligation (Figure 4.21) the analytical RP-HPLC chromatogram shows the hydrolysis of MBP-Nt-Fas-DD H285G and product peaks to be of similar height. However in the reactions containing the concentration ratios of 1:2 (Figure 4.20) and 1:1 (Figure 4.19), this species distribution was not observed until four, possibly eight hours. This suggests that at a lower concentration of MBP-Nt-Fas-DD H285G more ligation product is made in a shorter period of time. What is also notable when comparing these three ligations (Figure 4.19-4.21) is that once this 1:1:1 distribution of peaks is established, there in no further increase in product formation, as if there were no more reagents available. After this point only N-terminal thioester hydrolysis is observed. This observation suggests that one of the reagents is undergoing a change and becoming inactive during the experiment.

A possibility was that the reactive thiol group of Htmb was oxidising during the ligation. If so, this would have prevented the ligation reaction from occurring. To test this, an aliquot of Htmb-Ct-pY-Fas-DD was assayed by analytical HPLC and the chromatogram overlaid with the corresponding chromatogram from the ligation reaction. If Htmb-Ct-pY-Fas-DD had oxidised, the peak observed by HPLC would have shifted. No peak shift was observed for the peptide (data not shown) so Htmb oxidation appear to not be the cause of the unexpected lack of ligation activity.

4.6.2 Neither the N nor C terminus are a limiting factor to the reaction

To test whether either the MBP-Nt-Fas-DD H285G thioester or the Htmb-Ct-pY-Fas-DD peptide were limiting the progression of the ligation, two ligations were prepared as described in Section 2.10.3, both containing 0.5 mM MBP-Nt-Fas-DD H285G thioester and 1 mM Htmb-pY-Fas-DD peptide. To one of them, fresh MBP-Nt-Fas-DD H285G thioester was added into the reaction at several time points, and to the other fresh Htmb-pY-Fas-DD peptide was added. In order to minimise the change in the concentration of reagents, this was done by removing an aliquot of the reaction and replacing it with equivalent volume of the fresh reagent at the same concentration. These ligations are shown in Figures 4.22 and 4.23, respectively.

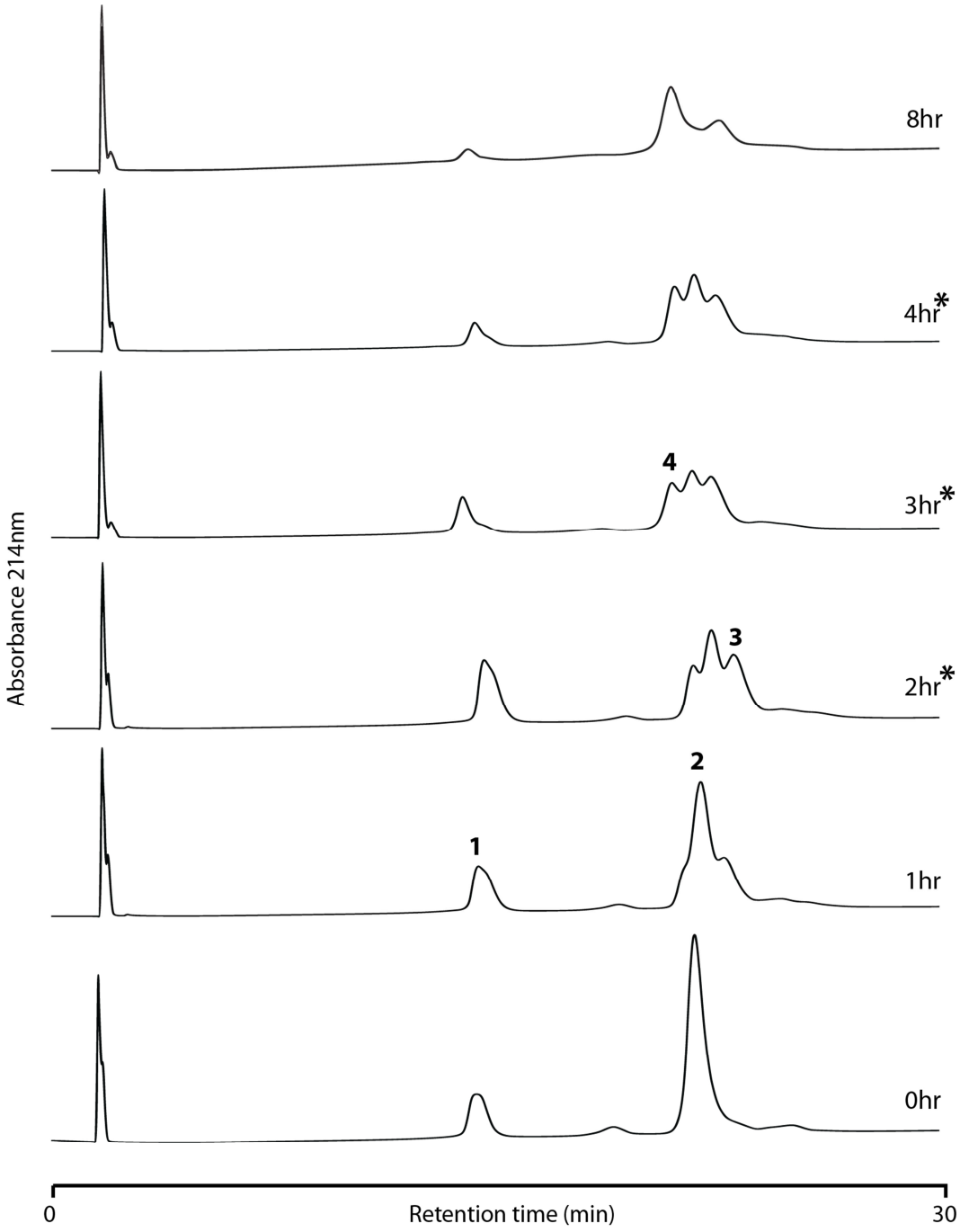

Figure 4.22 The readdition of MBP-Nt-Fas-DD-H285G protein, increases the amount of product from the ligation but does not reduce the amount of hydrolysis occurring

Analytical C4 HPLC (gradient: of 30-50%B in 30 minutes) of the time-course for a ligation reaction between 0.5mM MBP-Nt-Fas-DD-H285G and 1mM Htmb-pY-Ct-Fas-DD with TCEP in degassed 200mM NaH_2PO_4 and 6 M Guanidine chloride at pH 7. N-terminal Fas protein was added at the same 0.5mM concentration at time points 2hr, 3hr and 4hr, this is illustrated by the *. Peaks are numbered corresponding to the species that were present; 1, Htmb-pY-Ct-Fas-DD, 2, MBP-Nt-Fas-DD-H285G thioester, 3, hydrolysed MBP-Nt-Fas-DD-H285G, 4, ligated pY291 MBP-Fas-DD-H285G product.

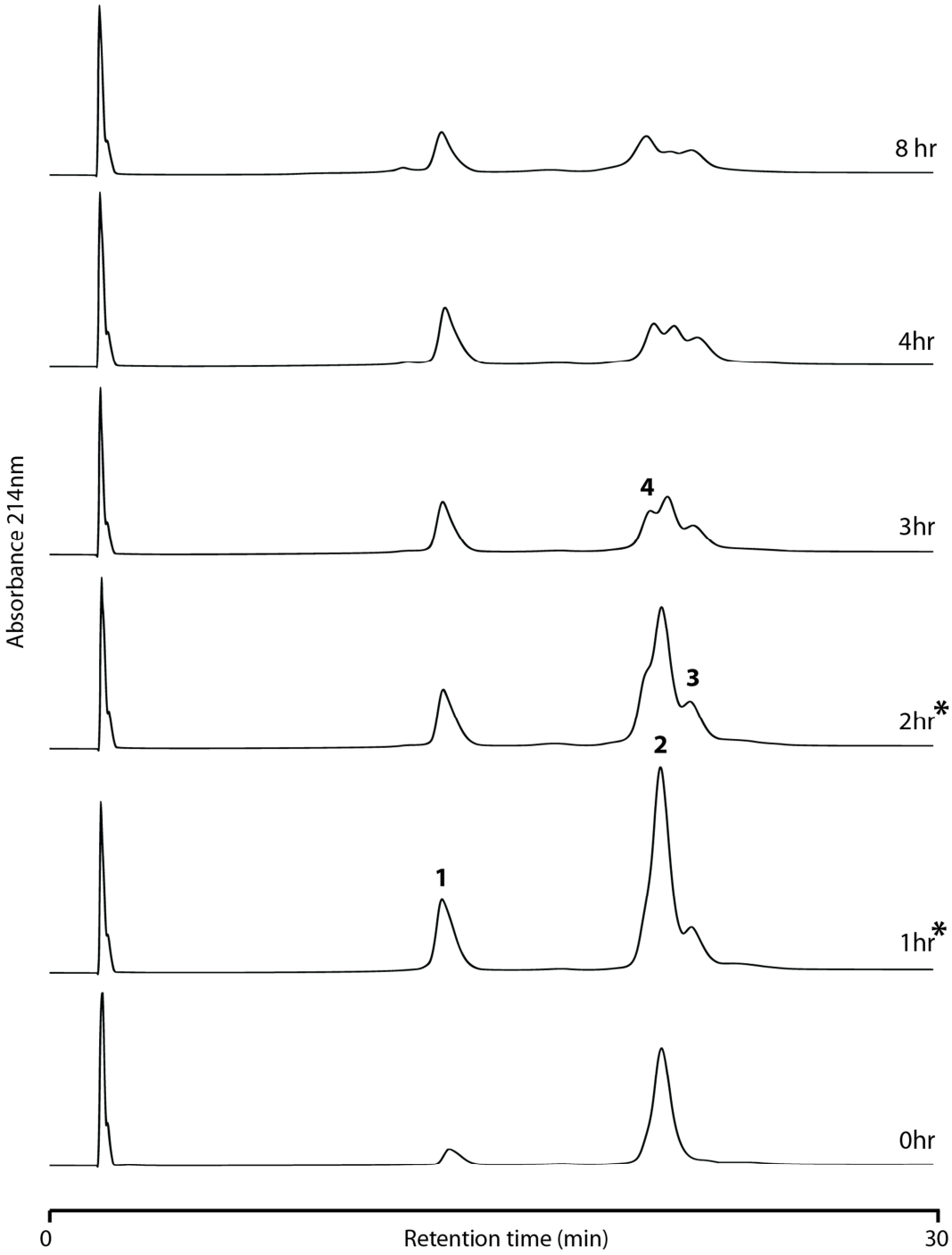

Figure 4.23 The readdition of Htmb-pY-Ct-Fas-DD, increases the rate of the ligation but does not reduce the amount of hydrolysis occurring

Analytical C4 HPLC (gradient: of 30-50%B in 30 minutes) of the time-course for a ligation reaction between 0.5mM N-terminal MBP-Fas-DD-H285G and 1mM C-terminal Fas phosphopeptide with TCEP in degassed 200mM NaH_2PO_4 and 6 M Guanidine chloride at pH 7. Peptide was added to the same 1mM concentration at time points 1hr and 2hr, this is illustrated by the *. Peaks are numbered corresponding to the species that were present; 1, C-terminal Fas-DD phosphopeptide, 2, N-terminal MBP-Fas-DD-H285G, 3, hydrolysed N-terminal MBP-Fas-DD-H285G, 4, ligated phospho-Y291 MBP-Fas-DD-H285G product.

When fresh MBP-Nt-Fas-DD H285G thioester was added into the ligation (shown in Figure 4.22) at the two, three and four hour time points, the addition of extra thioester increased the amount of product formed. However, this had no effect on the onset of hydrolysis, the distribution 1:1:1 was achieved once more and if anything, we observed even more hydrolysis than in the previous cases. When fresh Htmb-pY-Fas-DD peptide was added into the ligation at one and two hours (shown in Figure 4.23), there was less of an effect on product formation when compared to the re-addition of the MBP-Nt-Fas-DD H285G thioester. The overall progression of the ligation was similar to the 1:10 concentration ratio ligation shown in Figure 4.21. Together with the hydroxylamine result discussed above, this outcome shows that lack of Htmb-pY-Fas-DD peptide is not what is causing the ligation reaction to falter.

4.6.3 Optimisation of the reaction conditions using traditional NCL procedures does not reduce hydrolysis

Thiol additives are commonly included within a NCL reaction, to enhance the rate of ligation by catalysing in situ transthioesterification. One of the most common thiol additives is mercaptophenulacetic acid (MPAA)[224]. A ligation was performed with 0.5 mM MBP-Nt-Fas-DD H285G and 1 mM Htmb-Ct-pY-Fas-DD peptide in pH 7 ligation buffer, containing 5 mg/ml MPAA. The aim of this experiment was to increase the rate of ligation so that it would take place quicker than the hydrolysis. The reaction was monitored over a time course in which the ligation was followed by analytical HPLC, as illustrated in Figure 4.24.

The addition of MPAA to the ligation did speed up the rate of the ligation but also the rate of hydrolysis. All of the MBP-Nt-Fas-DD H285G thioester had been either hydrolysed or reacted to form pY291-Fas-DD product within an hour. There was no change in the HPLC chromatogram for the ligation time points after two hours. The ratio of peak heights of hydrolysed MBP-Nt-Fas-DD H285G to the product was even greater than was observed when all of the thioester has been hydrolysed in the previous ligations. The addition of MPAA and elevated temperature did not mitigate the hydrolysis problem within this ligation.

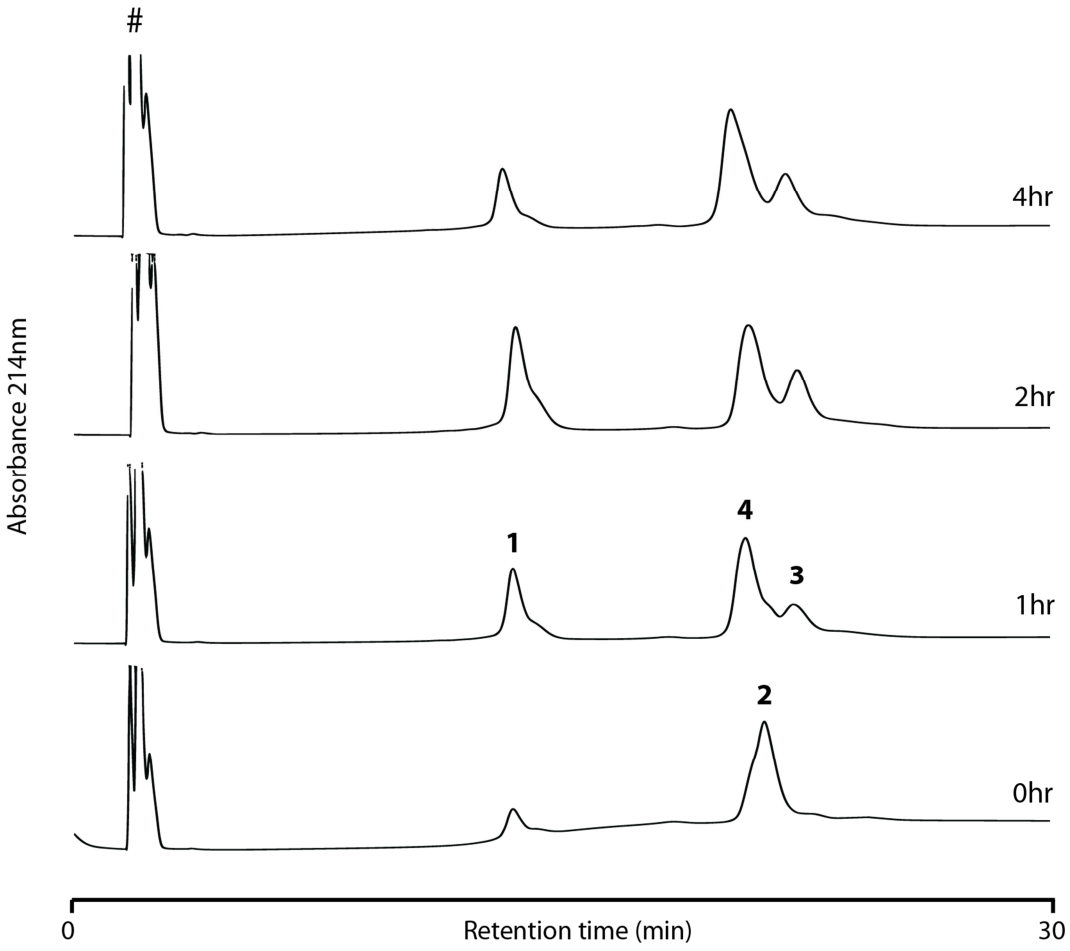

Figure 4.24 Addition of the cofactor MPAA and elevating the temperature of the ligation reaction speeds up the ligation as well as the hydrolysis.

Analytical C4 HPLC (gradient: of 30-50%B in 30 minutes) of the time-course for a ligation reaction between 0.5mM MBP-Nt-Fas-DD-H285G and 1mM Htmb-pY-Ct-Fas-DD with TCEP, 5mg/ml MPAA (mercaptophenylacetic acid) in degassed 200mM NaH_2PO_4 and 6 M Guanidine chloride at pH 7, incubated at 40^{o}C. # identifies the MPAA in the injection peak. Peaks are numbered corresponding to the species that were present; 1, Htmb-pY-Ct-Fas-DD, 2, MBP-Nt-Fas-DD-H285G thioester, 3, ligated pY291 MBP-Fas-DD-H285G product, 4, hydrolysed MBP-Nt-Fas-DD-H285G..

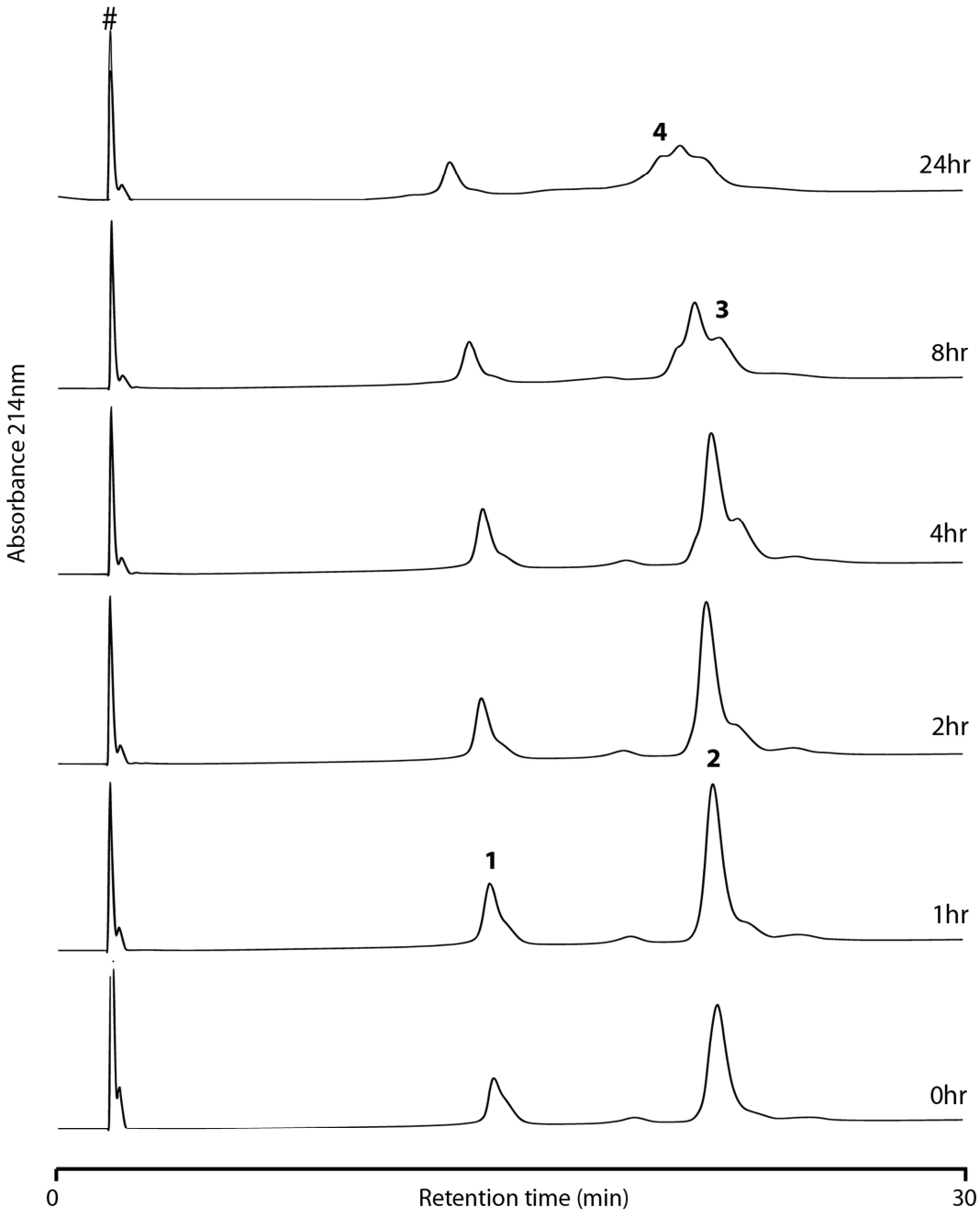

Figure 4.25 Reducing the phosphate buffer concentration reduces the rate of the ligation and appears to not affect the solubility of the reaction components.

Analytical C4 HPLC (gradient: of 30-50%B in 30 minutes) of the time-course for a ligation reaction between 0.5mM MBP-Nt-Fas-DD-H285G and 1mM Htmb-pY-Ct-Fas-DD with TCEP, in degassed 20mM NaH_2PO_4 and 6 M Guanidine chloride at pH 7, incubated at 30^{o}C. # identifies the guanidine in the buffer to halt the reaction in the injection peak. Peaks are numbered corresponding to the species that were present; 1, Htmb-pY-Ct-Fas-DD, 2, MBP-Nt-Fas-DD-H285G thioester, 3, ligated pY291 MBP-Fas-DD-H285G product, 4, hydrolysed MBP-Nt-Fas-DD-H285G.

It was suggested that high concentrations of phosphate can adversely affect the ligation efficiency of NCL reactions. To test whether this was the case I set up a ligaton with 0.5 mM MBP-Nt-Fas-DD and 1 mM Htmb-pY-Ct-Fas-DD in a buffer containing 20 mM NaH_2PO_4 50 mMTCEP and 6 M guanidinium hydrochloride at pH 7. The ligation reaction was followed over time by analytical RP-HPLC as can be seen in Figure 4.25. This had an interesting effect, in that although compared to other cases the same amount of ligation product was observed, the rate of hydrolysis was somehow reduced. Even after 24 hours we could still detect the peak corresponding to the thioester. However, this new result did not offer sensible clues as to explain why the side reaction takes place.

4.7 Optimised ligation conditions for phosphorylated-Y291-Fas-DD

From the experiments outlined above, the conditions which the greatest yield of ligation product could be obtained were 0.5 mM MBP-Nt-Fas-DD and 1 mM Htmb-Ct-pY-Fas-DD in ligation buffer at pH 7 for two hours. The analytical RP-HPLC chromatograms of the ligation reactions of MBP-Nt-Fas-DD and MBP-Nt-Fas-DD H285G are shown in Figure 4.26. It is evident when seeing these traces side by side that the yield with the H285G mutant is higher compared to the wild type construct. However, due to the lack of resolution between the product and the NT-Fas-DD thioester peaks, the reaction yield could not be properly quantified, as attempts to separate this species using different flow rates and solvent gradients were unsuccessful (data not discussed). QTOF-MS spectra confirmed that the mass of these peaks correspond to fully ligated MBP-Nt-Fas-DD and MBP-Nt-Fas-DD H285G (Figure 4.27). Table 4.3 shows a comparison of the predicted and observed masses for the ligation products.

Table 4.4 Predicted and observed masses of ligation products

N-terminal Fas construct	**Predicted ligation product mass (Da)**	**Observed ligation product mass (Da)**
Nt-Fas-DD	12352	12252
MBP-Nt-Fas-DD	55252	55189
MBP-Nt-Fas-DD H285G	55170	55108

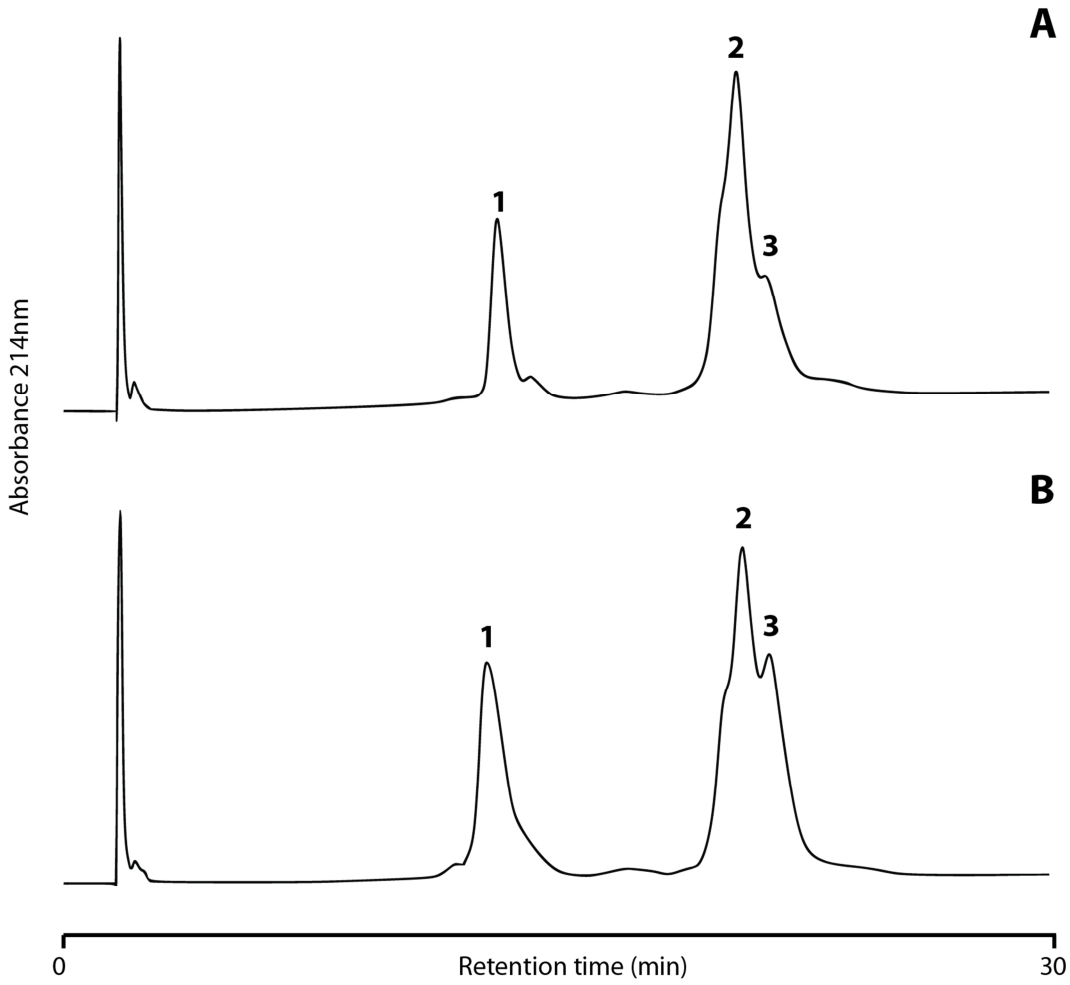

Figure 4.26 'Optimal' MBP-Nt-Fas-DD and Htmb-Ct-pY-Fas-DD ligation

Analytical C4 HPLC (gradient: of 30-50%B in 30 minutes) of the time-course for a ligation reaction between 0.5mM MBP-Nt-Fas-DD-H285G and 1mM Htmb-pY-Ct-Fas-DD with TCEP, in degassed 20mM NaH_2PO_4 and 6 M Guanidine chloride at pH7, incubated at 30^{o}C for two hours. # identifies the guanidine in the buffer to halt the reaction in the injection peak. A, shows optimal HPLC trace for WT MBP-Nt-Fas-DD, B, shows optimal HPLC trace for MBP-Nt-Fas-DD- H285G. Peaks are numbered corresponding to the species that were present; 1, Htmb-pY-Ct-Fas-DD, 2, MBP-Nt-Fas-DD thioester, 3, ligated pY291 MBP-Fas-DD product

.

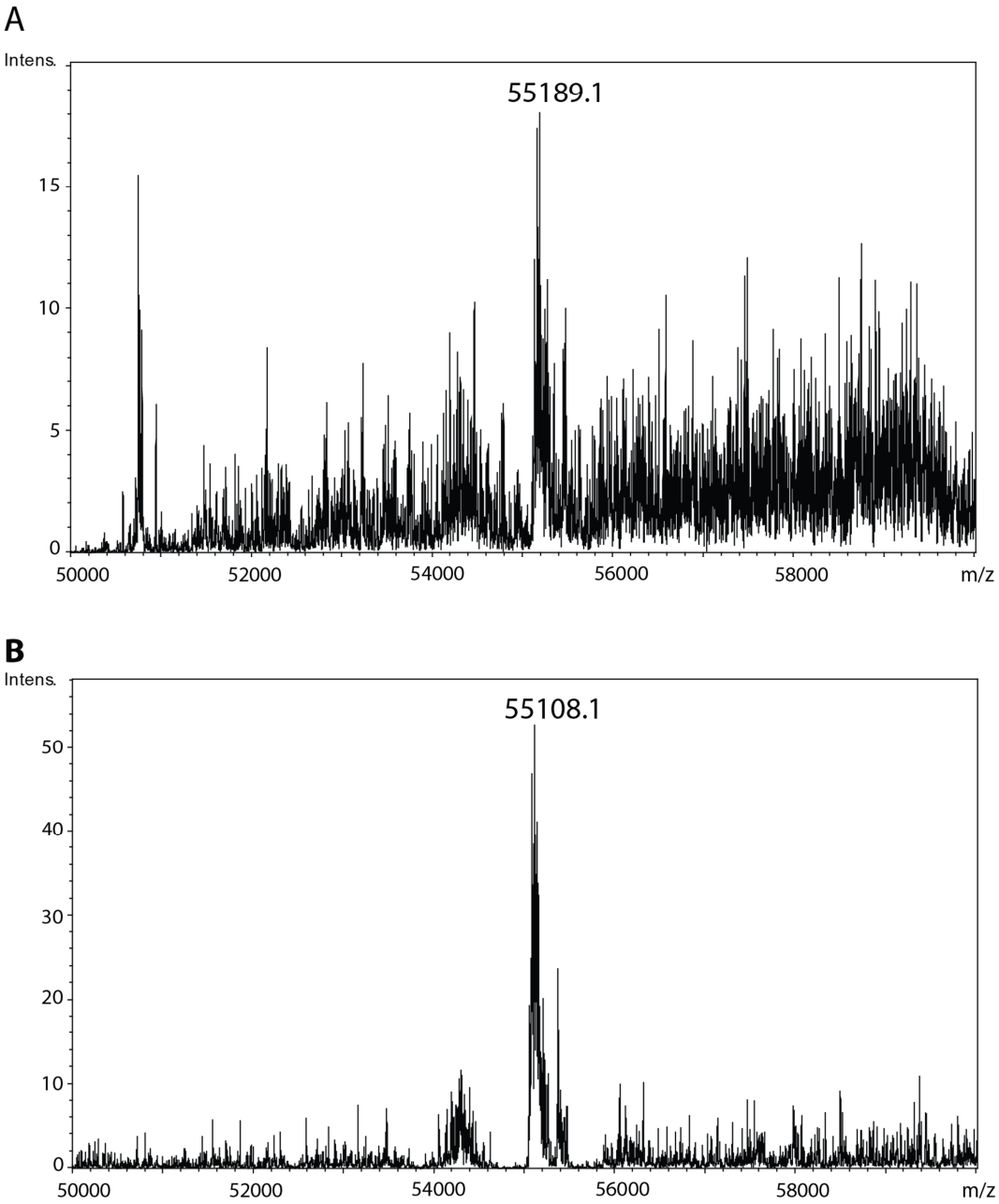

Figure 4.27 ESI-MS results from the products formed from the 'optimal' reaction conditions.

Low resolution ESI-MS for the product peaks shown in Figure 4.26. A. mass spectrum of the product from the ligation of MBP-Nt-Fas-DD and Htmb-pY-Ct-Fas-DD. B, Mass spectrum of ligated product from the ligation of MBP-Nt-Fas-DD H285G and Htmb-pY-Ct-Fas-DD.

4.8 Discussion

Expressed protein ligation is becoming widely used to semi-synthesise proteins containing post translational modifications and site-specific labelling. I report here the development of an EPL technique to prepare a Fas death domain containing a pY at position 291. An Nα auxiliary cysteine mimic (developed in the Offer laboratory at NIMR) was used to bypass the usual for a cysteine at the N-terminus of the ligation junction. If successful, this technique could be the platform on which to begin *in vitro* structural, functional and dynamic studies to further probe the effects of this post translational modification on the death domain of Fas in particular, but also in death domains in general.

The approach that was selected to produce Fas-DD pY291 was to generate an N-terminal recombinant Fas-DD thioester and a C-terminal synthetic Fas phospho-peptide. The ligation junction was chosen to be between residues H285 and G286. This position was considered the most promising in terms of previous knowledge of success rate of the occurrence of different amino acids at the ligation junction.

The Nt-Fas-DD thioester was generated using the NEB-IMPACT system. A construct was cloned and expressed containing the Mxe intein followed by a chitin binding domain at the C-terminus. The expression yield of this construct was good and no *in vivo* proteolysis of the construct was observed. Intein cleavage had to be induced in denaturing conditions, because otherwise the Nt-Fas-DD thioester did not elute from the chitin beads, presumably because it is very hydrophobic and/or insoluble.

The pY-Ct-Fas-DD peptide was successfully synthesised by SPPS in four stages. Two pseudo-proline dipeptide units were incorporated to prevent aggregation of the growing peptide chain. The novel Htmb auxiliary was coupled to the N-terminus of the peptide to act as a cysteine mimic necessary for the ligation reaction to occur. The auxiliary can be removed at the end of the ligation leaving no chemical scars in the created semi-synthetic protein.

The initial ligation of Nt-Fas-DD thioester and Htmb-Ct-pY-Fas-DD was successful in that it generated a fragment of the anticipated molecular weight for pY291-Fas-DD. However, only a small amount of product was formed and most of the thioester

was degraded by hydrolysis. To try to discourage hydrolysis of the Nt-Fas-DD thioester, the ligation buffer conditions were carried out at higher pH and in the presence of a high concentration of organic solvent. Increasing the pH of the ligation buffer to pH 8 did not have any effect on thioester hydrolysis, suggesting it is being catalysed by bases. Unfortunately it was not possible to reduce the pH below 7 due to the auxiliary being incompatible with a lower ligation reaction pH (John Offer, personal communication).

Dittman *et al.* (2010)[217] have previously reported the use of organic solvents for native chemical ligation of hydrophobic peptides. We predicted that an environment with a high concentration of organic solvent would prevent hydrolysis and also improve the solubility of the N and C-terminal components. A ligation was set up in 80% NMP v/v, conditions similar to those described by Payne *et al.* (2007) for sugar-assisted ligation (SAL) reactions[219]. None of the previously observed reactions (hydrolysis or ligation) occurred within the reaction carried out in organic solvent (NMP) until the concentration of NMP was reduced to 40% (v/v) at which thioester hydrolysis was observed. It is believed that a base additive is required to ensure thiol reduction and enable thioester exchange in an organic solvent environment[217]. Dittman *et al.* (2010) used the base triethyamine as well as a thiol additive to catalyse a ligation reaction in DMF, this is because thiol additives catalyse the ligation reaction by in situ transesterification[224]. Perhaps the lack of base additive was the reason I did not observe a Fas-DD ligation in these conditions.

At this point, it was clear that not only the ligation had to be optimised, but also that the yield of Nt-Fas-DD thioester needed to be improved. I decided to try to make a more soluble construct by insertion of maltose binding protein (MBP) at the N-terminus of the Nt-Fas-DD construct. This strategy was successful in that the fusion construct eluted from the chitin beads under non-denaturing conditions both increasing yield and simplifying the preparation. However, the behaviour of MBP-Nt-Fas-DD thioester during ligation was not different and if anything a little worse than that of untagged Nt-Fas-DD thioester. An unexpected precipitate was formed during the reaction and the quenched aliquots gellified on addition of TFA, presumably because the quenching reduces the concentration of guanidinium hydrochloride, and/or because the acid precipitated the protein. Several other death

domain polypeptides also create gels in various situations (TJ Ragan, Lily Nematollahi, Christine Richter, personal communications), and we believe this is a consequence of the domains' inability to fold efficiently leaving the hydrophobic core exposed. Of course, in this case results are too preliminary to assess whether precipitation was related to the prevalence of the hydrolysis reaction or not.

Another strategy that could increase the ligation rate and in this way outcompete hydrolysis was to replace the His at the ligation junction for Gly. A C-terminal glycine thioester results in slower thioester rearrangements[193] but there is less steric hindrance, therefore potentially increasing the rate and yield of ligation. In a review of published Nα auxiliary-mediated NCL reactions[127], it was highlighted that the most frequently used ligation junction is glycine-glycine for this reason. This mutation might favour ligation, but it also disfavours intein-mediated cleavage. Glycine is the least favourable amino acid to have positioned immediately N-terminal to the Mxe intein[223], greatly reducing the speed of the cleavage reaction. The overnight cleavage protocol had to be extended to 72 hours in order to obtain comparable amounts of MBP-Nt-Fas-DD H285G thioester. Despite this unanticipated hiccup, incorporation of the H285G mutation did increase the rate and yield of product formed in the ligation reaction, although the formation of product was still being outcompeted by the hydrolysis reaction.

Ligation reactions, in which the concentration of MBP-Nt-Fas-DD was reduced while that of Htmb-Ct-pY-Fas-DD was kept constant, made clear that the reaction always reached a point in which no more product was formed and only thioester hydrolysis occurred. Reducing the concentration of MBP-Nt-Fas-DD resulted in the reaction reaching this point a lot quicker than in the previous ligations. This posed the question of whether one of the components was losing its ability to react over time. To investigate this, ligations in which fresh MBP-Nt-Fas-DD or Htmb-Ct-pY-Fas-DD were added into the ligation at different time points were carried out. As expected, the addition of fresh MBP-Nt-Fas-DD thioester increased the amount of product, for as long as more fresh thioester was added. Whereas the addition of fresh Htmb-Ct-pY-Fas-DD peptide made no difference to the distribution of the reaction species visible in the RP-HPLC chromatogram. This outcome also suggests that the lack of reactive Ct fragment is not what is leading to thioester hydrolysis. It was also

confirmed that the Htmb auxiliary was not oxidising and thereby becoming unreactive over time. Each of these ligation conditions displayed the same behaviour; namely, a ligation product started forming, but when reaching a certain concentration the ligation halted and the hydrolysis became dominant. It is important to point out that the only evidence (we have at this point) that this is a hydrolysed thioester are previous observations in the Offer lab, and the fact that the retention time is not very different to that of the N-terminal fragment, only slightly less hydrophobic. More detailed analysis of this peak would need to be carried out to really understand what is the side reaction that is taking place.

After identifying that neither the N- nor C-terminal components were a limiting factor in the decay of product formation, the addition of additives was tested. It is common to include a thiol additive during NCL reactions, but we discovered that the addition of MPAA was able to both increase the rate of hydrolysis and of ligation. Johnson and Kent (2006) also observed this effect upon ligations when using MPAA as a catalyst[224].

Despite being unable to prevent hydrolysis using several strategies, I regarded that it was important to generate enough sample to characterise the peaks by MS. The best conditions found were to be incubating 0.5 mM MBP-Nt-Fas-DD and 1 mM Htmb-pY-Fas-DD for two hours at 30 ^{o}C in ligation buffer at pH 7. From side-to-side comparison under these conditions it was clear that the H285G mutant performed better than the wild type thioester.

The next possible strategy to tackle the hydrolysis problem, would be to vary the thiol used to prepare the thioester, as perhaps the benzyl mercaptan thioester is not stable under these conditions. Benzyl mercaptan has been found to perform poorly during ligation reactions. This is thought to be the case because under the conditions of the reactions the benzyl group is a non-optimal leaving group[224]. Johnson and Kent (2006) suggested that the MPAA thioesters would outperform others in expressed protein ligation reactions, because of their superior stability and ease of storage[224].

More data would have to be obtained using other systems to validate Htmb for EPL applications. It could well be that the Htmb auxiliary is suitable for NCL using peptides, however proteins are more challenging in terms of the possible

conformations present, steric hindrance, and solubility limitations. Whether Htmb is the cause or not of the poor yields and hydrolysis that I observed, it could be assessed by attempting the ligation without the use of an auxiliary, by synthesising a peptide with a cysteine at the G286 position. It could also be that the ligation is inhibited by changes in pH or the presence of other products. This could be tackled by doing the ligation in an open system in which the buffer was constantly being replenished and small molecules would diffuse rapidly, e.g. a microdialysis chamber. Other alternatives include carrying out the reaction in organic solvents, addition of alternative additives and attempting ligations in other sites within the domain and/or other death domains.

In summary, this chapter has demonstrated that a 55 kDa MBP-tagged phosphorylated Fas-DD can be generated by expressed protein ligation. Although attempts to optimise the ligation reaction yield and limit hydrolysis of the thioester were made, I was unable to satisfactorily overcome these limitations. However, the results have set the basis to further optimise conditions to be able to perform this reaction at a preparative scale in the future.

Chapter 5

Molecular investigations of a potential direct Fas:ezrin interaction

5.1 Introduction

The first step of Fas-mediated apoptosis is the aggregation of Fas upon activation by its ligand. Fas clusters trigger the formation of the Death Inducing Signalling Complex (DISC) by recruitment of Fas-associated protein with death domain (FADD), procaspase-8 and cellular-FLICE inhibitory protein (c-FLIP).

There is controversy about the nature of the involvement of the cytoskeleton in the formation of the DISC. Actin interacts with membrane proteins via the linker protein ezrin or other members of the ERM family of proteins (ezrin, radixin and moesin). Early reports suggested that ezrin was required for the Fas apoptotic pathways to be initiated[114], this was further supported by the observation that Fas ligation stimulated ezrin recruitment[225]. However, others have observed that siRNA-mediated knockdown of ezrin facilitates DISC formation, increasing the level of apoptosis[116].

An interaction between Fas and ezrin has been observed mainly in mammalian cells and lysates by co-localisation and co-immunoprecipitation. However, two independent groups have reported a specific direct interaction between recombinant Fas and recombinant ezrin using GST pull down assays[116,117]. Luzopone and collaborators mapped the interaction to a nineteen amino acid region in the central lobe of the FERM domain of ezrin (residues 149-168)[117]. Using different constructs of recombinant Fas and mammalian cell lysates, Ruan *et al.* mapped the interaction site in Fas to a region, predicted to be unstructured, between the transmembrane domain and the death domain (residues 191-204); they named this region the membrane proximal domain (MPD)[118]. Moreover, ezrin and other ERM proteins are

known to recognise twenty to thirty amino acid stretches with little regular secondary structure[110,111], a description that could be applied to the MPD of Fas.

In this chapter I describe the development of methodologies for biophysical studies of the putative interaction between the cytoplasmic region of Fas and the FERM domain of ezrin. This involved the cloning, expression and purification of constructs of Fas and ezrin, followed by the characterisation of the interaction using pull-down assays, isothermal titration calorimetry (ITC), analytical ultracentrifugation (AUC) biolayer interferometry (BLI), and nuclear magnetic resonance (NMR). Particular attention was paid to confirmation of 'non-specific' ezrin interactions and to verify NMR spectroscopy results.

5.1.2 Biophysical techniques used to characterise the Fas-ezrin interaction

5.1.2.1 Isothermal titration calorimetry - ITC

Isothermal titration calorimetry is a physical technique which is used to characterise the thermodynamics of a binding event in solution. The method provides a direct measurement of the binding energies of biological processes that is widely implemented to characterise protein:protein, protein:ligand, protein:DNA and antigen:antibody interactions. ITC measures the heat which is produced (exothermic) or taken (endothermic) from the environment as an interaction occurs, exploiting the fact that the production or absorption of heat is an intrinsic property of virtually all biochemical reactions. The change in enthalpy (ΔH) can be used to precisely calculate the changes of Gibbs free energy (ΔG), entropy (ΔS) and heat capacity upon macromolecules binding. These parameters are then used to determine the stoichiometry and binding affinity of the interaction being studied. ITC is carried out in a matrix free environment requiring no immobilisation or modification of binding partners which are only required at low concentrations. Experiments can be carried out in a range of salt concentrations, pHs and temperatures, making ITC a robust assay for any interaction.

ITC analysis is carried out using a heat flux calorimeter which operates under a dynamic power compensation principle. The calorimeter itself is made up of a syringe to enable binding partner titration and two cells, one for the sample and one for a buffer reference which are contained in an adiabatic jacket. The temperature of

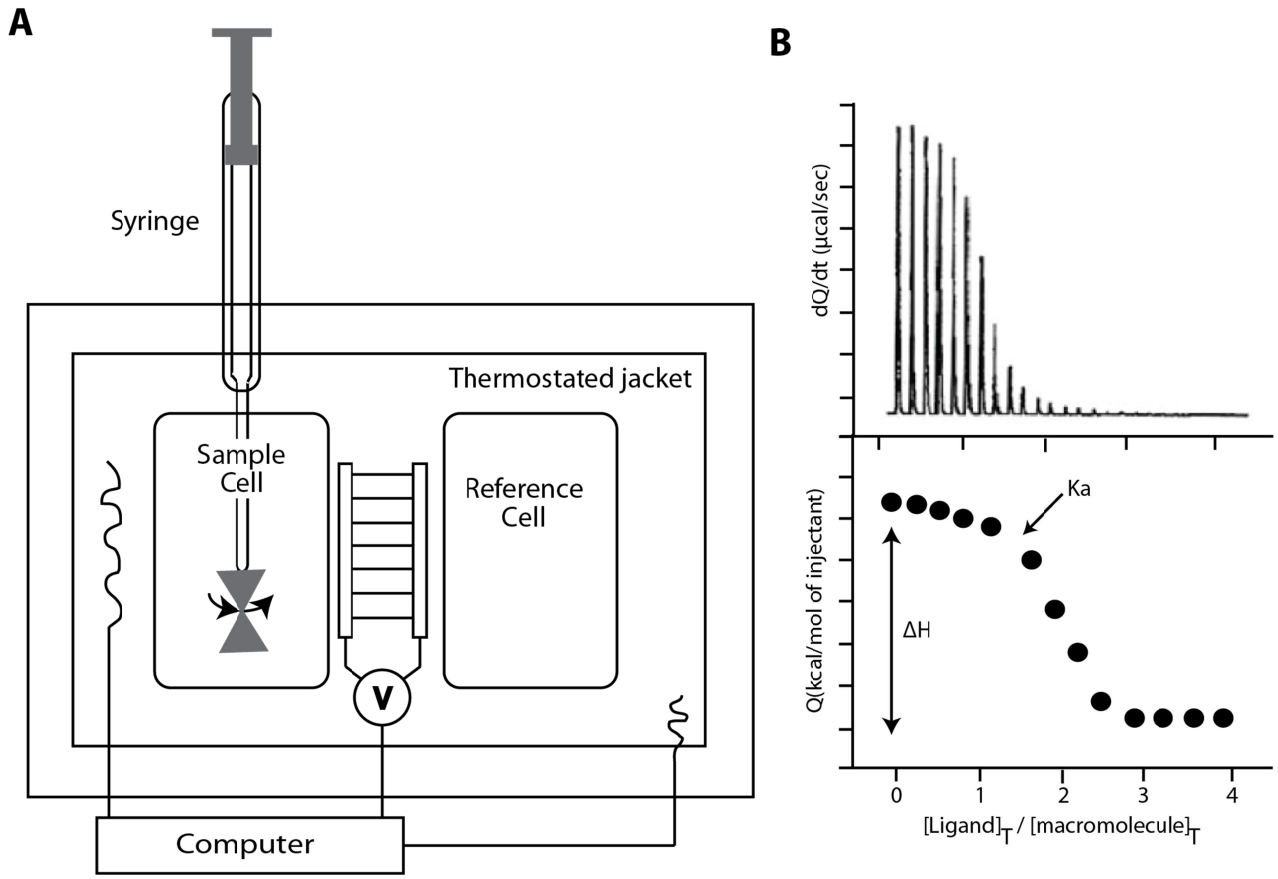

Figure 5.1 Basic illustration of ITC instrument and example of typical endothermic binding plot.

A, basic illustration of an ITC instrument, showing two cells surrounded by a thermostated jacket, the injection syringe, a stirring device and the computer controlled thermostatic feedback systems. B, Typical ITC experimental data for an endothermic reaction. Top panel shows the monitored signal over time with spikes in power upon each injection point. The bottom panel shows the integrated heat plot, indicating the ΔH and where the K_a is calculated from. Figure adapted from Velazquez-Campo*y et al*. (2004).

the cells are constantly monitored and upon temperature changes in the cell, the calorimeter implements a feedback control system to maintain the same temperature between cells. The instrument output is a measure of the amount of power (in μcal/sec) which is required to maintain a constant temperature between the two cells (dynamic power compensation). Temperature control is monitored by the presence of a semiconductor sensor which is sandwiched between the cells. A schematic diagram of an isothermal calorimeter is shown in Figure 5.1A.

For the experiment, one reactant is placed within the sample cell, whereas the other is placed in the syringe. The reference cell only contains the buffer that the reaction is being carried out in, which acts as the temperature reference. Over the course of the experiment, known aliquots of the reactant from the syringe are titrated into the sample cell and the reaction is mixed. If a complex is formed, the extent of binding is dependent upon the concentration and binding affinity of the reactants. Upon complex formation, heat is either released (exothermic reaction) or absorbed (endothermic reaction) resulting in a temperature difference between the reference and the sample cells. The feedback system within the instrument increases or decreases the thermal power deposition to the sample cell to restore the temperature balance between the two cells following each injection. The deflection in the power input to the sample cell to maintain a constant temperature constitutes the reported signal. This is plotted as a series of peaks against the concentration of reactant added from the syringe. An example of raw ITC data is illustrated in Figure 5.1B. Titration of the reactant from the syringe into the sample cell is continued until the binding is observed as saturated. Saturation is achieved when the heat signal diminishes so much so that only the background heat from dilution or unspecific buffer factors are detectable.

To analyse the raw data, the area under each of the peaks of instrument power is calculated and normalised to the quantity of the ligand injected in each step of the titration. This is plotted against the molar ratio of the reaction components as an integrated heat plot, as illustrated in Figure 5.1B (bottom panel). From this graph, thermodynamic parameters such as binding affinity and stoichiometry of the complex can then be extracted by applying a specific analytical model. The analysis and fitting functions of the raw data are usually carried out within the control and analysis software of the calorimeter.[226–228]

5.1.2.2 Analytical ultracentrifugation – AUC

Analytical ultracentrifugation is a useful tool for the study of protein:protein interactions. AUC monitors the sedimentation of macromolecules through a solvent over time within a centrifugal field. It is a technique which enables the hydrodynamic and thermodynamic characterisation of a macromolecule (or complex) in solution without the interference or interaction with a matrix. In general terms, during AUC, a sample is spun (encased in a transparent cell) at a very high speed in which real time monitoring is carried out by an optical detection system. The concentration of a sample is observed verses the distance it is from the axis of the centrifugal field. Real time detection can take the form of UV/visible spectrophotometric absorption or collection by an interference optical refraction index (RI) system. There are two main types of AUC experiment which can be carried out to study macromolecules in solution, sedimentation velocity (SV) and sedimentation equilibrium (SE) experiments.

Within sedimentation velocity experiments, high speed centrifugation results in a centrifugal force which depletes macromolecules at the meniscus of the sample cell resulting in a concentration boundary which moves to the base of the cell as a function of time. The recording of this process is illustrated by a response spectrum (Figure 5.2) which plots the variation in concentration of the macromolecule that is formed throughout the axis of the cell during centrifugation as a function of time. The concentration is plotted in units of ‘fringe displacement’ which is taken from the interference optical system and translates into a specific analyte concentration value per unit. With this response spectrum it is then possible to determine the sedimentation coefficient (S) of a molecule. The sedimentation coefficient (S) is used as a parameter that characterises the molecules translated hydrodynamic behaviour during the sedimentation process. S is defined as the ratio of a particles sedimentation velocity to the force of acceleration applied to it. With the molecules S value it is possible to begin to model the hydrodynamic shape, including the oligomeric state and if a heterogeneous interaction the stoichiometry of the macromolecules under investigation.

In sedimentation equilibrium (SE) AUC experiments, the absolute molecular weight and stoichiometry of a complex mixture can be obtained. SE-AUC experiments are

carried out at a lower rotor speed establishing an equilibrium across the cell in which sedimentation diffusion can be monitored. These experiments are run for several days during which the distribution of molecules along the cell reaches an equilibrium state. The distribution formed is sensitive only to the molecular mass and not the shape. To study the interaction between Fas and ezrin described in this chapter, sedimentation velocity experiments were carried out.

As mentioned above, the molecular sedimentation coefficient (S) can be obtained from the SV-AUC experimental data. Another parameter, the translational diffusion coefficient (D_T) can also be calculated. D_T gives an estimate of the molecular weight of a macromolecule independent of its shape. These parameters are calculated using the Svedberg equation, which takes into account the buoyant force (F_b), the frictional force (F_f) and the centrifugal force (F_c) which the macromolecule experiences, along with the mass of the displaced solution and the density of the solution itself. The Svedberg equation to calculate S is shown in Equation 1 below:

$$M(1-\tilde{v}\rho)/N_A f = v/\omega^2 r = S \qquad \textit{Equation 5.1}$$

The diffusion coefficient (D_T) can be determined using Equation 5.2.

$$D_T = RT/ N_A f \qquad \textit{Equation 5.2}$$

Where v is the radial velocity, ω is the angular velocity, M is the molar mass, ρ is the solvent density, *f* is the frictional coefficient, R is the gas constant, r is the radial position, $\omega^2 r$ is the centrifugal field, $\tilde{v}$ is the partial specific volume, N_A is Avagadro's constant and D_T is the diffusion coefficient.

At the beginning of a SV-AUC experiment, the analyte macromolecules are positioned at a uniform concentration throughout the solvent. As the sample is centrifuged, macromolecules sediment leading to the formation of a concentration boundary in which there is a depletion of the macromolecules between the boundary and the meniscus of the cell. The concentration boundary moves through the cell as a function of time; it is the position of this boundary which is recorded in the response spectrum. The data from the entire SV-AUC experiment is fitted to the Lamm equation (Equation 5.3) to obtain values for D_T and S.

$$\left(\frac{\partial C}{\partial r}\right) r = -\frac{1}{r}\left\{\frac{\partial}{\partial r}\left[s\omega^2 r^2 C - D_T r\left(\frac{\partial c}{\partial r}\right)_t\right]\right\}_t \qquad \textit{Equation 5.3}$$

The Lamm equation takes into account the variation in the rate of concentration of the particles along the radius of the cell in conjunction with the movement of the components in the sample. In a multicomponent system a range of sedimentation coefficients contribute to the observed behaviour.

In these circumstances the correct analysis involves the calculation of the continuous size distribution factor C(s) which allows for the sedimentation coefficient to vary within a defined range. The C(s) value is plotted against the sedimentation coefficient resulting in the formation of a peak for each of the components present in the sample.

The frictional coefficient (f_o) gives information about the shape of the protein within a sample, which can be used to calculate the molecular weight of the macromolecule using the Stokes equation (Equation 5.4), which for a spherical object takes the following form:

$$f_o = 6\pi\eta R_0 \qquad \textit{Equation 5.4}$$

Where f_o is the frictional coefficient of a spherical particle, ŋ is the viscosity of the solution and R_0 is the radius of the spherical particle. Shape anisotropy of the macromolecule causes the measured friction coefficient (f) to be different from f_o. Hence, the frictional ratio f/f_o which is obtained during fitting of the SV-AUC data can provide an indication of the shape of the investigated protein.[229,230] Within this study, the AUC data analysis program Sedfit was employed to calculate the sedimentation coefficient (S) and associated parameters using the observed sedimentation boundary measurements at a specific centrifugal field by fitting the data to the Lamm equation

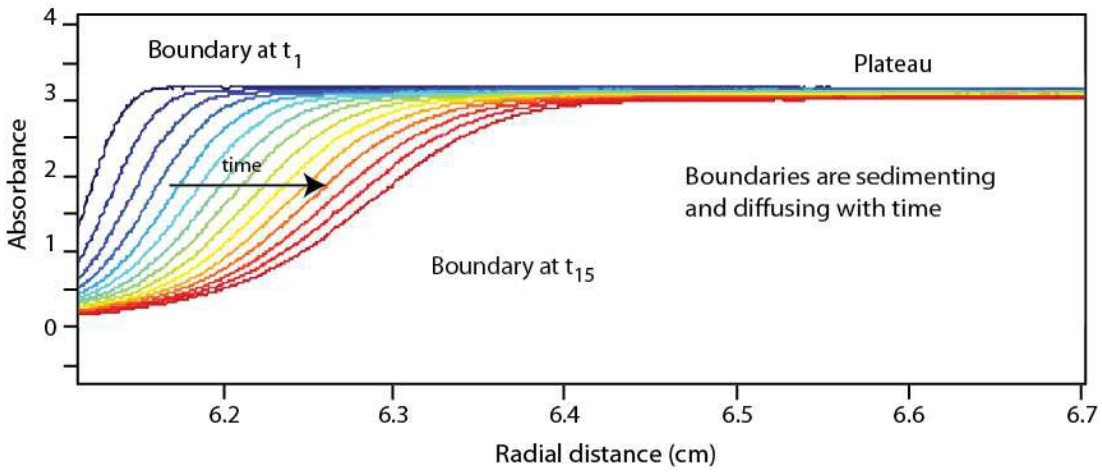

Figure 5.2 Schematic representation of the experimental output from a sedimentation velocity-analytical ultracentrifugation experiment.

The absorbance boundaries across fifteen consecutive time points (denoted t1-t15) are illustrated as a function of the radial distance in the cell. Colour of the boundary is representative of the first fifteen time points of the experiments from t_1 in blue to t_{15} in red.

5.1.2.3 Biolayer interferometry – BLI

Biolayer interferometry (BLI) is a label free technique for real time monitoring of molecular interactions based upon the interference of reflected white light in a form of interference spectroscopy/reflectomeric interferometry spectroscopy (RIfS). It can be used to measure several aspects of biomolecular interactions such as binding kinetics, concentration and affinity. BLI involves the use of proprietary technology in the form of disposable detector tips (biosensors) developed by ForteBio that enable a binding reaction to be analysed in real time upon the Octet instrumentation. The tip of a biosensor is the location for the binding reaction to be monitored. Biosensors have an optical coating with a biocompatible matrix which enables the immobilisation of a variety of different biomolecules. A range of standard surface chemistries are available to enable sample immobilisation, such as protein A and protein G for antibody binding and glutathione biosensors to bind the GST tag. Within this study, streptavidin sensors were used to immobilise biotinylated proteins.

BLI is carried out upon the Octet system in which up to eight biosensors can be used to analyse eight samples in parallel in an automated manner. This enables multiple conditions, proteins or concentrations to be analysed at one time. Experiments/assays are carried out across the columns of a standard 96 well plate in which the instrument moves the biosensors across and into separate wells for each step of the binding assay. Bringing the biosensor to the sample of interest removes the need for microfluidics systems which is common in other known real time binding assays such as Biacore/surface plasmon resonance instruments. To remove the effects of diffusion, the sample plate is maintained on a shaker throughout the experiment which can be set to oscillate between 100-1500 rpm.

BLI measurements are carried out in real time, as binding is monitored by the building up of a protein layer upon the surface of the biosensor (schematic illustration shown in Figure 5.3A). During an assay, white light is shone down the long axis of the biosensor, with the instrument collecting the light which is reflected back from the end of the sensor. Protein binding to the biosensor tip, shifts the interference pattern of white light. The instrument measures and reports the change in wavelength as a function of time, with the wavelength shift ($\Delta\lambda$) being a direct measurement of the optical thickness of the biological layer. Therefore only if one or

more species are binding to the biosensor tip it affects the trace from the instrument. The observed interference pattern is analysed as a comparison between two surfaces: the immobilised protein layer upon the biosensor, and an internal reference layer within the tip itself, illustrated in Figure 5.4. This interference data create a unique spectral signal within the visible spectrum which is reported in relative intensity units (nm). [231,232] In this study, BLI was utilised as a kinetic binding study to monitor protein:protein interactions and to calculate dissociation constants between putative binding partners. To enable this calculation, each step of the binding assay (e.g. loading, association, dissociation) was carried out across five columns of a 96 well plate, with seven different concentrations of binding partner. The traditional steps of the experiment, the status of the biosensor tip and example data read outs are shown in Figure 5.3.

The experimental assay was initiated with the establishment of a buffer baseline in which the sensors are equilibrated in the buffer solution which is used throughout the whole experiment (Step 1). Biosensors are then moved to the next column of the plate containing the tagged protein which is immobilised upon the biosensor until a.new baseline optical readout has been achieved (Step 2). The bait-loaded sensor is then equilibrated in the buffer used in the experiment to establish an experimental baseline (Step 3). The association step is initiated by shifting the biosensors into wells containing the binding partner of interest (Step 4) which is followed by moving the sensor into buffer enabling dissociation to occur (Step 5). The association and dissociation events are observed by a change in the optical readout. To calculate the dissociation constant from the relative intensity units, serial dilutions of the protein binding partner were tested in parallel by aliquoting them down a column of wells in the plate. Following subtraction of the baseline reading (Figure 5.3C), the change in relative intensity units for each analyte concentration were extracted and a dissociation constant (K_d) calculated by fitting the data to a one to one binding model using the program Sedfit

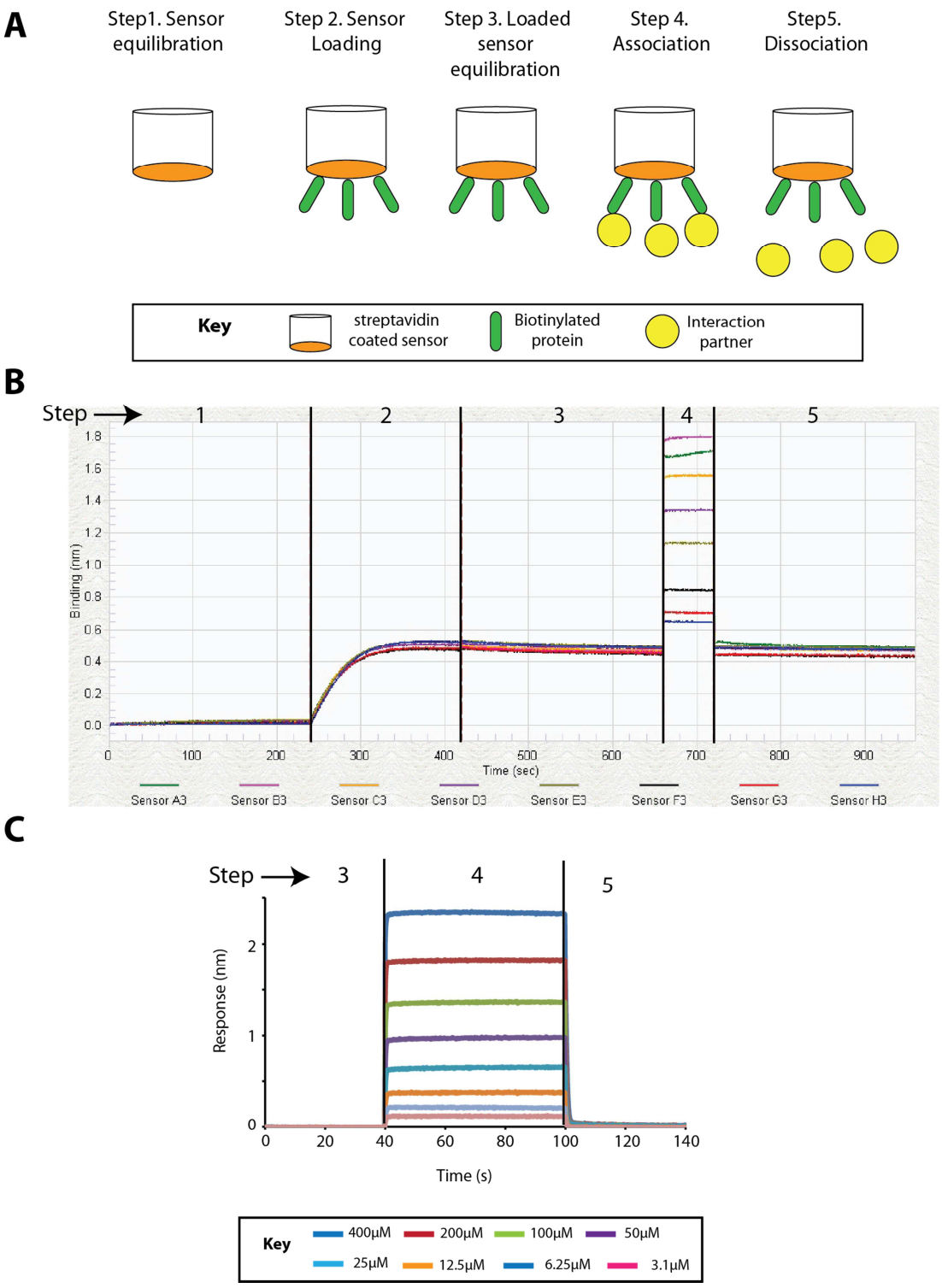

Figure 5.3 Schematic representations of the steps involved in the biolayer interferometry assays.

A, Schematic representation of streptavidin biosensors throughout the course of one binding experiment. Briefly, the sensor is equilibrated (1) followed by loading of the sensor with the tagged protein of interest (2). The loaded sensor is equilibrated in the buffer to be used throughout the experiment (3), prior to association with the protein of interest (4) which is followed by a dissociation step (5). B, Experimental binding assay raw data taken from the Octet instrument. Steps in the experiment are indicated by the numbers above the trace. C, An example of processed BLI data. The raw data has been truncated to just include the binding events and the baseline normalised to the absorbance of the loaded biosensor.

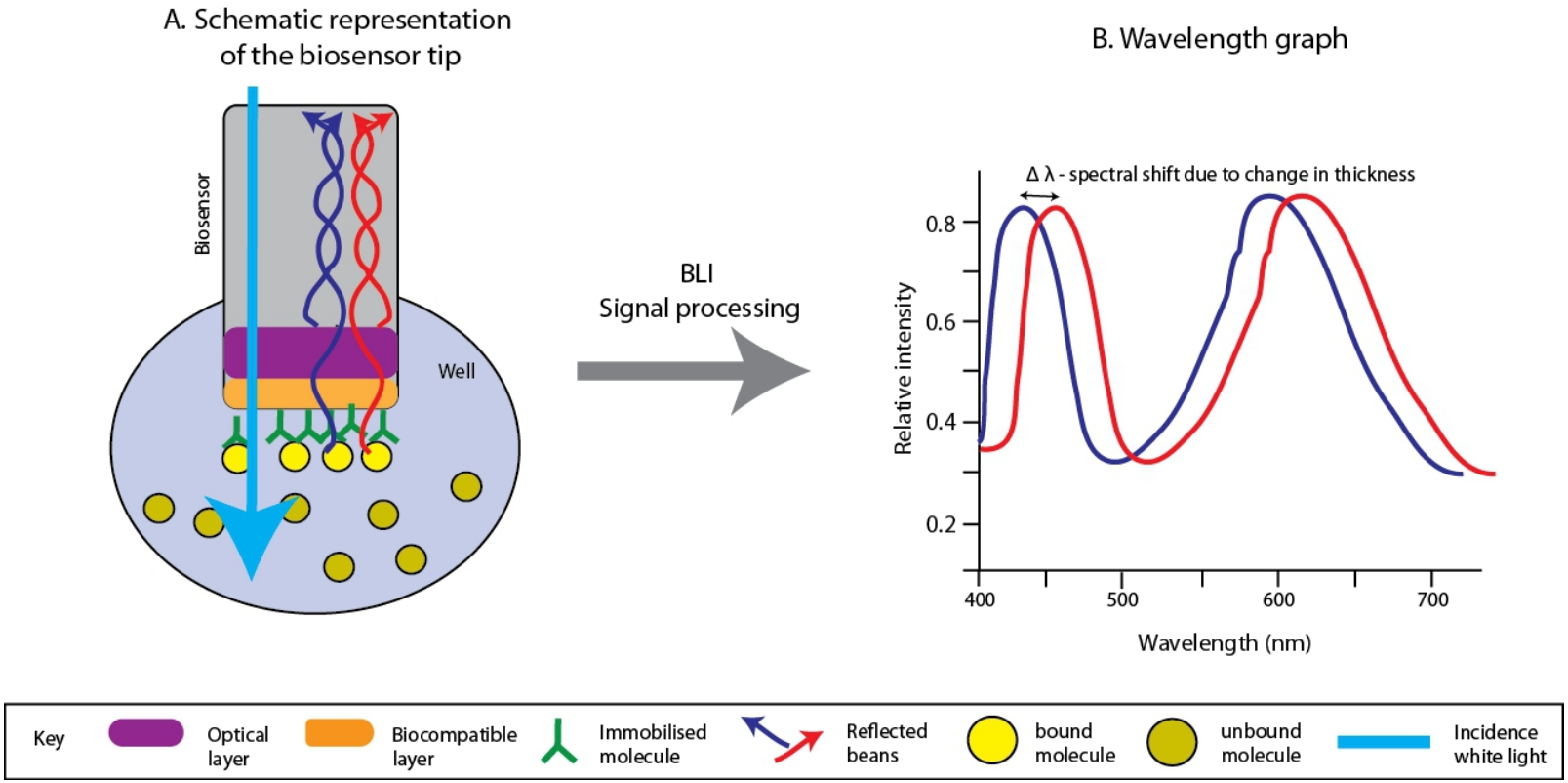

Figure 5.4 Principles behind the biolayer interferometry assay

A. Schematic representation of a biosensor within a well. The immobilised protein upon the biosensor binds to molecules in solution increasing the biological layer upon the tip of the biosensor. White light is shone down the biosensor, the instrument collects the light which is reflected back from the surface of the sensor The effect of a biomolecule binding to the sensor surface is detected from the difference in the reflected light from a reference/optical layer and the biocompatible layer. A comparison between these two signals (spectral shift) is used to calculate biomolecule binding. This is illustrated via the wavelength graph (B) which the instrument generates during processing reporting the difference as a standardised unit. Adapted from Concepcion et al. (2009)

5.1.2.4 NMR titrations with ^{15}N-labelled protein samples

The most common method of studying protein:protein interactions by NMR is to monitor the two dimensional ^{1}H/^{15}N-HSQC spectrum of a labelled protein as an (unlabelled) putative binding partner is titrated into the sample. This method is known as a '^{15}N titration' experiment. A ^{15}N titration enables the monitoring of resonance frequencies and line widths of the spectrum upon addition of binding partners. If the chemical shift assignments are known for the ^{15}N-labelled protein, the effect of the addition of an unlabelled binding partner upon the cross peaks in the spectrum can be related to the protein structure. This approach is referred to as 'chemical shift mapping', in which the affected cross peaks can be used to map a putative binding site upon the structure of the protein of interest.

A change in the chemical environment of the nuclei that give rise to a cross peak typically results in chemical shift perturbation. Perturbation reflects a change in the atoms which are in close proximity to the nuclei which gave rise to the cross peak, which could be caused by a change in the local atomic configuration, an induced conformational change which has been brought about by the presence of a binding partner, at a more or less remote site or a combination of the two. The protein surface which corresponds to the location of perturbed cross peaks is commonly interpreted as revealing the binding site of an interaction partner but the effects upon a ^{1}H/^{15}N-HSQC can radiate beyond the contact surface upon the labelled protein[233].

Chemical shift mapping is a method which can also be used to characterise the kinetic process of two site exchange between two molecules. Two site exchange is characterised by an exchange rate constant (k_{ex}), which is sum of the forward (binding) and reverse (unbinding) of a reaction. A simple ligand two-site exchange binding can be considered as:

$$P + L \underset{k_{off}}{\overset{k_{on}}{\leftrightarrows}} PL \qquad \textit{Equation 5.5}$$

P represents the free protein, L is the ligand (or protein binding partner) and PL is the bound form of the protein, ligand complex. k_{on} represents the binding of the ligand to the protein as a biomolecular second order rate constant, whereas k_{off}

represents dissociation of the complex as a first order rate constant. Therefore k_{ex} is characterised as:

$$k_{ex} = k_{on} + k_{off} \qquad \textit{Equation 5.6}$$

Within the NMR spectrum, both the free and bound forms of the protein have resonance frequencies, represented as ν_P and ν_{PL}, which result in a chemical shift difference, reported in angular frequency units – s^{-1}.

$$\Delta\nu = \nu_P - \nu_{PL} \qquad \textit{Equation 5.7}$$

The appearance of the corresponding features in the $^{1}H/^{15}N$-HSQC spectrum is dependent upon the populations of each state, the magnitude of the exchange rate constant and the chemical shift difference $\Delta\nu$. The exchange rate corresponds to the average number of exchange events per unit time which enables comparison with $\Delta\nu$. The nature of the observed chemical exchange is typically characterised as belonging to one of three exchange regimes, slow exchange ($k_{ex} < \Delta\nu$), fast exchange ($k_{ex} > \Delta\nu$) and intermediate exchange ($k_{ex} \sim \Delta\nu$). Each regime is associated with a pattern of ligand concentration dependent effects on the appearance of the corresponding NMR resonances (and cross peaks).

When an interaction is undergoing slow exchange, separate signals are observed which represent both the free and bound states of the protein (and/or ligand). This is due to the exchange rate being lower than the frequency differences within the spectrum. The linewidth of each resonance/cross peak is not materially affected by exchange in this case. In this instance, a bound state spectrum may need its own set of assignments to be carried out. Peaks undergoing fast exchange are the easiest to follow when implementing chemical shift mapping as only a single peak is observed. The chemical shifts of the affected spectral features change as a function of the concentration of the binding partner. The behaviour enables the affected peaks to be easily followed and mapped back to the original peaks in the free state spectrum and then onto the three dimensional structure of the protein. This occurs because the exchange rate constant k_{ex} is greater than then chemical shift difference between the two states. Binary systems interacting in intermediate exchange regimes are characterised by the observation of overall line broadening of the affected peaks and dependent on ligand concentration, the broadening of spectral lines, resulting in loss

of signals within the spectrum. In these circumstances, the exchange rate constant is within the same order as the chemical shift differences. Assignment is more or less straight forward depending upon the overall effect of signal loss, the extent of binding and spectral overlap.

Throughout a ^{15}N-titration, the cross peak intensity can be affected by any one of these exchange regimes, which is ultimately dependent upon the binding properties (K_{on}/K_{off}) of the ligand to the ^{15}N-labelled protein. In principle it is possible for all three exchange mechanisms to occur within the same experiment, through different binding sites on the molecule undergoing different exchange regimes. However simultaneous fast and slow behaviours occurring from the same interaction are highly unlikely[234].

5.2 DNA cloning of constructs of intracellular Fas and ezrin FERM domain into *E. coli* protein expression vectors

The expression constructs of Fas Death Domain (DD) (residues 218-319) and Fas DD+C-terminal region (CTD) (residues 218-335) were kindly provided by Dr Diego Esposito. All other constructs were made by cloning into pNIC-NTH vectors (detailed methodology in Section 2.4.2). pNIC-NTH are vectors for ligation independent cloning developed at the Oxford site of the Structural Genomics Consortium[221]. They encode the introduction of an N-terminal hexa-histidine tag for affinity purification, either a GB1 or a GST fusion tag for immobilisation and/or solubility enhancement and a tobacco-etch virus (TEV) protease cleavage site. The pNIC-NTH vector with a GB1 tag was developed in our laboratory.

Fas constructs were subcloned from existing plasmid vectors available in our laboratory. Ezrin was cloned from human neural cDNA (DV Biologics). The ezrin FERM-truncated coiled coil (tCC) construct (residues 1-362) is equivalent to the construct used in the pull-down experiments carried out by Louzepone *et al.* (2004).

A schematic diagram illustrating the protein constructs used throughout this chapter are shown in Figure 5.5. The molecular weight and extinction coefficient for each construct was estimated using the EXPASY ProtParam server, this information is shown in Table 5.1 below. Throughout this chapter, different constructs are referred

to by the construct names listed in Table 5.1. Fas residues are numbered according to UniProt:P25445.

Table 5.1 Properties of Fas and ezrin constructs

Construct name	**Residues**	**Predicted molecular mass***	**Extinction coefficient (M^{-1} cm^{-1})**	**tag**		
				GST	**GB1**	**H_6Avi**
Fas-DD	218-319	13315	8480			
Fas-DD+CTD	218-335		8480			✓
Fas-JM(-MPD)-DD+CTD	208-335	14335	8480	✓	✓	
Fas JM+DD+CTD	194-335	16101	8480	✓	✓	✓
Fas-TM+IC	185-335	17221	13980	✓	✓	
Ezrin FERM+tCC	1-362	43170	53860	✓	✓	
Ezrin FERM	1-297	35026	52370		✓	

DD, death domain; CTD, C-terminal domain; JM juxtamembrane; MPD, membrane-proximal domain; IC intracellular, tCC, truncated coiled coil domain; FERM, four point one ezrin radixin moesin domain

* following removal of the affinity tag by TEV protease cleavage

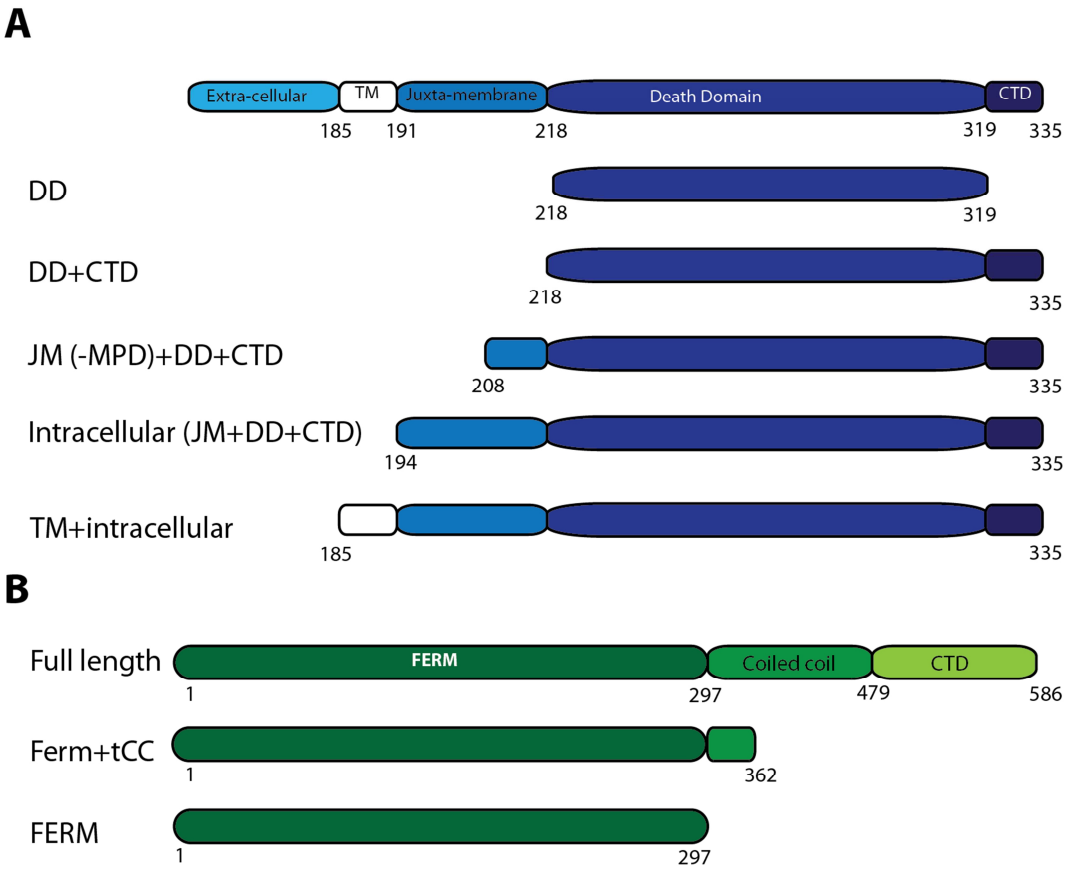

Figure 5.5 Schematic representation of Fas and ezrin proteins and construct design.

A, Full length Fas indicating the domain architecture and numbering used throughout this chapter. The extracellular region is present to illustrate the shape of the whole molecule and is not to scale. TM -, transmembrane domain, JM - juxtamembrane domain, MPD - membrane proximal domain, CTD - C-terminal domain. Shorter Fas truncation constructs are shown below the full length diagram. B, Full length ezrin indicating the domain orientation and numbering used throughout this chapter. FERM - band four point one ezrin radixin moesin, tCC – truncated coiled coil domain, CTD – C-terminal domain. Ezrin truncation constructs are shown below the full length diagram.

5.3 Expression and purification of Fas and ezrin constructs

The *E. coli* strain BL21 (DE3) Gold was used for the expression of all Fas and ezrin constructs. An expression test for each construct was performed as described in Section 2.5.2, assaying expression by SDS-PAGE. Expression for all constructs was optimal when cells were induced with 0.5 mM IPTG for sixteen hours at 22 ^{o}C. These were the conditions used for large scale expression of the proteins, as described in Section 2.5.3.

When fused to an N-terminal hexa-histidine tag, expressed proteins were initially purified by immobilised metal affinity chromatography (Ni-IDA, Generon). Then solubility and purification tags were removed by cleavage with TEV protease. A final purification step was carried out using size exclusion chromatography (SEC; Superdex75, GE Healthcare) (Section 2.6). SDS-PAGE analysis and SEC chromatograms of typical Fas and ezrin preparations are shown in Figures 5.6 and 5.7.

When fused to an N-terminal GST tag, expressed proteins were initially purified by glutathione sepharose (GE healthcare) affinity chromatography using a batch binding method to load the beads. Then solubility and purification tags were removed by treatment with TEV protease. A final purification step was carried out using size exclusion chromatography (SEC; Superdex75, GE Healthcare) (Section 2.6).

The solubility of Fas constructs was enhanced by the presence of the K263A mutation which has been shown to enable Fas-DD constructs to be concentrated up to 800 μM without aggregation. This enabled preparation of protein at concentrations suitable for NMR samples. The Fas constructs containing more of the intracellular and transmembrane domain were less stable and could not be concentrated to such a high concentration due to protein precipitation. Ezrin constructs were stable up to 600 μM with no solubility problems. The FERM-tCC construct formed a dimer observable upon a SDS-PAGE gel as well as by SEC. This limited concentration to ~400 μM.

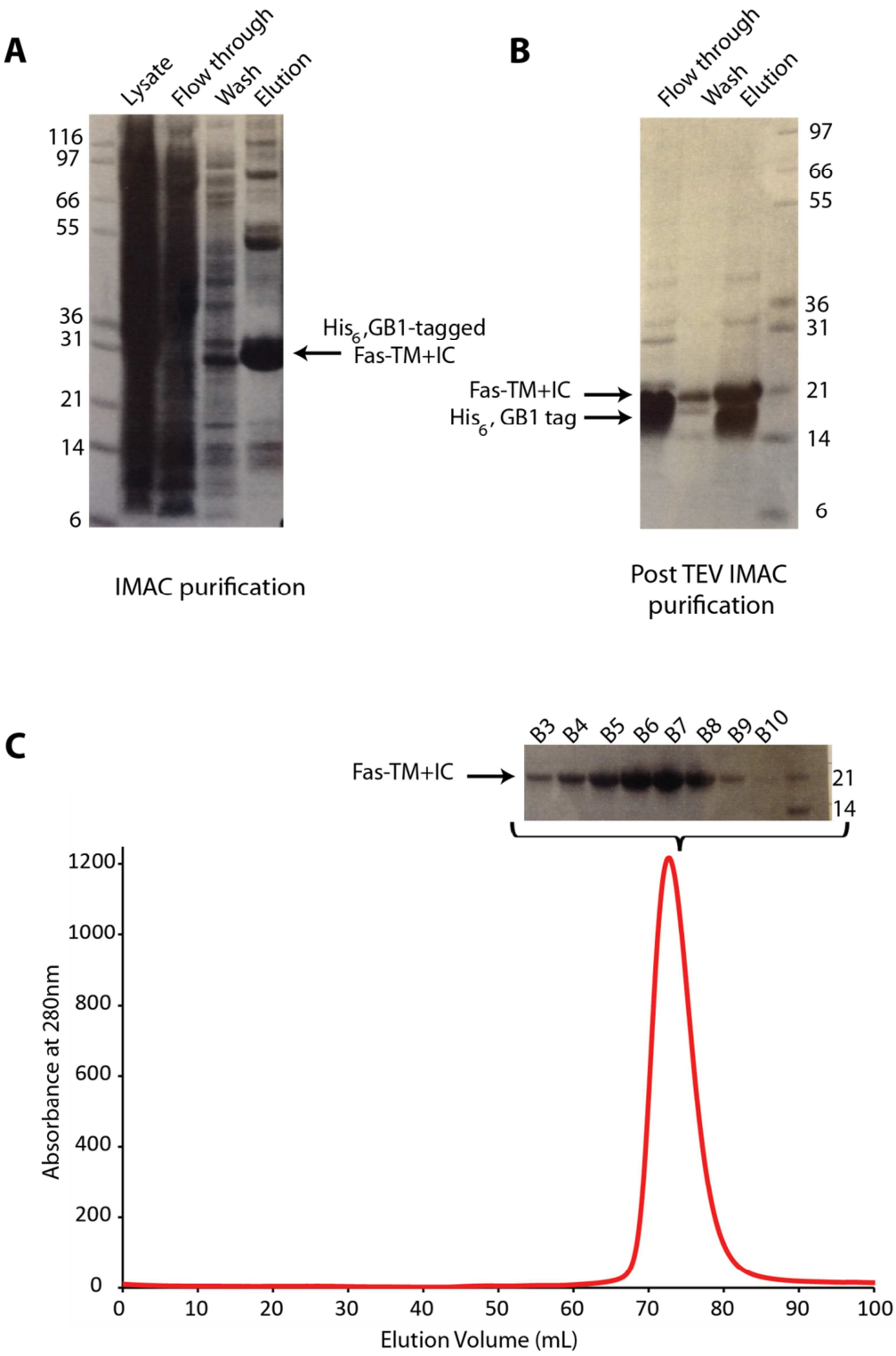

Figure 5.6 Fas 185-335 purification

A, SDS-PAGE analysis of the IMAC purification of Fas-TM+IC. B, SDS-PAGE analysis post TEV cleavage. C, The elution profile (monitored by UV absorbance at 280nm) and SDS-PAGE analysis of Superdex 75 SEC.

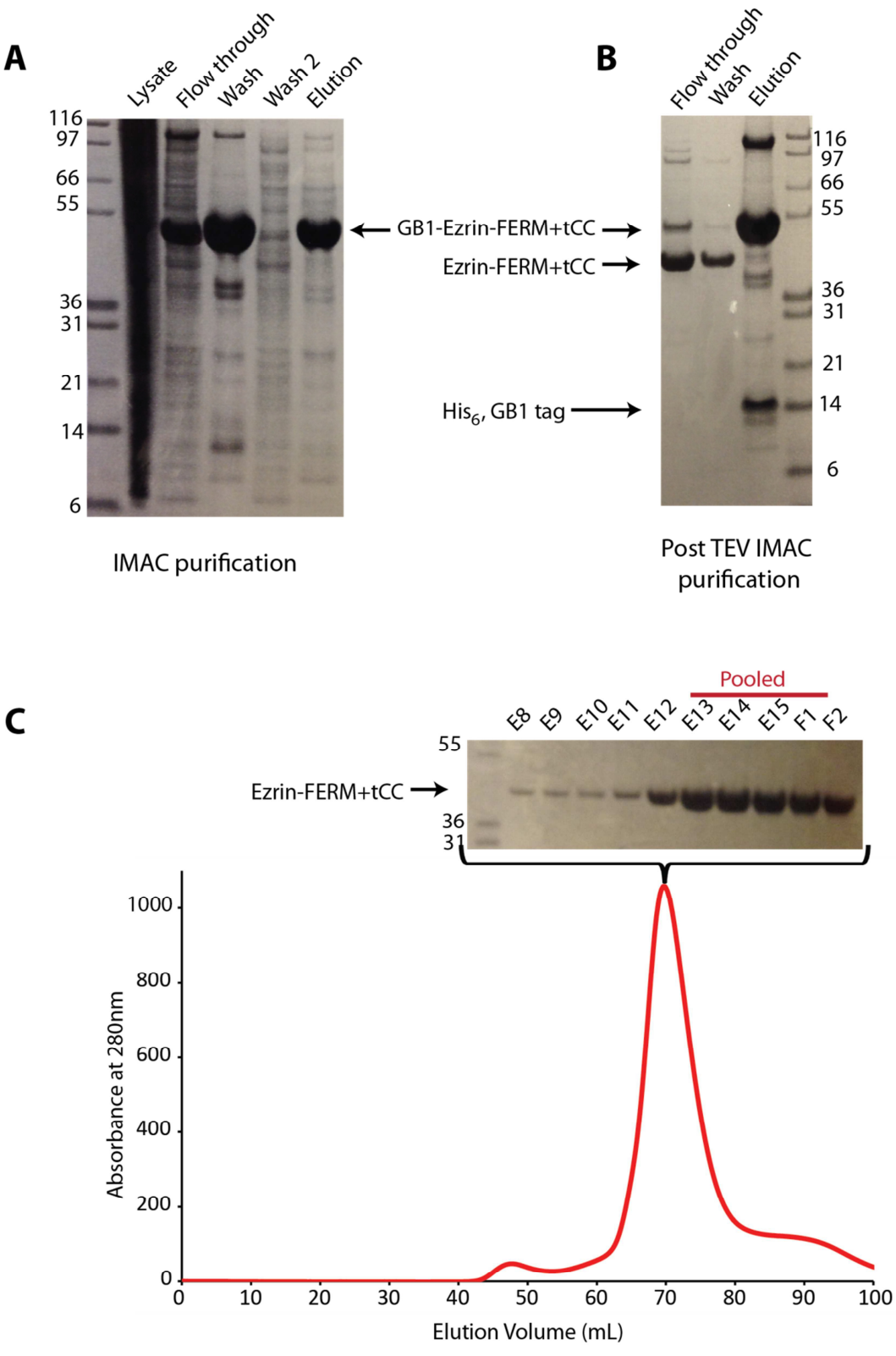

Figure 5.7 Ezrin 1-362 purification

A, SDS-PAGE analysis of the IMAC purification of Ezrin-FERM+tcc. B, SDS-PAGE analysis post TEV cleavage. C, The elution profile (monitored by UV absorbance at 280nm) and SDS-PAGE analysis of Superdex 75 SEC. The red line indicates the fractions that were pooled.

5.4 An interaction between intracellular Fas and ezrin is not observed in a number of conventional biophysical assays

5.4.1 A variety of pull-down assays with Fas-JM+DD+CTD and ezrin FERM+tCC failed to detect an specific interaction

In an attempt to replicate the GST pull-down assay carried out by Lozupone *et al*. (2004)[117], GST-tagged ezrin FERM+tCC was immobilised onto glutathione sepharose beads as bait and Fas-JM+DD+CTD was used as prey. Lozupone and coworkers used a variety of ezrin constructs to map the binding site, but because the purpose of this study was to validate the fundamental result of their study, only the longest ezrin construct in their assay (FERM+tCC) was tested.

Preliminary GST-pull down experiments were attempted with these two protein constructs but they failed to show a Fas and ezrin interaction (data not shown). To ensure that the expressed and purified Fas and ezrin constructs were correctly folded, a number of controls were added to the experiment. As a positive control for Fas binding, the GST-FADD:Fas pull down previously published by our laboratory[123] was used. As a positive control for ezrin binding, we selected an 18 amino acid sequence corresponding to the region of Na^+/H^+ exchange regulatory factor 2 (NHERF2) that has been crystallised bound to the radixin FERM domain[111]. The sequence of the peptide was introduced into the pNIC-GB1 vector, and the GB1-NHERF2 (residues 320-337) fusion protein expressed and purified. To control for Fas binding to GST as opposed to ezrin, a stop codon was inserted into the pNIC-GST vector to enable the expression and purification of GST alone. Fas-JM+DD+CTD was also incubated with the glutathione sepharose beads on its own to control for non-specific binding. GST-tagged proteins were incubated with 50 μg of their respective binding partner for sixteen hours. Beads were equilibrated and washed in 20 mM MES, 100 mM NaCl, 1 mM EDTA, 0.5 mM TCEP, pH 6.2 and then added to the protein mix. Pull downs were then analysed by SDS-PAGE analysis followed by Coomassie Blue or silver staining (Figure 5.8).

Evidence of a productive interaction was detected for both positive controls GST-FADD:Fas and GST-Ezrin:GB1-NHERF2 (residues 320-337). This pull down confirmed that the conditions of the assay were appropriate to detect protein:protein interactions and that both Fas and ezrin were in a suitable conformation to be able to

bind their well-documented binding partners. However, Fas was also pulled down by GST and by the gluthatione sepharose beads. To try and reduce this non-specific binding, the assay was repeated with the addition of 0.1% NP40 detergent and 1 mg/ml BSA, but this did not prevent this non-specific binding (data not shown).

Due to Fas binding to the gluthatione sepharose beads, an alternative pull down using immobilised hexahistidine-tagged Fas-JM+DD+CTD was tested. Lysate of cells which express H_6-GB1-Fas-JM+DD+CTD was used to load the Ni-NTA beads which were then incubated with 25 μM of purified ezrin FERM domain for sixteen hours. Beads were equilibrated and washed in 30 mM Tris-HCl, 150 mM NaCl, 10% glycerol, 1% Triton, 1 mM EDTA, 10 mM imidazole, pH 7.5. The results can be seen in Figure 5.9. Fas was successfully loaded onto the beads and appeared to have pulled down ezrin. However, the unloaded bead control had also pulled down ezrin, suggesting that this untagged ezrin construct can bind to these beads in a non-specific manner. These pull down conditions were not further optimised as the buffer conditions already contained additives to reduce non-specific binding.

As a third option, co-immunoprecipitation of H_6-GB1-Fas ezrin was attempted with an anti-H_6 antibody. Cell lysate containing H_6-GB1-Fas-JM+DD+CTD was precleared by incubation with Protein G magnetic beads for one hour. After preclearing, anti-H_6 antibody (5 μg/ml) was added to the lysate and the mixture was incubated overnight with ezrin (25 μM). Following ezrin incubation, the conjugate was incubated with Protein G magnetic beads for one hour, the beads were then washed with PBS and finally analysed by SDS-PAGE and silver staining (Figure 5.10). Unfortunately, like the two previous pull downs detailed above, ezrin bound to the beads with or without Fas, so presumably in a non-specific manner. Furthermore, it was not possible to observe a band on the gel corresponding to H_6-GB1-Fas-JM+DD+CTD. Perhaps the light chain of the antibody and the tagged Fas construct migrate on the gel at a similar rate. Being unable to observe Fas is sub-optimal for a pull down because it would be impossible to prove that it was the Fas that gave rise to the pull down of a binding partner rather than the antibody and due to this the immunoprecipitation approach was not further explored.

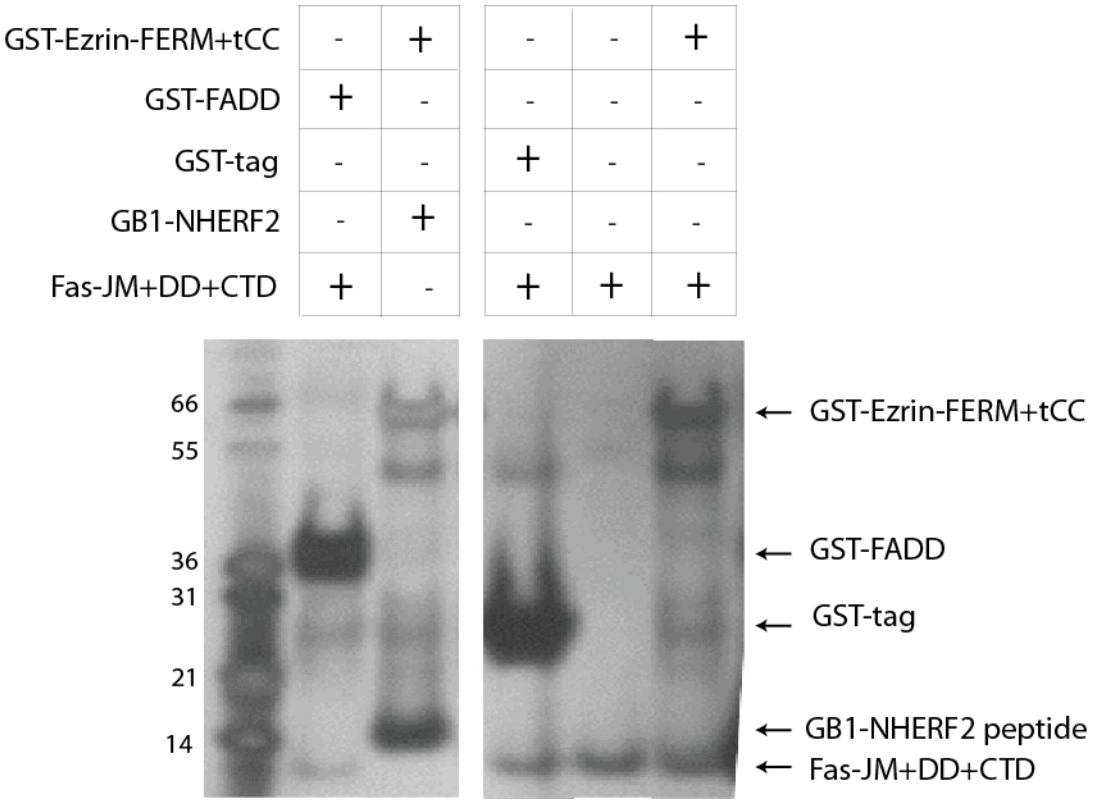

Figure 5.8 Silver stained pull down using Glutathione sepharose beads to immobilise GST-ezrin-FERM+tCC to pull down Fas-TM+IC

GST ezrin-FERM+tCC was immobilised upon glutathione sepharose beads and incubated with Fas or a number of binding partners to control for whether Fas and ezrin were able to bind to known binding partners (GST-FADD to ensure the Fas construct bound and GB1-NHERF2 to ensure GST-ezrin could pull down protein) as well as whether Fas bound to the beads or the GST tag upon the ezrin construct. Beads were equilibrated and washed in 20mM MES, 100mM NaCl, 1mM EDTA, 0.5mM TCEP, pH6.2. 50µg of each protein partner was incubated for sixteen hours prior to washing and analysis.

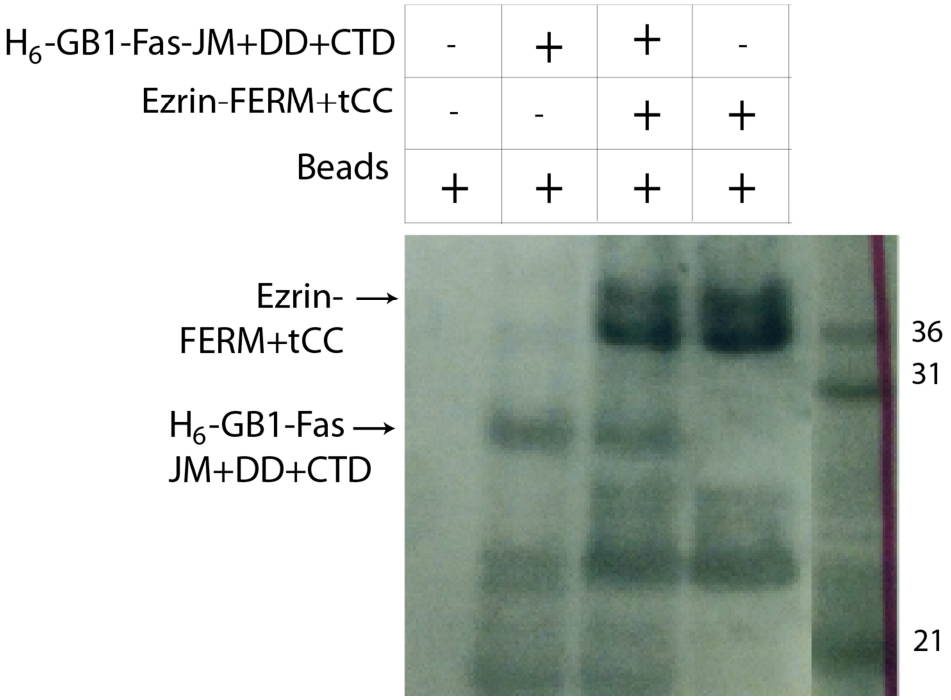

Figure 5.9 Silver stained pull down using Ni-NTA beads to immobilise H_6-GB1-Fas-JM+DD+CTD to pull down ezrin-FERM

H_6-GB1-Fas-JM+DD+CTD was immobilised upon Complete Ni-NTA beads and incubated with 25μM ezrin-FERM for sixteen hours. Beads were equilibrated and washed in 30mM Tris-HCl, 150mM NaCl, 10% glycerol, 1% Triton, 1mM EDTA, 10mM imidazole, pH7.5. Unfortunately ezrin was observed to bind to the Ni-NTA beads therefore this would not be a suitable method for observing any interactions. Bands which are unlabelled are non-specific binding from the H_6-GB1-Fas cell lysate used to load the beads.

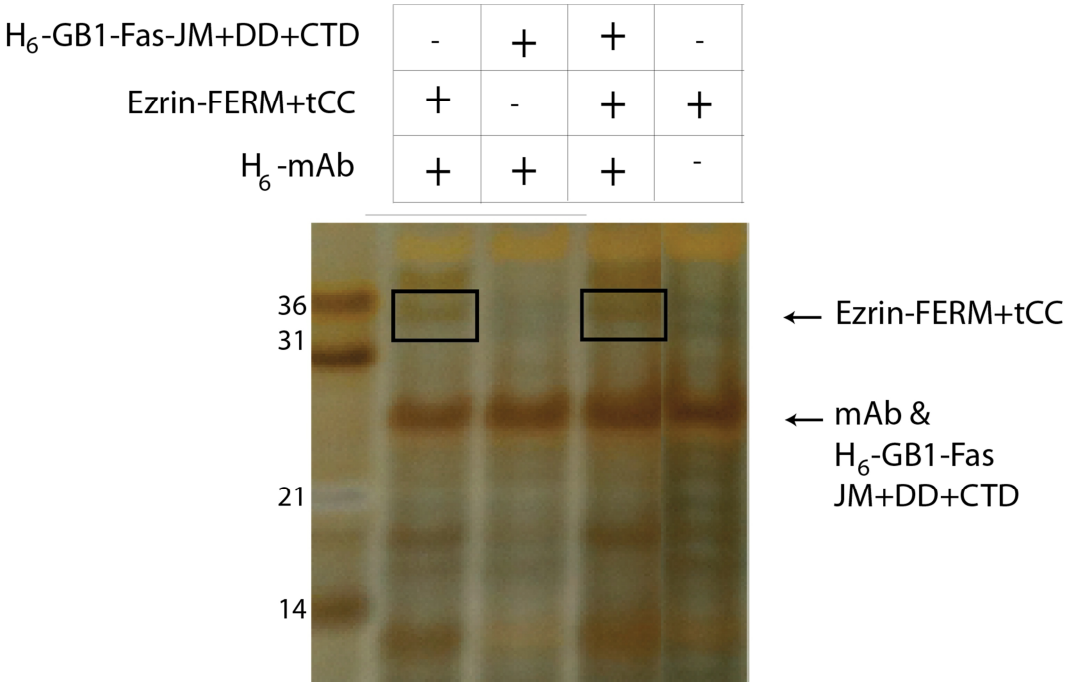

Figure 5.10 Silver stained immunoprecipitation using H_6 antibody coupled to protein G magnetic beads to pull down ezrin FERM with H6-GB1-Fas-JM+DD+CTD

H_6-GB1-Fas-JM+DD+CTD was immobilised upon Complete Ni-NTA beads and incubated with 25μM ezrin-FERM for sixteen hours. Beads were equilibrated and washed in 30mM Tris-HCl, 150mM NaCl, 10% glycerol, 1% Triton, 1mM EDTA, 10mM imidazole, pH7.5. Unfortunately ezrin was observed to bind to the Ni-NTA beads therefore this would not be a suitable method for observing any interactions. Bands which are unlabelled are non-specific binding from the H_6-GB1-Fas cell lysate used to load the beads.

5.4.2 Size exclusion chromatography does not show co-elution of Fas-JM+DD+CTD and ezrin FERM

To assess the ability of intracellular Fas and ezrin to form a higher molecular weight complex, purified Fas-JM+DD+CTD and ezrin FERM were combined with a molar excess of the Fas construct and loaded into an analytical SEC column (Superdex 75 10/300GL; GE Healthcare) that had been calibrated using the following molecular weight standards: lysozyme (15 kDa), RNase (25 kDa), cytochrome C (29 kDa), ovalbumin (45 kDa) and BSA (66 kDa) (Figure 5.11).

Purified ezrin-FERM and Fas-JM+DD+CTD constructs, both in 20 mM Tris, pH 7.4, 150 mM NaCl, 1 mM EDTA, 1 mM TCEP, 3 mM NaN_3, were mixed in a 1:4 ratio and concentrated to a final protein concentration of 1 mM (200 μM ezrin:800 μM Fas). A hundred μl of the solution were injected onto the analytical SEC column previously equilibrated in the same buffer. As shown in Figure 5.4, the co-concentrated Fas and ezrin sample eluted as two separate peaks with no indication of a higher molecular weight complex being formed. The elution volumes of the two peaks in the mixed protein sample overlaid perfectly with the elution volumes of the proteins obtained when they were individually injected (at 10.18 ml and 12.05 ml). This behaviour suggests that Fas and ezrin do not form a high molecular weight complex when mixed at this concentration or that the association constant for any such complex formation is too low to be observed by analytical SEC.

5.4.3 Isothermal titration calorimetry measures no heat of exchange upon mixing Fas-JM+DD+CTD with ezrin FERM+tCC

Isothermal titration calorimetry (ITC) experiments were carried out at 10 ^{o}C, 20 ^{o}C and 25 ^{o}C. The sample cell contained ezrin FERM+tCC (50 μM) and the syringe contained Fas-JM+DD+CTD (500 μM). No heat of interaction was observed suggesting that if an interaction occurs, it does not absorb or emit a significant amount of any heat. Interestingly, other confirmed protein-protein interactions involving death domains do not have any observable heat exchange (Dr Diego Esposito and Dr Lily Nematollahi, personal communication).

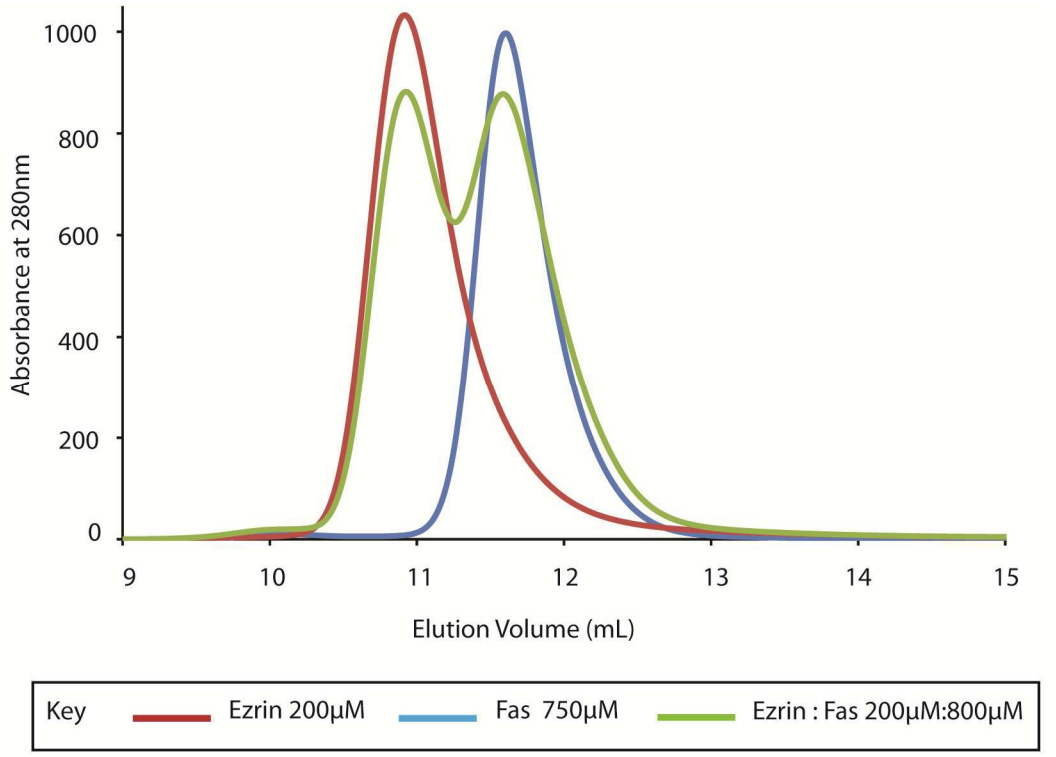

Figure 5.11 Fas and ezrin do not co-elute from an analytical size exclusion column suggesting a weak interaction

Ezrin-FERM and Fas-JM+DD+CTD were co-injected onto an analytical Superdex 75 size exclusion column (in ezrin NMR buffer) to see whether an interaction could be observed by the presence of co-elution. The three runs are overlaid, with Fas (750µM) in blue, ezrin (200µM) in red and the co-concentrated ezrin:fas (200µM:800µM) in green.

5.4.4 Sedimentation velocity analytical ultracentrifugation experiments of Fas-DD+CTD with ezrin FERM+tCC gives no definitive suggestion of complex formation

Sedimentation velocity analytical ultracentrifugation (SV-AUC) experiments were carried out as described in Section 2.7.5, with all samples dialysed overnight into 20 mM Tris, 150 mM NaCl, 0.5 mM TCEP, pH 7.4. Initially, data for Fas and ezrin samples alone were collected at concentrations ranging from 0.5 mg/ml to 2 mg/ml. Figures 5.12 and 5.13 show representative data analyses for Fas (0.5 mg/ml) and ezrin (1 mg/ml), showing the experimental time-dependent sedimentation profiles, the residuals and the derived sedimentation coefficient distributions c(S) (graph in B) obtained after fitting the data with the program SEDFIT. These data show the Fas-DD+CTD and ezrin FERM+tCC are both monomeric when alone in solution and have a sedimentation coefficient (S value) of 1.6 S and 2.8 S, respectively. These sedimentation coefficients were reproducible across all concentrations tested. The Fas experiments predicted the molecular weight to be ~18 kDa, about 6 kDa larger than the expected mass for this construct. The predicted molecular weight for ezrin was ~43 kDa which is around the expected monomeric weight for this construct. Table 5.2 lists the ultracentrifugation experiments carried out and the results obtained.

Table 5.2 Summary of the SV-AUC experiments for Fas and ezrin

Concentration (mg/ml)	**S**	**f/f_o**	**Mw (kDa)**	**Fit (RMSD)**
Fas-DD+CTD				
0.5	1.62	1.32	18.2	0.003
2.0	1.61	1.41	18.2	0.004
Ezrin-FERM+tCC				
0.5	2.88	1.38	44.9	0.008
1.0	2.83	1.36	43.9	0.006
2.0	2.89	1.31	42.7	0.010

S, sedimentation coefficient; MW, molecular weight in kDa; %, % of that species present;, f/f_0, frictional ratio.

SV-AUC experiments were also carried out for Fas and ezrin mixed at equimolar concentrations of 20 μM, 50 μM and 100 μM. Figure 5.14A shows a representative experiment including experimental time-dependent sedimentation profiles, the residuals and the derived sedimentation coefficient distribution c(S). A summary of the SV-AUC experiments of mixed Fas and ezrin can be seen in Table 5.3. As can be seen from Figure 5.14B and Table 5.3, the majority of the Fas and ezrin within the sample appeared to remain in its monomeric form at all three concentrations with ~20% sample being monomeric Fas and ~76% of the sample being monomeric ezrin. Sedfit estimates the contribution that each species has on the total absorbance observed. Therefore this distribution of components would be expected if there was no interaction as ezrin has a molecular weight approximately three times that of Fas, therefore there would be approximately three times as much present at an equi-molar concentration. A third species was shown to have formed, with a sedimentation coefficient of ~5, however this only makes up around 2% of the species present for each experiment. This new species has an estimated molecular weight close to 100 kDa which would suggest that a number of ezrin monomers would be involved or a high molecular weight platform of Fas could have formed. However as it is such a small proportion of the sample it is difficult to say whether it has any bearing on Fas and ezrin interacting as the majority of the sample is still made up of Fas and ezrin in a monomeric form, at all three concentrations.

Table 5.3 Summary of the SV-AUC experiments for Fas-DD+CTD and ezrin-FERM+tCC mixture.

Concentration (μM)	**Fas-DD+CTD**			**Ezrin-FERM+tCC**			**Oligomer**			**f/f_0**	**Fit (RMSD)**
	S	**MW**	**%**	**S**	**MW**	**%**	**S**	**MW**	**%**		
20	1.4	13.0	21	2.8	37.5	76	5.3	97.3	1.3	1.226	0.009
50	1.4	13.2	20	2.9	38.9	76	5.8	110.3	2.3	1.211	0.016
100	1.5	14.1	15	3	42	80	5.3	95.3	2.2	1.211	0.018

S, sedimentation coefficient, MW, molecular weight in kDa, %, % of that species present, f/f_0, frictional ratio.

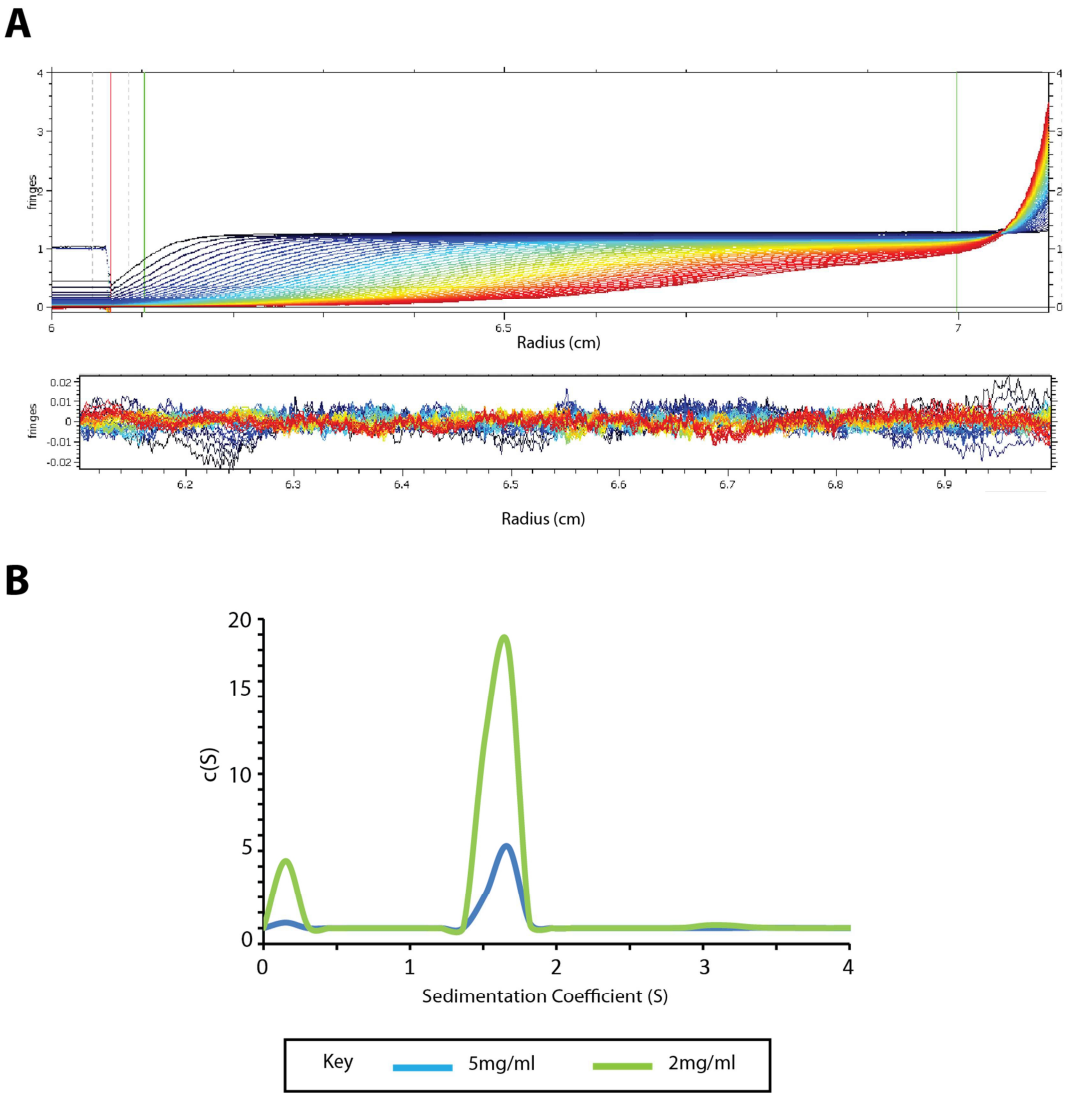

Figure 5.12 Sedimentation velocity profiles, c(S) distribution and residuals for Fas-DD+CTD

Sedimentation velocity measurements were performed on Fas-DD+CTD at concentrations of 0.5mg/ml and 2mg/ml in buffer containing 20mM Tris, 150mM NaCl, 0.5mM TCEP at pH7.4. A, Time-dependent sedimentation velocity profiles and the fit residuals. The meniscus (red line) and fitted data range (between the green lines) are highlighted. B, The c(S) distribution plot showing that Fas is monomeric and sediments with the sedimentation coefficient of 1.6S at the two concentrations of 0.5mg/ml (blue line) and 2mg/ml (green line).

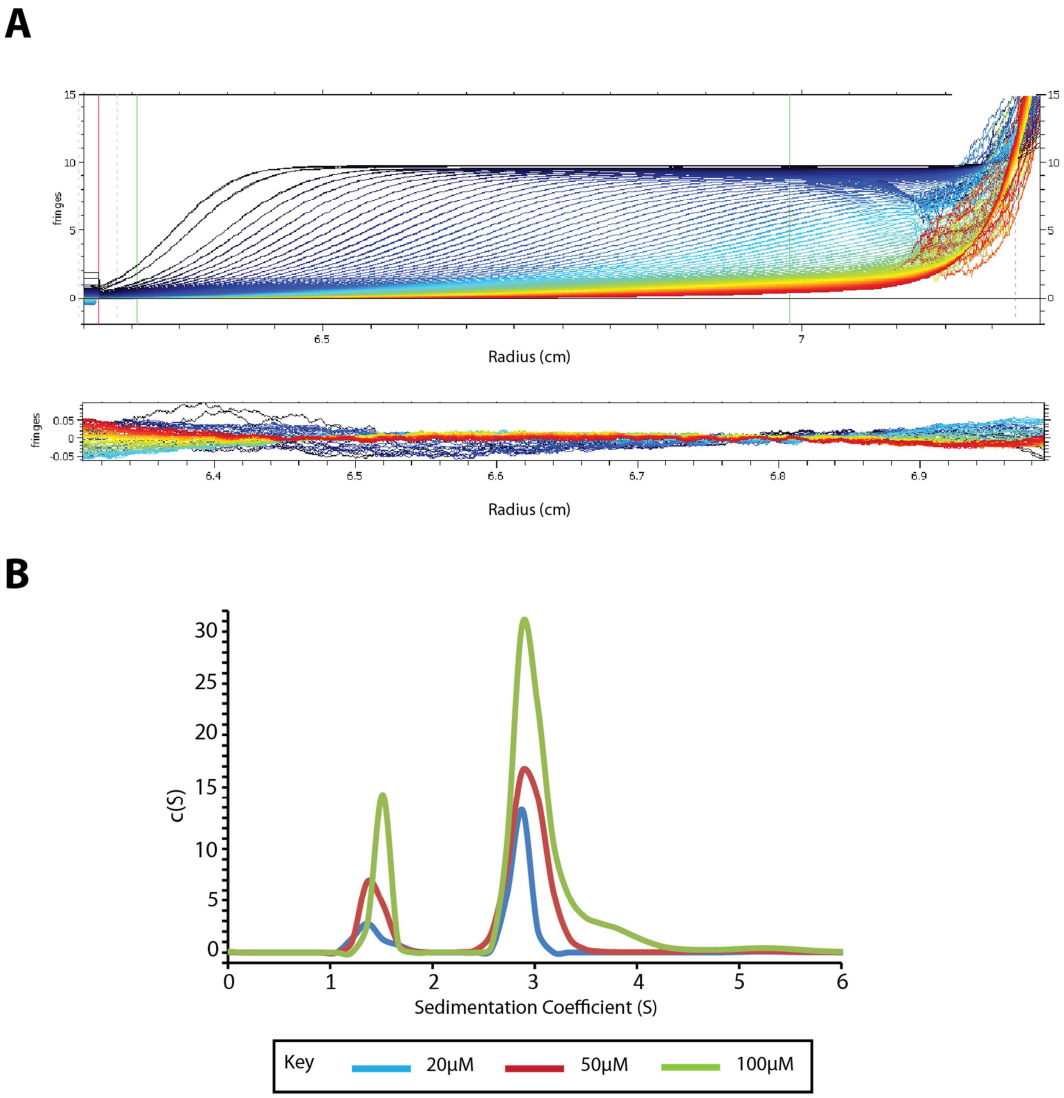

Figure 5.13 Sedimentation velocity profiles, c(S) distribution and residuals for ezrin-FERM+tCC

Sedimentation velocity measurements were performed on ezrin-FERM+tCC at concentrations of 0.5mg/ml, 1mg/ml and 2mg/ml in a buffer containing 20mM Tris, 150mM NaCl, 0.5mM TCEP at pH7.4. Time-dependent sedimentation velocity profiles and the fit residuals are shown in A. The meniscus (red line) and fitted data range (between the green lines) are highlighted. The c(S) distribution plot showing that ezrin is monomeric and sediments with the sedimentation coefficient of 2.8S at the three concentrations of 0.5mg/ml (blue line), 1mg/ml (red line) and 2mg/ml (green line) as shown in B.

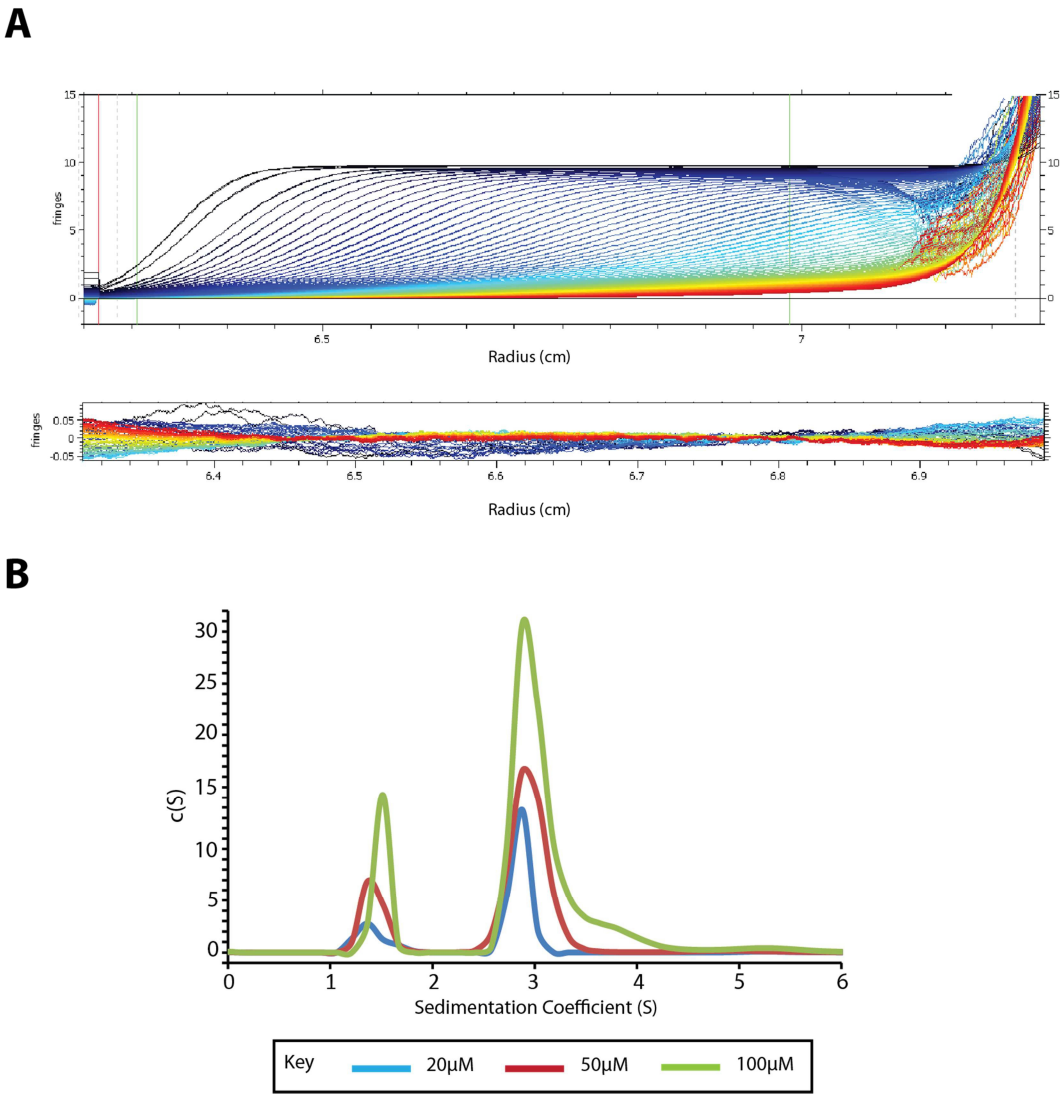

Figure 5.14 Sedimentation velocity profiles, c(S) distribution and residuals for Fas:ezrin complex

Sedimentation velocity measurements were performed on Fas-DD+CTD and ezrin-FERM+tCC mixed at a 1:1 ratio at concentrations of 20µM, 50µM and 100µM, in buffer containing 20mM Tris, 150mM NaCl, 0.5mM TCEP at pH7.4. Time-dependent sedimentation velocity profiles and the fit residuals is shown in A. The meniscus (red line) and fitted data range (between the green lines) are highlighted. The c(S) distribution plot showing the Fas and ezrin monomers at 1.6S and 2.8S respectively, as well as the formation of a larger species between 4 and 5S is shown in B. The third species was more prominent at the higher concentrations. Concentrations represented as, 20µM, blue line, 50µM, red line and 100µM, green line.

5.5 An interaction between Fas constructs and ezrin is observed by BLI

Biolayer Inteferometry (BLI) measures molecular interactions indirectly through changes in the interference pattern of white light between an immobilised protein and an internal reference[231]. Proteins can be immobilised using several chemistries, we were advised to use streptavidin-biotin chemistry due to its robust non covalent immobilisation properties. Because the intensity of the signal depends on the thickness of the biolayer upon binding, it is better to immobilise the smallest protein to the sensor, in this case, Fas. To obtain biotinylated Fas, the Fas-DD+CTD and Fas-JM+DD+CTD DNA constructs were cloned into a vector constructed in our laboratory to allow the expression of proteins with an N-terminal hexa-histidine tag followed by the *E. coli* biotin ligase (BirA) recognition sequence (GLNDIFEAQK*IEWHE - * denotes site of biotin attachment), commonly named by its commercial name Avi-tag. After purification of the protein, the lysine in the recognition sequence can be biotinylated *in vitro* by incubation of the recombinant protein with BirA, biotin and ATP, as described in Section 2.7.3. From here onwards, the tag H_6-linker-TEV-Avi (MKHHHHHHPMSDYDIPTT ENLYFQ GLNDIFEAQKIEWHE GSGSGA), will be referred to as H_6Avi without biotin attached and H_6Avi*, when biotin-labelled.

The setting of a typical BLI experiment was as follows: First, the H_6Avi* Fas constructs are immobilised onto the surface of the sensors using streptavidin. Next the sensors are equilibrated in binding buffer, and then immersed in buffer with the potential binding partner. Finally the sensors are dipped into buffer again in order to measure the dissociation kinetics. The experiment was repeated using different concentrations of ezrin FERM+tCC (from 3.1 to 400 μM) in the plate wells, and also FADD as a positive control, as in the pull down experiments. The interaction was recorded over time and is shown in Figure 5.15. The time-dependent BLI profiles (Figure 5.15A and 5.15C) show that Fas and ezrin associate and dissociate very quickly. The initial baseline in the profile is obtained when the biotinylated protein is being equilibrated in the binding buffer. When the sensor is immersed into the solution with the potential binding partner, the response increases as more protein is bound to the sensor. Finally the response decreases during the dissociation step. The effective dissociation constant was calculated by fitting the experimental data to an A + B heterodimerisation model in SEDPHAT.

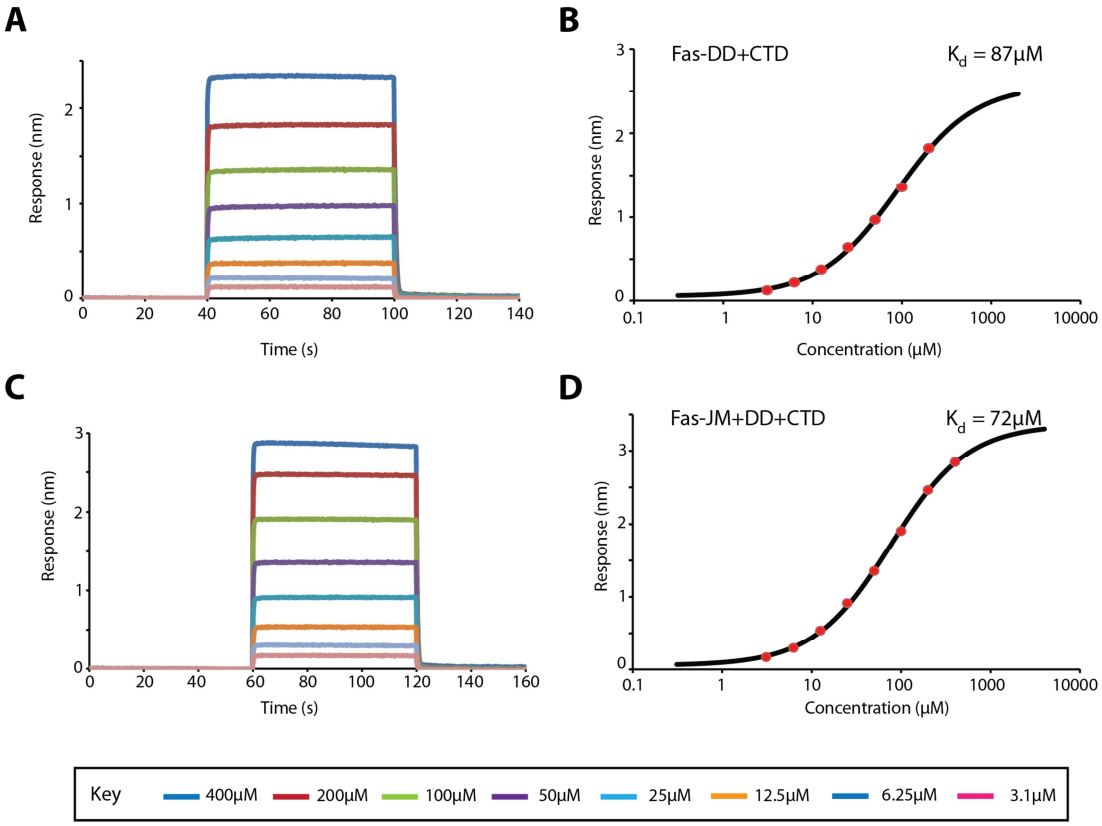

Figure 5.15 Biolayer interferometry show that the Fas:ezrin interaction has a K_d around 100μM

BLI analysis was used to see if different immobilised Fas constructs associated to ezrin. The colours used in the time response data (A and C) corresponds to the concentrations illustrated below the graphs. Experimental data is shown as the red points, fitted trend as a black line (B and D).
A, Bio-Fas-DD+CTD interaction with ezrin-FERM-tCC background corrected time response data. B, Bio-Fas-DD+CTD interaction with ezrin-FERM+tCC data fitted to A + B heterodimerisation model using SEDPHAT, giving a Kd of 87μM. C, Bio-Fas-JM+DD+CTD interaction with ezrin-FERM+tCC background corrected time response data. D, Bio-Fas-JM+DD+CTD interaction with ezrin-FERM+tCC data fitted to A + B heterodimerisation model using SEDPHAT, giving a Kd of 75μM.

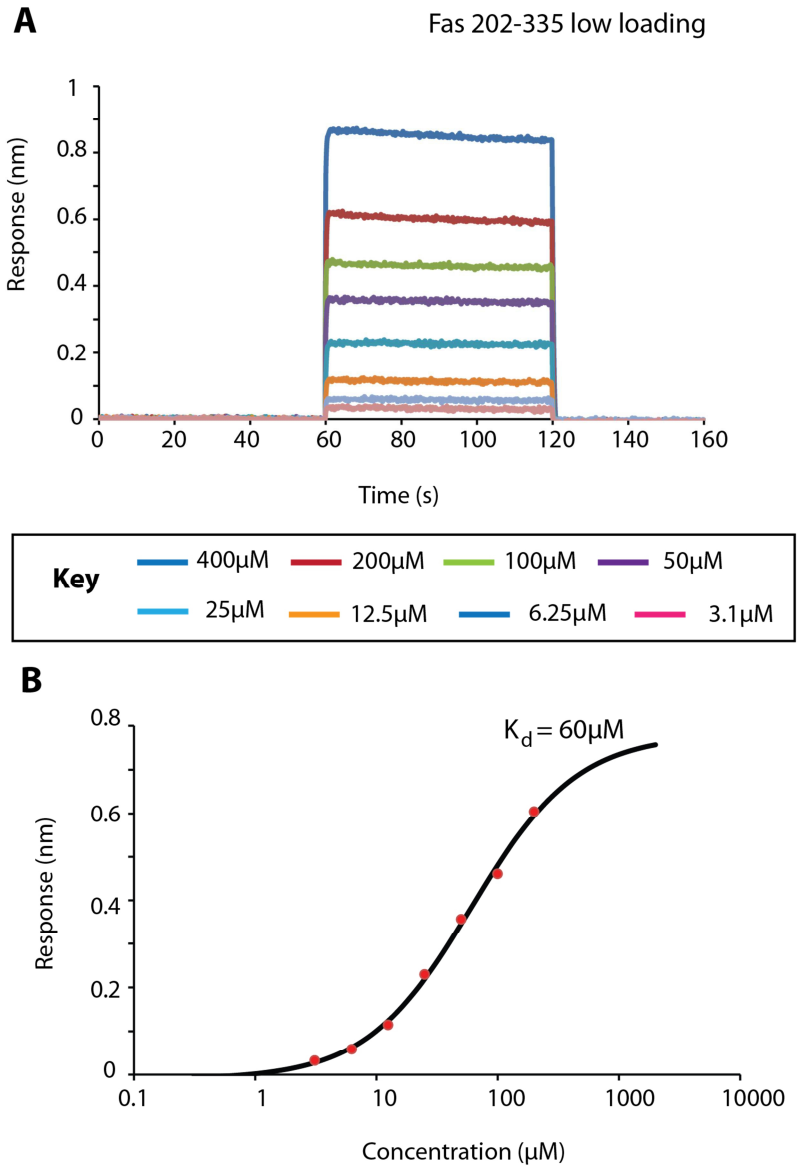

Figure 5.16 Biolayer interferometry shows that Fas immobilisation onto the sensor does not affect the observation of the interaction

The colours used in the time response data (A) corresponds to the concentrations illustrated below the graphs. Experimental data is shown as the red points, fitted trend as a black line (B).a) low loaded Bio-Fas(202-335) interaction with ezrin (1-297) background corrected time response data. b) low loaded Bio-Fas-202-335 interaction with ezrin (1-297) data fitted to A + B heterodimerisation model using SEDPHAT, giving a Kd of 60µM.

The fitted K_d for the interaction with H_6Avi*-Fas-DD-CTD was predicted to be 87 μM (Figure 5.15B) and with H_6Avi*-Fas-JM+DD+CTD at 75 μM (Figure 5.15D). These results indicate that the Fas death domain interacts with ezrin with little dependence on the presence of the juxtamembrane/membrane proximal domain upon the apparent dissociation constant.

The experiment using H_6Avi*-Fas-DD+CTD was repeated with a shorter immobilisation time in order to verify that the amount of loaded Fas did not affect the results. With a reduced amount of Fas on the sensor surface, the derived ezrin dissociation constant was 60 μM, which is of the same order of magnitude as the other experiments (Figure 5.16).

5.6 Ezrin interaction observed by Biolayer Interferometry is mapped to the purification/biotinylation tag

5.6.1 Fas-DD+CTD surface mutants all show similar dissociation constants

Having detected an apparent interaction between Fas and ezrin which did not include the Fas juxtamembrane region, we thought it important to map the binding site in the Fas death domain. Six solvent exposed residues located across the whole surface of the death domain surface were chosen for mutation. These residues were identified from the published structure of the Fas death domain (PDB code 1DDF) using the program MOLMOL. Mutations were introduced in the H_6Avi-Fas-DD+CTD construct by site directed mutagenesis, as described in Section 2.4.3.

BLI experiments were carried out as with the wild-type Fas constructs, with the H_6Avi*-Fas mutants immobilised onto streptavidin sensors. Sensors were immersed in samples containing different concentrations of ezrin (FERM+tCC), (from 3.1 to 400 μM). The interactions were recorded over time and the effective dissociation constant was calculated by fitting the experimental data to an A + B heterodimerisation model in SEDPHAT. As can be seen from Figure 5.17 and Table 5.4, the dissociation constants for each of the mutants (except K231D) were within the same range as the initial wild-type Fas BLI experiments shown in Figure 5.11. The K231D mutant showed a much higher predicted dissociation constant which could have suggested that Fas K231 was in the ezrin interaction site. However, the

time-dependent signal, shown in Figure 5.17A, shows that the 400 μM and 200 μM ezrin binding curves do not follow the trend of the other six concentrations assayed suggesting that an experimental artifact was the source of the anomalous behaviour.

Table 5.4 BLI calculated dissociation constants for Fas surface mutants.

Fas surface mutant	Dissociation constant K_d (μM)
K231D	240*
D260K	64
Q268K	85
E272K	79
K287Q	80
K309D	74

*Unreliable result, see main text.

5.6.2 Ezrin interacts with a variety of unrelated proteins with only the H_6Avi tag in common

Having obtained little variance with Fas surface mutants and due to the non-specific binding observed during pull-down experiments, it was decided to conduct more detailed control BLI experiments. The following H_6Avi biotinylated proteins were used as negative controls: (a) the death domain of the protein PIDD (kindly provided by Dr Lily Nematollahi); (b) the glycogen binding domain of AMPK (kindly provided by Dr Matthew Sanders) and; (c) *E. coli* frataxin (CyaY), (kindly provided by Dr Clara Iannuzzi).

A full dilution series of ezrin (0-400 μM) was assayed for H_6Avi*-PIDD which showed a similar association/dissociation profile (Figure 5.18A, B) to the Fas constructs with a calculated dissociation constant of 80 μM. Ezrin also bound to H_6Avi*-AMPK-GBD and H_6Avi*-CyaY at the assayed concentrations (Figure 5.18C-F and Table 5.5). It could be concluded that ezrin is a very promiscuous binding partner, however, all of the constructs being assayed had the H_6Avi tag in common. The higher dissociation constants for H_6Avi*-CyaY and H_6Avi*-AMPK-GBD could indicate that, being of higher molecular weight, these proteins hinder the interaction between ezrin and the H_6Avi* to a greater extent.

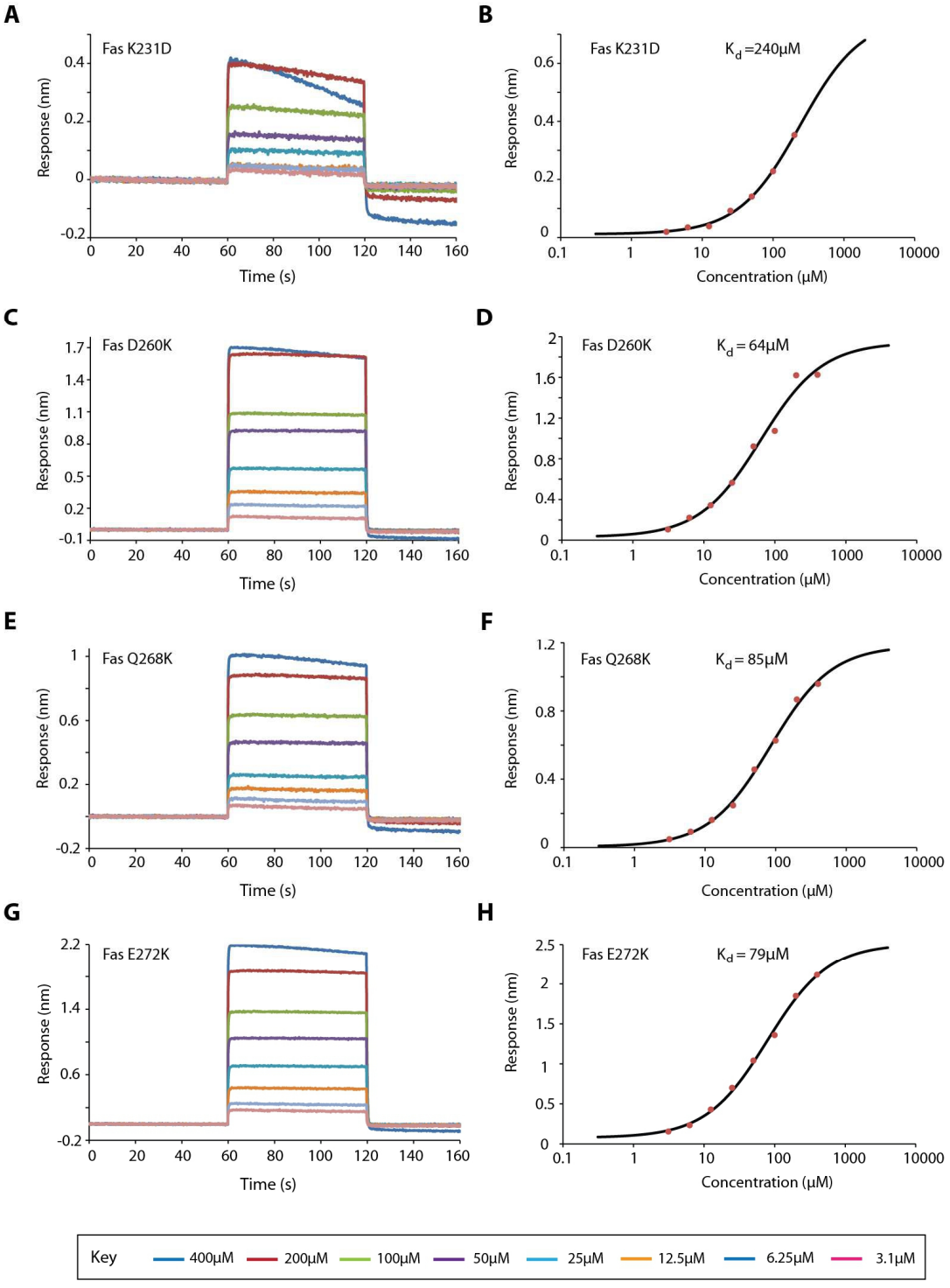

Figure 5.17 Biolayer interferometry shows that ezrin interacts with a variety of Fas surface mutants with similar dissociation constants

BLI analysis was used to see if immobilised Fas constructs with different surface mutations associate to ezrin-FERM+tCC with different affinities. The colours used in the time response data (A and C) corresponds to the concentrations illustrated below the graphs. Experimental data is shown as the red points, fitted trend as a black line (B and D). The ezrin construct was kept constant throughout these experiments.
A,C,E, G, I and K show the time response data (background corrected) for varying Fas-DD+CTD mutants interaction with ezrin. The mutation being tested is shown above the graph. B, D, F, H, J, and L, show the data collected for each mutant fitted to an A + B heterodimerisation model using SEDPHAT. Dissociation constants and the mutant Fas tested are shown above each of the curves.

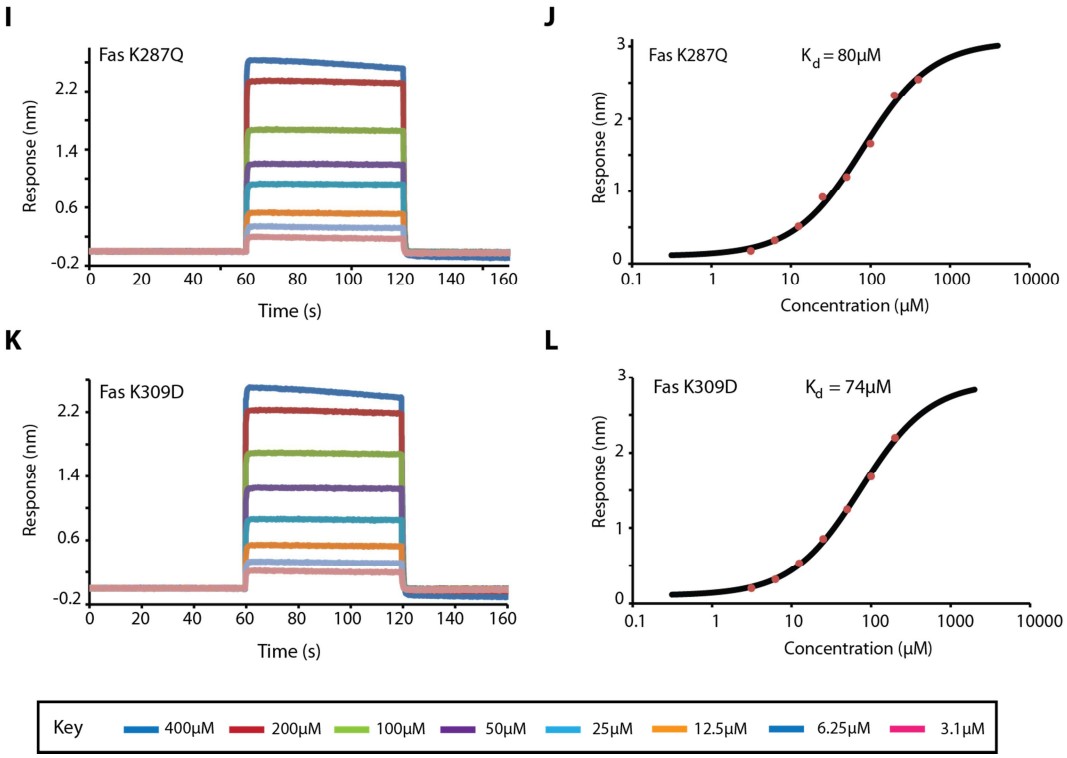

Figure 5.17 (continued) Biolayer interferometry shows that ezrin interacts with a variety of Fas surface mutants with similar dissociation constants

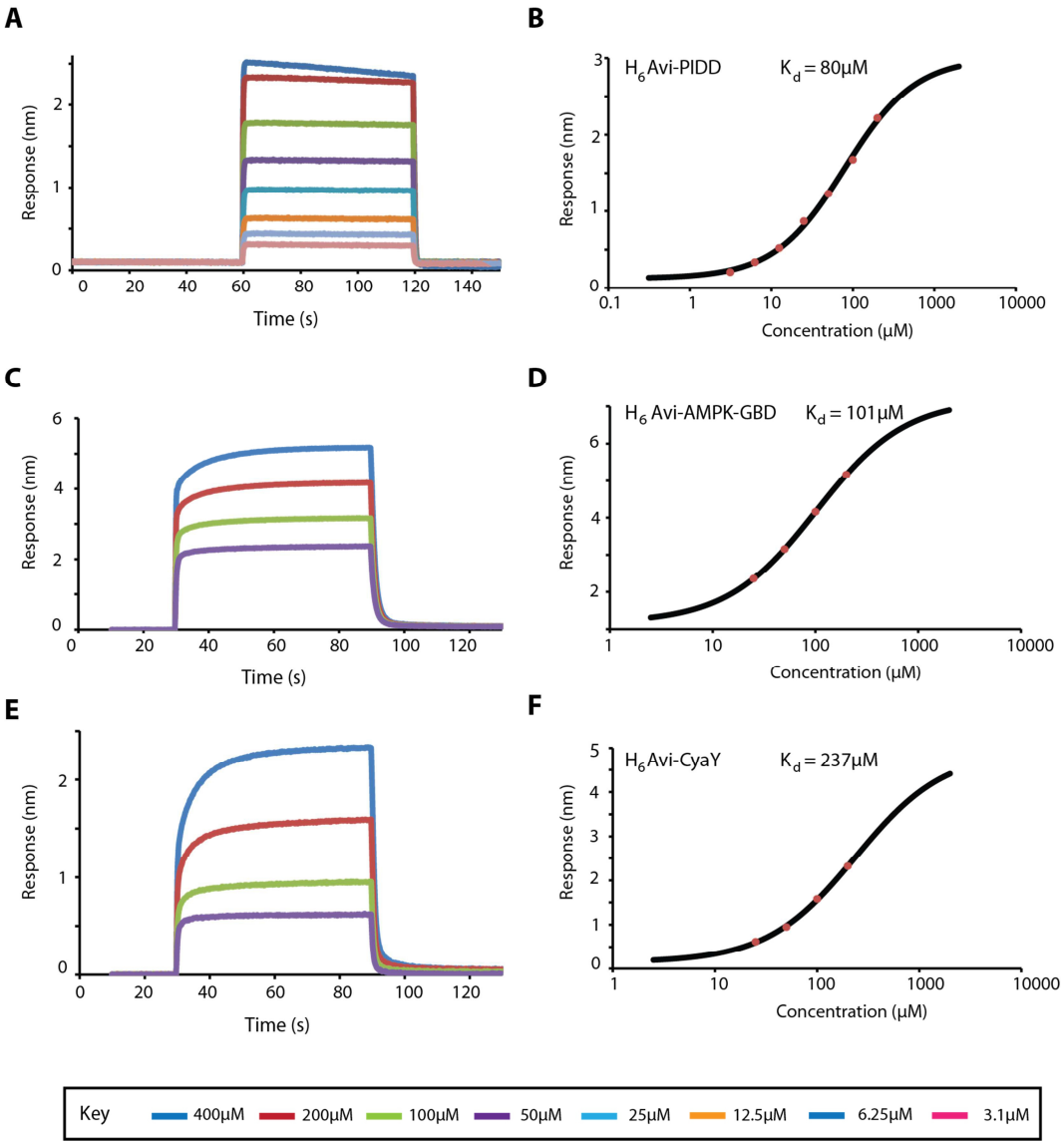

Figure 5.18 Ezrin shows binding to unrelated proteins by biolayer interferonmetry

A and B, show the time response data (background corrected) (A) and the data fitted to a A + B heterodimerisation model using SEDPHAT (B) for immobilised Biotinylated-PIDD and ezrin-FERM+tCC. C and D show the time response data (background corrected) (C) and the data fitted to a A + B heterodimerisation model using SEDPHAT (D) for immobilised Biotinylated-AMPK-GBD and ezrin-FERM+tCC. E, F show the time response data (background corrected) (E) and the data fitted to a A + B heterodimerisation model using SEDPHAT (F) for immobilised Biotinylated-CyaY and ezrin-FERM+tCC.

The next section describes how the association of ezrin and H_6Avi was further confirmed by both BLI and NMR and can also be observed by GST pull down assays.

Table 5.5 BLI calculated dissociation constants for ezrin-FERM+tCC and alternative binding partners.

Binding partner	Dissociation constant K_d (μM)
H_6Avi*-PIDD	80
H_6Avi*-AMPK-GBD	101
H_6Avi*-CyaY	237

5.7 BLI, NMR and GST pull-down assays show that ezrin recognises the purification tag

5.7.1 H_6Avi tagged proteins compete ezrin off the BLI sensor

To test the hypothesis that ezrin could be interacting with the H_6Avi tag and not with the proteins themselves, a competition assay was designed in order to see whether mixing free non-biotinylated H_6Avi-Fas with ezrin in the association step would compete with the H_6Avi*-Fas immobilised in the streptavidin sensor.

Figure 5.19 shows the time dependent binding profile for the ezrin and H_6Avi*- Fas-DD+CTD competition assay. The binding profile shows four steps of the assay separated by dashed lines. After being loaded with biotinylated protein, the sensors were moved into wells containing only binding buffer (step 1). Next, the sensors were moved into wells containing 50 μM ezrin FERM+tCC (step 2), causing an increase in the optical response due to the ezrin binding. The sensors were then transferred into wells containing a fixed concentration of ezrin with a serial dilution of either non-biotinylated H_6Avi-Fas (bottom panel) or un-tagged Fas-DD+CTD (top panel) (step 3). The final step was to dissociate ezrin from the sensors by moving the sensors into wells containing only buffer (step 4).

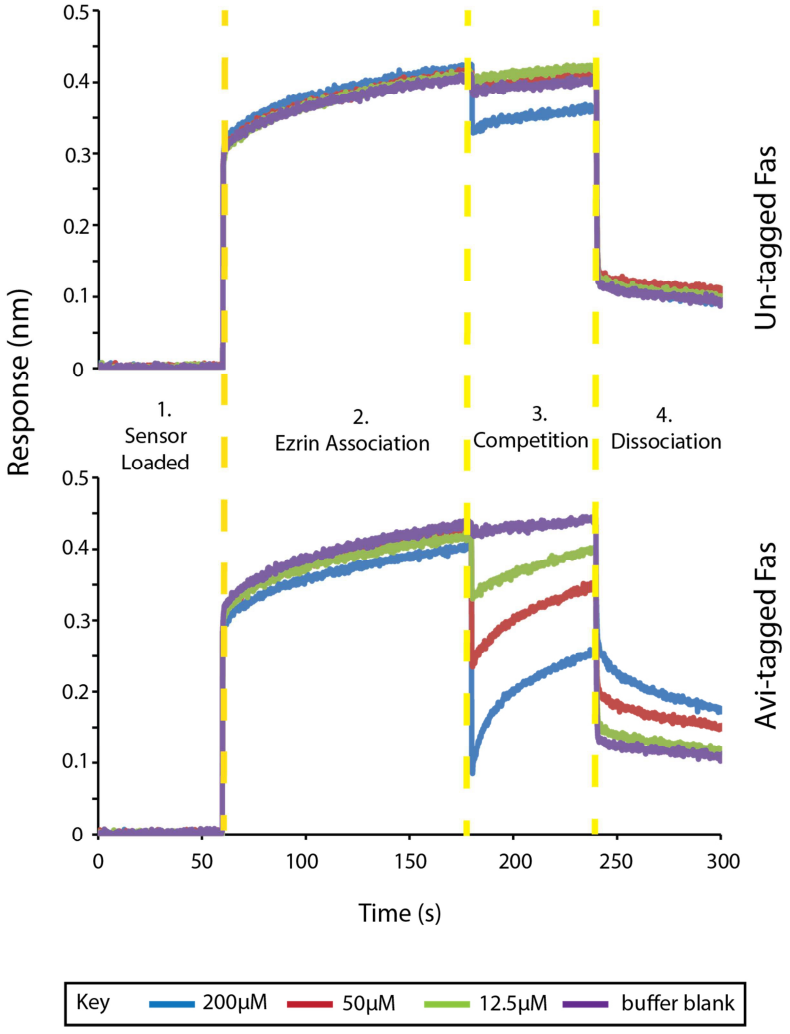

Figure 5.19 Biolayer interferometry competition assay, competing ezrin off the biosensor using H_6Avi-tagged Fas-DD+CTD

BLI was used to see whether H_6Avi-tagged proteins could compete ezrin-FERM+tCC off the streptavidin sensors it was already bound to. There were five steps to the experiment, loading the sensor with biotinylated Fas (not shown), equilibrating a baseline with the loaded sensor (1), associating ezrin to the Fas on the sensor (2), competition (3) in which the sensor was moved into a well containing the Avi or untagged protein and dissociation (4) where the sensor was moved into a well containing buffer to dissociate the remaining ezrin from the sensor. These steps are separated by the dashed yellow lines. The top panel is the time response data for untagged Fas being used to compete ezrin from the sensors. The bottom panel shows the time response data when H_6Avi-tagged Fas was used to compete ezrin form the sensor. Each competition was carried out at four concentrations, 200µM (blue line), 50 µM (red line), 12.5µM (green line) and a buffer blank (purple line).

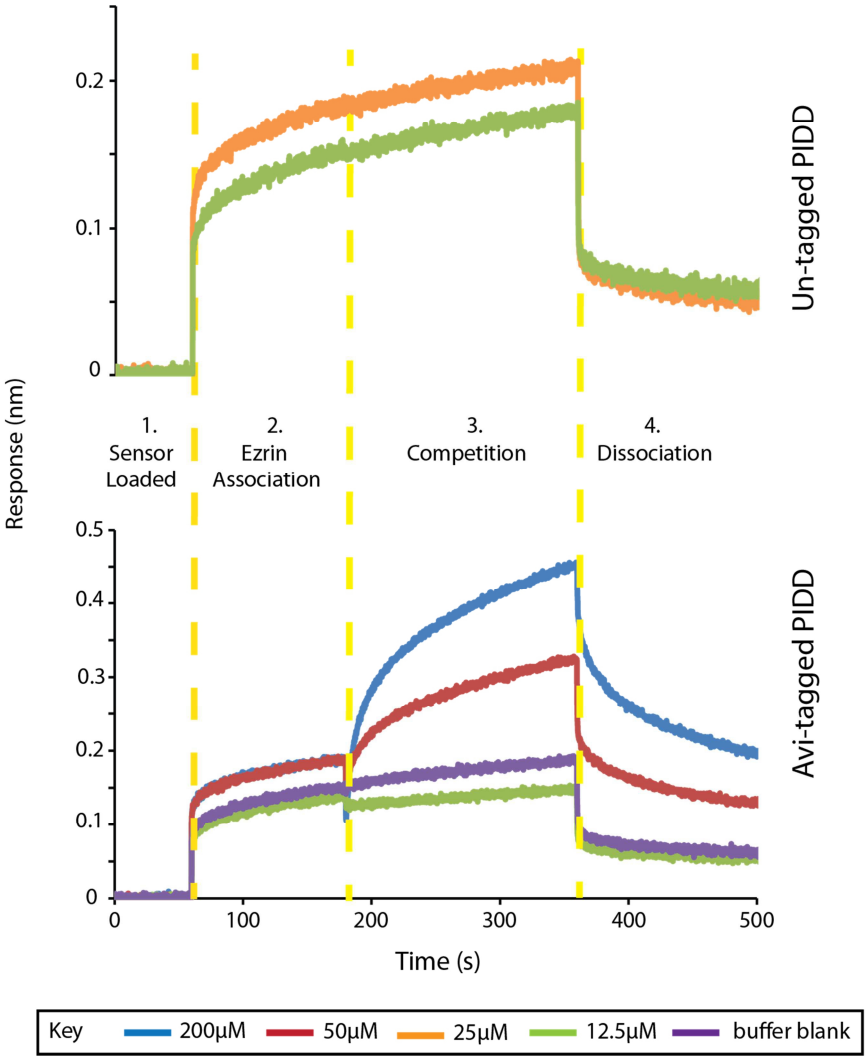

Figure 5.20 Biolayer interferometry competition assay, competing ezrin off the biosensor using H_6Avi-tagged PIDD

BLI was used to see whether H_6Avi-tagged PIDD could compete ezrin FERM+tCC off the streptavidin sensors it was already bound to. There were five steps to the experiment, loading the sensor with biotinylated Fas (not shown), equilibrating a baseline with the loaded sensor (1), associating ezrin to the PIDD on the sensor (2), competition (3) in which the sensor was moved into a well containing the avi or untagged protein and dissociation (4) where the sensor was moved into a well containing buffer to dissociate the remaining ezrin from the sensor. These steps are separated by the dashed yellow lines. The top panel is the time response data for untagged PIDD being used to compete ezrin from the sensors. The bottom panel shows the time response data when H_6Avi-tagged PIDD was used to compete ezrin from the sensor. Each competition was carried out at four concentrations, 200µM (blue line), 50 µM (red line), 25µM (orange line) 12.5µM (green line) and a buffer blank (purple line).

The time response data show that as the concentration of H_6Avi-Fas in the well increases, ezrin detaches from sensor, presumably because the free H_6Avi tag outcompetes the immobilised H_6Avi* tag for ezrin binding. Only the highest concentration of un-tagged Fas seems to be able to show some competition but not to the same extent as the H_6Avi-Fas protein. The competition assay was also repeated with immobilised H_6Avi*-Fas-DD+CTD using H_6Avi-PIDD and un-tagged PIDD to compete. This assay showed the same behaviour between the H_6Avi tagged protein competing and removing ezrin from the sensor and the un-tagged protein not being able to do so, shown in Figure 5.20. This competition assay confirms that the previous BLI results are not detecting ezrin interacting with Fas, but ezrin interacting with the H_6Avi tag.

5.7.2 A variety of proteins with H_6Avi tags perturbed the $^{2}H^{15}N$ ezrin $^{1}H/^{15}N$-HSQC spectrum

To verify whether the H_6Avi interaction with ezrin could be monitored using other techniques, a number of NMR titration end points were collected for $^{2}H^{15}N$ labelled ezrin mixed with non-isotope labelled proteins with and without H_6Avi tags.

The ezrin FERM construct is 35 kDa and non-deuterated samples show a $^{1}H/^{15}N$-HSQC spectrum of very poor quality (shown in appendix), most probably because of signal broadening due to slow tumbling. To enable suitable visualisation of ezrin FERM by NMR, the construct was expressed in $^{2}H/^{15}N$ labelled minimal medium as described in Section 2.5.3. Following expression in $^{2}H_2O$-labelled medium, purification was carried out in the same manner as for the other H_6-tagged proteins as described in Section 2.5.3.

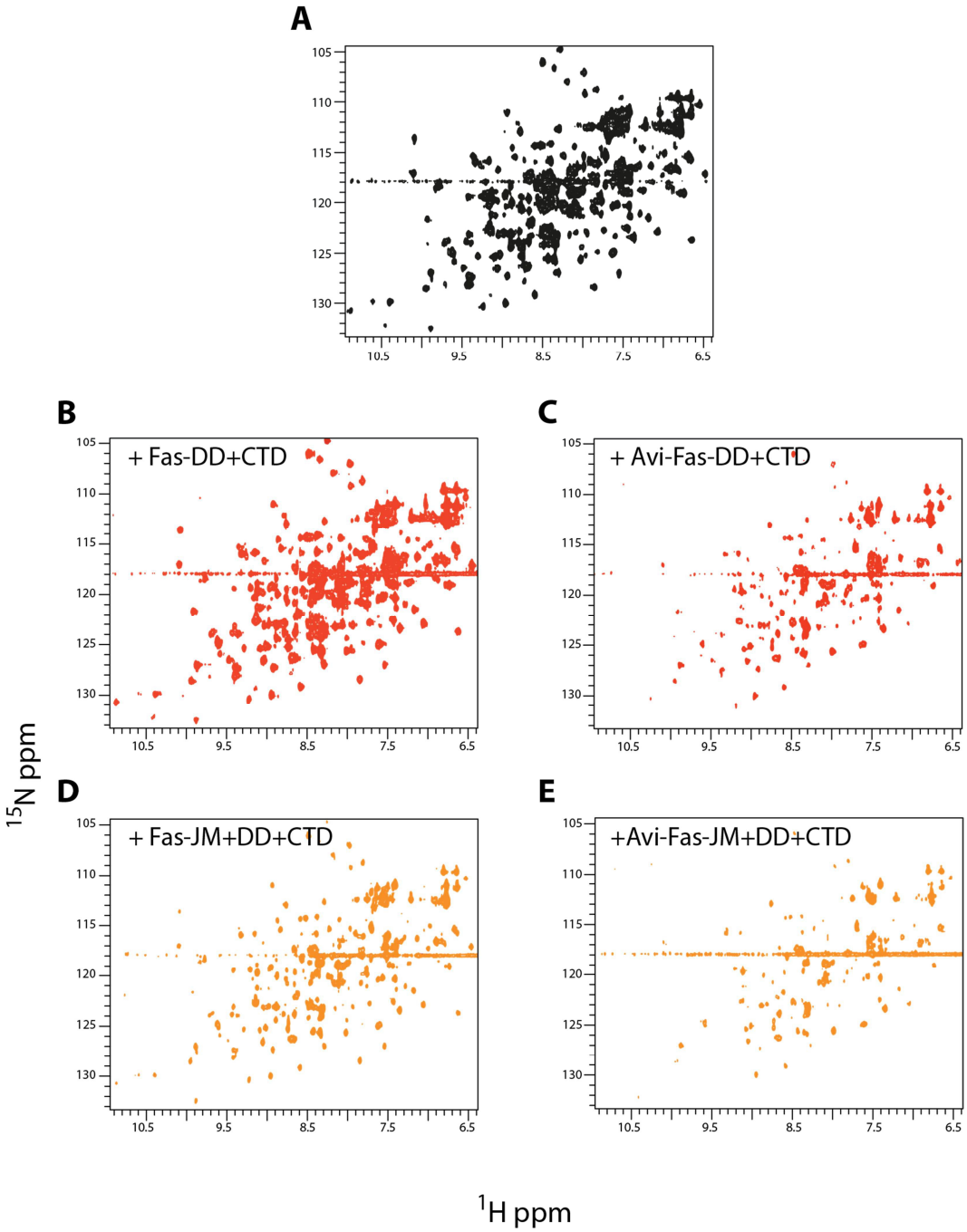

Figure 5.21 H_6Avi-tagged proteins perturb the $^{1}H/^{15}N$-HSQC spectrum of $^{2}H/^{15}N$ ezrin-FERM whereas non H_6Avi-tagged proteins do not

$^{1}H/^{15}N$-HSQC spectra of 200μM $^{2}H/^{15}N$ ezrin-FERM mixed with 400μM of binding partners stated upon each spectra. The left side of the figure shows ezrin spectra mixed with untagged proteins, whereas the right side of the figure shows ezrin spectra when mixed with tagged proteins. A, 200μM $^{2}H/^{15}N$ ezrin-FERM; B, 200 μM $^{2}H/^{15}N$ ezrin-FERM with 400μM Fas-DD+CTD; C, 200μM $^{2}H/^{15}N$ ezrin-FERM with 400μM H_6Avi-Fas-DD+CTD; D, 200μM $^{2}H/^{15}N$ ezrin-FERM with 400μM Fas-JM+DD+CTD; E, 200μM $^{2}H/^{15}N$ ezrin-FERM with 400μM H_6Avi-Fas-JM+DD+CTD; F, 200μM $^{2}H/^{15}N$ ezrin-FERM with H_6Avi-D;1G, 200μM $^{2}H/^{15}N$ ezrin-FERM with 400μM Rab-GFP; H, 200μM $^{2}H/^{15}N$ ezrin-FERM with 400μM H_6-GFP. All of the spectra were recorded at 25°C at 800MHz.

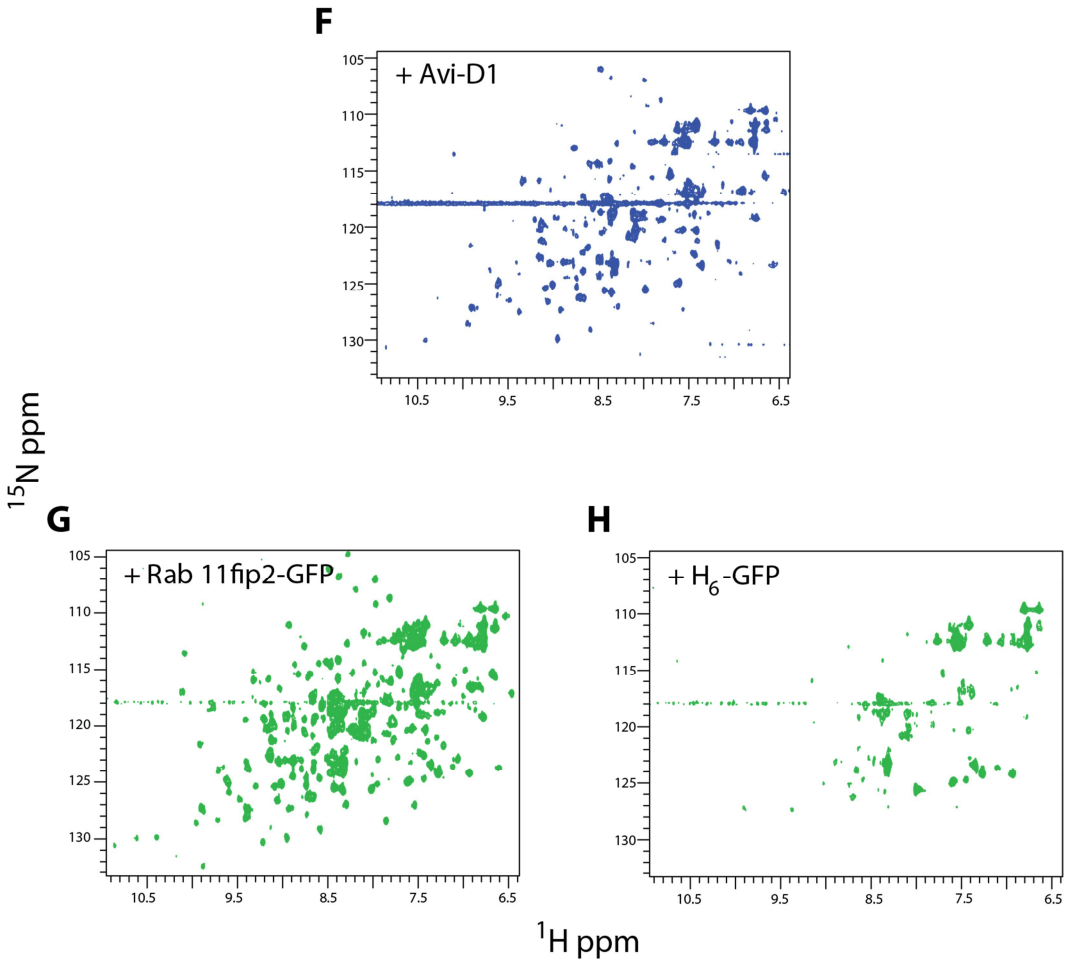

Figure 5.21 (continued) H_6Avi-tagged proteins perturb the $^{1}H/^{15}N$-HSQC spectrum of $^{2}H/^{15}N$ ezrin-FERM whereas non H_6Avi-tagged proteins do not

Each sample contained 200 μM $^{2}H^{15}N$ ezrin FERM and 400 μM of the test protein. The samples were prepared by co-concentrating both proteins to 500 μl. $^{1}H/^{15}N$-HSQC spectra were collected at 25 ^{o}C at 800 MHz as described in Section 2.9. Figure 5.21 shows the $^{1}H/^{15}N$-HSQC spectrum of 200 μM $^{2}H^{15}N$ ezrin on its own (panel A) as well as mixed with a variety of proteins with and without the H_6Avi tag (panels B-H). Panel A shows a well dispersed spectrum consistent with globular structure, as expected from the crystal structure. The overall trend observed is that, irrespective of the nature of the protein, the presence of the H_6Avi tag broadens the cross peaks resulting in an overall reduction in the intensity of the spectrum (panels C, E and F).

These effects are indicative of an interaction occurring in a millisecond, slow, timescale ($k_{ex} << \Delta\upsilon$). The $^{1}H/^{15}N$-HSQC spectra of ezrin in the presence of untagged proteins (panels B and D) also show broadening, but to a lesser extent. Although the longer H_6Avi-Fas-JM+DD+CTD (panel D) construct appears to show more line broadening than the shorter H_6Avi-Fas-DD+CTD construct (panel B), the unrelated protein H_6Avi-DI (DI is the N-terminal sushi domain of beta-2 glycoprotein 1, kindly provided by Lucy Murfitt) affects the spectrum to a similar extent, so the line-broadening effect cannot be solely attributed to the presence of Fas (Figure 5.21F).

In an effort to find a possible biological significance of ezrin biding the H_6Avi tag a BLAST search was carried out, which highlighted that the Avi peptide, the BirA recognition sequence LNDIFEAQKIEWHE, shares 50% identity with a fragment (LNDIFEDKQRRTE) of the protein Rab11fip2 (Rab11 family-interacting protein 2; UniProt: Q7L804), a protein involved in receptor-mediated endocytosis and membrane trafficking of recycling endosomes. A construct of GFP containing the Rab11bp (residues 105-118) fragment instead of the Avi tag was generated by site-directed mutagenesis of an H_6Avi-Green Fluorescent Protein (GFP) construct available in our laboratory. However when titrated into ezrin, the presence of this construct had no effect on the ezrin spectrum (Figure 5.21G) suggesting that it did not interact with ezrin. To test for the effect of the hexa histidine tag, $^{2}H^{15}N$ ezrin was mixed with H_6-GFP as shown in Figure 5.21 (panel H). Surprisingly, this construct perturbed the ezrin NMR spectrum more than the constructs containing the H_6Avi tags, showing a larger number of peaks broadening to the noise level and

essentially disappearing. This result led us to conclude that the interaction between ezrin and the H_6Avi tag would be restricted to the hexa histidine purification tag.

To quantify these observations (and for a more visual representation of the result), the decrease in peak intensity was assessed for each of the end point spectra (Figure 5.21 panels B-H) relative to the intensity of the starting spectrum (Figure 5.21 panel A). A set of 60 well-resolved peaks was selected and the decrease in intensity in the spectra recorded for these peaks in each of the spectra is shown in Figure 5.21. This change in peak intensity is represented in Figure 5.22 as a bar chart illustrating which binding partner had induced the greatest relative decrease in peak intensity compared to the starting spectra. The bar chart representation highlights the trends described above, showing that H_6-GFP and H_6Avi-Fas-JM+DD+CTD had the greatest effect on the spectrum with 90% and 80% loss of peak intensity, respectively.

5.7.3 The H_6Avi tag ezrin interaction is also observed by GST pull down assays

In order to verify that the results obtained by NMR, GST-tagged ezrin was used as bait and the same protein constructs used in the NMR experiments were used as prey in a GST pull down assay (Figure 5.23). The results of this pull down were in agreement with the NMR results. The most intense band, suggesting stronger binding, was that of H_6Avi-Fas-JM+DD+CTD, followed by H_6-GFP.

Intriguingly, the pull down assay also shows GST tagged ezrin interacting with untagged Fas-JM+DD+CTD, in agreement with the $^{1}H/^{15}N$ HSQC spectrum in Figure 5.21 (panel E). Although more controls are needed at this point, these two results still suggest that ezrin and Fas were capable of binding, but that, until this moment, this interaction was being masked by that of ezrin and the hexa histidine tag. Therefore, I set out to test this hypothesis by NMR using only untagged proteins

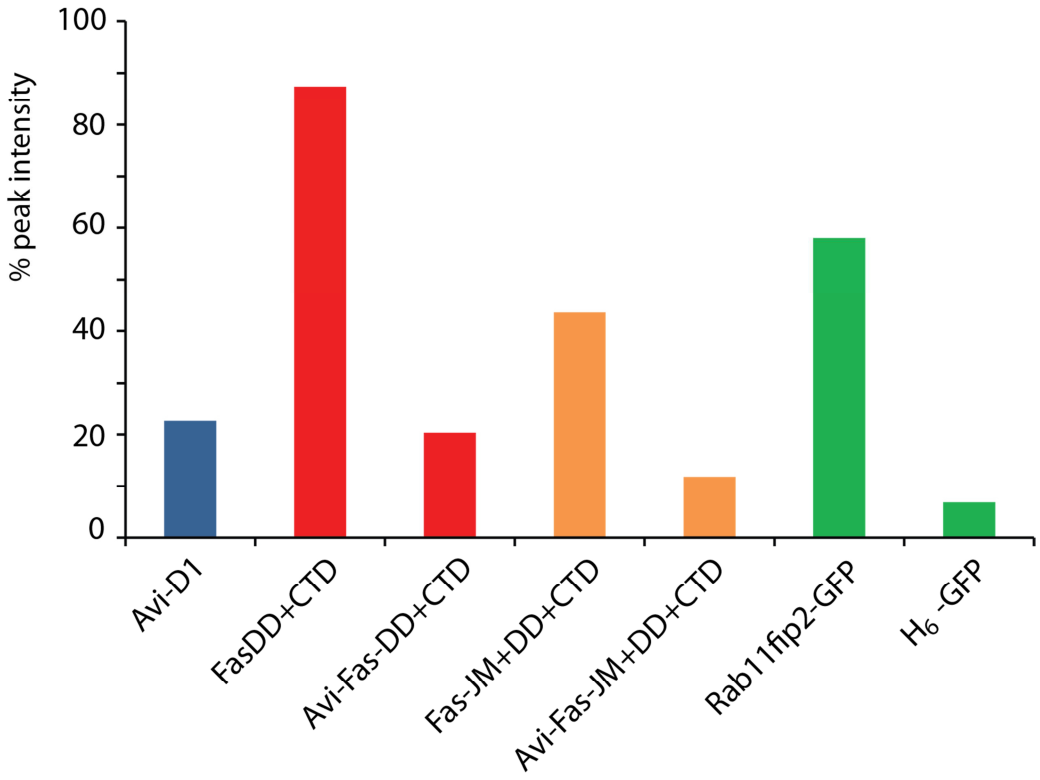

Figure 5.22 Percentage decrease in peak height across the spectra shown in 5.15 when $^{2}H/^{15}N$ ezrin-FERM is mixed with alternatively tagged proteins.

Bar chart showing the decrease in percentage of peak height (for a selection of 60 well resolved peaks) for each of the binding partners added to $^{2}H/^{15}N$ ezrin-FERM and recorded by $^{1}H/^{15}N$ HSQC shown in Figure 5.15.

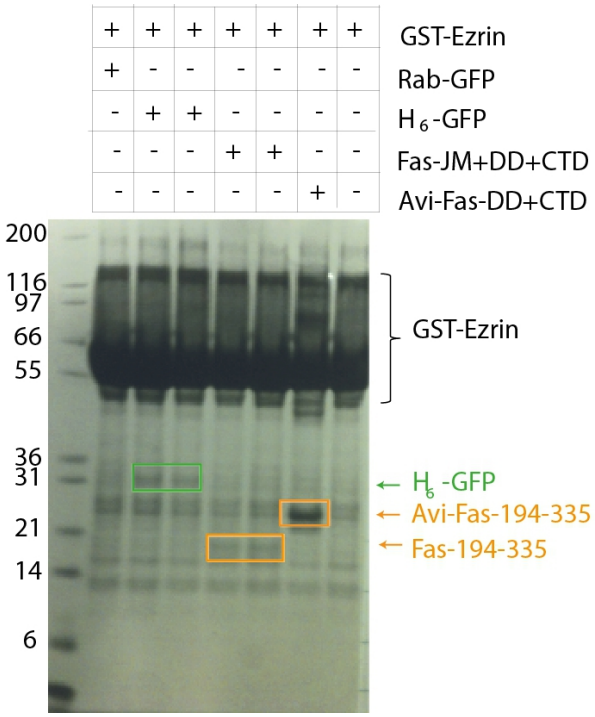

Figure 5.23 Ezrin: H_6Avi-tagged protein interaction can also be observed by GST-ezrin pull down

To verify the effects seen by $^{1}H/^{15}N$ HSQC, the same protein combinations were used in a GST-pull down. GST-ezrin-FERM+tCC was immobilised upon glutathione beads and incubated overnight with between 5μM and 50μM of possible ezrin binding partners (all pre-purified, lanes labelled above the gel). Following three washes beads were denatured in SDS-loading buffer and visualised upon a SDS-PAGE gel with comassie staining. Pull down was only observed for the H6Avi-tagged constructs and the GFP containing constructs. The buffer used to equilibrate and wash the beads was 30mM Tris-HCl, 150mM NaCl, 10% glycerol, 1% triton, 1mM EDTA, pH 7.5. Proteins pulled down by GST-ezrin are highlighted with coloured boxes. The colours reflect the colours used for each construct in the NMR spectra in Figure 5.21.

5.8 A weak and unspecific interaction between intracellular Fas and ezrin is observed by NMR

5.8.1 The presence of ezrin FERM+tCC broadens the signals in the $^{1}H/^{15}N$ HSQC spectrum of all constructs of intracellular Fas

Signal broadening due to the presence of untagged Fas in the $^{1}H/^{15}N$ HSQC spectrum of $^{2}H^{15}N$ ezrin FERM was observed during the investigation of the H_6Avi tag: ezrin interaction (Figure 5.21 panels D and F). To investigate this further, I performed the inverse experiment, to test the effect of unlabelled ezrin FERM+tCC on the $^{1}H/^{15}N$ HSQC spectrum of Fas.

The four ^{15}N-labelled Fas intracellular domain truncation constructs were expressed and purified as described in Section 2.5. For each of the Fas constructs, two NMR samples were prepared: one with 200 μM ^{15}N-labelled Fas only, and the second with 200 μM ^{15}N-labelled Fas mixed with 300 μM ezrin FERM+tCC. Figure 5.24 shows the eight $^{1}H/^{15}N$-HSQC spectra corresponding to four different Fas intracellular domain constructs (panels A, C, E and G) on their own and the same proteins mixed with ezrin FERM+tCC (panels B, D, F and H).

All untagged Fas intracellular domain constructs show a reduction in the intensity of the peaks across the spectrum when mixed with untagged ezrin. The majority of the cross peaks were broadened to the noise level and effectively disappeared. The only remaining cross peaks correspond to the flexible N- and C- termini of the molecule, based on known assignments and the characteristic chemical shifts of Fas-DD. The most straightforward interpretation of this behaviour is that untagged ezrin does interact with untagged Fas, forming a protein complex which tumbles slowly in solution leading to an overall increase in the line widths of all peaks except those corresponding to atoms located in regions that retain high internal mobility in the complex. However, the fact that the effect of ezrin is observed irrespective of the precise nature of the Fas construct used is in disagreement with the observations by Ruan and coworkers, who mapped the ezrin binding site to the so-called membrane proximal domain in the juxtamembrane region[118]. Although there is a possibility that the interaction is happening elsewhere within the intracellular region of Fas, given our previous experience with the promiscuous binding tendency's for ezrin FERM proteins, leads us to interpret this result as a non-specific binding event.

5.8.2 ICAM2 peptide counteracts the effect of ezrin FERM+tCC on the $^{1}H/^{15}N$ HSQC of Fas DD+CTD

To test the hypothesis that ezrin interaction with Fas was non-specific, we designed a competition experiment using a peptide we hypothesised will bind ezrin with high affinity. Some of the interactions of the FERM domain (residues 1-297) of ERM proteins are well characterised, as a number of FERM domains have successfully co-crystallised with a variety of binding partners. For example, the radixin FERM domain has been crystallised with peptides from NHERF2, ICAM2 and CD44,[111,112,235] each showing a strong binding affinity. Specifically, a 26 residue peptide of ICAM2 (QHLRQQRMGTYGVRAAWRRLPQAFRP) has been previously shown to interact with the radixin FERM domain (PDB: 1J19) with a dissociation constant of 3.3 μM[235]. As the level of sequence identity between radixin and ezrin in the region of the interaction with the ICAM2 peptide is very high, we hypothesised that the interaction would also be observed with ezrin.

To test the interaction between the ezrin FERM and the ICAM2 peptide, a NMR titration was carried out in which two samples were made, one containing 100 μM $^{2}H^{15}N$ ezrin (sample A) and one containing 100 μM $^{2}H^{15}N$ ezrin and 100 μM of the ICAM2 peptide (sample B). To obtain the intermediate points of the titration without dilution, samples of intermediate concentrations were prepared by simultaneously swapping equivalent volumes between sample A and sample B. This was followed by the recording of a $^{1}H/^{15}N$ HSQC spectrum for each of the sample tubes. As the concentration of the ICAM2 peptide was increased, signals form the cross peaks became broader, resulting in an overall reduction in intensity of the spectrum, which is indicative of an interaction occurring. This is shown in the appendix.

Once the interaction between ezrin and the ICAM2 peptide was confirmed, three NMR samples were prepared. One contained 135 μM ^{15}N Fas-DD+CTD (sample C). The second and third samples were prepared in the same way: two aliquots of 135 μM Fas-DD+CTD and 270 μM ezrin FERM+tCC were concentrated to 400 μl by centrifugal concentration. To one sample 100 μl of buffer were added (sample D) and to the other ICAM2 peptide and buffer were added to make the final volume 500 μl with 270 μM of peptide (sample E). $^{1}H/^{15}N$-HSQC experiments were recorded at 800 MHz and 25 ^{o}C for each sample, illustrated in Figure 5.25. As before, sample D,

containing only unlabelled ezrin showed a decrease in the intensity of the majority of the folded peaks in the spectrum in the presence of Fas-DD+CTD only. However, in sample E with Fas, ezrin and ICAM2 peptide a number of Fas cross-peaks are recovered in the spectrum. These features are highlighted by residue type and number in Figure 5.25C. The recovery of peaks suggests that the binding observed between Fas and ezrin was not a strong interaction and that a significant fraction of Fas was being displaced by the small peptide at equimolar concentration. When the residues whose peaks are recovered are plotted on the Fas structure, these residues do not cluster to suggest a binding site (data not shown) which could also be interpreted as arising from non-specific interactions with ezrin.

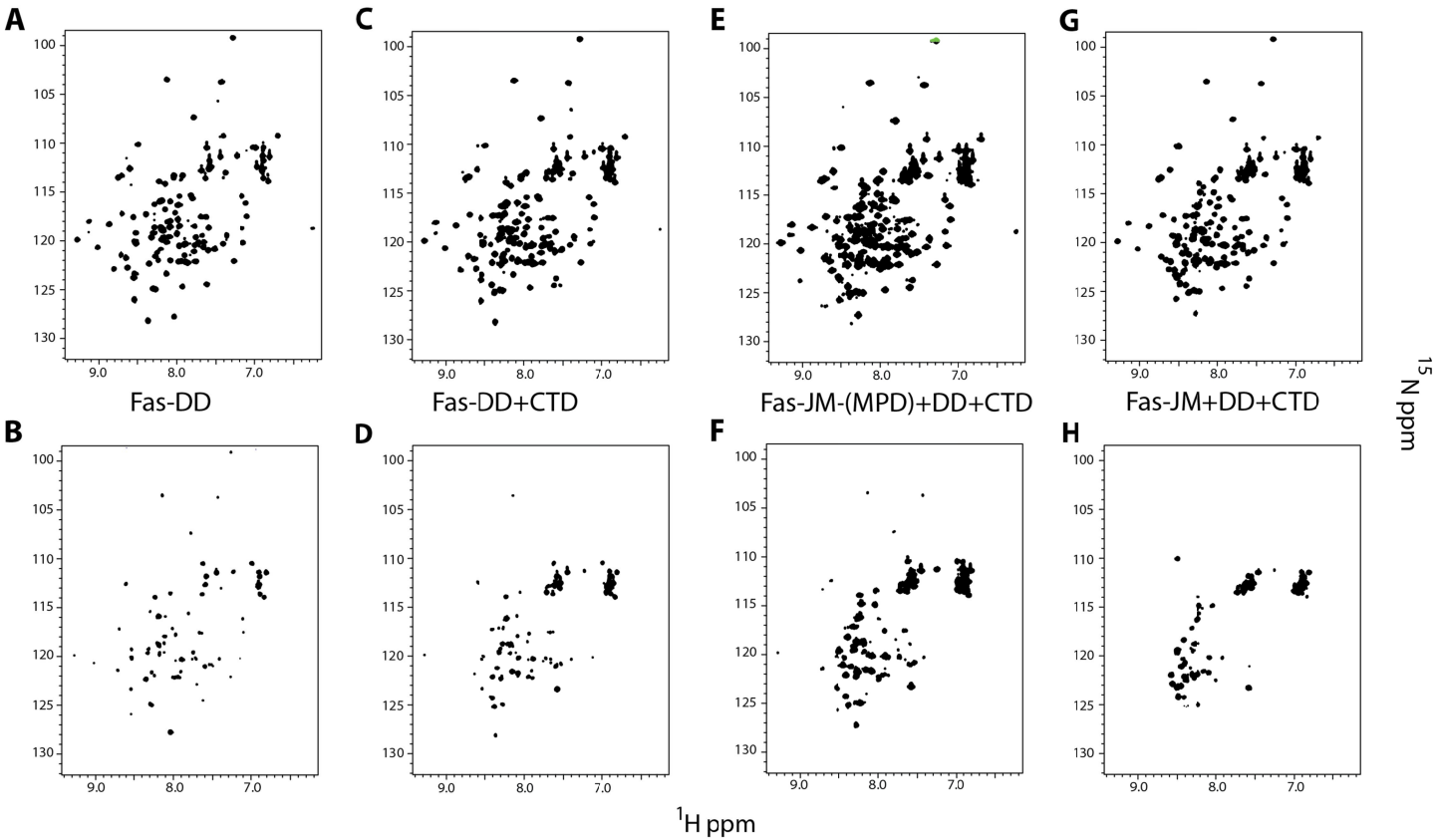

Figure 5.24 ^{1}H/^{15}N-HSQC spectra showing ezrin affecting the ^{15}N Fas spectrum for four Fas truncation constructs

Four Fas intracellular truncations were ^{15}N labelled, with one sample containing the Fas alone and another containing double the concentration of ezrin. These spectra would correspond to the end points of a titration . A, ^{1}H/^{15}N-HSQC spectrum of 200μM ^{15}N Fas DD. B, ^{1}H/^{15}N-HSQC spectrum of 200μM ^{15}N Fas DD with 400μM ezrin-FERM+tCC . C, ^{1}H/^{15}N-HSQC spectrum of 200μM ^{15}N Fas DD-CTD, D, ^{1}H/^{15}N-HSQC spectrum of 200μM ^{15}N Fas DD-CTD with 400μM ezrin-FERM+tCC. E, ^{1}H/^{15}N-HSQC spectrum of 200μM ^{15}N Fas JM(-MPD)-DD- CTD. F, ^{1}H/^{15}N-HSQC spectrum of 200μM ^{15}N Fas JM(-MPD)-DD- CTD with 400μM ezrin-FERM+tCC. G, ^{1}H/^{15}N-HSQC spectrum of 200μM ^{15}N Fas JM-DD-CTD. H, ^{1}H/^{15}N-HSQC spectrum of 200μM ^{15}N Fas JM-DD-CTD with 400μM ezrin-FERM+tCC. All of the spectra were recorded at 25^{o}C at 800MHz.

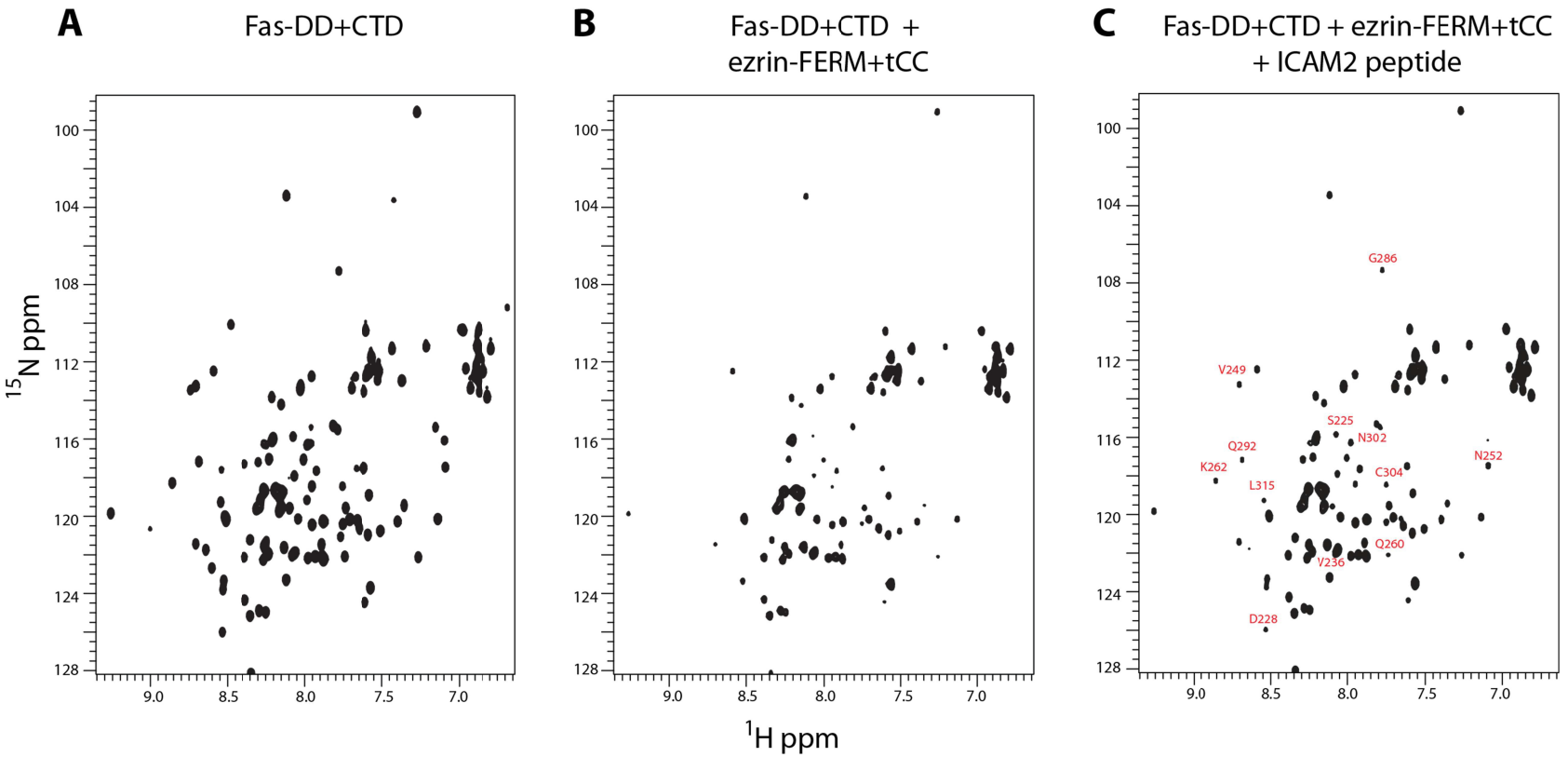

Figure 5.25 ICAM2 peptide competes ezrin-FERM+tCC off ^{15}N Fas-DD+CTD

A, ^{1}H/^{15}N HSQC spectrum of 135µM ^{15}N Fas-DD+CTD, B, ^{1}H/^{15}N HSQC spectrum of 135µM ^{15}N Fas-DD+CTD with 270µM ezrin-FERM+tCC. C, ^{1}H/^{15}N HSQC spectrum of 135µM ^{15}N Fas-DD+CTD with 270µM ezrin-FERM+tCC and 270µM of ICAM2 peptide. Fas peaks which were recovered following ICAM2 peptide addition are highlighted with the assignment for that peak in red. Those without assignment are in the more overlapped region of the spectrum therefore difficult to identify when peaks have shifted.

5.8.3 Addition of ezrin does not perturb the $^{13}CH_3$-ILV-labelled Fas-DD methyl-TROSY spectrum

The addition of unlabelled ezrin to ^{15}N Fas results in the decrease in intensity of cross peaks throughout the $^{1}H/^{15}N$-HSQC spectrum. Irrespective of the nature of this interaction, this behaviour could be indicative of the formation of a high molecular weight complex. Even a 1:1 complex of aproximately 47 kDa might be invisible in a $^{1}H/^{15}N$-HQSC experiment due to signal broadening as a result of slow tumbling. The combination of novel NMR experiments such as TROSY (Transverse Relaxation-Optimised Spectroscopy) pulse sequences combined with specific labelling of atoms within a construct are technologies which allow information about high molecular weight macromolecular complexes to be elucidated by NMR[236]. Previous work in our laboratory has used TROSY-based experiments to analyse the formation of the Fas:FADD death domain complex[123]. This was achieved using a Fas death domain construct which had been specifically ^{13}C-labelled on the methyl groups of the isoleucine, leucine and valine (ILV) residues in an otherwise uniformly deuterated background. As the $^{13}CH_3$ ILV-labelling and methyl-TROSY experiments have already been optimised for the Fas system in our lab, probing the possible Fas:ezrin interaction in this way was relatively straightforward.

Dr Diego Esposito kindly provided some ILV-labelled Fas-DD to be used for this work. To prepare samples for this experiment, the ILV-labelled Fas and unlabelled ezrin were buffer exchanged into ezrin NMR buffer prepared in 99% $^{2}H_2O$, as the experiment requires a fully deuterated background for optimal performance. Two samples were prepared: one containing 125 μM ILV-Fas-DD (sample A) and one containing 125 μM ILV-Fas-DD with 125 μM unlabelled ezrin-FERM (sample B). Methyl-TROSY spectra were recorded for these two samples, shown in Figure 5.26A and B. As can be seen, there was no change in the spectrum containing both ezrin and Fas. Due to no difference being observed, sample B was modified by the addition of more unlabelled ezrin and re-concentrated to 500 μl so that the sample then contained 450 μM ezrin, shown in Figure 5.26C. Even at the higher concentration of ezrin, it had no effect upon the spectrum suggesting that no higher molecular weight complex was being formed between Fas and ezrin.

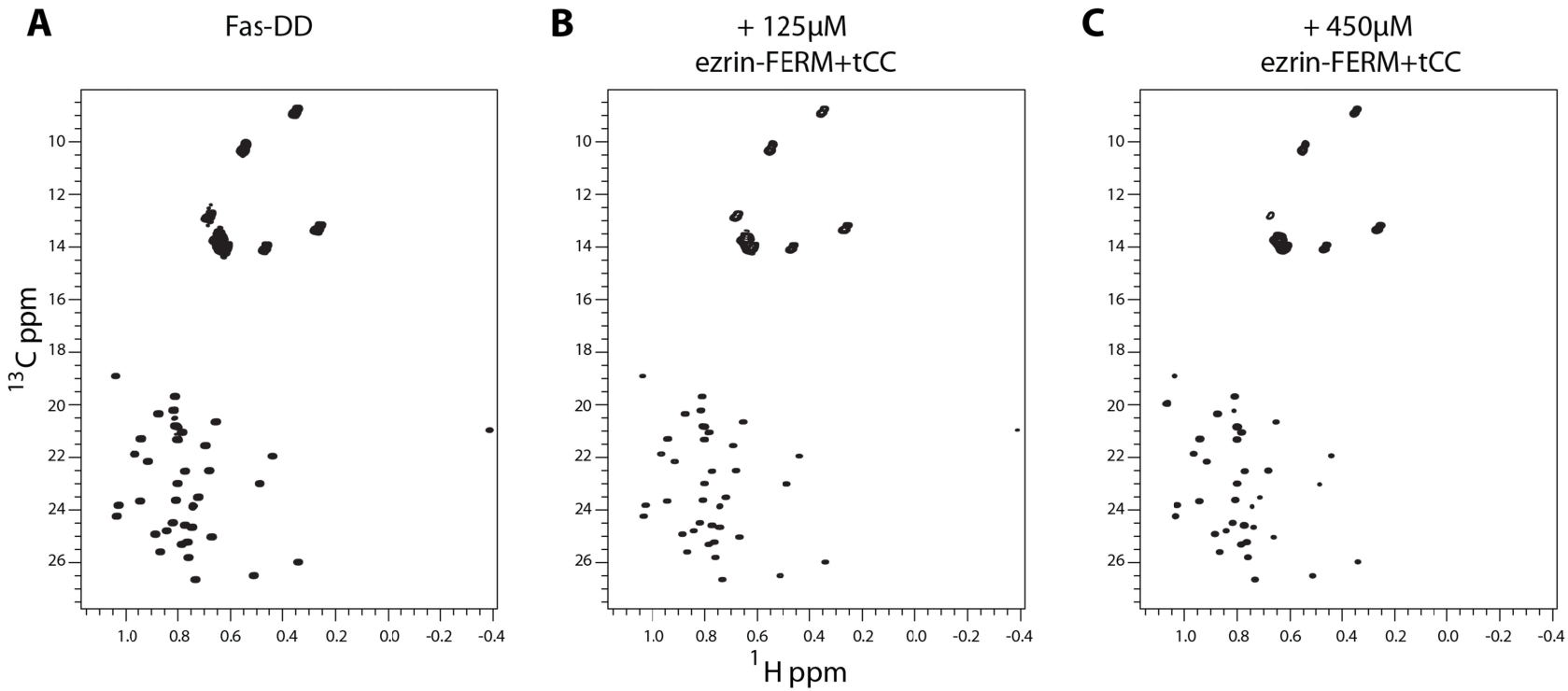

Figure 5.26 Addition of Ezrin does not perturb the methyl-TROSY spectrum of ILV-labelled Fas-DD

Methyl-TROSY spectra were acquired on an ILV labelled Fas-DD sample mixed with ezrin at two concentrations, to observe whether a complex too large to see by a traditional $^{1}H/^{15}N$ HSQC was formed between Fas and ezrin. A, Methyl-TROSY spectrum of 110µM ILV labelled Fas-DD. B, Methyl-TROSY spectrum of 110µM ILV labelled Fas-DD with 125µM ezrin-FERM+tCC. C, Methyl-TROSY spectrum of 110µM ILV labelled Fas-DD with 450µM ezrin-FERM+tCC. All of the spectra were recorded at 25°C at 800MHz.

5.8.4 Addition of Fas-JM+DD+CTD does not perturb the $^{1}H/^{15}N$ HSQC of $^{2}H^{15}N$ ezrin

Section 5.7.2 shows the presence of Fas constructs has a moderate effect on the ^{15}N HSQC spectrum of $^{2}H^{15}N$ ezrin. This experiment was revisited with the addition of twice as much unlabelled Fas to the $^{2}H^{15}N$ ezrin in an attempt to encourage a stronger effect on the spectrum compared to that observed in Section 5.7.2.

As in the previous NMR titration end point experiments, two samples were prepared, one containing 200 μM $^{2}H^{15}N$ ezrin (sample A) and one containing 200 μM $^{2}H^{15}N$ ezrin mixed with 800 μM Fas-JM+DD+CTD (sample B). A $^{1}H/^{15}N$-HSQC spectrum was collected for each sample at 25 ^{o}C at a field strength of 800 MHz. The resulting spectra are shown in Figure 5.27. Unfortunately, in this case, the effect was minimal compared to that observed previously. It could be argued that these results are not comparable, as in this experiment the signal to noise ratio in not as good as the one obtained in Figure 5.21, this is possibly due to less efficient deuterium exchange between the solvent and the protein during expression in *E.coli*.

5.9 Different pH or presence of other proteins does not have the same effect as ezrin on the $^{1}H/^{15}N$-HSQC of Fas

The results of the previous section suggest that the effect of ezrin on the NMR spectra of Fas is reproducible, but weak and non-specific and that the intensity of such effect is variable. A couple of experiments were devised to test whether this effect could be due to a failure of the experimental design or a result of molecular crowding at high protein concentration and/or a viscosity effect.

5.9.1 Increasing the sample pH does not fully re-create the ezrin effect on the 15N Fas 1H/15N-HSQC

Samples in solution NMR spectra of proteins are particularly sensitive to changes in the sample buffer, particularly pH. For example when working on a new protein construct, some of the parameters to assay for an optimal NMR spectrum (in terms of line widths, peak dispersion and resolution) is the pH of the sample, temperature and salt concentration. It could have been possible that slight variations in the pH of ezrin samples might have a strong effect on the ^{15}N Fas $^{1}H/^{15}N$-HSQC spectrum.

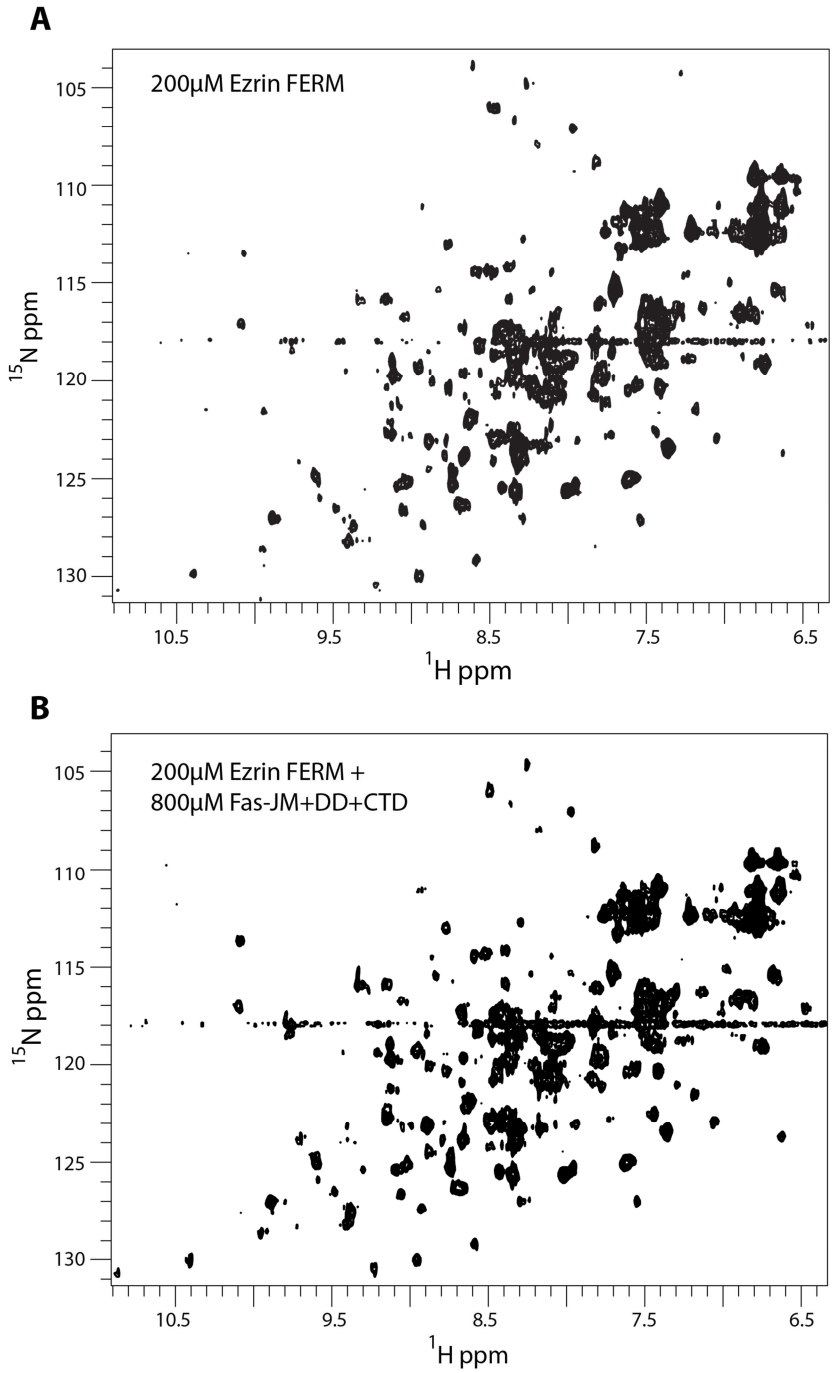

Figure 5.27 $^{1}H/^{15}N$-HSQC spectra of $^{2}H/^{15}N$ ezrin-FERM mixed with 800µM Fas-JM+DD+CTD.

As no effect upon the ezrin spectra had been observed with the addition of double the concentration of Fas, four times the concentration of Fas 194-335 was added to $^{2}H/^{15}N$ ezrin. A, $^{1}H/^{15}N$-HSQC spectrum of 200µM $^{2}H/^{15}N$ ezrin-FERM. B, $^{1}H/^{15}N$-HSQC spectrum of 200µM $^{2}H/^{15}N$ ezrin-FERM with 800µM Fas-JM+DD+CTD. All of the spectra were recorded at 25^{o}C at 800MHz.

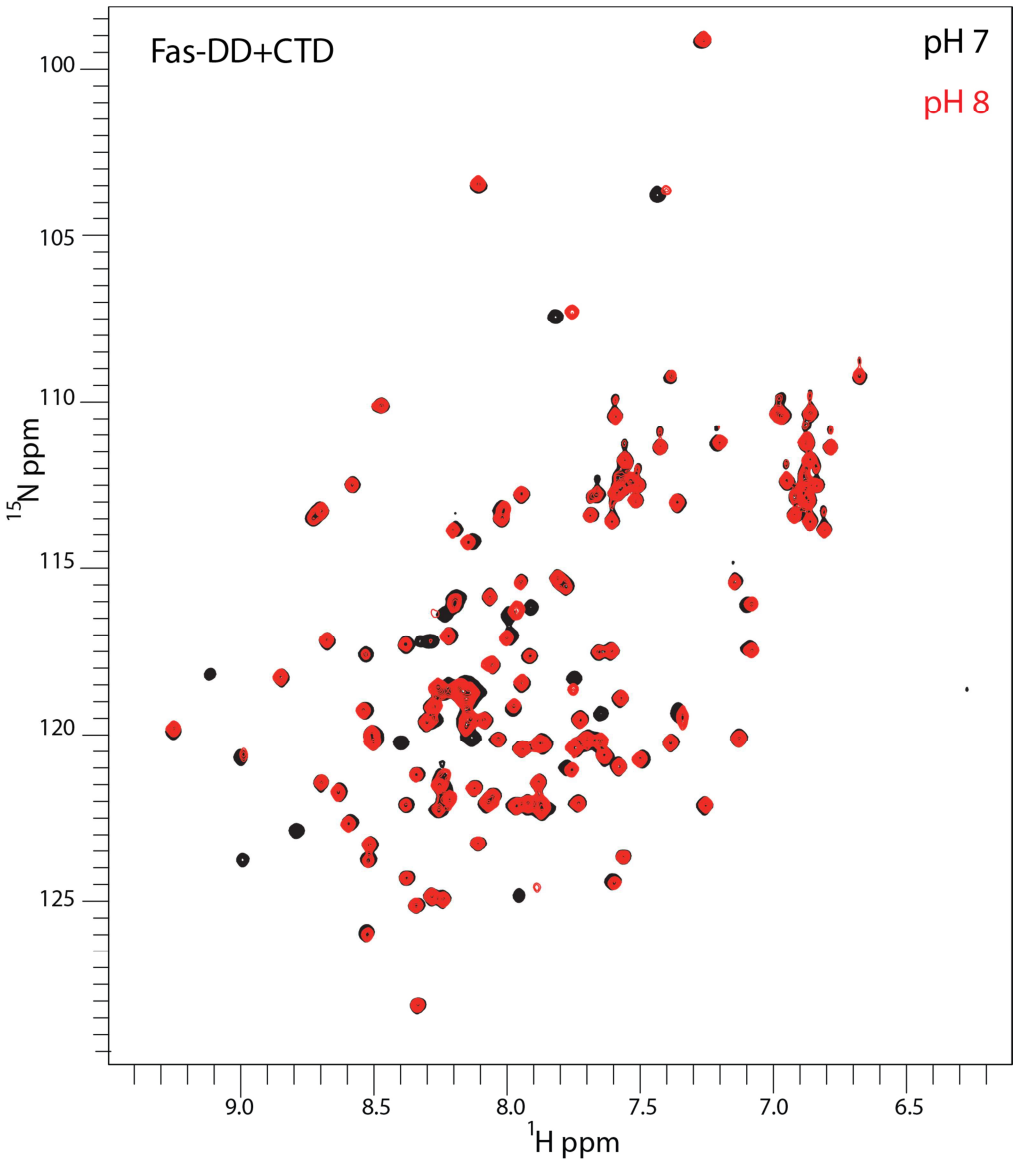

Figure 5.28 Superimposed $^{1}H/^{15}N$ HSQC spectra of Fas-DD+CTD at pH7 and pH8

$^{1}H/^{15}N$ HSQC spectrum of 200µM ^{15}N Fas-DD+CTD at pH7 is shown in black and the $^{1}H/^{15}N$ HSQC spectrum of 200µM ^{15}N Fas-DD+CTD at pH8 is overlaid in red.

To test whether the variation of the pH of the sample could induce the same effects as ezrin addition upon the ^{15}N Fas HSQC spectrum, two ^{1}H/^{15}N-HSQC datasets were recorded for the same sample. Initially, a ^{1}H/^{15}N-HSQC spectrum of 200 μM Fas-DD+CTD in ezrin NMR buffer at pH 7 was recorded, shown in black contours in Figure 5.28. This sample was then dialysed into ezrin NMR buffer at pH 8 and another ^{1}H/^{15}N-HSQC spectrum was recorded, overlaid in red contours in Figure 5.28. When comparing these two NMR spectra at different pH it is notable that some peaks are not present in the pH 8 spectrum compared to the pH 7 spectrum. However these effects upon the spectrum are quite minor compared to the effect when ezrin was added. The effect of pH variation cannot explain the effects seen for the ^{1}H/^{15}N-HSQC spectrum of Fas after ezrin addition.

5.9.2 Addition of high molecular weight proteins does not fully re-create the ezrin effect on the ^{15}N Fas ^{1}H/^{15}N-HSQC

In general one might expect that the ^{1}H/^{15}N-HQSC spectrum of a protein is sensitive to the viscosity of a sample. High viscosity slows the tumbling time of the observed protein, which would translate to broadening of the signals. Adding ezrin did not cause any effect on the methyl-TROSY spectrum of $^{13}CH_3$ ILV-labelled Fas, suggesting that there was no complex formation, but the addition of ezrin could have caused an increase in the viscosity and/or crowding of the samples observed by ^{1}H/^{15}N-HSQC experiments, therefore perturbing the spectra of interactions assayed in this manner. To test for this effect, two NMR samples were prepared, one containing 200 μM ^{15}N Fas-DD+CTD and one which contained 200 μM ^{15}N Fas-DD+CTD and 400 μM bovine serum albumin (BSA). The two ^{1}H/^{15}N-HSQC spectra are shown overlaid in Figure 5.29 with an equivalent spectrum which was recorded for a sample containing Fas-DD+CTD and ezrin FERM+tCC. As can be seen in Figure 5.29, a number of the peaks which are not present in the ezrin spectrum are also not present in the spectrum containing BSA, however the effect is not as extensive as it is with ezrin. Therefore the addition of a large protein to ^{15}N Fas does not fully explain the changes induced in the spectrum by the presence of ezrin.

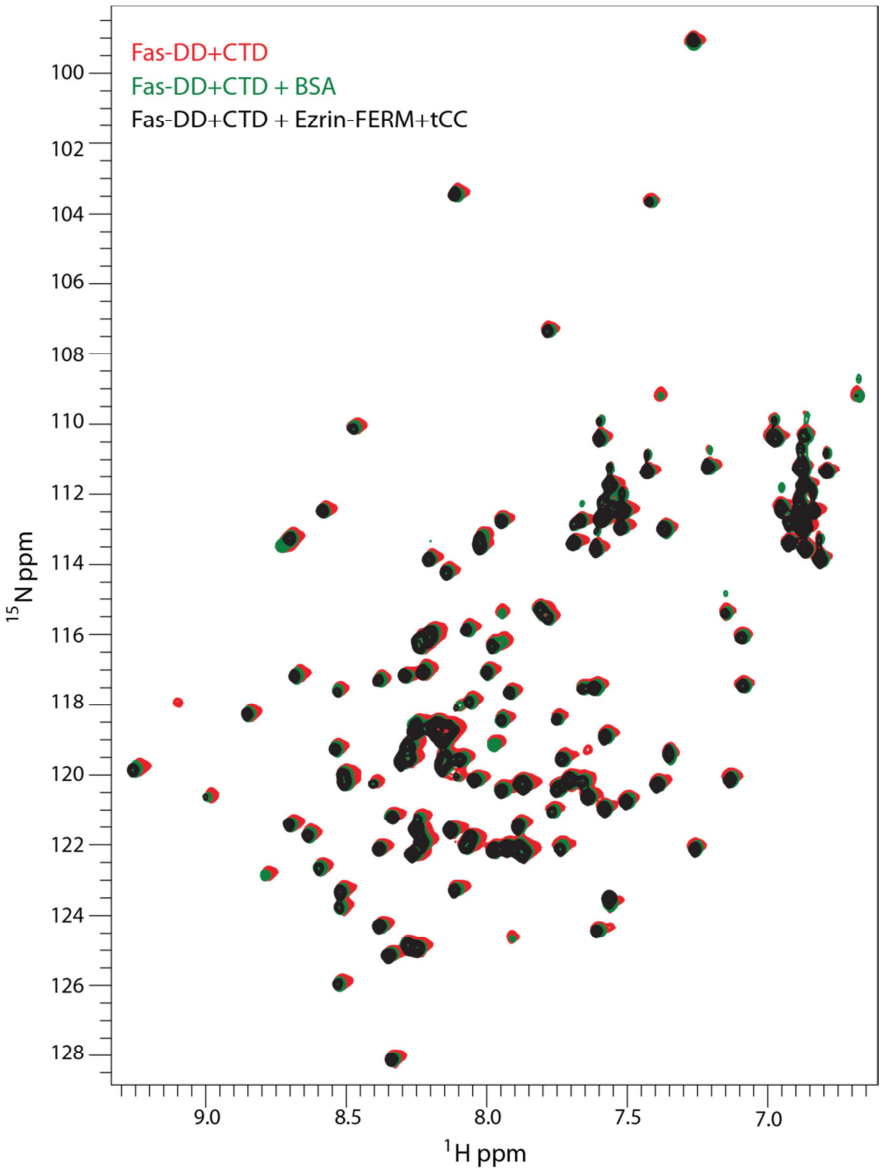

Figure 5.29 Superimposed 1H/15N HSQC spectra of 200µM 15N Fas-DD+CTD, 200µM 15N Fas-DD+CTD and 400µM ezrin-FERM+tCC and 200µM 15N Fas-DD+CTD and 400µM BSA

To see whether the effects of ezrin upon the Fas $^{1}H/^{15}N$ HSQC could be due to the addition of a larger protein to the sample, thus changing the viscosity and the environment of the protein rather than showing an interaction, 400µM BSA was added to 200µM ^{15}N Fas 202-335.
200µM ^{15}N Fas-DD+CTD spectrum in red, with 200µM ^{15}N Fas-DD+CTD, 200µM ^{15}N Fas-DD+CTD and 400µM BSA spectrum overlaid in green and 400µM ezrin-FERM+tCC overlaid in black. All spectra are shown at a low contour level at which you recover the majority of the Fas HSQC spectrum when ezrin is present. The addition of BSA to the sample alters the spectrum in a similar manner to the addition of ezrin does, however not as many peaks disappear.

5.10 Discussion

An interaction between Fas and ezrin has been highly documented in the literature with conflicting opinions of its involvement in the positive or negative regulation of apoptosis. The interaction has mainly been observed *in vivo* by co-localisation and *in vitro* by co-immunoprecipitation[114] or by using GST tagged recombinant proteins as bait and mammalian cell lysates as prey[117,118]. GST pull downs using only recombinant proteins have been reported by two different groups. In both cases, the construct of Fas was roughly equivalent to Fas-JM+DD+CTD, but while Kuo and coworkers used full-length ezrin, Lozupone *et al.* (2004) used a variety of ezrin constructs with the aim of mapping the Fas binding site. They concluded that it consisted of a nineteen-amino acid region of the ezrin FERM domain (residues 149-168). However no structural, thermodynamic or kinetic binding data have been published regarding this interaction.

The first step towards attempting to characterise the Fas:ezrin interaction was to express and purify truncations of the intracellular region of Fas as well as the ezrin FERM domain and the coiled coil region. Fas constructs were loosely based around those used previously within the laboratory in the work published by Esposito *et al.* (2010). The Fas protein constructs contained a K263A mutation which increases the solubility and stability of the constructs. The ezrin FERM domain construct consisting of residues 1-362 was based on the longest construct used by Lozupone and collaborators. The ezrin FERM domain has been highly characterised and a crystal structure has been solved[97], therefore expression and purification was not expected or observed to be problematic. The analysis of the analytical SEC chromatograms of both proteins at concentrations similar to those used in the NMR experiments, show that both proteins exist in a monomeric state in solution, as has been previously reported from other biophysical investigations of these proteins[96,122].

Within this study it was not been possible to fully recapitulate the pull-down results obtained by Lozupone and collaborators. Although it appeared at first glance that both GST-ezrin could pull down Fas and immobilised H_6-GB1-Fas could pull down ezrin, in both of these assays, the un-tagged binding partner was observed to associate with the beads in a non-specific manner. The non-specific interaction observed in the negative control could be caused by the addition of high, non-

physiological, concentrations of un-tagged protein resulting in non-specific binding to the beads. However the conditions used within the binding assays in this study and those used by Lozupone *et al.* are very similar. It is possible that what these researchers interpreted as an interaction was a result of non-specific binding. This possibility cannot be discarded as the authors failed to show the results of ezrin binding to the glutathione-sepharose beads in the absence of Fas.

Likewise, Fas and ezrin were not found to co-elute from an analytical SEC column which suggested the corresponding dissociation constant is too high for complex formation to be observable by this technique. However, the SEC results were also supported by analytical ultracentrifugation measurements which can access lower affinity protein protein complex formation. The SV-AUC experiments also showed that both Fas and ezrin were monomeric in solution and that the majority of the sample maintained the dissociated monomeric forms after mixing the two proteins.

Biolayer interferometry (BLI) is an optical analytical technique which offers a real time binding assay in which you can detect the build-up of a protein complex on the sensor by analysing the interference pattern of white light with an internal reference[231]. Initial BLI experiments were very encouraging, suggesting that the dissociation constant between Fas and ezrin was between 70 μM and 90 μM. The first doubts about this conclusion were cast with the realisation that similar binding constants were obtained with or without the juxtamembrane region of Fas, which has previously been reported by Ruan *et al.* (2008) to be crucial for binding. In an effort to map the ezrin binding site, BLI experiments were also conducted with six mutants of Fas with conservative point mutations that spanned the solvent exposed surface of the death domain. Derived dissociation constants for the mutants were also between 60 μM and 90 μM, suggesting that the interaction did not map to the Fas death domain. To test for binding to the purification/biotinylation tag (H_6Avi), which was common to all constructs, a variety of H_6-Avi tagged proteins unrelated to Fas were also tested and they all interacted with ezrin, adding further support to the idea that ezrin was recognising the H_6Avi region of the constructs. Ezrin binding to the H_6Avi tag was further investigated by a number of NMR titration experiments and by a GST-pull down assay of the corresponding proteins (Figures 5.21 and 5.23). The results of these assays also supported the hypothesis that ezrin recognises the H_6Avi tag. Because the same effect on the $^{1}H/^{15}N$-HSQC spectrum of $^{2}H^{15}N$ ezrin occurred

with H_6-GFP, the conclusion is that ezrin is able to bind the hexa histidine tag alone. The possibility that it also binds some region of GFP cannot be excluded but it was decided not to pursue this avenue any further.

The fact that ezrin may be able to recognise a variety of targets with different levels of affinity as well as in a non-specific manner may be a feature of the FERM domain family binding, as their role is to bind a wide variety of proteins in the membrane to actin. Even the well-documented FERM binding ligands of ICAM2, CD44, NHERF2 and EBP50 do not share a common binding motif. Results obtained so far did not exclude the possibility that ezrin and Fas were interacting but that this interaction was masked by the binding to the H_6Avi tag, so that further experiments would have to be done with fully untagged proteins to prevent further non-physiological interference.

NMR is a powerful technique to observe protein-protein interactions in solution because, in principle, it can permit analysis of interactions at the residue level. The requirement for high protein concentrations to observe sufficient signal enables the study of weak binding events. $^{1}H/^{15}N$-HSQC experiments recorded with ^{15}N-labelled Fas in the presence or absence of non-isotopically labelled ezrin initially appeared to indicate that an interaction was taking place, as addition of ezrin caused broadening of the Fas signals consistent with the formation of a high molecular weight complex. Because NMR cross peaks corresponding to the structured death domain were also affected, this putative interaction did not seem to be limited to the MPD of Fas. Unfortunately, the inverse NMR experiment using $^{2}H^{15}N$ ezrin and non-isotopically labelled Fas was not successful as the spectrum remained unperturbed on the addition of Fas.

So far, I could not exclude the possibility that a Fas-ezrin interaction was occurring but was not being detected using the HSQC experiment due to the size of the complex formed. This was addressed by recording a methyl-TROSY experiment with $^{13}CH_3$ ILV-labelled Fas and non-labelled ezrin. The advantage of collecting a methyl-TROSY spectrum over a $^{1}H/^{15}N$ spectrum is that the methyl-TROSY experiment is less sensitive to the tumbling time of the molecule; therefore if a large complex is formed which tumbles slowly, an interaction between the two interaction partners would still be observable. The resulting spectra (shown in Figure 5.26)

showed no indication of a decrease in cross peak intensity or chemical shift perturbation allowing us to conclude that in our experimental setting no high molecular weight complex was being formed between Fas and ezrin. In light of these results, sample pH and the addition of BSA to increase viscosity were explored as possible causative agents of the signal broadening of the ^{15}N-Fas signals in the ^{1}H/^{15}N-HSQC, but this did not seem to be the case.

In summary, exhaustive exploration of a possible direct binding interaction between a variety of intracellular Fas constructs and the FERM domain of ezrin has revealed that there is no strong evidence for an interaction occurring in these conditions. Instead, ezrin has shown promiscuous interactions with a number of different solid supports used for pull down assays as well as the H_6Avi tag, most probably the hexa histidine region. These results have led us to the conclusion that the Fas, ezrin interaction that has been observed by co-localisation and co-immunoprecipitation experiments[114] cannot be reliably reproduced *in vitro* using recombinant proteins. It is essentially impossible to reconcile my findings with all reports in the literature. However it is possible that productive Fas ezrin interaction of the type claimed by multiple research groups for in-cell type experiments may require an element that my experimental approach could not straightforwardly take into account. Such as (a) the requirement of other regions of ezrin besides the FERM domain; (b) the involvement of a third interaction partner and/or; (c) the requirement of a post translational modification of Fas. It has previously been reported that Fas is palmitoylated prior to the binding of ezrin[25]. It is possible that this lipid modification upon Fas could be the missing aspect within this interaction study.

Chapter 6

In vitro palmitoylation of the cytoplasmic region of Fas

6.1 Introduction

6.1.1 Palmitoylation functions as a switch to modulate protein association with cell membranes

S-palmitoylation is the addition of palmitate, the sixteen carbon fatty acid, by thioesterification of a cysteine residue side chain within a protein[237]. More accurately it should be referred to as protein S-acylation, as depending on availability, other fatty acids can also be attached to a protein in this fashion and with similar results[238]. Throughout this chapter acylation and palmitoylation will be used interchangeably to refer to palmitoylation – the covalent addition of a palmitate fatty acid to a protein via a cysteine residue side chain.

Post translational palmitoylation is a reversible modification that is used as a switch-like mechanism, much like other, better understood, post translational modifications such as ubiquitinylation and phosphorylation[239,47]. In humans, protein palmitoylation is widespread throughout a number of cell types, with more than 1000 human proteins showing some evidence of palmitoylation[240], this is approximately 10% of the human proteome[241]. The substrate for palmitoylation is the activated form of the palmitate fatty acid, palmitoyl-coenzyme A (CoA); the structure of both palmitate and its activated form are shown in Figure 6.1. *In vivo*, the palmitoyl group is transferred from the palmitoyl-CoA to the target cysteine by a class of enzymes known as palmitoyl transferases (PAT). It had been known for a long time that an enzyme existed carry out this role, but the first PAT were not identified until 2002[242,243] possibly due to their membrane association. Depalmitoylaton is catalysed by the protein palmitoyl thioesterases/acyl protein thioesterases (PPT/APT), which hydrolyse the thioester bond to generate a cysteine thiol and palmitate[244].

The addition of a palmitoyl group to a protein increases its hydrophobicity which mainly functions as a protein trafficking mechanism. Both soluble and integral membrane proteins have been shown to be palmitoylated *in vivo*. Palmitoylation of a soluble protein targets the protein to membrane environments inside the cell[238]. It acts as a temporary transmembrane domain, tethering the protein to the cytoplasmic side of the cell membrane, or to other membrane compartments such as the Golgi apparatus or endosomes. The consequences of adding palmitoyl groups to integral membrane proteins are less obvious, but it seems that palmitoylation can regulate recruitment of proteins to lipid rafts or to other cholesterol-rich membrane regions such as tetraspanin-rich microdomains[245]. Driving palmitoylated proteins into lipid rafts has been suggested to be necessary for events such as endocytosis[38] and massive endocytosis (MEND)[246]. Palmitoylation can also alter protein conformation, for example by 'tilting' the transmembrane domain which in turn can affect the local shape of the membrane and/or promote the formation of protein complexes[47].

Protein palmitoylation also influences protein:protein interactions. A number of studies have identified an increased affinity between both tetraspanins and integrin subunits upon palmitoylation as a mode of regulating their interactions[48,247]. Palmitoylation of GPCR components has also been shown to maintain receptor signalling. For example, palmitoylation prevents desensitisation of the β2-adrenergic receptor, which is involved in the production of cyclic adenosine monophosphate (cAMP), by maintaining subunit interaction[248]. Other studies have highlighted a role for palmitoylation in protein signalling and ion transport into the cell[241].

6.1.2 Protein palmitoylation can take place both enzymatically and non-enzymatically depending on the concentration of the activated fatty acid

There is not a specific consensus sequence which targets specific cysteines for palmitoylation by PAT. Bizzozero *et al.* (2001) found that stretches of basic amino acids, similar to those commonly found close to the membrane, were preferentially palmitoylated *in vitro*. The same sequences that could be chemically palmitoylated *in vitro* were found to be palmitoylated *in vivo,* suggesting that it is not the protein structure that is recognised by the PAT, but the environment in which the cysteine is located[249]. Prior to the identification of PAT a number of *in vitro* autoacylation/*in vitro* palmitoylation (IVP) assays were used to look into the possible mechanisms of

palmitoylation. This section serves as a brief review of both *in vitro* palmitoylation/autoacylation as well as some background about the PAT enzymes.

6.1.2.1 Autoacylation only takes place at millimolar concentrations of activated fatty acid

The autoacylation reaction is the spontaneous addition of a palmitoyl group to a cysteine within a protein or a peptide when incubated with the activated form of the acid: palmitoyl-CoA[49]. It has been shown to be an effective method to palmitoylate both short peptides and proteins *in vitro*. It was primarily used to study palmitoylation prior to the identification of the PAT enzymes, both to elucidate the mechanism of the reaction and to identify palmitoylation sites within proteins.

The first autoacylation reaction was carried out by Bizzozero and colleagues in 1987. In this experiment they observed that a peptide corresponding to a region of myelin proteolipid protein was acylated on the correct cysteine when incubated with palmitoyl-CoA. They hypothesised that the mechanism with which the reaction occurred by could be physiological and therefore an enzyme may not be necessary for the reaction to occur[250]. Building upon this, a number of different groups successfully used IVP on peptides corresponding to palmitoylated regions of proteins, furthering debate over the need for an enzyme for palmitoylation to occur at all[136,249]. Interestingly, a number of these peptides could only be palmitoylated when they had been previously lipid modified with a myristoyl group[136,250–252]. IVP was also used to develop a fluorescence-based assay to identify palmitoylated peptides *in vitro*[252] as well as a method to correctly acylate full proteins such as the $G_{i\alpha1}$ subunit of a GPCR[251] and SNAP-25[253] *in vitro*.

By using autoacylation reactions on short peptides corresponding to know palmitoylation sites, the basic mechanism of palmitoylation was elucidated. There is limited sequence similarity between the locations that proteins are palmitoylated. Bizzozero and colleagues[254] used the IVP assay to identify the specificity of the amino acids surrounding the palmitoylation site and the role which this would play within the process of palmitoylation. They identified that in close proximity to or surrounding the cysteine there were always a number of basic amino acids, it was unclear whether these were the same basic residues usually observed in near proximity to the cell membrane. The sulfhydryl group of a free cysteine has a pKa of

7.2-7.4 rendering it unable to react with palmitoyl-CoA at physiological pH. The presence of the basic amino acids in close proximity to the cysteine results in the reduction in the pKa of the thiol to around 3[254]. Therefore, palmitoylation targets exist as thiolates in physiological conditions. The thiolate ion can then attack the carbonyl of the thioester between CoA and the palmitoyl group resulting in the formation of a new thioester bond between the cysteine of interest and the palmitoyl group and the release of HSCoA[49]. This reaction is shown in figure 6.2, illustrated using IC-Fas-DD as the target protein.

The spontaneous acylation of proteins is an unlikely mechanism of palmitoylation *in vivo* due to the presence of acyl-CoA binding protein (ACBP). This 10 kDa protein sequesters activated fatty acids (such as palmitoyl-CoA) to prevent them from reacting. ACBP has a strong affinity for activated fatty acids and the ability to remove them from the cell membrane. The presence of ACBP maintains the concentration of free acyl-CoA within a cell at the nanomolar concentration range, ACBP itself is present at micromolar range of concentrations inside cells[255,256]. In the assays described above, the palmitoyl-CoA was always present at an excess concentration to the peptide or protein to be palmitoylated; *in vivo*, the autoacylation reaction could take days to occur and would not be a viable mechanism. Despite this, it has been suggested that autoacylation could play a role in the modulation of mitochondrial metabolic enzymes, because there are no known PAT in the mitochondria. For example, it is known that substrate binding in methylmalonate semialdehyde dehydrogenase is controlled by S-acylation[239] .

6.1.2.2 Palmitoylation is catalysed by the DHHC family of transmembrane proteins

The first PAT, Akr1p[242] and Erf2[243] were discovered using classical genetic screens in yeast. By now, seven yeast and twenty three metazoan PAT have been identified and a sufficient number of studies on these enzymes have been reported in order to draw some generalisations. PAT are multipass alpha helical proteins containing four or six transmembrane helices. Through cell based tests of both yeast and human PAT, a large number were shown to localise to the endoplasmic reticulum or the Golgi body, with very few locating to the plasma membrane[257]. This could further suggest that following protein synthesis, palmitoylation can act to target the protein to the membrane, rather than protein palmitoylation occurring at the membrane.

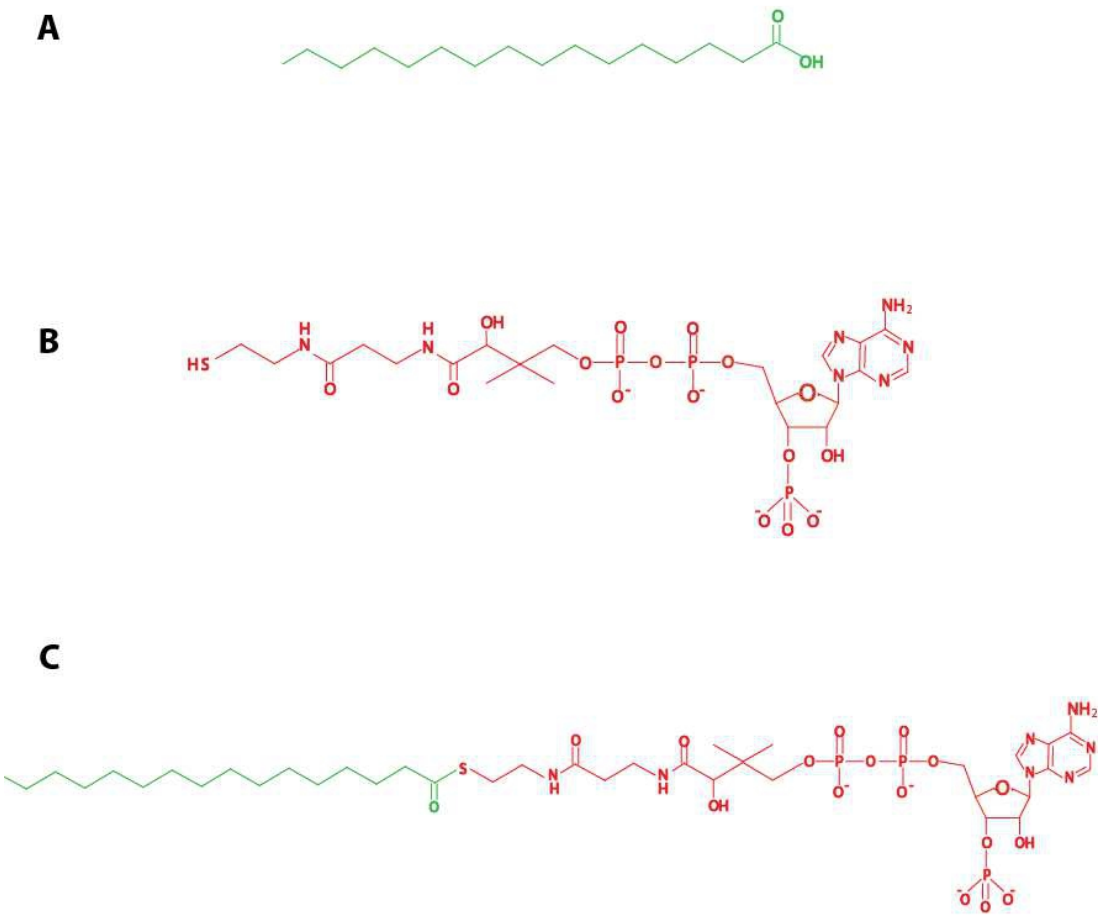

Figure 6.1 Structures of the small molecules used throughout chapter 6

A, Palmitate/palmitic acid. B, coenzyme A. C, palmitoyl-coenzyme A

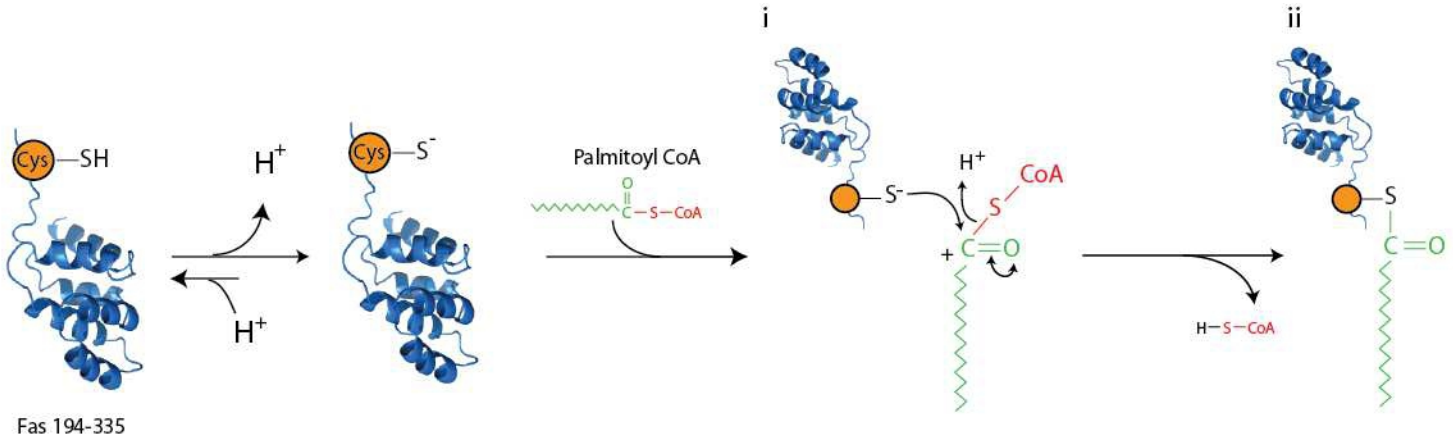

Figure 6.2 The chemical palmitoylation reaction used to palmitoylate Fas-JM+DD+CTD

Schematic diagram of the mechanism of chemical palmitoylation used to palmitoylate Fas-JM+DD+CTD. In brief, Fas Cysteine 199 is amongst basic residues resulting in the reduction and deprotonation of the sulphydryl group forming a thiolate ion. This enables nucleophilic attack of the thiolate upon the alpha-carbon of palmitoyl-CoA (i), which forms a thioester bond between Fas and the palmitic acid group (ii). Adapted from Dietrich & Ungermann 2004. PDB:1DDF

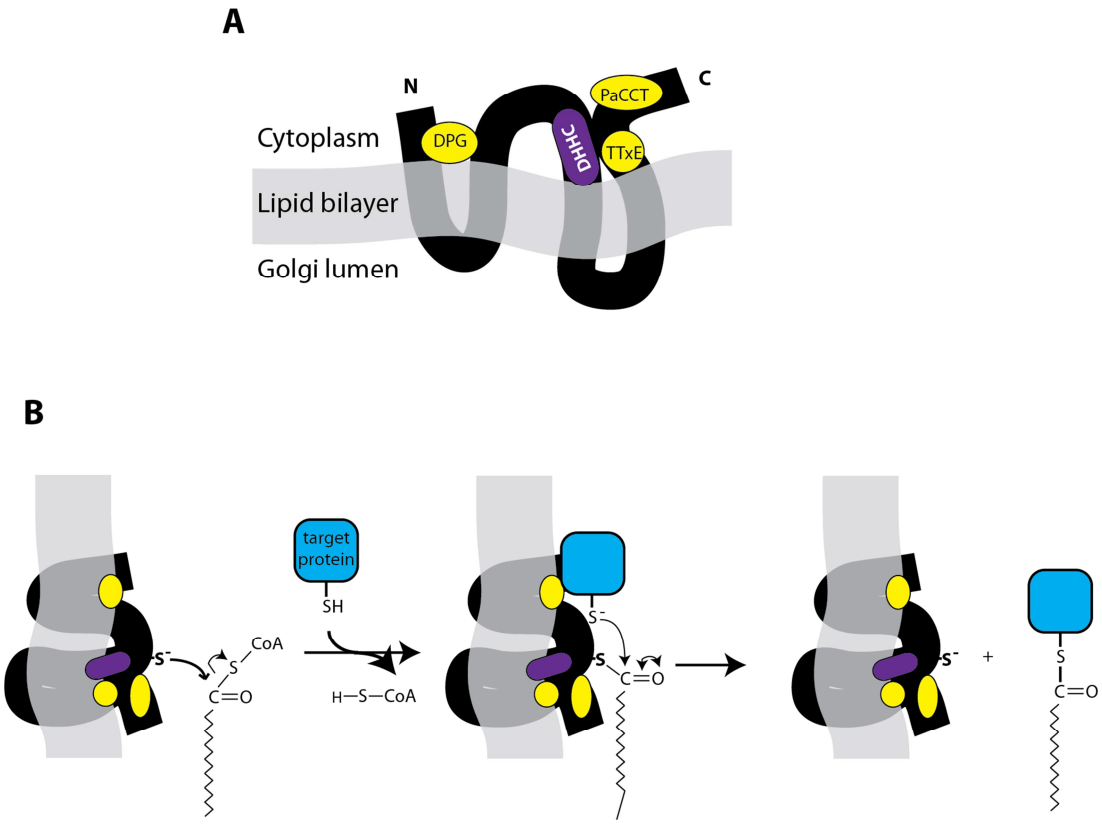

Figure 6.3 DHHC palmitoyl transferase mechanism of palmitoylation

A, Schematic representation of a palmitoyl transferase enzyme. B, Schematic representation of the suggested DHHC mechanism of palmitoylation. The palmitoyltransferase enzyme (yellow) forms a thioester intermediate with palmitate.A target protein can bind to the pamlitoyltransferase, which then catalyses the transfer of palmitate onto the target protein.

PATs are characterised by the presence, in the cytoplasmic-facing site of the molecule, of a highly conserved 50-residue cysteine rich domain referred to as the DHHC (Asp-His-His-Cys)[258,241,237]. The DHHC sequence is very hydrophobic and folds forming a zinc finger thought to be able to co-ordinate two Zn^{2+} ions. The hydrophobicity of the DHHC is necessary in order to be able to exclude H_2O, thus preventing side reactions from occurring during palmitoyl transfer[237]. Three other conserved motifs, all facing the cytoplasm, are present in known PAT, a Thr-Thr-X-Glu (TTxE motif); a Asp-Pro-Gly (DPG motif) and a 16-residue motif named palmitoyl transferase conserved C-terminal (PaCCT)[259]. The human PATs are referred to by a number following the DHHC name, e.g. DHHC17.

The role of a PAT is to recognise the target cysteine on the protein to be palmitoylated and then to catalyse the acyl transfer[49]. The mechanism of action has been described as 'ping pong' kinetics[260], in which the enzyme first becomes autoacylated by palmitoyl-CoA, and then transfers the palmitoyl group to the protein of interest[260] (Figure 6.3). This site of autoacylation is still unknown.

Although the DHHC domain and the other motifs are relatively well conserved between all known PATs, there is a high level of substrate specificity between the enzyme and the protein targets. This substrate specificity is conferred by regions of the protein distinct from the DHHC domain. N- and C- terminal extensions of the DHHC have been shown to contain a variety of distinct protein-protein interaction domains; evidence has been found to suggest that it is these domains which recruit the protein to be acylated. For example, the C-terminal extension of DHHC3 contains a Src homology 3 (SH3) domain[261] and in the same region of DHHC13 and DHHC17 ankirn repeats have been predicted[262]. However, it is not just the protein sequence which modulates the activity of DHHC-PAT, but also protein-protein interactions between different DHHCs themselves. It has been shown that DHHC2 and DHHC3 can homodimerise, affecting the reactivity of each of the enzymes. When dimers, these enzymes are catalytically inactive, suggesting that oligomerisation could be a mechanism of self-regulation for DHHC protein activity[263]. DHHC proteins have not only been reported to self-associate, but there are also reports that DHHC activity is modified through interactions with other proteins in regions which are not being palmitoylated, for example the cysteine rich

domain of SNAP25 which is not palmitoylated is important for the recruitment of DHHC15 at the membrane, enabling palmitoylation to occur[261].

6.1.3 Palmitoylation is required for the activity of Fas and many other pro-apoptotic proteins

Palmitoylation has a prominent role in both intrinsic and extrinsic apoptosis. BCL-2-associated X (BAX) protein is recruited to the membrane of mitochondria by palmitoylation where it permeabilises the mitochondrial outer membrane and leads to the release of cytochrome C into the cytoplasm[264]. The netrin receptor UNC5H, which induces apoptosis when netrin is not available, also requires palmitoylation and lipid raft localisation in order to induce caspase activation and apoptosis[265]. Palmitoylation is also essential for Fas ligand (FasL) activity, as the addition of a palmitoyl group is required for recruitment to lipid rafts prior to proteolysis[52]. The death receptor DR4, but not DR5 or TNFR1, requires palmitoylation for DISC formation and commitment to cell death[51].

Initiation of Fas-mediated apoptosis occurs by receptor oligomerisation and lipid raft recruitment followed by DISC internalisation[38]. The palmitoylation of the membrane proximal cysteine (Cys199) is believed to be the targeting signal for Fas to be directed into lipid rafts[266]. Lipid raft recruitment of activated Fas has been observed prior to the internalisation of the DISC[50]. It has been reported that Fas palmitoylation is a requirement for the formation of the ezrin-mediated cytoskeleton association of the DISC. Without such association, internalisation does not occur reducing the onset of the caspase cascade[25].

This chapter documents an approach to *in vitro* palmitoylate a recombinant intracellular Fas construct and to characterise it using biophysical and binding studies. Furthermore, I present my attempts to validate the location of the palmitoyl group by NMR spectroscopy, site-directed mutagenesis and mass spectrometry (MS) techniques. The development of these techniques was in line with efforts in our lab to set the methodology for studying transmembrane domains in lipid bilayers by solution NMR.

Furthermore, the previous chapter detailed comprehensive *in vitro* studies of the interaction between Fas and ezrin, all of which did not give evidence of a specific

interaction, suggesting that something could be missing in our *in vitro* system which would allow this interaction to occur. As palmitoylation is one of the first events that take place before receptor clustering, we hypothesised that Fas might need to be palmitoylated in order to interact with ezrin.

6.2 Palmitoyl-Coenzyme A palmitoylates Fas-JM+DD+CTD on Cys 199

6.2.1 Fas-JM-DD+CTD preparation

Fas-JM+DD+CTD (residues 194-335) was prepared using the H_6-GB1-Fas-JM-DD+CTD construct introduced in Chapter 5. The construct was expressed in either LB or ^{15}N-labelled minimal medium (as described in Section 2.5), purified by IMAC and cleaved with TEV protease. The tag was then removed by a second IMAC step and a final purification step was carried out by SEC. SDS-PAGE analysis and the SEC chromatogram of a typical purification is shown in Figure 6.4. Table 6.1 shows the predicted properties of Fas-JM+DD+CTD.

6.2.2 Palmitoyl-CoA incubation causes broadening of the ^{1}H/^{15}N-HSQC signals due to the formation of two products

In vitro palmitoylation of Fas-JM+DD+CTD was initially carried out using a ^{15}N-labelled protein in an attempt to track the reaction using a ^{1}H/^{15}N-HSQC experiment.

Two NMR samples were prepared, each containing 200 μM ^{15}N Fas-JM+DD+CTD in acylation buffer (10 mM HEPES, pH 7, 1m M EDTA, 1 mM $MgCl_2$, 10 mM NaCl, 130 mM KCl, 1 mM DTT) at a volume of 550 μl (containing 10% $^{2}H_2O$). Palmitoylation was initiated in one of the samples by addition of a final concentration of 1 mM palmitoyl-CoA dissolved in acylation buffer. The equivalent volume of acylation buffer was added to the other sample (Section 2.8). ^{1}H/^{15}N-HSQC spectra were collected periodically over five hours for ^{15}N Fas-JM+DD+CTD mixed with palmitoyl-CoA. By the time it took from adding the palmitoyl-CoA to inserting the sample in the spectrometer, the changes in the ^{1}H/^{15}N-HSQC had been quite dramatic, there was no further change to the spectra in subsequent time points, suggesting that the reaction was occurring very fast. The comparison of the ^{1}H/^{15}N-HSQC spectra before and after palmitoyl-CoA addition (Figure 6.5 A and B, respectively) reveals that addition of palmitoyl-CoA causes significant broadening of the cross peaks corresponding to the folded regions of the protein.

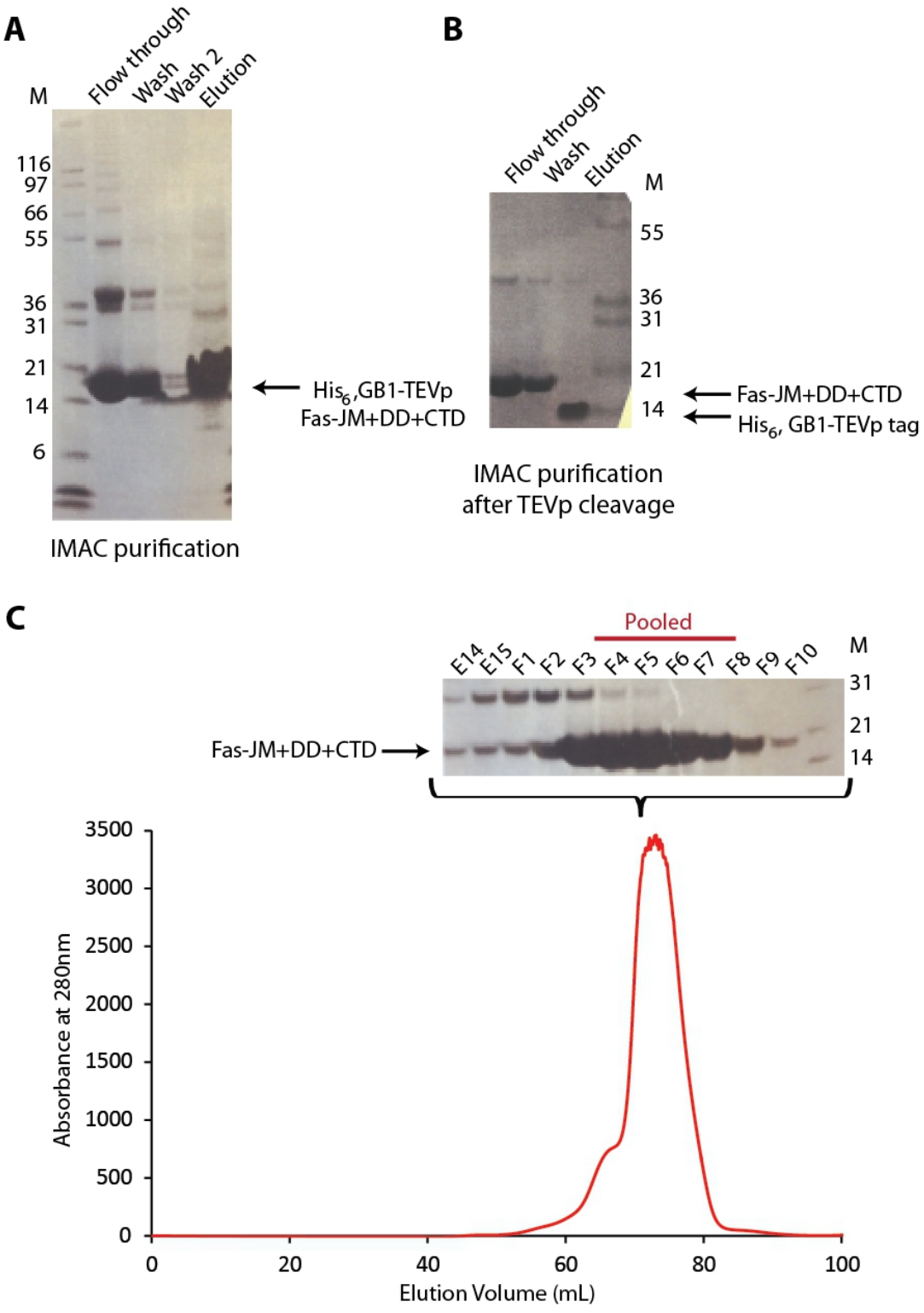

Figure 6.4 Fas-JM+DD+CTD purification

A, SDS-PAGE analysis of the IMAC purification of Fas-JM+DD+CTD (residues 194-335). Wash 2 corresponds to the high imidazole wash. The elution was taken and TEV cleaved prior to running back over an IMAC column. B, SDS-PAGE analysis post TEV cleavage. C, The elution profile (monitored by UV absorbance at 280nm) and SDS-PAGE analysis of post TEV flowthrough and washes from Superdex 75 size exclusion column. The red line indicates the fractions that were pooled and concentrated to be used throughout these experiments.

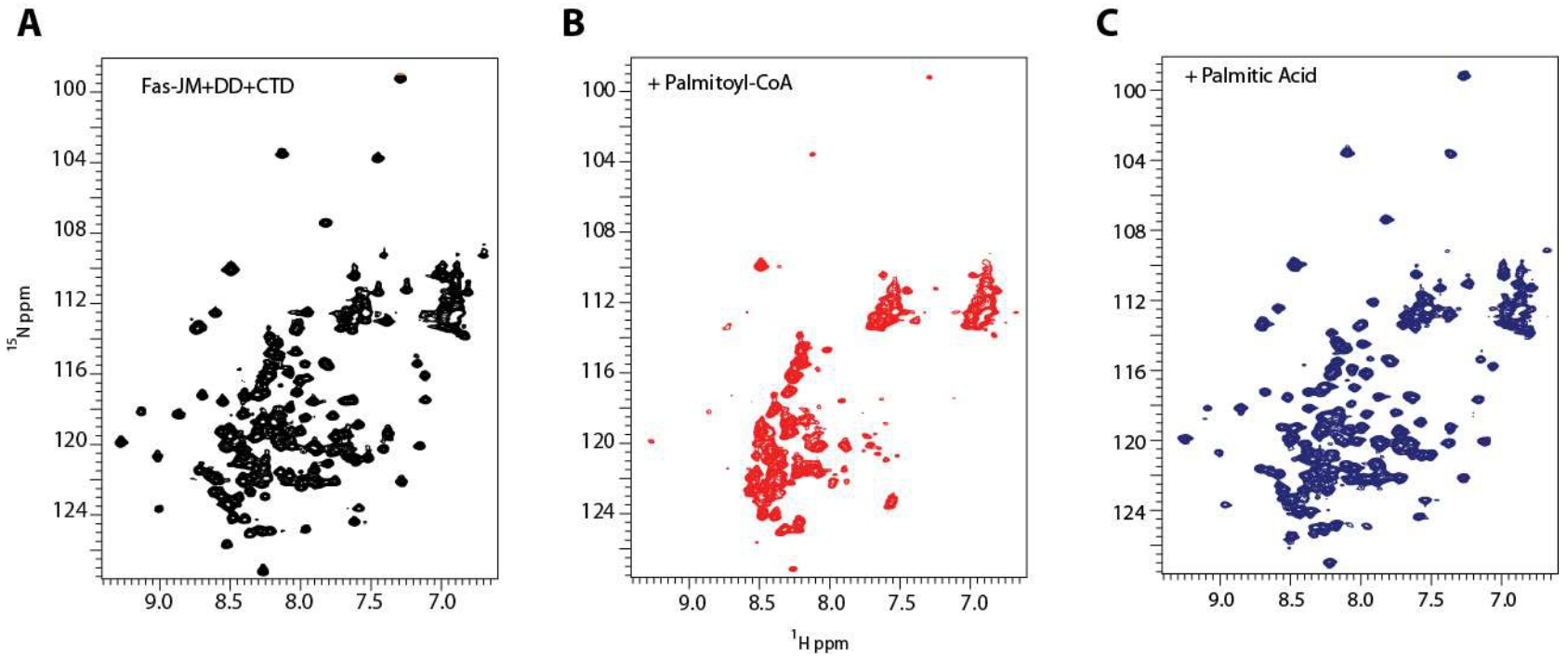

Figure 6.5 Palmitoyl CoA incubation generates a larger Fas species invisible to NMR

A, $^{1}H/^{15}N$-HSQC spectra of 200µM ^{15}N Fas-JM+DD+CTD. B $^{1}H/^{15}N$-HSQC spectra of 200µM, ^{15}N Fas-JM+DD+CTD with 1mM palmitoyl CoA. C, $^{1}H/^{15}N$-HSQC spectra of 200µM ^{15}N Fas-JM+DD+CTD with 5mM palmitic acid. Incubation with palmitoyl CoA resulted in a decrease in peak intensity which was not observed with palmitic acid alone

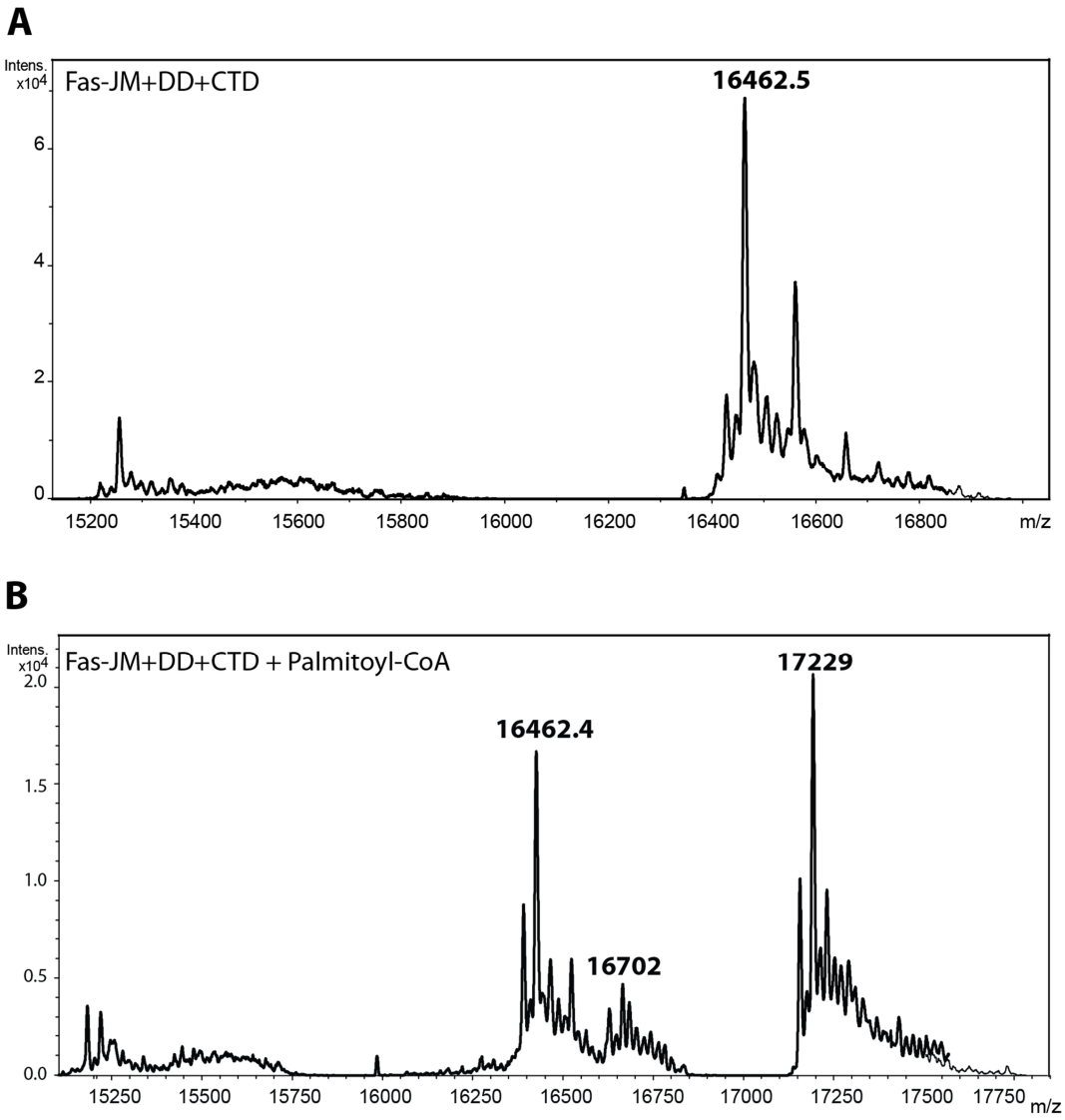

Figure 6.6 The Fas species invisible to NMR is confirmed to be palmitoylated Fas-JM+DD+CTD by ESI-TOF-MS

Mass spectra of samples of NMR samples shown in Figure 6.5. A, QTOF mass spectra of unreacted ^{15}N Fas-JM+DD+CTD. B, QTOF mass spectra of ^{15}N Fas-JM+DD+CTD with 1mM Palmitoyl CoA. Masses corresponding to the addition of a palmitoyl group or coenzyme A to Fas-JM+DD+CTD were observed. N.B. ^{15}N Fas-JM+DD+CTD shown in this spectrum yields a higher molecular weight than previously noted within this study. This is due to the ^{15}N labelling used for NMR spectroscopy.

This was not observed in the sample containing no palmitoyl-CoA (Figure 6.5A). The observed broadening of $^{1}H/^{15}N$-HSQC peaks can be a result of the formation of a high molecular-weight Fas oligomer, conformation exchange and/or protein denaturation.

To test whether the effect of adding palmitoyl CoA to Fas-JM+DD+CTD on the $^{1}H/^{15}N$ HSQC was the result of a specific palmitoylation event or palmitoyl-CoA aggregating around Fas, a third set of conditions were tested. $^{1}H/^{15}N$-HSQC spectra were collected for ^{15}N-Fas-JM+DD+CTD (200 μM) samples mixed with 1 mM or 5 mM free palmitic acid. It was expected that if aggregation was occurring it would be due to the lipid component. Therefore the addition of the fatty acid should control for this effect. The $^{1}H/^{15}N$-HSQC spectra recorded for these samples looked identical to when no palmitoyl-CoA was present (Figure 6.5C). This suggested that the effects observed were specific to the addition of palmitoyl-CoA reacting with Fas and not just the presence of a hydrophobic group in the sample.

The samples were left at room temperature for sixteen hours to assess the stability of the newly produced construct compared to an unmodified Fas-JM+DD+CTD. After this time, a precipitate formed in the sample containing palmitoyl-CoA but not in the sample without the lipid additive. Lipid modified proteins are known to be less soluble in aqueous conditions and require detergent or other lipid micelles to stay in solution. The acylation buffer used contained no detergent additives to increase solubility. Therefore, this is a separate indication that a lipid modified product is being generated over time.

To confirm that palmitoylation of Fas-JM+DD+CTD had taken place, aliquots of the NMR samples were analysed by ESI-QTOF MS. The mass spectra for ^{15}N Fas-JM+DD+CTD and ^{15}N Fas-JM+DD+CTD, which had been incubated with palmitoyl-CoA, are shown in Figure 6.6 and the predicted masses of the constructs are shown in Table 6.1. The incubation with palmitoyl-CoA resulted in the formation of two additional masses different from the free Fas-JM+DD+CTD. The mass of 16702 is consistent with the addition of a single palmitoyl group (which has a molecular weight of 240) to Fas-JM+DD+CTD. The mass of 17229 would be consistent with the addition of coenzyme A (molecular weight 766.5) or the addition of more than one palmitoyl group to the construct; due to the presence of a second

cysteine (C304) in the Fas construct, it was possible that at least one other palmitoyl group could be added to Fas-JM+DD+CTD.

As can be seen from Figure 6.6B, the 16702 peak is very weak, compared to the others, suggesting that the proportion of palmitoylated Fas-JM+DD+CTD was quite low. However, this is probably just an artefact of the sample preparation for mass spectrometry. Samples have to be desalted and concentrated using a ziptip - a tip packed with C4 resin, and there is a high probablility that being more hydrophobic, the palmitoylated protein binds quite strongly to the C4 tips. Another possibility is that the palmitoylated Fas could be less soluble than non-palmitoylated Fas and could have precipitated prior to desalting. This way there would be less present for the mass spectrometry analysis.

6.2.3 Limited digestion of palmitoylated Fas-JM+DD+CTD does not enable mapping of the palmitoylation site due to heterogeneity

In order to map the location and number of palmitoyl groups which had been added to Fas-JM+DD+CTD on incubation with palmitoyl-CoA, a limited trypsin proteolysis was carried out on both palmitoyl-CoA reacted and unreacted samples. *In vitro* palmitoylation had to be repeated using an unlabelled sample to enable identification of peptide masses. The trypsin digested samples were analysed by ESI-QTOF MS. The theoretical peptide masses of Fas-JM+DD+CTD were calculated using 'Peptidemass' in the Expasy server. A coverage of 85% of the Fas-JM+DD+CTD sequence was achieved. An alignment of the peptides corresponding to the masses observed by MS is shown in Figure 6.7.

Cys199 is the residue that is palmitoylated *in vivo*[30]. Two peptides were detected for this region in the non-palmitoylated Fas-JM+DD+CTD (corresponding to masses of 927.5 and 1501.7). In the palmitoylated sample, both of these peptide fragments were no longer detectable which could suggest that there was a palmitoyl group attached to this peptide.

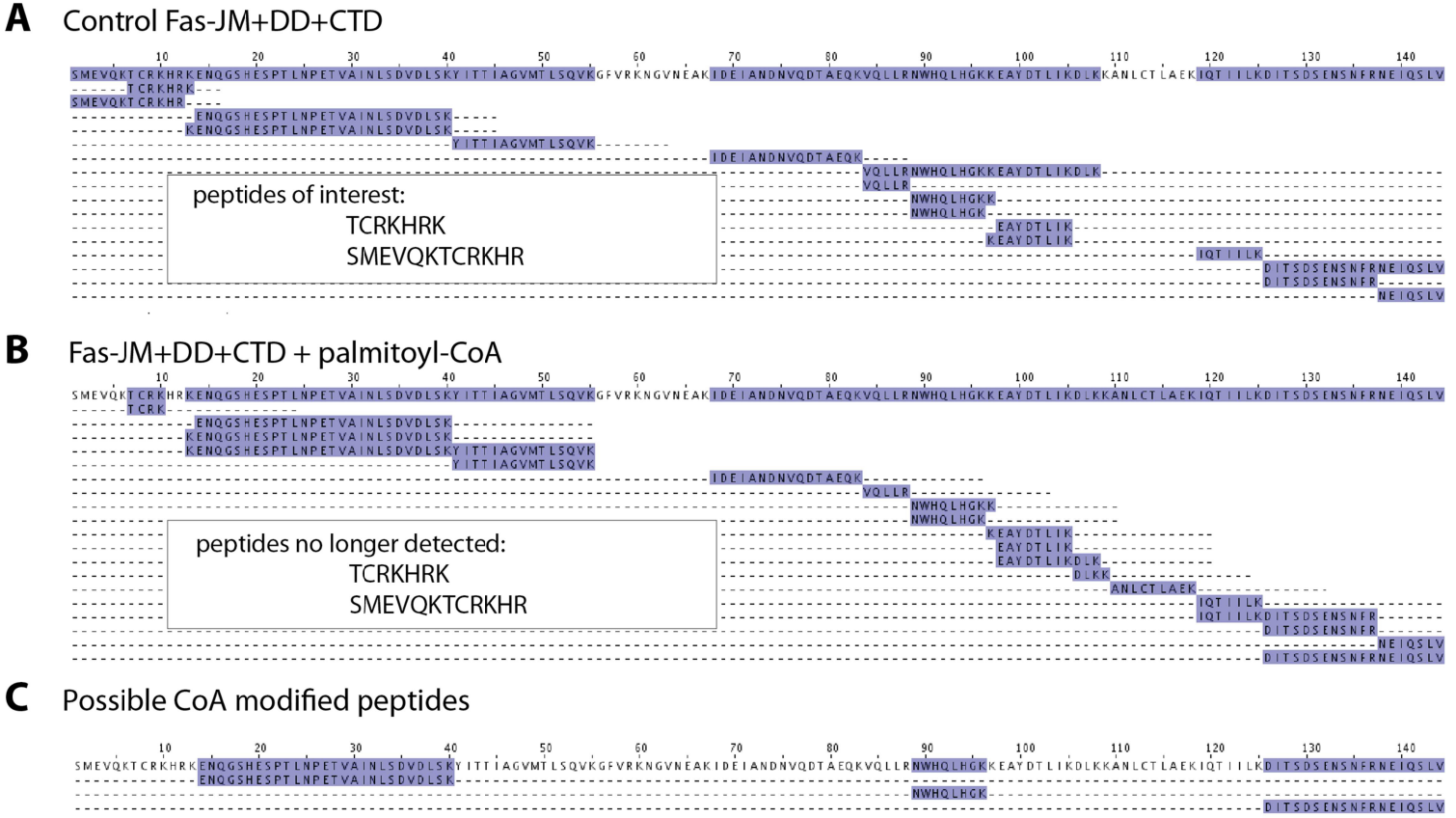

Figure 6.7 Tryptic digest of palmitoylated Fas suggests that C199 is being palmitoylated – visual representation of recovered peptide masses

A, Alignment of peptide fragments corresponding to the masses achieved following tryptic digestion of unreacted Fas-JM+DD+CTD. The highlighted peptide mass corresponds to the region of interest around cysteine 199. B, Alignment of peptide fragments corresponding to the masses achieved following tryptic digestion of Fas-JM+DD+CTD which had been incubated with palmitoyl-CoA. Peptide masses around cysteine 199 were no longer detected C, Alignment of the peptide fragments corresponding to peptide fragments detected with the mass of CoA attached.

A different peptide corresponding to the region containing Cys199 was identified: TCRK with a molecular weight of 506, suggesting that the digestion had not gone to completion; an expected result given that the mass spectrum had already shown that there are at least three species in the sample. Unfortunately, all my attempts to separate the three species using RP-HPLC had been unsuccessful (data not shown). The non-palmitoylated peptides may also be positively selected for during desalting following limited proteolysis due to the hydrophobic nature of palmitoylated peptides as described in Section 6.2.2.

To detect whether or where CoA could be reacting with Fas-JM+DD+CTD, the mass of CoA (677.5) was added to the mass of the peptide fragments observed in the control sample and the palmitoylated peptide fragments analysed for these masses. Three peptide fragments were identified as possible peptides with a CoA modification; these are illustrated in Figure 6.7C. These peptide fragments span a large proportion of the protein and do not highlight one specific location which CoA is reacting with.

In the control sample (Figure 6.7A) two regions of the protein were not detected, one of which contained the second possible palmitoylation site, Cys304. A peptide corresponding to this region was detected in the sample which had been incubated with palmitoyl-CoA (Figure 6.7B), suggesting that at least part of the protein had not been palmitoylated on Cys304.

6.2.4 Site-directed mutagenesis confirms palmitoylation occurs on Cys199

Given that the results of limited proteolysis of palmitoyl-CoA treated Fas-JM+DD+CTD were inconclusive, I turned to site directed mutagenesis to further characterise the reaction. Both Cys199 and Cys304 were mutated to serine using the method described in Section 2.4.3. The cysteine to serine mutation removes the reactive thiol of cysteine while maintaining the size and polar character of the amino acid, it is a conservative mutation that is not expected to have a significant effect on the 3D structure of the domain. A C199S/C304S double mutant was also generated to investigate whether palmitoylation could occur elsewhere in the construct. These mutants behave the same as the original construct during expression and purification, and have a very similar $^{1}H/^{15}N$-HSQC spectra. Table 6.1 shows the properties of each of the constructs.

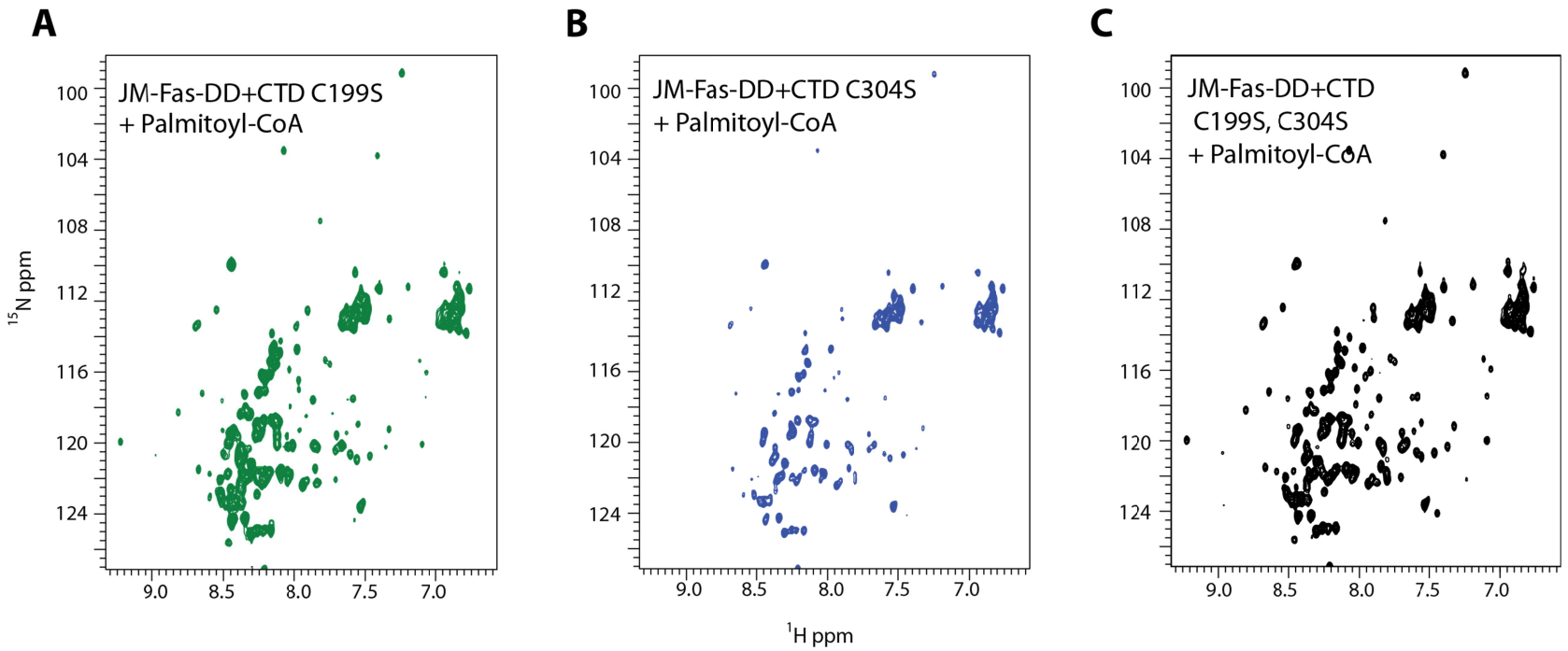

Figure 6.8 Fas C199S mutation removes the effect of Palmitoyl CoA on the NMR spectrum whereas C304S mutation does not

A, 1H/15N-HSQC spectra of 200µM 15N Fas-JM+DD+CTD C199S with 500µM palmitoyl CoA . B, 1H/15N-HSQC spectra of 200µM 15N Fas-JM+DD+CTD C304S with 500µM palmitoyl CoA. C, 1H/15N-HSQC spectra of 200µM 15N Fas-JM+DD+CTD C199S, C304S 500µM palmitoyl CoA (C). The C199S mutation removed any effect of incubation with palmitoyl-CoA upon the spectra. Spectra without palmitoyl-CoA was identical to the spectra in Figure 6.5A.

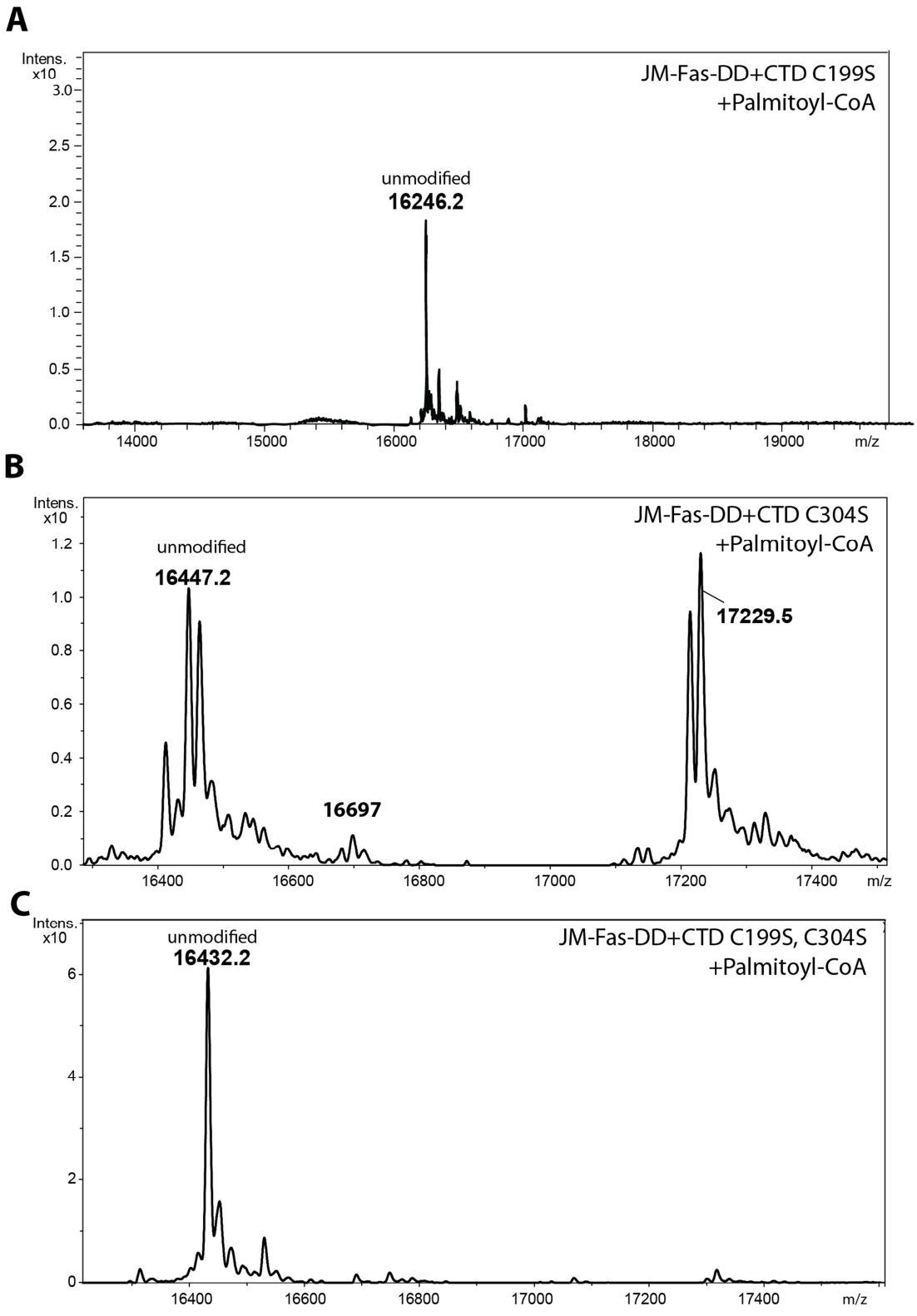

Figure 6.9 QTOF mass spectra of JM-Fas-DD+TD cysteine mutants which had been incubated with palmitoyl-CoA

Mass spectra of the samples shown in Figure 6.8. A, QTOF mass spectra of Fas-JM+DD+CTD C199S incubated with pamitoyl-CoA. B, QTOF mass spectra of Fas-JM+DD+CTD C304S incubated with pamitoyl-CoA. C, QTOF mass spectra of Fas-JM+DD+CTD C199S, C304S incubated with pamitoyl-CoA. ^{15}N Fas-JM+DD+CTD constructs shown in this spectrum yield a higher molecular weight than previously noted within this study, see Table 6.1.

Table 6.1 Properties of Fas-JM+DD+CTD mutants after cleavage with TEV protease

Construct name	Residues of Fas	Mutation	Molecular weight (Da)	^{15}N averaged molecular weight* (Da)	Extinction coefficient (M^{-1} cm^{-1})
Fas-JM+DD+CTD	194-335	K263A	16262	16464	8480
Fas-JM+DD+CTD C199S	194-335	K263A, C199S	16246	16448	8480
Fas-JM+DD+CTD C304S	194-335	K263A, C304S	16246	16448	8480
Fas-JM+DD+CTD C199S, C304S	194-335	K263A C199S, C304S	16230	16432	8480

*^{15}N averaged molecular weight calculated using the Scripps Mass calculator

Three NMR samples were made in acylation buffer, each containing 200 μM of the cysteine mutants of Fas-JM+DD+CTD and 500 μM palmitoyl-CoA at a volume of 550 μl (containing 10% $^{2}H_2O$). For each sample, a $^{1}H/^{15}N$-HSQC spectrum was recorded, shown in Figure 6.8. C199S and C199S/C304S show no effect after incubation with palmitoyl-CoA on the $^{1}H/^{15}N$-HSQC spectrum (Figure 6.8A,C). On the other hand, when incubated with palmitoyl-CoA, the $^{1}H/^{15}N$-HSQC spectrum of Fas-JM+DD+CTD C304S showed the same behaviour as the one seen for the original construct (Figure 6.5). In both cases the spectrum showed line broadening, resulting in a marked decrease in intensity of the peaks corresponding to the folded region of the protein.

Aliquots of these NMR samples were desalted and analysed by ESI-QTOF MS. The mass spectra for ^{15}N Fas-JM+DD+CTD cysteine mutants incubated with palmitoyl-CoA are shown in Figure 6.9. In agreement with the $^{1}H/^{15}N$-HSQC spectra, both samples which contained a C199S mutation showed no chemical modifications, whereas in the mass spectrum for the sample containing the C304S mutation the main product peak observed contained a peak corresponding to the mass of 17229. This mass would correspond to the addition of 780Da that, as previously mentioned, could correspond to the addition of coenzyme-A to Fas. Its occurrence in the C304S mutant, and not in the C199S mutants, may suggest this is a reaction that takes place

after the thioesterification of Cys199, when HS-Co-A is released, so it might involve the thiol group. Altogether, the effects on the $^{1}H/^{15}H$-HSQC spectra and the mass spectra for the Fas-JM+DD+CTD cysteine mutants suggest that palmitoylation is occurring at the predicted site of Cys199. However, and perhaps not surprisingly, the palmitoylated Fas is not tractable by NMR in aqueous buffers lacking detergents.

6.3 Discussion

The process of palmitoylation is crucial for a number of different pro-apoptotic pathways. Palmitoylation of Cys199 in the intracellular region of Fas is necessary for the recruitment of Fas to lipid rafts and clustering of the receptors, an event that is necessary for the initiation of the caspase cascade[266,25,50]. This chapter documents the development of a protocol to palmitoylate Fas *in vitro* suitable for biophysical characterisation and protein-protein interaction studies. *In vitro* palmitoylation takes place spontaneously by incubating the protein of interest with the activated form of palmitate, palmitoyl-CoA. Not all cysteines can be palmitoylated using this method, as the pKa of the side chain thiol needs to be acidic for the reaction to occur[254]. Comparison of known palmitoylation sites indicate that the low pKa of palmitoylated cysteines is due to the presence of several basic residues in the vicinity, and this is the case for Fas Cys199, which is close to lysines at positions 194, 201 and 204 and arginines at position 200 and 203.

On addition of palmitoyl-CoA, the $^{1}H/^{15}N$-HSQC of ^{15}N Fas-JM+DD+CTD immediately showed a dramatic change. The majority of folded peaks became significantly broader, suggesting that a much larger species had been formed. MS detected the addition of at least one palmitoyl group to Fas-JM+DD+CTD, but also the presence of a second product corresponding to the addition of CoA to Fas-JM+DD+CTD; unreacted Fas-JM+DD+CTD was also detected. The amount of palmitoylated product detected by ESI-MS probably underestimates the actual yield of the reaction. To enable MS analysis the sample was desalted using a tip with C4 hydrophobic resin fixed inside (ZipTip). For ZipTip purification, the proteins are bound to the resin in aqueous solution and then eluted with 65% acetonitrile, 0.1% acetic acid. Given the hydrophobicity of palmitoylated Fas, it seems likely that these conditions may not have been sufficient to elute palmitoylated protein from the

ZipTip; more hydrophobic solvents may improve the recovery from the C4 resin or other methods of preparation of the sample for MS would have had to be explored.

As a first approach to map the palmitoylation site I carried out a limited trypsin digestion of Fas-JM+DD+CTD incubated with and without palmitoyl-CoA. A good coverage of the whole protein sequence was achieved following digestion, proving that the palmitoyl group was not being added to Cys304. However, results were ambiguous as to whether Cys199 was being palmitoylated. Although long peptides corresponding to the region containing this cysteine were not present in the palmitoylated sample, a short peptide including Cys199 was recovered. However, this peptide could have been derived from the unreacted Fas present in the sample. In order to overcome this problem, separation of palmitoylated and non palmitoylated Fas by RP-HPLC was briefly explored using a C18 column and an acetonitrile/0.1%TFA gradient (data not shown). The addition of the palmitoyl group increases the hydrophobicity of Fas, therefore the retention time of the palmitoylated construct in reverse phase chromatography would have been longer compared to the non palmitoylated protein. Unfortunately, there was little change in the retention time between the two species of Fas resulting in poor separation. The components of the acylation buffer absorb quite strongly at 220 nm, making it difficult to identify the protein components in the chromatogram. Further optimisation of the conditions used for RP-HPLC would be necessary for any further studies, for example by changing the hydrophobicity of the stationary phase, the ion pairing agent and/or the composition of the buffers[267].

Given the ambiguity of the peptide mapping experiment, the limitations of the detection methods and the intriguing fact that there seem to be two reaction products, I decided to tackle the problem using site directed mutagenesis experiments. Three mutants were generated; two single mutants with each one of the cysteines mutated to serine and a double mutant without any cysteines. Once the thiol group is absent the *in vitro* palmitoylation reaction should not take place. When the Cys199 was mutated to Ser, either on its own or in the double mutant, no changes to Fas-JM+DD+CTD were observed by NMR or MS. Only the C304S mutant showed similar behaviour as wild type Fas-JM+DD+CTD, *i.e.* a small peak corresponding to palmitoyl Fas-JM+DD+CTD, a peak corresponding to unreacted Fas and another peak corresponding to the added mass of Fas and CoA. This result suggests that only

Cys199 is being modified and that the formation of a CoA-protein adduct is either dependent on the breakage of the thioester bond between CoA and the palmitoyl group or competing with the acylation reaction for the Cys199 thiol. The pKa of HS-CoA is ~9.6, so that the expected species in solution would be the oxidised CoA-S-S-CoA dimer, but perhaps the presence of DTT in the buffer allows for some reactivity. It would be interesting to test whether this adduct can be obtained by incubating the protein with CoA-SH in the absence of acyl groups. This result was quite surprising, as the formation of a CoA-protein by-product has not been reported during *in vitro* palmitoylation reactions. Perhaps this is because in most studies *in vitro* palmitoylation has been assayed by reacting CoA with [H^3] or [^{14}C] palmitic acid before acylation and then tracking the product by scintillation or fluorography, a possible protein-CoA adduct would not be detectable by these methods. In 1996, Huth and coworkers reported the existence of CoA-modified proteins in the mitochondria, but there has not been any follow-up to this work[268]. To my knowledge this is the first report of the detection of CoA modified proteins produced by *in vitro* palmitoylation.

The increase in hydrophobicity of palmitoylated Fas-JM+DD+CTD would offer an explanation for protein precipitation when the samples were left at room temperature overnight. The IVP assay used within this study (adapted from Bano *et al.* (1998))[136] was carried out in aqueous solution, and although this seems to be adequate for peptides, it would not be surprising that a palmitoylated protein is not able to stay in solution. Reported IVP experiments using full proteins were carried out in the presence of detergent; IVP of GPCR Gα subunits was carried out in 7.5 mM CHAPS[251], and in the case of SNAP-25 IVP was initiated in 0.005% Triton X-100[253]. However, in both of these cases the palmitoylated samples were not used for any other assay in solution, in the case of the Gα subunit the protein was precipitated and assayed by scintillation and in the case of SNAP-25 it was analysed by western blot and fluorography. Therefore it could well be that these proteins were also insoluble.

The addition of detergent before palmitoylation was briefly tested. Three detergents (CHAPS, n-dodecyl-β-D-maltoside (DDM) and sodium cholate) were screened at both 20% above and below their critical micelle concentration (CMC) to see whether this would affect the $^{1}H/^{15}N$ HSQC spectrum observed on addition of palmitoyl-CoA

to ^{15}N Fas-JM+DD+CTD. Unfortunately, the HSQC spectrum of samples with detergent did not change at all after addition of palmitoyl-CoA (data not shown) and these detergent-containing samples could not be analysed by MS because a suitable protocol for detergent removal was not in place. It is possible that the concentration of detergent was inhibiting the reaction. During the palmitoylation of SNAP-25 0.1% Triton X-100 inhibited the reaction[253], also 0.1% Triton was enough to inhibit the acylation of rhodopsin[269]. On the other hand Bano and collaborators observed an increase in the yield of palmitoylated myristoylated Yes-peptides in the presence of 0.1% Triton X-100[136]. So it is difficult to draw any conclusions based on so few experiences. Detergent conditions were not further screened as at the time there was no feasible way to analyse them. Avoiding detergent contamination in MS samples is another reason why the development of a suitable HPLC method for the separation of the reaction products is necessary.

In light of these findings, it is possible that the only feasible method of preparing palmitoylated proteins for structural studies is to avoid the use of detergents during the reaction, and to further induce the palmitoylated protein precipitation in order to facilitate its recovery, purification and analysis. Once pure, the palmitoylated protein can then be resuspended in lipid bilayers[270,271] or detergent micelles[272]. Once solubilised palmitoylated Fas can be obtained, circular dichroism and NMR spectroscopy could be used to investigate the effects of the lipid modification on the folding of the cytoplasmic region of Fas and its interaction with the lipid phase. Binding experiments with ezrin and other better characterised Fas binding partners could also be assayed with a similar methodology as used in Chapter 5.

In retrospect, owing to these additional complications that arise from working with full protein domains instead of peptides, it would have been a better starting point to first assay palmitoylation of short peptides comprising Cys199 and Cys304. Peptides allow for greater flexibility regarding reaction conditions. For example, Yousefi-Sakakdeh *et al.,* reported 80% S-palmitoylation of a 17- residue peptide after 10 minute incubation with palmitoyl chloride in 100% TFA[273], and Vogt and collaborators palmitoylated a 14-residue peptide in benzene[274], and in a subsequent paper reconstituted the lyophilised acyl-peptide in lipid bilayers for NMR studies[275].

In summary, this chapter has illustrated that palmitoylation of Cys199 can be accomplished in sufficient amounts for structural studies, but that two problems need to be overcome before putting into practice this technique; first, separation of the palmitoylated product, and second the solubility of the palmitoylated product in aqueous conditions. It is almost certainly possible to separate the palmitoylated protein from the unreacted protein and CoA modified by-product by reversed or normal phase liquid chromatography. Solubility could be achieved by purification under denaturing conditions and subsequent reconstitution in lipid bilayers or micelles.

Chapter 7

Concluding remarks and perspectives

Death domains are protein:protein recognition platforms that enable specific and controlled modes of oligomerisation (aggregation) to allow the proximity activation of enzymes such as proteases and kinases. Although structures of members of the death domain family have been solved, many in isolation and some in oligomeric form, the molecular bases of their patterns of recognition have only just begun to be understood. Of particular interest for our laboratory was to develop methods to enable the biophysical characterisation of their dynamic behaviour and of the effects of post translational modifications on structure, dynamics and binding modes. This thesis describes my efforts to tackle some of these challenges using the cytoplasmic domain of the death receptor Fas as a test case.

In retrospect, it is precisely the ability of death domains to undergo organised aggregation that made progress so difficult. By developing these biophysical techniques in a more tractable system before applying them to death domains, it would have enabled the capabilities and reliability of the techniques to be established first, and clarified the questions of whether the problems encountered were inherent to the technique or the specific protein at hand. Nevertheless, I believe I have been able to improve the characterisation of the Fas death domain in solution and lay the foundations for future progress in the understanding of phosphorylated and palmitoylated proteins through the semi-synthetic methods that I have established for their production. I conclude by presenting my observations, general conclusions and perspectives of each chapter independently.

7.1 The Fas-DD adopts a compact configuration in solution with inconclusive evidence that it can also form an open conformation in the tested conditions

The canonical death domain (DD) fold is formed by a bundle of six alpha helices arranged in a Greek key motif. The structure of the 90 residue Fas death domain was published in 1996, it was the first of the DD structures to be solved and has formed the basis of a number of Fas and FADD protein-protein interaction studies[6,121–124]. The Fas-FADD interaction is of interest due to its role in the initiation of apoptotic pathways through the formation of the death inducing signalling complex (DISC).

In 2009 a crystal structure of the Fas-FADD complex was published which contained four Fas-DD and four FADD-DD subunits. In this structure the death domain of Fas showed an open conformation exposing the hydrophobic core of the domain to form the main interaction surface with FADD. Although this has since been shown to be a non-physiological arrangement of Fas and FADD-DD[123,124], probably induced by the crystallisation conditions (0.95 M citric acid, 1.9 M ammonium sulphate, pH 4), this non-canonical form fuels the debate over the ability of the Fas-DD to form alternative structures. A more open DD conformation would help rationalise the proposed phosphorylation site (Tyr291) and the recruitment of SH2 domain containing proteins to a region which is particularly buried in the current compact Fas-DD structure. Furthermore, structures of calmodulin with peptide corresponding to the death domains of some death receptors have been published[125,276]. If proven biologically relevant, the formation of these calmodulin complexes, both with Fas and with the neurotrophin receptor death domains, would require the opening of the death domain.

The Fas-DD structure presented in this thesis was calculated using data obtained from modern multidimensional NMR pulse programs. Due to the fact what I have yet to complete the assignment of all NOE peaks present for the residues in helices five and six, I am not yet in a position to calculate the structure without any input from prior structural information. However, by priming the calculation using a small subset of NOEs derived from the compact Fas-DD structure, a structural ensemble of twenty conformers is obtained, which shows a six helical canonical death domain type structure. While it could be argued that this protocol forced the structure into the canonical death domain fold, both the secondary structure predicted from

chemical shifts and the presence of NOEs between residues expected to be close in the compact structure indicate that, in our hands, Fas-DD forms the canonical fold in solution.

Fas-DD is not the only death domain that has been reported to experience a radical conformational change. The death domain of Pelle, a protein involved in dorsal-ventral patterning in *Drosophila* development, has also been seen to undergo structural rearrangement when crystallised. By crystallography methods, the death domain alone, formed an elongated helical structure[169] whereas in complex with its binding partner Tube[168], and when isolated in solution[170] it formed the expected six helical bundle. The authors of the crystal structure of isolated Pelle discuss how the cosolvent conditions (45% 2-methyl-2,4-pentanediol, MPD) could be responsible for the induction of the structural change. This change may illustrate the susceptibility of the death domains to rearrange when present in some conditions, perhaps because the hydrophobic core is quite minimal. In addition, this behaviour might provide some evidence that the death domains can be made to change their arrangement of alpha helices in certain physiologically relevant conditions as well.

Of the death domain structures that are deposited in the Protein Data Bank, there are examples of the DD undergoing small rearrangements. This is illustrated reasonably well by the alignment of a subset of the known DD structures (Figure 3.4). In particular for Fas, the lymphoproliferation mutation V254N is well known to disrupt the binding interface between Fas and FADD which when present *in vivo* results in the accumulation of autoreactive T cells characteristic of ALPS. Analysis of NMR chemical shifts and heteronuclear NOEs highlighted that the V254N mutation results in local destabilisation with possible unfolding of Fas-DD helix 3; the cause of the loss of FADD binding[277]. The mutation did not appear to rearrange the rest of the death domain in a similar manner; it could be possible that the death domain is able to tolerate some level of local rearrangement to its structure. This could be the mechanism used to enable the reported interaction with Fas and SH2 domain containing proteins. Perhaps once full assignments have been collected for Fas-DD Y291E and Fas-DD in crystallisation buffer the chemical shift mapping will enable us to draw further conclusions from the relaxation data; much like Eberstadt and colleagues did for the Fas V254N mutation.

In attempts to encourage conformational changes and probe the effects of phosphorylation upon the death domain we collected NMR relaxation data on Fas-DD, both with a phosphomimetic mutation and in the same buffer conditions used for crystallisation of the open conformation. In the case of the phosphomimetic Y291E mutation, considerable chemical shift changes were observed in the mutant compared to the wild type death domain and I was unable to transfer my assignments from wild type to Y291E HSQC. Lacking assignments, I can only make general observations of the differences between both HSQCs. Fas-DD Y291E appears to show localised changes in dynamics around the site of the mutation. From this we can infer that a phosphorylation event may encourage a local rearrangement to enable other proteins to bind. A more in depth study would be required to study the extent and the causes of this rearrangement. Chapter four documents an expressed protein ligation approach to generate a phosphorylated Fas-DD that would enable building upon this matter.

Relaxation measurements of Fas-DD in crystal buffer were significantly hampered by the poor signal to noise ratio caused by the partial precipitation of the protein. It is not surprising that the buffer used to crystallise Fas-DD induced precipitation in solution, as that is precisely the aim of such a buffer. However, even from the low quality data obtained, some tangible observations could be made. In all relaxation experiments an increased level of exchange was observed in these conditions, compared to the one observed in the NMR buffer (20 mM MES, 100 mM NaCl, pH 6.2). This increase could indicate that Fas-DD was opening, oligomerising, or affected by the viscosity of the solution, or a combination of these three possibilities. However, it is clear that the shape of the molecule is not particularly perturbed, as assignments could be transferred from those obtained in NMR buffer along the whole length of the construct.

It is possible that the Fas-DD does not undergo rearrangement unless in the presence of a specific binding partner. There are two schools of thought regarding the mechanisms and structural changes that can occur upon protein or ligand binding to its interaction partner: induced to fit and conformational selection. Proteins exist in more than one conformation in solution and conformational selection type binding occurs when a ligand binds to a sparsely populated/minor species of the protein, immediately forming the structure of the protein:ligand complex. In an induced fit

mechanism of binding a ligand binds to a protein, forming a weak intermediate complex that induces a conformational change to the whole protein[278]. However binding events may not be so straightforward, with more recent analysis suggesting an extended conformational selection model which encompasses selection and adjustment of protein structures in sites distinct from the binding site. For example an interaction may result in allosteric propagation throughout the molecule. Models of protein interactions increase in complexity when more than two binding partners are involved resulting in a large number of conditional steps that can affect the processing of the interaction[279]. It is possible that the open Fas conformation could form through the conformational selection process, in which only a small population of the death domain is in an alternative conformation at any given time. It is possible that the conditions used in the experiments presented in this thesis were not suitable for the detection of such minor alternative conformation of the Fas-DD. The addition of a binding partner could therefore be the trigger to cause global opening of the death domain.

Studies of the transient structures of proteins that exist prior to ligand binding are inherently difficult due to their low population and the fluctuations of such species. Transient protein conformations can be characterised using paramagnetic relaxation enhancement experiments (PRE), in which a paramagnetic spin label is incorporated onto an engineered or native cysteine and the relaxation rate is collected between the label and nuclei of interest. By NOE measurements only effects occurring within 6 Å can be observed, while PRE experiments, due to the fact that an unpaired electron has a very large magnetic moment, changes within 25-35 Å of the paramagnetic group can be observed. Because the increase in relaxation rate is strong but decays rapidly as the distance increases, in a case where there is a very low populated conformation in which a nucleus is closer to the paramagnetic group than in the main species, the presence of the rare conformation can be detected via the unusually fast relaxation of the nucleus[278]. PRE analysis of Fas-DD could be a good method to detect the possible existence of open conformations in solution that may provide more conclusive evidence about the plasticity of the domain.

7.2 Auxiliary mediated EPL is a viable platform for the preparation of phosphorylated death domains by semi-synthesis

Production of post translational modified proteins in bacterial expression systems in sufficient quantity for structural and functional studies is not a straightforward process. Protein post translational modifications are not genetically encoded but arise from sequence or structural motifs present in the protein itself. Bacterial expression systems such as *E. coli* often do not possess the necessary machinery to perform the desired modifications to an exogenous protein. To overcome these limitations, post translational modifications are usually performed in vitro during or after protein purification. In the specific case of phosphorylation, phosphorylated proteins are often prepared by the incubation of the purified protein with a suitable kinase and ATP. It not uncommon to find that the substrate recognition is highly specific, so that phosphorylation requires the use of a kinase that might not be commercially available, requiring additional cloning, expression and purification. Moreover, the *in vitro* phosphorylation reaction often results in low yields o product and it is difficult to control the specific site of phosphorylation without introducing mutations[280].

Expressed protein ligation (EPL) enables the production of phosphorylated proteins by semi synthesis. EPL produces a chemically defined protein construct which can contain a phosphate group on the amino acid residue of interest. This methodology has been successfully used to generate a number of phosphorylated proteins *in vitro*. For example, the molecular mechanism of Smad2 activation by type I transforming growth factor β receptor (TGFβR) was probed using a tetraphosphorylated EPL generated TGFβR construct[281,282]. The same research group also generated a phosphorylated Smad2 showing that upon phosphorylation the transcription factor induces the formation of a stable trimer[283]. In an unrelated study, the use of EPL to generate a phosphorylated fork head associated (FHA) domain of check point kinase 2 (Chk2) was used to illustrate that phosphorylation stabilises the FHA domain interactions *in vitro*[284].

Although EPL is a well-established technique proved to be amenable to the production of phosphorylated proteins for biophysical studies, it has one main limitation: the fragment at the C-terminus of the ligation junction needs to start with a cysteine. Cysteine is the second lowest abundant amino acid in cytoplasmic

proteins, it is unlikely that, if a cysteine is present, it will be in a convenient location in the polypeptide chain to constitute a suitable ligation junction. It is common for researchers to either mutate an amino acid to or insert a cysteine into the protein of interest to overcome this limitation, for example, to enable EPL using Chk2, Ser73 was mutated to Cys[284]. Insertion of a cysteine is not always feasible or could have knock on effects on the properties of the protein under investigation, and this is why the development of Nα-auxiliary technologies is a promising area of research. An Nα-auxiliary is a molecule able to mimic the function of the cysteine thiol, but after ligation can be removed by an acid treatment step, leaving no trace in the final protein construct[127]. The Nα-auxiliary tested in this study, Htmb, has been developed by the laboratory of Dr John Offer at the NIMR and is currently under investigation for performance and yield in different systems. The Offer group was particularly interested in assessing the performance of Htmb in systems of biological relevance, as their focus is traditional peptide chemistry ligation strategies.

My aim was to develop a protocol to semi-synthesise phosphorylated death domain constructs in order to probe the structural and functional effect of the presence of a phosphate group on the death domain of Fas. The Htmb-mediated expressed protein ligation approach was used to successfully generate a 55kDa MBP-tagged phosphorylated Fas-DD, but the methodology will requires substantial optimisation to enable the reaction to be performed on a preparative scale. The main problem observed during synthesis was the ongoing occurrence of N-terminal thioester hydrolysis and protein precipitation, both of which hampered the yield of ligated protein which was generated. Li and co-authors observed some thioester hydrolysis in the production of a phosphorylated semi synthesised Chk2, but not to an extent which impaired the ligation reaction itself such as we observed[284]. To overcome thioester hydrolysis, the influence of several parameters needs to be assessed. Reports show that native chemical ligation reaction (EPL between two peptides) can greatly be improved by performing the experiment in a solvent environment. In the case of our Fas-DD ELP this strategy was tested with little success, but the effect of base additives for catalysis in these conditions has not been tested. Protein precipitation has also been observed in the EPL reaction used to make a tetraphosphorylated TGFβR, which upon optimisation was overcome by the use of 1,6 hexanediol[281], solvent conditions may also aid to improve this difficulty. Another

important parameter that could have a great effect on hydrolysis is the use of thioesters different than benzyl mercaptan.

Unfortunately, given that Htmb has not been tested in a variety of systems, at this stage it is not possible to conclude if the problems encountered could be attributed to the auxiliary, or were an effect of the specific peptide sequence in the vicinity of the ligation junction or of the aggregation tendencies of the DDs. These effects will have to be studied independently to assess their importance. In order to test the limitations of the auxiliary, it would prove valuable to attempt a traditional EPL reaction by inserting a cysteine at the C-terminus of the junction. The effect of the residues at the ligation junction has been briefly explored by mutating the histidine at the N-terminus of the junction to glycine. The use of glycine as the preceding amino acid to the thioester is a popular choice throughout both NCL and EPL as it reduces the steric bulk which can interfere with the thioester exchange[193,194]. Indeed, the ligation yields of this mutant were better than in the wild type, however, the introduction of unnecessary mutations could have a great effect in the behaviour of the domain, and this is not a solution that we are keen to pursue. Another more suitable solution would be to explore other sites within the polypeptide chain that would perform better as ligation junctions. Whether the poor yields are due to the general behaviour of death domains could be assessed by attempting ligation of other death domain superfamily members, for example, the death domain of PIDD, which has been extensively characterised in our lab, has been reported to be Threonine phosphorylated[285].

EPL technologies have roots in native chemical ligation (NCL) of peptides to generate larger proteins than are unable to be synthesised using solid phase peptide synthesis alone. Protein based systems are more challenging to work with than peptides due to the increased size, steric hindrance, greater conformational variability and limitations on solubility observed in the larger molecules. For peptides, these problems are traditionally overcome by keeping peptides in a denaturing acidic environment, conditions that might not be suitable for a protein based system. However, EPL is not inherently unsuitable for large proteins, dimers of Hsp90 (heat shock protein 90) of approximately 80kDa, have been made by EPL[286]. Although the size of this construct is an attribute of having both the N and C

termini purified from bacteria, it shows that in principle the thioester exchange reaction mechanisms should not be limited by protein size.

The semi-synthesis of a protein is a laborious process that involves many steps. As with any multi-step protocol, the accumulating loss of material at each purification step results in low yields of ligation product[287]. To compound this challenge, millimolar concentrations of reactants are required to obtain suitable ligation yields[191]. For this multi-step process to be worthwhile for the production of a phosphorylated Fas-DD at a preparative scale, better yields at each step and/or fewer purification steps are necessary. It is not unreasonable to expect yields of several milligrams for ligated Fas-DD. The semi synthesised phosphorylated Chk2 and Smad2 proteins were generated at high enough yields to carry out analytical ultraentrifugation, surface plasmon resonance and size exclusion chromatography with multiangle laser light scattering analysis[283,284]. In the case of the semi-synthesis of TGFβ required much optimisation to reduce a side reaction and the non-specific aggregation observed when the ligation was initially carried out[282]. But following optimisation the authors reported a 16% yield of ligated product in the milligram quantities, enough to enable the implementation of kinase activity assays[281]. Expression levels of the Nt-Fas-DD intein conjugate were adequate, however purification from the chitin column was inefficient due to protein aggregation. The purification of Nt-Fas-DD was greatly improved by the presence of the MBP-solubility tag, but the introduction of the His to Gly mutation greatly reduced the yield of cleaved protein. The scaling up of Ct-pY-Fas-DD synthesis would also require optimisation, current yields are in the order of 5 mg on a 0.1 mmol scale reaction. With further handling practice and synthesis at a larger scale it should be possible to prepare the peptide in greater amounts. The ligation itself would require some optimisation primarily to avoid hydrolysis, but also to develop a suitable method for the efficient separation of the ligation product from the N-terminal fragment. There is no reason to believe that by implementing some of these changes pY-Fas-DD could not be produced in the hundreds of micromolar quantities required for assays such as circular dichroism and binding assays such as BLI.

7.3 The reported Fas ezrin interaction is unlikely to be direct or does not occur in the juxtamembrane region or the DD of Fas

It cannot be disputed that Fas and ezrin interact, as it has been observed independently by several groups using colocalisation or coprecipitation experiments[50,113–115]. Unfortunately, throughout the work carried out for this thesis, we have been unable to detect a direct Fas and ezrin interaction *in vitro* using purified recombinant proteins. In light of these results, either this interaction may not be direct, or it does not occur at the juxtamembrane region of Fas as suggested by Ruan and collaborators[118], or through the death domain.

Most previously reported co-immunoprecipitation and colocalisation experiments were carried out using mammalian cell extracts. Unlike the recombinant proteins used in our *in vitro* assays, the use of mammalian cell extracts allows for proteins being post translationally modified and/or for the presence of additional proteins from the ones being detected. All previous reports used antibody-based detection methods to analyse Western blots and/or co-immunoprecipitation experiments. These methods are targeted for the detection of what the researchers wish to observe, leaving them unaware of any other constituents that may have been present in their samples. It is conceivable that the interaction between Fas and ezrin could not have been reproduced *in vitro* because it is mediated by another protein, or because it requires a change in configuration as a result of a posttranslational modification.

The recombinant Fas and ezrin constructs in this study focused around the ezrin FERM domain and the Fas death domain with a proportion of the juxtamembrane region. Another possibility is that one or both of these constructs did not contain the region of interaction. Kuo *and coworkers.*[116] reported a direct interaction by pulling down recombinant full-length His-tagged ezrin with a recombinant GST-tagged Fas construct containing the transmembrane region and cytoplasmic domain (residues 185-328), and used anti-His and anti-GST antibodies for detection. Perhaps using these much longer constructs would have been sufficient to detect binding. However this reasoning does not fully justify why in our hands no direct interaction was detected, as Lozupone and coworkers[117] reported a successful pull down of cytoplasmic Fas construct (residues 191-335, three residues longer than the Fas-JM+DD+CTD (194-335) used in this study) by short truncations of GST-tagged

ezrin and using an anti-Fas antibody for detection. It is feasible that these three residues are necessary for binding. Another, more interesting, possibility is that, by using short truncations of the FERM domain, surfaces that are not exposed in the full length FERM are available for binding.

Crucially, neither Kuo nor Luzopone and collaborators included a negative control showing that ezrin is not associating with the bead matrix, and the possibility exists that they are only observing an artefact. In our hands, ezrin binding in a not specific manner was a substantial problem when using a number of matrixes and proteins. If is very unfortunate that a significant proportion of the literature regarding the direct interaction between Fas and ezrin has been published from the same research group, as it is possible that others have attempted to recreate these results and have stumbled across similar issues to those we encountered.

FERM domains are known to either directly interact with membrane proteins or indirectly interact via adaptor proteins of the NHERF family. NHERF (Na^+/H^+ exchanger regulatory factor) 1 and 2 (also known as ERM binding phosphoprotein 50 (EBP50) and E3KARP (NHE3 kinase A regulatory protein)) have been identified as a linker between the cytoplasmic tail of transmembrane proteins and the FERM domain of ERM proteins[288,107]. NHERFs are composed of a a C-terminal ERM binding domain, which has been shown to bind the F3 lobe of ezrin[289] and two PDZ domains, a protein:protein interaction fold that recognises short regions at the C-terminus of its targets. Upon scaffold protein binding, the FERM domain reduces its affinity for known direct membrane protein interactions which is suggested as a role for scaffold proteins in the regulation of the formation of ERM related signalling complexes[111]. Diverse transmembrane proteins such as the β2 adrenergic receptor[108], cystic fibrosis transmembrane conductance regulator (CFTR)[290], platelet derived growth factor receptor (PDGFR)[291] and EGFR[292] associate by EBP50 in this manner. Fas associated phosphatase-1 (FAP-1) is a PDZ domain containing enzyme that has been identified to bind to the C-terminal tail of Fas[293]. The PDZ domain of FAP-1 shows 49% similarity to the N-terminal PDZ domain of EBP50 and 45% similarity to its C-terminal PDZ domain, therefore it would not be surprising that EBP50 can also bind to the C-terminus of Fas. This mechanism of interaction would account for our inability to confidently observe a direct Fas and ezrin interaction *in vitro*.

Fas is not the only death receptor that has been shown to require a link to the actin cytoskeleton for DISC progression to apoptosis. A recent study has reported that the apoptotic pathways of the death receptors DR4 and DR5 can be regulated by an E-cadherin mediated link to the actin cytoskeleton. E-cadherin is known to be involved in the formation of adherens junctions, promoting cell adhesion and providing a link to cytoskeleton dynamics via the formation of a cadherin-catenin complex with β and α-catenin binding to actin. The authors report that, upon receptor ligation, E-cadherin links DR4/DR5 to the actin cytoskeleton, facilitating receptor clustering and efficient DISC formation. This effect was not observed on Fas receptor activation[294]. Parallels can be drawn between effects on a cytoskeletal link during DR4/DR5 activation and the DISC forming events involving Fas and ezrin. This new study shows that death receptors other than Fas require an association to the cytoskeleton to initiate apoptosis and that this link is not a direct link.

Ezrin is not the only protein with has been reported to mediate a linkage between Fas and the cytoskeleton. Del Rio and coworkers[295] observed that the death domain of ANKG190, a kidney ankyrin, interacts with the Fas death domain. Akyrins are a conserved family of proteins, known to link integral membrane proteins to the actin cytoskeleton. They are modular in structure, containing a number of ankyrin repeats, a spectrin domain and a C terminal death domain. In the renal cell line MDCK, ANKG190 overexpression resulted in an increase in cells undergoing apoptosis. A mutation in ANKG190, R1496 (similar to the FADD R234 mutation on the Fas binding surface) resulted in loss of the interaction[295]. This study illustrates an alternative mechanism of Fas linkage to the actin cytoskeleton that does not involve ezrin but exploits a death domain mediated interaction to reach the same ends. Like many other apoptotic related observations this is perhaps a cell type specific interaction and therefore may not be generally applied to the Fas apoptotic system. However it is an illustration that DISC formation can be flexible with the possibility of a variety of adaptor proteins being involved in the internalisation of the DISC.

7.4 *In vitro* palmitoylation of full length proteins proved more challenging than expected, but raises interesting possibilities

Much like the addition of a phosphate group to a protein, protein lipid modifications are not genetically encoded or easily obtainable through the use of bacterial expression systems. Unlike the phosphorylation of proteins, *in vitro* study of protein lipid modifications, particularly palmitoylation are highly underrepresented throughout the literature. The confirmation of the identity of palmitoyl transferase enzymes is a relatively recent discovery[242], the specificity and the transmembrane form[49] of these enzymes makes the use of enzymes to palmitoylate a protein *in vitro* almost impossible.

We hypothesised that one of the possible scenarios for an undetectable Fas and ezrin interaction *in vitro* was that our recombinant expressed Fas constructs were not palmitoylated. Fas palmitoylation upon Cys 199 is reported to redistribute and partition Fas into lipid raft regions of the cell membrane prior to receptor internalisation. Feig and colleagues reported that prior to Fas internalisation ezrin was recruited to Fas in a palmitoylation dependent manner, therefore we embarked on a method to try and recreate this process *in vitro*[30].

In vitro palmitoylation or autoacylation exploits the local sequence environment surrounding a cysteine to enable transfer of the lipid group from palmitoyl CoA (an activated fatty acid form) to the cysteine of interest[254]. It is a method which was favoured to study the mechanism of palmitoylation using primarily peptide targets prior to the discovery of the palmitoyl transferase enzymes. Our aim was to transfer this technique to a whole protein target which could be scaled up and used for structural and biophysical characterisation and interaction studies. Palmitoylation of Fas-DD at Cys 199 was indeed achieved using this *in vitro* palmitoylation technology. However, we also observed a side reaction with coenzyme A and significant precipitation of the presumably palmitoylated protein.

Many of the reported autoacylation studies of both peptides and recombinant proteins did not go onto use the palmitoylated target for anything other than identification of the palmitoylated target. Peptide targets were assayed using scintillation counting and HPLC based assays to confirm the incorporation of radiolabelled palmitate[252,254]. In the case of the G protein alpha subunit and SNAP-

25, the proteins were assayed for palmitoylation by precipitation in trichloroacetic acid or chloroform/methanol and assayed by western blot and scintillation counting[251,253]. At the time of their publication, these studies were focused upon characterising the mechanism of palmitoylation rather than in developing a preparative method, and no observations were made on the effects on the solubility of the proteins or other effects of the modification. This is why, perhaps, we were so naïve when we decided to follow their steps.

Although limited, there are examples of proteins that have been *in vitro* palmitoylated on a preparative scale and used for some other purpose. These experiences might prove more valuable in order to put our results in perspective. Robert and colleagues demonstrated that palmitoylation of proteins could be a method of enabling proteins to cross the blood brain barrier (BBB) by preparing *in vitro* N-palmitoylated RNase A and testing it in a BBB mimicking system [296,297]. Along similar lines, a palmitoylated gramicidin (a membrane channel-forming polypeptide) has been investigated using solution NMR spectroscopy to observe the effect of acylation on the position of specific side chain residues in a lipid bilayer[274,275]. Notable from these studies is that they both use a non-aqueous environment to palmitoylate and throughout analysis of the palmitoylated protein. Palmitoylated RNase A was prepared within reverse micelles, (small aqueous droplets in an apolar medium) followed by protein precipitation and resuspension prior to the assay[296]. In the case of gramicidin, the peptide was palmitoylated in a solvent environment containing free fatty acid, benzene, PPY (4, pyrolidinopyridine) and DDC (N,N,dicyclohexylcarbodiimide), precipitated, purified[274] and resuspended in SDS micelles or DPMC detergent bilayers for NMR experiments[275]. These examples highlight the requirement for a hydrophobic environment to be present to make lipidated proteins tractable for biophysical study. However in the autoacylation reaction used in this thesis, detergents were shown to inhibit the lipid transfer[253].

Ultimately, it would be interesting to see what palmitoylation would do to the structure and the interactions of intracellular Fas. A search of the Protein Data Bank for protein structures which contain a covalent palmitic acid modification showed that there is an abundance of structures of acyl binding proteins, acyltransferases and thioesterases in complex with palmitic acid, but there seem to be few structures that contained the fatty acid covalently linked to a protein chain. Acyl binding protein

and acyl transferase structures are of less interest in this analysis as these proteins tend to contain a hydrophobic binding cleft, that isolates the lipid from the aqueous environment. For example, the crystal structure of an atypical acetyltransferase domain from mycobacterial polyketide synthase Pks13 was solved showing palmitic acid present. This orientation was achieved by cocrystallision or crystals soaking with palmitoyl CoA to get the resulting complex[298]. This could illustrate a much easier structural methodology than a reaction such as the one we were attempting to optimise if our protein had such mode of binding to the fatty acid.

Of the structures deposited in the PDB which contained covalently linked palmitate, lipidation was either synthetic or unexpected. The structure of a lipidated thirty amino acid glucan analogue has been reported using solution NMR and characterised by circular dichroism, to investigate lipidation of peptides which could be used to stimulate weight loss[299]. Whereas another group reported the crystal structure of EVF, a Virulence Factor Produced by the *Drosophila* Pathogen *Erwinia carotovora* observing S-palmitoylation which was unexpectedly added to the protein during its expression in *E. coli*[300]. These examples highlight that structural studies containing covalently linked S-palmitoylation appear to be rarely approached in a way in which palmitoyl groups are added to a recombinant expressed protein that may further highlight the difficulties observed throughout chapter six.

Another approach that could be utilised to palmitoylate Fas would be the generation of a palmitoylated protein by expressed protein ligation. The lipidation of the GTP binding protein Ras has been studied in an S-palmitoylated and farnesylated form in which the lipidated C terminus of the protein was synthesised as a short lipidated peptide and ligated to the expressed N-terminus. The resulting construct was used in biophysical assays in which it was inserted into artificial lipid bilayers and assayed using surface plasmon resonance or utilised in cell based assays[301]. A similar technique was used to solve the structure of a prenylated Ras protein[302], illustrating that this is a possible technique to generate lipidated proteins at yields which are suitable for biophysical analysis

In light of these observations and the challenges of working with palmitoylated proteins, to progress with the palmitoylation of Fas *in vitro*, *in vitro* palmitoylation could be carried out using a Fas construct with solubility fusion proteins N and C-

termini, perhaps this could encourage the protein to remain in solution following palmitoylation. Also, as discussed at the end of chapter six, a feasible strategy would be to perform the reaction in aqueous buffer, induce precipitation, purify and finally encourage the protein to solubilise in the presence of a membrane mimicking environment such as lipid bilayers[270,271] or detergent micelles[272].

One of the grander aims of our laboratory is to work towards the full reconstitution of the Fas DISC in a membrane mimicking environment. Organisation of a membrane-confined DISC would constrain oligomerisation in an arrangement more similar to the one found *in vivo*. This extra level of constraint would possibly affect the structure of the DISC and shed light into some of the many mysteries that still puzzle the apoptosis community. In recent times the use of highly deuterated phospholipid bilayer nanodiscs has been presented as a promising tool for studying membrane proteins by solution NMR. A nanodisc is a small patch of phospholipid bilayer of defined size, held in place with apolipoprotein-1, into which membrane proteins of interest can be inserted. The use of nanodiscs avoids the associated problems of using detergents to mimic a membrane environment as detergents are well known to disrupt protein folding and protein interactions, making a detergent environment far from optimal for the study of protein complexes[303]. Nanodiscs would be an attractive system to study the effects of Fas palmitoylation on DISC formation, and I hope my work will be the first step towards such a fascinating achievement.

7.5 Final summary

In summary, this thesis demonstrates the implementation of a variety of structural and biophysical techniques, exploring aspects of the 3D-structure, dynamics, chemical modification and possible interactions of the cytoplasmic region of the death receptor Fas.This work has paved the way for the routine production of *E. coli*-expressed death domains with modifications incorporating the use of chemical biology methodologies. This approach constitutes an exciting development towards the in-depth biophysical study of the effect of post-translational modifications. Milligram amounts of post-translationally modified death domains would facilitate the understanding of new aspects in the behaviour of this intriguing protein family and its ability to initiate the dissimilar signalling events of cell survival and apoptosis

References

1. Igney, F. H. & Krammer, P. H. Death and anti-death: tumour resistance to apoptosis. *Nat. Rev. Cancer* **2,** 277–288 (2002).

2. Aggarwal, B. Signalling pathways of the TNF Superfamily: a double-edged sword. *Nat. Rev. Immunol.* **3,** 745–756

3. Elmore, S. Apoptosis: A review of Programmed Cell Death. *Toxicol. Pathol.* **35,** 495–516 (2007).

4. Kersse, K., Verspurten, J., Berghe, T. Vanden & Vandenabeele, P. The death-fold superfamily of homotypic interaction motifs. *Trends Biochem. Sci.* **36,** 541–552 (2011).

5. Park, H. H., Lo, Y., Lin, S.-C., Wang, L., Yang, J. K. & Wu, H. The Death Domain Superfamily in Intracellular Signaling of Apoptosis and Inflammation. *Annu. Rev. Immunol.* **25,** 561–586 (2007).

6. Huang, B., Eberstadt, M., Olejniczak, E. T., Meadows, R. P. & Fesik, S. W. NMR structure and mutagenesis of the Fas (APO-1/CD95) death domain. *Nature* **384,** 638–41

7. Eberstadt, M., Huang, B., Chen, Z., Measdows, Robert, P., Ng, S.-Ch., Zheng, L., Lenardo, M. J. & Fesik, S. W. NMR structure and the mutagenesis of the FADD (Mort1) death-effector domain. *Nature* **392,** 941–945 (1998).

8. Weber, C. H. & Vincenz, C. The death domain superfamily: a tale of two interfaces? *Trends Biochem. Sci.* **26,** 475–481 (2001).

9. Garvey, T. L., Bertin, J., Siegel, R. M., Wang, G., Lenardo, M. J. & Cohen, J. I. Binding of FADD and Caspase-8 to Molluscum Contagiosum Virus MC159 v-FLIP Is Not Sufficient for Its Antiapoptotic Function. *J. Virol.* **697,** 697–706 (2002).

10. Dickens, L. S., Boyd, R. S., Jukes-Jones, R., Hughes, M. a, Robinson, G. L., Fairall, L., Schwabe, J. W. R., Cain, K. & Macfarlane, M. A death effector domain chain DISC model reveals a crucial role for caspase-8 chain assembly in mediating apoptotic cell death. *Mol. Cell* **47,** 291–305 (2012).

11. Siegel, R. M., Martin, D. A., Zheng, L., Ng, S. Y., Bertin, J., Cohen, J. & Lenardo, M. J. Death-effector Filaments: Novel Cytoplasmic Structures that Recruit Caspases and Trigger Apoptosis. *J. Cell Biol.* **141,** 1243–1253 (1998).

12. Chou, J. J., Matsuo, H., Duan, H. & Wagner, G. Solution Structure of the RAIDD CARD and Model for CARD / CARD Interaction in Caspase-2 and Caspase-9 Recruitment. *Cell* **94,** 171–180 (1998).

13. Zhou, P., Chou, J., Sanchez Olea, R., Yuan, J. & Wagner, G. Solution structure of Apaf-1 CARD and its interaction with caspase-9 CARD : A structural basis for specific adaptor ¯caspase interaction. *Proc. Natl. Acad. Sci.* **96,** 11265–11270 (1999).

14. Kersse, K., Lamkanfi, M., Bertrand, M. J. M., Berghe, T. Vanden & Vandenabeele, P. Interaction Patches of Procaspase-1 Caspase Recruitment Domains (CARDs) Are Differently Involved in Procaspase-1 Activation and Receptor-interacting Protein 2 (RIP2) -dependent Nuclear Factor kB Signaling. *J. Biol. Chem.* **286,** 35874–35882 (2011).

15. Qi, S., Pang, Y., Hu, Q., Liu, Q., Li, H., Zhou, Y., He, T., Liang, Q., Liu, Y., Yuan, X., Luo, G., Li, H., Wang, J., Yan, N. & Shi, Y. Crystal Structure of the Caenorhabditis elegans Apoptosome Reveals an Octameric Assembly of CED-4. *Cell* **141,** 446–457 (2010).

16. Bertin, J. & DiStefano, P. The PYRIN domain : a novel motif found in apoptosis and inflammation proteins. *Cell Death Differ.* **7,** 1273–1274 (2000).

17. Hiller, S., Kohl, A., Fiorito, F., Herrmann, T., Wider, G., Tschopp, J., Grutter, M. G. & Wuthrich, K. NMR Structure of the Apoptosis- and Inflammation-Related NALP1 Pyrin Domain. *Structure* **11,** 1199–1205 (2003).

18. Liepinsh, E., Barbals, R., Dahl, E., Sharipo, A., Staub, E. & Otting, G. The Death-domain Fold of the ASC PYRIN Domain, Presenting a Basis for PYRIN/PYRIN Recognition. *J. Mol. Biol.* **332,** 1155–1163 (2003).

19. Park, H. H. PYRIN domains and their interactions in the apoptosis and inflammation signaling pathway. *Apoptosis* **17,** 1247–1257 (2012).

20. Siegel, R. M., Frederiksen, J. K., Zacharias, D. A., Chan, F. K., Johnson, M., Lynch, D., Tsien, R. Y. & Lenardo, M. J. Fas Preassociation Required for Apoptosis Signaling and Dominant Inhibition by Pathogenic Mutations. *Science* . **288,** 2354–2357 (2000).

21. Ferguson, T. A. & Griffith, T. S. A vision of cell death : Fas ligand and immune privilege 10 years later. *Immunol. Rev.* **213,** 228–238 (2006).

22. Tanaka, M., Itali, T., Adachi, M. & Nagata, S. Downregulation of Fas ligand by shedding. *Nat. Med.* **4,** 31–36 (1998).

23. Holler, N., Tardivel, A., Kovacsovics-Bankowski, M., Hertig, S., Gaide, O., Tinel, A., Deperthes, D., Calderara, S., Schulthess, T., Engel, J., Schneider, P. & Tschopp, J. Two Adjacent Trimeric Fas Ligands Are Required for Fas Signaling and Formation of a Death-Inducing Signaling Complex Two Adjacent Trimeric Fas Ligands Are Required for Fas Signaling and Formation of a Death-Inducing Signaling Complex. *Mol. Cell. Biol.* **23,** 1428–1440 (2003).

24. Trauth, B., Klas, C., Peters, A., Matzku, S., Moller, P., Falk, W., Debatin, K. & Krammer, P. Monoclonal antobody-mediated tumor regression by induction of apoptosis. *Science* . **245,** 301–305 (1989).

25. Chakrabandhu, K., Hérincs, Z., Huault, S., Dost, B., Peng, L., Conchonaud, F., Marguet, D., He, H. & Hueber, A. Palmitoylation is required for efficient Fas cell death signaling. *EMBO J.* **26,** 209–20 (2007).

26. Lee, K., Feig, C., Tchikov, V., Schickel, R., Hallas, C., Schütze, S., Peter, M. E., Chan, A. C. & Schutze, S. The role of receptor internalization in CD95 signaling. *EMBO J.* **25,** 1009–1023 (2006).

27. Carrington, P. E., Sandu, C., Wei, Y., Hill, J. M., Morisawa, G., Huang, T., Gavathiotis, E., Wei, Y. & Werner, M. H. The Structure of FADD and Its Mode of Interaction with Procaspase-8. *Mol. Cell* **22,** 599–610 (2006).

28. Sandu, C., Morisawa, G., Wegorzewska, I. & Huang, T. FADD self-association is required for stable interaction with an activated death receptor. *Cell Death Differ.* **13,** 2052–2061 (2006).

29. Hughes, M. A., Harper, N., Butterworth, M., Cain, K., Cohen, G. M. & MacFarlane, M. Reconstitution of the death-inducing signaling complex reveals a substrate switch that determines CD95-mediated death or survival. *Mol. Cell* **35,** 265–79 (2009).

30. Feig, C., Tchikov, V., Schütze, S. & Peter, M. E. Palmitoylation of CD95 facilitates formation of SDS-stable receptor aggregates that initiate apoptosis signaling. *EMBO J.* **26,** 221–31 (2007).

31. Peter, M. E. & Krammert, P. H. Mechanisms of CD95 (APO-1 / Fas) - mediated apoptosis. *Apoptosis* **95,** 545–551 (1998).

32. Krammer, P. H., Arnold, R. & Lavrik, I. N. Life and death in peripheral T cells. *Nat. Rev. Immunol.* **7,** 532–42 (2007).

33. Neumann, L., Pforr, C., Beaudouin, J., Pappa, A., Fricker, N., Krammer, P. H., Lavrik, I. N. & Eils, R. Dynamics within the CD95 death-inducing signaling complex decide life and death of cells. *Mol. Syst. Biol.* **6,** 1–17 (2010).

34. Schleich, K., Warnken, U., Fricker, N., Oztürk, S., Richter, P., Kammerer, K., Schnölzer, M., Krammer, P. H. & Lavrik, I. N. Stoichiometry of the CD95 death-inducing signaling complex: experimental and modeling evidence for a death effector domain chain model. *Mol. Cell* **47,** 306–19 (2012).

35. Strasser, A., Harris, A. W., Huang, D. C. S., Krammer, P. H. & Cory, S. Bcl-2 and Fas / APO-1 regulate distinct pathways to lymphocyte apoptosis. *EMBO J.* **14,** 6136–6147 (1995).

36. Lacronique, V., Mignon, A., Fabre, M., Viollet, B., Rouquet, N., Moline, T., Porteu, A., Henrion, Al., Bouscary, D., Varlet, P., Joulin, V. & Kahn, A. Bcl-2 protects from lethal hepatic apoptosis induced by an anti-Fas antibody in mice. *Nature* **2,** 80–86 (1996).

37. Barnhart, B. C., Alappat, E. C. & Peter, M. E. The CD95 Type I / Type II model. *Semin. Immunol.* **15,** 185–193 (2003).

38. Schütze, S., Tchikov, V. & Schneider-Brachert, W. Regulation of TNFR1 and CD95 signalling by receptor compartmentalization. *Nat. Rev. Mol. Cell Biol.* **9,** 655–662 (2008).

39. Algeciras-schimnich, A., Shen, L., Barnhart, B. C., Murmann, A. E., Burkhardt, J. K., Peter, M. E. & Marcus, E. Molecular Ordering of the Initial Signaling Events of CD95. *Mol. Cell. Biol.* **22,** 207–220 (2002).

40. Muppidi, J. R. & Siegel, R. M. Ligand-independent redistribution of Fas (CD95) into lipid rafts mediates clonotypic T cell death. *Nat. Immunol.* **5,** 182–9 (2004).

41. Rebillard, A., Jouan-Lanhouet, S., Jouan, E., Legembre, P., Pizon, M., Sergent, O., Gilot, D., Tekpli, X., Lagadic-Gossmann, D. & Dimanche-Boitrel, M.-T. Cisplatin-induced apoptosis involves a Fas-ROCK-ezrin-dependent actin remodelling in human colon cancer cells. *Eur. J. Cancer* **46,** 1445–55 (2010).

42. Tauzin, S., Debure, L., Moreau, J.-F. & Legembre, P. CD95-mediated cell signaling in cancer: mutations and post-translational modulations. *Cell. Mol. Life Sci.* (2011). doi:10.1007/s00018-011-0866-4

43. Eramo, A., Sargiacomo, M., Ricci-Vitiani, L., Todaro, M., Stassi, G., Messina, C. G. M., Parolini, I., Lotti, F., Sette, G., Peschle, C. & De Maria, R. CD95 death-inducing signaling complex formation and internalization occur in lipid rafts of type I and type II cells. *Eur. J. Immunol.* **34,** 1930–1940 (2004).

44. Chakrabandhu, K., Huault, S., Garmy, N., Fantini, J., Stebe, E., Mailfert, S., Marguet, D. & Hueber, A. The extracellular glycosphingolipid-binding motif of Fas defines its internalization route, mode and outcome of signals upon activation by ligand. *Cell Death Differ.* **15,** 1824–37 (2008).

45. Koncz, G., Kerekes, K., Chakrabandhu, K. & Hueber, A. Regulating Vav1 phosphorylation by the SHP-1 tyrosine phosphatase is a fine-tuning mechanism for the negative regulation of DISC formation and Fas-mediated cell death signaling. *Cell Death Differ.* **15,** 494–503 (2008).

46. Kulms, D., Düssmann, H., Pöppelmann, B., Ständer, S., Schwarz, A. & Schwarz, T. Apoptosis induced by disruption of the actin cytoskeleton is mediated via activation of CD95 (Fas/APO-1). *Cell Death Differ.* **9,** 598–608 (2002).

47. Blaskovic, S., Blanc, M. & Van Der Goot, F. G. What does S-palmitoylation do to membrane proteins? *FEBS J.* **280,** 2766–2774 (2013).

48. Delandre, C., Penabaz, T. R., Passarelli, A. L., Chapes, S. K. & Clem, R. J. Mutation of juxtamembrane cysteines in the tetraspanin CD81 affects palmitoylation and alters interaction with other proteins at the cell surface. *Exp. Cell Res.* **315,** 1953–1963 (2009).

49. Dietrich, L. E. P. & Ungermann, C. On the mechanism of protein palmitoylation. *EMBO Rep.* **5,** 1053–7 (2004).

50. Rossin, A., Kral, R., Lounnas, N., Chakrabandhu, K., Mailfert, S., Marguet, D. & Hueber, A.-O. Identification of a lysine-rich region of Fas as a raft nanodomain targeting signal necessary for Fas-mediated cell death. *Exp. Cell Res.* **316,** 1513–22 (2010).

51. Rossin, A., Derouet, M., Abdel-sater, F. & Hueber, A. Palmitoylation of the TRAIL receptor DR4 confers an efficient TRAIL-induced cell death signalling. *Biochem. J.* **419,** 185–192 (2009).

52. Guardiola-Serrano, F., Rossin, A., Cahuzac, N., Luckerath, K., Melzer, I., Mailfert, S., Merguet, D., Zornig, M. & Hueber, A.-O. Palmitoylation of human FasL modulates its cell death-inducing function. *Cell Death Dis.* **1,** 1–8 (2010).

53. Peter, M. E. & Krammer, P. H. The CD95(APO-1/Fas) DISC and beyond. *Cell Death Differ.* **10,** 26–35 (2003).

54. Gradl, G., Grandison, P., Lindridge, E., Wang, Y., Watson, J. & Rudert, F. The CD95 (Fas/APO-1) receptor is phosphorylated in vitro and in vivo and constitutively associates with several cellular proteins. *Apoptosis* **1,** 131–140 (1996).

55. Eberle, A., Reinehr, R., Becker, S. & H, V. K. D. CD95 tyrosine phosphorylation is required for CD95 oligomerization. *Apoptosis* **12,** 719–729 (2007).

56. Sharif-askari, E., Gaucher, D., Halwani, R., Ma, J., Jao, K., Haddad, E. K. & Sekaly, R.-P. p56 Lck Tyrosine Kinase Enhances the Assembly of Death-inducing Signaling Complex during Fas-mediated Apoptosis. *J. Biol. Chem.* **282,** 36048–36056 (2007).

57. Atkinson, E. A., Ostergaard, H., Kane, K., Pinkoski, M. J., Caputo, A., Olszowy, M. W. & Bleackley, R. C. A Physical Interaction between the Cell Death Protein Fas and the Tyrosine Kinase p59 fynT. *J. Biol. Chem.* **271,** 5968–5971 (1996).

58. Eberle, A., Reinehr, R., Becker, S. & Haussinger, D. Fluorescence Resonance Energy Transfer Analysis of Proapoptotic CD95–EGF Receptor Interactions in Huh7 Cells. *Heptology* **41,** 13–15 (2005).

59. Daigle, I., Yousefi, S., Colonna, M., Green, D. R. & Simon, H.-U. Death receptors bind SHP-1 and block cytokine-induced anti-apoptotic signaling in neutrophils. *Nat. Med.* **8,** 61–67 (2002).

60. Sato, T., Irie, S., Kitada, S. & Reed, J. FAP-1: a protein tyrosine phosphatase that associates with Fas. *Science (80-.).* **268,** 411–415 (1995).

61. Li, Y., Kanki, H., Hachiya, T., Ohyama, T., Irie, S., Tang, G., Mukai, J. & Sato, T.-A. Negative regulation of Fas-mediated apoptosis by FAP-1 in human cancer cells. *Int. J. Cancer* **479,** 473–479 (2000).

62. Kleber, S. *et al.* Yes and PI3K bind CD95 to signal invasion of glioblastoma. *Cancer Cell* **13,** 235–48 (2008).

63. Sancho-Matinez, I. & Martin-Villalba, A. Tyrosine phosphorylation and CD95: A FAScinating switch. *Cell Cycle* **8,** 838–842 (2009).

64. Schlottmann, K. E., Gulbins, E., Lau, S. M. & Coggeshall, M. K. Activation of Src-family apoptosis tyrosine kinases during Fas-induced apoptosis. *J. Leukoc. Biol.* **60,** 546–554 (1996).

65. Gulbins, E., Hermisson, M., Brenner, B., Grassme, H. U. C., Linderkamp, O., Dichgans, J., Weller, M. & Lang, F. Cellular stimulation via CD95 involves activation of phospho-inositide-3-kinase. *Pflugers Arch.* **435,** 546–54 (1998).

66. Chatfield, K. & Eastman, A. Inhibitors of protein phosphatases 1 and 2A differentially prevent intrinsic and extrinsic apoptosis pathways. *Biochem. Biophys. Res. Commun.* **323,** 1313–1320 (2004).

67. Harmala-Brasken, A.-S., Mikhailov, A., Soderstrom, T. S., Meinander, A., Holmstrom, T. H., Damuni, Z. & Eriksson, J. E. Type-2A protein phosphatase activity is required to maintain death receptor responsiveness. *Oncogene* **22,** 7677–7686 (2003).

68. Anathy, V., Aesif, S. W., Guala, A. S., Havermans, M., Reynaert, N. L., Ho, Y., Budd, R. C. & Janssen-Heininger, Y. M. W. Redox amplification of apoptosis by caspase-dependent cleavage of glutaredoxin 1 and S-glutathionylation of Fas. *J. Cell Biol.* **184,** 241–52 (2009).

69. Leon-Bollotte, L., Subramaniam, S., Cauvard, O., Colas, S. P., Paul, C., Godard, C., Ruiz, A. M., Legembre, P., Jeannin, J. F. & Bettaieb, A. S-Nitrosylation of the Death Receptor Fas Promotes Fas Ligand–Mediated Apoptosis in Cancer Cells. *Gastroenterology* **140,** 2009–2018.e4 (2011).

70. Talbott, S. J., Luanpitpong, S., Stehlik, C., Azad, N., Iyer, A. K. V, Wang, L. & Rojanasakul, Y. S-nitrosylation of FLICE inhibitory protein determines its interaction with RIP1 and activation of NF-kB. *Cell Cycle* **13,** Epub ahead of print (2014).

71. Martin-Villalba, A., Llorens-Bobadilla, E. & Wollny, D. CD95 in cancer: tool or target? *Trends Mol. Med.* **19,** 329–35 (2013).

72. Ahn, J., Park, S., Cho, H., Lee, M., Yoon, J., Vilcek, J., Lee, T. H., Kinases, M. P. & Expression, N.-B. G. Non-apoptotic Signaling Pathways Activated by Soluble Fas Ligand in Mitogen-Activated Protein Kinases and NF-κ B-dependent Non-apoptotic Signaling Pathways Activated by Soluble Fas Ligand in Serum-starved Human Fibroblasts. *J. Biol. Chem.* **274,** 47100–47106 (2001).

73. Kavuri, S. M., Geserick, P., Dimitrova, D. P., Siegmund, D., Neumann, M., Wajant, H. & Leverkus, M. Cellular FLICE-inhibitory Protein (cFLIP) Isoforms Block CD95- and TRAIL Death Receptor-induced Gene Induction Irrespective of Processing of Caspase-8 or cFLIP in the Death-inducing Signaling Complex. *J. Biol. Chem.* **286,** 16631–16646 (2011).

74. Kataoka, T., Budd, R. C., Holler, N., Thome, M., Martinon, F., Irmler, M., Burns, K., Hahne, M., Kennedy, N., Kovacsovics, M. & Tschopp, J. The caspase-8 inhibitor FLIP promotes activation of NF-κB and Erk signaling pathways. *Curr. Biol.* **10,** 640–648 (2000).

75. Chen, L., Park, S., Tumanov, A. V, Hau, A., Sawada, K., Feig, C., Turner, J. R., Fu, Y., Romero, I. L., Lengyel, E. & Peter, M. E. CD95 promotes tumour growth. *Nature* **465,** 492–6 (2010).

76. Matsumoto, N., Imamura, R. & Suda, T. Caspase-8- and JNK-dependent AP-1 activation is required for Fas ligand-induced IL-8 production. *FEBS J.* **274,** 2376–2384 (2007).

77. Qian, C., Qian, L., Yu, Y., Guo, Z., Han, Y., Bai, Y. & Wang, Q. Fas Signal Promotes the Immunosuppressive Function of Regulatory Dendritic Cells via the ERK / Beta-Catenin Pathway. *Journall Biol. Chem.* **288,** 27825–27835 (2013).

78. Wilson, N. S., Dixit, V. & Ashkenazi, A. Death receptor signal transducers: nodes of coordination in immune signaling networks. *Nat. Immunol.* **10,** 348–55 (2009).

79. Park, H. H., Logette, E., Raunser, S., Cuenin, S. & Walz, T. Death Domain Assembly Mechanism Revealed by Crystal Structure of the Oligomeric PIDDosome Core Complex. *Cell* 533–546 (2007). doi:10.1016/j.cell.2007.01.019

80. Kreuz, S., Siegmund, D., Rumpf, J., Samel, D., Leverkus, M., Janssen, O., Häcker, G., Dittrich-breiholz, O., Kracht, M., Scheurich, P. & Wajant, H. NFkB activation by Fas is mediated through FADD, caspase-8 and RIP and is inhibited by FLIP. *J. Cell Biol.* **166,** 369–380 (2004).

81. Ofengeim, D. & Yuan, J. Regulation of RIP1 kinase signalling at the crossroads of inflammation and cell death. *Nat. Rev. Mol. Cell Biol.* **14,** 727–736 (2013).

82. Iyer, A. K. V, Azad, N., Talbot, S., Stehlik, C., Lu, B., Wang, L. & Rojanasakul, Y. Antioxidant c-FLIP Inhibits Fas Ligand-Induced NF-κB Activation in a Phosphatidylinositol 3-Kinase/Akt-Dependent Manner. *J. Immunol.* **187,** 3256–3266 (2014).

83. Liu, F., Bardham, K., Yang, D., Thangaraju, M., Ganapathy, V., Liles, G., Lee, J. & Liu, K. Molecular Bases of Disease : NF- κ B directly regulates Fas transcription to modulate Fas-mediated apoptosis and tumor suppression Feiyan Liu , Kankana Bardhan , Dafeng Yang , Georgia Liles , Jeffrey Lee and Kebin Liu Supplemental material : *J. Biol. Chem.* 0–22 (2012). doi:10.1074/jbc.M112.356279

84. Schneider-brachert, W., Heigl, U. & Ehrenschwender, M. Membrane Trafficking of Death Receptors : Implications on Signalling. *Int. J. Mol. Sci.* **14,** 14475–14503 (2013).

85. Poppema, S., Maggio, E. & Van Den Berg, A. Development of Lymphoma in Autoimmune Lymphoproliferative Syndrome (ALPS) and its Relationship to Fas Gene Mutations. *Leuk. Lymphoma* **45,** 423–431 (2004).

86. Rieux-Laucet, F., Deist, F. Le & Fischer, A. Autoimmune lymphoproliferative syndromes : genetic defects of apoptosis pathways. *Cell Death Differ.* **10,** 124–133 (2003).

87. Fisher, G. H., Rosenberg, F. J., Straus, S. E., Dale, J. K., Middelton, L. A., Lin, A. Y., Strober, W., Lenardo, M. J. & Puck, J. M. Dominant interfering Fas gene mutations impair apoptosis in a human autoimmune lymphoproliferative syndrome. *Cell* **81,** 935–946 (1995).

88. Martin, D. A., Zheng, K., Sirgel, R. M., Huang, B., Fisher, G. H., Wang, J., Jackson, Christine, E., Puck, Jennifer, M., Dale, J., Straus, S. E., Peter, M. E., Krammer, P. H., Fesik, S. & Lenardo, M. J. Defective CD95/APO-1/Fas signal complex formation in the human autoimmune lymphoproliferative syndrome, type Ia. *Proc. Natl. Acad. Sci. USA* **96,** 4552–4557 (1999).

89. Bivona, T. G., Hieronymus, H., Parker, J., Chang, K., Taron, M., Rosell, R., Moonsamy, P., Dahlman, K., Miller, V. a, Costa, C., Hannon, G. & Sawyers, C. L. FAS and NF-κB signalling modulate dependence of lung cancers on mutant EGFR. *Nature* **471,** 523–6 (2011).

90. Straus, S. E. *et al.* The development of lymphomas in families with autoimmune lymphoproliferative syndrome with germline Fas mutations and defective lymphocyte apoptosis. **98,** 194–200 (2001).

91. Grønbæk, B. K., Straten, P., Ralfkiaer, E., Ahrenkiel, V., Andersen, M. K., Hansen, N. E., Zeuthen, J., Hou-jensen, K. & Guldberg, P. Somatic Fas

Mutations in Non-Hodgkin's Lymphoma: Association With Extranodal Disease and Autoimmunity. **92,** 3018–3024 (1998).

92. Bretscher, A., Edwards, K. & Fehon, R. G. ERM proteins and merlin: integrators at the cell cortex. *Nat. Rev. Mol. Cell Biol.* **3,** 586–99 (2002).

93. Doi, Y., Itoh, M., Ishihara, S., Takano, H., Noda, T., Tsukita, S. & Tsukita, S. Normal Development of Mice and Unimpaired Cell Adhesion/ Cell Motility/Actin-based Cytoskeleton without Compensatory Up-regulation of Ezrin or Radixin in Moesin Gene Knockout. *J. Biol. Chem.* **274,** 2315–2321 (1999).

94. Kikuchi, S., Hata, M., Fukumoto, K., Yamane, Y., Matsui, T., Yonemura, S., Yamagishi, H., Keppler, D., Tsukita, S. & Tsukita, S. Radixin deficiency causes conjugated hyperbilirubinemia with loss of Mrp2 from bile canalicular membranes. **31,** (2002).

95. Saotome, I., Curto, M. & Mcclatchey, A. I. Ezrin Is Essential for Epithelial Organization and Villus Morphogenesis in the Developing Intestine. **6,** 855–864 (2004).

96. Smith, W. J. & Cerione, R. A. Crystallization and preliminary crystallographic analysis of the ezrin FERM domain. *Acta Crystallogr. Sect. D Biol. Crystallogr.* **58,** 1359–1361 (2002).

97. Smith, W. J., Nassar, N., Bretscher, A., Cerione, R. a & Karplus, P. A. Structure of the active N-terminal domain of Ezrin. Conformational and mobility changes identify keystone interactions. *J. Biol. Chem.* **278,** 4949–56 (2003).

98. Pearson, M. A., Reczek, D., Bretscher, A. & Karplus, P. A. Structure of the ERM protein moesin reveals the FERM domain fold masked by an extended actin binding tail domain. *Cell* **101,** 259–270 (2000).

99. Chambers, D. N. & Bretscher, A. Ezrin mutants affecting dimerization and activation. *Biochemistry* **44,** 3926–32 (2005).

100. Yonemura, S., Hirao, M., Doi, Y., Takahashi, N., Kondo, T., Tsukita, S. & Tsukita, S. Ezrin/Radixin/Moesin (ERM) Proteins Bind to a Positively Charged Amino Acid Cluster in the Juxta-Membrane Cytoplasmic Domain of CD44, CD43, and ICAM-2. *J. Cell Biol.* **140,** 885–895 (1998).

101. Barret, C., Roy, C., Montcourrier, P., Mangeat, P. & Niggli, V. Mutagenesis of the Phosphatidylinositol 4, 5-Bisphosphate (PIP2) Binding Site in the NH 2 -Terminal Domain of Ezrin Correlates with Its Altered Cellular Distribution. *J. Cell Biol.* **151,** 1067–1079 (2000).

102. Hamada, K., Shimizu, T., Matsui, T., Tsukita, S. S. & Hakoshima, T. Structural basis of the membrane-targeting and unmasking mechanisms of the radixin FERM domain. *EMBO J.* **19,** 4449–4462 (2000).

103. Edwards, S. D. & Keep, N. H. The 2.7 Å Crystal Structure of the Activated FERM Domain of Moesin : An Analysis of Structural Changes on Activation. *Biochemistry* **40,** 7061–7068 (2001).

104. Hamada, K., Shimizu, T., Matsui, T., Tsukita, S. S. & Hakoshima, T. Crystallographic characterization of the radixin FERM domain bound to the cytoplasmic tail of the adhesion protein ICAM-2. *Acta Crystallogr. Sect. D Biol. Crystallogr.* **57,** 891–892 (2001).

105. Legg, J. W. & Isacke, C. M. Identification and functional analysis of the ezrin-binding site in the hyaluronan receptor , CD44. *Curr. Biol.* **8,** 705–708 (1998).

106. Helander, T. S., Carpen, O., Turunen, O., Kovanen, P., Vaheri, A. & Timonen, T. ICAM-2 residtributed by ezrin as a target for killer cells. *Nature* **282,** 265–268 (1996).

107. Reczek, D. & Bretscher, A. The Carboxyl-terminal Region of EBP50 Binds to a Site in the Amino-terminal Domain of Ezrin That Is Masked in the Dormant Molecule. *J. Biol. Chem.* **273,** 18452–18458 (1998).

108. Hall, R. A., Premont, R. T., Blitzer, J. T., Pitcher, J. A., Claing, A., Barak, L. S. & Lefkowitz, R. J. The B2-adrenergic receptor interacts with the Na+/H+-exchanger regulatory factor to control Na+/H+ exchange. *Nature* **392,** 626–630 (1998).

109. Takeda, T., Mcquistan, T., Orlando, R. A. & Farquhar, M. G. Loss of glomerular foot processes is associated with uncoupling of podocalyxin from the actin cytoskeleton. *J. Clin. Invest.* **108,** 289–301 (2001).

110. Hamada, K., Shimizu, T., Yonemura, S., Tsukita, S. & Hakoshima, T. Structural basis of adhesion-molecule recognition by ERM proteins revealed by the crystal structure of the radixin–ICAM-2 complex. *EMBO J.* **22,** 502–514 (2003).

111. Terawaki, S., Maesaki, R. & Hakoshima, T. Structural basis for NHERF recognition by ERM proteins. *Structure* **14,** 777–89 (2006).

112. Mori, T., Kitano, K., Terawaki, S., Maesaki, R., Fukami, Y. & Hakoshima, T. Structural basis for CD44 recognition by ERM proteins. *J. Biol. Chem.* **283,** 29602–12 (2008).

113. Kondo, T., Takeuchi, K., Doi, Y., Yonemura, S., Nagata, S. & Tsukita, S. ERM (ezrin/radixin/moesin)-based molecular mechanism of microvillar breakdown at an early stage of apoptosis. *J. Cell Biol.* **139,** 749–758 (1997).

114. Parlato, S., Giammarioli, A. M., Logozzi, M., Lozupone, F., Matarrese, P., Luciani, F., Falchi, M., Malorni, W. & Fais, S. CD95 (APO-1/Fas) linkage to the actin cytoskeleton through ezrin in human T lymphocytes: a novel

regulatory mechanism of the CD95 apoptotic pathway. *EMBO J.* **19,** 5123–5134 (2000).

115. Hébert, M., Potin, S., Sebbagh, M., Bréard, J., Hamelin, J., Bertoglio, J. & Bre, J. Rho-ROCK-dependent ezrin-radixin-moesin phosphorylation regulates Fas-mediated apoptosis in Jurkat cells. *J. Immunol.* **181,** 5963–73 (2008).

116. Kuo, W., Yang, K., Hsieh, S. & Lai, M. Ezrin is a negative regulator of death receptor-induced apoptosis. *Oncogene* **29,** 1374–83 (2010).

117. Lozupone, F., Lugini, L., Matarrese, P., Luciani, F., Federici, C., Iessi, E., Margutti, P., Stassi, G., Malorni, W. & Fais, S. Identification and relevance of the CD95-binding domain in the N-terminal region of ezrin. *J. Biol. Chem.* **279,** 9199–207 (2004).

118. Ruan, W., Lee, C. T. & Desbarats, J. A novel juxtamembrane domain in tumor necrosis factor receptor superfamily molecules activates Rac1 and controls neurite growth. *Mol. Biol. Cell* **19,** 3192–202 (2008).

119. Cheng, L., Itoh, K. & Lemmon, V. L1-Mediated Branching Is Regulated by Two Ezrin – Radixin – Moesin (ERM) -Binding Sites , the RSLE Region and a Novel Juxtamembrane ERM-Binding Region. **25,** 395–403 (2005).

120. Giammarioli, A. M. M., Garofalo, T., Sorice, M., Misasi, R., Gambardella, L., Gradini, R., Fais, S., Pavan, A. & Malorni, W. GD3 glycosphingolipid contributes to Fas-mediated apoptosis via association with ezrin cytoskeletal protein. *FEBS Lett.* **506,** 45–50 (2001).

121. Scott, F. L., Stec, B., Pop, C., Dobaczewska, M. K., Lee, J. J., Monosov, E., Robinson, H., Salvesen, G. S., Schwarzenbacher, R. & Riedl, S. J. The Fas-FADD death domain complex structure unravels signalling by receptor clustering. *Nature* **457,** 1019–22 (2009).

122. Ferguson, B. J., Esposito, D., Jovanović, J., Sankar, A., Driscoll, P. C. & Mehmet, H. Biophysical and cell-based evidence for differential interactions between the death domains of CD95/Fas and FADD. *Cell Death Differ.* **14,** 1717–9 (2007).

123. Esposito, D., Sankar, A., Morgner, N., Robinson, C. V, Rittinger, K. & Driscoll, P. C. Solution NMR investigation of the CD95/FADD homotypic death domain complex suggests lack of engagement of the CD95 C terminus. *Structure* **18,** 1378–90 (2010).

124. Wang, L., Yang, J. K., Kabaleeswaran, V., Rice, A. J., Cruz, A. C., Park, A. Y., Yin, Q., Damko, E., Jang, S. B., Raunser, S., Robinson, C. V, Siegel, R. M., Walz, T. & Wu, H. Supplementary information The Fas – FADD death domain complex structure reveals the basis of DISC assembly and disease mutations. *Nat. Struct. Mol. Biol.* **17,** 1324–9 (1920).

125. Cao, P., Zhang, W., Gui, W., Dong, Y., Jiang, T. & Gong, Y. Structural insights into the mechanism of calmodulin binding to death receptors. *Acta Crystallogr. Sect. D Biol. Crystallogr.* **70,** 1604–1613 (2014).

126. Severinov, K. & Muir, T. W. Expressed Protein Ligation , a Novel Method for Studying Protein-Protein Interactions in Transcription. *J. Biol. Chem.* **26,** 16205–16209 (1998).

127. Offer, J. Native chemical ligation with Nalpha acyl transfer auxiliaries. *Pept. Sci.* **94,** 530–41 (2010).

128. Katoh, K. & Standley, D. M. MAFFT multiple sequence alignment software version 7: improvements in performance and usability. *Mol. Biol. Evol.* **30,** 772–80 (2013).

129. Waterhouse, A. M., Procter, J. B., Martin, D. M. A., Clamp, M. & Barton, G. J. Jalview Version 2--a multiple sequence alignment editor and analysis workbench. *Bioinformatics* **25,** 1189–91 (2009).

130. Edelhoch, H. Spectroscopic determination of tryptophan and tyrosine in proteins. *Biochemistry* **6,** 1948–54 (1967).

131. Pace, C. N., Vajdos, F., Fee, L., Grimsley, G. & Gray, T. How to measure and predict the molar absorption coefficient of a protein. *Protein Sci.* **4,** 2411–23 (1995).

132. Kibbe, W. A. OligoCalc: an online oligonucleotide properties calculator. *Nucleic Acids Res.* **35,** W43–6 (2007).

133. Maniatis, T., Fritsch, E. F. & Sambrook, J. *Molecular cloning : a laboratory manual*. (Cold Spring Harbor Laboratory Press, 2001).

134. Ulrich, A., Andersen, K. R. & Schwartz, T. U. Exponential megapriming PCR (EMP) cloning--seamless DNA insertion into any target plasmid without sequence constraints. *PLoS One* **7,** e53360 (2012).

135. Studier, F. W. Protein production by auto-induction in high density shaking cultures. *Protein Expr. Purif.* **41,** 207–34 (2005).

136. Bano, M. C., Jackson, C. S. & Magee, A. I. Pseudo-enzymic S-acylation of a myristoylated Yes protein tyrosine kinase peptide in vitro may reflect non-enzymic S-acylation in vivo. *Biochem. J.* **330,** 723–731 (1998).

137. Delaglio, F., Grzesiek, S., Vuister, G. W., Zhu, G., Pfeifer, J. & Bax, A. NMRPipe: a multidimensional spectral processing system based on UNIX pipes. *J. Biomol. NMR* **6,** 277–93 (1995).

138. Vranken, W. F., Boucher, W., Stevens, T. J., Fogh, R. H., Pajon, A., Llinas, M., Ulrich, E. L., Markley, J. L., Ionides, J. & Laue, E. D. The CCPN data

model for NMR spectroscopy: development of a software pipeline. *Proteins* **59,** 687–96 (2005).

139. Mori, S., Abeygunawardana, C., O'Neil Johnson, M. & M. van Zul, P. Improved sensitivity of HSQC spectra of exchanging protons at short interscan delays using a new fast HSQC detection scheme that avoids water saturation. *J. Magn. Reson. Ser. B* **108,** 94–98 (1995).

140. Grzesiek, S. & Bax, A. Amino acid type determination in the sequential assignment procedure of uniformly 13C/15N-enriched proteins. *J. Biomol. NMR* **3,** 185–204 (1993).

141. Wittekind, M. & Mueller, L. HNCACB, a high sensitivity 3D NMR Experiment to Correlate amide-proton and nitrogen resonances with the Alpha and Beta-Carbon resonances in proteins. *J. Magn. Reson. Ser. B* **101,** 201–205 (1993).

142. Grzesiek, S. & Bax, A. Improved 3D triple-resonance NMR techniques applied to a 31 kDa protein. *J. Magn. Reson.* **96,** 432–440 (1992).

143. Grzesiek, S. & Bax, A. Correlating Backbone Amide and Side Chain Resonances in Larger Proteins by Multiple Relayed Triple Resonance NMR. *J. Am. Chem. Soc.* **114,** 6291–6293 (1992).

144. Marion, D., Driscoll, P. C., Kay, L. E., Wingfield, P. T., Bax, A., Gronenborn, a M. & Clore, G. M. Overcoming the overlap problem in the assignment of 1H NMR spectra of larger proteins by use of three-dimensional heteronuclear 1H-15N Hartmann-Hahn-multiple quantum coherence and nuclear Overhauser-multiple quantum coherence spectroscopy: application to. *Biochemistry* **28,** 6150–6 (1989).

145. Bax, A., Clore, G. M. & Gronenborn, A. 1H- 1H Correlation via Isotropic Mixing of 13C a New Three-Dimensional Approach for Assigning lH and 13C Spectra of 13C-Enriched Proteins. *J. Magn. Reson.* **88,** 425–431 (1990).

146. Olejniczak, E. T., Xu, R. X. & Fesik, S. W. A 4D HCCH-TOCSY experiment for assigning the side chain 1H and 13C resonances of proteins. *J. Biomol. NMR* **2,** 655–659 (1992).

147. Orekhov, V., Ibraghimov, I. & Billeter, M. Optimizing resolution in multidimensional NMR by three-way. *J. Biomol. NMR* **27,** 165–173 (2003).

148. Jaravine, V., Ibraghimov, I. & Orekhov, V. Removal of a time barrier for high-resolution multidimensional NMR spectroscopy. *Nat. Methods* **3,** 605–607 (2006).

149. Hansen, M. R., Mueller, L. & Pardi, A. Tunable alignment of macromolecules by filamentous phage yields dipolar coupling interactions. *Nat. Struct. Mol. Biol.* **5,** 1065–1074 (1998).

150. Ottiger, M., Delaglio, F. & Bax, A. Measurement of J and Dipolar Couplings from Simplified Two-Dimensional NMR Spectra. *J. Magn. Reson.* **131,** 373–378 (1998).

151. Dosset, P., Hus, J. C., Marion, D. & Blackledge, M. A novel interactive tool for rigid-body modeling of multi-domain macromolecules using residual dipolar couplings. *J. Biomol. NMR* **20,** 223–31 (2001).

152. Tugarinov, V., Hwang, P. M., Ollerenshaw, J. E. & Kay, L. E. Cross-Correlated Relaxation Enhanced 1H - 13C NMR Spectroscopy of Methyl Groups in Very High Molecular Weight Proteins and Protein Complexes. *J. Am. Chem. Soc.* **125,** 10420–10428 (2003).

153. Farrow, N. a, Muhandiram, R., Singer, a U., Pascal, S. M., Kay, C. M., Gish, G., Shoelson, S. E., Pawson, T., Forman-Kay, J. D. & Kay, L. E. Backbone dynamics of a free and phosphopeptide-complexed Src homology 2 domain studied by 15N NMR relaxation. *Biochemistry* **33,** 5984–6003 (1994).

154. Linge, J. P., O'Donoghue, S. I. & Nilges, M. Automated assignment of ambiguous nuclear overhauser effects with ARIA. *Methods Enzymol.* **339,** 71–90 (2001).

155. Linge, J. P., Williams, M. A., Spronk, C. A. E. M., Bonvin, A. M. J. J. & Nilges, M. Refinement of Protein Structures in Explicit Solvent. *Proteins Struct. Funct. Genet.* **50,** 496–506 (2003).

156. Rieping, W., Habeck, M., Bardiaux, B., Bernard, A., Malliavin, T. E. & Nilges, M. ARIA2: automated NOE assignment and data integration in NMR structure calculation. *Bioinformatics* **23,** 381–2 (2007).

157. Schroll, A. L., Hondal, R. J. & Flemer, S. 2,2'-Dithiobis(5-nitropyridine) (DTNP) as an effective and gentle deprotectant for common cysteine protecting groups. *J. Pept. Sci.* **18,** 1–9 (2012).

158. Schroll, A. L., Hondal, R. J. & Flemer, S. The use of 2,2'-dithiobis(5-nitropyridine) (DTNP) for deprotection and diselenide formation in protected selenocysteine-containing peptides. *J. Pept. Sci.* **18,** 155–62 (2012).

159. Handa, N., Kukimoto0Niino, M., Akasaka, R., Murayama, K., Terada, T., Aoki, M., Seki, E., Matsuda, T., Nunokawa, E., Tanaka, A., Hayashizaki, T., Kigawa, T., Shirouzu, M. & Yokoyama, S. Structure of the UNC5H2 death domain. *Acta Crystallogr. Sect. D Biol. Crystallogr.* **D62,** 1502–1509 (2006).

160. Sukits, S. F., Lin, L., Hsu, S., Malakian, K., Powers, R. & Xu, G. Solution Structure of the Tumor Necrosis Factor Receptor-1 Death Domain. *J. Mol. Biol.* **310,** 895–906 (2001).

161. Feinstein, E. & Kimchi, A. The death domain: a module shared by proteins with diverse cellular functions. *Trends Biochem. Sci.* **20,** 342–344 (1995).

162. Berglund, H., Olerenshaw, D., Sankar, A., Federwisch, M., McDonald, N. Q. & Driscoll, P. C. The three-dimensional solution structure and dynamic properties of the human FADD death domain. *J. Mol. Biol.* **302,** 171–88 (2000).

163. Jeong, E., Bang, S., Lee, T. H., Park, Y. I., Sim, W. & Kim, K. The Solution Structure of FADD Death Domain: Structural basis of death domain interactions of Fas and FADD. *J. Biol. Chem.* **274,** 16337–16342 (1999).

164. Liepinsh, E., Ilag, L. L., Otting, G. & Ibanez, C. F. NMR structure of the death domain of the p75 neurotrophin receptor. *EMBO J.* **16,** 4999–5005 (1997).

165. Lasker, M. V, Gajjar, M. M. & Nair, S. K. Cutting Edge: Molecular Structure of the IL-1R-Associated Kinase-4 Death Domain and Its Implications for TLR Signaling. *J. Immunol.* **175,** 4175–4179 (2005).

166. Lin, S., Lo, Y. & Wu, H. Helical assembly in the MyD88 – IRAK4 – IRAK2 complex in TLR / IL-1R signalling. *Nature* **465,** 885–891 (2010).

167. Park, H. H. & Wu, H. Crystal Structure of RAIDD Death Domain Implicates Potential Mechanism of PIDDosome Assembly. *J. Mol. Biol.* **357,** 358–364 (2006).

168. Xiao, T., Towb, P., Wasserman, S. A. & Sprang, S. R. Three-Dimensional Structure of a Complex between the Death Domains of Pelle and Tube. *Celll* **99,** 545–555 (1999).

169. Xiao, T., Gardner, K. H. & Sprang, S. R. Cosolvent-induced transformation of a death domain tertiary structure. *Proc. Natl. Acad. Sci.* **99,** 11151–11156 (2002).

170. Moncrieffe, M. C., Stott, K. M. & Gay, N. J. Solution structure of the isolated Pelle death domain. *FEBS Lett.* **579,** 3920–3926 (2005).

171. Wishart, D. S. & Sykes, B. D. The 13C Chemical-Shift Index : A simple method for the identification of protein secondary structure using. *J. Biomol. NMR* **4,** 171–180 (1994).

172. Wishart, D. S., Sykes, B. D. & Richards, F. M. The Chemical Shift Index: a fast and simple method for the assignment of protein secondary structure through NMR spectroscopy. *Biochemistry* **31,** 1647–1651 (1992).

173. Linge, J. P., Habeck, M., Rieping, W. & Nilges, M. ARIA: automated NOE assignment and NMR structure calculation. *Bioinformatics* **19,** 315–6 (2003).

174. Nilges, M. Calculation of protein structures with ambiguous distance restraints. Automated assignment of ambiguous NOE crosspeaks and disulphide connectivities. *J. Mol. Biol.* **245,** 645–60 (1995).

175. Schwieters, C. D., Kuszewski, J. J., Tjandra, N. & Clore, G. M. The Xplor-NIH NMR molecular structure determination package. *J. Magn. Reson.* **160,** 65–73 (2003).

176. Cheung, M., Maguire, M. L., Stevens, T. J. & Broadhurst, R. W. DANGLE : A Bayesian inferential method for predicting protein backbone dihedral angles and secondary structure. *J. Magn. Reson.* **202,** 223–233 (2010).

177. Linge, J. P. & Nilges, M. Influence of non-bonded parameters on the quality of NMR structures : A new force field for NMR structure calculation. *J. Biomol. NMR* **13,** 51–59 (1999).

178. Laskowski, R. A., Macarthur, M. W., Moss, D. S. & Thornton, J. M. PROCHECK: a program to check the stereochemical quality of protein structures. (1993). doi:10.1107/S0021889892009944

179. Voehler, M. W., Collier, G., Young, J. K., Stone, M. P. & Germann, M. W. Performance of cryogenic probes as a function of ionic strength and sample tube geometry. *J. Magn. Reson.* **183,** 102–9 (2006).

180. Kay, L. E., Torchia, D. a & Bax, A. Backbone Dynamics of Proteins As Studied by 15N Inverse Detected Heteronuclear NMR Spectroscopy : Application to Staphylococcal Nuclease ? *Biochemistry* **28,** 8972–8979 (1989).

181. Palmer, A. G., Grey, J. M. & Wang, C. Solution NMR spin relaxation methods for characterizing chemical exchange in high-molecular-weight systems. *Methods Enzymol.* **394,** 430–465 (2005).

182. Palmer, A. G., Kroenke, C. D. & Loria, J. P. Nuclear Magnetic Resonance Methods for Quantifying Microsecond-to-Millisecond Motions in Biological Macromolecules. *Methods Enzymol.* **339,** 204–238 (2001).

183. Tollinger, M., Skrynnikov, N. R., Mulder, F. A. A., Forman-Kay, J. D. & Kay, L. E. Slow Dynamics in Folded and Unfolded States of an SH3 Domain. *J. Am. Chem. Soc.* **123,** 11341–11352 (2001).

184. Korzhnev, D., Salvatella, X., Vendruscolo, M., Di Nardo, A. A., Davidson, A. R., Dobson, C. M. & Kay, L. E. Low-populated folding intermediates of Fyn SH3 characterized by relaxation dispersion NMR. *Nature* **430,** 586–590 (2004).

185. Neudecker, P., Lundstrom, P. & Kay, L. E. Relaxation Dispersion NMR Spectroscopy as a Tool for Detailed Studies of Protein Folding. *Biophys. J.* **96,** 2045–2054 (2009).

186. Hyberts, S. G., Arthanari, H., Robson, S. A. & Wagner, G. Perspectives in magnetic resonance: NMR in the post-FFT era. *J. Magn. Reson.* **241,** 60–73 (2014).

187. Tikole, S., Jaravine, V., Orekhov, V. & Guntert, P. Effects of NMR Spectral Resolution on Protein Structure Calculation. *PLoS One* **8,** 1–10 (2013).

188. Wohr, T. & Mutter, M. Pseudo-Prolines in Peptide Synthesis : Direct Insertion of Serine and Threonine Derived Oxazolidines in Dipeptides. *Tetrahedron Lett.* **36,** 3847–3848 (1995).

189. Haack, T. & Mutter, M. Serine derived oxazolidines as secondary structure disrupting, solubilising building blocks in peptide synthesis. *Tetrahedron Lett.* **33,** 1589–1592 (1992).

190. White, P., Keyte, J. W., Bailey, K. & Bloomberg, G. Expediting the Fmoc solid phase synthesis of long peptides through the application of dimethyloxazolidine dipeptides. *J. Pept. Sci.* **10,** 18–26 (2004).

191. Muralidharan, V. & Muir, T. W. Protein ligation: an enabling technology for the biophysical analysis of proteins. *Nat. Methods* **3,** 429–438 (2006).

192. Offer, J. & Dawson, P. E. N α -2-Mercaptobenzylamine-Assisted Chemical Ligation. *Org. Lett.* **2,** 23–26 (2000).

193. Canne, L. E., Bark, S. J., Kent, S. B. H. & Jolla, L. Extending the Applicability of Native Chemical Ligation. *J. Am. Chem. Soc.* **7863,** 5891–5896 (1996).

194. Botti, P., Carrasco, M. R. & Kent, S. B. . Native chemical ligation using removable Nα-(1-phenyl-2-mercaptoethyl) auxiliaries. *Tetrahedron Lett.* **42,** 1831–1833 (2001).

195. Elleuche, S. & Pöggeler, S. Inteins, valuable genetic elements in molecular biology and biotechnology. *Appl. Microbiol. Biotechnol.* **87,** 479–89 (2010).

196. Perler, F. B., Olsen, G. J. & Adam, E. Compilation and analysis of intein sequences. *Nucleic Acids Res.* **25,** 1087–93 (1997).

197. Perler, F. B. Protein splicing mechanisms and applications. *IUBMB Life* **57,** 469–76 (2005).

198. Xu, M. Q. & Perler, F. B. The mechanism of protein splicing and its modulation by mutation. *EMBO J.* **15,** 5146–53 (1996).

199. Chong, S., Mersha, F. B., Comb, D. G., Scott, M. E., Landry, D., Vence, L. M., Perler, F. B., Benner, J., Kucera, R. B., Hirvonen, C. a, Pelletier, J. J., Paulus, H. & Xu, M. Q. Single-column purification of free recombinant proteins using a self-cleavable affinity tag derived from a protein splicing element. *Gene* **192,** 271–281 (1997).

200. Evans, T. C., Benner, J. & Xu, M. Q. The in vitro ligation of bacterially expressed proteins using an intein from Methanobacterium thermoautotrophicum. *J. Biol. Chem.* **274,** 3923–6 (1999).

201. Welker, E. & Scheraga, H. A. Use of benzyl mercaptan for direct preparation of long polypeptide benzylthio esters as substrates of subtiligase. *Biochem. Biophys. Res. Commun.* **254,** 147–51 (1999).

202. Watanabe, T., Ito, Y., Yamada, T., Hashimoto, M., Sekine, S. & Tanaka, H. The roles of the C-terminal domain and type III domains of chitinase A1 from Bacillus circulans WL-12 in chitin degradation. *J. Bacteriol.* **176,** 4465–72 (1994).

203. Chong, S., Mersha, F. B., Comb, D. G., Scott, M. E., Landry, D., Vence, L. M., Perler, F. B., Benner, J., Kucera, R. B., Hirvonen, C. a, Pelletier, J. J., Paulus, H. & Xu, M. Q. Single-column purification of free recombinant proteins using a self-cleavable affinity tag derived from a protein splicing element. *Gene* **192,** 271–81 (1997).

204. Telenti, A., Southworth, M., Alcaide, F., Daugelat, S., Jacobs, W. R. & Perler, F. B. The Mycobacterium xenopi GyrA Protein Splicing Element : Characterization of a Minimal Intein. *J. Bacteriol.* **179,** 6378–6328 (1997).

205. Southworth, M. P., Amaya, K., Evans, T. C., Ming-Qun, X. & Perler, F. B. Purification of proteins fused to either the amino or carboxy terminus of the Mycobacterium xenopi Gyrase A intein. *Biotechniques* **27,** 110–120 (1999).

206. R.B., M. Solid Phase Peptide Synthesis. I. The Synthesis of. *J. Am. Chem. Soc.* **85,** 2149–2154 (1963).

207. Perich, J. W., Ede, N. J., Eagle, S. & Bray, A. M. Synthesis of phosphopeptides by the Multipin method : Evaluation of coupling methods for the incorporation of Fmoc-Tyr(PO3Bzl,H)-OH , Fmoc-Ser(PO3Bzl,H)-OH and Fmoc-Thr(PO3Bzl,H)-OH. *Lett. Pept. Sci.* **6,** 91–97 (1999).

208. Fields, G. B. & Noble, R. L. Solid phase peptide synthesis utilizing 9-fluorenylmethoxycarbonyl amino acids. *Int. J. Pept. Protein Res.* **35,** 161–214 (1990).

209. Kent, S. B. *Chemical synthesis of peptides and proteins. Annual review of biochemistry* **57,** 957–89 (1988).

210. Stawikowski, M. & Fields, G. B. Introduction to Peptide Synthesis. *Curr. Protoc. Protein Sci.* **18,** 1–13 (2012).

211. Dawson Philip, E., Muir Tom, W., Clarke-Lewis, I. & Kent, S. B. H. Synthesis of proteins by native chemical ligation. *Science.* **266,** 776–779 (1994).

212. Bang, D. & Kent, S. B. H. A One-Pot Total Synthesis of Crambin. *Angew. Chem. Int. Ed. Engl.* **43,** 2534–2538 (2004).

213. Villain, M., Gaertner, H. & Botti, P. Native Chemical Ligation with Aspartic and Glutamic Acids as C -Terminal Residues : Scope and Limitations. *European J. Org. Chem.* 3267–3272 (2003). doi:10.1002/ejoc.200300032

214. Low, D. W., Hill, M. G., Carrasco, M. R., Kent, S. B. H. & Botti, P. Total synthesis of cytochrome b562 by native chemical ligation using a removable auxiliary. *Proc. Natl. Acad. Sci. U. S. A.* **98,** 5–10 (2001).

215. Offer, J., Boddy, C. N. C. & Dawson, P. E. Extending Synthetic Access to Proteins with a Removable Acyl Transfer Auxiliary terminal cysteine peptide is an established methodology for the. *J. Am. Chem. Soc.* **124,** 4642–4646 (2002).

216. Isidro-Llobet, A., Alvaraz, M. & Albericio, F. Amino Acid-Protecting Groups. *Chem. Rev.* **109,** 2455–2504 (2009).

217. Dittmann, M., Sauermann, J., Seidel, R., Zimmermann, W. & Engelhard, M. Native chemical ligation of hydrophobic peptides in organic solvents. *J. Pept. Sci.* **16,** 558–62 (2010).

218. Dittmann, M., Sadek, M., Seidel, R. & Engelhard, M. Native chemical ligation in dimethylformamide can be performed chemoselectively without racemization. *J. Pept. Sci.* **18,** 312–6 (2012).

219. Payne, R. J., Ficht, S., Tang, S., Brik, A., Yang, Y., Case, D. A. & Wong, C.-H. Extended Sugar-Assisted Glycopeptide Ligations: Development, Scope, and Applications. *J. Am. Chem. Soc.* **129,** 13527–13536 (2007).

220. Esposito, D. & Chatterjee, D. K. Enhancement of soluble protein expression through the use of fusion tags. *Curr. Opin. Biotechnol.* **17,** 353–8 (2006).

221. Savitsky, P., Bray, J., Cooper, C. D. O., Marsden, B. D., Mahajan, P., Burgess-brown, N. A. & Gileadi, O. High-throughput production of human proteins for crystallization: The SGC experience. *J. Struct. Biol.* **172,** 3–13 (2010).

222. Low, D. W., Hill, M. G., Carrasco, M. R., Kent, S. B. & Botti, P. Total synthesis of cytochrome b562 by native chemical ligation using a removable auxiliary. *Proc. Natl. Acad. Sci. U. S. A.* **98,** 6554–9 (2001).

223. New England Biolabs Inc. *IMPACT Kit Instruction Manual Version 1.1*. 9 (2009).

224. Johnson, E. C. B. & Kent, S. B. H. Insights into the Mechanism and Catalysis of the Native Chemical Ligation Reaction. *J. Am. Chem. Soc.* **128,** 6640–6646 (2006).

225. Hebert, M., Potin, S., Sebbagh, M., Bertoglio, J., Breard, J. & Hamelin, J. Rho-ROCK-dependent ezrin-radixin-moesin phosphorylation regulates Fas-mediated apoptosis in Jurkat cells. *J. Immunol.* **181,** 5963–5973 (2008).

226. Velazquez-Camooy, A., Ohtaka, H., Nezami, A., Muzammil, S. & Freire, E. Isothermal Titration Calorimetry. *Curr. Procols Cell Biol.* **Supplement,** 1–24 (2004).

227. Freyer, M. W. & Lewis, E. a. Isothermal titration calorimetry: experimental design, data analysis, and probing macromolecule/ligand binding and kinetic interactions. *Methods Cell Biol.* **84,** 79–113 (2008).

228. Liang, Y. Applications of isothermal titration calorimetry in protein science. *Acta Biochim. Biophys. Sin. (Shanghai).* **40,** 565–576 (2008).

229. Lebowitz, J., Lewis, M. S. & Schuck, P. Modern analytical ultracentrifugation in protein science: a tutorial review. *Protein Sci.* **11,** 2067–2079 (2002).

230. Schuck, P. Size-distribution analysis of macromolecules by sedimentation velocity ultracentrifugation and lamm equation modeling. *Biophys. J.* **78,** 1606–19 (2000).

231. Concepcion, J. *et al.* Label-Free Detection of Biomolecular Interactions Using BioLayer Interferometry for Kinetic Characterization. *Comb. Chem. High Throughput Screen.* **12,** 791–800 (2009).

232. Cooper, M. A. Current biosensor technologies in drug discovery. *Biosensor* 68–82 (2006).

233. Rajagopal, P., Waygood, B., Reizer, J., Saier, M. H. & Klevit, R. E. Demonstration of protein-protein interaction specificity by NMR chemical shift mapping. *Protein Sci.* **6,** 2624–2627 (1997).

234. Williamson, M. P. Using chemical shift perturbation to characterise ligand binding. *Prog. Nucl. Magn. Reson. Spectrosc.* **73,** 1–16 (2013).

235. Heiska, L., Alfthan, K., Gro, M., Vilja, P., Vaheri, A. & Carpe, O. Association of Ezrin with Intercellular Adhesion Molecule-1 and -2 (ICAM-1 and ICAM-2). *Biochemistry* **273,** 21893–21900 (1998).

236. Sprangers, R., Velyvis, A. & Kay, L. E. Solution NMR of supramolecular complexes : providing new insights into function. *Nat. Methods* **4,** 697–703 (2007).

237. Gonzalez Montoro, A., Rodrigo, Q. & Valdes Taubas, J. Zinc co-ordination by the DHHC cysteine-rich domain of the DHHC cysteine-rich domain of the palmitoyltransferase Swf1. *Biochem. J.* **454,** 427–435 (2013).

238. Greaves, J. & Chamberlain, L. H. DHHC palmitoyl transferases: substrate interactions and (patho)physiology. *Trends Biochem. Sci.* **36,** 245–253 (2011).

239. Smotrys, J. E. & Linder, M. E. Palmitoylation of Intracellular Signaling Proteins: Regulation and Function. *Annu. Rev. Biochem.* **73,** 559–87 (2004).

240. Martin, B. R., Wang, C., Adibekian, A., Tully, S. E. & Cravatt, B. F. Global profiling of dynamic protein palmitoylation. *Nat. Methods* **9,** 84–89 (2012).

241. Blaskovic, S., Adibekian, A., Blanc, M. & Van Der Goot, G. F. Mechanistic effects of protein palmitoylation and the cellular consequences thereof. *Chem. Phys. Lipids* **180,** 44–52 (2014).

242. Roth, A. F., Feng, Y., Chen, L. & Davis, N. G. The yeast DHHC cysteine-rich domain protein Akr1p is a palmitoyl transferase. *J. Cell Biol.* **159,** 23–8 (2002).

243. Lobo, S., Greentree, W. K., Linder, E. & Deschenes, R. J. Identification of a Ras Palmitoyltransferase in Saccharomyces cerevisiae. *J. Biol. Chem.* **277,** 41268–41273 (2002).

244. Resh, M. D. Palmitoylation of ligands, receptors, and intracellular signaling molecules. *Sci. STKE* **2006,** re14 (2006).

245. Yang, W., Vizio, D. Di, Kirchner, M., Steen, H. & Freeman, M. R. Proteome Scale Characterization of Human S -Acylated Proteins in Lipid Raft-enriched and Non-raft Membranes. *Molecualr Cell. proteomics* **9,** 54–70 (2010).

246. Hilgemann, D. W., Fine, M., Linder, M. E., Jennings, B. C. & Lin, M. Massive endocytosis triggered by surface membrane palmitoylation under mitochondrial control in BHK fibroblasts. *Elife* **2,** 1–16 (2013).

247. Yang, X., Kovalenko, O. V, Tang, W., Claas, C., Stipp, C. S. & Hemler, M. E. Palmitoylation supports assembly and function of integrin-tetraspanin complexes. *J. Cell Biol.* **167,** 1231–1240 (2004).

248. O'Dowd, B. F., Hnatowicht, M., Caron, M. G., Lefkowitz, R. J. & Bouviern, M. Palmitoylation of the Human B2-Adrenergic Receptor. *J. Biol. Chem.* **264,** 7564–7569 (1989).

249. Bharadwaj, M. & Bizzozero, O. a. Myelin P0 glycoprotein and a synthetic peptide containing the palmitoylation site are both autoacylated. *J. Neurochem.* **65,** 1805–15 (1995).

250. Bizzozero, O. A., Mcgarry, J. F. & Lees, M. B. Autoacylation of myelin proteolipid protein with acyl coenzyme A. *J. Biol. Chem.* **262,** 13550–7 (1987).

251. Duncan, J. a & Gilman, a G. Autoacylation of G protein alpha subunits. *J. Biol. Chem.* **271,** 23594–600 (1996).

252. Varner, A. S., De Vos, M. L., Creaser, S. P., Peterson, B. R. & Smith, C. D. A fluorescence-based high performance liquid chromatographic method for the characterization of palmitoyl acyl transferase activity. *Anal. Biochem.* **308,** 160–7 (2002).

253. Veit, M. Palmitoylation of the 25-kDa synaptosomal protein (SNAP-25) in vitro occurs in the absence of an enzyme, but is stimulated by binding to syntaxin. *Biochem. J.* **345,** 145–151 (2000).

254. Bizzozero, O. A., Bixler, H. A. & Pastuszyn, A. Structural determinants influencing the reaction of cysteine-containing peptides with palmitoyl-coenzyme A and other thioesters. *Biochim. Biophys. Acta* **1545,** 278–88 (2001).

255. Dunphy, J. T., Schroeder, H., Leventis, R., Greentree, W. K., Knudsen, J. K., Silvius, J. R. & Linder, M. E. Differential effects of acyl-CoA binding protein on enzymatic and non-enzymatic thioacylation of protein and peptide substrates. *Biochem. Biophys. Acta* **1485,** 185–198 (2000).

256. Leventis, R., Juel, G., Knudsen, J. K. & Silvius, J. R. Acyl-CoA Binding Proteins Inhibit the Nonenzymic S-Acylation of Cysteinyl-Containing Peptide Sequences by Long-Chain Acyl-CoAs. *Biochemistry* **36,** 5546–5553 (1997).

257. Ohno, Y., Kihara, A., Sano, T. & Igarashi, Y. Intracellular localization and tissue-specific distribution of human and yeast DHHC cysteine-rich domain-containing proteins. *Biochem. Biophys. Acta* **1761,** 474–483 (2006).

258. Putilina, T., Wong, P. & Gentleman, S. The DHHC domain : A new highly conserved cysteine-rich motif. *Mol. Cell. Biochem.* **195,** 219–226 (1999).

259. Gonzalez Montoro, A., Quiroga, R., Macciono, H. & Valdez Taubas, J. A novel motif at the C-terminus of palmitoyltransferases is essential for Swf1 and Pfa3 function in vivo. *Biochem. J.* **419,** 301–308 (2009).

260. Jennings, B. C. & Linder, M. E. DHHC Protein S -Acyltransferases Use Similar Ping-Pong Kinetic Mechanisms but Display Different Acyl-CoA Specificities. *J. Biol. Chem.* **287,** 7236–7245 (2012).

261. Greaves, J., Gorleku, O. A., Salaun, C. & Chamberlain, L. H. Palmitoylation of the SNAP25 Protein Family: specificity and regulation by DHHC palmitoyl transferases. *J. Biol. Chem.* **285,** 24629–24638 (2010).

262. Huang, K., Sanders, S., Singaraja, R., Orban, P., Cijsouw, T., Arstikaitis, P., Yanai, A., Hayden, M. R. & El-husseini, A. Neuronal palmitoyl acyl transferases exhibit distinct substrate specificity. *FASEB J.* **23,** 2605–2615 (2009).

263. Lai, J. & Linder, M. E. Oligomerization of DHHC Protein S-Acyltransferases. *J. Biol. Chem.* **288,** 22862–22870 (2013).

264. Frohlich, M., Dejanovic, B., Kashkar, H., Schwarz, G. & Nussberger, S. S-palmitoylation represents a novel mechanism regulating the mitochondrial targeting of BAX and initiation of apoptosis. *Cell Death Dis.* **5,** 2041–4889 (2014).

265. Maisse, C., Rossin, A., Cahuzac, N., Paradisi, A., Klein, C., Haillot, M., Hérincs, Z., Mehlen, P. & Hueber, A. Lipid raft localization and palmitoylation : Identification of two requirements for cell death induction by the tumor suppressors UNC5H. *Exp. Cell Res.* **4,** 2544–2552 (2008).

266. Fais, S., De Milito, a & Lozupone, F. The role of FAS to ezrin association in FAS-mediated apoptosis. *Apoptosis* **10,** 941–7 (2005).

267. Ji, Y., Leymarie, N., Haeussler, D. J., Bachschmid, M. M., Costello, C. E. & Lin, C. Direct Detection of S-Palmitoylation by Mass Spectrometry. *Anal. Chem.* **85,** 11952–11959 (2013).

268. Huth, W., Pauli, C. & Moller, U. Immunochemical detection of CoA-modified mitochondrial matrix proteins. *Biochem. J.* **320,** 451–457 (1996).

269. Veit, M., Sachs, K., Heckelmann, M., Maretzki, D., Hofmann, K. P. & Y, M. F. G. S. Palmitoylation of rhodopsin with S-protein acyltransferase: enzyme catalyzed reaction versus autocatalytic acylation. *Biochem. Biophys. Acta* **1394,** 90–98 (1998).

270. Page, R. C., Moore, J. D., Nguyen, H. B., Sharma, M., Chase, R., Gao, F. P., Mobley, C. K., Sanders, C. R., Ma, L., Sönnichsen, F. D., Lee, S., Howell, S. C., Opella, S. J. & Cross, T. a. Comprehensive evaluation of solution nuclear magnetic resonance spectroscopy sample preparation for helical integral membrane proteins. *J. Struct. Funct. Genomics* **7,** 51–64 (2006).

271. Krueger-Koplin, R. D., Sorgen, P. L., Krueger-Koplin, S. T., Rivera-Torres, I. O., Cahill, S. M., Hicks, D. B., Grinius, L., Krulwich, T. a & Girvin, M. E. An evaluation of detergents for NMR structural studies of membrane proteins. *J. Biomol. NMR* **28,** 43–57 (2004).

272. Yu, T.-Y., Raschle, T., Hiller, S. & Wagner, G. Solution NMR spectroscopic characterization of human VDAC-2 in detergent micelles and lipid bilayer nanodiscs. *Biochim. Biophys. Acta* **1818,** 1562–9 (2012).

273. Yousefi-Salakdeh, E., Johansson, J. & Strömberg, R. A method for S- and O-palmitoylation of peptides: synthesis of pulmonary surfactant protein-C models. *Biochem. J.* **343 Pt 3,** 557–62 (1999).

274. Vogt, T. C. B., Killian, J. A., Demel, R. A. & Kruijff, B. De. Synthesis of acylated gramicidins and the influence of acylation on the interfacial properties and conformational behavior of gramicidin A. *Biochem. Biophys. Acta* **1069,** 157–164 (1991).

275. Koeppe II, R. E., Killian, J. A., Vogt, T. C. B., Kruijff, B. De, Taylor, M. J., Mattice, G. L. & Greathouset, D. V. Palmitoylation-Induced Conformational Changes of Specific Side Chains in the Gramicidin Transmembrane Channel. *Biochemistry* **34,** 9299–9306 (1995).

276. Fernandez, T. F., Samal, A. B., Bedwell, G. J., Chen, Y. & Saad, J. S. Structural and biophysical characterization of the interactions between the death domain of Fas receptor and calmodulin. *J. Biol. Chem.* **288,** 21898–908 (2013).

277. Eberstadt, M., Huang, B., Olejniczak, E. T. & Fesik, S. W. The lymphoproliferation mutation in Fas locally unfolds the Fas death domain. *Nat. Struct. Biol.* **4,** 983–985 (1997).

278. Clore, G. M. Interplay between conformational selection and induced fit in multidomain protein-ligand binding probed by paramagnetic relaxation enhancement. *Biophys. Chem.* **186,** 3–12 (2014).

279. Csermely, P., Palotai, R. & Nussinov, R. Induced fit, conformational selection and independent dynamic segments: an extended view of binding events. *Trends Biochem. Sci.* **35,** 539–546 (2010).

280. Muir, T. W. Semisynthesis of proteins by expressed protein ligation. *Annu. Rev. Biochem.* **72,** 249–89 (2003).

281. Flavell, R. R., Huse, M., Goger, M., Trester-zedlitz, M., Kuriyan, J. & Muir, T. W. Efficient Semisynthesis of a Tetraphosphorylated Analogue of the Type I TGF Receptor. *Org. Lett.* **4,** 165–168 (2002).

282. Huse, M., Holford, M. N., Kuriyan, J. & Muir, T. W. Semisynthesis of Hyperphosphorylated Type I TGFB Receptor : Addressing the Mechanism of Kinase Activation. *J. Am. Chem. Soc.* **122,** 8337–8338 (2000).

283. Ottesen, J. J., Huse, M., Sekedat, M. D. & Muir, T. W. Semisynthesis of Phosphovariants of Smad2 Reveals a Substrate Preference of the Activated T beta RI kinase. *Biochemistry* **43,** 5698–5706 (2004).

284. Li, J., Taylor, I. A., Lloyd, J., Clapperton, J. A., Howell, S., Macmillan, D. & Smerdon, S. J. Chk2 oligomerisation studied by phosphopeptide ligation: Implications for regulation and phosphodependent interactions. *J. Biol. Chem.* **282,** 36019 (2008).

285. Ando, K., Kernan, J. L., Liu, P. H., Sanda, T., Logette, E., Tschopp, J., Look, a T., Wang, J., Bouchier-Hayes, L. & Sidi, S. PIDD death-domain phosphorylation by ATM controls prodeath versus prosurvival PIDDosome signaling. *Mol. Cell* **47,** 681–93 (2012).

286. Karagoz, G. E., Sinnige, T., Hsieh, O. & Ru, S. G. D. Expressed protein ligation for a large dimeric protein. *Protein Enginering, Des. Sel.* **24,** 495–501 (2011).

287. Zhao, W., Zhang, Y., Cui, C., Li, Q. & Wang, J. An efficient on-column expressed protein ligation strategy : Application to segmental triple labeling of human apolipoprotein E3. *Protein Sci.* **17,** 736–747 (2008).

288. Fehon, R. G., McClatchey, A. I. & Bretscher, A. Organizing the cell cortex: the role of ERM proteins. *Nat. Rev. Mol. Cell Biol.* **11,** 276–87 (2010).

289. Ye, F. & Zhang, M. Structures and target recognition modes of PDZ domains: recurring themes and emerging pictures. *Biochem. J.* **14,** 1–14 (2013).

290. Wang, S., Raab, R. W., Schatz, P. J., Guggino, W. B. & Li, M. Peptide binding consensus of the NHERF-PDZ1 domain matches the C-terminal sequence of cystic fibrosis transmembrane conductance regulator (CFTR). *FEBS* **427,** 103–108 (1998).

291. Maudsley, S., Zamah, A. M., Rahman, N., Blitzer, T., Luttrell, L. M., Lefkowitz, R. J. & Hall, A. Platelet-Derived Growth Factor Receptor Association with Na+/H+ Exchanger Regulatory Factor Potentiates Receptor Activity. *Mol. Cell. Biol.* **20,** 8352–8363 (2000).

292. Lazar, C. S., Cresson, C. M., Lauffenburger, D. A. & Gill, G. N. The Na+/H+ Exchanger Regulatory Factor Stabilizes Epidermal Growth Factor Receptors at the Cell Surface. *Mol. Biol. Cell* **15,** 5470–5480 (2004).

293. Yanagisawa, J., Takahashi, M., Yano-yanagisawa, H., Sawa, E., Nishitoba, T. & Sato, T. The Molecular Interaction of Fas and FAP-1: A tripeptide blocker of human Fas interaction with FAP-1 promotes Fas-induced Apoptosis. *J. Biol. Chem.* **272,** 8539–8545 (1997).

294. Lu, M., Marsters, S., Ye, X., Luis, E., Gonzalez, L. & Ashkenazi, A. E-Cadherin Couples Death Receptors to the Cytoskeleton to Regulate Apoptosis. *Mol. Cell* **54,** 1–12 (2014).

295. Rio, M. D. E. L., Imam, A., Deleon, M., Gomez, G., Mishra, J., Ma, Q., Parikh, S. & Devarajan, P. The Death Domain of Kidney Ankyrin Interacts with Fas and Promotes Fas-Mediated Cell Death in Renal Epithelia. *J. Am. Soc. Nephrol.* **14,** 41–51 (2004).

296. Robert, S., Domurado, D., Thomas, D. & Chopineau, J. Fatty acid acylation of Rnase A using reversed micelles as microreactors. *Biochem. Biophys. Res. Commun.* **196,** 447–454 (1993).

297. Chopineau, J., Robert, S., Fenart, L., Cecchelli, R., Lagoutte, B., Paitier, S., Dehouck, M. & Domurado, D. Monoacylation of ribonuclease A enables its transport across an in vitro model of the blood – brain barrier. *J. Control. release* **56,** 231–237 (1998).

298. Bergeret, F., Gavalda, S., Chalut, C., Malaga, W., Quémard, A., Pedelacq, J., Daffé, M., Guilhot, C., Mourey, L. & Bon, C. Biochemical and Structural Study of the Atypical Acyltransferase Domain from the Mycobacterial Polyketide. *J. Biol. Chem.* **287,** 33675–33690 (2012).

299. Ward, B. P., Ottaway, N. L., Perez-Tilve, D., Ma, D., Gelfanov, Vasily, M., Tschop, Matthias, H. & DiMarchi, R. D. Peptide lipidation stabilises structure to enhance biological function. *Mol. Metab.* **2,** 468–479 (2013).

300. Quevillon-cheruel, S., Leulliot, N., Muniz, C. A., Vincent, M., Gallay, J., Argentini, M. & Cornu, D. Evf , a Virulence Factor Produced by the Drosophila Pathogen Erwinia carotovora, Is an S -Palmitoylated Protein with a New Fold That Binds to Lipid Vesicles. *J. Biol. Chem.* **284,** 3552–3562 (2009).

301. Bader, B., Kuhn, K., Owne, D. J., Waldermann, H., Wittinghofer, A. & Kuhlmann, J. Bioorganic synthesis of lipid-modified proteins for the study of signal transduction. *Nature* **403,** 223–226 (2000).

302. Pylypenko, O., Rak, A., Kushnir, S., Dursina, E., Thomae, N. H., Constantinescu, T., Brunsveld, L., Watzke, A., Waldmann, H., Goody, R. S. & Alexandrov, K. Structure of doubly prenylated Ypt1 : GDI complex and the mechanism of GDI-mediated Rab recycling. *EMBO J.* **25,** 13–23 (2006).

303. Hagn, F., Etzkorn, M., Raschle, T. & Wagner, G. Optimized Phospholipid Bilayer Nanodiscs Facilitate High-Resolution Structure Determination of Membrane Proteins. *J. Am. Chem. Soc.* **135,** 1919–1925 (2013).

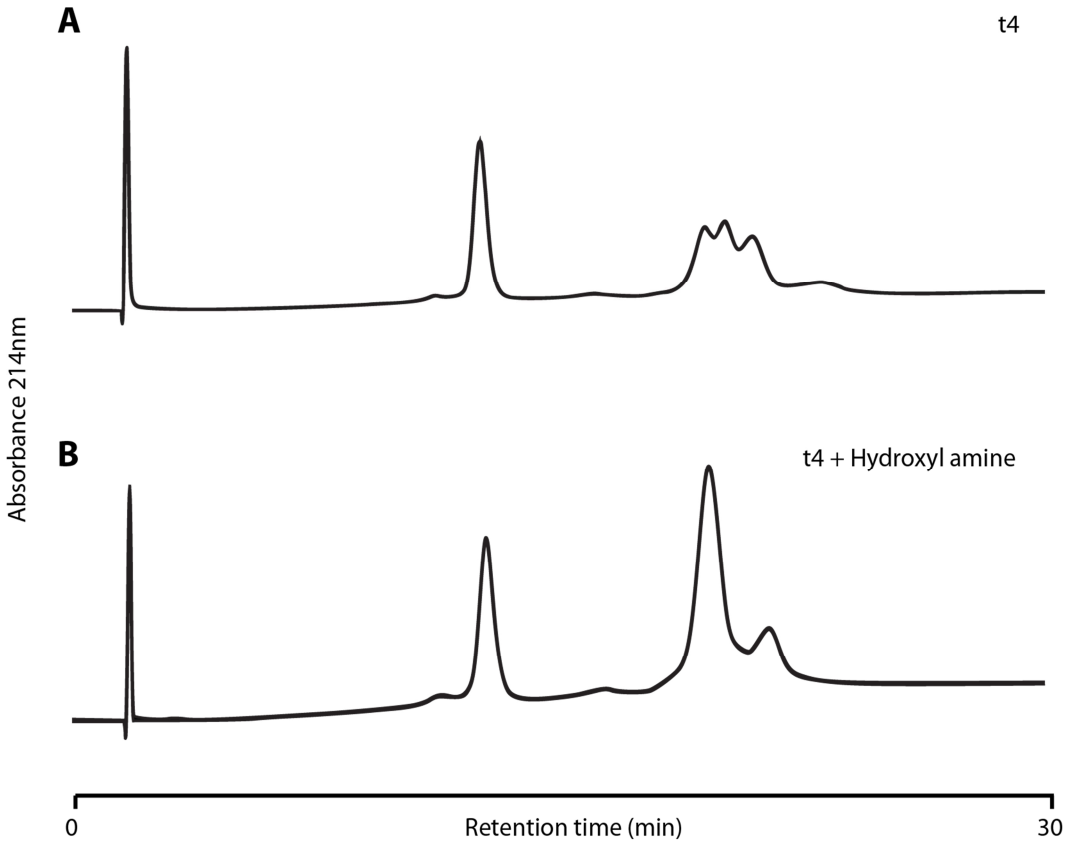

Appendix A - Hydoxylamine treatment of L11 t4 to prove the product is product not unrearranged intermediate

Chromatograms showing the four hour timepoint from the ligation in which 1mM MBP-Nt-Fas-DD H285G thioester was incubated with1mM Hmb-pY-Ct-Fas-DD peptide at pH 7 in ligation buffer. A, shows with no additives. B, shows with the addition of hydroxyl amine, reducing any non-amide bonded thioester components

Appendix B - $^{1}H/^{15}N$-HSQC spectrumof 15N ezrin 1-297

Recorded at 298K, 600MHz ^{1}H frequency.

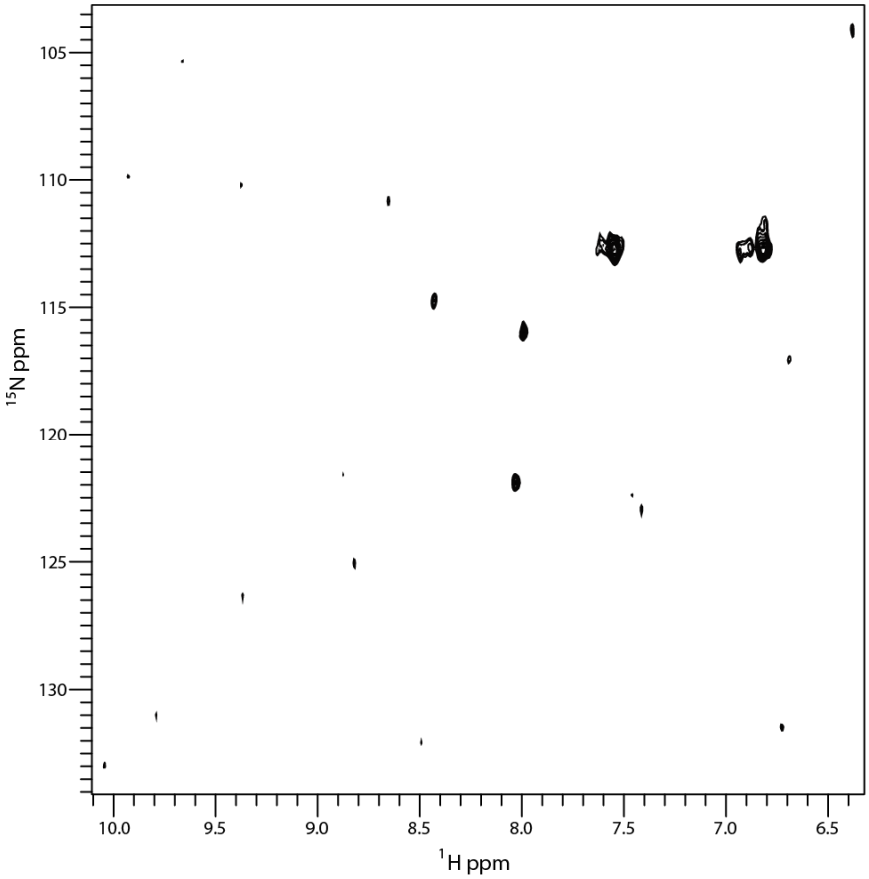

Appendix C - $^{2}H/^{15}N$ ezrin 1-297 titration with ICAM2 peptide

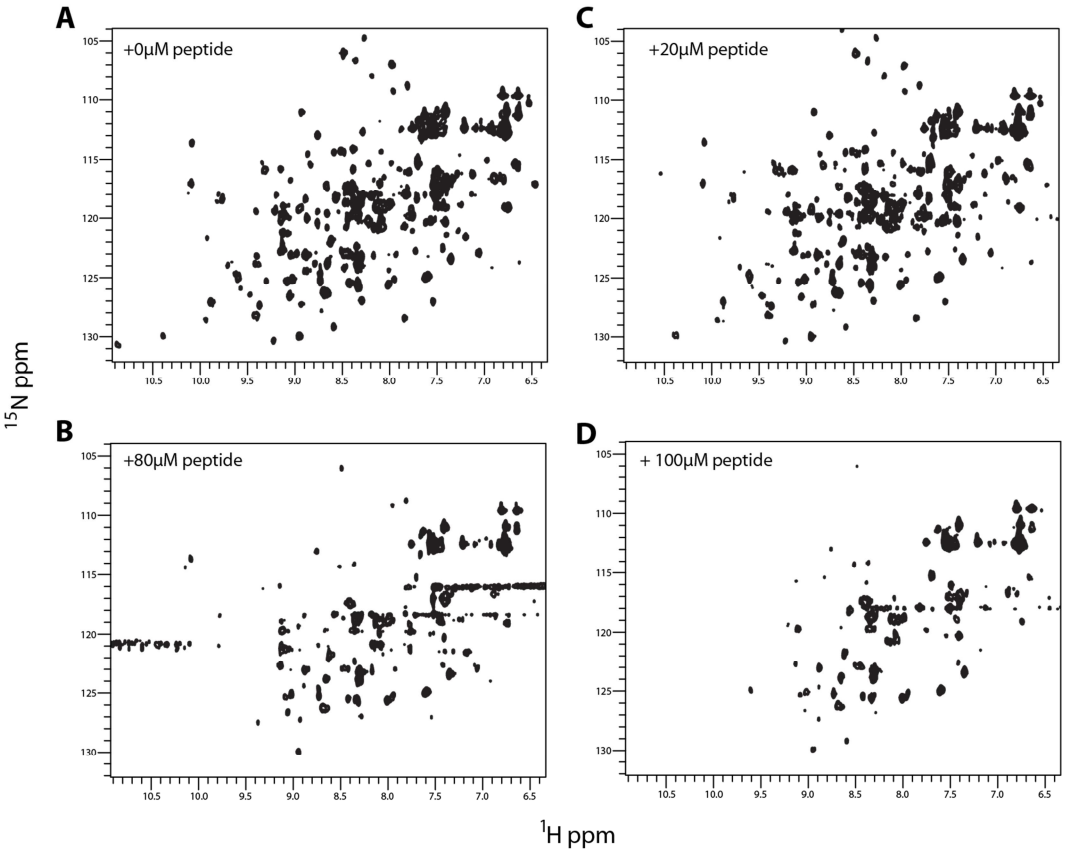

$^{1}H/^{15}N$-HSQC spectra of 100 μM : $^{2}H/^{15}N$ ezrin with: A, 0 μM ICAM2 peptide, B, 20 μM ICAM2 peptide, C, 80 μM ICAM2 peptide, D 100 μM ICAM2 peptide. The ICAM2 peptide causes line broadening in the $^{1}H/^{15}N$ HSQC spectrum of ezrin FERM